Investigation into Environmental Stress Cracking in Processed Food Cans.

P.J.Smith

Abstract

This study followed instances of filled can leakage in the late 1990s – 2000, affecting steel cans packed with high protein meats or fish. Such foods typically contain at least one anion promoting susceptibility, phosphate, and low levels of some promoters of hydrogen ingress into steel.

Experiments utilised product brines from cans of tuna and red salmon, bulked and deep frozen. Tuna has some history of stress corrosion in steel cans but no cases were known for salmon. DC polarisation tests did not reveal conclusive evidence of passive conditions on the anodic polarisation curves.

Slow strain rate tests including current measurement were conducted at the Open Circuit Potential, for three cold reduced 620MPa nominal yield strength steels of Al killed type, tested as notched specimens. Each steel showed loss of ductility at the notch region under high or low air (N_2 flush) test conditions with either product. Discrete regions of environmental stress cracking were observed using SEM, for each steel type with salmon brine under high and low air conditions, with more limited evidence for tuna. Loss of ductlity and environmental stress cracking were partial effects. The features observed were consistent with hydrogen cracking; analytical work revealed headspace hydrogen in the cans of each product type.

Regression relationships for time to failure were derived combining the direct effect of mechanical work up to maximum load, and the inverse effect of the integrated current-time parameter.

FEA modelling for prediction of stresses was carried out for the notched tensile sample, a drawn redrawn fish can and an easy open end shell. The predictions permitted comparisons to be drawn between the different cases in the absence of corrosion. Further work e.g. by changing notch angles may help identify any threshold stress levels affecting this failure type.

Table of Contents

1 SECTION 1: INTRODUCTION 15

1.1 BACKGROUND TO THE PROJECT 15
1.2 METAL CONTAINERS AND MATERIALS FOR PROCESSED FOODS: TYPES CONSIDERED 16
1.2.1 Three Piece Round Processed Food Cans : Body plus two Ends. 16
1.2.2 Two Piece Drawn and Redrawn Cans 19
1.3 MATERIALS CHARACTERISTICS 21
1.4 PRODUCTS AND ENVIRONMENTS: GENERAL FEATURES OF COMPOSITION. 24
1.5 STRESSES PRESENT IN CANS AND COMPONENTS : INITIAL OBSERVATIONS 26
1.6 FOOD PRODUCTS : SOME CASES OF COMMERCIAL FAILURES REPORTED. 27
1.7 SOME COMPOSITIONAL ASPECTS OF MEAT INCLUDING MYOGLOBIN 28
1.8 ENVIRONMENTAL FACTORS: COMMON ANIONS AND CARBON DIOXIDE. 30
1.9 SULPHIDE ENVIRONMENTS AND TYPES OF HYDROGEN CRACKING EFFECTS 34
1.10 SULPHIDES: BREAK DOWN BEHAVIOUR INVOLVING AMINO ACIDS IN FOODS 37
1.11 SUMMARY OF INFORMATION: VOLATILES FROM COOKING OF MEAT AND FISH. 44
1.12 COMPOSITIONAL ASPECTS OF FOOD: FISH PRODUCTS. 45
1.13 DISCUSSION OF DIFFERENCES OBSERVED IN THE COMPOSITION BETWEEN TUNA AND SALMON IN BRINE, AND CONSIDERATION OF OTHER FISH. 47
1.14 MEAT ANALYSIS. 52
1.15 METALLURGICAL ASPECTS OF STRESS CORROSION CRACKING. 56
1.15.1 Fracture Mechanics and Surface Energy related Effects 56
1.15.2 Measurement of Internal Stresses in Metals 64
1.15.3 Material Forming Strains and Stresses : The Finite Element Method 67
1.15.4 Metallurgical Aspects: Effects of Steel Composition. 69
1.15.5 Stacking Fault Energy and Chemical Composition of Steels 74
1.15.6 Metallurgical Aspects : Hydrogen Cracking and The Troiano Theory. 76
1.15.7 Surface Energy Theory , Coleman et al; Stroh and Petch. 80
1.16 ELECTRO CHEMICAL ASPECTS 81
1.16.1 Electro Chemical Theory: E.H. Dix 81
1.16.2 Cracking of Carbon Steels by Nitrate : Henthorne and Parkins 82
1.16.3 Electrochemical Aspects : Cracking Studies in Phosphate Solutions 82
1.16.4 Electrochemical Aspects: Localised Corrosion and Pitting. 83
1.16.5 Electrochemical Aspects: Further Observations: J.C. Scully 85
1.17 FACTORS AFFECTING CRACK GROWTH KINETICS: PARKINS 86
1.18 CORROSION FATIGUE. 88
1.18.1 Corrosion Fatigue: Testing and Fracture Mechanics Aspects 90
1.19 STRESS CORROSION SPECTRUM 91
1.20 DISCUSSION OF POTENTIAL CONTRIBUTORY CONDITIONS TO ENVIRONMENTAL STRESS CRACKING IN MEAT AND FISH CANS. 92
1.20.1 Chemical Species in Meat and Fish. 92
1.20.2 Chemisorption Behaviour: Selenium and Sulphur Compounds 95
1.20.3 Fats , Sugars and Vitamins. 98

1.20.4 Synergistic Effects *100*
1.20.5 Failure Mechanisms and Metallurgical Aspects *101*
1.21 CONCLUSIONS 116
1.22 SECTION 1, APPENDIX 1. 120
1.23 SECTION 1, APPENDIX 2, PAGE 1 121
1.24 SECTION 1, APPENDIX 2, PAGE 2 123

2 SECTION 2: EXPERIMENTAL STUDIES : INITIAL WORK AND FINDINGS. 124

2.1 INTRODUCTION 124
2.2 EXPERIMENTAL WORK AND PROCEDURES. 125
2.2.1 Parameters Determined During Slow Strain Rate Test Work. *126*
2.3 RESULTS 129
2.3.1 Initial Observations from Slow Strain Rate Tests using Product Brine from individual Drained Cans. *129*
2.3.2 DC Polarisation Tests. *132*
2.3.3 Pitting Loop Tests. *134*
2.4 SLOW STRAIN RATE TEST FINDINGS FROM EXPERIMENTS USING BULKED TUNA BRINE. 135
2.4.1 Correlations Data from Slow Strain Rate Test Data: Combined Acid Types. 135
2.4.2 Correlation and Regression Predictions of 'Time of Test': Tuna Brine with Added Acetic Acid. *140*
2.4.3 Discussion of Statistical Information from Initial Slow Strain Rate Tests 151
2.4.4 Observations from Microscopy on Slow Strain Rate Tested Samples: 'Non Scratched' Sub Groups. *153*
2.4.5 Observations from Microscopy on Slow Strain Rate Tested samples: 'Scratched' Sub Groups. *166*
2.4.6 Product Analysis: Tuna Brine: Anions and Cations. *170*
2.4.7 Tensile Properties of eccs Test Material *171*
2.4.8 Steel Composition Analysis *173*
2.5 DISCUSSION OF INITIAL RESULTS. 174
2.6 CONCLUSIONS FROM INITIAL EXPERIMENTAL FINDINGS. 176
2.7 SECTION 2, APPENDIX 1, PAGE 1 179
2.8 SECTION 2, APPENDIX 1, PAGE 2 180

3 SECTION 3: EXPERIMENTAL WORK 181

3.1 INTRODUCTION: SLOW STRAIN RATE TESTING AND TEST PROGRAMME 181
3.2 RESULTS 187
3.2.1 Notes on Statistical Methods used *187*
3.2.2 Statistical Correlations : Tuna Brine : Slow Strain Rate Tests: Air Conditions *188*
3.2.3 Statistical Correlations : Tuna Brine : Slow Strain Rate Tests: Nitrogen Flushing Conditions. See Appendix 3 Pages 1 and 2 for Data. *189*
3.2.4 Statistical Correlations : Salmon Brine : Slow Strain Rate Tests: Air Conditions. See Appendix 4, Pages 1 and 2. ..... *190*
3.2.5 Statistical Correlations : Salmon Brine : Slow Strain Rate Tests: Nitrogen Flushing Conditions. See Appendix 5, Pages 1 and 2. ..... *191*
3.2.6 Summary of Main Points of Correlation Evidence for Tuna and Salmon Brines 192

3.2.7 Regression Predictions for Time to failure using 'Best Subsets' Method: Tuna Brine Product *193*
3.2.8 Regression Predictions for Time to failure using 'Best Subsets Method: 201
3.2.9 Summary Comments on Regression Data: Tuna and Salmon Brines...211
3.2.10 Estimation of Crack Growth Rate for Tuna Brine samples tested under Air Conditions using Slow Strain Rate Test Data *214*
3.3 MICROSCOPY: 225
3.3.1 General Observations on Development of Fractures *225*
3.3.2 Observations on Control Samples Tested in Oil. *227*
3.3.3 Observations on Slow Strain Rate Tested Samples in Tuna Brine: Air Conditions. *231*
3.3.4 Slow Strain Rate Tensile Load - Extension Plots for Tuna Brine Tests: Air and Nitrogen Flushing Conditions *238*
3.3.5 Microscopy Observations on Slow Strain Rate Tested Samples in Tuna Brine: Nitrogen Flush Conditions *240*
3.3.6 Microscopy: Slow Strain Rate Tested Samples: Salmon Brine: Air Conditions. *242*
3.3.7 Microscopy: Observations on Samples subject to Slow Strain Rate Tests in Salmon Brine: Nitrogen Flush Conditions. *247*
3.3.8 Tensile Load – Extension Plots for Salmon Samples Subject to Plots for Samples Subject to also Strain Rate Tests in salmon Brine and control Samples Tested in Oil *250*
3.4 METAL THICKNESS REDUCTION DATA AT NOTCH REGIONS FOR SAMPLES SUBJECT TO SLOW STRAIN RATE TESTS. 254
3.5 OBSERVATIONS FROM PEAK LOAD VALUES FOR SLOW STRAIN RATE TEST GROUPS TESTED IN PRODUCT BRINES. 259
3.6 PREDICTIVE ESTIMATION OF STRAINS AND STRESSES BY FINITE ELEMENT ANALYSIS (FEA) STUDIES. 261
3.6.1 Explanatory Introduction *261*
3.6.2 Plate Tensile Properties: Engineering-Stress Strain Plots and True Stress Strain Estimation Studies on DR620 CA Plates used in Product Brine Slow Strain Rate Tests. *266*
3.6.3 Final Estimate of True-Stress-Strain Plots achieved. *273*
3.7 MODEL EXAMPLES SELECTED FOR THE STUDY : 274
3.7.1 Model 1: Notch Tensile Sample Used in Slow Strain Rate Testing Under Tension. 274
3.7.2 Model 2: 83mm Dia Drawn Redrawn Can with Redraw Height of 50mm. 284
3.7.3 Model 3: 73mm Dia Easy Open End Shell for Processed Foods *293*
3.8 PRODUCT TESTS AND ANALYSES. 303
3.8.1 Electrochemical Tests on Tuna and Salmon Brine Products. *303*
3.8.2 Experimental Details *303*
3.8.3 Discussion of Results *305*
3.8.4 Observations from XRA Studies using SEM equipment on Electrodes from Electrochemical tests in Salmon and Tuna Brines : *313*
3.8.5 Chemical Analyses of Product Brines for Anions and Cations. *320*
3.8.6 Headspace Gas Analysis Data from Tuna and Salmon Can Stock used to Provide Product Brine Bulks. *322*
3.8.7 Steel Analyses for 0.16mm , 0.18mm and 0.235mm Gauge DR620CA eccs Plates used in Slow Strain Rate Test Programme. *323*

3.8.8 Microstructural Characterisation of Steels Used in Slow Strain Rate Test Programme, and Comments. *324*
3.9 DISCUSSION OF INVESTIGATIONS 327
3.9.1 The Development of Cracking and Failure: Initial Observations on Corrosion Behaviour. *327*
3.9.2 Behaviour at Notches *330*
3.9.3 Evidence from Fractography. *331*
3.9.4 Evidence from Product Chemistry and X Ray Analysis(XRA). *331*
3.9.5 Evidence from Correlation and Regression Information from Slow Strain Rate Tests. *334*
3.9.6 Regression Predictions for Time to Failure in slow Strain rate tests, Based upon Integrated Current-Time Data and Mechanical Work. *335*
3.9.7 Stress Prediction Studies by Finite Element Modelling *344*
3.9.8 83mm Diameter Draw-Redrawn Can Model: Base Rim and Wall Stresses and Comparison with Notch Tensile Test Piece Results. *345*
3.9.9 73mm Diameter Model for Easy Open end Shell: Comments. *346*
3.9.10 Stress Predictions from Notched Tensile Models. *346*
3.10 SECTION 3, APPENDIX 1. 348
3.11 SECTION 3, APPENDIX 2, PAGE 1 352
3.12 SECTION 3, APPENDIX 2, PAGE 2 353
3.13 SECTION 3, APPENDIX 3, PAGE 1 354
3.14 SECTION 3, APPENDIX 3, PAGE 2 355
3.15 SECTION 3, APPENDIX 4, PAGE 1 356
3.16 SECTION 3, APPENDIX 4, PAGE 2 357
3.17 SECTION 3, APPENDIX 5, PAGE 1 358
3.18 SECTION 3, APPENDIX 5, PAGE 2 359
3.19 SECTION 3, APPENDIX 6 360
3.20 SECTION 3, APPENDIX 7 361
3.21 SECTION 3, APPENDIX 8 362
3.22 SECTION 3, APPENDIX 9 363
3.23 SECTION 3, APPENDIX 10 364
3.24 SECTION 3, APPENDIX 11, PAGE 1 OF 3 365
3.25 SECTION 3, APPENDIX 11, PAGE 2 OF 3. 366
3.26 SECTION 3, APPENDIX 11, PAGE 3 OF 3 367
4 SECTION 4: CONCLUSIONS AND RECOMMENDATIONS 368
4.1 CONCLUSIONS. 368
4.2 RECOMMENDATIONS 375
5 ACKNOWLEDGEMENTS 376
6 REFERENCE LIST 377

Supplementary List of Figures in order of appearance.

FIGURE 1: EXTERIOR SURFACE OF 83MM DIAMETER TUNA IN BRINE CAN SHOWING CRACKING AT BASE RIM, PARTLY ASSOCIATED WITH DENTING IN RIM. 15
FIGURE 2: SECTION FROM REGION NEAREST INTERIOR SURFACE OF TUNA IN BRINE CAN FROM LOT CORRESPONDING TO FIGURE 1, SHOWING BRANCHING CRACKS AT BASE RIM REGION 16
FIGURE 3: NITROGENISED 0.235MM DR620CA PACKAGING STEEL EX SOURCE A, SECTIONED PARALLEL TO THE PLATE GRAIN DIRECTION. 23
FIGURE 4: NON NITROGENISED 0.235MM DR 620 CA STEEL EX SOURCE B, SECTIONED PARALLEL TO THE GRAIN DIRECTION, SHOWING INCREASED COLD WORK RELATIVE TO NITROGENISED MATERIAL. 23
FIGURE 5: GENERAL STRUCTURE OF AMINO ACID AND CHAIN WITH PEPTIDE LINKAGES. 25
FIGURE 6: CHEMICAL STRUCTURE OF CYSTINE 37
FIGURE 7: VOLATILE SUBSTANCES ARISING FROM THE PROCESSING OF MEAT. 39
FIGURE 8 SCHEMATIC ILLUSTRATION OF SLOW STRAIN RATE TEST SAMPLE NOTCH USED IN INITIAL SLOW STRAIN RATE STUDIES. 107
FIGURE 9: 0.235MM DR620CA MALEIS STEEL STRUCTURE FROM A SECTION PARALLEL TO THE GRAIN, SHOWING LOCAL CARBIDES, BUT HAVING A LOW DENSITY OF CARBIDE STRINGERS. A RELATIVELY GOOD RESULT WAS OBTAINED IN A STRESS CORROSION PACK TEST. THE % ELONGATION WAS 2.3. THE GRAIN SIZE MEASUREMENT WAS 32,200GRAINS PER MM^2. 113
FIGURE 10: NITROGENISED ECCS MATERIAL FROM SOURCE 1 GIVING A RELATIVELY GOOD PACK TEST RESULT AND HAVING A LOW DENSITY OF GRAIN BOUNDARY CARBIDES. THE %ELONGATION WAS 3.3% AND THE GRAIN SIZE MEASUREMENT WAS 43,472 GRAINS /MM^2. 113
FIGURE 11: DR620 CA NITROGENISED MATERIAL FROM SOURCE 2 GIVING A MEASURABLY LESS GOOD PACK TEST RESULT THAN FOR MATERIALS IN FIGURES 9 AND 10 AND HAVING A HIGHER DENSITY OF GRAIN BOUNDARY CARBIDES THAN THE NITROGENISED MATERIAL IN FIGURE 13 TOGETHER WITH A MORE IRREGULAR GRAIN SIZE. THIS MATERIAL HAD LOW ELONGATION OF 1.1% AND GRAIN SIZE MEASUREMENT OF 45,680GRAIN /MM^2 114
FIGURE 12: STANDARD DR 620 CA MATERIAL, NON NITROGENISED, AGAIN GIVING A LESS GOOD PACK TEST RESULT THAN MATERIALS SHOWN IN FIGURES 9 AND 10 , WITH A RESULT SIMILAR TO FIGURE 14 MATERIAL. THIS MATERIAL HAS SHOWN GREATER COLD WORK EFFECTS IN THE GRAIN STRUCTURE THAN FOR NITROGENISED STEELS ABOVE TOGETHER WITH GRAIN BOUNDARY CARBIDES AND SOME CARBIDE STRINGERS. THE MATERIAL HAD AN ELONGATION OF 1.81% AND A GRAIN SIZE MEASUREMENT OF 42,030 GRAINS /MM^2. 114
FIGURE 13: EXAMPLE OF CRACKING IN PACK TEST FAILURE SAMPLE FILLED WITH ANIMAL FOOD PRODUCT. THE MATERIAL IN THIS CASE CORRESPONDED TO THAT CHARACTERISED IN FIGURE 11 115
FIGURE 14: TUNA BRINE SAMPLE SRTTU47 JAN 2003 , TESTED UNDER AIR CONDITIONS BY THE SLOW STRAIN RATE METHOD. CRACKING ON WALL OF SPECIMEN CLOSE TO THE FRACTURE EDGE. 129
FIGURE 15: TUNA BRINE SAMPLE SSRTTU51 JAN 2003, TESTED UNDER AIR CONDITIONS BY SLOW STRAIN RATE METHOD. CRACKING ON WALL OF SPECIMEN CLOSE TO FRACTURE EDGE 130
FIGURE 16: METALLOGRAPHIC MICRO SECTION ACROSS SAMPLE SSRTTU51 FRACTURE,CUT PARALLEL TO THE AXIS OF THE TEST SAMPLE JUST BELOW THE NOTCH APEX 131
FIGURE 17: FAST AND SLOW SWEEP POLARISATION: AIR CONDITIONS : 0.19MM DR520 CA ECCS MATERIAL. 132
FIGURE 18: FAST AND SLOW SWEEP POLARISATION: NITROGEN FLUSHING CONDITIONS: 0.19MM DR520 CA ECCS MATERIAL. 133
FIGURE 19: PITTING LOOP : TUNA BRINE: 0.19MM DR520 CA ECCS MATERIAL : NON ABRADED: AIR CONDITIONS. 134
FIGURE 20: PITTING LOOP : TUNA BRINE: 0.19MM DR520 CA ECCS MATERIAL: NON ABRADED: NITROGEN FLUSH CONDITIONS. 135
FIGURE 21: IMAGE OF FAILURE REGION ADJACENT NOTCH ON CONTROL SAMPLE N16, AFTER SLOW STRAIN RATE TESTING UNDER AIR CONDITIONS. 155
FIGURE 22: IMAGE OF FAILURE REGION ASDJACENT NOTCH ON CONTROL SAMPLE N16, AFTER SLOW STRAIN RATE TESTING UNDER AIR CONDITIONS: LARGER MAGNIFICATION. 156
FIGURE 23: IMAGE OF FAILURE REGION ASDJACENT NOTCH ON CONTROL SAMPLE N7, AFTER SLOW STRAIN RATE TESTING UNDER AIR CONDITIONS: LARGER MAGNIFICATION. 157

FIGURE 24: SAMPLE SSRTTU047: SLOW STRAIN RATE TESTED SAMPLE: TUNA BRINE ACIDIFIED WITH ACETIC ACID TO PH 4.68. NOTCH AREA FRACTURE SURFACE SHOWING REGIONS OF VERY LOW DUCTILITY BELOW PITTING ZONE. 158
FIGURE 25: SAMPLE SSRTTU047: SLOW STRAIN RATE TESTED SAMPLE: TUNA BRINE ACIDIFIED WITH ACETIC ACID TO PH 4.68. FRACTURE SURFACE NEAR NOTCH AREA SHOWING REGIONS OF ENVIRONMENTAL STRESS CRACKING. LARGER MAGNIFICATION 159
FIGURE 26: SAMPLE SSRTTU047: SLOW STRAIN RATE TESTED SAMPLE: TUNA BRINE ACIDIFIED WITH ACETIC ACID TO PH 4.68. FRACTURE SURFACE NEAR NOTCH AREA SHOWING STEP REGIONS OF ENVIRONMENTAL STRESS CRACKING. LARGER MAGNIFICATION: 2ND VIEW 159
FIGURE 27: SAMPLE SSRTTU049. SLOW STRAIN RATE TESTED SAMPLE: TUNA BRINE ACIDIFIED WITH ACETIC ACID TO PH 4.68. FRACTURE SURFACE NEAR NOTCH AREA SHOWING ZONE OF LOW DUCTILITY. 161
FIGURE 28: SAMPLE SSRTTU049 LARGER MAGNIFICATION OF FIGURE 30 SHOWING STEP FRACTURE CONSISTENT WITH TRANS-GRANULAR ENVIRONMENTAL STRESS CRACKING NEAR FRACTURE EDGE. 162
FIGURE 29: SAMPLE SSRTTU049. SLOW STRAIN RATE TESTED SAMPLE: TUNA BRINE ACIDIFIED WITH HYDROCHLORIC ACID TO PH 5.01. FRACTURE SURFACE NEAR NOTCH AREA SHOWING ZONE OF LOW DUCTILITY 163
FIGURE 30: SAMPLE SSRTTU054. SLOW STRAIN RATE TESTED SAMPLE: TUNA BRINE ACIDIFIED WITH HYDROCHLORIC ACID TO PH 5.01. LARGER MAGNIFICATION VIEW OF FRACTURE SURFACE NEAR NOTCH AREA SHOWING ZONE OF LOW DUCTILITY, AND LEDGES CONSISTENT WITH TRANSGRANULAR ENVIRONMENTAL STRESS CRACKING EFFECTS. 164
FIGURE 31: SAMPLE SSRTTU055. SLOW STRAIN RATE TESTED SAMPLE: TUNA BRINE ACIDIFIED WITH HYDROCHLORIC ACID TO PH 4.56. VIEW OF FRACTURE SURFACE NEAR NOTCH AREA SHOWING ZONE OF LOW DUCTILITY, AND LEDGES CONSISTENT WITH TRANSGRANULAR ENVIRONMENTAL STRESS CRACKING EFFECTS. MORE DUCTILITY WAS INDICATED AT THE OPPOSITE FRACTURE EDGE. 165
FIGURE 32: SAMPLE SSRTTU055. LARGER MAGNIFICATION VIEW SHOWING LOW DUCTILITY BEHAVIOUR AND STEP FRACTURE CONDITIONS CONSISTENT WITH TRANS-GRANULAR ENVIRONMENTAL STRESS CRACKING. 165
FIGURE 33: SAMPLE SSRTTU041. SLOW STRAIN RATE TESTED SAMPLE: TUNA BRINE NON ACIDIFIED. VIEW OF FRACTURE SURFACE NEAR NOTCH AREA SHOWING ZONE OF LOW DUCTILITY, AND LEDGES AND FAN SHAPES CONSISTENT WITH TRANSGRANULAR ENVIRONMENTAL STRESS CRACKING. 166
FIGURE 34: SAMPLE SSRTTU041. SLOW STRAIN RATE TESTED SAMPLE: TUNA BRINE, NON ACIDIFIED. LARGER MAGNIFICATION VIEW OF LEDGES AND FAN SHAPES CONSISTENT WITH TRANSGRANULAR ENVIRONMENTAL STRESS CRACKING 167
FIGURE 35: SAMPLE SSRTTU043. SLOW STRAIN RATE TESTED SAMPLE: TUNA BRINE ACIDIFIED WITH ACETIC ACID TO PH 4.67. VIEW OF FRACTURE SURFACE NEAR NOTCH AREA SHOWING ZONE OF LOW DUCTILITY, AND SOME LEDGES CONSISTENT WITH TRANSGRANULAR ENVIRONMENTAL STRESS CRACKING. 168
FIGURE 36 SAMPLE SSRTTU040: SLOW STRAIN RATE TESTED SAMPLE: TUNA BRINE ACIDIFIED WITH HYDROCHLORIC ACID TO PH 4.66. VIEW OF FRACTURE SURFACE NEAR NOTCH AREA SHOWING ZONE OF LOW DUCTILITY, AND SOME LEDGES. 169
FIGURE 37: SLOW STRAIN RATE TESTER CELL FOR AIR, OR NITROGEN FLUSHING CONDITIONS 181
FIGURE 38: TENSILE TEST SPECIMEN FOR STRESS CORROSION CRACKING: SCHEMATIC 185
FIGURE 39: NOTCH AND STRESS INTENSITY FACTOR CALCULATIONS 217
FIGURE 40: EXAMPLE OF CRACKS DEVELOPING FROM ELONGATED PITS IN SALMON BRINE SAMPLE SSRTSAL215 TESTED UNDER AERATED CONDITIONS 225
FIGURE 41: SSRT 260 CONTROL AT NOTCH END B 228
FIGURE 42: SSRT 260 CONTROL AT NOTCH END G 228
FIGURE 43: SSRT 260 CONTROL AT NOTCH END C 228
FIGURE 44: SSRT 260 CONTROL AT NOTCH END H 228
FIGURE 45: SSRT 261 CONTROL AT NOTCH END G 229
FIGURE 46: SSRT 261 CONTROL AT NOTCH END B. 229
FIGURE 47: SSRT 261 CONTROL AT NOTCH END H 229
FIGURE 48: SSRT 261 CONTROL AT NOTCH END C 229
FIGURE 49: SSRT 262 CONTROL AT NOTCH END B 230
FIGURE 50: SSRT 262 CONTROL AT NOTCH END G 230
FIGURE 51: SSRT 262 CONTROL AT NOTCH END C 230
FIGURE 52: SSRT 262 CONTROL AT NOTCH END H 230
FIGURE 53: TEST SAMPLE SRTTUO116: TUNA SAMPLE AT NOTCH 'GH': AIR CONDITIONS. LOW DUCTILITY AT FRACTURE. 0.18MM PLATE 232
FIGURE 54: TEST SAMPLE SSRTTU0116 : TUNA SAMPLE AT NOTCH 'BC' SHOWING A DUCTILE CONDITION. 0.18MM PLATE 232

FIGURE 55: TEST SAMPLE SSRTTUO163:HA: TEST PIECE FROM TUNA BRINE: X650. 0.235MM PLATE..... 233
FIGURE 56: TEST SAMPLE SSRTTUO163:NOTCH CA X650: TUNA TEST PIECE 0.235MM PLATE..... 234
FIGURE 57: TUNA SAMPLE SSRTTUO163BC ; AIR CONDITIONSX4000: BRITTLE ZONE NEAR NOTCH ALONG SPECIMEN EDGE, APPEARANCE OUT OF CHARACTER WITH GENERAL EVIDENCE. 0.235MM PLATE..... 234
FIGURE 58: TEST SAMPLE SSRTTUO163GE X3000: LOW DUCTILITY ZONE ALONG FRACTURE EDGE WITH STEP FRACTURE. 0.235MM PLATE 235
FIGURE 59: TUNA SAMPLE 116GB X2500: FRACTURE ZONE SHOWING DISCRETE AREA OF PROBABLE ENVIRONMENTAL STRESS CRACKING INITIATION. 0.18MM PLATE. 236
FIGURE 60: TUNA SAMPLE 116GC X5000 TUNA : HIGHER MAGNIFICATION: FRACTURE ZONE SHOWING DISCRETE AREA OF PROBABLE ENVIRONMENTAL STRESS CRACKING INITIATION- MULTIPLE SITES AND DISCRETE LEDGES. 0.18MM PLATE. 236
FIGURE 61: TEST SAMPLE SSRTTU0164BA X650: TUNA PRODUCT : AIR TEST CONDITIONS, SHOWING LOW DUCTILITY: 0.235MM PLATE 237
FIGURE 62: TEST SAMPLE SSRTTU0164GA X650: TUNA PRODUCT , OPPOSITE END NOTCH FROM FIGURE 25 SHOWING DUCTILE BEHAVIOUR WITH CONE / CUP REGIONS IN THE CENTRAL BAND. 237
FIGURE 63: SLOW STRAIN RATE TESTED TUNA SAMPLE SSRTT TU150 HA: X600. 0.16MM PLATE. 240
FIGURE 64: SLOW STRAIN RATETEST SAMPLE: SSRTTU150HA X3500: TOP EDGE. 241
FIGURE 65: SSRTTU150NN2 080409HC X 8000..... 241
FIGURE 66: SALMON BRINE SLOW STRAIN RATE TEST SAMPLE: SSRTSAL211CA:DUCTILE CONDITION..... 242
FIGURE 67: SALMON BRINE SLOW STRAIN RATE TEST SAMPLE: SSRTSAL211, HA: LOSS OF DUCTLITY AT NOTCH GH 243
FIGURE 68: TEST SPECIMEN SSRT SAL211, GB0.18M DR 620CA PLATE IMAGE SHOWING REGIONS OF TRANSGRANULAR ENVIRONMENTAL STRESS CRACKING. 0.18MM PLATE. 244
FIGURE 69: SSRTSAL211HB090109X2000 TOP EDGE FROM FIGURE 68TRANSGRANULAR ENVIRONMENTAL STRESS CRACKING. LEDGES AND RIVER PATTERN EFFECTS 244
FIGURE 70: SAL211,HC X200. LOWER EDGE FROM FIGURE 68, SHOWING SMALL BAND OF ENVIRONMENTAL STRESS CRACKING NEAR SURFACE. 245
FIGURE 71: SALMON SAMPLE SSRTSAL 0206HA: TESTED IN AIR: 0.16MM DR 620 CA PLATE, SHOWING FRACTOGRAPHY NEAR NOTCH INCLUDING FRATOGRAPHY CHARACTERISTIC OF TRANSGRANULAR ENVIRONMENTAL STRESS CRACKING..... 245
FIGURE 72:SALMON SAMPLE SSRT SAL 0206H: TESTED IN AIR: 0.16MM DR 620 CA PLATE; LARGER MAGNIFICATION VIEW OF THE FRACTOGRAPHIC CHARACTERISTIC OF ENVIRONMENTAL STRESS CRACKING FROM FIGURE 35, WITH MORE DUCTILE CONDITIONS BENEATH. 246
FIGURE 73: SALMON SAMPLE SSRTSAL 0218H, TESTED IN AIR: 0.235MM DR 620 CA PLATE, SHOWING FRACTOGRAPHY NEAR NOTCH CHARACTERISTIC OF TRANS-GRANULAR ENVIRONMENTAL STRESS CRACKING. 246
FIGURE 74: SALMON SAMPLE SSRT SAL 0218H: TESTED IN AIR: 0.235MM DR 620 CA PLATE, LARGER MAGNIFICATION VIEW OF FRACTOGRAPHY CHARACTERISTIC OF ENVIRONMENTAL STRESS CRACKING FROM FIGURE 37, WITH MORE DUCTILE CONDITIONS BENEATH..... 247
FIGURE 75: SALMON SAMPLE SSRT SAL 228HE: X1000 : TEST UNDER NITROGEN FLUSHING CONDITIONS: 0.18MM DR 620 CA PLATE, SHOWING TRANS-GRANULAR CRACKING REGIONS CHARACTERISTIC OF ENVIRONMENTAL STRESS CRACKING AT EITHER EDGE, WITH MORE DUCTILE REGIONS IN BETWEEN. 248
FIGURE 76: SALMON SAMPLE SSRT SAL 228H: X2500. TEST UNDER NITROGEN FLUSHING CONDITIONS: 0.18MM DR 620 CA PLATE, LARGER MAGNIFICATION VIEW OF FRACTOGRAPHY AT TOP EDGE FROM FIGURE 39, WITH EVIDENCE OF TRANS-GRANULAR ENVIRONMENTAL STRESS CRACKING 248
FIGURE 77: SALMON SAMPLE SSRT SAL 232BCX2500: NITROGEN FLUSHING CONDITIONS: 0.16MM DR 620 CA PLATE, LARGE MAGNIFICATION VIEW OF FRACTOGRAPHY AT EDGE , WITH INDICATIONS OF TRANS-GRANULAR ENVIRONMENTAL STRESS CRACKING NEAR EDGE. 249
FIGURE 78: SALMON SAMPLE SSRT SAL 238BCX2000: NITROGEN FLUSHING CONDITIONS: 0.235MM DR 620 CA PLATE, LARGE MAGNIFICATION VIEW OF FRACTOGRAPHY AT EDGE , WITH INDICATIONS OF TRANS-GRANULAR ENVIRONMENTAL STRESS CRACKING NEAR EDGE 249
FIGURE 79: DIAGRAM OF MODEL SET UP 275
FIGURE 80: SALMON BRINE : AIR CONDITIONS: FAST AND SLOW SWEEP DC POLARISATION CURVES FOR 0.18MM DR620CA ECCS MATERIAL. 306
FIGURE 81: SALMON BRINE: REDUCED AIR CONDITIONS: (NITROGEN FLUSHED CELL). FAST AND SLOW SWEEP DC POLARISATION CURVES FOR 0.18MM DR620CA ECCS MATERIAL..... 307
FIGURE 82: TUNA BRINE : AIR CONDITIONS: FAST AND SLOW SWEEP DC POLARISATION CURVES FOR 0.18MM DR620CA ECCS MATERIAL. 308
FIGURE 83: TUNA BRINE TESTED UNDER NITROGEN FLUSHING CONDITIONS. FAST AND SLOW SWEEP DC POLARISATION CURVES FOR 0.18MM DR620CA ECCS MATERIAL..... 309
FIGURE 84: SALMON BRINE : AIR CONDITIONS: DC POLARISATION PITTING LOOP CURVES FOR 0.18MM DR620CA ECCS MATERIAL. DUPLICATE RUNS. 311

FIGURE 85: SALMON BRINE : NITROGEN FLUSH CONDITIONS: DC POLARISATION PITTING LOOP CURVES FOR 0.18MM DR620CA ECCS MATERIAL. DUPLICATE RUNS 311
FIGURE 86: TUNA BRINE : AIR CONDITIONS: DC POLARISATION PITTING LOOP CURVES FOR 0.18MM DR620CA ECCS MATERIAL. DUPLICATE RUNS. 312
FIGURE 87: TUNA BRINE : NITROGEN FLUSH CONDITIONS: FAST AND SLOW SWEEP DC POLARISATION CURVES FOR 0.18MM DR620CA ECCS MATERIAL. DUPLICATE RUNS. 312
FIGURE 88: TUNA BRINE: CELL 253: ELECTRODE 1: ABRADED ECCS , SCAN 1B, SHOWING INTERMEDIATE PHOSPHORUS PEAK. 314
FIGURE 89: CELL 254: SALMON BRINE: AIR CONDITION PITTING TEST SAMPLE ECCS ELECTRODE. SCAN S5 SHOWING MAJOR PHOSPHORUS PEAK ASSOCIATED WITH PRECIPITATE ON SURFACE 317
FIGURE 90: SALMON SAMPLE 254 , AIR CONDITIONS TEST , SHOWING PRECIPITATIONS FOUND TO BE PHOSPHORUS RICH. 318
FIGURE 91: TUNA SAMPLE 255, AIR CONDITIONS TEST, SHOWING CORRODED AND PITTED SURFACE 318
FIGURE 92: 0.16MM DR 620CONTINUOUSLY ANNEALED ECCS STEEL. THIS MATERIAL WAS A LOW CARBON MATERIAL SUITABLE FOR FABRICATING INTO DRAWN REDRAWN CANS. 325
FIGURE 93: 0.18MM DR 620CONTINUOUSLY ANNEALED ECCS STEEL. THIS MATERIAL WAS A STAMPING QUALITY TYPE 325
FIGURE 94: 0.235MM DR 620 CONTINUOUSLY ANNEALED NITROGENISED ECCS STEEL. THIS MATERIAL WAS A STAMPING QUALITY TYPE 326

Supplementary List of Tables in order of appearance.

TABLE 1: LIST OF SOME EXAMPLES OF ENVIRONMENTAL STRESS CRACKING INCIDENTS IDENTIFIED INVOLVING CANNED FOODS. 27
TABLE 2: EMPIRICAL COMPOSITION OF MEATS PER 100G 29
TABLE 3: MYOGLOBIN CONTENT OF SOME MEATS 30
TABLE 4: EMPIRICAL APPROXIMATE COMPOSITION OF SOME FISH TYPES 45
TABLE 5: ADDITIONAL VITAMINS NOT INCLUDED IN PLOT 53
TABLE 6: PARAMETERS DETERMINED DURING SLOW STRAIN RATE TEST WORK. 126
TABLE 7: CORRELATION MATRIX: NON SCRATCHED SAMPLES TESTED IN ACIDIFIED MEDIA: COMBINED ACID TYPES 138
TABLE 8: CORRELATION MATRIX : ACIDIFIED MEDIA : SCRATCHED SAMPLES: COMBINED ACID TYPES 139
TABLE 9: CORRELATION MATRIX FOR TIME OF TEST APPLIED TO NON SCRATCHED SAMPLES TESTED IN TUNA MEDIA ACIDIFIED WITH ACETIC ACID TO PH 4.5-5.0 141
TABLE 10: DATA FROM STEPWISE REGRESSION PROCEDURE APPLIED TO 7 PREDICTORS FROM CORRELATION MATRIX: NON SCRATCHED SAMPLES. 142
TABLE 11: REGRESSION TABLE FOR REGRESSION 1 143
TABLE 12: ANALYSIS OF VARIANCE FOR REGRESSION 1 143
TABLE 13: DETAILS OF UNUSUAL OBSERVATION FOR REGRESSION 1 143
TABLE 14: BEST SUBSETS REGRESSION TABLE FOR THREE CHOSEN PARAMETERS SUBSEQUENT TO THE STEPWISE REGRESSION PROCEDURE: NON SCRATCHED SAMPLES: ACETIC ACID ADDITION. 145
TABLE 15: REGRESSION TABLE FOR REGRESSION 2 146
TABLE 16: ANALYSIS OF VARIANCE FOR REGRESSION 2 146
TABLE 17: CORRELATION SUBSET MATRIX FOR TUNA BRINE SAMPLES TESTED, AFTER ACIDIFICATION WITH ACETIC ACID TO PH 4.5-5.0 : SCRATCHED SAMPLES 148
TABLE 18: DATA FROM STEPWISE REGRESSION PROCEDURE APPLIED TO 7 PREDICTORS FROM CORRELATION MATRIX: SCRATCHED SAMPLES 149
TABLE 19: BEST SUBSETS REGRESSION TABLE FOR FOUR CHOSEN PARAMETERS SUBSEQUENT TO THE STEPWISE REGRESSION PROCEDURE: SCRATCHED SAMPLES. 149
TABLE 20: REGRESSION TABLE FOR REGRESSION 3 : SCRATCHED SAMPLES 150
TABLE 21: ANALYSIS OF VARIANCE TABLE FOR REGRESSION 3: SCRATCHED SAMPLES 150
TABLE 22: ANION ANALYSIS DATA FOR TUNA BRINE USED IN SLOW STRAIN RATE TESTS.DATA IN PARTS PER MILLION. 170
TABLE 23: CATION ANALYSIS DATA FOR TUNA BRINE USED IN SLOW STRAIN RATE TESTS.DATA IN PARTS PER MILLION. 170
TABLE 24: STEEL COMPOSITION ANALYSIS BY WT% FOR 0.19MM DR520CA PLATE USED FOR TESTS ON TUNA BRINE IN SECTION 2 WORK. 173
TABLE 25: PARAMETERS DETERMINED IN THE COURSE OF SLOW STRAIN RATE TESTING. 186
TABLE 26: PARAMETERS DETERMINED IN THE COURSE OF SLOW STRAIN RATE TESTING. 187
TABLE 27: REGRESSION MATRIX: TUNA BRINE : AIR CONDITIONS : COMPLETELY FAILED SPECIMENS.... 194
TABLE 28 REGRESSION MATRIX : TUNA BRINE : NITROGEN FLUSH CONDITIONS: COMPLETELY FAILED SPECIMENS. 194
TABLE 29: SUBSET 4 : REGRESSION STATISTICS/ 195
TABLE 30: SUBSET 4: ANALYSIS OF VARIANCE FOR REGRESSION 196
TABLE 31: SUBSET 4: UNUSUAL OBSERVATIONS 196
TABLE 32: SUBSET 7 : REGRESSION STATISTICS 197
TABLE 33: SUBSET 7 : ANALYSIS OF VARIANCE 197
TABLE 34: BLANK 197
TABLE 35: SUBSET 7 : REGRESSION STATISTICS 199
TABLE 36: SUBSET 7 : ANALYSIS OF VARIANCE 199
TABLE 37: SUBSET 7 : UNUSUAL OBSERVATIONS 199
TABLE 38: SUBSET 9 : REGRESSION STATISTICS 200
TABLE 39: SUBSET 9 :ANALYSIS OF VARIANCE 200
TABLE 40: SUBSET 9 : UNUSUAL OBSERVATIONS 200
TABLE 41: REGRESSION MATRIX: SALMON BRINE : AIR CONDITIONS : COMPLETELY FAILED SPECIMENS 202
TABLE 42: REGRESSION MATRIX: SALMON BRINE : NITROGEN FLUSH CONDITIONS : COMPLETELY FAILED SPECIMENS. 203

TABLE 43: SUBSET 7 REGRESSION TABLE 205
TABLE 44: SUBSET 7 ANALYSIS OF VARIANCE 205
TABLE 45: SUBSET 7 UNUSUAL OBSERVATIONS: MECHANICAL WORK: M1 205
TABLE 46: SUBSET 8 REGRESSION TABLE 206
TABLE 47: SUBSET 8 ANALYSIS OF VARIANCE 206
TABLE 48: SUBSET 5 REGRESSION TABLE 208
TABLE 49: SUBSET 5 ANALYSIS OF VARIANCE 208
TABLE 50: SUBSET 5 UNUSUAL OBSERVATIONS 208
TABLE 51: SUBSET 7 REGRESSION TABLE 209
TABLE 52: SUBSET 7 ANALYSIS OF VARIANCE 209
TABLE 53: SUBSET 7 UNUSUAL OBSERVATIONS 210
TABLE 54: SUBSET 8 REGRESSION TABLE 210
TABLE 55: SUBSET 8 ANALYSIS OF VARIANCE 211
TABLE 56: REGRESSION TABLE 214
TABLE 57: ANALYSIS OF VARIANCE 214
TABLE 58 UNUSUAL OBSERVATIONS. 215
TABLE 59: STATISTICAL CORRELATION MATRIX FOR CRACK GROWTH RATE INCLUDING ESTIMATED STRESS INTENSITY FACTOR. 220
TABLE 60: BEST SUBSETS REGRESSION FOR LOG_{10}CRACK GROWTH RATE 221
TABLE 61: REGRESSION TABLE 222
TABLE 62: ANALYSIS OF VARIANCE. 222
TABLE 63: SUMMARY STATISTICS FOR PLOT 29 LOTS: % METAL THICKNESS REDUCTION AT NOTCH..... 255
TABLE 64: SUMMARY STATISTICS FOR PLOT 30 LOTS: % METAL THICKNESS REDUCTION AT NOTCH..... 257
TABLE 65: TABLE OF ANALYSIS OF VARIANCE DATA: CONTROL SAMPLES TOTALLING SIX, TWO PER PLATE TYPE..... 258
TABLE 66: STATISTICAL DETAIL 259
TABLE 67: FINAL FRACTURE STRESS OF STANDARD TENSILE 'DOG BONE' TEST PIECES: NO NOTCHES. . 268
TABLE 68: DATA: FINAL FRACTURE STRESS OF STANDARD TENSILE 'DOG BONE' TEST PIECES, HAVING TWO NOTCHES, EACH 1.06MM DEEP. 269
TABLE 69: DATA FROM ERICHSEN CUP DRAW TEST: 6 SAMPLES PERTEST 270
TABLE 70: NOTCH HEIGHT STRAIN FROM TENSILE TESTS 274
TABLE 71: DETAILS OF THE MODEL ARE SHOWN IN THE TABLE BELOW 275
TABLE 72: 0.16MM DR 620 CA SAMPLE. DATA ARE : STRESSES IN MPA 277
TABLE 73: 0.16MM DR 620 CA SAMPLE. DATA ARE : STRESSES IN MPA 278
TABLE 74: 0.18MM DR 620 CA SAMPLE. DATA ARE : STRESSES IN MPA 279
TABLE 75: 0.18MM DR 620 CA SAMPLE. DATA ARE : STRESSES IN MPA 279
TABLE 76: 0.235MM DR 620 CA SAMPLE. DATA ARE : STRESSES IN MPA 280
TABLE 77: 0.235MM DR 620 CA SAMPLE. DATA ARE : STRESSES IN MPA 281
TABLE 78: STRESS PREDICTIONS FOR NOTCHED SPECIMENS COMPARED WITH TRUE FRACTURE STRESSES MEASURED ON STANDARD UN -NOTCHEDTENSILE SPECIMENS. 282
TABLE 79: STAGES OF FORMATION AND TIMES 284
TABLE 80: MODEL DETAILS 285
TABLE 81: TABLE OF S33 (HOOP STRESSES) ON DRAWN REDRAWN CAN 289
TABLE 82: STRESS PREDICTIONS : MPA: +VE = TENSION , -VE = COMPRESSION 290
TABLE 83: STRESS PREDICTIONS : MPA : +VE = TENSION , -VE = COMPRESSION 291
TABLE 84: STRESS PREDICTIONS :MPA : +VE = TENSION , -VE = COMPRESSION 292
TABLE 85: EASY OPEN SHELL FORMATION SEQUENCE AND TIMING 294
TABLE 86: EASY OPEN END SHELL MODEL MODEL DETAILS 294
TABLE 87: MODEL 3, IMAGE 2: SUMMARY OF S11 ('X' DIRECTION) STRESS PREDICTIONS: 297
TABLE 88: MODEL 3, IMAGE 3: SUMMARY OF S22 ('Y' DIRECTION) STRESS PREDICTIONS:..... 298
TABLE 89: MODEL 3, IMAGE 4: SUMMARY OF S33 ('Z' DIRECTION) STRESS PREDICTIONS: 299
TABLE 90: SUMMARY TABLE COMBINING ALL STRESS PREDICTIONS AND COMMENTS ON MODEL 3..... 300
TABLE 91: PITTING LOOP TESTS. 305
TABLE 92: LIST OF OBSERVATIONS OF ELEMENTS IDENTIFIED 313
TABLE 93: XRA OBSERVATIONS ON ELECTRODES FROM PITTING LOOP TESTS. 316
TABLE 94: CHEMICAL ANALYSES OF PRODUCT BRINES FOR ANIONS AND CATIONS 320
TABLE 95: HEADSPACE GAS ANALYSIS DATA 323
TABLE 96: REGRESSION EQUATIONS FOR TIME TO FAILURE IN SLOW STRAIN RATE TESTS. 335
TABLE 97: STATISTICAL PARAMETERS FOR RESPECTIVE DATA SETS IN GROUPS 1 TO 4. 338
TABLE 98: UNUSUAL OBSERVATIONS 339
TABLE 99: UNUSUAL OBSERVATIONS 341

Supplementary List of Plots in order of appearance.

PLOT 1: INORGANIC CONSTITUENTS OF THREE FISH TYPES. 47
PLOT 2: VITAMIN CONTENTS OF THREE FISH TYPES 48
PLOT 3: FATS, SUGARS AND OTHER CONSTITUENTS IN THREE FISH TYPES. 50
PLOT 4: OX LIVER, LAMB AND CHICKEN: INORGANIC CONSTITUENTS. 52
PLOT 5: MEAT ANALYSIS : VITAMIN CONTENTS FOR THREE MEAT TYPES. 53
PLOT 6: MEAT ANALYSIS: FATS AND OTHER CONSTITUENTS FOR THREE MEAT TYPES 55
PLOT 7: RESIDUALS PLOT FOR CANDIDATE REGRESSION 1, USING 3 PREDICTORS 144
PLOT 8: PARTIAL LEAST SQUARES RESPONSE PLOT OF CALCULATED VS ACTUAL TIME OF TEST VALUES FOR REGRESSION 1 WITH OCV, E_{RMS2} AND IA_2 FOR NON SCRATCHED SAMPLES TESTED IN TUNA BRINE ACIDIFIED WITH ACETIC ACID. 144
PLOT 9: RESIDUALS FOR SUBSET 1, TABLE 14 : REGRESSION OF TIME OF TEST WITH E_{RMS2} FOR TUNA BRINE ACIDIFIED USING ACETIC ACID. 146
PLOT 10: PARTIAL LEAST SQUARES REGRESSION RESPONSE FOR REGRESSION 3: SCRATCHED SAMPLES 151
PLOT 11: ENGINEERING STRESS STRAIN PLOTS FOR 0.19MM DR 520 MATERIAL USED IN INITIAL SLOW STRAIN RATE TESTS IN TUNA BRINE UNDER AIR CONDITIONS. 172
PLOT 12: TUNA BRINE : AIR CONDITIONS: ANALYSIS FOR RESIDUALS: SUBSET 4 196
PLOT 13: TUNA BRINE : AIR CONDITIONS: ANALYSIS FOR RESIDUALS: SUBSET 7 197
PLOT 14: TUNA BRINE : NITROGEN FLUSH : ANALYSIS FOR RESIDUALS: SUBSET 7 199
PLOT 15: TUNA BRINE : NITROGEN FLUSH : ANALYSIS FOR RESIDUALS: SUBSET 9 201
PLOT 16: SALMON BRINE : AIR CONDITIONS : ANALYSIS FOR RESIDUALS: SUBSET 7 206
PLOT 17: SALMON BRINE : AIR CONDITIONS : ANALYSIS FOR RESIDUALS: SUBSET 8 207
PLOT 18: PLOT 6: SALMON BRINE : NITROGEN CONDITIONS : ANALYSIS FOR RESIDUALS:SUBSET 5 209
PLOT 19: SALMON BRINE: NITROGEN CONDITIONS: ANALYSIS FOR RESIDUALS: SUBSET 7 210
PLOT 20: SALMON BRINE: NITROGEN CONDITIONS : ANALYSIS FOR RESIDUALS: SUBSET 8 211
PLOT 21: LOAD VS EXTENSION AND TIME FOR TUNA SAMPLE SSRT 135 TESTED UNDER NITROGEN FLUSH CONDITIONS. 213
PLOT 22: TUNA BRINE: AIR CONDITIONS : ANALYSIS FOR RESIDUALS: 215
PLOT 23: RESIDUAL PLOT FOR LOG_{10} CRACK GROWTH RATE FOR TUNA BRINE IN AIR. 223
PLOT 24: LOAD VS EXTENSION PLOTS FROM TESTS FOR TESTS IN TUNA BRINE; NUMBER 116: 0.18MM PLATE , NO 132: 0.16MM PLATE AND NO 163: 0.235MM PLATE: AIR CONDITIONS. 238
PLOT 25: LOAD VS EXTENSION PLOTS FROM TESTS FOR SLOW STRAIN RATETESTS IN TUNA BRINE (NITROGEN FLUSHING CONDITIONS); SSRT NO 135: 0.18MM PLATE , NUMBER 142: 0.235MM PLATE AND NO 150: 0.16MM PLATE. 239
PLOT 26: TENSILE SLOW STRAIN PLOTS FOR SAMPLE SSRT SAL 0206 (0.16MM DR 620CA PLATE; 0211 (0.18MM DR 620CA PLATE) AND 0218 (0.235MM DR 620CA PLATE), TESTED IN SALMON BRINE UNDER AIR CONDITIONS. 250
PLOT 27: TENSILE SLOW STRAIN PLOTS FOR SAMPLE SSRT SAL 232 (0.16MM DR 620CA PLATE; 228 (0.18MM DR 620CA PLATE) AND 238 (0.235MM DR 620CA PLATE), TESTED IN SALMON BRINE UNDER AIR CONDITIONS. 251
PLOT 28: TENSILE SLOW STRAIN PLOTS FOR CONTROL SAMPLES TESTED IN OIL: NO 260: 0.18MM , NO 261, 0.235MM , NO 262 : 0.16MM. 252
PLOT 29: SUMMARY DATA BOXPLOT FOR % METAL THICKNESS REDUCTION AT NOTCH SHOWING THE MOST THINNING AFTER FRACTURE FOLLOWING SLOW STRAIN RATE TESTS. 255
PLOT 30: SUMMARY DATA BOXPLOT FOR % METAL THICKNESS REDUCTION AT NOTCH SHOWING THE MOST THINNING AFTER FRACTURE FOLLOWING SLOW STRAIN RATE TESTS. 256
PLOT 31: SUMMARY DATA BOXPLOT FOR % METAL THICKNESS REDUCTION AT NOTCHES FOR CONTROL SPECIMENS AFTER FRACTURE FOLLOWING SLOW STRAIN RATE TESTS IN MACE FOOD OIL. 258
PLOT 32: SUMMARY OF PEAK LOADS RECORDED IN SLOW STRAIN RATE TESTS FOR MATERIAL GAUGES, PRODUCTS AND EVIRONMENTAL CONDITIONS USED 260
PLOT 33: ENGINEERING TENSILE STRESS STRAIN PLOTS FOR 0.16MM , 0.18MM AND 0.235MM DR620CA MATERIALS USED. 267
PLOT 34: TRUE STRESS STRAIN ESTIMATES UP TO THE POINT OF NECKING, BASED UPON EQUATION A1 AND EQUATION B1. 271
PLOT 35: TRUE STRESS- TRUE STRAIN ESTIMATES. PLOTS COMBINING PRACTICAL FRACTURE STRESS DETERMINATIONS WITH ENGINEERING STRESS STRAIN DATA MODIFIED USING THE CONSTANT VOLUME ASSUMPTION FOR PLASTIC STRAIN. FINAL STRAIN VALUES ARE MEANS FROM THE ERICHSEN PLASTIC STRAIN DATA DETERMINED. 273

PLOT 36: NOTCH TENSILE SPECIMEN MODEL: PREDICTED PEAK STRESES FOR LOADS APPLIED TO A FULL WIDTH TENSILE SPECIMEN, FOR EACH OF THE DR620CA MATERIALS MODELLED , 0.16MM , 0.18MM AND 0.235MM. 283
PLOT 37: REGRESSION RESIDUALS FOR TIME TO FAILURE IN HOURS OF SALMON BRINE, SUBJECT TO SLOW STRAIN RATE TESTING UNDER AIR CONDITIONS AS A FUNCTION OF MECHANICAL WORK, M1, AND INTEGRATED CURRENT, IA_1. 339
PLOT 38: REGRESSION RESIDUALS FOR TIME TO FAILURE OF SALMON BRINE UNDER NITROGEN FLUSHING CONDITIONS AS A FUNCTION OF MECHANICAL WORK,M1, AND INTEGRATED CURRENT,IA_1 UP TO THE POINT OF MAXIMUM LOAD. 341

Supplementary List of Diagrams in order of appearance.

DIAGRAM 1: STAGES IN THE MANUFACTURE OF 3 PIECE WELDED SIDESEAM CANS 18
DIAGRAM 2: TWO PIECE DRAWN AND RE-DRAWN (DRD) FOOD CAN E.G. FOR FISH: SCHEMATIC REPRESENTATION OF FORMING STAGES 20

1 Section 1: Introduction

1.1 Background to the Project

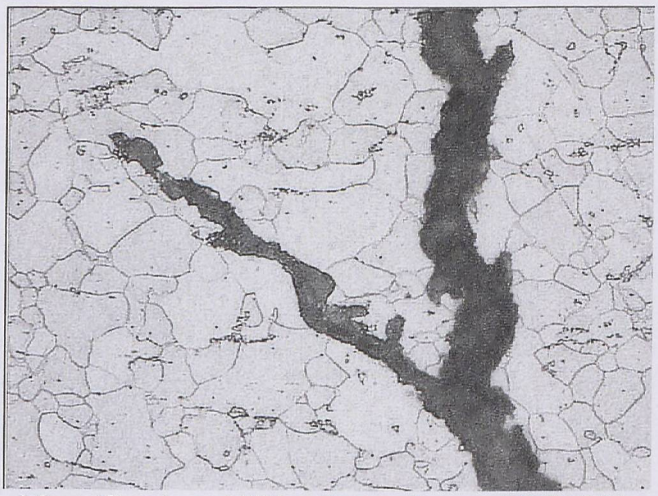
During the past 20 years or more the processed food can sector of the Metal Packaging Industry has experienced a significant incidence of environmental stress cracking failures in metal containers, having either tinplate or electro chrome coated steel components (henceforth abbreviated eccs), and packed mainly with fish or meat based products. The time to failure has varied significantly from less than one year following packing to 3 years or more. Investigations have been undertaken by can makers[1] and steel suppliers[2,3] , but more understanding of the subject was believed to be necessary. The present study was initiated to attain a better knowledge of risk factors and potential means to reduce risks. The micrographs below, Figures 1 and 2, illustrate an example of cracking in the dented base rim of a Tuna in Brine 83mm dia drawn can.

Figure 1: Exterior surface of 83mm Diameter Tuna in Brine can showing cracking at Base rim, partly associated with denting in rim.



Magnification : 4x : Crown Report TR10899

Figure 2: Section from region nearest interior surface of Tuna in Brine can from lot corresponding to Figure 1, showing branching cracks at base rim region



Magnification x1200 : Crown Report TR10899

The term 'environmental stress cracking' is commonly used to describe failures involving the combination of stress and a corrosive environment, which include stress corrosion cracking, hydrogen embrittlement and corrosion fatigue. Definitions of these individual failure modes are included on **Appendix 1** of this section.

1.2 Metal Containers and Materials for Processed Foods: Types Considered

Two main container types are considered for the purposes of this study, namely, three piece round cans and two piece drawn and redrawn (DRD) containers, the essential features of which are briefly described below:

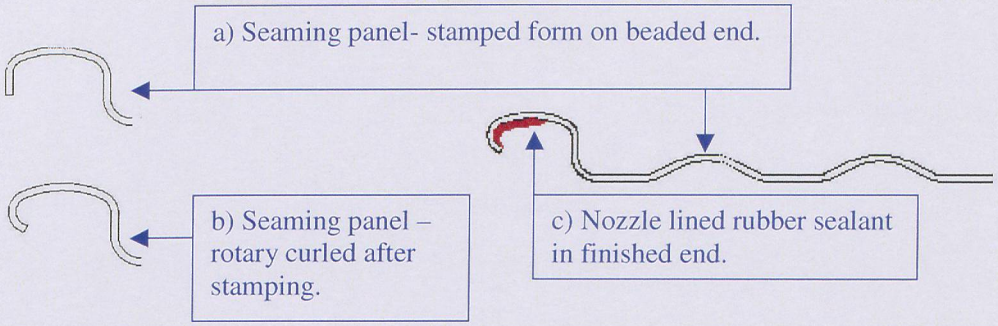
1.2.1 Three Piece Round Processed Food Cans : Body plus two Ends.

This container type comprises a body cylinder having a soudronically welded side seam (electric resistance welding), after which body flanges are formed, followed by the mechanical process of double seaming to ends previously fabricated by stamping, curling of the rim, and compound lining of the seam area. The seaming process causes end and body hooks to engage, the joint then being compressed to form a hermetic seal by virtue of the rubber based sealing compound applied to the perimeter of the end

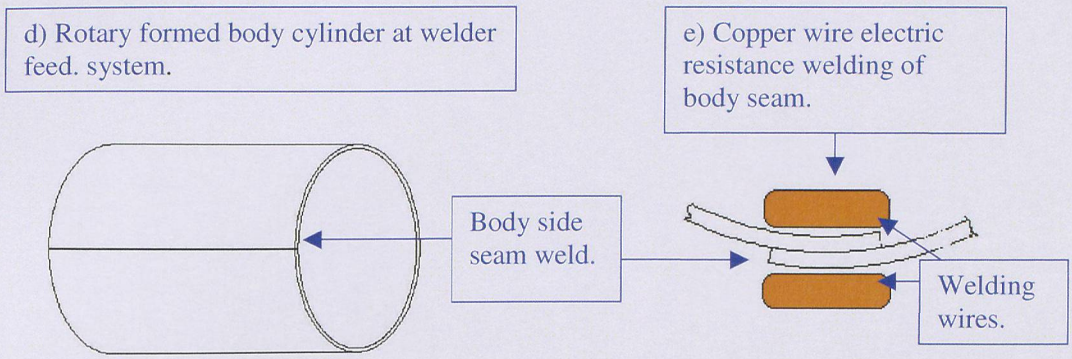
component. Ends are profiled with beading during stamping to withstand the pressures generated by heat processing and these pressures may be up to around 2.5 bars for meat and fish products. The three-piece can has a body manufactured from tinplate, the tin-coating being necessary to enable the electric resistance welding operation to function effectively. A common level of tin-coating for food bodies is an electrodeposited level of 2.8 grams. metre^{-2} (henceforth gsm) per surface. The ends may be produced from tinplate or **e**lectro **c**hrome **c**oated **s**teel , the '**eccs**' coating thickness being around 15nm, the total mass of chromium on each surface being typically between 50 and 130mg/m^2. Ends and bodies are internally lacquered prior to the fabrication process, so there is an inherent susceptibility to coating damage, and a variable level of metal exposure resulting from fabrication processes is very likely to be generated. An exception to this is the treatment of the side- seam, which is internally spray coated with lacquer immediately after the side seam weld is formed, to protect the weld and adjacent areas, but this process may be less than fully effective in affording total protection to these areas, especially the weld edge. A polyester powder coating may be applied instead of a liquid lacquer, and the powder system generally leads to better protection. The manufacturing sequence is shown in Diagram 1 below.

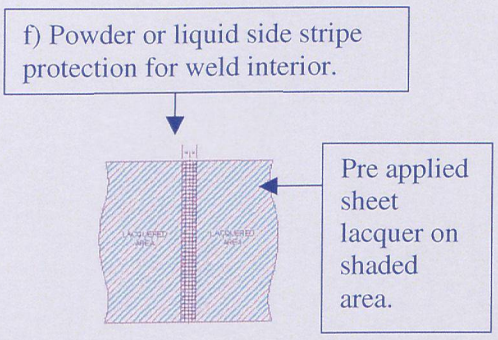
Diagram 1: Stages in the Manufacture of 3 Piece Welded Sideseam Cans:

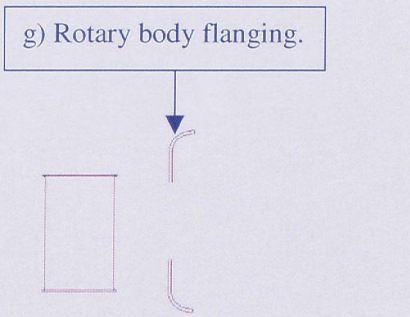
Ends: Stamping , Curling and Lining.

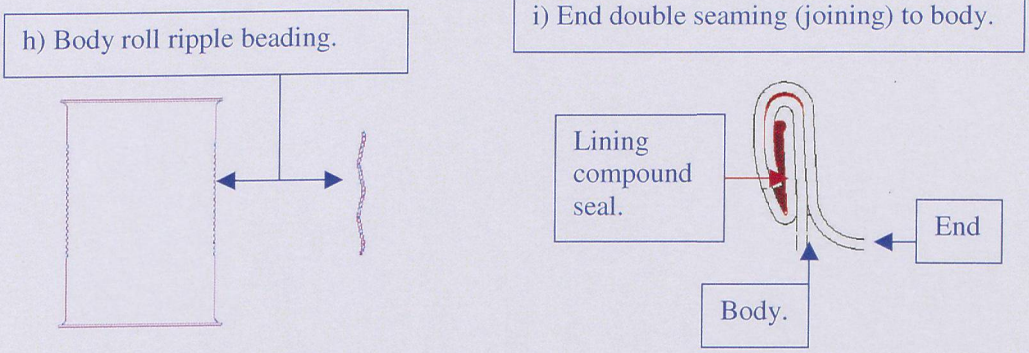


Body Forming, Sidseam Welding, Side Striping , Flanging , Beading and Seaming









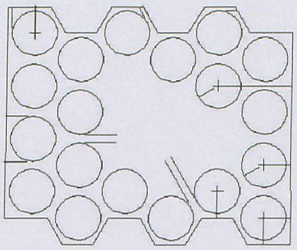
1.2.2 Two Piece Drawn and Redrawn Cans

This container type has a body most commonly manufactured from pre lacquer coated eccs sheet material, and is formed by one cupping operation followed typically by one or two redrawing stages. The body is then flanged by a die or rotary process. After filling, the container is closed by double seaming with either a non easy open or an easy open end type, which can be manufactured from either eccs or tinplate materials. The pre-applied sheet lacquer coatings are present on both surfaces of the body and of the end materials when 'eccs' material is used in manufacture. The manufacturing sequence is illustrated in Diagram 2 below.

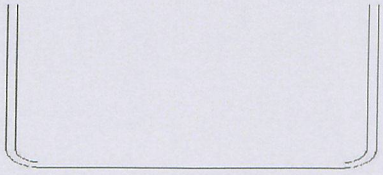
Both the above mentioned container types have been found to show susceptibility to environmental stress cracking failures at the more heavily worked areas, when packed with fish or meat based products. This usually means the end component for 3 piece cans, but there have been occasional instances of weld failures. For 2 piece cans the bottom rim, beading or any roll bead used to accommodate stacking may be vulnerable, as well as the seamed top end.

Diagram 2: Two Piece Drawn and Re-drawn (DRD) Food Can e.g. for Fish: Schematic Representation of Forming Stages:

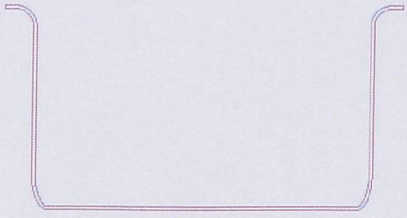
1. Sheets are Pre-lacquered and Scroll Cut for the Cupping Press..



2. The first draw stage takes place.



3. The initial cup is redrawn and flanged.



4. The base is profiled and beaded by additional stamping tools, to provide pressure resistance after the can has been filled with product and closed for heat sterilisation. The base rim is designed to interstack to help prevent rim damage.



5. The finished can having redrawn and flanged body with base profiling is ready for product filling and end seaming as for the 3 piece can. The drawn can tooling used is of very high quality to minimise coating damage risks.



1.3 Materials Characteristics

The steel used in Western Europe as well as the US for the above types of container at the present day is most commonly an aluminium killed type, and of a grade having very low levels of residual elements as well as very low levels of inclusions, with tensile properties significantly determined by cold reduction. The temper classification is frequently a 'double cold reduced' (DR) grade of steel, indicating that after hot and cold rolling and annealing, the plate is given a final cold rolling pass causing a gauge reduction of, for example 30% for the DR550 grade, to achieve the required properties. The annealing process is carried out typically at 660 deg C in an atmosphere of either pure hydrogen or nitrogen /5% hydrogen. The overall process enables temper grades having alternative yield strength levels of 520N/mm^2, 550 N/mm^2, or 620N/mm^2 to be supplied for different applications. The number designations after the letters 'DR' e.g. 'DR550' normally refer to the yield strength. Plate gauges relevant to this study are typically in the range from 0.24mm to 0.16mm. The temper grades may be supplied using a Batch Annealed (BA) or Continuously Annealed (CA) production process. The CA process is the most common at the present day as the BA process becomes phased out other than for some special product requirements. The CA process leads to a hexagonal grain structure and the material having a distinctive yield point, and typical elongation values are between 1 and 3% for coated and stoved double cold reduced plates. The BA process leads to a more pan-caked grain structure with a less distinctive yield point; this plate is slightly more ductile and sometimes has advantages of being more tolerant of certain forming operations such as flanging of welded side-seam cylinders to avoid splitting risks. The great bulk of production of food can steel is by a continuous casting process and the steel is aluminium killed. The chemical composition of these plates is characterised by a low carbon level of 0.13% maximum by weight and an aluminium content of 0.02-0.08%.

These plates also have a much lower level of non metallic inclusions relative to earlier ingot cast 'rimming' steels and this would be expected to benefit general corrosion resistance, as any large inclusions close to the plate surface may promote metal exposure following stretching and bending on fabrication.

Continuously cast double cold reduced steel plates are characterised by finely distributed carbides, which are present both within the grains and discontinuously at grain boundaries. In studies by Cron C. J., Payer J. H. and Staehler[4], on conditions giving rise to chemical attack on carbides in carbon steel, or of the ferrite matrix or at the ferrite carbide interface, the region of attack was found to be a complex function of anion type, pH and electrochemical potential. The grain size for CA DR packaging steel plates is fine i.e. greater than that 20,000 grains per mm^2, but is expected to be below 60,000 grains/mm^2, compared with below 20,000 grains/mm^2 i.e. relatively larger, for batch annealed (BA) DR materials. Certain suppliers of DR steels manufacture grades having a nitrogen addition at 0.010-0.015% by weight, termed nitrogenised steel, whereas conventional plate has total nitrogen level below 0.008wt%. Nitrogen is an element imparting additional strength to steel by virtue of its interstitial solubility in a manner similar to carbon. The use of nitrogen means that it is feasible to have a less heavily cold worked grain structure than with a non nitrogenised CA plate which derives its high strength predominantly from cold work, so that a slightly better elongation may be possible with the nitrogenised plate e.g. up to close to 3% for certain manufacturers processing. Examples showing the micro-structural comparison are illustrated in **Figures 3 and 4** where the grain structures of nitrogenised and non nitrogenised CA double cold reduced packaging steels are compared.

Figure 3: Nitrogenised 0.235mm DR620CA Packaging Steel ex Source A, sectioned parallel to the plate grain direction.

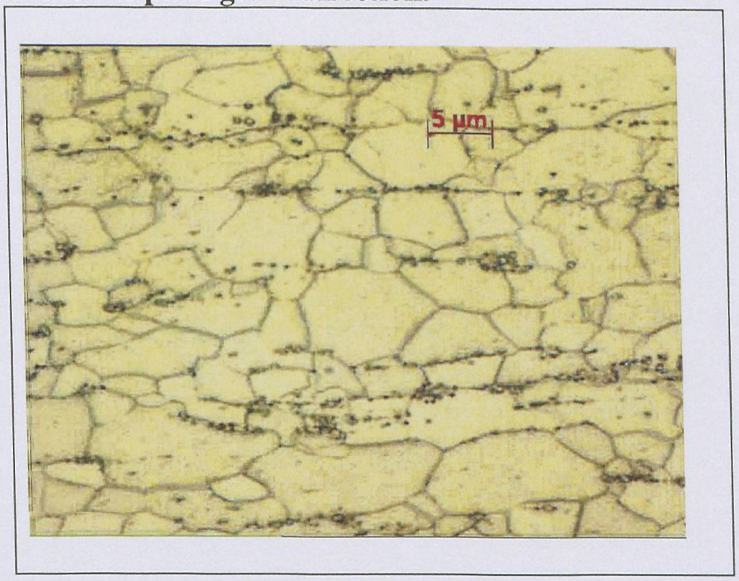
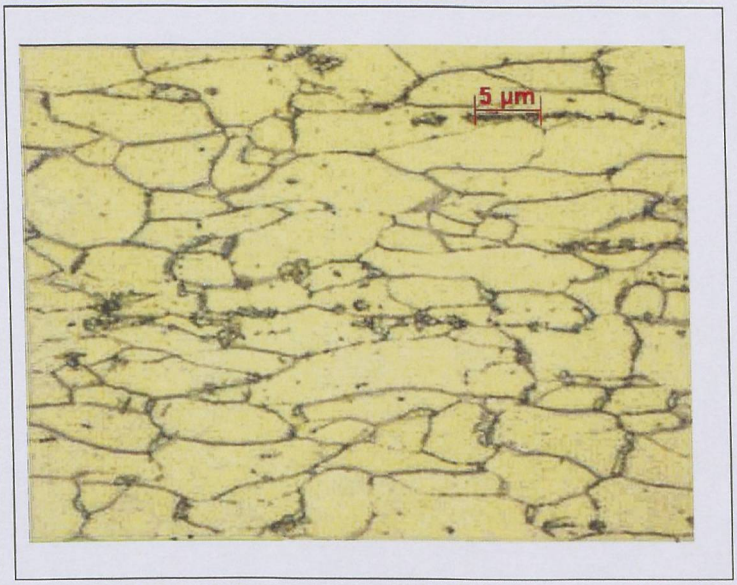


Figure 4: Non nitrogenised 0.235mm DR 620 CA steel ex Source B, sectioned parallel to the grain direction, showing increased cold work relative to nitrogenised material.



Depending on the steel manufacturing process, a high elongation for DR steels such as close to 3% may not be attained and figures closer to 1% may be observed, even for a nitrogenised steel process.

Iron with very low levels of carbon, e.g. <0.002%, has been found to have very low susceptibility to stress corrosion cracking in nitrates[5], whereas iron with low levels of carbon added e.g. above 0.002%, becomes increasingly susceptible.

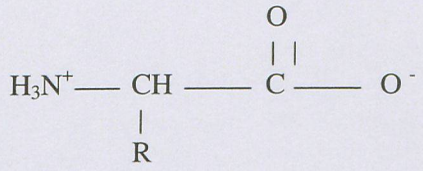
While the literature refers to an association of nitrogen with stress corrosion cracking of carbon steels[5], no evidence found in searches during this study has indicated susceptible effects associated with the levels of nitrogen specified for can making steels. Practical testing by Arcelor[6] in a beef liver medium has not indicated increased susceptibility resulting from the use of nitrogenised steels having nitrogen levels at 0.010-0.015 wt% compared with non nitrogenised DR steels having nitrogen level below 0.01wt%.

1.4 Products and Environments: General Features of Composition.

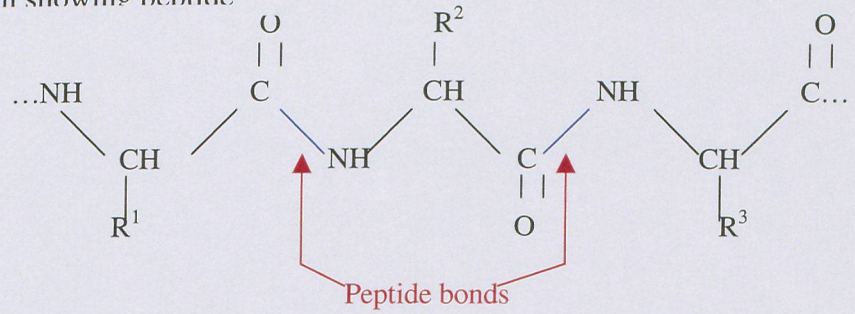
Lean meat is the muscle tissue of animals and contains around 20-25% of proteins and as much as around 70% water. The remainder essentially encompasses fats, carboxylic acids, mineral salts, vitamins and sugars. The proteins are complex chain structures of amino acids having 'peptide linkages' between the carboxylic group (COO-) of one amino acid molecule and the amino group of another. The general structure of an amino acid is shown in Figure 5a, with the peptide linkage in Figure 5b.

Figure 5: General Structure of Amino Acid and Chain with Peptide Linkages.

a) Basic



b) Chain showing peptide



While the amino acid molecule has an overall charge of zero it can contain within the same molecule two groups of opposite charge. In a metal corrosion context this implies that the basic polar structure from a fragmented chain would be capable of adsorbing on to surface points having opposite charge and acting in an inhibitive way.

Phosphates are contained within phospho-proteins and also the DNA (deoxyribonucleic acid) genetic structure. A further source of phosphate can be deliberate additions e.g. of bone to animal foods. Sulphur-containing amino acids are cystine, cysteine and methionine. These acids are capable of releasing volatile sulphur-containing species during heat processing e.g. hydrogen sulphide is cited by Schutte[7] , as a breakdown product of beef and fish on heat processing. Canned food products including meats, may also contain some nitrate anions, notably if they have been formulated with an added sauce having constituents where nitrate containing fertilizers have been used. Salts including chlorides are also constituents of canned meat and fish products. Sodium chloride is a preservative for cured meats. Examples of other additions are ascorbic acid

as an oxygen scavenger and nitrite salts such as potassium or sodium nitrite [8] as curing agents for meat which provide inhibitory effects on micro organisms. The use of nitrate was reported to serve as a reservoir for nitrite. It is apparent from very limited consideration of product contents that a number of species e.g. phosphate and nitrate anions, and volatile sulphides known from experience in the petrochemical industry to be associated with risks of environmental stress cracking in carbon steel, are present in meat and fish based high protein foods. The identification of any individual species associated with critical effects in a particular case(s) of Stress Corrosion Cracking, (SCC) failure, is likely to be extremely difficult in any post mortem analysis.

1.5 Stresses Present in Cans and Components : Initial Observations

Stresses which lead to environmental stress cracking may be residual, applied or a combination. Fabrication of can ends is by stamping at high speed e.g. 500 components per minute, and involves plate commonly having yield stresses between 520 and 620N/mm^2. Experience indicates that the component geometry[1] plays a significant part in determining risk areas for corrosion and stress corrosion initiation. Areas such as end countersink radii, countersink walls and bead radii where stretching occurs during fabrication, occasionally leading to degrees of necking behaviour, become vulnerable to environmental stress cracking failures, while flat panel areas such as the centre panel have no history of such failures.

1.6 Food Products : Some Cases of Commercial Failures Reported.

A summary of some examples from internal investigations involving the writer and some by other workers is given in **Table 1** below:

Table 1: List of Some Examples of Environmental Stress Cracking Incidents identified Involving Canned Foods.

Item	Product	Container	Time to failure (where stated)	Other information
1.	Tuna in Brine	End failures: countersink radius	-	Reference 1, 1992 paper, Japan
2.	Mackerel in Tomato sauce	Internally lacquered tin free steel ends	Around 1 year	Reference 1, 1992 paper, Japan
3.	Chicken in Brown sauce	Internally liquid side striped tinplate side-seam welds	Around 2 years	CMB report. TR5966, 1992
4.	Steak and onion	Internally liquid side striped tinplate side-seam welds	Around 2 years	CMB report. TR5966, 1992
5.	Beef product	Hot dipped and electrolytically coated plate	Around 2 years	Reference 2, 1992 paper, Czechoslovakia
6.	Mackerel in Tomato sauce	Internally lacquered tinplate side-seam welds	9 months	Poor internal side stripe protection; nitrate 20-40ppm. Report TR(MP) 19946
7..	Tuna in Brine	Internally lacquered tin free steel DRD drawn bodies having roll bead cracks.	Around 1 year	Crown report .TR8153, 1998.
8.	Dog Food	Internally lacquered double cold reduced tin free steel ends.	Around 3 months.	Polyester phenolic end lacquer. Crown report TR7831,1997.
9.	Tuna in Brine	Internally lacquered eccs drawn bodies	Around 1 year	Base rim denting and borderline lacquer protection. Crown UK report. TR10899, 2002

The above serves to indicate that these failures were associated with meat and fish products and that failure times have ranged from a few months to 2 years. No consistent cause has been identified, but in individual cases various conditions

associated with breakdown of the internal protective coating have been observed. Additional cases of failure recorded include vegetables e.g. potatoes, sweet-corn and mushrooms in brine, but these appear to have been comparatively rare occurrences, whereas fish and meat products appear to fail more commonly. Regarding the items 3 and 4 in Table 1, the laboratory investigations were followed up by additional slow strain rate testing by Newman[9] at UMIST on Chicken in Brown Sauce which had failed, and Stewed Steak Product which had not. Both products were reported to have given indications of hydrogen embrittlement in these tests. J Nekvasil and J Pitter[2] reported on a series of outbreaks of stress corrosion cracking in food cans packed with meats in Czechoslovakia including beef which started to crack after 2 years when moved between stores. Both hot dipped tinplate (made by dipping of steel sheet into a tin bath) and electrolytic tinplates (having an electro deposited tin coating) were reported to have been involved.

The authors[2] also reported that "cracking of beef preserves was more frequent than pork preserves, and cracking time was always shortest with liver in sauce. Luncheon meat cracked only very occasionally and paste products including liver paste never cracked." In the case of fish, mackerel and tuna in brine account for several incidents reported whereas for salmon in brine, no case has been identified by the author. Similarly, the author has not found cases of environmental stress cracking involving milk products.

1.7 Some Compositional aspects of Meat including Myoglobin

Meat is the muscle tissue of animals and comprises proportions of up to around three quarters water and one quarter proteins. For high fat meats the protein content may drop as low as 8-9%. Other constituents comprise small amounts of fat, 1% of mineral elements and some vitamins. Typical compositions[10] are summarised in **Table 2** below.

Table 2: Empirical Composition of Meats per 100g

	Beef		Lamb		Pork		Chicken
	lean	fat	lean	fat	lean	fat	
Energy (kj)	517	2625	679	2762	615	2757	508
Protein (g)	20	9	21	6	21	7	21
Fat (g)	5	67	9	72	7	71	4
Calcium(mg)	7	10	7	7	8	7	10
Iron (mg)	2	1	2	1	1	1	1
Niacin (mg)	5	-	6	-	6	-	8

In addition to evidence from Nekvasil and Pitter [2], laboratory evidence for the propensity of cracking with beef liver has been produced by Arcelor [6] in pack tests. For white meats, rather less evidence of records of failure has been found by the author e.g. only one case in the 10 items quoted involved white meat alone, Table1, Item 3. Bodwell and McClain[11] have described the chemistry of animal tissue within which the protein myoglobin "controls the colour of red meat and contains as much as 95% or more of the iron present." Organs such as the heart and liver of animals have greater blood supplies than skeletal muscles. During slaughter bleeding removes much iron as hemoglobin but liver retains more blood and hence more hemoglobin and iron after bleeding. The colour of the meat is determined by the oxidation state of iron and the ferrous iron associated with red meat is converted to brown ferric iron on cooking. If the heme iron in the cooked ferric state is capable of reduction to ferrous iron it may react with sulphides such as H_2S to liberate atomic hydrogen. The myoglobin contents of some meats quoted [11] are listed in **Table 3** below, revealing higher content for red meats than white meats, and a suggested animal age influence on the level in beef.

Table 3: Myoglobin Content of Some Meats

Meat Type	Myoglobin : mg per gram of wet tissue
Beef	4-10
Beef from older animals	16-20
Veal	1-3
Pork	1-3

A further important property of myoglobin is its function in binding oxygen within muscle tissue for use in aerobic metabolism. It can form ionic complexes with water. However, when meat has been cooked leading to de-naturing of the protein, the ferrous iron is converted to the ferric state, and it is reported[11] that the oxidised form of myoglobin containing ferric iron cannot bind oxygen.

Essential proteins in muscle fibre are actin and myosin at levels of around 2.5% and 7.5% respectively. Myosin is a fibrous protein and these tend to have poor solubility, whereas actin can be fibrous or globular and globular proteins tend to be soluble in water.

1.8 Environmental Factors: Common Anions and Carbon Dioxide.

Anions:

It is established knowledge that for carbon steels, the anions nitrate, phosphate and carbonate/bicarbonate as well as hydroxide are each associated with susceptibility to stress corrosion cracking in aqueous media. The pH ranges associated with susceptibility have been defined [12,13] for each of the above species. For carbonate/bicarbonate anions, the pH range indicated was >7.0 to 10.5 at 90°C [12] and from just below 7.0 to 10.0 at 25°C [13].

Meat and fish media considered in this work have pH values typically around 6.0-6.4 or slightly below 6.0. If the cracks initiate from pits, then the local pH values for chloride containing solutions, such as meat or fish packs, may be reduced to e.g. possibly below pH 5.0. In these cases, the involvement of carbonate/bicarbonate anions in the cracking

process appears improbable. Further comment on the pH influence appears under discussion of individual anions.

Nitrate:

Henthorne and Parkins[14] have studied the influence of some metallurgical features on cracking in nitrate solutions. They used machined and vacuum annealed samples to vary grain size. They observed that inter-granular cracking of low carbon steel (0.08%C) could be initiated at the grain boundaries in the absence of applied stress, but the process was arrested. The function of stress was considered to be to facilitate maintenance of an active path, through breakdown of any surface film at the crack tip. Tests showed that the mechanism was not strain rate dependent, but that there was a time dependency.

Chemical tests in nitrate indicated that the grain boundaries were cathodic to the grains and that carbide particles were cathodic to the adjacent matrix. However, the carbide particles were not continuous at the grain boundaries and therefore not sufficient to explain the effect. The TEM evidence showed that the grain boundary corrosion was just adjacent to the boundaries. It was deduced that interstitial carbon (and also nitrogen) would segregate to the grain boundaries and that if carbon could act in a similar fashion to the carbides, this would explain the attack just adjacent to the grain boundaries. Electron microscopy work had shown that there was an absence of grain boundary ridges or mounds at dislocations on samples, which were quenched from 690 °C and had received wet hydrogen treatment to reduce carbon and nitrogen contents. The latter treatment was reported to render mild steels resistant to stress corrosion cracking. The pH range for nitrate attack indicated was very approximately from below 3.0 to slightly above 5.0 at 25 deg C, from diagrammatic information.

Nekvasil and Pitter [2] used a test for SCC, starting by deforming samples with a 4mm ball indenter and then heating them for 40 hours in 55% aqueous calcium nitrate

solution in a refluxing vessel, followed by washing and examination for cracks. This method was used to select an improved steel grade, not specified in detail. This work concerned single reduced steels of relatively low yield strength around 300MPa

Phosphate:

Stress corrosion cracking of carbon manganese steels in phosphate solutions, was examined by Parkins, Holroyd and Fessler [15]. Trans-granular cracking in the pH range 3.0-7.0 was demonstrated when accompanied by an appropriate potential range. The solutions used were 1N $Na_3 PO_4$ or 1N Na_2HP0_4. NaH_2PO_4 did not produce cracking. The authors noted that determining the lower potential boundary for scc effects was complicated by the incidence of failure due to the ingress of hydrogen into the specimens; this was associated with reduced ductility in slow strain rate tests. The steel compositions of the alloys used were outside those for typical tinplate or eccs packaging steels, with carbon at 0.14% to 0.23% and manganese and silicon also higher. One steel was cold worked by 2% and a second was annealed.

Smart, Scott and Procter[16] investigated re-passivation kinetics and stress corrosion cracking of mild steel in phosphate solutions. This work employed 0.13% C steel with Si at 0.2% and Mn 0.6%, all these levels being above those normal for present day double reduced eccs materials.

Unstressed specimens did not suffer cracking, and several observations including current fluctuation measurement led to the proposal that cracking only occurred when the yield point had been exceeded. 'Active' deaeration was found to stifle cracking. Cracking occurred at potentials associated with an intermediate repassivation rate having $t^{-1/2}$ power law. At potentials more negative than -550mV (vs a saturated calomel electrode), a considerable loss of ductility was observed and the authors deduced that hydrogen embrittlement was possible at these potentials.

It was concluded that under anodic conditions and at potentials more positive than -550mV (vs a saturated calomel electrode), the data supported a mechanism of crack growth by a dissolution controlled model.

Carbonate/Bicarbonate Solutions:

Sutcliffe, Fessler, Boyd and Parkins[17] reported on stress corrosion cracking of carbon steels in carbonate solutions. Cracking could be made to occur with NH_4^+, Na^+ or K^+ as cations. Cracking took place at potential ranges identified during sweeps from a negative to positive direction and coinciding with a region where the anodic current peak reduced as the rate of sweep slowed.

The test solutions used were found to contain CO_3^- and HCO_3^- anions with cations defined above such that the initial pH was 8.0 to 10.5. Inter-granular cracking occurred where the anodic peak gave way to a rapid repassivation condition. The pH range quoted in this work was well above that for foodstuffs with which this study is concerned.

The same authors referred to work by Parkins and Usher [18] related to substances from coal gas cleaning plants, showing that inter-granular cracking involving NH_3 and HCN with either or both H_2S and CO_2 present, could occur.

Carbon Dioxide Environments:

Kowaha and Nagata [19] reported on SCC in mild steels and low alloy steels in an H_2O-CO-CO_2 system following tests at 40°C over 168 hours and pH 6.0. The gas pressures were 12.5kg/cm^2 of CO and 2.5kg/cm^2 of CO_2. The steels tested were not fully defined, but were described as commercial pipes and plates comprising mild steel and stainless steel. The authors reported that cathodically polarised steel did not give rise to cracking and that cracking only occurred in the presence of tensile stress. Cracking was trans-granular, and if one of the constituents was missing no cracking occurred. The order of gas pressures quoted for CO_2 were far in excess of any partial pressure likely for this

gas in food processing, although some residues of CO_2 are present in meat and fish packs. The net internal can pressure on cooking would only be sustained in small cans for up to around 1 hour, at around 2.0 bars maximum or slightly more, and the CO_2 levels after processing should not lead to positive pressures.

1.9 Sulphide Environments and Types of Hydrogen Cracking Effects

While the subject of volatile sulphides and their potential contribution to cracking in processed fish and meat cans is discussed in certain papers, the information found by the author is lacking very clear data on the subject. Schutte[7] has quoted hydrogen sulphide levels of 0.2-1.0mg/kg in cooked chicken meat.

Attempts by Campden and Chorley-Wood Food Research Association[20] to measure the volatile sulphides present in canned meats and fish during the present work were unsuccessful in terms of identification of the specific species present. A number of peaks corresponding to sulphur containing species were identified by gas chromatography-mass spectrometry, but could not be associated with specific substances.

Much background information concerning the influence of sulphides on environmental stress cracking relates to papers from the oil and petrochemical industry. While these studies have concerned processes and steels that differed from those used in steel cans, there may be a parallel information regarding environments and /or material factors which should not be overlooked in the present work.

Kane, Wilhelm and Oldfield [21] have reported on hydrogen induced cracking in wet petrochemical refinery service. These authors referred to hydrogen sulphide together with carbon dioxide, ammonia, cyanide and organic amine compounds. Environments giving least attack are described as having pH 7.0-8.0. The pH could fall to 4.0 with high acid gas and rise above 8.0 with increasing CN^- ions. Either condition was suggested as increasing corrosion, blistering and cracking.

The same paper[21] reported on five alternative environmental stress cracking modes, as follows:

- Stress Corrosion Cracking (SCC)
- Hydrogen Induced Cracking (HIC)
- Stress Orientated Hydrogen Induced Cracking (SOHIC)
- Hydrogen Blistering
- Sulphide Stress Cracking.

Testing quoted as applicable to steel for sour H_2S refinery environments utilised NACE information concerning the TMJ-02-84 HIC test procedure with the TM-01-77 solution (5% sodium chloride, 0.5% acetic acid, pH 2.7). Stress Corrosion Cracking is defined in **Appendix 1.**

Germit N Buchheim[22] gives views on several mechanisms of cracking referred to above. He stated that the refinery industry considers that there are three types of cracking arising from wet H_2S environments, namely: sulphide stress cracking, hydrogen induced cracking (also referred to as hydrogen blistering or hydrogen damage), and stress orientated hydrogen induced cracking.

In each case, it is required that hydrogen atoms are produced at the steel surface by a corrosion reaction in an H_2S containing aqueous solution. Buchheim indicated that the oil industry assumes a 50ppm threshold for H_2S below which cracking does not occur. In the presence of FeS and /or cyanides, the hydrogen re-combination reaction to form hydrogen gas is poisoned, allowing some of the hydrogen atoms to diffuse into the steel. Buchheim explains **sulphide stress cracking** as due to the hydrogen atoms affecting the flow and fracture behaviour of the steel, leading to hydrogen embrittlement, and being very dependent on composition, microstructure, strength and residual stress level. In the petrochemical industry, macro hardness control had been an insufficiently sensitive method to control cracking.

Hydrogen induced cracking (HIC) is described by the same author in terms of the hydrogen atoms collecting at imperfections or at in-homogeneities in the microstructure, such as elongated sulphide inclusions or oxides. Hydrogen atoms then combine at these sites to form hydrogen gas, but the molecules are too large to escape. Pressure then causes yielding or laminate type fissures parallel to the steel surface. This can lead to hydrogen blistering. As sulphides are regarded as catalytic recombination poisons preventing the generation of hydrogen gas in aqueous media at least, this aspect requires further consideration. Elboujdaini[23] describes a similar process, referring to "accumulation of hydrogen atoms at hydrogen traps, such as voids around inclusions", and later mentions manganese sulphide inclusions in this context. The hydrogen molecules were said to nucleate at traps or voids around inclusions. A further mechanism involves pits within which manganese sulphide inclusions can react to form HS^- ions, which can cause embrittlement by acting as a catalytic poison, leading to atomic hydrogen in the metal. This is considered later in this report.

For the **stress orientated hydrogen induced cracking mechanism (SOHIC)**, hydrogen atoms were said by Buchheim[22] to collect at imperfections just as in HIC, but fissures formed in the through thickness direction. The effect was reported to occur typically in "heat affected zones or other areas of high stress concentration". Buchheim also observed that while cleaner steels may be less susceptible to HIC or SOHIC, some data suggests that such steels may be more prone to sulphide stress cracking.

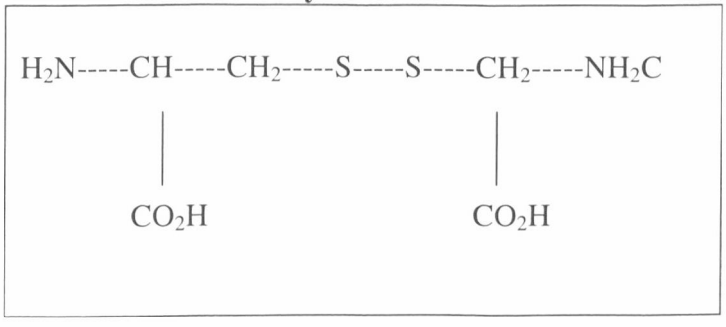
A further author in this field, Gutzeit[24], commented on the metallurgical nature of the cracking observed. He stated that hydrogen stress cracking, which he associated with H_2S environments, was primarily trans-granular. The stress orientated hydrogen induced cracking was present in trans-granular or inter-granular forms.

1.10 Sulphides: Break Down Behaviour Involving Amino Acids in Foods

Meat and fish products contain three amino acids within the protein contents that are sulphur bearing, namely, cystine, cysteine and methionine. Cystine is a dimer of cysteine. The role of sulphides and H_2S has been highlighted from Petro- Chemical Industry literature studies as instrumental in the promotion of hydrogen cracking in carbon steels. In the context of food, the question then arises as to the evidence for the generation of this substance as well as the level, and any other sulphide species that might assist the process.

Bjarnason and Carpenter[25] studied mechanisms of heat damage in proteins and the chemical changes that occurred. The material used was bovine plasma albumin (BPA) containing 14% moisture. This was heated for 27 hours at 115°C and later at 145°C. Much the greatest loss of amino acid by type was found to occur from cystine, amounting to 50% at 113°C, or 3.3gms per 100gms ash-free dry matter. Methane was found to have shown an apparent increase of 14% on heating at 115°C and a 12% increase at 145°C. It was also observed that 0.23g of free ammonia was liberated per 100g ash free dry matter. The structure of cystine having the disulphide bridge is shown below in Figure 6.

Figure 6: Chemical Structure of Cystine



Bjarnasson and Carpenter[25] recorded that hot water releases some H_2S from wool protein and that Schoberl[26], 1941, had attributed this to the reaction of the water with the disulphide bridges of cystine. The authors quote a hydrolysis reaction between hot

water and cystine postulated by Schoberl and Eck[27], 1936, leading to the liberation of hydrogen sulphide, as follows:

$$R\text{-}CH_2\text{-}S\text{-}\sim S\text{-}CH_2\text{-}R + H_2O \longrightarrow R\text{-}CH_2\text{-}SH + HOS - CH_2 - R \quad (1)$$

$$HOS - CH_2 - R \longrightarrow H_2S + OCH - R \quad (2)$$

These reactions have been suggested by Bjarnasson and Carpenter[25] as at least partly responsible for the loss of cystine which occurs on heating of proteins in the absence of oxygen. However, the processing of meat in cans does not take place in the complete absence of oxygen.

Carpenter et al[25] reported that the exact mechanism was still hypothetical, but indicated that breakdown of S-S bonding with formation of a carbonyl group would be a mechanism in conjunction with a maillard reaction involving lysine.

The maillard reaction describes a non-enzymic browning process. This is defined by deMan[28] as a series of reactions beginning with that of the amino group of an amino acid e.g. within a peptide of protein, with the glycosidic hydroxyl group of sugars. These reactions end with the formation of brown nitrogenous polymers, otherwise called meladoins.

Volatile Substances arising from the Processing of Meat.

Varnam and Sutherland[29] have described substances associated with meat like aromas. They identified such substances as being associated with "A ring containing at least one double bond and a methyl group adjacent the thiol group". Seven compounds were recorded "as being of greatest importance in determining meat flavour". These are listed below in Figures 7a-7g.

Figure 7: Volatile Substances arising from the Processing of Meat.

Figure7a: 2-methyl-3-(methylthio) Furun

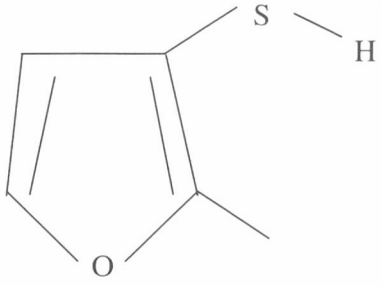


Figure 7b: 2-methyl –furan-3-thiol

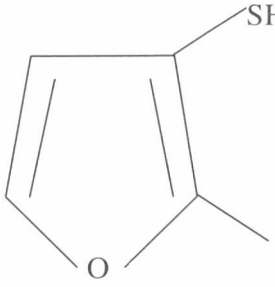


Figure 7c: bis (2-methyl –3-furyl) disulphide

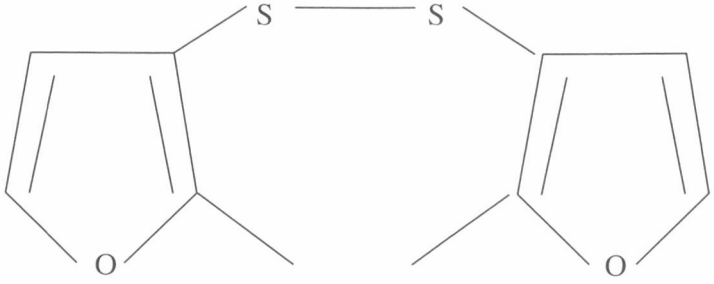


Figure 7d: 2-Furfuryl 2- methyl-3-furyl disulphide

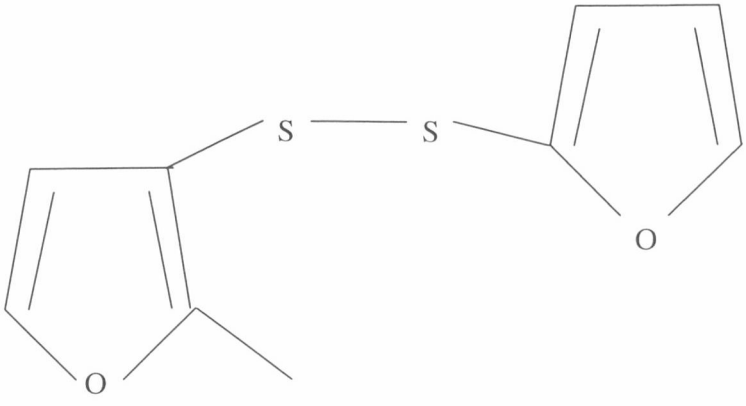


Figure 7e: bis (2-furfuryl) disulphide

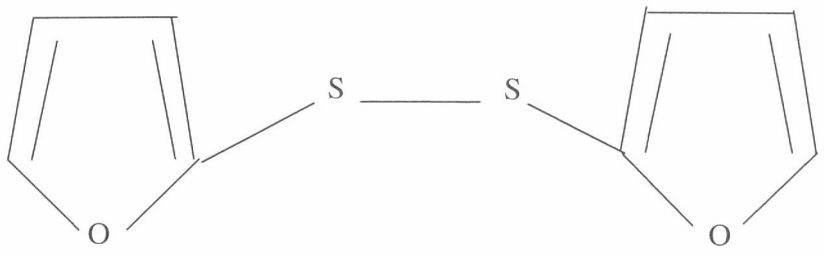


Figure 7f: dimethylfuryl 2-methyl-3-furyl disulphide

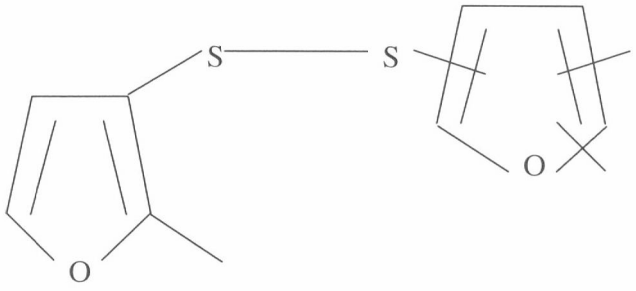
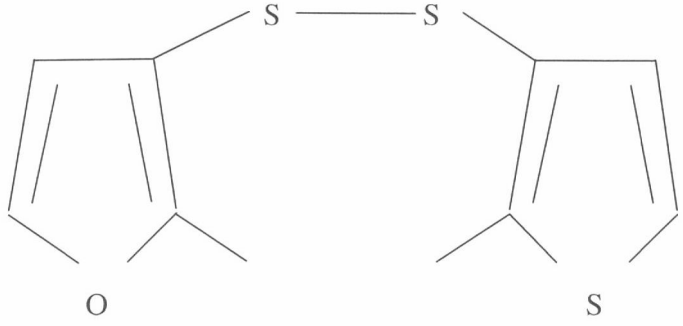


Figure 7g: 2-methyl – 3 – furyl 2 – methyl – 3 – thienyl disulphide



Heterocyclic structures such as furan, pyrrole and thiophene have chemical properties somewhat similar to those of benzene. Substitution in each ring can take place at the 2, 3 or 5 positions.

These are polar molecules. The dipole moment which signifies the relative polar character of the molecule is affected by two main factors, namely the –ve charge generated by the attraction of the sigma carbon electron towards the second hetero atoms, e.g. the sulphur of thiophene, and the counteracting resonance structure effect of delocalisation of the unshared electrons into the ring structure. The thiophene structure has a bond angle of 91 degrees at the sulphur atom, lower than for oxygen in furan, on account of the involvement of 3d orbitals in the resonance bonding, whereas for oxygen only 2d electrons are involved. Thiophene is not miscible with water, but it may contribute to corrosion chemistry through adsorption behaviour.

Organic hetero-cyclic molecules having free donor electron pairs, which exist for oxygen, sulphur and nitrogen containing compounds, can act as inhibitors where the surface has an opposite charge. For adsorption of polar molecules containing sulphur and oxygen this requires a positive charge on the metal surface, i.e. above the zero charge potential, which would apply to steel corroding at a significant rate. The result of adsorption of the organic molecule may then be a barrier to diffusion of other competing species of required to sustain the corrosion process e.g. oxygen at cathodic sites or other reducible species such as ferric ions, supposing nitrogen were the adsorbed species. At anodic sites the effect may be reduction in the access of aggressive anions such as chlorides which otherwise assist corrosion by forming soluble species and obstructing protective film formation. Polar compounds containing sulphur which are immiscible in water may conceivably act as catalytic poisons through heterogeneous behaviour, but failing identification of such behaviour so far, relating to the above materials, the effect would need to be tested.

In the case of the immiscible hetero cyclic molecules having a disulphide bond, or for a thio-furan , corrosion activity of the former is likely to depend primarily on the cleavage of the disulphide bond e.g. by hydrogenation, as suggested by Bjarnasson and

Carpenter[25] for cystine, and for the thio furan a similar result would depend on reduction reaction involving the HS group to liberate hydrogen sulphide.

M Elboujdaini[23] explains that hydrogen atoms produced at a steel surface may combine to form hydrogen gas, but that in the presence of a sulphide or cyanide, "the hydrogen recombination reaction is poisoned so that the nascent hydrogen atoms diffuse into the steel to form hydrogen gas". The chemical reaction sequence is explained as follows:

$$H_2S = H^+ + HS^-$$

Cathodic reaction $2H^+ + 2e = 2H$

The HS- ion is indicated as the poison. The overall reaction involving iron is shown as:

$$Fe^{2+} + H_2S = FeS + 2H^o$$

The "poisoning" action of HS- ions described by Elboujdaini[23] is related to the ability of these ions to raise the over-potential for discharge of hydrogen gas in the cathodic reaction under acid conditions. Evans[34] describes the effect as hydrogen sulphide acting as a poison for the second stage of the cathodic process i.e. recombination of hydrogen atoms to form hydrogen gas. The reaction has also been expressed as a re-combination of hydrogen atom and an ion plus electron to form hydrogen gas in certain cases, whereas in others there combination of two atoms was said to predominate. Evans[33] also refers to selenium as well as phosphorus amongst other elements that behave as catalytic poisons to the hydrogen evolution reaction on steel.

The possibility of enzymatic catalysis processes acting as poisons to hydrogen evolution has not been resolved in this study.

Hydrogen damage was stated by M Elboujdaini[23] to be accelerated by H_2S, CO_2, Cl^-, cyanide (CN-) and ammonium ions (NH_4^+). The breakdown products of processed meat and fish have been found to include hydrogen sulphide, carbon dioxide and ammonia. Salt, and hence chloride is also present in significant quantities.

Dimethyl Sulphide and Methane Thiol

These substances have been identified by Schutte[7] as volatiles liberated in the cooking of meat such as beef chicken and also from fish. Dimethyl disulphide and dimethyl trisulphide are cited as liberated in the cooking of beef and chicken but not fish. Alkyl sulphides are insoluble on water but soluble in organic solvents, and chemically comparatively inert. They form addition products e.g. with bromine and iodine. The molecules have a structure with sulphur at the apex of a bend. The apex angle for sulphur is found to be smaller than for oxygen. This has been attributed to the unshared electron pair on sulphur occupying orbitals based on quantum level 3, creating repulsive forces with the chemical bonds and forcing them closer together. While these sulphides are polar molecules, they not soluble and thus not ionic in an aqueous phase.
Thiols resemble alcohols but are more acidic. They are less soluble in water than alcohols. Reactions of thiols in a food context can be with carboxylic acids to form thiol esters, and mild oxidation with air can lead to disulphide formation.

Further Observations on the Formation of Volatile Sulphur Compounds in Meat and Fish.

The subject of precursors of sulphur containing flavour compounds in food stuffs has been considered in depth in a review by L Schutte[7]. Hydrogen sulphide and methanethiol are indicated as formed by maillard reactions in beef and fish as well as for di methyl sulphides. Schutte[7] described reactions by which these compounds can be generated in processed foods, and proposed a 'Strecker' degradation reaction involving cystine for the generation of H_2S . The cysteine molecule first synthesises with a di-ketone, following which it splits into a mercapto- aldehyde and hydrogen sulphide.

1.11 Summary of Information: Volatiles from Cooking of Meat and Fish.

From the above review a number of points are clear as follows:

1. Volatiles produced in the cooking of meat include sulphides, and among these hydrogen sulphide as well as other organic sulphides and mercaptans are cited. A great number of other volatile organic substances are also produced, certain of which e.g. alcohols are referred to in other literature as promoters of scc.

2. Bjarnasson and Carpenter[25] showed that cystine was a key source of protein loss in the prolonged heating of Bovine Albumin plasma, and that some ammonia was generated.

3. The breakdown of cystine was indicated as capable of generating hydrogen sulphide, but while Bjarnasson and Carpenter[25] have suggested a hydrolysis mechanism, no conclusive evidence of the mechanism was understood to have been established.

4. The literature evidence found was not definitive concerning the level of hydrogen sulphide in processed high protein food, but Schutte[7] identified 0.2-1.0mg per kg in cooked chicken meat.

5. Examination of environmental stress cracking of steels reported in literature published by the oil industry indicated that in addition to hydrogen sulphide, chloride anions, CO_2 and ammonium ions can be accelerating substances for hydrogen cracking.

6. Among the wide range of volatiles stated by Price[30] to be generated in the cooking of beef , alcohols are included and certain of these have been investigated in a different

context from the oprsent investigation, and shown to be capable of causing environment stress cracking[35] in packaging steels when combined with chloride and organic acids such as acetic acid. Acetic acid as well as other organic acids have been reported by Price to be present in the volatiles of cooked meat (beef).

7. The observations of Bjarnason and Carpenter[25] concerning hydrogen sulphide and ammonia as substances liberated on heating of meat may have added significance in view of those of Kane, Wilhelm and Oldfield[21] that hydrogen sulphide and ammonia were among substances associated with cracking of steels in wet petrochemical refinery equipment.

1.12 Compositional Aspects of Food: Fish Products.

Maurice E Standsby[31] give information concerning the approximate composition of fish shown in Table 4 below:

Table 4: Empirical Approximate Composition of some Fish Types

			Weight %			
	Type	**Species**	**% Moisture**	**% Protein**	**% Oil**	**% Ash**
A	Low Oil - High Protein <5% 15-20%	Pacific Cod	81.5	17.9	0.6	1.6
B	Medium Oil – High Protein 5-15% 15-20%	Mackerel	67.5	18.0	13.0	1.3
C	High Oil – Low Protein >15% <15%	Sisacowet Lake Trout	52.5	11.3	36.0	0.53
D	Low Oil–Very High Protein <5% >20%	Skipjack Tuna	72.4	26.2	0.7	1.5
E	Low Oil – Low Protein <5% <15%	Butter Clams	83.0	13.3	1.3	1.9

Composition categories of some important species.

Herring (B).	Some caught in certain seasons or localities will fall in category **C.**
Mackerel (B)	Some caught in certain seasons or localities will fall in category **C.**
Salmon (B).	Some species of salmon, Chum Atlantic and Pink may border on category **A.**
Sardines (B)	Some caught in certain seasons or localities will fall in category **C.**
Tuna (D)	Albacore Tuna when caught in certain areas is in category **B.** Bluefin Tuna borders on category **B.**

The author has not so far found reference to cases of recorded failures through environmental stress cracking of steel cans involving salmon, cod, trout, clams or herring, but cases were found for tuna in brine product and for mackerel in tomato sauce, including failures produced in lab test work. For the mackerel in tomato sauce product, the authors of the study, M Tsurumaru, K Masuda and Y Yamamoto[1], commented that for the failing product "pH was slightly lower, with phosphate higher, chloride less, fructose more than for the non failing mackerel in brine". It was also commented that hydrogen sulphide was significantly higher in the failing product, but the precise levels were not apparent from the detail. However, dimethyl sulphide was slightly higher for the failing product.

From the table above, it is apparent that the tuna product, D, combined the highest protein and lowest oil contents, with the mackerel showing the second highest protein content, but also the second highest oil level. Tsurumara[1] et al found the Mackerel product to fail with tomato sauce added associated with reduced pH, but did not detect cracking in lab tests with the mackerel product in brine.

Both mackerel and tuna products were noted by Fox and Cameron[10] to be high in histidine. The histidyl residue also forms part of the porphyrine ring of myloglobin which is common to fish and mammals, and is linked to the iron complex structure of fish and meat.

1.13 Discussion of Differences Observed in the Composition between Tuna and Salmon in Brine, and Consideration of Other Fish.

Searches by the writer so far have not revealed a history of cases of SCC type failure involving salmon products, whereas some cases have been reported for Tuna in Brine (See Section 1.6, Page 27, Table 1).

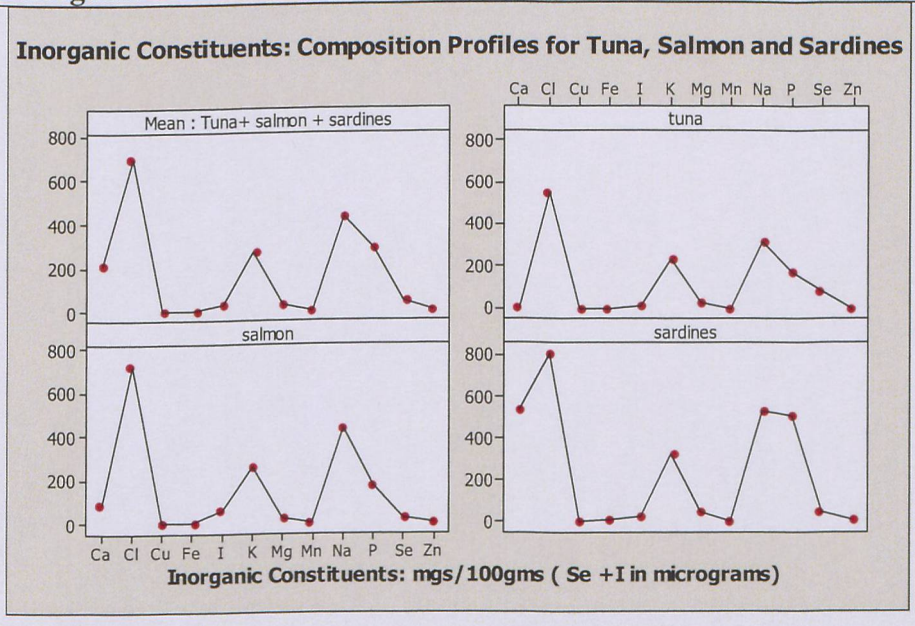
The literature also records SCC cases involving Mackerel and Pilchards, but none have so far been found by the author for sardine , kipper or herring products. This does not necessarily mean that none have occurred in the types mentioned , or could not occur. Some compositional aspects have been examined.

Salmon and Tuna Product

A comparison has been made of Canned Tuna with Salmon and Sardine products using compositional data[32] for canned fish. Full details are recorded in Appendix 2, pages 1 and 2.

A summary discussion with charted information is given below.

Plot 1: Inorganic Constituents of Three Fish Types.



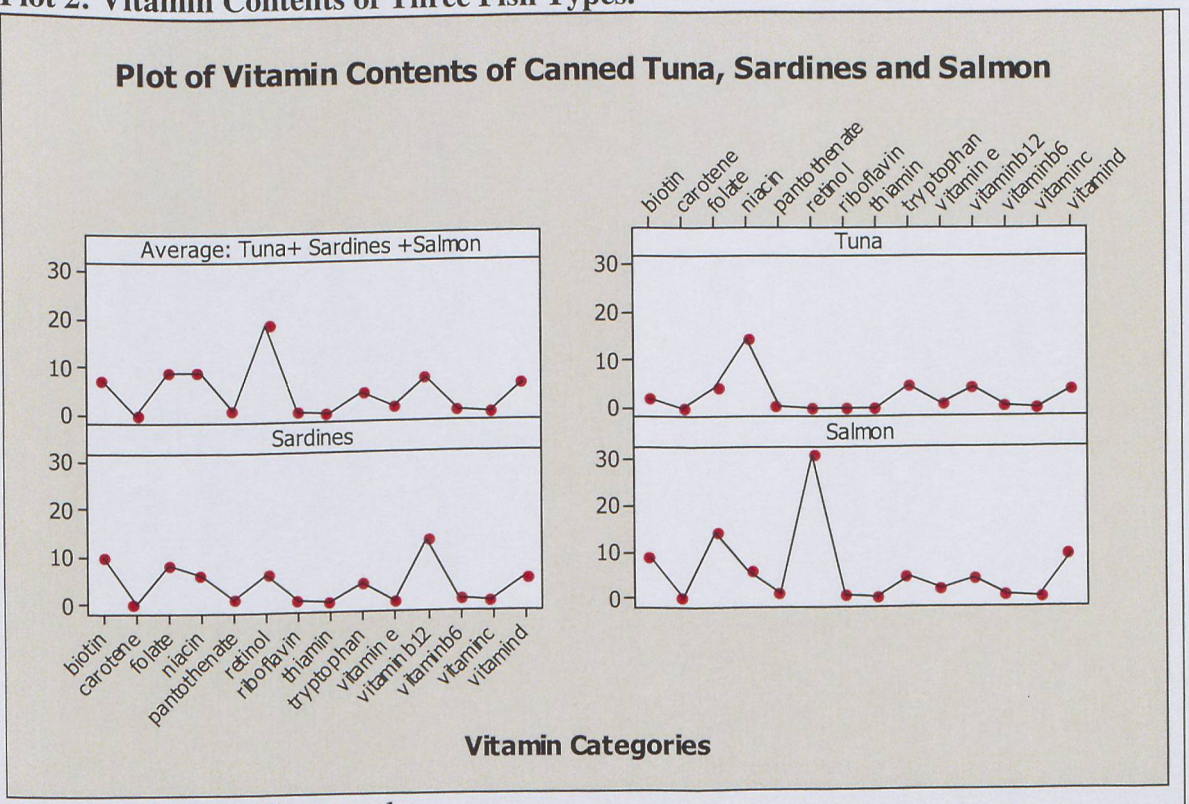
Notes : Units for ordinate scale:
Inorganic elements in mgs per 100 grams edible portion.
Exceptions: Selenium and Iodine : units µgms per 100 grams edible portion.

From these compositional profiles for Inorganic Constituents , Plot 1, the chlorine and sodium contents of salmon and sardine products were higher than for tuna, and for sardines phosphorus was above that for the other two variables. Potassium was quite similar in Tuna and Salmon.

Iodine was higher in salmon than for either of the other two fish. This being a halide, if present as an ion it may be expected to assist pitting, but chlorine is already rather high in all three products and the net effect due to iodine may not be noticed.

Selenium was highest in tuna. This substance is mentioned in literature as conferring some anti oxidant properties which parallel Vitamin E. Selenium is an element identified by Evans[33] as a catalytic poison linked to hydrogen entry into steel. This is conceivably important, although only a limited difference existed between products, given the very low levels.

Plot 2: Vitamin Contents of Three Fish Types.



Notes : Units for ordinate scale:
Vitamins in mgs per 100gms edible portion, except as below
Exceptions : in µgms per 100gms edible portion.
Retinol, Carotene , Vitamin D, Vitamin B12, Folate, Biotin.

The composition profiles for Vitamin Contents, Plot 2, showed that tuna and salmon each displayed some measurable differences for individual species from the average values, but all species were present at relatively low concentrations after canning, so that observations about possible chemical influences on corrosion will be rather speculative.

Tuna had less folate present and less Vitamin D than salmon, but more niacin than salmon. For retinol, salmon was higher than average and above that for sardines, but there is no data for tuna. Retinol is an aryl based alcohol. Certain alcohols e.g. aliphatic types, can promote SCC in conjunction with organic acids and chlorides. In this case salmon, without history of failure, was higher than the average for fish in the alcohol type present. The role of folate is metabolic, related to amino acids and indirectly to hemoglobin. Tetra-hydrofolate rings contain nitrogen substituents, which can lead to inhibiting properties through chemi-sorption, but the concentration relative to that of aggressive species such as chloride was very small, so the effect is more likely to be very weak, if any at all.

Sardines were lower in retinol than salmon, and similar to salmon in niacin, but were slightly higher than the former two in vitamin B12. This vitamin, Cobalamin, is a highly complex molecule where Cobalt is a coordinating atom at the centre of a ring system resembling porphyrine, but having substituents which are mostly amides. The liberation of ammonia via breakdown products on processing might be interpreted as providing generation of an accelerator to hydrogen cracking.

Ascorbic acid (Vitamin C), was only recorded in trace amounts in any of the products. This substance when present as ascorbate which was reported by HO Hultin[34] to be a reducing component of fish tissue, has been indicated as capable of reducing iron from the inactive ferric state to active ferrous iron. It was also recorded that reactive non

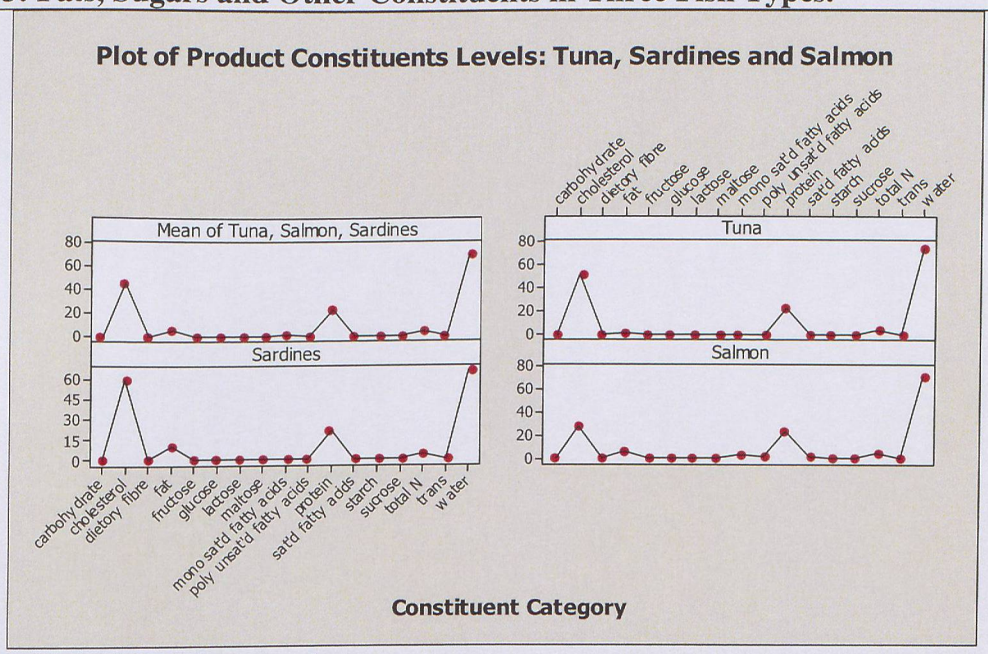
haem iron can be obtained by release of iron from haemoglobin pigments or from the iron storage protein ferritin.

The generation of ferrous ions is potentially of some significance to Environmental Stress Cracking of carbon steel if the level is sufficiently great to assist either of the effects of:

a) The formation of magnetite under anodic conditions, know to assist scc

b) The liberation of atomic hydrogen by reaction with H_2S[23].

Plot 3: Fats, Sugars and Other Constituents in Three Fish Types.



Notes : Units for ordinate scale
Data : in gms per 100gms edible portion
Exceptions below : in mgs per 100gms edible portion:
Cholesterol

Among the remaining constituent categories compared in Plot 3, it can be seen that no sugars were present in any of the products.

Cholesterol is termed a sterol, which is a polar lipid signifying solubility in organic liquids. It has a complex ring structure with an OH^- group joined to an aromatic ring.

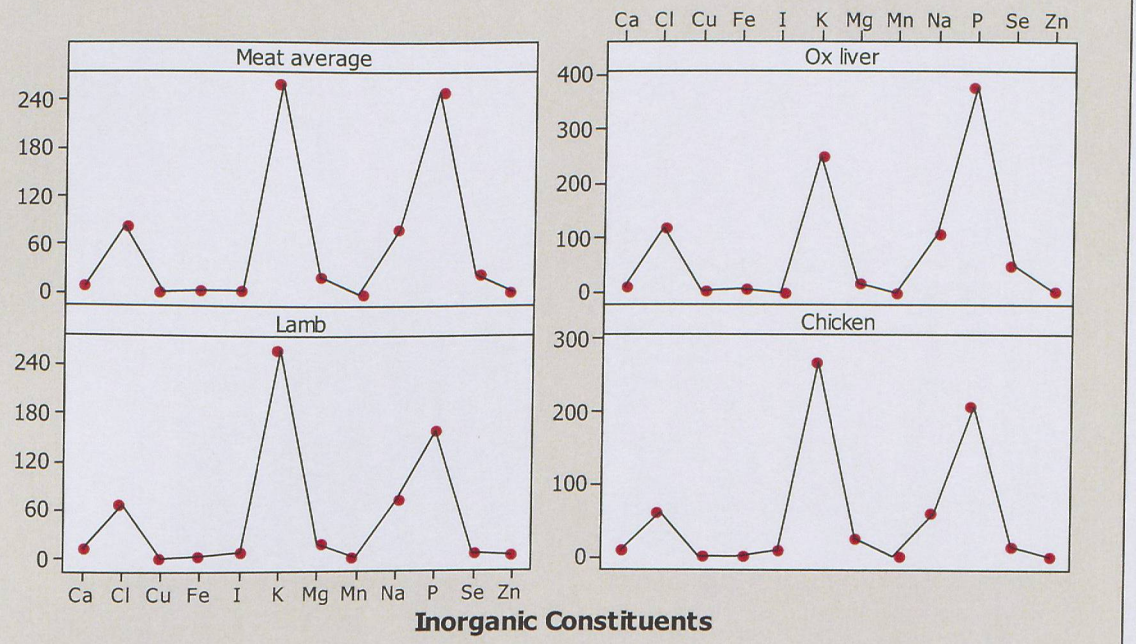
While higher in level in tuna and sardines than in salmon, it is not of very obvious significance to SCC behaviour given the lack of solubility. Aqueous alkalis, or alcohols[32] miscible with water can lead to SCC in carbon steels under certain conditions.

However, any effect of cholesterol would need to be established by testing. The overall content of fat was measurably higher in salmon than in tuna with sardines higher still than salmon. It is again conceivable that this aspect is of some relevance to the apparent difference in stress corrosion susceptibility history between tuna and salmon based upon commercial packing experience alone given the observations of Schutte[7]. Schutte's analysis quotes work by Pippen and Mecchi concerning the contribution of hydrogen sulphide to cooked chicken aroma, and these authors reported that hydrogen sulphide was bound to the fat phase if aldehydes were present . It was inferred that as hydrogen sulphide was only partly recovered from the fat, the remainder must have reacted with the aldehydes. "A homolog of one of the products they propose i.e. trimethyl-s-triathane, has been identified in cooked chicken." Hence if a mechanism similar to that proposed for chicken could occur in salmon having higher fatty acid content than tuna, then a lowering of activity of H_2S may result, and susceptibility to environmental stress cracking may then be lowered.

1.14 Meat Analysis.

Meat compositions have been compared for Ox liver, Lamb and Chicken. These are considered below.

Plot 4: Ox liver, Lamb and Chicken: Inorganic Constituents.

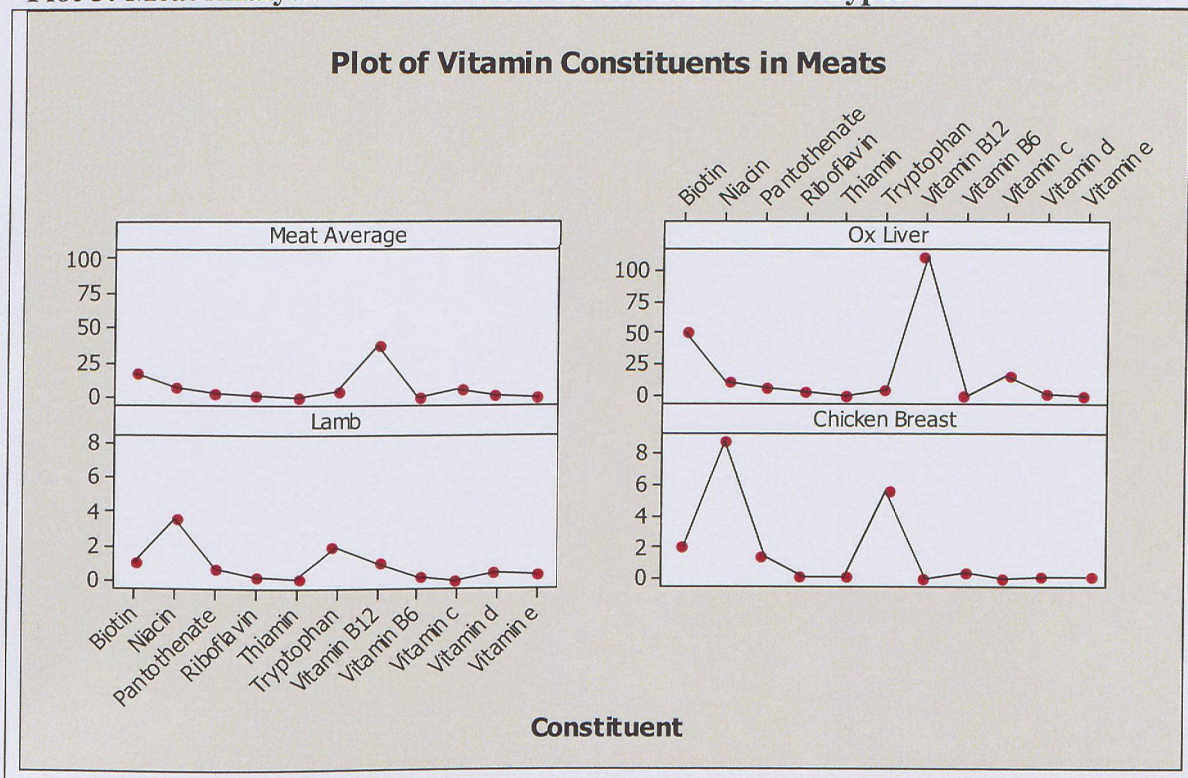


Notes : Units for ordinate scale: Element levels in mgs per 100gms edible portion
Exceptions are: Se and Zn in μ gms per 100gms edible portion
Meat average means the average for cooked ox liver chicken and lamb
A full table of element levels is shown in Appendix 2.

From these composition profiles for Inorganic Constituents, Plot 4, it can be seen that the liver was slightly higher in phosphorus and chlorine and sodium than the average for the meats, as well as being higher in iron, copper, zinc, manganese and selenium. Note that selenium is a promoter of hydrogen ingress into steel as a catalytic poison[33] , although the level present in micrograms was very small . Evans[33] also identified zinc as

a promoter of hydrogen entry into steel. In the tuna vs salmon comparison, iodine was higher and selenium lower in the apparently less susceptible salmon.

Plot 5: Meat Analysis : Vitamin Contents for Three Meat Types.



Notes : Units for ordinate scale on plot : Vitamins listed in mgs per 100gms edible portion:

Vitamin E, Thiamin, Riboflavin ,Niacin, Tryptophan 60, Vitamin B6,

Panto-thenate, Vitamin C.

Vitamins listed in μ gms per 100gms edible portion

Vitamin D, Vitamin B12, Biotin.

Additional Vitamins not included in plot are shown in the table 5 below:

Table 5: Additional Vitamins not included in plot

Vitamin	Meat average (μ gms per 100gms edible portion)	Ox liver (μ gms per 100gms edible portion)	Lamb (μ gms per 100gms edible portion)	Chicken (μ gms per 100gms edible portion)
Retinol	5776	17300	29	Trace
Carotene	500	1500	0.0	Trace
folate	100	290	4	6

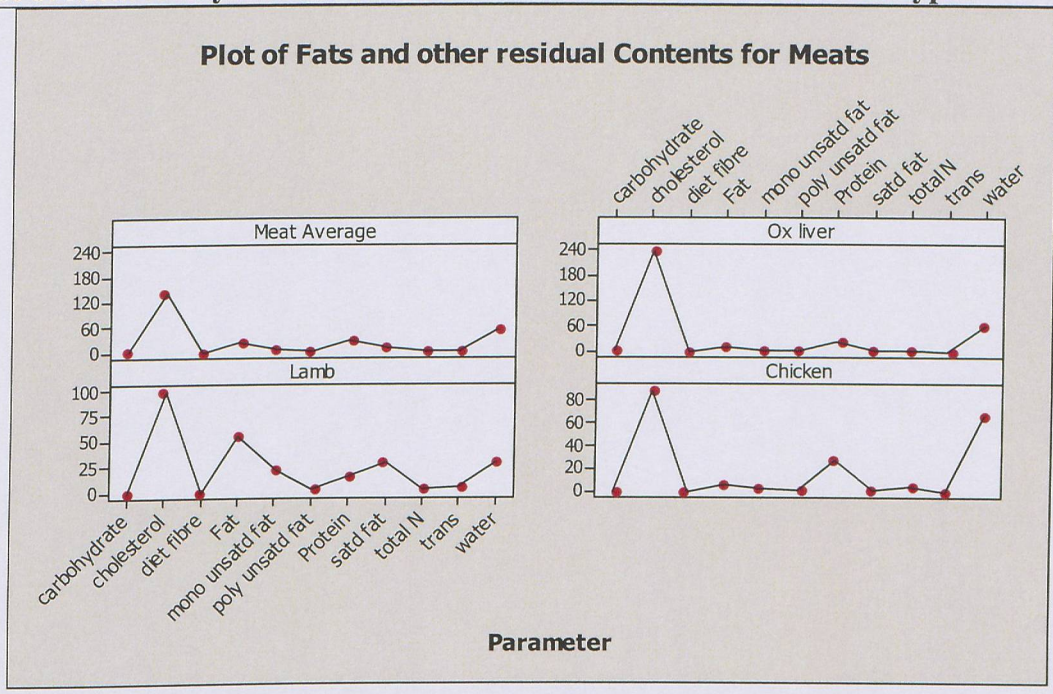
From the above information in Plot 5 and Table 5, the tabulated data are considered first. Retinol, an aryl based alcohol as discussed in the section on fish, was much higher in liver than for lamb or chicken. Specific alcohols[35] have been shown to lead to SCC in carbon steel in association with other constituents, but the work referenced concerned aliphatic alcohols, so any effect is subject to corroboration. Carotene is an anti oxidant which would retard oxidation of fats and de-activate 'singlet' oxygen. Biological systems can contain certain highly reactive forms of oxygen such as $.O_2^-$, an oxygen molecule with an unpaired electron giving it a negative charge. Carotene can react with singlet oxygen returning it to an un-reactive state. Folates form hetero-cyclic ring compounds having nitrogen substituents, and hence may have inhibiting properties through adsorption at negative metal potential regions relative to that of the zero charge potential charge (zcp). For the other vitamins, ox liver clearly had a higher level of vitamin B12 (Cobalamin) relative to the other meats.

Cobalamin is a complex ring compound with cobalt as the coordinating atom. Cobalamin promotes synthesis of the haem species in haemoglobin, hence its logical association with the liver possessing high iron content, but still present at a relatively low level. No reference has been found indicating cobalt as a promoter of hydrogen ingress to steel.

Possibly a very important aspect is the increased Vitamin C content of liver accompanying the increased iron level. Vitamin C (ascorbic acid) when present as ascorbate in animal tissue is reported as commented under fish aspects, as reducing the ferric iron, for example in ferritin, to the ferrous state, then creating the possibility that the ferrous iron could react with sulphides such as H_2S to promote ingress of atomic hydrogen . The thiamine breakdown is an additional potential source of hydrogen sulphide, as indicated by Schutte[7]. Biotin is a complex ring compound containing a sulphur substituent, but is reported as being stable under cooking and processing

conditions. Comparing the composition profiles further, regarding the lamb and chicken products, Niacin and Tryptophan were at higher levels in ox liver than in the afore-mentioned two, but no reason to implicate these in an SCC process has been identified.

Plot 6: Meat Analysis: Fats and Other Constituents for Three Meat types



Notes on table: Substances listed are in gms per 10gms edible portion
Exception is cholesterol in mgs per 10gms edible portion
Sugars not included as either nil or a trace level (in ox liver)

The data for Fats and Other Constituents, Plot 6, showed that ox liver was slightly higher in fat level than chicken but far lower than lamb, and below the average for meat. Fat has been commented on by Schutte[7] as a reservoir for sulphides, e.g. in Chicken. Cholesterol (having an OH^-) group was highest in liver, but as this is a lipid, it would not be soluble in water and hence not thought a very prominent candidate likely to be significant to the SCC problem. For other categories, no significance has been identified at this stage.

From the above analyses, those factors which could be considered as potential candidate contributors to an scc process involving carbon steel at this stage concerning ox liver

would be the increased levels of phosphorus, iron, selenium , retinol and ascorbic acid , and possibly zinc each of which has some link to one or other characteristic capable of promoting of loss of ductility or environmental stress cracking of carbon steel, or in the case of ascorbate, indirectly via a reported capability to reduce iron in myoglobin, then facilitating a reaction with hydrogen sulphide to liberate atomic hydrogen. The compositional data obtained has not included sulphur levels.

1.15 Metallurgical Aspects of Stress Corrosion Cracking.

1.15.1 Fracture Mechanics and Surface Energy related Effects

Environmental stress cracks, when examined metallurgically by sectioning are commonly noted to have an appearance suggesting little plastic deformation of grains visible either side of the crack, and plastic deformation is only visibly present at the region of final fracture. Fracture mechanics facilitates the definition of relationships which govern the occurrence of cracking including stress corrosion cracks. Herzberg[36] explains the Griffith crack theory concerning the introduction of a crack into a stressed plate of elastic material. According to the theory, an energy balance exists, between a decrease of potential energy resulting from introduction of the crack plus work done by external loads, and the increase in surface energy arising from crack formation.

These concepts lead to an equation of the form below:

$$U - U_0 = -\frac{\pi \sigma^2 a^2 t}{E} + 4at\gamma S$$

Change of energy = decrease in potential energy of cracked plate + surface energy increase due to crack

where U = Potential energy of the body with crack

Uo = Potential energy of the body without the crack

σ = Applied stress.

a = One half of crack length.

t = The thickness of the material.

E = The modulus of elasticity of the material.

γS = Specific surface energy.

The surface energy of a solid is the work required to increase the surface area by $1cm^2$.

At equilibrium, the energy state is determined by differentiating U with respect to 'a' and setting the value equal to zero. This leads to the following equations:

$$\frac{du}{da} = 4t\gamma S - \frac{2\pi\sigma^2 at}{E} = o$$

From which

$$2\gamma S = \frac{\pi\sigma^2 a}{E}$$

$$\sigma = \sqrt{\frac{2E\gamma S}{\pi a}}$$

This is the Griffith equation.

The second differential of U with respect to 'a' gives:

$$\frac{d^2u}{da^2} = -\frac{2\pi\sigma^2 t}{E}$$

This would be a negative value i.e. corresponding to a maximum rate of growth, from which it is deduced that the crack is unstable and would continue to grow.

The Griffith equation applies to brittle solids such as glass. The crack tip radius was not included in the Griffith equation but was assumed to be very sharp. Typical alloys such as carbon steels in cold reduced form have finite ductility, and the theoretical prediction requires inclusion of a term to encompass the energy used in plastic deformation. King and Jarman[37] explain the inclusion of the plastic work term by substitution of the parameter G for $2\gamma S$, where :

$$G = 2\gamma S + p,$$

p being the energy required to cause plastic deformation during fracture, and γS being the surface energy.

Packaging steels are of low gauge, and during forming processes, plane stress conditions will be a close approximation. King and Jarman[37] described the plastic zone size as :

$$rp_x \text{ (plane stress)} = a/2 \times (\sigma_{app}/\sigma_y)^2$$

where:

rp is the plastic zone size along the plane of the crack and perpendicular to the applied stress.

The stress intensity factor, K_I ,defines the 'fracture toughness parameter', and a value K_{Ic}

(K_I critical) can be determined, above which unstable crack propagation occurs. The K_I parameter is a numerical value representing a stress condition affecting a local

geometric region such as a notch containing a finite crack, where the value obtained is a function of the applied stress, the crack length and the specific geometry. King and Jarman[37] define the relationship of K_I to geometry, stress and crack length in terms of the equation:

$$K_I = Y^{*}\sigma\,(\pi a)^{1/2}$$

where :

Y is a constant related to specimen dimensions and specific geometry.

σ is the applied stress.

a is the crack length.

The stress intensity factor, K_I, can then be determined according to the geometric factor from reference book formulas, the applied stress and the crack length. The equation then allows the maximum flaw size to be determined for a particular geometry, above which unstable crack growth is predicted, associated with the K_{1c} value.

Notched specimens have been used as test pieces in slow strain rate tests in the course of this study, and packaging steels have a measure of ductility. Whereas the parameter K_{1c} is applicable to brittle materials, a general yielding fracture mechanics solution taking account of ductility would be applicable to packaging steels. Also, the energy balance involved in creation of an environmental stress crack requires modification to include chemical / electrochemical aspects. Parkins[38] has expressed the energy balance as:

Surface energy change + Plastic work done = Change in initial stored energy + Electro-chemical energy released.

A number of approaches have been used to take into account the plasticity element in the fracture of alloys:

Crack tip opening displacement: delta (δ)

King and Jarman[34] describe the relationship of G to delta as $G = 4/3 * \sigma * \delta$

This solution would probably be difficult to apply to samples of packing steel in the context of environmental stress cracking failure measurement, due to the difficulties in making the δ observation, although the method might be used for a model.

J integral method. This method explained by Rice[39] relates a line integral surrounding a notch to the strain energy required to intiate the crack at the notch tip. The expression related to the path length Γ is:

$$J = \int_{\Gamma} (W\,dy - T\,du / dx.\,ds)$$

W is the strain energy density.

dy is the strain in direction y parallel to the notch surface.

du is the displacement vector for the integral.

dx is the strain increment in the x direction.

ds is the increment along the line contour.

T is the stress vector acting on the contour.

Rice showed that for a closed loop around the notch, the line integral was equal to zero. The integral was initially devised for elastic materials, and Rice adapted it also to elastic –plastic cases.

For small scale yielding in elastic-plastic materials, such as where the yield zone near the tip is small in comparison with the un-notched specimen width , and having polar coordinates r, θ, Rice defined the stresses, $\sigma_{i,j}$ in the vicinity of the notch tip as having an inverse square root dependence on r, expressed as:

$$\sigma_{i,j} = \frac{K_I}{(2\pi r)^{1/2}} * f_{i,j}(\theta)$$

+ other terms which are bounded at the crack tip.

K_I is the stress intensity factor.

Rice deduced the J integral for this case as:

$$J = \frac{(1-\nu^2)}{E} * K_I^{\,2}$$ for small scale yielding, where :

K_I = The stress intensity factor.

ν = Poisson's ratio.

E = Young's modulus.

Given the use of notched specimens in slow strain testing reported later in this work, the J integral method is a further candidate method for defining conditions leading to cracking at the notch, where small scale yielding initially takes place. However, this is a

purely physical relationship, and would require additional parameters to be added to take into account any significant electro-chemical behaviour.

N J Petch[40] studied the relationship of fracture strength and yield strength to grain size. A fundamental relationship established was:

$$\sigma_c = \sigma_0 + K^* l^{-1/2}$$

where : σ_c = fracture strength

σ_0 = constant

K = constant

l = grain diameter

A linear regression relationship of fracture strength to grain size was established based on testing. The relationship was well supported by a regression plot. Petch[40] put forward an explanation of the process based on dislocation movement along glide planes, but where no dislocation movement across a grain boundary took place, this was equated to elastic movement conditions, which could be associated with a brittle fracture mode. The above equation was formulated to define the cleavage strength to grain size relationship for zero plastic deformation. Parkins[38] has further shown that finer grain size steels were more prone to inter-granular cracking in nitrate solutions. Where a hydrogen embrittlement mechanism is postulated, the Griffith relationship has again been invoked by certain authors. Petch and Stables[41] considered the Griffith equation and the observations of Orowan that gas adsorption would lead to a lowering of surface energy; this could then facilitate crack growth at reduced stress levels.

Petch and Stables[41] tested the rate dependency of hydrogen cracking by comparing tensile test results with tests using a falling weight test for sudden loading. Whereas the tensile test differentiated hydrogen charged from non charged material by reduction of area differences with lower values for brittle material, the falling weight test did not.

The proposal was based upon the concept of accumulation of molecular hydrogen adsorbed on to the new surfaces produced by a Griffith crack model. The proposal did not deal with the possible role of atomic hydrogen behaving as an interstitial element.

Other authors, R N Parkins et al[15], and Scott, Smart and Procter[16] have reported on loss of ductility of steels exposed to aqueous phosphate media at low anodic over-potentials and attributed this to the possible role of hydrogen.

Parkins[38] adapted the energy balance approach to fracture mechanics theory to take account of an electrochemical aspect entering into stress corrosion cracking as follows:

Surface energy change + the Plastic work done = Change in initial stored energy + Electrochemical energy released.

The plastic work term , P, encompassing the electrochemical energy is expressed as :

$$P = K_I^2(1-\nu^2) / E + (zF\rho\delta/M)\eta$$

Where:

K_I = the stress intensity factor.

ν = Poisson's ratio.

E = Young's modulus.

z = the valency of the ions in solution.

F = the Faraday.

ρ = the density of the alloy.

δ = the crack tip opening displacement.

M = the molecular mass of the metal.

η = the anodic over-potential.

The minimum value of K_I for stress corrosion cracking was stated as:

$$K_{Iscc} = ((E/1-\nu^2) (P - zF\rho\delta\eta/M) \text{ min})^{1/2}$$

As the material strength increases and the plastic work term P falls, and for a given over-potential , K_{Iscc} will then fall, so that susceptibility to scc will increase.

Parkins states that this relationship is appropriate to a dissolution model, but that an equivalent expression could be written for a hydrogen cracking mechanism.

1.15.2 Measurement of Internal Stresses in Metals

Internal stresses in can components will be generated both in the plate fabrication process by cold rolling, and later in the container manufacturing process by stamping e.g. of end components. Such stresses if leading to net tensile effects of sufficient magnitude on the component produced, can assist the occurrence of environmental stress cracking, perhaps even if there is no further stress added due to external factors. Jian Lu[42] et al defines three types of residual stress according to the range over which they are observed:

A: Macroscopic residual stress is that extending over several grains or more

B: Structural micro stress is that covering one grain part of a grain

C: Stress acting over several atomic distances within the grain.

In stamped end components, for example, it might well be expected that all three conditions may be present due to the large non uniformities in the effects of working e.g. at the countersink wall and around the radius of a stamped end where the through section effects may vary widely.

Dieter[43] stated that residual stresses were to be considered only as elastic stresses, since the maximum value which can be obtained is the elastic limit and above this it will relieve itself by plastic deformation until it falls to the yield stress.
One prominent measurement method for residual stress is the X ray method which is described as having the advantage of real time analysis of the stress, and that using a layer removal technique it is possible to obtain a depth profile of the stress.

The X ray Diffraction Principle.

A monochromatic X ray beam irradiating a solid material undergoes scatter by the atoms.
For a perfectly crystalline material a 3 dimensional lattice exists having defined inter-atomic spacing d. The X ray beams are diffracted by atoms and form a pattern which can be used to characterise the material.

The intensities of the scattered waves lead to a constructive interference when the following relationship, known as Bragg's law is satisfied:

$$n\lambda = 2d \sin \theta$$

where:

n is an integer

λ = the wavelength of the X ray beam.

d = the inter atomic spacing.

θ = the angle of incidence of the X ray beam.

The diffraction pattern of a polycrystalline material leads to a series of cones of diffracted rays being emitted, each corresponding to particular lattice planes.

These diffractions can be recorded, for example, on photographic film and the combination of characteristic spacings used to identify the material.

The Effect of Stress on The X ray Pattern

If the polycrystalline material is stress free, then for a given set of planes, the lattice spacing does not vary with the orientation of the planes. If the specimen is under the influence of elastic stress then the inter-planar spacing changes according to the orientation of the planes to the direction of stress. If a uni-axial tension is applied, then the planes normal to the direction of stressing will increase in inter-atomic distance and those parallel to the direction of stressing will reduce in spacing.

The elastic strain of the material can be estimated from the change in crystal lattice spacing measured by the position of the Bragg peak(s), as follows:

$$E = \frac{d-d_0}{d_0}$$

Where d_0 is the lattice spacing corresponding to a stress free specimen, and d is the strained lattice spacing.

A X ray method can therefore be used to determine elastic strain from shifts in the diffraction peaks. The diffraction peaks are the result of X rays being scattered by atoms in many grains, and the change in lattice spacing will depend on the uniformity of effect over the volume involved; the strain measured under these conditions will be macroscopic. The strain determined can be related to the stress from the stress strain relationship for the material for elastic conditions.

1.15.3 Material Forming Strains and Stresses : The Finite Element Method

A brief description only is given in this section. A much more detailed consideration together with 3 examples modelled relevant to this study is given in Section 3.

The Abaqus manual[44] describes the application of this method to the solution regarding material deformation models. The finite element analysis method is widely used in industrial sectors, but cross validation should be carried out in relation to model estimates. It is a method designed to give good approximations to true behaviour. In the case of metal forming for packaging, the method lends itself to relatively rapid estimates of behaviour of stamped components.

The geometry of the structure is broken down into discrete elements called finite elements, which are joined at node points. This elemental structure forms a mesh.

Deformation of the material may be defined as 2 dimensional e.g. plane stress, axi-symmetric e.g. for a round component such as a can end, or 3 dimensional forming for more complex cases.

The mechanical properties of the material must be defined, which for can plates means a true stress strain curve, Young's modulus and Poisson's ratio. If anisotropic effects are to be examined this must be repeated e.g. for tests parallel to the grain direction, at 90 degrees to the grain direction and at 45 degrees to the grain direction, and repeat models run , or a more complex version of a single model generated. Again the mechanical properties of the forming tools must be defined, but this is often simplified by the description 'analytical rigid'. All of the interactive conditions between the material and the forming components require to be defined, such as tool movement speeds and clearances, the types of interactive contacts between surfaces, and friction coefficients. When the structure is deformed, this is carried out in a sequence of model steps defining any multiple stages in the forming process, and within each steps, normally a multiplicity of small increments is required. In association with the material properties and fabrication conditions set up, the node points within the mesh are displaced and the FEA method calculates these movements, The strains and resulting stresses in each element are determined. The mesh may have a simple rectangular structure or a more complex form.

Two types of fundamental analysis are used in FEA modelling of material deformation processes, as follows:

The Implicit Method

In this form of model, the equilibrium equations linking loads, strains and stresses are solved simultaneously to obtain the displacements at all the nodes, at the end of each solution increment. The equations referred to are those which define the stiffness of the elemental structure. This method is suitable for modelling stresses and strains in slow strain rate test specimens.

The Explicit Method.

In this method the ideal solution increment time is based upon a stress wave speed in the material, which is linked to Young's modulus and the density of the material. **See Section 3.** The advantage is that the equilibrium equations linking loads strains and stresses do not require to be solved at the end of each increment, and this makes the model more adaptable to forming operations such as end stamping or deep drawing of a drawn redrawn container, than is the implicit method. In these types of model, local deformations such as at surfaces interactions with tools, may give rise to non linear effects such that the stiffness equations used in the implicit method are not in equilibrium and the model fails to function. Section 3 provides additional detail on the use and limitations of the explicit model related to the increment time and any resulting mass scaling effects.

1.15.4 Metallurgical Aspects: Effects of Steel Composition.

Parkins Slattery and Poulson[42] have described investigations into the effects of chemical composition on the stress corrosion cracking behaviour of ferritic steels. These authors also reviewed information from elsewhere in the literature. Much of the comment relates to environments involving boiling nitrate or caustic solutions, and concerns carbon steels in many cases not having the composition or state of working

representative for packaging, so that the observations may not be applicable to food packaging environments, or to cold reduced packaging steels. Comments relating to boiling caustic solutions have been omitted as these environments would not relate to processed food.

Food environments do, however, frequently contain low levels of nitrate e.g. 10-200ppm, but typically not exceeding around 50ppm in processed meat and fish products.

Further comments concerning steel composition below relate to the paper by Parkins et al[45], except as indicated.

Carbon: Relatively pure iron was stated not to have been caused to fail by SCC in boiling nitrate solutions; Flis had reported cracking in an iron whisker, but owing to the very small cross section this might have been due to pitting. Cracking became apparent in boiling nitrate solutions as carbon was introduced, but susceptibility passed through a maximum as the carbon content was increased. Parkins[45] quoted work by Long and Uhlig indicating very long failure times in nitrate solution tests when the carbon content fell below around 0.002 wt%. A value of carbon content in the order of 0.1% was quoted, above which greater resistance to cracking may be expected.
Carbon levels used in double reduced packaging steels at the present day are specified at 0.12% maximum and typical levels in double reduced packaging steels may be expected to be in the order of 0.05-0.07%.

Nitrogen. It is suggested as likely that nitrogen can act in a manner similar to carbon; both elements show interstitial behaviour as well as forming precipitates with iron. The

author[45] quoted work by Uhlig and Sava which showed that decarburised electrolytic iron was resistant to cracking, but became susceptible when 0.043% nitrogen was added.

This level of nitrogen was significantly in excess of that present in any packaging steels for light gauge metal cans which is either below 0.01% in nitrogen content for non nitrogenised steels, or if nitrogen has been added to enhance strength properties, a normal order of limits is 0.010-0.015%.

Pack test data which has been gathered from within the industry concerning nitrogenised steels does not support the case that nitrogen at the levels used in these steels is likely to have been influential. It should be noted that the type of cracking observed with meat and fish is typically trans-granular, whereas much comment on the behaviour of carbon and nitrogen e.g. by R N Parkins, relates to intergranular cracking studies involving nitrate environments.

Aluminium: Studies were reported mainly related to the use of Al as a de oxidant in steels. The evidence in terms of an effect on SCC was conflicting. While some data suggested a benefit to resistance to cracking from such additions, other work including a steel where half the heat was cast without Al addition and the other with 0.089% added, recorded no obvious improvement resulting from the Al addition.

The Al level in packaging steels for food cans is in the range 0.02-0.08%. Kim and Helwig[3] investigated cracking susceptibility in different steel types and concluded that neither aluminium killed nor non killed carbon steel nor whether continuous cast or ingot cast affected the cracking behaviour based upon slow strain tests in air using meat and fish products.

Titanium: A beneficial effect of titanium addition at 0.46% to very low carbon steel (0.016%C) in a nitrate environment was recorded.

Chromium: Chromium additions have been observed to have a beneficial effect on cracking in nitrate solutions, but whereas the chromium additions considered were in the range from 0.5% to 2% or above, the chromium level in a Packaging steel is typically under 0.03%, but 0.08% is permitted.

Nickel: Uhlig had studied cracking in nitrate solutions and found that maximum susceptibility occurred at about 2% nickel, whereas immunity was obtained at around 8% addition. Nickel is at a very low level in packaging steel of 0.08% maximum and typical levels are under 0.02%.

The broad indications from the survey were that Al, Ti , Cr, Mo and possibly Mn and V additions in sufficient amounts had a beneficial effect on cracking resistance. Carbon , nitrogen, Ni and Si additions give rise to maximum susceptibility at intermediate levels, and copper additions were deleterious. Most trends observed concerned tests in nitrate solutions.

In relation to copper especially, the findings concerning cracking in nitrate solutions may not be relevant to food packing involving sulphide environments where copper could be expected to react with sulphides. The work of J Haggman[46] relating to pitting studies in tinplates showed beneficial effects with copper at 0.08-0.12%.

Tests conducted by RN Parkins et al[45], concerned additions of : Al, Cr, Cu, Mo, Ni , Si and Ti added to low residual mild steel. The tests utilised tensile rods made by drawing followed by high temperature annealing at 950°C for 1 hour.

Regarding composition, phosphorus levels for practically all steels were above the maximum normally used for double reduced continuously cast packaging steels , normally 0.025%. Testing was by a combination of slow strain rate tests and constant load tests together with electrochemical measurements.

The author observed that the effect of the alloying elements varied with the environment as well as with the level of the element, but alloying additions were only concluded to be likely to improve cracking resistance if present in amounts in excess of 1% , and in some cases notably higher levels. Such additions have never been considered practical for packaging steels, which are produced to relatively high purity levels to ensure a combination of good mechanical performance, satisfactory corrosion resistance and economics. Chromium and Titanium consistently produced significant improvements in cracking response.

Hume Rothery[47] reported observations concerning grain boundaries in iron. These included a transmission electron microscope observation from work by McLean, of an iron 0.01% nitrogen alloy. Light bands on either side of the grain boundary indicated that these regions were thinner and had dissolved more rapidly during electrolytic polishing.

Hume Rothery suggested that this observation supported the notion that the grain boundary had a different chemical composition from the grain interiors and as no precipitation was revealed, it was evidence for adsorption of nitrogen at grain boundaries.

Hume Rothery[47] also discussed the inter-metallic chemistry of iron and the lattice distortions which result from the addition of alternative transition elements. He stated that there were uncertainties at low concentrations, but that the general effect was for

lattice expansion at constant atomic percentage of solute to increase in the order Mn<Cr<V<Ti and Co<Ni<Cu.

These observations may be considered alongside the susceptibility information reported by Parkins, Slattery and Poulson[45]. These authors reported that Cr and Ti were elements that consistently produced improvements in cracking response of ferritic steels, a large number of which were carbon steels. It was commented that Mn was not varied sufficiently to reach a conclusion on effect. In nitrate solutions it was concluded that alloying additions which altered susceptibility did not do so until present in amounts exceeding around 0.75%, and copper additions were detrimental. Based upon this comparison there does not seem to be a high consistency between the relative order of lattice expansion resulting from alloying additions commented on by Hume Rothery[47], and the beneficial effect of certain alloying additions to resistance to stress corrosion cracking commented on by Parkins et al[45].

Harada , Kochizuku and Ban[48] studied the effects of surface enriched elements on killed steel, and examined performance using special property measurements in addition to characterisation by spectroscopy methods such as EPMA. They concluded that during the annealing of low carbon steels for tinplate manufacture, the elements such as silicon, manganese and chromium segregate to the steel surface and that oxides are formed both at the grain boundaries and at the free grain surface. The oxides were concluded not to be removed by pickling before electro plating, and adversely affected the iron solution value property test for the materials.

1.15.5 Stacking Fault Energy and Chemical Composition of Steels

Within a metal lattice structure a dislocation can separate into a pair of partial dislocations, associated with a reduction of strain energy. The energy of the dislocation

is proportional to the square of the burgers vector and the total energy is reduced for the partial dislocations, between which a repulsive force exists. Discontinuities then arise in the stacking order of atoms which are called stacking faults, with the atoms at either end of the fault not being in normal lattice positions and giving rise to a finite surface energy.

The separation between the partial dislocations is an equilibrium between the repulsive energy of the dislocations and the surface energy of the stacking fault. Swann[49] examined the relationship of stacking fault energy to stress corrosion cracking behaviour of a number of single phase alloys, but the only body centred cubic metal tested was beta brass and relatively little information on this was presented. However, much information of the fcc and hexagonal metal alloys was presented which revealed the following:

a) Increased resistance to scc related to a dislocation structure having a cellular form associated with high stacking fault energy.

b) More susceptible conditions were associated with planar dislocation distributions where the stacking fault energy was lower and cross slip would tend not to occur.

c) Carbon steel was not investigated but in examining austenitic stainless steel, nitrogen was found to promote planar dislocations in an FCC structure, but the effects on performance were concluded to be overridden by heavy deformation and high stress.

The nitrogen test levels were at 0.04% and 0.12% well above that in packaging steels. Phosphorus was also deleterious, evaluated at 0.3%, again far higher than in food packaging steels where it is limited to 0.02% maximum. It was deduced that while

phosphorus and nitrogen promoted planar dislocation structures this was not by way of lowering of stacking fault energy.

1.15.6 Metallurgical Aspects : Hydrogen Cracking and The Troiano Theory

Troiano[50] describes a theory of hydrogen cracking related to its behaviour as an interstitial element. The failure may be termed delayed failure embrittlement or slow strain embrittlement. Such failure typically affects high strength steels e.g. martensitic types. The process commences with an incubation period during which the atomic hydrogen which has been generated in the metal diffuses under the influence of an activity gradient created by tensile stress, to a highly stressed region. This diffusion is explained by the following effects :

i) Tensile stress application will multiply dislocations, and these will concentrate at sites such as grain boundaries, and at sites of stress concentration such as notch regions.

ii) This effect will increase vacancies in these locations creating an activity gradient, causing interstitial atoms to move into the vacancies to reduce free energy.

Governing equations for this diffusion are given as :

$$V = \frac{D}{kT} * F$$

Terms are not fully listed but were interpreted as:

V= Velocity of the interstitial

D= Diffusion coefficient

F= Strain gradient

k= Constant

T= Absolute temperature

and

$$D = A\, e^{-Q/RT}$$

Where

D = Diffusion coefficient

A = constant

Q = Activation energy for diffusion

R = Gas constant

T = absolute temperature

The above stage is followed by crack initiation, slow crack propagation, and finally catastrophic failure. The fracture surface typically revealed distinctions between embrittled conditions near the surface and final tensile effects. The examples shown of embrittled zones appeared to be up to e.g. about 20% of the specimen radius in depth. Supporting data included tests at –321°F, where the hydrogen diffusion rate is effectively nil, resistivity measurements which identified discontinuous crack growth, and current density measurements to indicate proportionate levels of hydrogen uptake required to effect the failure mode based on reduction of area.

Using the above supporting data, the case was developed that crack propagation was a discontinuous process, requiring a critical concentration of hydrogen to be developed, ahead of the crack tip, involving an interaction energy based upon a Boltzmann distribution function, according to:

$$C = C_o e^{-U/kT}$$

Where:

C = Interstitial hydrogen concentration

C_0 = Average interstitial concentration

U = Interaction energy between the interstitial and the stress field

k = Boltzmann's constant

T = Absolute temperature

The interaction energy is expressed as:

$$U = P \Delta V$$

Where :

$$P = -1/3 (\sigma_{xx} + \sigma_{yy} + \sigma_{zz})$$

ΔV = the change in volume produced in the lattice by the interstitial element.

P = the average hydrostatic stress but not explained fully, the interpretation made here being that the hydrostatic component arises due to the forces necessary to counteract lattice strains generated by the interstitial hydrogen.

Taking into account a stress concentration factor for a notch (K_f), it was deduced that the product of the applied stress (σ_a) and the stress concentration factor is constant at the maximum interaction energy U:

$$\sigma_a * K_f = \text{constant}$$

It is then taken into account that the yield stress will be the limiting parameter in brittle fracture, and that any finite plastic deformation will lower the stress concentration factor, K_f. Thus, as the material strength increases and plastic strain (ductility) reduces, K_f increases and hence the applied stress to achieve the interaction energy for critical hydrogen concentration falls. It was reported that this was consistent with practical observations involving materials.

Troiano[50] suggested that the ultimate failure mechanism may involve entry of electrons from the hydrogen atoms into the d electron states of the iron, so increasing repulsive forces in the lattice, and enabling de-cohesion failure.

Cases of similar failure involving FCC alloys such as nickel based materials were discussed, and further arguments developed that adding elements of lower atomic number may can lower susceptibility by enlarging the unfilled d electron states the alloy.

This paper was thought well supported by experimental data, although the ultimate mechanism suggested may be beyond existing technology to prove. There was some uncertainty remaining regarding the link between electrical current data and hydrogen adsorbed, which was not explained.

1.15.7 Surface Energy Theory , Coleman et al; Stroh and Petch.

Coleman Weintein and Rostocker[51] described a surface energy related model for cracking initially in the context of liquid metal embrittlement, and had noted that Petch had proposed that hydrogen embrittlement arose from adsorption of hydrogen on to dislocations formed at crack nuclei, causing reduction of surface energy and permitting cracks to propagate at stresses lower than normal. Cases of mild steel exposed to molten lithium, and brass with liquid mercury were tested[51] against the Stroh-Petch relationship and this was found to be followed. The reduction in surface energy in each case was found to be over 50%. The mechanism considered is often termed the 'Stress-Sorption Cracking' Theory.

When the method was applied to a stainless steel and a Magnesium – Al alloy in aqueous media, the brittle cracking observed was only of limited depth up to 0.7mm on 0.25inch diameter samples the region beyond this being ductile i.e. quite similar effects to those observed by Troiano[50].

The findings of Coleman et al[51] did not eliminate electrochemical functions from the cracking process. The authors also stated that a dislocation and surface energy model could not yet be applied to delayed failure embrittlement because the function of time in dislocation assemblies had not been treated sufficiently. However, the function of time has been discussed by Troiano[50], to explain diffusion, stress gradient and temperature effects involving the behaviour of hydrogen.

Stroh[52] had put forward mechanism for purely physical crack formation under plastic flow conditions, in which a piled up group of dislocations could generate a crack, from short range non elastic interactions. Stroh also proposed that a crack could be initiated by a smaller number of dislocations in each of several slip planes. The mechanism is described on the basis that a crack arises from the interaction of a few dislocations in a

pile up, the remainder producing the stress concentration to force the interaction of a few. If this mechanism is true for purely physical fracture under plastic flow conditions, then in the context of environmental stress cracking involving hydrogen embrittement of materials normally displaying measurable ductility, the local difference in behaviour between the initiation region at a surface and the more ductile failure some distance away requires to be accounted for. Troiano has put forward an explanation for this behaviour supported by test evidence for high strength metal alloys, but it could be suggested that the mechanism for crack initiation may include behaviour proposed by Stroh, assuming that some finite ductility still exists, or an alternative decohesion mechanism, one of which was suggested by Troiano.

1.16 Electro Chemical Aspects

1.16.1 Electro Chemical Theory: E.H. Dix

Dix [53] had discussed many aspects of the stress corrosion cracking phenomena in an earlier paper on the subject, and this paper was almost exclusively concerned with inter-granular cracking. However, it was also acknowledged that in some cases of inter-granular cracking involving cold worked materials, cracks may also follow the slip planes which can be sites for precipitation. A fundamental observation concerned potential differences detected in non ferrous alloys between the grain and grain boundary regions. This work was carried out by preparing separate samples of the same alloy by masking grains and grain boundaries with enamel following which comparative potentials were measured. These included an aluminium copper alloy in which the grains were cathodic to the grain boundaries on account of precipitation of $CuAl_2$. This would lead to grain boundary zones denuded of copper. By contrast, an Aluminium-10% Magnesium alloy was found to show anodic behaviour of the beta phase Mg_5Al_8 particles precipitated at the grain boundaries.

As compared with these cases, Al –Mg alloys containing Mg_2Si did not show similar galvanic effects, and a corresponding observation was made regarding Al Mn alloys.

Discussion also included of the case of a nickel chrome stainless steel, where chromium carbide can be precipitated at the grain boundaries leading to susceptibility to inter-granular attack and a parallel case was made that the grain boundaries would be anodic.

Dix's case for an electrochemical mechanism involving selective corrosion along continuous paths resulting from galvanic action involving secondary phases, can be supported for a number of such cases which have been practically demonstrated. However, it did not account well enough for the specific nature of SCC.

1.16.2 Cracking of Carbon Steels by Nitrate : Henthorne and Parkins

M. Henthorne and R.N. Parkins[14] investigated the stress corrosion behaviour of annealed mild steels produced to a range of grain sizes in nitrate solutions using two alternative carbon steels having 0.08 and 0.3% carbon respectively. The yield stress, 5% or 10% flow stress and stress corrosion fracture stresses were determined and followed the Petch relationship for brittle fracture as a function of grain size. Parkins also calculated the surface energy values, and these indicated a reduction for both steel types, but in the case of a spherodised structure for the pearlitic steel, a negative value of k and hence a negative surface energy would result.

Parkins deduced a mechanism based on elemental carbon as well as carbides showing cathodic behaviour at the grain boundaries.

1.16.3 Electrochemical Aspects : Cracking Studies in Phosphate Solutions.

Parkins , Holroyd and Fessler[15] carried out studies on carbon manganese steels initially using the method of fast and slow polarisation sweeps to identify stress corrosion

potentials and slow strain rate test to perform susceptibility tests. A similar approach was indicated as having been used in tests using nitrate solutions. The behaviour in the fast sweep was expected to be such that the speed of the sweep was too rapid to allow passive films to form. Trans-granular cracking of the steels prepared either from 1N $Na_3 PO_4$ or 1N Na_2HPO_4 and acidified to the pH range 3-7 was observed. The domain of cracking was stated as probably associated with the formation of mixed iron oxide /phosphate films with SCC ceasing where only Fe_2O_3 films were produced.

Stress Corrosion behaviour and re-passivation kinetics involving phosphate solutions, were also studied by Smart Scott and Procter[16]. These authors reproduced cracking including that with fan shaped forms, and low ductility contours having small steps. In this work it was observed that fast and slow sweeps were not considered a good prediction method for conditions giving rise to SCC. Comment made was that with phosphate media the cracking could occur in the active loop and de-aeration was stated to stifle cracking, but this was further qualified by the term active de-aeration. Static de-aeration was described as giving rise to more potency than de-aeration under stirred conditions.

A potential step and current decay method was considered more effective than fast and slow sweep tests in identifying electro-chemical conditions associated with cracking.

1.16.4 Electrochemical Aspects: Localised Corrosion and Pitting.

M Pourbaix[54] explained the localised corrosion chemistry associated with the development of pits which are commonly observed as a precursor to many cases of stress corrosion cracking. The basic corrosion reactions involving iron were explained as follows:

Anodic dissolution:

$$Fe = Fe^{2+} + 2e^{-}$$

Cathodic reduction : neutral solutions

$$½\ O_2 + 2H^{+} + 2e^{-} = H_20$$

Cathodic reduction under more acidic conditions;

$$2H^{+} + 2e^{-} = H_2$$

If the volume of solution in a cavity was small, the solution could become saturated and oxides or hydroxides may be precipitated through reactions which cause acidification, such as:

$$Fe^{3+} + 3H_2O = Fe_2O_3 + 6H+ + 3e^{-}$$

$$3Fe^{2+} + 4H_20 = Fe_3O_4 + 8H^{+} + 2e^{-}$$

Pourbaix indicated that important factors concerning acidification included the separation of preferred sites for oxidation and reduction reactions. If dissolved oxygen or other oxidants were present and preferred sites for oxidation and reduction existed, acidification was said not to occur unless negative ions such as chloride or sulphate are present in cavities to balance the positive charges created by metal dissolution.

The simultaneous presence of an oxidant combined with negative ions other than OH^- such as Cl^-, SO_4^{2-} or NO_3^- was said to be necessary to promote localised attack and accompanying acidification.

1.16.5 Electrochemical Aspects: Further Observations: J.C. Scully

JC Scully[55] reviewed some elements of behaviour likely to be influential in determining the tendency for cracking to occur. This predominantly concerned passive alloy cases such as stainless steels and titanium alloys and the emergent slip step concept related to trans-granular cracking. Key points included the following:

i) Stringent conditions were likely related to the specificity of effect involving anion types.

ii) Re-passivation rates would be critical to prevention of crack progression, and these would require a critical current density, the value of which can depend on the speed of determination of the polarisation curve, environment and direction of sweep.

iii) At a certain potential level above the Flade potential, a sufficient current will be reached for effective passivity. Relating these effects to the situation in a stress corrosion crack, a potential drop will exist down the crack resulting from factors such as resistance polarisation, differential aeration and concentration changes in the environment. This drop would relate to the difference between the Flade potential and that at a higher potential region where stable passivation existed.

iv) As the strength of the aggressive anion is raised towards the minimum to cause trans-granular stress corrosion cracking, it is likely that there will be a transition from shallow to deep pitting to fissures and finally branching cracks.

This paper was predominantly a theoretical treatment of the subject area, requiring more experimental follow up to translate the ideas into outputs of practical use.

1.17 Factors Affecting Crack Growth Kinetics: Parkins

This subject area was explored in a wide ranging treatment by Parkins[56], which took into account fluctuating stresses, protective film rupture/ repair effects, crack tip strain rates, multiple cracks and coalescence, and current decay behaviour. Testing was in carbonate bicarbonate solutions. Important points included the following:

i) Predicting real effects and timescales required consideration that the stresses in common situations will fluctuate but will be rather less severe than many lab test conditions involving high stresses and strain rates rapidly exceeding $K_{Iscc.}$

ii) For a single crack model with fluctuating stress, crack tip strain rates were found to equate to experimental observations reasonably using the formula below:

$$\dot{\delta}_{AV} = \frac{1}{2T} * \frac{(\Delta K)^2}{G \times \sigma_y}$$

where:

$\dot{\delta}_{AV}$ = Average crack tip strain rate

T = Loading time

ΔK = Stress intensity factor range

G = Shear modulus

σ_y = yield stress

A formula was also given for the multiple crack case taking into account number of cracks generated and the applied strain rate. This would be difficult to apply where the number of cracks is uncertain or cannot be established reasonably. Consideration of current decay lead to the observation that the slope of the current decay curve was less important than the maximum current passed by a bare surface.

It was further noted that integration of current transients over time provided a relevant anodic charge density reflecting the discontinuous nature of crack propagation.

This lead to the following formula related to the electrochemical function.

$$\frac{da}{dt} = \frac{Q_f}{E_f} * \dot{E}_{CT} * \frac{M}{zFd}$$

where

a = crack length

t = time

Q_f = charge density passed

E_f = strain for fracture

$\dot{E}_{CT}$ = crack tip strain rate

M = atomic weight of the metal

z = valency of the metal

F = the Faraday

d = the Specimen diameter

Parkins emphasised the importance of taking into account the number of cracks, and that some may cease to propagate, with new ones may be generated over time, and that coalescence can occur. Shallow cracks in pipeline steels were noted to be relatively long.

The work concluded with a complex formula in stages related to a pipeline case.

The current aspects are potentially capable of measurement in this study, but there is little knowledge at the present time of numbers of cracks in testing, and this would require significant work, unless the condition can be limited perhaps by notching, and then used for the development of a model.

1.18 Corrosion Fatigue.

Corrosion fatigue defines the failure of a metallic material under the simultaneous action of corrosion and fluctuating or cyclic stresses. This results in failure below that which occurs under constant load. It may have relevance to food cans and steels used mainly in circumstances of transport where cyclic stresses are likely to occur, for example in stacks, which may lead to the generation of fatigue effects on body beads or at sites such as rim dents on 2 piece cans, these dents being generated by offset loading. Another possibility is that the fluctuating load triggers an onset of another form of environmental stress cracking through breakdown of the protective system e.g. at a weakened site.

Wang[57] describes 4 stages of the corrosion fatigue process as follows:

i) Pre-crack cyclic deformations causing mechanical damage such as local intrusions or extrusions of the metal.

ii) Crack initiations and stage 1 growth. The cracks initiate and grow on planes of high shear stress.

iii) Stage II crack propagation. Well defined cracks propagate on planes of high tensile stress in directions normal to the maximum tensile stress.

iv) Ductile crack growth leading to failure.

Corrosion fatigue is not material and environment specific in the manner of stress corrosion cracking. Two main mechanisms have been cited by Wang:

a) Anodic Slip Dissolution: The active corrodent diffuses to the crack tip, where corrosion takes place following rupture of surface films, or extension of the crack or following fretting contact of the faces.

b) Hydrogen Embrittlement during Corrosion Fatigue.

In this case the mechanisms will be similar to those considered in earlier sections, namely hydrogen is generated at the crack region through development of a pit or crevice leading to acidic conditions. The hydrogen ions are then considered to be reduced to the atomic form in the presence of a catalytic poison and can be adsorbed into the metal and concentrate at stressed regions, leading to embrittlement.
Wang discusses the role of inclusions. In the case of sulphide inclusions, local acidification at pits enhances the dissolution of sulphides and accumulation of HS^- ions which can act as catalytic poisons. The sulphide inclusions can contribute to pits and sites for crack initiations and calcium aluminates are responsible for fatigue crack initiation in air, but were not found to affect corrosion fatigue in high strength steels

1.18.1 Corrosion Fatigue: Testing and Fracture Mechanics Aspects

Testing methods typically involve the generation of S-N curves meaning S- stress and N number of cycles to failure. Tests may be performed in air and in the corrosive environment to show any lowering of fatigue performance on account of the corrosion effect.

P.M. Scott[58] described the fracture mechanics aspects by which the crack growth rate per cycle of the test was expressed as a function of the cyclic crack tip stress intensity value ΔK by the equation:

$$da/dn = c\,(\Delta K)^m$$

where:

c and m are constants.

da/dn is the crack growth per cycle.

$\Delta K = K_{max} - K_{min}$

where

$$K_{max} = \sigma_{max} \sqrt{\pi a}$$

and $$K_{min} = \sigma_{min} \sqrt{\pi a}$$

ΔK has units of MPa $\sqrt{m}$

These formulae can be used to generate plots of crack growth rate as a function of Delta K so that prediction of conditions for high crack growth rates and alternative safe conditions can be made.

1.19 Stress Corrosion Spectrum

R.N. Parkins[59] in a review of stress corrosion considered that localised corrosion may be distributed in a number of ways to promote stress corrosion cracking and that changes from a pre existing path mechanism to a strain generated mechanism may be possible resulting from either physical conditions, a metallurgical change in the state of the alloy, or a change in the environment. The subject had not been rationalised to a single mechanism, the logic being that several mechanisms may be operative.

1.20 Discussion of Potential Contributory Conditions to Environmental Stress Cracking in Meat and Fish Cans.

1.20.1 Chemical Species in Meat and Fish.

From the literature review, a number of species exist in meat and fish packs which it is known may cause or accelerate environmental stress cracking of carbon steel, as follows:

Anions: phosphate[15,16], low amounts of nitrates[14] and HS- ions [21,23] in solution from hydrogen sulphide, which literature reports as leading to one or other form of environmental stress cracking.

Promoters of hydrogen ingress into steel other than hydrogen sulphide: e.g. Selenium and Phosphorus [33].

Other substances reported as Accelerators of hydrogen cracking modes: CO_2, chloride anions and ammonium cations[23].

Other volatile organic sulphides from processing (either insoluble or of low solubility in aqueous media), about which there is uncertainty concerning the effects e.g. thiophenes, alkyl sulphides, and mercaptans. These are polar compounds, but would require to act in a heterogeneous fashion to contribute to hydrogen ingress into steel due to lack of solubility.

Regarding carbonate/bicarbonate anions, these are promoters of environmental stress cracking effects in carbon steels in aqueous media within a pH range[12] from slightly below 7.0 to around 10.0, and over a restricted potential range. This appears not to be applicable to meat or fish packs, which typically have a bulk pH close to 6.0, or slightly below in the case of acidified products. For these anions to be active, local increases in pH towards 7.0 or above would be required, such as by cathodic reactions. As the environment within a pit leads to local reduction of pH[54] in aqueous salt containing media, and cathodic species external to a pit can more readily undergo diffusion to or from the bulk, it is improbable that local pH would rise such that any carbonate/ bicarbonate media present would be sufficiently active to promote stress corrosion effects.

Nitrate anion levels in meat and fish packs were typically below 100ppm in cases examined by the author, see section 1.6, and cracking effects with this anion are commonly inter-granular[14]. However, Parkins et al [38] have reported evidence of trans-granular cracking in a carbon steel in nitrate solution at the free corrosion potential.

Phosphate media have been associated with two alternative failure conditions in carbon steel, namely:

a) Stress corrosion cracking under anodic conditions[15] at over-potentials leading to active/ passive states of the electrode determined from dc polarisation curves.

b) Loss of ductility[15,16] or hydrogen induced cracking at low anodic over-Potentials under active conditions.

No evidence was found to indicate a likelihood of anodic active /passive conditions during initial dc polarisation tests on Tuna Brine in this study (See Section 2), but the

further tests under acidified conditions to reflect what can exist within a pit may be beneficial, given also the findings of Parkins[15] related to pH effect with phosphate solutions.

Evans[33] indicated that catalytic poisons occupy sites where reactions involving other adsorbed atoms e.g. hydrogen would occur, such as in an activated complex process. The adsorbed catalytic poisons thus impede the ability of hydrogen to recombine at the metal surface. Hydrogen sulphide, which liberates HS^- ions in solution, was indicated by Evans[33] to be a catalytic hydrogen recombination poison and Evans also stated that selenium and phosphorus can act in this way.

In meat processing a principle source of hydrogen sulphide was deduced to be via the breakdown of cystine or cysteine[25,7], but the mechanism appears not to have been conclusively established. Hydrolysis has been proposed [25] and Schutte[7] has discussed an alternative degradation process, as well as reactions of cysteine and thiamine with sugars.

Furthermore, it is understood that some products such as tuna may be precooked and frozen before transit for canning elsewhere, while some may be processed 'raw'.

RB Hughes[60] carried out studies on volatiles from herring. This work showed that among three sulphur compounds identified: hydrogen sulphide, methyl mercaptan and di-methyl sulphide, on heating up to 75°C , hydrogen sulphide production was greatest during the first 30 minutes of cooking, then dropped off and ceased completely after 45 minutes. Methyl mercaptan showed similar behaviour, and di-methyl sulphide was evolved mostly after between 30 and 45 minutes, then reduced. Thus the potency of the media could be affected by any pre-processing history.

1.20.2 Chemisorption Behaviour: Selenium and Sulphur Compounds

Organic molecules having reactive functional groups are considered capable of chemi-sorption on to metal surfaces. One theory is that the chemi-sorption involves formation of coordinate bonds with the metal by donation of electron pairs. Sastri[61] quoted inhibition efficiency for molecules containing different donor atoms to have relative effectiveness Se > S > N > O. Selenium was present at a very low levels generally in the foods considered. Electro-static adsorption of inhibiting species can also take place on account of polar characteristics of the reactive functional species within a molecular type, but dependent also on the existence of an opposite charge between the metal surface and the atomic species in the molecule. Sastri[61] indicated that electrostatic adsorption is a weaker effect than chemi-sorption.

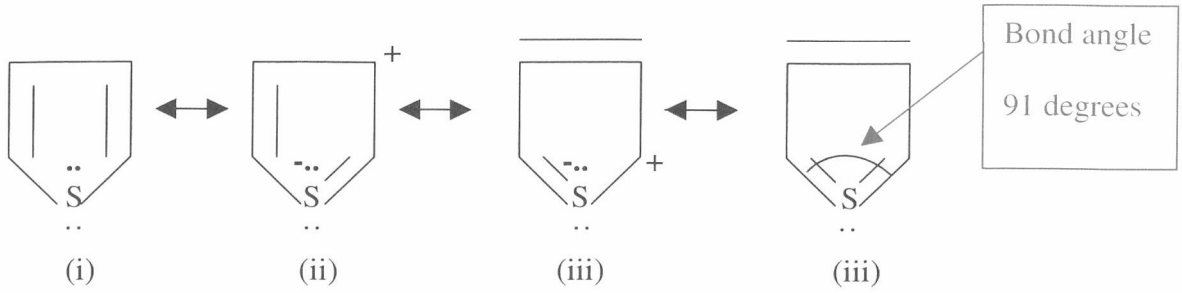
Within the element series listed above, the atomic volumes run in order from largest to smallest following the same sequence above, selenium to oxygen , but with limited differences. The ionisation energies show nitrogen highest with both nitrogen and oxygen above sulphur and selenium, with selenium lowest. Finally electro negativities showed that nitrogen was greatest with oxygen second and selenium least. These observations are consistent with the most favourable conditions for chemi-sorption existing for the order cited, selenium followed by sulphur and these elements will be expected to donate electrons to a metal surface more readily than nitrogen or oxygen. A larger atomic volume having less electro negativity will allow more ready electron donation to a metal surface, and also be consistent with lower ionisation energy.

From this reasoning it can be considered that hetero-cyclic molecules containing sulphur, such as thiophenes, and also furan derivatives would be expected to show some chemisorption behaviour of sulphur and oxygen respectively on to the surface of steel. The dipole moment is weakened in a hetero cyclic molecule when the resonance effect

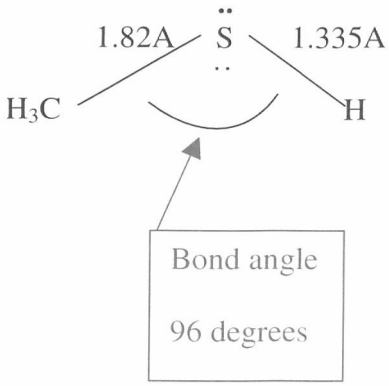
in the molecule leads to delocalisation of one pair of unbonded electrons e.g. for oxygen or sulphur.

The structures of thiophene, methyl mercaptan and dimethyl sulphide are shown below. The angular molecular structure involving sulphur on the latter two compounds results from repulsive forces created by the two un-bonded electron pairs, and the same effect would be expected to be influential in determining the bond angle at the sulphur atom of thiophene.

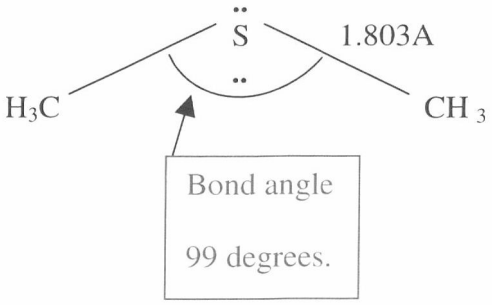
A) Resonance Structure of Thiophene (taken from Finar [62])



B) Structure of Methane Thiol (according to G Marc Loudon[63])



C) Structure of Di-Methyl Sulphide (according to G Marc Loudon[63])



Each of the above molecules can be expected to give rise to adsorption effects due to a combination of dipole moments and chemi-sorption involving the sulphur atom.

In the case of thiophene, resonance structures (ii) and (iii) are expected to give rise to enhanced negative charges favouring electrostatic adsorption effects at potentials more positive than the zero charge potential. Loudon[63] explains the structures of CH_3SH and

CH_3CH_3S based upon the ability of sulphur to accommodate unshared electron pairs in the 3d orbital, which takes up more space than for oxygen , where electrons are in quantum levels 1 and 2. This results in greater repulsive force from the un-bonded electron pairs, which decreases the bond angle for sulphur relative to similar structures involving oxygen. Similar comment is made by Finar[62] regarding the structure of thiophene.

Dipole moments were highest for methane thiol (1.52) and dimethyl sulphide (1.50) relative to thiophene (0.55). The higher dipole moment will signify a stronger electrostatic effect.Thiols and sulphides were quoted by Thomas [6] as inhibitors for acid solutions related to their adsorption characteristics, but the species shown above were not listed as soluble in water by Weast. [65]

Testing of these substances would be required to determine their behaviour as possible catalytic poisons in a hydrogen cracking context, due to the combination of their chemistry and adsorption characteristics. Other sulphides may also need to be considered.

1.20.3 Fats , Sugars and Vitamins.

Fats:

Regarding the fat content of the foods considered, Schutte[7] records that fat can bind H_2S if aldehydes are present, and may thus reduce its aqueous activity as a hydrogen recombination poison. Fat content was one significant difference between tuna (low fat) which does promote environmental stress cracking behaviour, and salmon which does not have a documented history of this type of failure occurrence in steel cans.

Sugars:

For sugars, either no compositional data were available for the foods considered, or no sugar levels could be measured, and these might have been affected by processing reactions. The reaction of proteins with sugars is called the maillard reaction and the products of the reaction are a route by which hydrogen sulphide can be produced. Sugar is included in certain laboratory formulations for the packing of fish which may be to balance flavour, and if this is also the case for commercial practice then a further route to hydrogen sulphide production can exist.

Vitamins:

Vitamin contents can also have been reduced by heat processing. Vitamins divide into fat soluble and water soluble types, and some amongst each contain the OH grouping(s). Among the fat soluble types, vitamin A has an alcohol group and vitamin D a phenol group. Among the water soluble types, Vitamin C, Vitamin B1, Vitamin B2 and B6 have alcohol groupings.

Certain alcohols are known to be capable of promoting SCC effects [35], but this is reported as involving very low water presence, combined with some organic acid and chloride anions. For meat and fish, while the latter two conditions exist, water presence is very high. Based upon these observations, an scc effect due to alcohol is not a foremost prediction, especially as some vitamins are fat soluble rather than water miscible.

Niacin is an organic acid, and possible effects due to pH reduction may assist a hydrogen related cracking mechanism.

Regarding other features of the vitamins, thiamine can release hydrogen sulphide on heating, and ascorbic acid is a reducing agent with capability to reduce iron in food from Fe^{3+} to Fe^{2+}, with potential to then assist release of hydrogen from H_2S [23].

1.20.4 Synergistic Effects

Several species have been identified which can promote forms of environmental stress Cracking in carbon steel. If one is at a reduced level e.g. through any pre-cooking losses of volatile sulphides from tuna, the risk may be less. Elboujdaini[23] quotes a pH level of 5.8 for plain carbon steel, below which hydrogen evolution may be sufficient for an embrittlement effect.

Whereas tuna brine has a pH around 5.9, salmon product measured had pH around 6.3-6.4. It is established knowledge that due to effects such as hydrolysis of metal cations and diffusion of halide anions into pits, pH in pits reduces, but the drop will require to be larger for a hydrogen cracking risk with salmon. The pH effect is likely to be important related to those product types having acid sauces added. As fat can reduce activity of H_2S by a binding action in certain circumstances, the risk of hydrogen cracking may then be reduced. Sugar if added to a formulation would facilitate a mechanism for the generation of volatile sulphides[7,66].

CO_2 [19] has been found to be a promoter of SCC under significant pressures and exposure times and in conjunction with other constituents, and is not an obvious candidate for promoting longer term can failures under vacuum. To establish an effect of NH^{4+} ions will require further study related to food environments.To enumerate the effect of species systematically, an experiment is required involving additions initially of the more prominent candidates based on established knowledge and using a protein base of high purity.

1.20.5 Failure Mechanisms and Metallurgical Aspects.

1.20.5.1 Delayed Failure Embrittlement of High Strength Steel: A.R. Troiano[50]

Troiano showed that embrittlement of high strength steel occurred when specimens were charged with hydrogen. Embrittlement conditions were displayed at surface regions, but not throughout the sample sections. Evans[33] stated that "There is little doubt that hydrogen passes through iron as atoms, and that molecular hydrogen cannot pass through unless definite pores are present". The mechanism explained for embrittlement by Troiano fundamentally depended on the generation of an activation energy, U, for hydrogen diffusion by local stress build up at sites such as at notches. The diffusion process requires an activity gradient generated by a non uniform stress state, and this process has temperature, concentration and time (diffusion coefficient) dependencies. De-cohesion is then postulated on a basis of repulsive forces due to entry of electrons from hydrogen atoms into unfilled d states of iron. A limitation of the theory was the indirect quantitative information for hydrogen, based upon electric current data.

1.20.5.2 Surface Energy Theory: Coleman , Weinstein and Rostoker [51].

The theory put forward by these authors concerned a lowering of surface energy such as by hydrogen adsorption, but the cracks reported in materials tests stainless steel and Mg-Al alloy) in aqueous media, for example, were only partly brittle, and the remaining tensile fracture behaviour based on lowering of surface energy was not fully explained. The Troiano model appears more substantive, and adsorption, diffusion and

cracking behaviour associated with local build up of atomic hydrogen would be consistent with lowering of surface energy through lattice de-cohesion.

1.20.5.3 Brittle Fracture Studies: N J Petch [40]

The Petch relationship related studies of brittle fracture of iron and carbon steel at liquid nitrogen temperatures to grain size, and the related theory involving dislocation build up at grain boundaries, has been extended to consideration of embrittlement caused by hydrogen [38]. However, this model appears to be an incomplete description of what takes place where environmental stress cracking or delayed failure embrittlement promoted by hydrogen occurs.

An energy balance approach including the electrochemical energy release is likely to be a more complete description of the process.

1.20.5.4 Energy Balance Approach: West.

Parkins summarised this approach from work by West[67] deriving an expression for electrochemical energy released in joules per mole starting from the expression

$$\Delta G = -zFE \quad \text{Joules/mole} \qquad (\text{Joules} = \text{coulombs} \times \text{volts})$$

where F is the Faraday, z is the valency and E is the electrochemical potential, to convert moles of energy to volume of metal released by dissolution requires the expression below:

$$\Delta G = - (z F \rho \delta .da /M) \eta$$

Where

ρ is density of the metal

δ the crack tip opening displacement

da increase of surface area

M is the molecular mass

η is the electro- chemical over potential

This expression describes the energy change associated with the number of moles of metal which have been liberated by anodic dissolution by electrochemical energy at the anodic over-potential η. In order to generate hydrogen for an embrittlement effect, anodic dissolution must take place to provide electrons required to reduce hydrogen ions to atomic hydrogen.

West[67] proposed that in the case of hydrogen embitterment, the surface energy will be zero or negative and that the plastic work term expressed here as P, will be reduced, deducing the equation:

$$K_{Iscc} = ((E/1- \nu^2) (P - z F \rho \delta \eta /M)_{min})^{1/2}$$

where the terms are as defined earlier, except that in this equation E is Young's modulus.

1.20.5.5 Notched samples and plastic work term : J Integral. Rice

In order to estimate the plastic work term for a geometry, such as in the case of a notched sample in a slow strain rate test, an estimate of the strain behaviour in the notch

region is required by measurement and/or modelling. Rice's application of the J integral [39] is a method which can be applied to local strains at notch areas. The cases covered did not match the geometry of a 90 degree v notch which has been used in this study.

However, Herzberg[68] explains an iterative procedure by which this may be done involving crack measurements on specimens loaded to different displacements, and determining the associated area under the load displacement curve, utilising ASTM standard E813-89, the basic equation being:

$$J = J_{elastic} + J_{plastic}$$

$$J = \frac{K_I^2 \times (1 - \nu^2)}{E} + J_{plastic}$$

where the terms are as previously described. The units of J are then Kn/m which equate to work units when the area parameter of stress is included.

The $J_{plastic}$ term must be established by a function from reference information involving the geometry of the test/ piece, and parameters including the displacement of the cracked sample and unbroken crack ligament dimension. Hence it may be attempted to model these key parameters, subject to either a reasonable estimate of the local anodic over-potential or altering the test potential from OCV conditions used so far in this work. Hertzberg[68] has reported that in relation to hydrogen cracking, the mode of failure can change between inter and trans-granular according to the value of K, with low K accompanying inter-granular attack and intermediate levels giving trans-granular cracking with high values giving micro void coalescence.

The Griffith model[36] for brittle crack development (derived for glass) is not applicable to the circumstances of the present study, as it did not encompass finite plastic strain

which can still exist in embrittled metal, and does not include electrochemical considerations.

The Dix[53] theory of stress corrosion was mainly concerned with stress accompanying galvanic corrosion behaviour related to second phases associated with inter-granular failure, and also looks improbable in application to the present case.

1.20.5.6 Stresses in Metal Components: Sheet Rolling Effects

A residual stress is described in literature by Dieter as an elastic stress[43] and where such a stress occurs and exceeds the yield point, it will be relieved by plastic deformation until it falls to the yield stress. For rolled sheet the sign of the stress will be expected to be opposite to the sign of the plastic stain which produced it. This suggests that the surface of cold reduction sheet leading to grain elongation will leave the surface in a state of compression. However, in the case of rolled sheet products, the level of cold reduction[69] can determine the existence of tensile or compressive residual stress, in that where this reduction is very low affecting the outer surface layers only, the surface is expected to be in a state of compression and the central region of the strip in a state of tension.

For larger reductions, the literature[69] indicates that the reverse situation is expected.

In the case of double reduced packaging steels, it is understood that the thickness reduction can be at least as high as 15%, and the latter situation would be thought more likely, but this would require to be verified, for example, by X ray measurement.

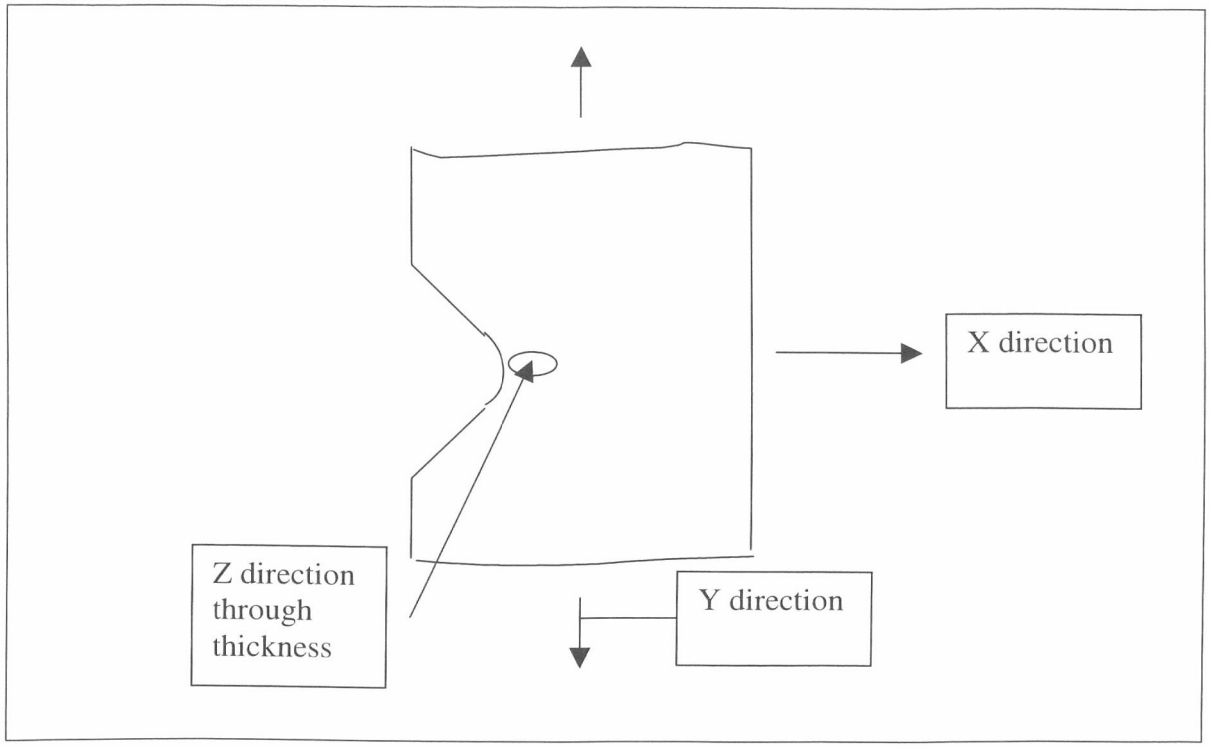
Forces such as vacuum, internal pressure or static load on cans or components may add to residual stress levels. Although fatigue does not appear to have figured significantly in studies related to packaging examined, effects such as vibration in transit under top

loads especially, cannot be disregarded as possible contributors to sites of crack initiation at points of tensile stress.

1.20.5.7 Slow Strain Rate Testing.

The slow strain rate test is aimed at simulating stress conditions which may exist in a container component in a short time and in the presence of a chosen environment such as one which may cause environmental stress cracking. A schematic illustration of the type of test sample used in this study at the outset is shown in Figure 8 below. For a thin plate loaded in the plane of the surface, the existence of plane stress conditions are described in the literature, on the basis that negative strains in the z direction are counteracted by induced stresses. Practical observation of notched samples tested in this work indicated that observable strains in the z (through thickness) direction, implying that some through thickness stress had existed at least locally near the notch apex.

Figure 8 Schematic illustration of Slow Strain rate test sample notch used in initial slow strain rate studies.



Regarding fracture in very thin sheets, Felbeck and Atkins [70] have explained that for the case involving notch areas, shear stresses may be produced that cause slip at 45 degrees in the thickness direction rather than across the width. Degrees of this effect were observed in initial slow strain rate tested samples. To make the most effective use of testing by the slow strain method using notched specimens in the context of environmental stress cracking requires a parallel assessment of stresses produced , primarily at the notched area. In this study Finite element modelling has been used as described in detail in section 3, and the means of attempting a form of cross validation was to relate the true failure stresses of a standard parallel sided dogbone specimen of the same material to the predicted peak notch stresses on a modelled specimen which were attained under the action of the practical specimen maximum load causing failure of the notched specimen. Using this approach the modelling package has taken account of the stresses due to the notch geometry. A further alternative would be to use

information for the stress concentration factor arising due to the notch geometry. This is considered below.

Stress Concentration Factor

Dowling[71] defined the elastic stress concentration factor K_t by the formula:

$$K_t = \sigma / S$$

where :

σ is a locally defined notch point stress

and

S is the average stress.

In the present study it is important to know the local stress at the apex of the notch, but while this can be estimated for an un-corroded specimen, the change resulting from any corrosion will be unknown.

Herzberg[72] explains the case of an elliptical hole in a plate analysed by Inglis, leading to the formula:

$$\sigma_{max} = \sigma_a (1+ 2 \sqrt{a/\rho})$$

where:

σ_{max} is the max is the maximum stress at the end of the major axis

σ is the applied stress normal to the major axis

a is half the major axis length.

ρ is the radius of curvature at the end of the ellipse.

In most cases $a >> \rho$ and the equation approximates to $\sigma_{max} = 2\sigma_a\sqrt{a/\rho}$.

For this case $2\sqrt{a/\rho}$ is the stress concentration factor.

The peak stress and the stress raiser or notch is thus the product of the stress and the stress concentration factor which has to be defined for a particular specimen and geometry, and the smaller the crack tip radius the larger the stress concentration factor. For ductile materials which would include the types of steels used in this study, increased stress at a notch can be relieved by the occurrence of plastic strain at this point. Reference information provides detail of stress concentration factors for a variety of different specimens and cases. Peterson[73] includes the case used in most of this study, where a double 90 degree angle v notch has been used. Using the data from Peterson which refers back to Appl & Koerner for the case for a double V notched plate, the ratio of the un-notched to notched widths could not be precisely matched to the data given, but it appeared that the difference would be small. The true ratio was 1.202 and the lowest given at by Appl & Koerner was 1.66. The stress concentration factor for the 1.66 ratio was estimated at $Kt_{\alpha}=3.48$ for the case of 90 degree double V notches used in the work reported in section 3 of this study, having a notch depth of 1.06mm and root radius 0.15mm for the two 90 degree v notches applied. Thus, on the assumption that the Peterson data is a close approximation to the correct value, then for a nominal stress of $620N/mm^2$ assumed elastic, the peak stress at the notch would be estimated to be in the order of $2158N/mm^2$. Section 3 gives Finite element estimates for the case which can be compared. Peterson states that the KT values for flat members covered are for 2 dimensional plane stress conditions and apply strictly to very thin sheets.

1.20.5.8 Possible Means to reduce Failure Risks : Steel Composition

As a reference comparison the steel composition for the 0.19mm DR 520CA material used in initial studies during the present work is is shown in Section 2 para 2.4.8 . This

analysis was conducted by Corus at Scunthorpe. The results confirm the very high purity of the type of steel used in terms of residual element levels.

Comments on Effects of Alloying Additions to Carbon Steels

Titanium and Chromium

Substantial work by Parkins et al[45] on annealed carbon steel materials broadly showed that where added elements improved SCC behaviour, the level required tended to be as much as 1% or more, and that titanium and chromium were found to show most consistency in behaviour. Ti and Cr are transition elements of lower atomic number than iron, and Troiano[50] reported test some evidence to support the case that addition of d block elements of lower atomic number than for the d block 'solvent'element can lower embrittlement susceptibility. He suggested that a reduction of density of the electron d states by such additions may influence this effect by lowering repulsive electron forces. It is apparent from the eccs plate compositions quoted later in this document, that the levels of the above two elements were each far below 1% in packaging steels.

Earlier work by Haggman[46] indicated that increased copper levels in packaging steel gave beneficial pack test results in relation to pitting performance of tinplate food cans. Further reading indicates that the evidence concerning copper has been inconsistent, and it has been reported[74] that in steels containing low amounts of sulphur and phosphorus, an increase in copper content can reduce the life of some packs, such as certain fruits. Because copper reacts with sulphur and phosphorus its function may have been most effective where steels with higher levels of these elements had been employed in the past.

Impurity Elements : Sulphur and Phosphorus and Segregation

Cron[4] et al commented on the important influences of sulphur and phosphorus in promoting pitting especially at the carbide ferrite matrix interface where these elements are segregated when iron carbide forms. Levels of these elements in present day packaging steels are very low (P: 0.02 wt %max; S : 0.03 wt% max).

Westerbrook's review[75] of segregation at grain boundaries discusses the effects of 3rd element modifiers in this context, recording that related to phosphorus segregation, molybdenum additions alleviate it and chromium aggravates it; in the case of sulphur segregation, carbon alleviates it.

Parkins et al [38] found that for certain carbon steel, molybdenum aggravated pitting, revealing the complexity of interactions which may exist.

Others

No substantive evidence has been found that the nitrogen at the level used in the 'Nitrogenised' packaging steel type (0.010-015wt%) has been influential in causing scc failures in meat or fish packs, or has been implicated in research elsewhere at this level. Neither has information reviewed from the literature shown that Aluminium used as a de-oxidant was fundamental to the problem. Parkins[45] et al indicated insufficient data on the effect of manganese.

Information reviewed related to changes in performance due to compositional factors affecting stacking fault energy concerned face centred cubic alloys as opposed to body centred alpha iron.

1.20.5.9 Metallurgical Microstructure

Practical studies which have taken place in parallel with this work involving alternative materials (TR11405[76], and TR11710[77] and TR12077 draft [78], reported by the author),

and have included pack tests with animal food involving double reduced eccs steels having different micro-structural conditions and properties, the variables reported in TR11710 being:

Standard cold reduced DR620CA eccs steel ; Nitrogenised DR620CA eccs steel(from two different sources) , and a 'maleis' type DR620CA eccs steel having a measurably larger grain size recorded that for the other steels, all materials being tested as lacquered ends, and all being of 0.235mm gauge.

From this work, aspects on which it is possible to comment regarding materials and performance are discussed below :

i) The better performing materials in this test were the 'maleis' type, Figure 9 below, and one of the nitrogenised variants, Figure 10 below, each showing limited degrees of improvement in % elongation measured parallel to the grain direction in comparison with the other two materials. Each of these two materials gave quite similar results with 13% and 17% failures respectively. The 2nd nitrogenised variant, Figure 11 below, and a standard DR620CA type, Figurec 12 below, each having lower % elongation levels than the former two materials, performed much less well under the particular 'design' conditions of the pack test, giving 54% and 50% failure rates respectively, in test sample sizes of 20 per sub group. It must be made clear that the pack test conditions were designed to be highly abnormal, involving artificially generated conditions representing a severe test. The test was done twice and the first occasion involving the most severe conditions showed up some differences between material performances as indicated above. When the test was repeated under a lesser degree of severity but a still highly abnormal condition, no failures occurred with any material. The microstructures of the four materials tested are shown below. These are followed by one additional

micrograph, Figure 13, showing the type of trans-granular environmental stress cracking condition observed in an animal food test pack

Figure 9: 0.235mm DR620CA Maleis steel structure from a section parallel to the grain, showing local carbides, but having a low density of carbide stringers. A relatively good result was obtained in a stress corrosion pack test. The % elongation was 2.3. The grain size measurement was 32,200grains per mm^2.

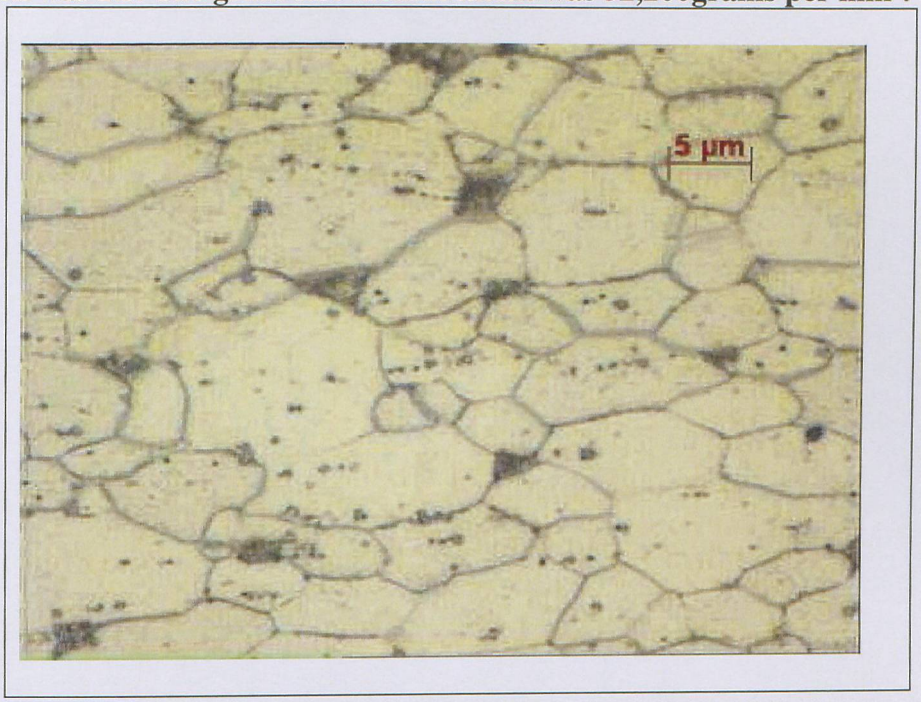


Figure 10: Nitrogenised eccs material from source 1 giving a relatively good pack test result and having a low density of grain boundary carbides. The %elongation was 3.3% and the grain size measurement was 43,472 grains /mm^2.

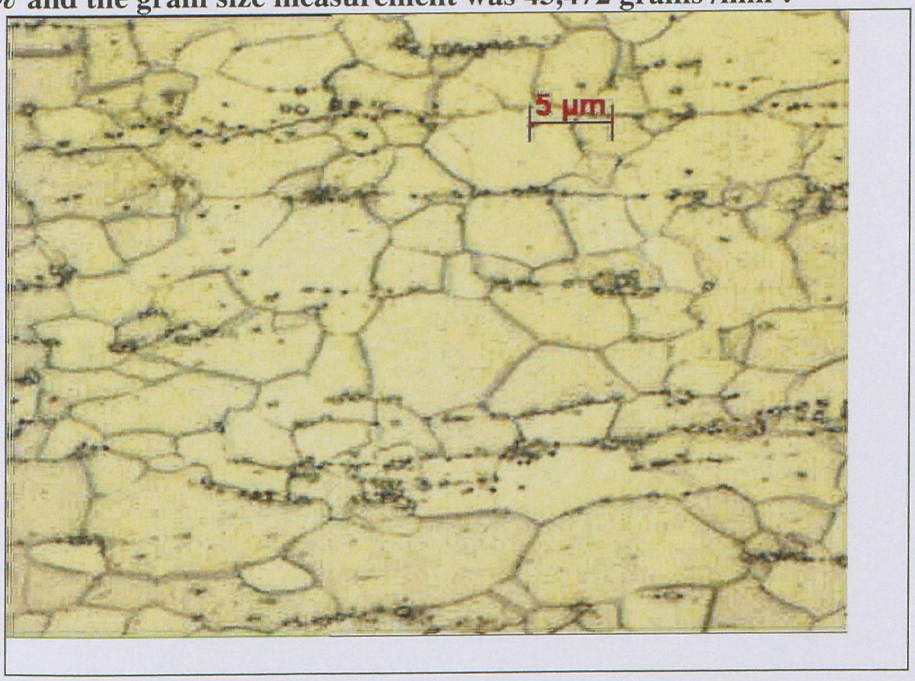


Figure 11: DR620 CA nitrogenised material from source 2 giving a measurably less good pack test result than for materials in Figures 9 and 10 and having a higher density of grain boundary carbides than the nitrogenised material in Figure 13 together with a more irregular grain size. This material had low elongation of 1.1% and grain size measurement of 45,680grain /mm^2

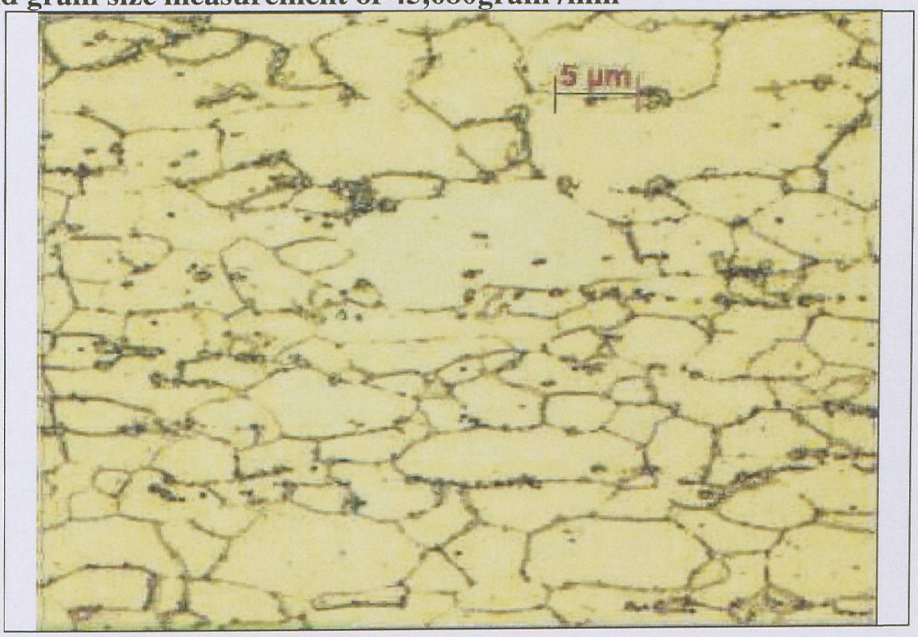
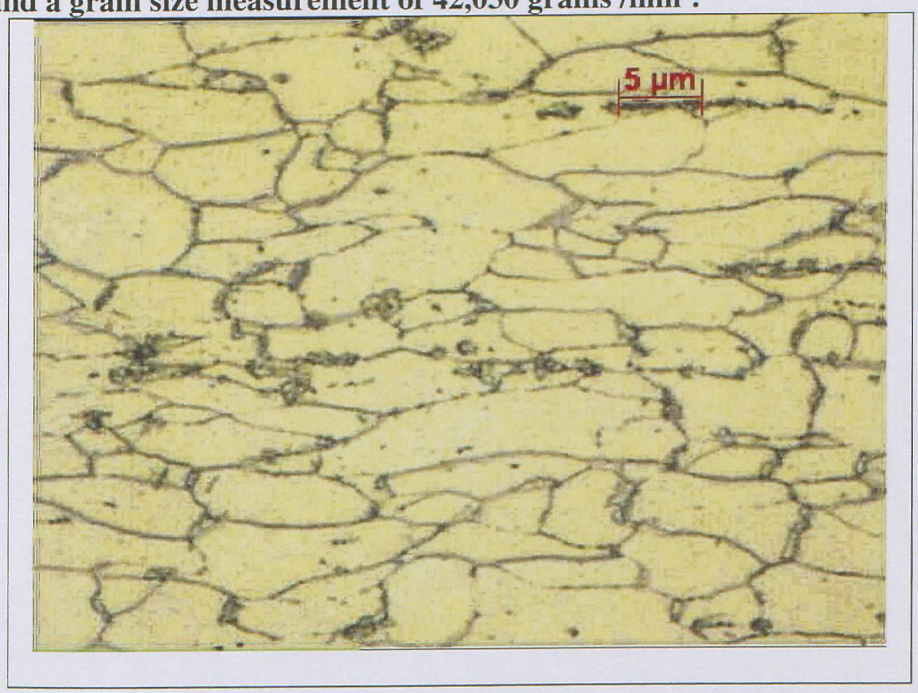
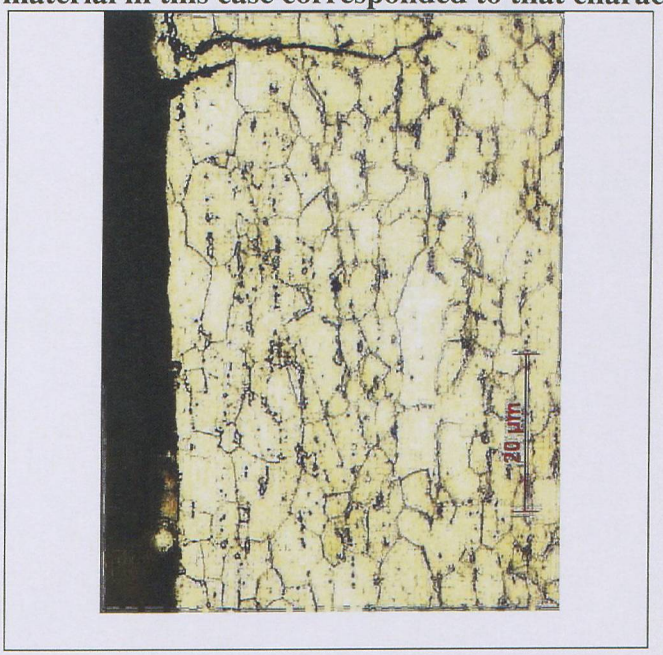


Figure 12: Standard DR 620 CA material, non nitrogenised, again giving a less good pack test result than materials shown in Figures 9 and 10 , with a result similar to Figure 14 material. This material has shown greater cold work effects in the grain structure than for nitrogenised steels above together with grain boundary carbides and some carbide stringers. The material had an elongation of 1.81% and a grain size measurement of 42,030 grains /mm^2.



An example of the environmental stress-cracking effect observed is shown in Figure 13 below. The indication was of trans-granular environmental stress cracking and the test involved the use of an animal food product.

Figure 13: Example of Cracking in Pack test failure sample filled with animal food product. The material in this case corresponded to that characterised in Figure 11.



ii) From the above test an observation was that the two materials showing lower elongation levels, Figures 11 and 12, performed less well in the first pack test relative to the maleis variable, Figure 9, and the nitrogenised group having the better elongation value, Figure 10, the former material having a distinctively larger grain size than the other 3 materials.

The results of these tests were not regarded as conclusive of the performances of the steel types tested, especially as test conditions were rather more severe than would exist in normal packing, but the data did provide indications of certain attributes to examine further. The 0.235mm steel used in the Slow Strain Rate Test work in Section 3 was a parallel lot from the same source as that shown in Figure 11.

The observations of Nekvasil and Pitter[2] in relation to stress corrosion cracking in meat cans included that of "poor formability" and "low elongation" of some materials and

the introduction of a test to measure plasticity reserve as one attribute to improve performance. From the tensile information quoted single reduced plates were deduced as the materials in use.

Coating Protection Aspects: Reference information

Studies of these aspects have taken place in parallel work reported in TR11405[76] and this has given indications of the level of coating protection for minimum risk in controlled lab pack tests. The performance of tin-coated plate was also discussed.

Other guidance was given by the work of M Tsurumaru, K Masuda and Y Yamamoto[1]. The detail of coating protection performance is outside the scope of this study.

1.21 Conclusions

1. **Type of Failure indicated as likely in Tuna Brine:** In parallel with the literature study initial test work reported in Section 2 of this investigation took place by the slow strain rate method using tuna brine and acidified tuna brine product, after initially conducting fast and slow sweep dc polarisation tests on DR550CA eccs plate. This work had not indicated passive conditions on the anodic polarisation curves for tuna, and some evidence of loss of ductility and environmental stress cracking was then shown using the slow strain rate method at the Open Circuit Potential. This would point to a hydrogen cracking mechanism for this product. Meat product was not tested.
2. **Related Food Aspects:** For a hydrogen embrittlement effect to occur, based on the mechanism put forward by Troiano, pitting and the presence of catalytic poisons is required to attain sufficient ingress of hydrogen to promote the effect. Products such as fish and meat containing brines are expected to show a variable pitting tendency and heat processing can be expected to generate low levels of sulphides such as hydrogen sulphide as well as other organic sulphides. Loss of ductility has been observed in tests

involving phosphate media alone[16], and phosphorus itself has been cited by Evans[33] as a promoter of hydrogen ingress into steels. This apart, arsenic, antimony bismuth and selenium are expected to act as catalytic poisons[33], and again zinc is mentioned as a hydrogen ingress promoter. Literature also indicates that carbon dioxide , chlorides and ammonia are accelerators of hydrogen cracking mechanisms. Carbon dioxide has been recorded as a constituent in the headspace of processed food cans and in certain instances may arise due to additives in animal food products. Salt has a normal presence in fish and meat and ammonia has been identified during heat processing studies on bovine albumin plasma[25].

3. **Sulphides, Meats and Fish and Myoglobin:** Regarding sulphides there is much uncertainty concerning the real influence on such a process in canned foods, because the level of hydrogen sulphide is likely to be low, and other volatile sulphides are not soluble and would require to act in a heterogeneous manner to act as catalytic poisons. The history of the subject gives rise to the observation that more instances appear to have been highlighted with red meat than white, and the possible role of myoglobin arises, this being as the source of red meat colour. Ferric ions will be generated by this substance during heat processing, and a mechanism may be postulated involving reduction of ferric to ferrous ions and reaction with a catalytic poison e.g. hydrogen sulphide to promote hydrogen ingress into the metal. However, any iron from a pitting reaction on steel might perform the same function, so an experiment would be necessary to determine any contribution of myoglobin to the environmental stress cracking effect. In the courcse of the study it was learned that products such as tuna may be precooked, frozen and transported for later canning or packed as raw product. Literature information for other fish indicated that precooking could lead to a significant loss of volatile sulphides.

4. **Materials:** Packaging steels are most typically Al killed type and are of high purity with low levels of residual elements, (illustrated by data in Sections 2 and 3), as well as having low levels of inclusions. Research reviewed on steel chemistry mainly involved materials with compositions far removed from normal packaging steels, and for those additions reported to reduce susceptibility to at least some types of stress corrosion, addition of elements such as titanium and chromium at as much as 1% was indicated. This would represent a major departure from present packaging steel compositions, quite apart from any effects on formability. Given the relatively high purity steel used for packaging, it is suggested that the stresses arising from the combination of use of double reduced tempers and forming behaviour look to be a more promising area for research to reduce failure risks. There was some indication of the potential importance of this factor from tests reported from references[76,78] and from the observations of Nekvasil and Pitter[2] on what were interpreted as single reduced steels. This is because the interactive effects involved can lead to variable gauge reduction and necking on forming, which may then affect internal stress and /or void levels, and provide sites for hydrogen nucleation, as well as metal exposure through the pre applied coating. The 'necking' behaviour of double reduced packaging steels is considered in more depth in Section 3 of this study.

5. **Corrosion and Protection Aspects:** This has been the subject of separate studies and reporting. Because end component manufacture as well as that of 3 piece can bodies and drawn redrawn container bodies, involves pre-applied organic sheet lacquer coatings, complete protection after fabrication is not achieved and the stress points such as tooling radii for ends are likely to be a source of metal exposure. If the substrate has suffered more than usual amount of stretching and some necking the metal exposure may be increased, or even if not the protective coating stretched and weakened. Localised attack may be enhanced by an excess of cathodic reactant such as too much

air in the pack, or by any cathodic behaviour of a surface such as a can wall, should the coating become readily permeable to product species e.g. due to undercuring or marginal suitability in respect of choice of type or level of the coating. A large cathode area may then be generated which causes rapid attack at a minute exposure site at a stress point.

Particular cases of failure have been triggered by external sources of added or exceptional stress causing e.g. base rim denting of 2 piece tuna cans, as shown in Figures 1 and 2, causing weakening of internal protection, and by design features such as roll beads in these cans which provide nested stacking. Other cases have involved circumferential scratching at end countersink regions combined with residual CO_2 in can pressure in an animal food which was thought to be a source of enhanced stress.

Experience over many years suggests that the prevention of any metal exposure at stress points is not an attainable goal for fabricated packaging steel components having pre applied coatings, and that the control of forming stresses and the interaction with material properties to minimise any 'necking' is a very important aspect, together with the avoidance of abnormal added sources of stress in service. The basic choice of coating must nevertheless be such that no undue permeability of product species occurs. These observations assume that product composition in terms of recognised anion and cation species which may contribute to a stress corrosion mechanism are within a normal order of values for the products packed, and that packing and processing conditions conform to industrial good practises.

1.22 Section 1, Appendix 1.

Definitions:

(Taken from Shreir, Jarman and Burstein, Corrosion 3rd Edition)

Stress Corrosion Cracking

Stress Corrosion Cracking is cracking produced by the combined action of corrosion and static tensile stress.

Hydrogen Embrittlement

Hydrogen embrittlement is embrittlement caused by entry of hydrogen into a metal.

Corrosion Fatigue

Corrosion fatigue is failure by cracking, caused by reversing alternating stress in the presence of a corrosive environment.

Table of Food Compositions for Selected Fish and Meat Categories:

(Data for constituent levels is in milligrams per 100grams edible portion, except for the following in-organics : Selenium and Iodine, and vitamins: Retinol, Carotene, VitaminD, Vitamin B12, Folate, Biotin and Vitamin C in µg per 100grams grams edible portion).

Parameter	Units	Fish average	Tuna	Salmon	Sardines	Meat average	Ox liver	Chicken	Lamb :fat cooked
Inorganic									
Sodium	mg	426.7	320	430	530	80.07	110	60	72
Potassium	mg	270	230	260	320	260	250	270	260
Calcium	mg	213	8	91	540	10.3	11	9	11
Magnesium	mg	32.3	27	25	45	20.7	19	25	18
Phosphorus	mg	283	170	170	510	250	380	210	160
Iron	mg	1.3	1.0	0.6	2.3	3.13	7.8	0.5	1.1
Copper	mg	0.0867	0.05	0.05	0.16	0.803	2.3	0.06	0.05
Zinc	mg	1.267	0.7	0.8	2.3	2.3	4.3	1.1	1.5
Chlorine	mg	696.7	550	730	810	82.3	120	60	67
Manganese	mg	(0.0673)	Tr	Tr	0.2	0.153	0.44	0.01	0.01
Selenium	µg	48	78	25	41	22.3	50	13	4
Iodine	µg	31.7	13	59	23	4.7	0.0	8	6
Vitamins									
Retinol	µg	(18.5)	N	31	6	(5776)	17300	Tr	29.0
Carotene	µg	-	Tr	Tr	Tr	(500)	1500	Tr	0.0
VitaminD	µg	5.8	3.6	9.2	4.6	0.57	1.1	0.10	0.50
Vitamin E	mg	(1.035)	0.55	1.52	N	0.26	0.44	0.07	0.28
Thiamin	mg	0.01667	0.02	0.02	0.01	0.11	0.18	0.06	0.09
Riboflavin	mg	0.1967	0.11	0.22	0.26	1.3	3.6	0.13	0.17
Niacin	mg	8.8	14.4	5.9	6.1	7.6	10.3	8.8	3.6
Tryptrophan 60	mg	4.267	4.4	4.4	4.0	4.3	5.3	5.6	2.0
Vitamin B6	mg	0.28	0.47	0.21	0.16	0.36	0.52	0.36	0.20
Vitamin B12	µg	7.0	4	4	13	(37.0)	110.0	Tr	1.0
Folate	µg	8.67	4	14	8	100	290	6	4
Pantothenate	mg	0.597	0.29	0.74	0.76	2.59	5.70	1.34	0.74

Parameter	Units	Fish average	Tuna	Salmon	Sardines	Meat average	Ox liver	Chicken	Lamb :fat cooked
Biotin	µg	7.0	2	9	10	17.7	50	2	1.0
Vitamin C	µg	-	Tr	Tr	Tr	5	15	0	0.0

Notes: Values in brackets denote average of 3 where one or more values were denoted Tr (= trace).
Values in brackets denote average of two where one point was denoted N (=no data available).

Table of Food Compositions for Selected Fish and Meat Categories

(Data is in grams per 100 grams edible portion, except for cholesterol which is in milligrams per 100 gra ms edible portion).

Parameter	Units	Fish average	Tuna	Salmon	Sardines	Meat average	Ox liver	Chicken	Lamb
Starch	g	0	0	0	0	1.2	3.6	0	0
Total sugars	g	0	0	0	0	0	0	0	0
Glucose	g	0	0	0	0	-	No data	No data	No data
Fructose	g	0	0	0	0	-	No data	No data	No data
Sucrose	g	0	0	0	0	-	No data	No data	No data
Maltose	g	0	0	0	0	-	No data	No data	No data
Lactose	g	0	0	0	0	-	No data	No data	No data
Water	g	70.7	74.6	71.3	66.2	52.9	62.6	67.7	28.3
Total N	g	3.66	3.76	3.79	3.44	3.71	3.96	4.54	2.64
Protein	g	22.8	23.5	23.5	21.5	22.9	24.8	28.4	15.4
Fat	g	5.6	0.6	6.6	9.6	23.7	9.5	5.2	56.3
Carbohydrate	g	0	0	0	0	1.2	3.6	0	0
Dietary fibre	g	0	0	0	0	0.0	0	0	0
Fatty acids									
Saturated	g	(0.75)	0.2	1.3	N	11.1	3.5	1.5	28.4
Mono-unsaturated	g	(1.25)	0.1	2.4	N	8.5	1.5	2.4	21.6
Poly-unsaturated	g	(1.05)	0.2	1.9	N	1.8	2.0	1.0	2.4
Trans	g	0.0	0	0	0	(1.8)	Tr	0.1	5.3
Cholesterol	mg	46	51	28	60	143	240	90	100

Notes: Values in brackets denote average of 3 where one values was denoted Tr (= trace).

Values in brackets denote average of two where one point was denoted N (=no data available).

2 Section 2: Experimental Studies : Initial Work and Findings.

2.1 Introduction.

This section summarises the initial experimental work and findings. The objectives at this stage were:

a) To reproduce environmental stress cracking by the slow strain rate test method.

b) To establish a procedure which could be used for more systematic studies of contributory conditions.

These objectives were attained to the extent of determining a procedure to follow for later work, but the data while indicating trends did not provide enough statistical output to enable conclusive findings on contributory effects. This section explains the methods in an abbreviated way, having some limited differences explained from the later work. The main findings are described, preparatory to a more thorough experimental study reported in Section 3. To avoid repitition, reference is made to the detailed explanation of the experiments in the later section, and any differences in earlier work are identified. Statsistical terms and methods are explained in detail in Section 3 Appendix 1 as well and in the introductory part of Section 3 . Statistical correlation test data using the Minitab package give the Pearson correlation value, and the P value indicating the significance level, with P values of 0.1 or below, i.e. significant at 10%, being considered as significant for the purposes of this study.

2.2 Experimental Work and Procedures.

Electrochemical Tests .

All of these tests were performed in a temperature controlled laboratory at 20°C. The material used for this phase of work was 0.19mm DR520 CA eccs continuous cast steel. Specimens were coupled to a Solatron 1286 potentiostat which was interfaced with an HP compaq computer equipped with DC Corrware Software.

Slow Strain Rate Testing.

The slow strain rate test cell used is illustrated in **Section 3, Figure 37**, with the test specimen illustrated in **Section 3, Figure 38.** The test specimen was a standard 175mm long dumbell shaped sample, to which at this stage a *single* v notch was applied at the mid point of one edge, having a 90 degree angle, 1.06mm depth and notch radius 0.15mm. Specimen edges were sealed with a brush applied lacquer. Each specimen was assembled into a bakelite test cell containing the test liquid and subject to tensile loading created by a crosshead movement of $5.7*10^{-6}$ mm.sec^{-1}. The bakelite test cell was equipped with a counter electrode, and a liquid junction for a reference electrode, which was of an N/10 calomel type. These were connected to a Solartron 1286 electro-chemical interface linked to a computer utilising Corrware DC electrochemical software supplied by Solartron. This enabled tests under conditions of defined potential, that used being the Open Circuit Voltage, as determined prior to each test over 30 minutes. At this stage slow strain rate tests were only performed under air conditions in tuna brine and acidified tuna brine variables. The parameters measured and analysed are described in Table 6 below. In the course of the test programme sub groups were also tested after application of one scratch across the specimen to see whether any environmental stress cracking effects could be enhanced. This was carried out using a standard tool made of hardened steels and operated in a specimen holder in a frame to

enable sliding and to provide a constant mass of 527grams as the tool was moved manually across one specimen width at the notch region. The tool had free upward movement in its holder under the mass, so that the load was constant.

2.2.1 Parameters Determined During Slow Strain Rate Test Work.

Table 6: Parameters Determined During Slow Strain Rate Test Work.

Item	Symbol	Unit	Description
	Dimensions		
1.	BC	cm	Starting height of notch .
2.	Delta BC	cm	Change of notch height following test.
3.	gauge	ins	Thickness of sheet material used.
	Other physical parameters		
4.	Initial load	Newtons (KN)	Initial reference value from tensometer, taken as zero.
5.	Maximum load	Newtons (KN)	Peak value in slow strain rate test.
6.	Change of load	Newtons (KN)	Nett load applied in course of test.
7.	d	mm	Starting cross-head displacement value before test.
8.	D1	mm	Final displacement.
9.	Ef	mm	Extension at failure.
	Chemical and		
	electrochemical		
	parameters		
10.	pH start	-	pH at start of test.
11.	pH end	-	pH at end of test.
12.	T1	deg C	Product temperature at time of initial pH.
13.	T2	deg C	Product temperature at time of final pH.
14.	T	deg C	Ambient room temperature during test, controlled to 20 deg C.
15.	OCV	Millivolts.	Open circuit voltage of specimen determined over 30 minutes before test, with reference to N/10 calomel reference electrode.
16.	E_{rms2}	Volts.	Root mean square value determined for the potential distribution during the entire time of the test.
17.	I_{rms2} ***	Amps/ cm^2	Root mean square value for current density determined during the entire test time.
18.	Ia_2 ***	Log_{10} current density (amps/cm^2) x time (seconds) .	Integrated current (density) -time value over the entire test time.

* The notch height gap correction is the subtraction of the gap which exists after testing between the fractured components at the notch, due to the greater ductility of behaviour away from the notch region. This gives a revised notch extension value according to fracture behaviour at the notch region only.
**M1=M*C, where M is the area under the tensile load-extension plot up to maximum load, and C is a calibration factor for the KH Slow Strain Rate Tester Load Cell. This is recorded in Section 3.
*** Electrochemical parameters were normalised to a surface area of $1cm^2$.
In section 3, the parameters E_{rms2}, I_{rms2} and I_{a2} each have suffix 2 replaced with suffix 1, as these parameters were then determined up to the time of maximum load only.
It should be explained that the integrated current values, $I_{a2,}$ recorded in this work using the $\log_{10}$ values for current were invariably negative, so that where an inverse correlation with this parameter is shown, the net effect on the dependent variable would be direct.

DC Potentiodynamic Polarisation Tests.

DC polarisation tests took place using an alternative cell, comprising $1cm^2$ electrodes of the same material as that used in the slow strain rate tests, and the same reference electrode. These tests comprised fast and slow sweep polarisations to examine for the existence of any active/ passive potential zones on the anodic curves, and later pitting loop tests to examine the propensity for this form of attack.

DC Fast and Slow Sweep Polarisation Tests

These took place under air and nitrogen flushing conditions, starting from 250mV active of OCV and running to 500mV noble of OCV, but with an intermediate holding time at 250mV active of OCV (vs an N/10 calomel reference electrode), derived from a procedure identified by Scott, Smart and Procter[16]. Fast sweeps were at 1000mV per minute and slow sweeps at 10mV per minute. Nitrogen flushing conditions were for 12 hours at a minimum flow rate of $3cm^3$ per minute through the liquid which was changed to flushing through the headspace during the test.

Pitting Loop Tests

These were performed at an intermediate sweep rate of 0.4mV/s (with respect to an N/10 Calomel reference electrode) operating from OCV, determined after monitoring

over 600 seconds, initially sweeping from OCV to 500mV noble of OCV, followed by a reverse sweep to 250mV active of OCV. Again, the tests were performed on eccs and abraded eccs and under high air and low air (nitrogen flushing) test conditions, as for the fast and slow sweep polarisation tests.

Product and Preparation

Initially, the product used was tuna brine from individual drained cans. This was followed by preparation of a bulk supply from purchase of a batch of tuna in brine cans, which were drained into a 5 litre beaker, stirred, and poured into 125ml analytical pots before freezing at –20°C. This was the same purchase lot as is identified in Section 3 of the report, but a new frozen bulk was later made from the same purchase for the Section 3 work. The bulked brine was used for the fast and slow sweep polarisation tests, the pitting loop tests and the main body of tests described for the slow strain rate method. However, in the slow strain tests only, as a great diffuculty had been encountered in the early stages of the study in reproducing environmental stress cracking, samples constituting the majority of tests performed were acidified using acetic acid or hydrochloric acid as small sub groups, to pH level 4.5-5.0, again in an attempt to enhance the effect.

2.3 Results

2.3.1 Initial Observations from Slow Strain Rate Tests using Product Brine from individual Drained Cans.

The first distinctive examples of failures of notched samples subject to slow strain rate testing under air conditions and involving loss of ductility at the surface, were produced with tuna brine using individual drained cans, and examples are illustrated in the Figures 14 and 15 below. The tests were performed at the open cicuit voltage, and loss of ductility or loss of ductility with degrees of environmental strsss cracking were judged to have occurred as a partial failure effect.

Figure 14: Tuna brine sample srttu47 Jan 2003 , tested under air conditions by the slow strain rate method. Cracking on wall of specimen close to the fracture edge.

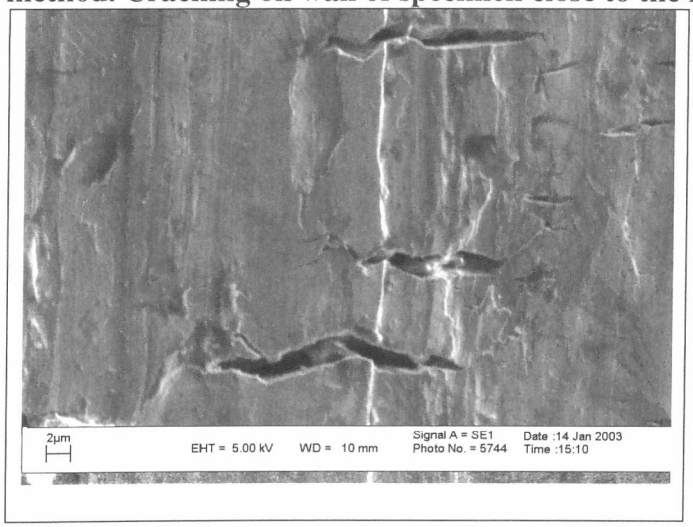
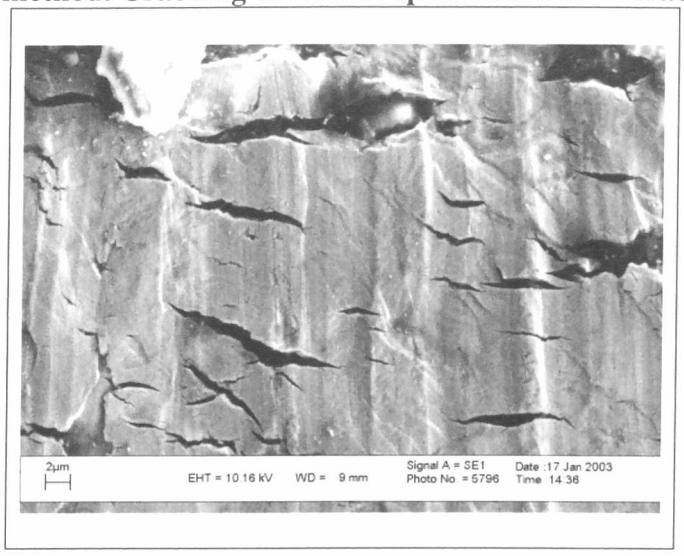
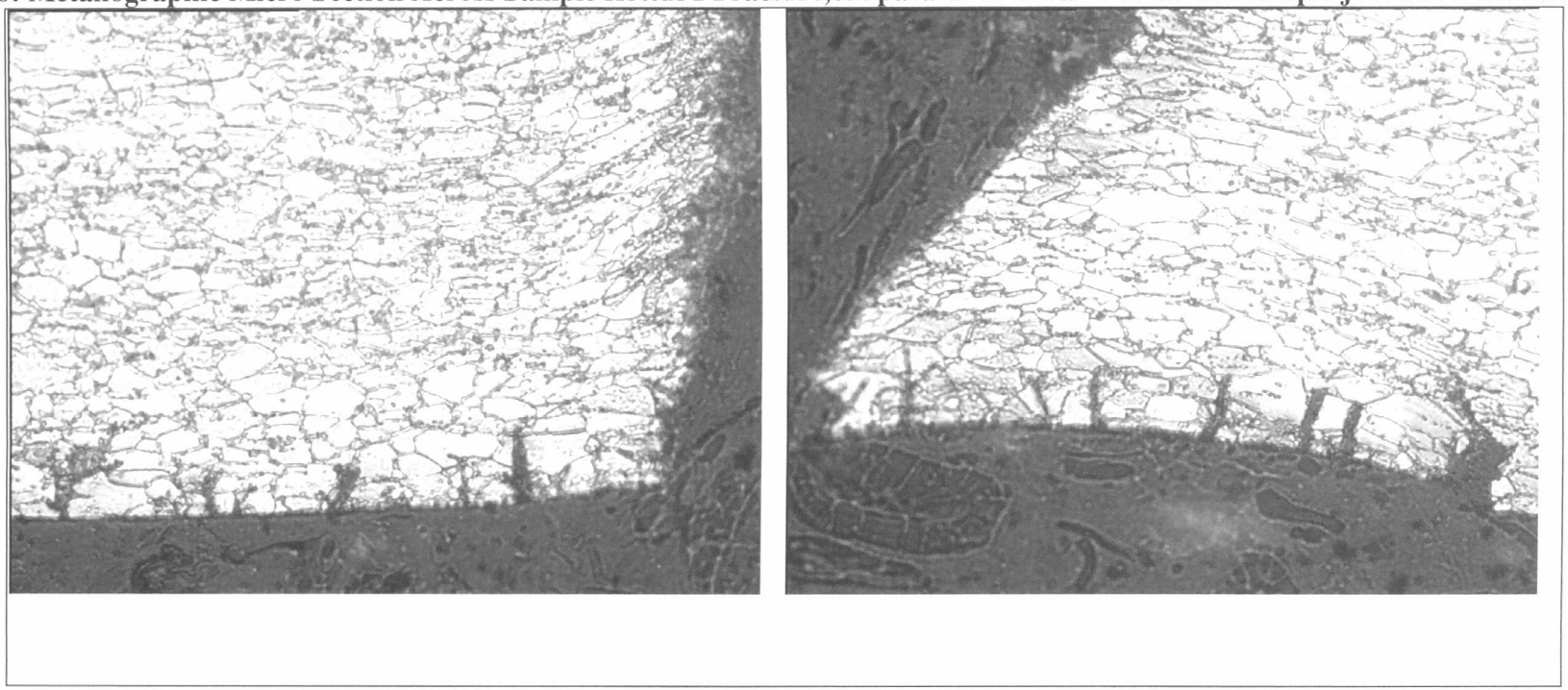


Figure 15: Tuna brine sample ssrttu51 Jan 2003, tested under air conditions by slow strain rate method. Cracking on wall of specimen close to fracture edge.



Despite many test since the above involving tuna brine , with some cases of environmental stress cracking identified, the particularly distinctive surface cracks above did not tend to be observed as clearly as in these cases. Figure 16 below shows the metallographic section on one of the above samples indicating local penetrating crack initiations at the surface, and for the left hand micrograph relatively limited plastic strain.

Figure 16: Metallographic Micro Section Across Sample ssrttu51 Fracture,cut parallel to the axis of the test sample just below the notch apex



2.3.2 DC Polarisation Tests.

The product was thawed to around 20°C and filtered before introduction to the test cell. Typical results are shown below for tuna brine tested under air conditions, and under nitrogen flushing conditions for eccs non abraded material. See Figures 17 and 18 for eccs non abraded material.

Figure 17: Fast and Slow Sweep Polarisation: Air conditions : 0.19mm DR520 CA eccs material.

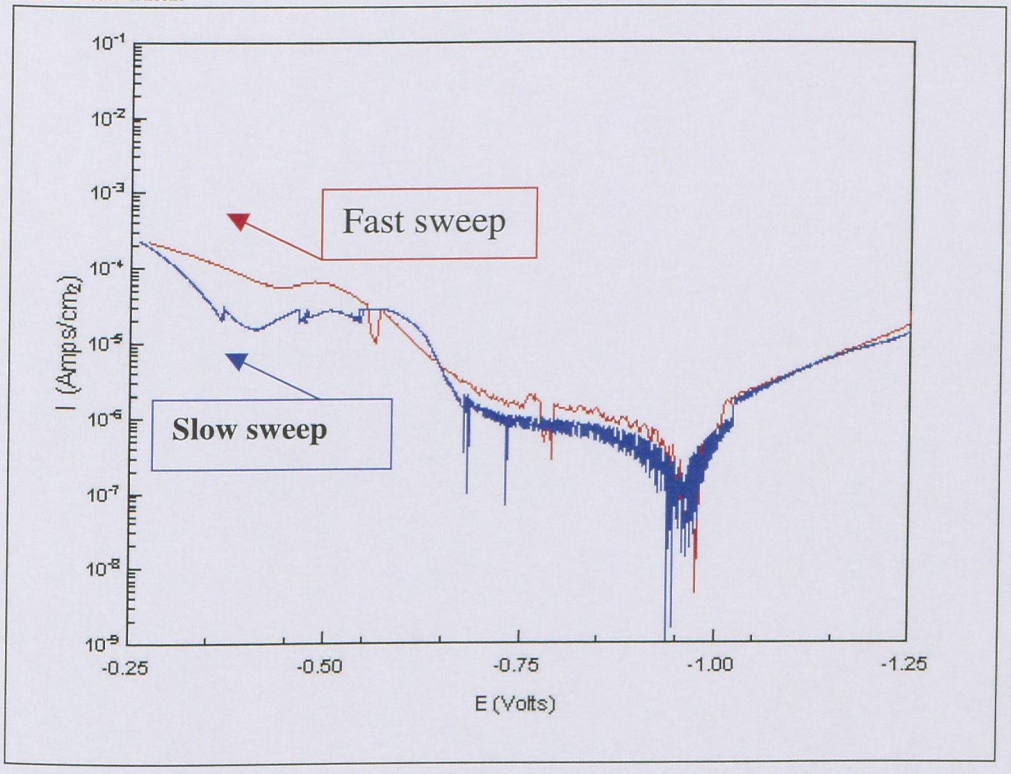
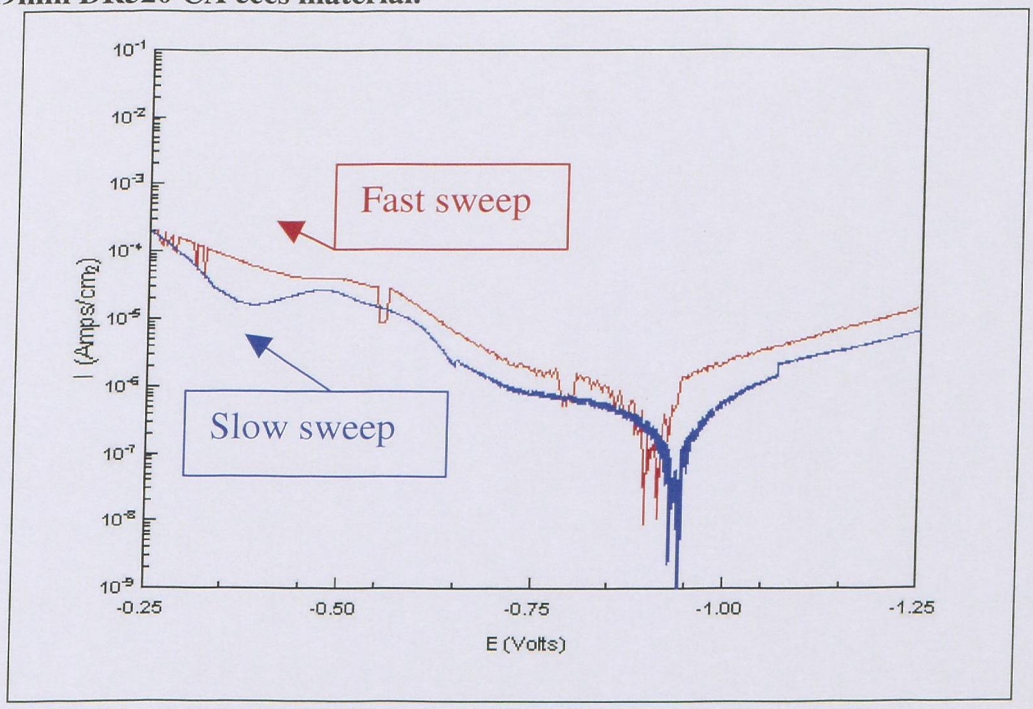


Figure 18: Fast and Slow Sweep Polarisation: Nitrogen flushing conditions: 0.19mm DR520 CA eccs material.



These curves showed that under air or nitrogen flushing conditions, no distinctive passivation conditions were apparent on the eccs material under slow sweep conditions. The peak currents at the maximum anodic overpotential were similar for air and nitrogen flushing conditions, but more noise was observed under air conditions at low cathodic overpotentials, and at low to intermediate anodic overpotentials. In the Tafel region the slow sweep curves appeared close to mixed cathodic/anodic control conditions. At high anodic overpotential there were arrests on the anodic curves for the slow sweep condition, but the current densities recorded were still at or above 10^{-4} amps /cm^2, so there was no passive condition observed, which would require a level at least below 10^{-6} amps/cm^2 if not lower.

2.3.3 Pitting Loop Tests.

The examples below, in Figures 19 and 20, were for non abraded eccs material under high and low air conditions respectively.Under high or low air conditions, the pitting loops displayed positive hysteresis, so that a pitting tendency was indicated.

Again, there was more noise at low cathodic and anodic over potentials for the curves obtained under air conditions. In the Tafel region under low air conditions, the indications from slopes were of close to mixed cathodic/anodic control for low air conditions, but were less clear for high air due to current noise. A feature of the comparison shown was that the low air condition variable did not show an 'arrest' on the anodic polarisation curve, whereas the high air sample did show the arrest. The oxygen level may have affected behaviour on this test interactively with sweep rate, but the fast and slow sweep polarisation curves had not shown a very marked difference between high air and low air conditions.

Figure 19: Pitting Loop : Tuna Brine: 0.19mm DR520 CA eccs material : Non abraded: Air conditions.

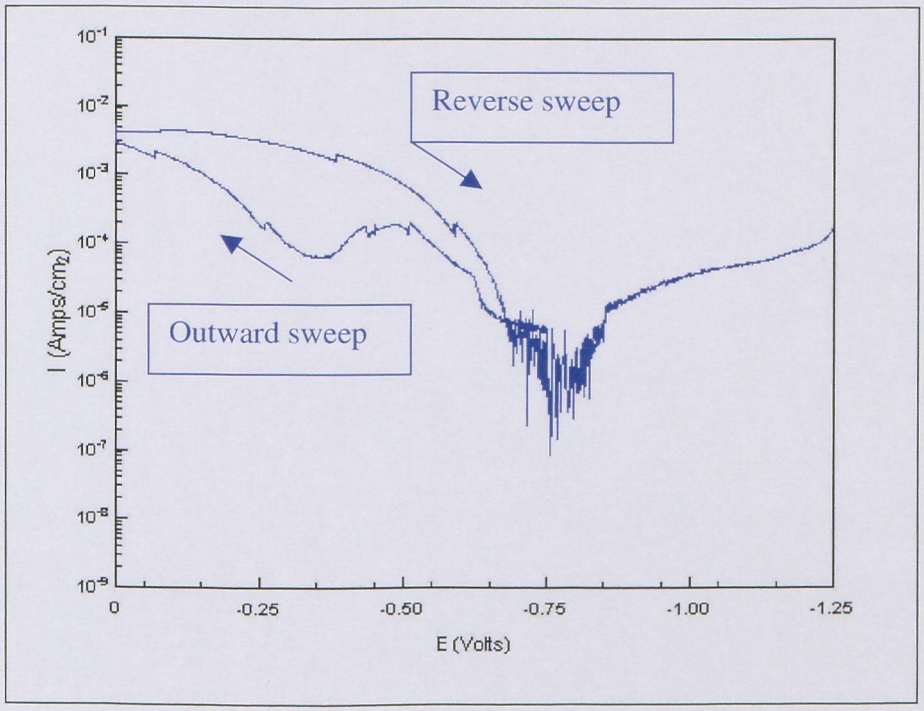
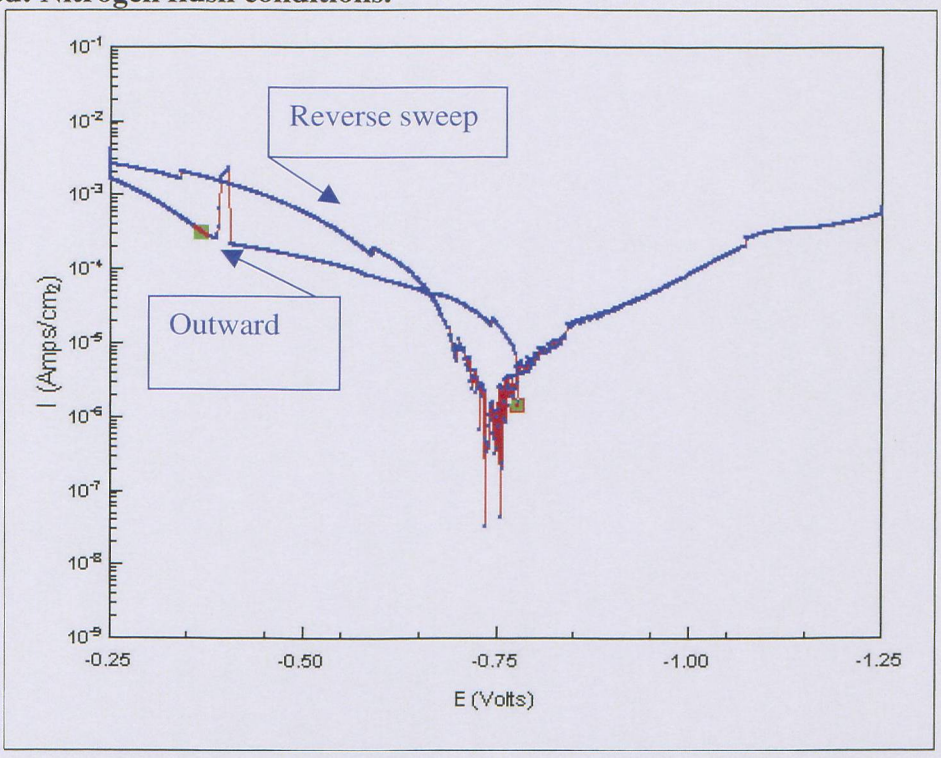


Figure 20: Pitting Loop : Tuna Brine: 0.19mm DR520 CA eccs material: Non abraded: Nitrogen flush conditions.



2.4 Slow Strain Rate Test Findings from Experiments using Bulked Tuna Brine.

The detailed results of data are recorded on Appendix 1 and Appendix 2 of this section for samples tested in the 'non scratched' and 'scratched' conditions respectively.

2.4.1 Correlations Data from Slow Strain Rate Test Data: Combined Acid Types.

The Minitab statistical Correlation Matrix is shown on Tables 7 and 8, for 'non-scratched' and 'scratched' samples respectively for tests using acidified media only, as these constituted the majority of tests performed. The correlation matrix included a 'Media Difference' parameter, which identified the hydrochloric acid dosed samples as

'zero' and acetic acid dosed samples as 1. Significant correlation was considered to exist when P values were at or below 0.1.

2.4.1.1 Correlations for Non Scratched Samples: See Table 7.

'Media difference' did not show significance with time of test or change of load, but there was a direct correlation with I_{a2}, significant at 5%, so any regression analyses would need to take this into account. As the correlation was positive the interpretation was higher values of the I_{a2} parameter on changing from brines treated with hydrochloric acid to acetic acid treatment.

The principal correlations concerning the integrated current parameter Ia_2, were inversely with time of test and with maximum load.

Time of test was also correlated directly with extension, but not maximum load.

pH start, representing a narrow range used, correlated with test parameters of extension and change of load directly , was on the borderline of significance for correlation (P= 0.1), for time of test, and showed an inverse relationship with Integrated current, Ia_2. pH start also correlated with pH end, but otherwise pH end did not show significant correlations. At this stage the correlation between $Irms_2$ and notch change does not have obvious importance in the analysis, neither parameter showing any other correlations.

2.4.1.2 Correlations for Scratched Samples: See Table 8.

For acidified media difference the results once again showed that a correlation existed with integrated current, I_{a2}. There was a reversal of the correlation between I_{a2} and time of test. Examination of the relationship via a plot suggested that this was significantly influenced by one data point. Any candidate regressions for time of test involving Ia_2 at least, would need to be considered with respect to individual acids.

Investigation of the relation of time of test to I_{a2} for this data indicated that the effect was biased to a degree by one result, number 34 showing a disproportionately high failure time relative to other samples. This might have been due to a finite slippage of the sample in the tensile grips. When result 34 was removed from the data set to test the influence the correlation of I_{a2} with failure time was lost. All analyses have nevertheless included this result, and I_{a2} showed additional correlations with extension and notch height change.

Time of test has again shown a strong direct correlation with extension and inversely with notch height change, delta BC, which are logical. pH has shown a small number of correlations for reasons which are not obvious, but it was not correlated with time of test.

Table 7: Correlation Matrix: Non Scratched Samples Tested in Acidified Media: Combined Acid Types

Factors Correlation values P values	Acidified media difference	Delta BC (cms)	Extension (mm)	Maximum load. KN	Time of test (hours)	OCV: (Milli-volts)	E rms_2* (Volts)	I rms_2* (Amps/ cm^2)	Ia_{2*} $log_{10}I$ (amps/cm^2) x time: s	pH start
P										
Delta BC	-0.049									
P	0.907									
Extension	-0.126	-0.046								
P	0.765	0.915								
Change of load	-0.383	0.178	0.465							
P	0.349	0.673	0.246							
Time of test	-0.415	-0.090	**0.861**	0.593						
P	0.306	0.832	**0.006**	0.122						
OCV	0.325	0.032	-0.201	-0.132	-0.529					
P	0.432	0.940	0.634	0.756	0.177					
E_{rms2}	-0.008	-0.472	-0.022	-0.298	-0.106	-0.060				
P	0.985	0.237	0.959	0.474	0.802	0.887				
I_{rms2}	0.521	**-0.839**	0.143	-0.378	0.023	-0.016	0.398			
P	0.185	**0.009**	0.735	0.356	0.956	0.969	0.329			
I_{a2}	**0.714**	-0.096	-0.597	**-0.799**	**-0.761**	0.354	-0.091	0.388		
P	**0.047**	0.821	0.118	**0.017**	**0.028**	0.390	0.831	0.342		
pH start	-0.138	-0.272	**0.674**	**0.805**	0.628	0.100	0.014	0.137	**-0.663**	
P	0.744	0.515	**0.067**	**0.016**	0.102	0.814	0.975	0.746	**0.073**	
pH end	0.269	-0.585	0.390	0.323	0.200	0.479	0.020	0.553	-0.066	**0.762**
P	0.520	0.128	0.339	0.435	0.634	0.230	0.962	0.155	0.877	**0.028**

Table 8: Correlation Matrix : Acidified Media : Scratched Samples: Combined Acid Types

Factors Correlation values P values	Acidified media difference	Delta BC. (cms)	Extension (mm)	Maximum of load: KN	Time of test: (hours).	OCV: (Milli-volts)	E rms* (Volts)	I rms* (Amps)	$Ia_{2:}$ $\log_{10}I$ (amps/cm^2) x time: s)	pH start
P										
Delta BC	-0.502									
P	0.139									
Extension	0.150	**-0.756**								
P	0.680	**0.011**								
Change of load	-0.066	-0.259	0.538							
P	0.857	0.470	0.108							
Time of test	0.140	**-0.777**	**0.997**	0.540						
P	0.700	**0.008**	**0.000**	0.107						
OCV	0.364	-0.385	0.447	-0.171	0.450					
P	0.301	0.271	0.195	0.638	0.192					
E_{rms2}	-0.219	0.237	-0.317	**-0.551**	-0.297	0.239				
P	0.542	0.509	0.372	**0.099**	0.404	0.505				
I_{rms2}	0.229	-0.390	0.024	0.111	0.039	-0.206	0.181			
P	0.524	0.266	0.948	0.761	0.916	0.569	0.617			
I_{a2}	**0.584**	**-0.799**	**0.575**	0.278	**0.571**	0.335	-0.262	0.447		
P	**0.076**	**0.006**	**0.082**	0.436	**0.085**	0.343	0.464	0.195		
pH start	-0.004	-0.096	0.351	**0.656**	0.341	-0.276	**-0.617**	-0.375	0.206	
P	0.991	0.793	0.320	**0.039**	0.335	0.440	**0.058**	0.286	0.568	
PH end	0.247	-0.358	-0.068	0.261	-0.042	-0.489	-0.055	**0.873**	0.394	-0.015
P	0.491	0.310	0.851	0.467	0.908	0.152	0.881	**0.001**	0.259	0.967

2.4.2 Correlation and Regression Predictions of 'Time of Test': Tuna Brine with Added Acetic Acid.

It had been shown in the correlation matrix that the media factor regarding acidification with acetic acid or hydrochloric acid revealed a significant correlation with integrated current I_{a2}, which in turn was correlated with time to failure. The candidate regression predictors therefore required examination by individual acid type. Due to the limitation of numbers in this exercise, this work was restricted to the acetic acid sub group, described below. Prior to regression analyses these sub groups were re-examined for correlations.

The regression options were examined for their relationship to 'time of test' by the methods of stepwise regression, best subsets and in certain individual cases, the partial least squares method within the Minitab statistical package. Because of the limited number of results, only a very small number of candidate predictors could be used among the total for the best subsets method. These were chosen to represent a combination of electro-chemical and physical parameters, where this was consistent with the evidence from the stepwise method and ther correlation information.

2.4.2.1 Non Scratched Samples: Sub Group Acidified with Acetic Acid : Correlations, and Regression Prediction for Time to Failure

The correlation matrix was re-examined for this sub group using a subset of physical and electrochemical parameters, namely: extension, maximum load, time of test, OCV, E_{rms2}, I_{rms2}, I_{a2} and pH start. Notch change is a difficult measurement to make which will be prone to error.

The subset correlation matrix is shown in Table 9 below:

Table 9: Correlation Matrix for Time of test applied to Non Scratched samples Tested in Tuna Media acidified with Acetic Acid to pH 4.5-5.0

Parameter	Extension	Maximum load	Time of test	Open Circuit Voltage	E_{rms2}	I_{rms2}	I_{a2}	pH start
Extension								
P value								
Maximum load	0.470							
P value	0.425							
Time of test	**0.945**	0.580						
P value	**0.015**	0.305						
OCV	-0.763	-0.170	-0.527					
P value	0.134	0.785	0.362					
E_{rms2}	**-0.975**	-0.496	**-0.988**	0.635				
P value	**0.005**	0.395	**0.002**	0.250				
I_{rms2}	-0.380	-0.406	-0.262	0.310	0.237			
P value	0.528	0.498	0.671	0.611	0.702			
I_{a2}	-0.356	**-0.931**	-0.418	0.108	0.329	0.671		
P value	0.557	**0.022**	0.483	0.862	0.589	0.215		
pH start	0.199	**0.888**	0.413	0.142	-0.311	0.022	-0.720	
P value	0.748	**0.044**	0.490	0.820	0.611	0.972	0.170	

It can be seen that there were significant inverse correlations between E_{rms2}, extension and time of test. Regarding maximum load, the correlation with integrated current, I_{a2}, has been retained from the original combined acids matrix, but not that with time of test. The stepwise regression procedure within the Minitab package revealed the following combinations of candidate regression predictors from the above matrix selected, as best choices based upon the P values. See Table 10 below.

Table 10: Data from Stepwise Regression Procedure applied to 7 predictors from Correlation Matrix: Non Scratched Samples.

Number of predictors in regression	Best Predictor options	P value given
1	a) E_{rms2}	0.002
	b) extension	0.015
2	E_{rms2}	0.005
	OCV	0.153*
3	E_{rms2}	0.001
	OCV	0.005
	Ia_2	0.007

* P> 0.100, therefore not significant at 10%.

Other predictors had P values above 0.1 i.e. not significant at 10%.

E_{rms2} as a single predictor is considered later in this section.

The candidate regression from the above combination of 3 predictors is shown below together with statistical details in Tables 11-13.

Regression 1: Time of test: hours = 125 + 0.127*OCV – 17025* E_{rms2}

- $5*10^{-6}$ *Ia_2.

Table 11: Regression Table for Regression 1

Predictor	Coefficient	Standard error of coefficient	T	P value
Constant	125.067	0.654	191.16	0.003
OCV	0.127330	0.000933	136.41	0.005
E_{rms2}	-17025.0	19.2	-888.93	0.001
I_{a2}	-0.00000482	0.00000005	-94.60	0.007

R-Sq = 100% R-Sq(adj) = 100 R-Sq (pred) = 99.97%.

Table 12: Analysis of Variance for Regression 1

Source	Degrees of freedom	Sum of squares	Mean square	F value	P value
Regression	3	120.671	40.224	446103.64	0.001
Residual error	1	0.000	0.000		
Total	4	120.671			

The P values from the regression table indicated that all predictors were significant at 1%, and the R^2 adjusted value shows that for predictions was very high. However, this is based on very limited data of 5 results and is over fitted but has been included as a candidate because of the very high R^2 value for predictions.

The ANOVA table confirmed significance of the regression at 1%. In this case the

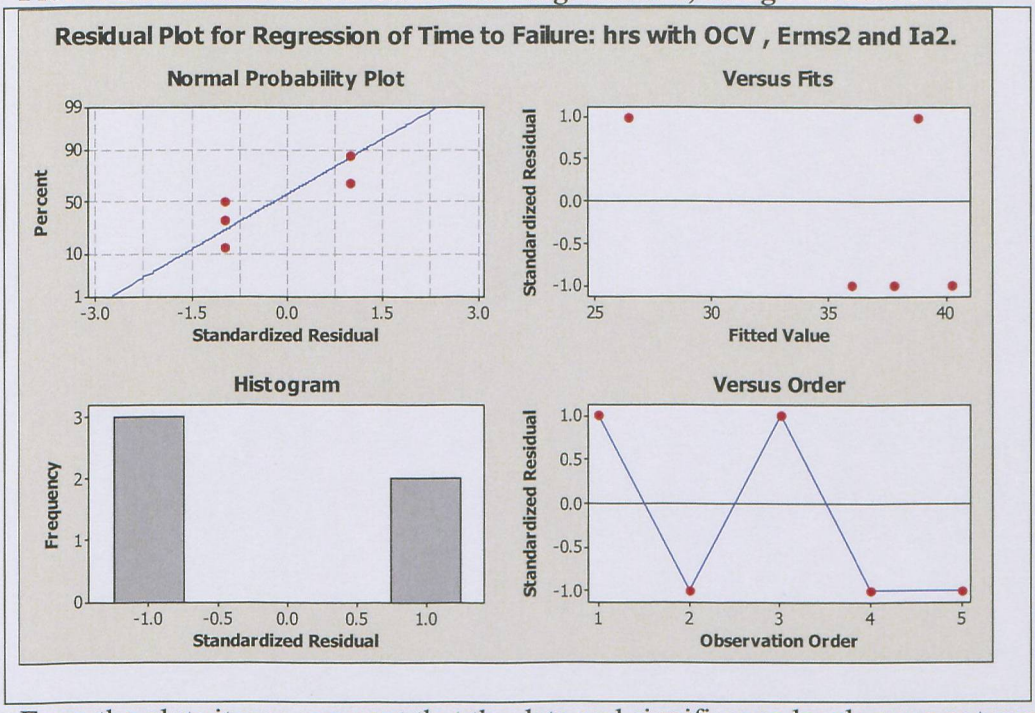
residuals did not follow close to a normal pattern and the statistical package indicated one unusual observation giving a large leverage. This is shown below:

Table 13: Details of unusual observation for Regression 1

Observation	OCV	Time of test: hours	Fit: hours	Standard error of fit	Residual	Standardised residual
5.	-687	40.25	40.2505	0.0095	-0.0005	-1.00

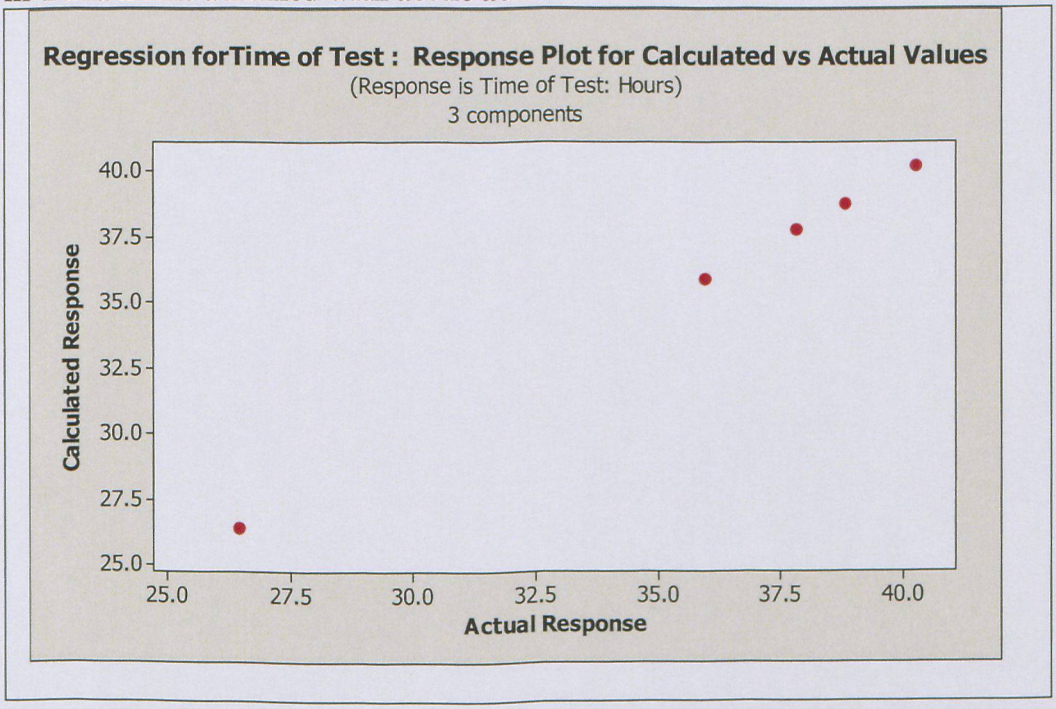
This appears to have arisen because a different result at similar OCV was associated with a very short test time. The residuals plot, Plot 7, is shown below:

Plot 7: Residuals Plot for Candidate Regression 1, using 3 Predictors



From the plots it was apparent that the data and significance levels were not supported by a central tendency of the residuals. Nevertheless, the partial least squares response, Plot 8, below would still suggest that the prediction is a candidate for further study using the acidified media, since linearity between calculated and actual responses was apparent.

Plot 8: Partial Least Squares Response Plot of Calculated vs Actual Time of Test values for Regression 1 with OCV, E_{rms2} and Ia_2 for Non Scratched Samples tested in Tuna Brine acidified with acetic acid.



Referring back to the stepwise regression significance table it was clear that E_{rms2} emerged as a strong predictor in this particular analysis. Given the objective of the study to better understand an environmental stress cracking failure, a primary candidate regression option should be one combining a physical parameter related to stress and a chemical or electrochemical parameter, assuming that a degree of environmental stress cracking took place. For best subsets, a combination of predictors not exceeding 3 required to be chosen and additional cases were examined by iteration of candidate regressions. The best subsets results are shown below, Table 14, for the candidate predictors of extension, $Erms_2$ and Integrated current, Ia_2.

Table 14: Best Subsets Regression table for three chosen parameters subsequent to the Stepwise Regression Procedure: Non Scratched Samples: Acetic acid addition.

Subsets	Rsq	Rsq adj	Mallows Cp	Standard deviation	Extension.	E rms_2	Ia_2
1	97.6	96.89	6.6	0.97634		x	
2	89.3	85.7	33.6	2.0786	x		
3	98.6	97.2	5.5	0.91593		x	x
4	98.4	96.7	6.3	0.99265	x	x	
5	99.7	98.8	4.0	0.61228	x	x	x

From this regression table, while R^2 adjusted values were all high, the Mallows Cp values were too high except for subset 5, relative to the guideline of 'number of predictors plus one'. This commonly indicates that other factors required to be taken into account. It was found that for subsets 4 and 5, the inclusion of extension was associated with an inverse effect on time to failure, whereas a direct effect was indicated from correlation data. For subset 3 the addition of E_{rms2} to I_{a2} lead to the latter not being significant within the regression. For subset 2, a very low R^2 adjusted value for prediction was in accord with a high Mallows value indicating other missing parameters. On this basis, the regression equation for subset 1 appeared to be the best candidate and is shown below, together with statistical details in Tables 15-16.

Regression 2: Time of test = 39.7 - 15911* E_{rms2}

Table 15: Regression Table for Regression 2

Predictor	Coefficient	Standard error of coefficient	T	P value
Constant	39.6615	0.5550	71.46	0.000
E_{rms2}	-15911	1431	-11.12	0.002

R-Sq = 98.4% R-Sq(adj) = 96.7% R-Sq (pred) = 89.21%

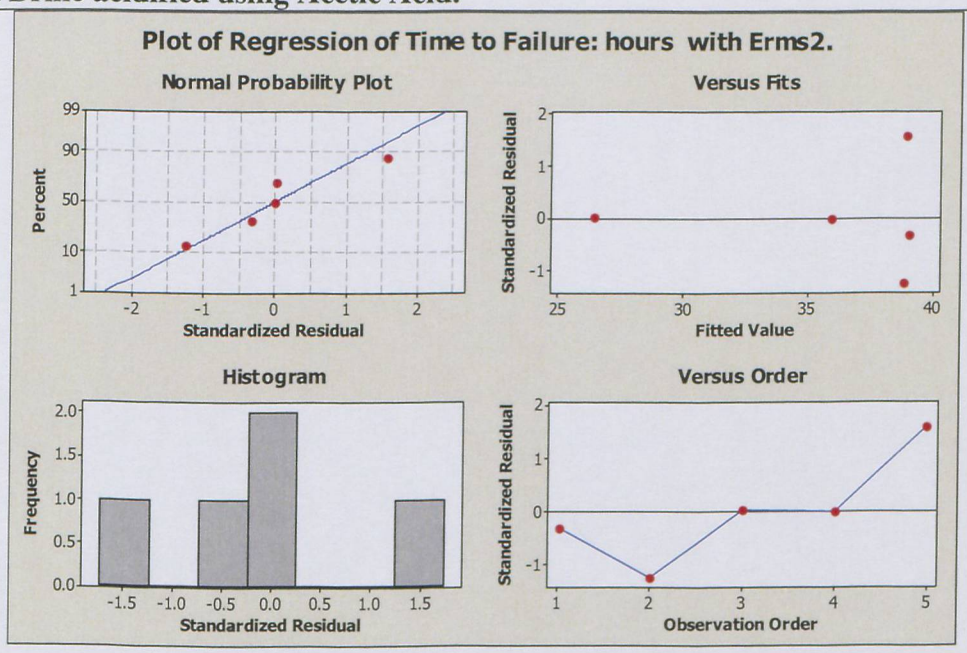
Table 16: Analysis of Variance for Regression 2

Source	Degrees of freedom	Sum of squares	Mean square	F value	P value
Regression	1	117.81	117.81	123.59	0.002
Residual error	3	2.86	0.95		
Total	4	120.67			

There was no evidence of lack of fit in the lack of fit test (P >= 0.1).

The regression table P values showed that E_{rms2} was significant at the 1% level , and the ANOVA test showed that regression as a whole was significant at the 1% level. The R^2 adjusted value showed that over 89% of the variability in time of test could be accounted for by the E_{rms2} parameter. The residual plots are shown in Plot 9 below.

Plot 9: Residuals for Subset 1, Table 14 : Regression of Time of Test with E_{rms2} for Tuna Brine acidified using Acetic Acid.



The residual plots above indicated that although data were limited, the residuals showed quite close conformance to the normal probability plot, also having a central tendency, and so this regression would be a candidate for further study.

Regarding the likely reasons why E_{rms2} would show an inverse influence on time to failure at constant cross head speed, the E_{rms2} changes signify the effect of local potential variations of the test sample, which lead to instantaneous current changes, requiring balancing currents to be provided by the potentiostat to restore the potential to the set value of the OCV determined at 30 minutes. These effects lead to a finite distribution of OCV and the larger the E_{rms2} value, the greater the likely current variation. However, I_{rms2} has not correlated with failure time; this might have depended on the balance between positive and negative current pulses which is not identified by I_{rms2} as a root mean square parameter.

2.4.2.2 Correlation and Regression Predictions: Tuna Brine with Acetic Acid added: 'scratched' samples.

The subset of correlations for scratched samples were re-examined as for non scratched samples for the group acidified with acetic acid. This gave the following matrix shown as Table 17. There were 6 test data points.

Table 17: Correlation Subset Matrix for Tuna Brine Samples Tested, after Acidification with Acetic Acid to pH 4.5-5.0 : Scratched Samples.

Parameter	Extension	Maximum load	Time of test	Open Circuit Voltage	E_{rms2}	I_{rms2}	I_{a2}	pH start
Extension								
P value								
Maximum load	0.580							
P value	0.227							
Time of test	**0.998**	0.570						
P value	**0.001**	0.238						
OCV	**0.787**	0.099	**0.784**					
P value	**0.063**	0.852	**0.065**					
E_{rms2}	-0.365	-0.666	-0.339	-0.325				
P value	0.477	0.149	0.511	0.529				
I_{rms2}	-0.016	0.170	0.006	-0.523	0.539			
P value	0.975	0.747	0.991	0.287	0.270			
I_{a2}	0.607	0.479	0.617	-0.261	-0.270	0.390		
P value	0.202	0.337	0.192	0.617	0.605	0.444		
pH start	0.435	0.617	0.409	0.366	**-0.981**	-0.469	0.427	
P value	0.389	0.192	0.421	0.476	**0.001**	0.349	0.399	

From this matrix it was apparent that only four correlations existed which were significant at the 10% level or higher, involving the direct effect of extension and OCV on time of test, the inter-correlation of OCV with extension, and the inverse relationship of pH to E_{rms2}. The stepwise regression procedure revealed just two individual significant parameter effects from the above candidates, as shown in the Table 18 below.

Table 18: Data from Stepwise Regression Procedure applied to 7 predictors from Correlation Matrix: Scratched Samples

Number of predictors in regression	Best Predictor options	P value given
1	a) Extension	0.000
	b) OCV	0.065

All other parameter effects gave P values > 0.100.

The best subsets regression was tested as for the non scratched samples but adding further variables of pH and E_{rms2}, each of these having shown significance in the correlation table. This following matrix, Table 19, was obtained.

Table 19: Best Subsets Regression Table for four chosen Parameters subsequent to the Stepwise regression Procedure: Scratched Samples.

Subsets	Rsq	Rsq adj	Mallows Cp	Standard deviation	Extension	OCV	E_{rms2}	pH
1	99.7	99.6	-0.7	0.64742	x			
2	61.5	51.9	149.9	0.69717		x		
3	99.7	99.6	1.0	0.65343	x			x
4	99.7	99.6	1.0	0.65610	x		x	
5	99.7	99.4	3.0	0.80013	x	x		x

From this matrix, therefore, extension remained the dominant predictor. OCV by itself was a relatively weak predictor with R^2 adjusted only just above 50%. Although E_{rms2} when combined with extension gave a similar standard deviation, the regression would not be enhanced. In terms of examining whether a purely electrochemical combination

of parameters could be fitted to a regression for time to failure as for the non scratched samples, iterative work using combinations of OCV, E_{rms2}, I_{rms2} and pH revealed the best fit for data recorded was obtained using OCV, E_{rms2} and I_{rms2}.

The Regression 3 equation is shown below together with statistical details in tables 20-21.

Regression 3: Time ot test : hours (scratched) = 828 + 1.12*OCV – 147517*E_{rms2} + 13529*I_{rms2}

Table 20: Regression Table for Regression 3 : Scratched samples

Predictor	Coefficient	Standard error of coefficient	T	P value
Constant	828.21	92.69	8.94	0.012
OCV	1.1166	0.1336	8.36	0.014
E_{rms2}	-14517	45404	-3.25	0.083
I_{rms2}	13529	2453	5.51	0.031

R^2 = 97.7% R^2 (adj) = 94.2 R^2 (predictions) = 0.00%.

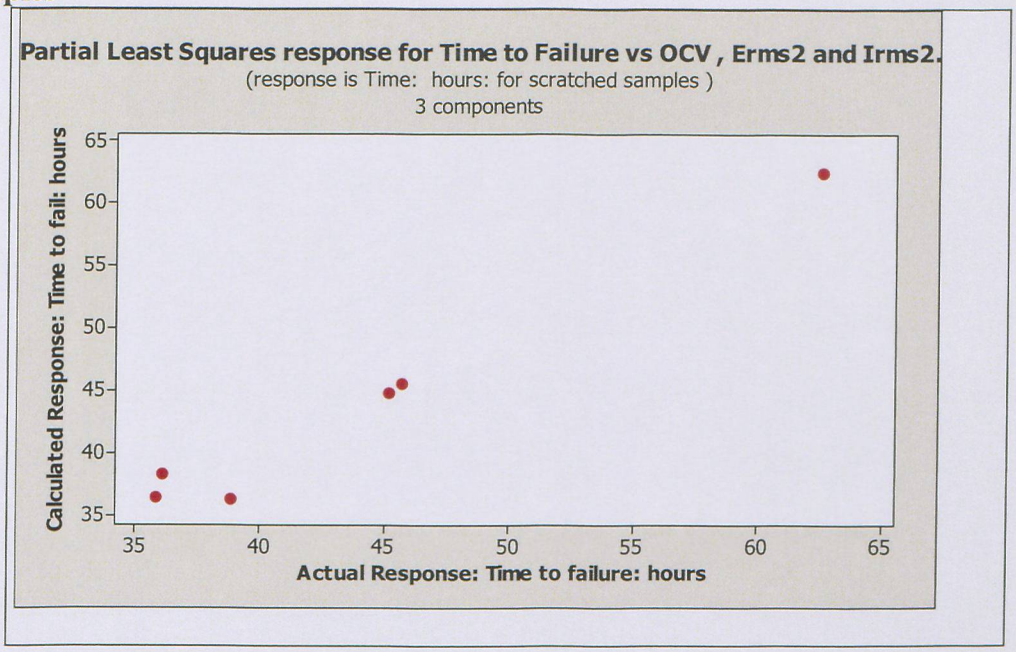
Table 21: Analysis of Variance Table for Regression 3: Scratched samples

Source	Degrees of freedom	Sum of squares	Mean square	F value	P value
Regression	3	493.68	164.56	28.0	0.035
Residual error	2	11.76	5.88		
Total	5	505.44			

The P values in the regression table 20 showed that all individual parameters were significant at 10%, P< 0.100 or a higher level. From R^2 values, the regression was sufficient to explain around 94% of variability in time to failure from the data obtained, but had no capability regarding prediction. The Analysis of variance table 21 indicated that the regression was significant at the 5% level (P =0.035).

The partial least squares response, Plot 10, is shown below for Regression 3.

Plot 10: Partial Least Squares Regression Response for Regression 3: Scratched samples



As the failure time became longer, this plot was sufficiently supportive of the linear relationship, to suggest that it would be a candidate for further examination should the work on scratched samples be taken further.

2.4.3 Discussion of Statistical Information from Initial Slow Strain Rate Tests

The mean failure time for 6 non scratched samples was 35.86 hours as compared with 42.29 hours for the mean of 5 scratched samples tested. A two sample statistical t test comparison of means was not significant at 10% on the hypothesis of no difference, using a 2 tail test. Nevertheless, a measurable indication of a greater mean failure time for scratched samples has been suggested by the data, although not sufficient for significance. The logic of this is considered below.

The failure time will almost certainly be critically determined by the combination of stress and corrosion effects at the notch area including any 'conjoint' action, leading to failure initiation. This is because of stress concentration created by a notch and the

initiation of corrosion, as passivation protection on the eccs surface breaks down under plastic strain just ahead of the notch. Once a crack at the notch vicinity has commenced, the stress intensity factor K_I rises in proportion to $\sqrt{a}$, a being the crack length, so that the propagation rate will accelerate with crack length. Regarding the test data for the non scratched samples, albeit limited, regressions with substantial R^2 values for predictions were possible involving electrochemical parameters, as well as for extension, although when combinations of extension and electrochemical parameters were attempted the fit was poor. This is not surprising, in view of the limited data and that at this stage, computation of the 'work of deformation' had not been made, this being a more complete description of what takes place than load or extension effects alone. This parameter is included in Section 3 studies. The non-scratched samples e.g. for the acetic acid sub group, had shown significant inverse correlations involving some electrochemical parameters, including E_{rms2} with time of test and Ia_2 with maximum load. Larger E_{rms2} values would imply the occurrence of spontaneous and increasing balancing current requirements to maintain the set potential, while increasing integrated current can indicate more dissolution which could reduce maximum load achieved. There was significant evidence of pitting attack on the test samples. In the event of negative current, decomposition of cathodic species at the metal surface is implied, which could include that of hydrogen gas in acidified brines, but for complex food media other reactions may be possible.

Considering the scratched samples for the acetic acid sub group, the only electrochemical parameter correlating with time of test was Open Circuit Voltage and this was found to be a relatively weak predictor of time to failure based on the best subsets statistics data. An implication, therefore, was that resulting from scratching, corrosion was more widely distributed on the sample at this region than for the non-scratched samples, where attack in the notch vicinity would have predominated.

Hence, it can be suggested that less locally intense corrosion took place at the notches to assist the onset of failure in scratched samples leading to longer failure times, and for non scratched samples, more localised attack at these regions assisted failure initiation, and reduced mean failure times observed. Greater correlation evidence of electro-chemical parameters with failure time was also observed e.g. for the acetic acid sub group on non scratched samples, and this could be translated into significant regression equations with more predictive capability than was the case for corresponding non scratched samples.

On the evidence considered at this stage, it appeared preferable to use 'non-scratched' samples in further work for this type of test where regression predictions for time of failure including electrochemical parameters are sought.

2.4.4 Observations from Microscopy on Slow Strain Rate Tested Samples: 'Non Scratched' Sub Groups.

Samples representative of each condition tested using the slow strain rate method were examined using the Scanning Electron Microscope for indications of loss of ductility and environmental stress cracking. The evidence is summarised in the following paragraphs:

There were visual indications of loss of ductility affecting both the two acidified categories of sample. No conclusive evidence was established for environmental stress cracking concerning the two non acidified samples tested, nos ssrttu 056 and 057; one of these was an incompletely failed sample. Loss of ductility was apparent at the notch region for the acidified samples by comparison with the two control samples tested in air, i.e. not in contact with any product brine media. Examples are discussed below.

Figure 21 and 22 show images of a control sample of the the same 0.19mm DR 520 CA material as was used in the tests, displaying ductile failure at the notch region. The % thickness reduction at the fracture area adjacent to the notch relative to the mid point of the notch region was approximately 59.52%. Figure 23 shows an image of a duplicate test sample N7, using the same material, showing an estimated % thickness reduction at the fracture of 55.7% relative to the mid region of the notch.

Figure 21: Image of Failure region adjacent notch on Control Sample N16, after Slow Strain Rate Testing under Air Conditions.

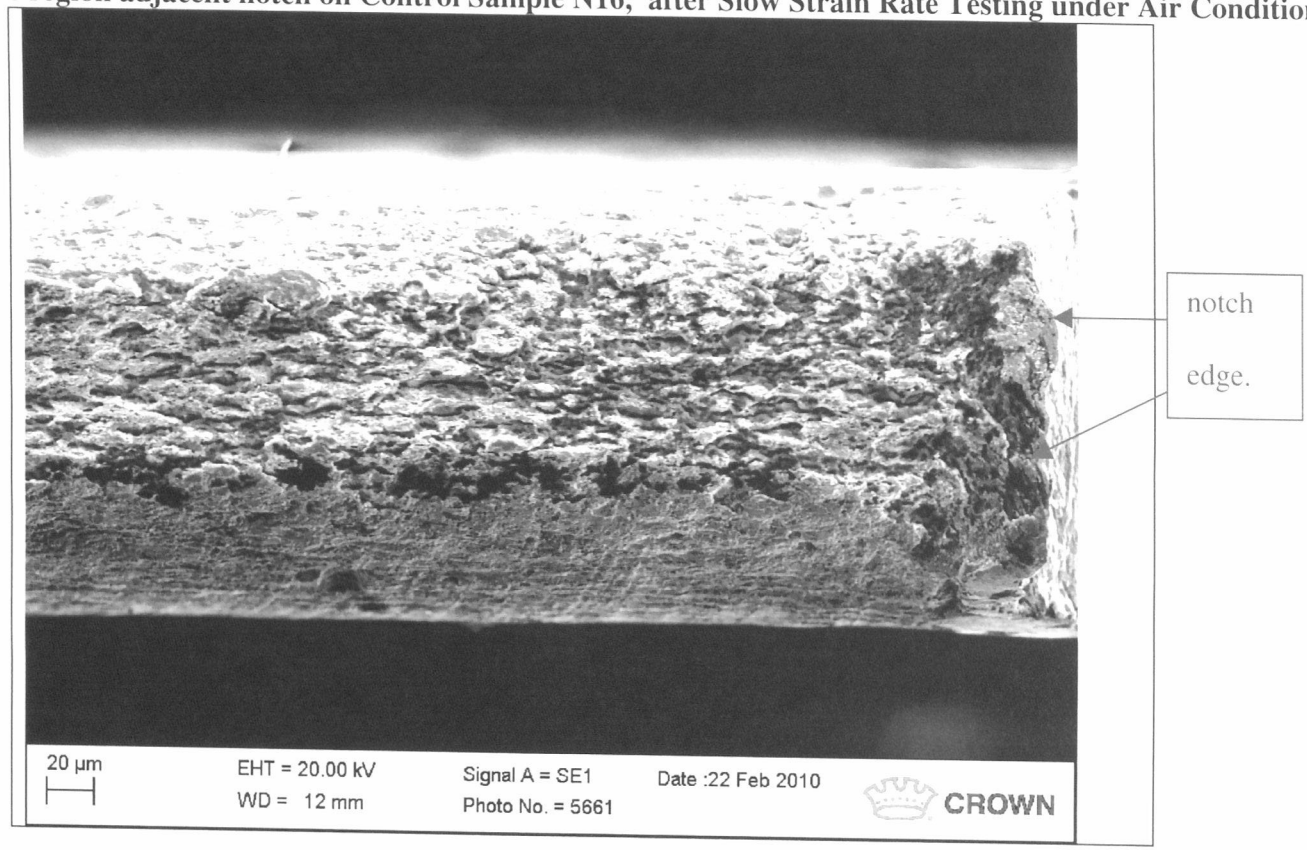


Figure 22: Image of failure region asdjacent notch on Control Sample N16, after slow strain rate testing under Air Conditions: Larger magnification.

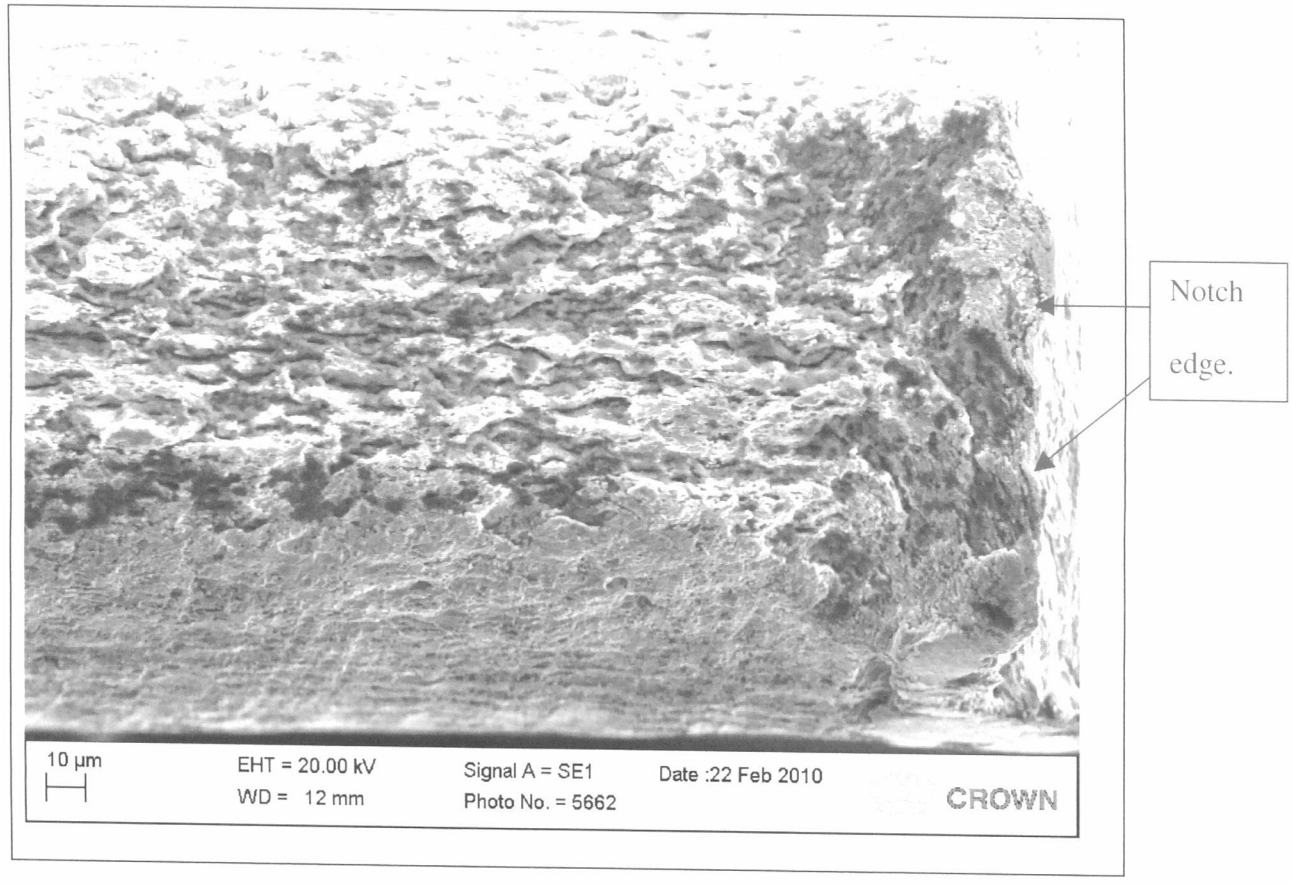
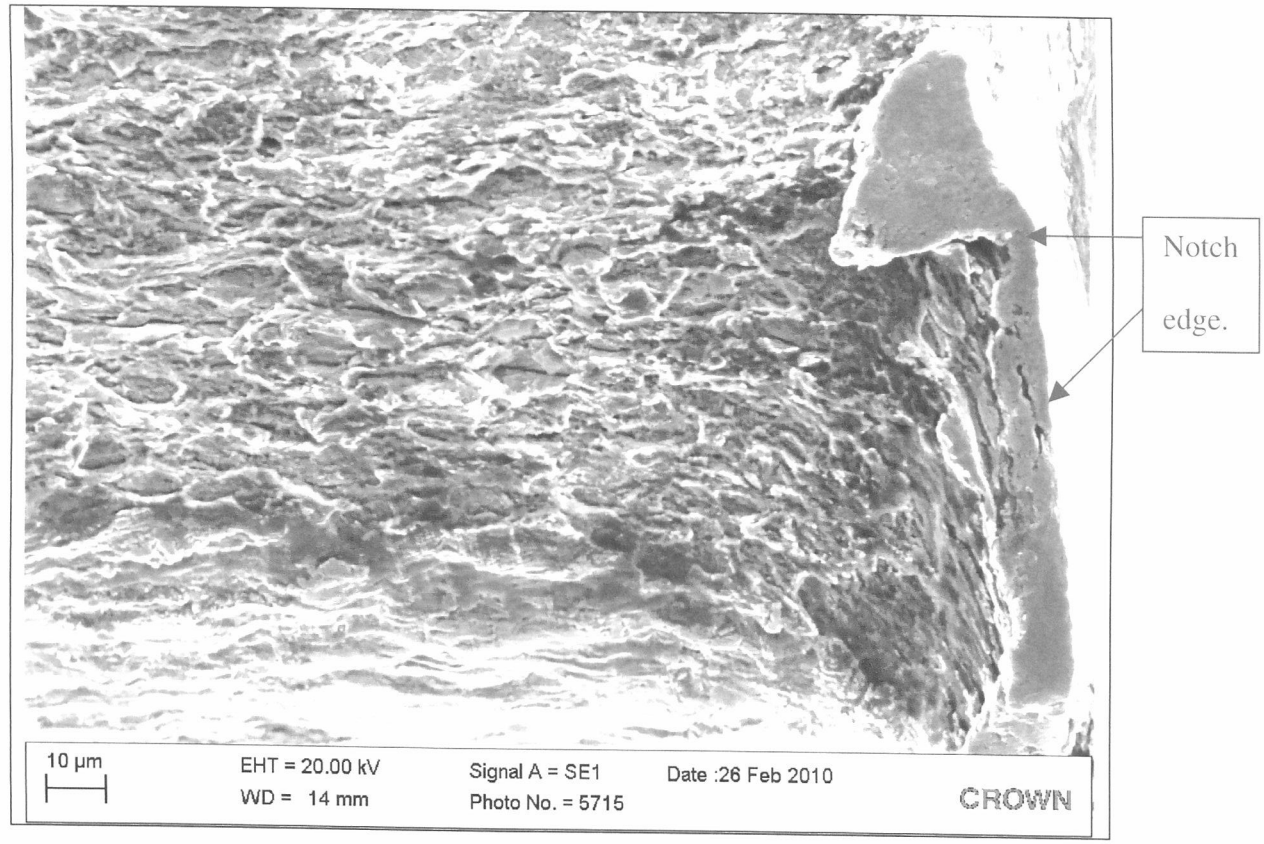


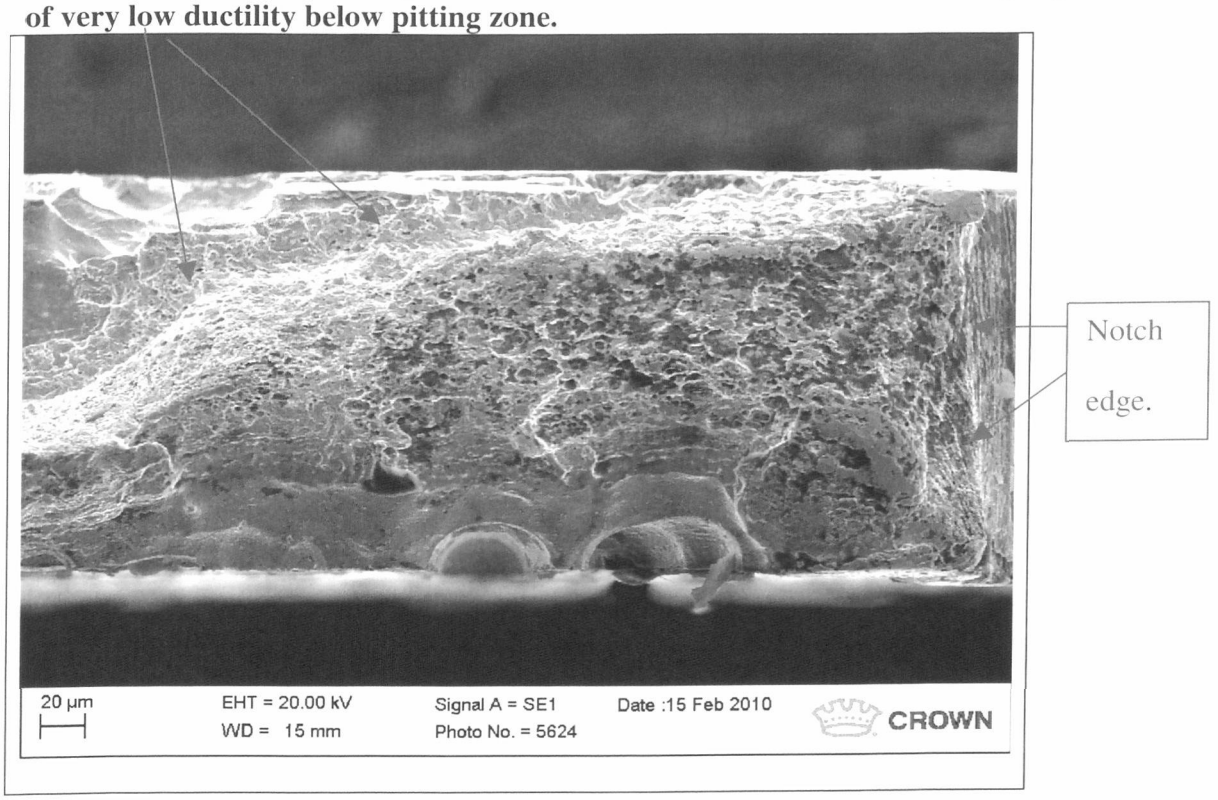
Figure 23: Image of failure region asdjacent notch on Control sample N7, after slow strain rate testing under Air Conditions: Larger magnification.



Images obtaned from corresponding samples tested in tuna brine and acidified tuna brine were compared with the above. For the tuna samples tested without acidification and without scratching it was not conclusively shown that envirnomental stress cracking was present on the two samples tested, but for acidified samples a number of significant observations were made. Examples from tests using the tuna brine acidified with acetic acid are shown in Figures 24-26 below.

Figure 24 illustrates some regions of low ductility at low magnification on sample ssrttu047

Figure 24: Sample ssrttu047: Slow Strain Rate Tested Sample: Tuna Brine acidified with acetic acid to pH 4.68. Notch area fracture surface showing regions of very low ductility below pitting zone.



Figures 25 and 26 below illustrate the corresponding sample at higher magnification. These show more distinctive evidence of steps and ledges, consistent with trans-granular environmental stress cracking.

Figure 25: Sample ssrttu047: Slow Strain Rate Tested Sample: Tuna Brine acidified with acetic acid to pH 4.68. Fracture surface near notch area showing regions of Environmental Stress Cracking. Larger magnification.

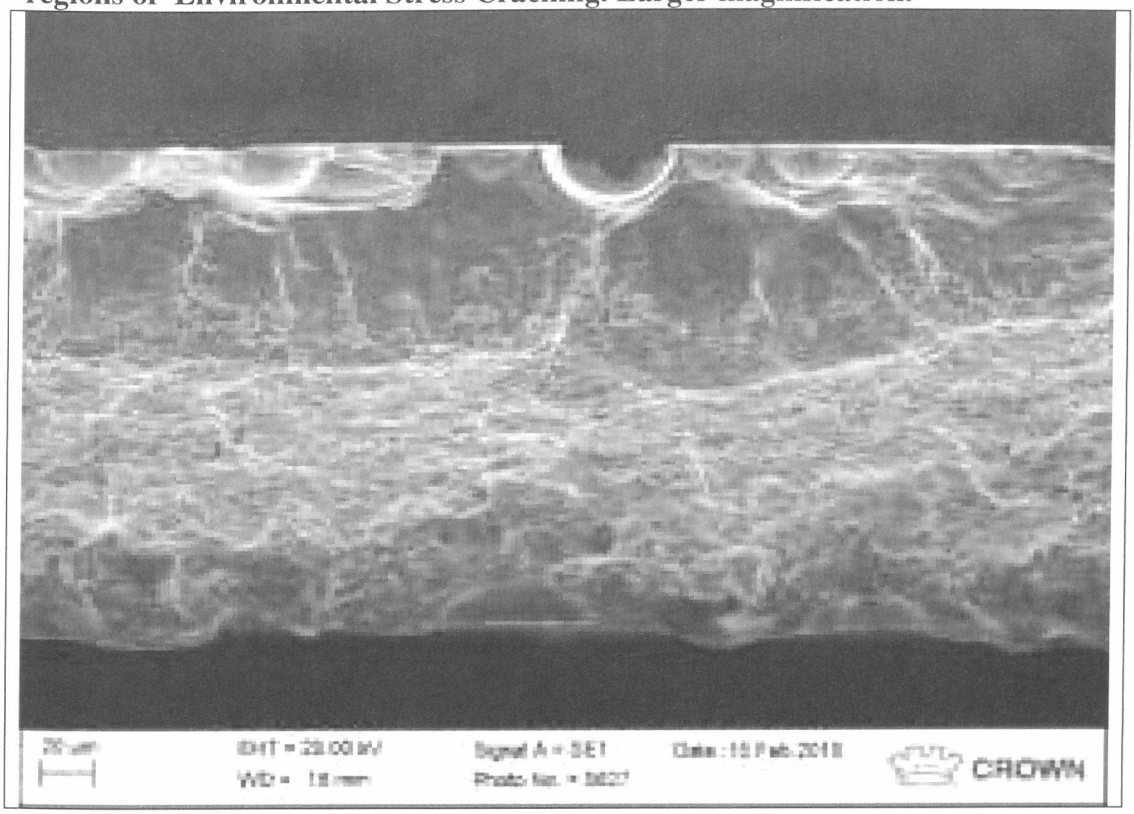
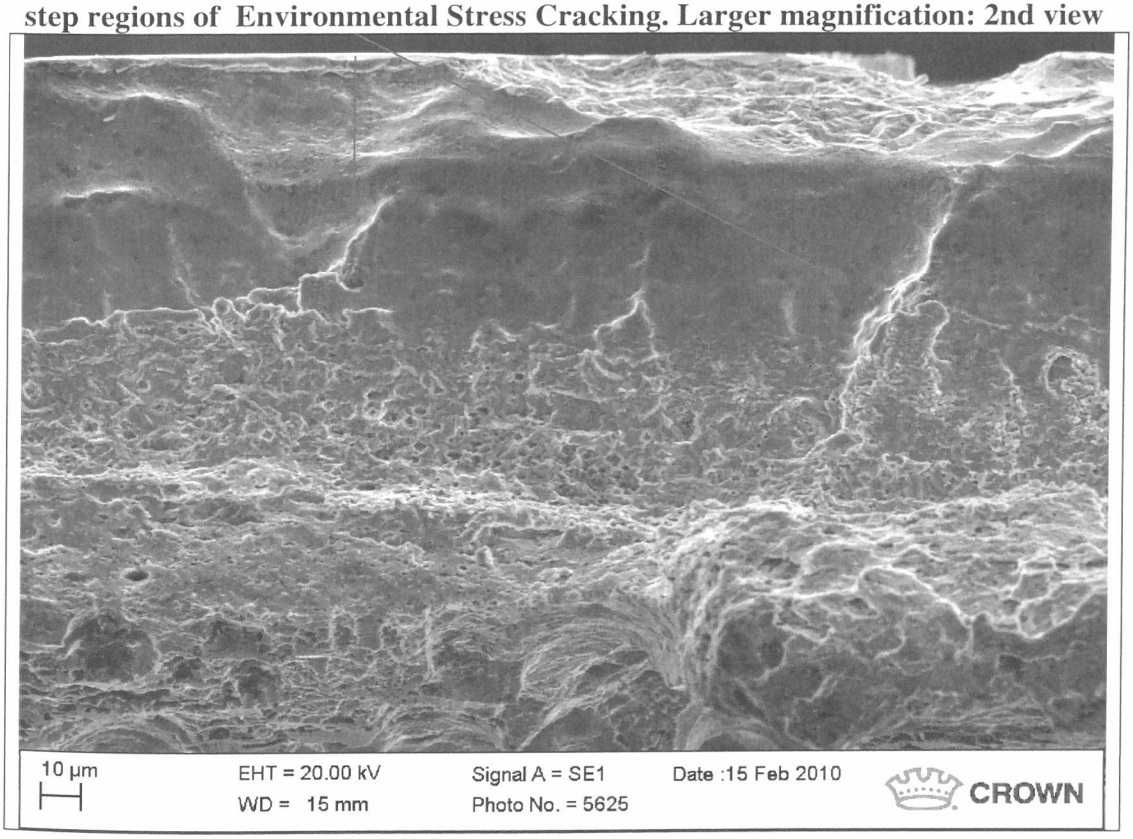


Figure 26: Sample ssrttu047: Slow Strain Rate Tested Sample: Tuna Brine acidified with acetic acid to pH 4.68. Fracture surface near notch area showing step regions of Environmental Stress Cracking. Larger magnification: 2nd view



Figures 27 and 28 below show that similar observations were replicated on sample ssrttu049 belonging to the same group acidified with acetic acid.

Figure 27: Sample ssrttu049. Slow Strain Rate Tested Sample: Tuna Brine acidified with acetic acid to pH 4.68. Fracture surface near notch area showing zone of low ductility.

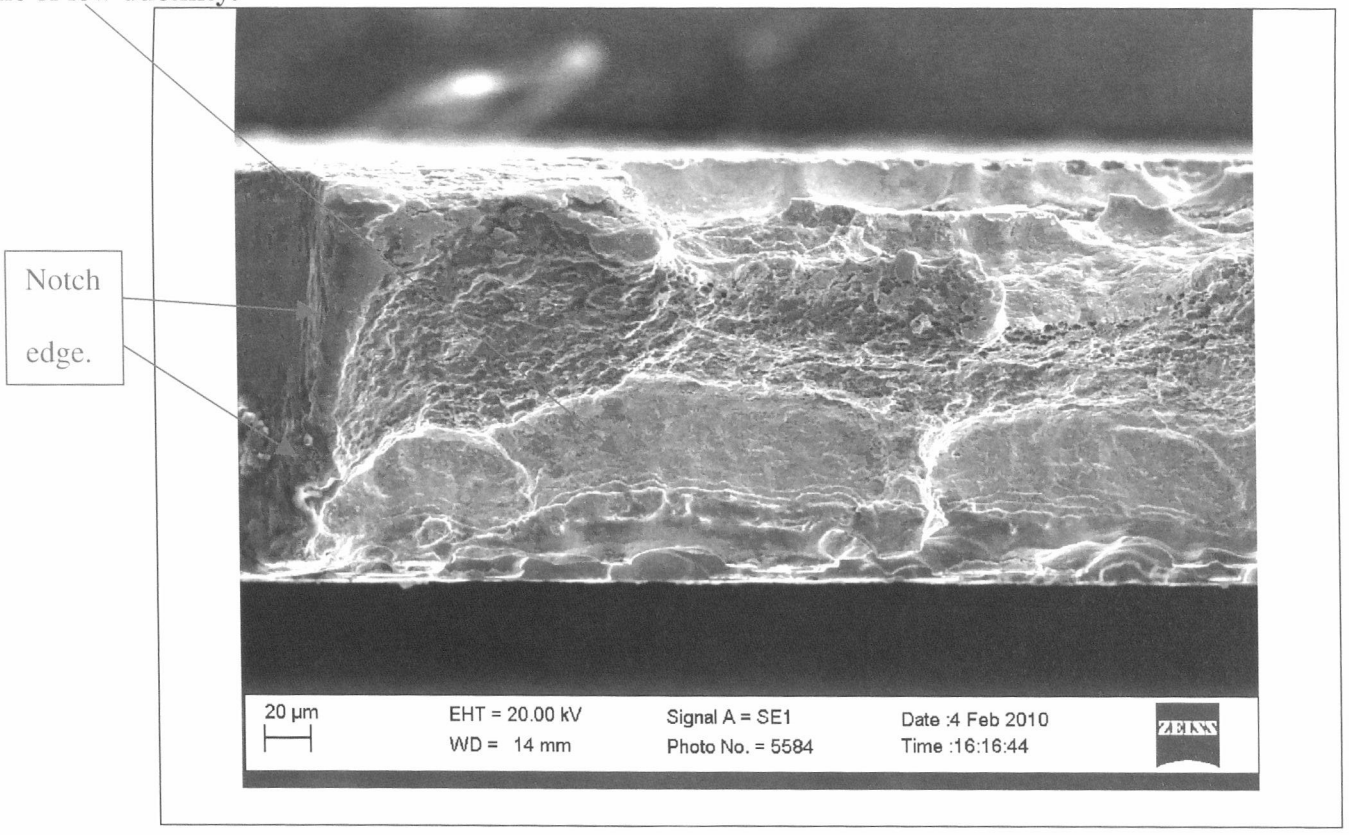
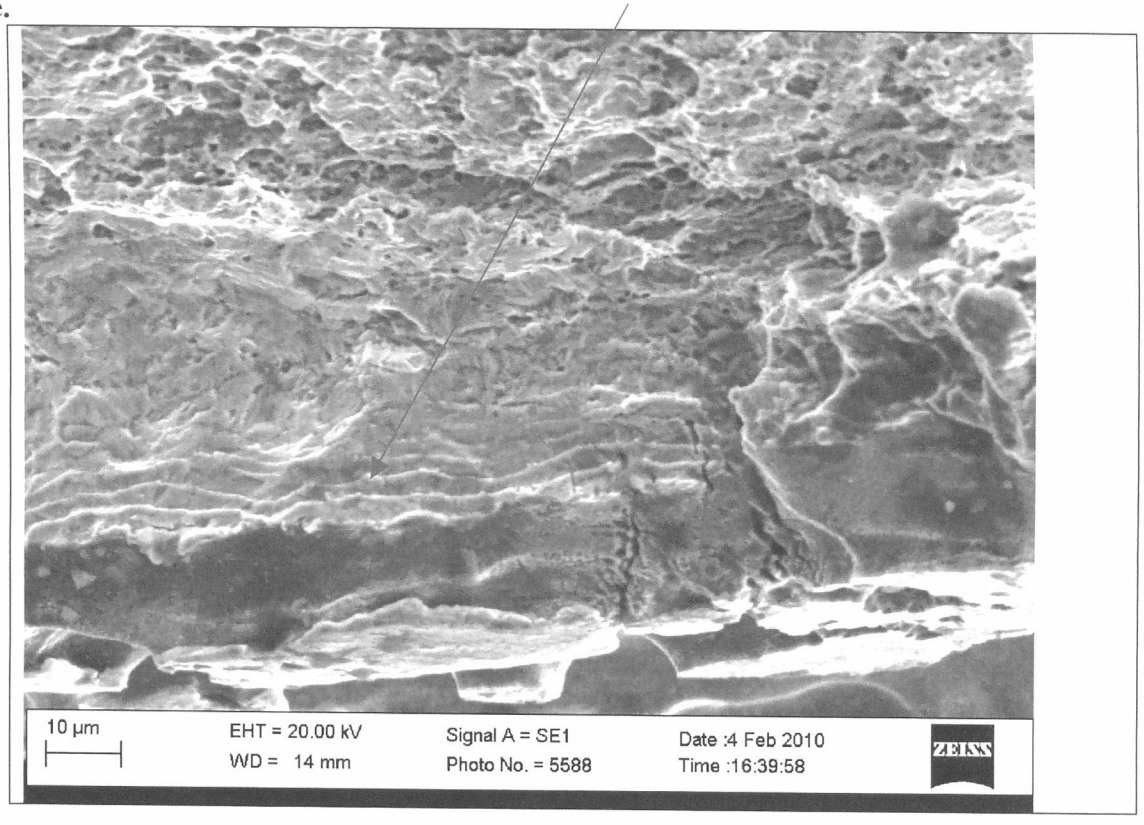


Figure 28: Sample ssrttu049 Larger magnification of Figure 30 showing step fracture consistent with trans-granular environmental stress cracking near fracture edge.



For samples tested after acidification of tuna brine with hydrochloric acid, degrees of quite similar effects to those reported above have been observed, as shown in Figures 29 and 30 for sample ssrttu049 and ssrttu054 respectively, each to a limited extent. More distinctive evidence can be seen in Figures 31 and 32 for sample ssrttu055 where both loss of ductility and environment stress cracking characteristics were clearly discernible from fracture steps or ledges.

Figure 29: Sample ssrttu049. Slow Strain Rate Tested Sample: Tuna Brine acidified with hydrochloric acid to pH 5.01. Fracture surface near notch area showing zone of low ductility.

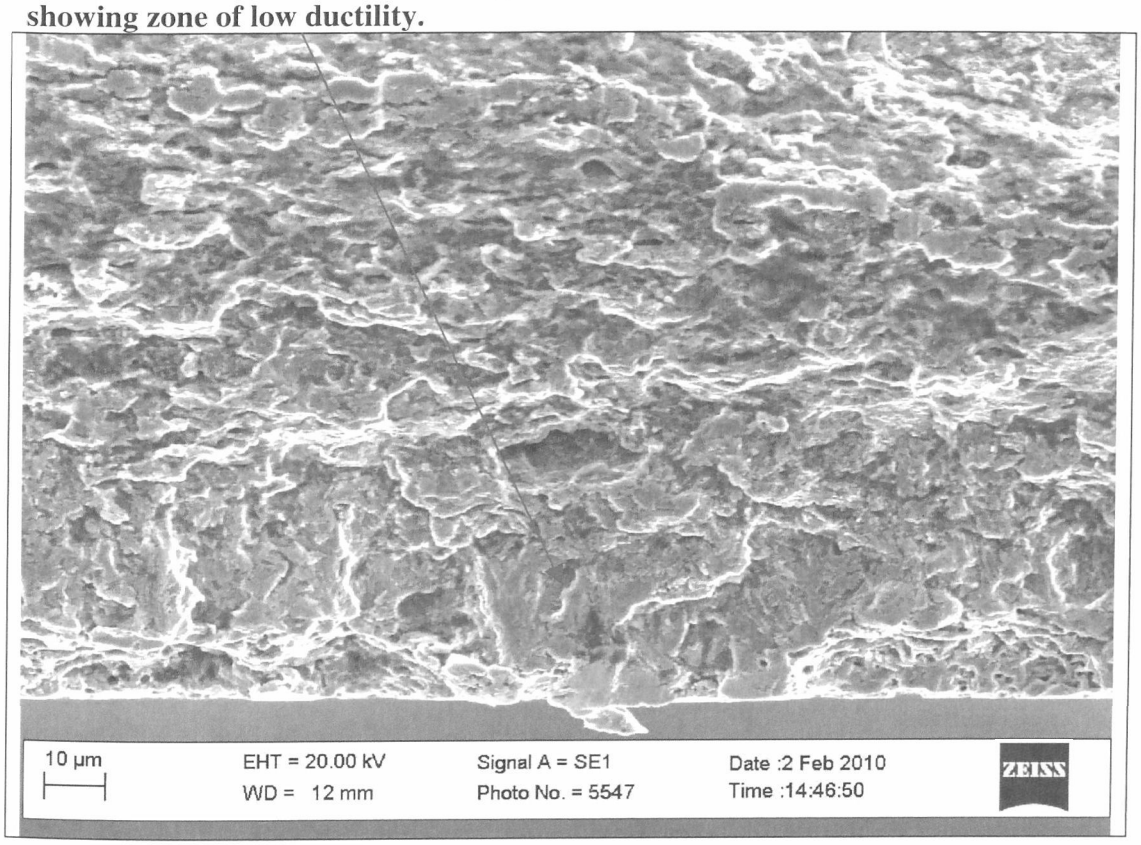
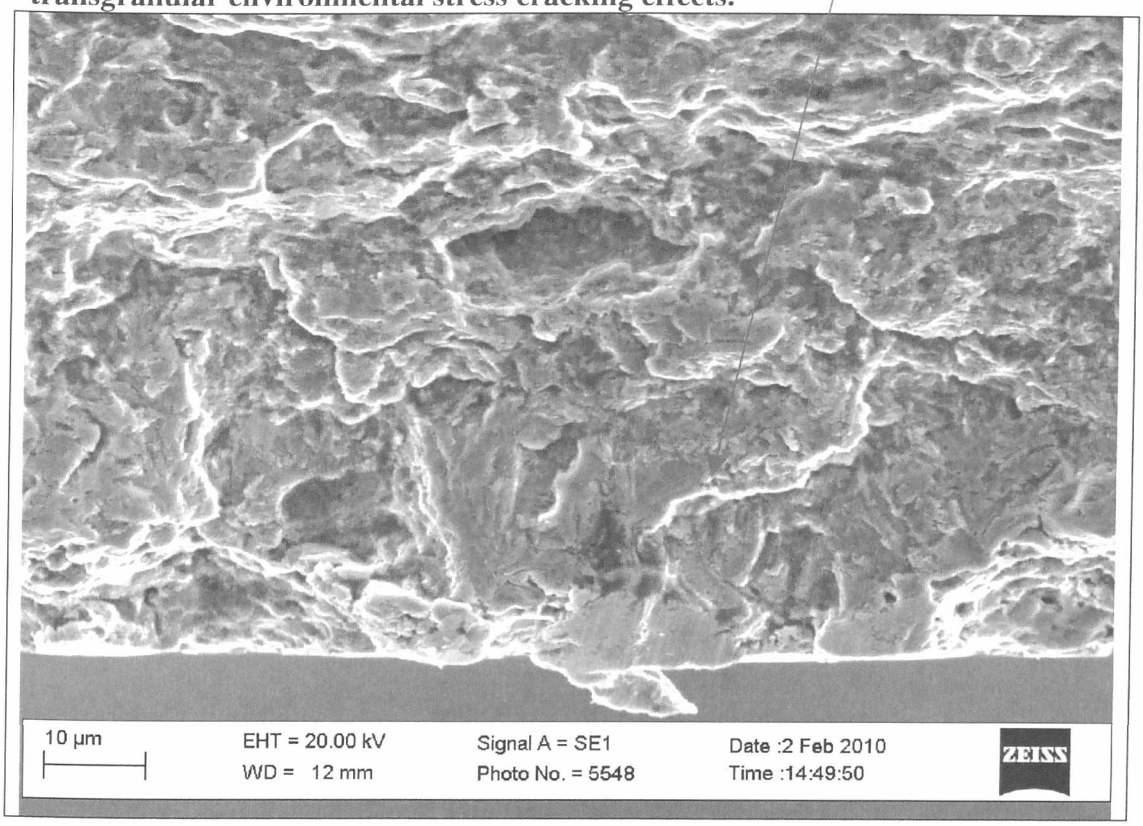


Figure 30: Sample ssrttu054. Slow Strain Rate Tested Sample: Tuna Brine acidified with hydrochloric acid to pH 5.01. Larger magnification view of fracture surface near notch area showing zone of low ductility, and ledges consistent with transgranular environmental stress cracking effects.



The sample shown below, Figures 31 and 32, representing a duplicate case for sample ssrt tu054 revealed another aspect that has been observed intermittently, namely that loss of ductility was not always apparent uniformly across the entire specimen section thickness, but may predominate towards one edge. Because the specimens had one face towards the counter electrode, there was a tendency for more corrosion to take place at this face and in the event of a hydrogen embrittlement phenomenon, this could contribute to different behaviour across the section thickness.

Figure 31: Sample ssrttu055. Slow Strain Rate Tested Sample: Tuna Brine acidified with hydrochloric acid to pH 4.56. View of fracture surface near notch area showing zone of low ductility, and ledges consistent with transgranular environmental stress cracking effects. More ductility was indicated at the opposite fracture edge.

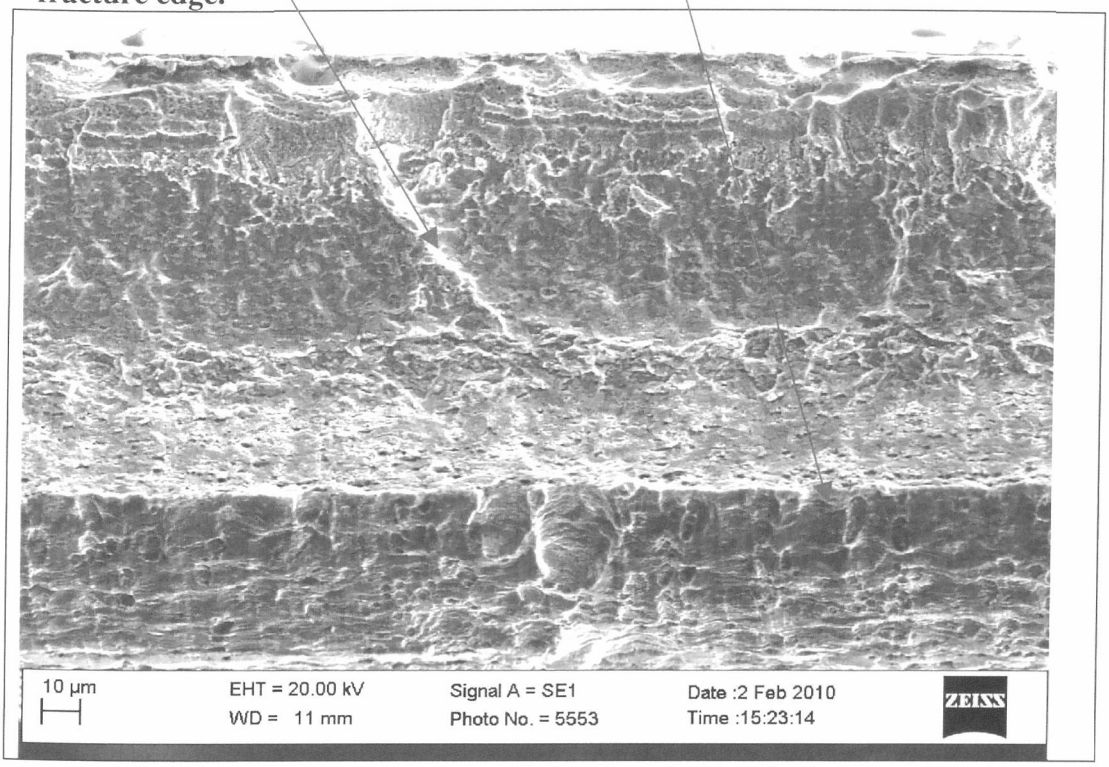
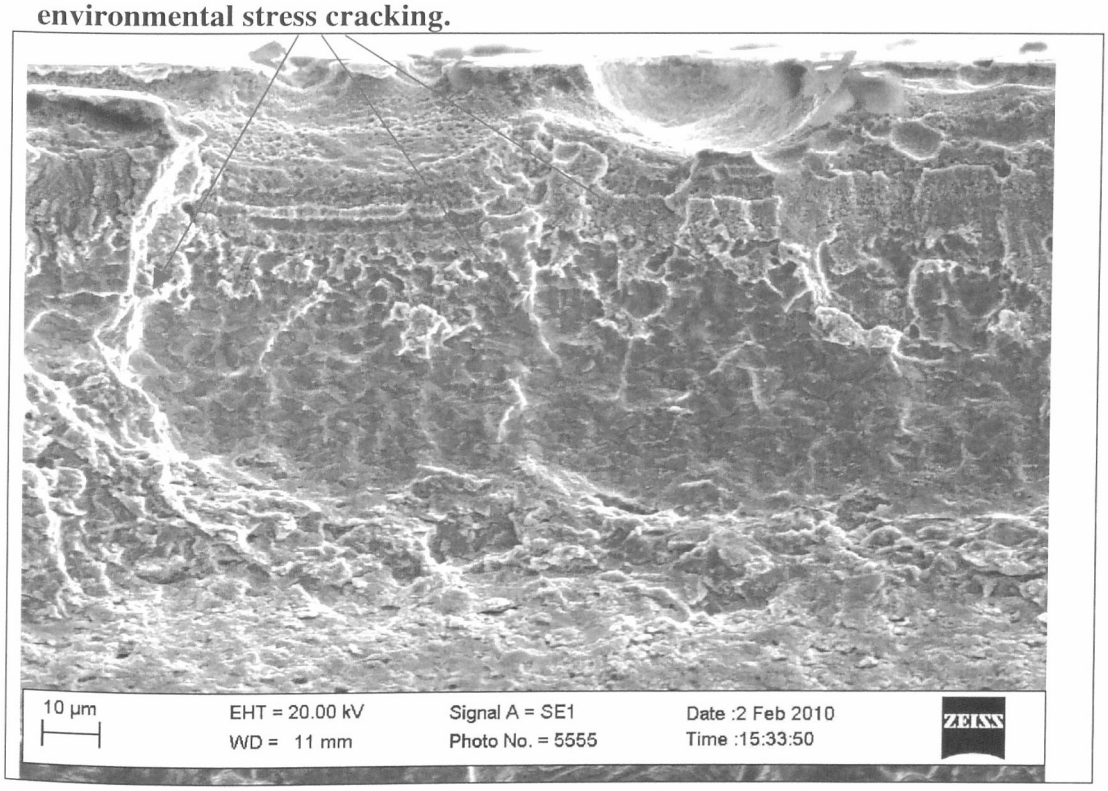


Figure 32: Sample ssrttu055. Larger magnification view showing low ductility behaviour and step fracture conditions consistent with trans-granular environmental stress cracking.



2.4.5 Observations from Microscopy on Slow Strain Rate Tested samples: 'Scratched' Sub Groups.

In this case, one of the tuna samples tested without acidification displayed a rather distinctive loss of ductility with a small area of fan shaped cracking. See Figures 33 and 34. While it has not been proved that the fan shapes could not possibly be product residues, these areas did not show evidence of very light regions characteristic of surface contaminaton giving rise to charging effects, although some such effects were apparent adjacent to these areas.

Figure 33: Sample ssrttu041. Slow Strain Rate Tested Sample: Tuna Brine non acidified. View of fracture surface near notch area showing zone of low ductility, and ledges and fan shapes consistent with transgranular environmental stress cracking.

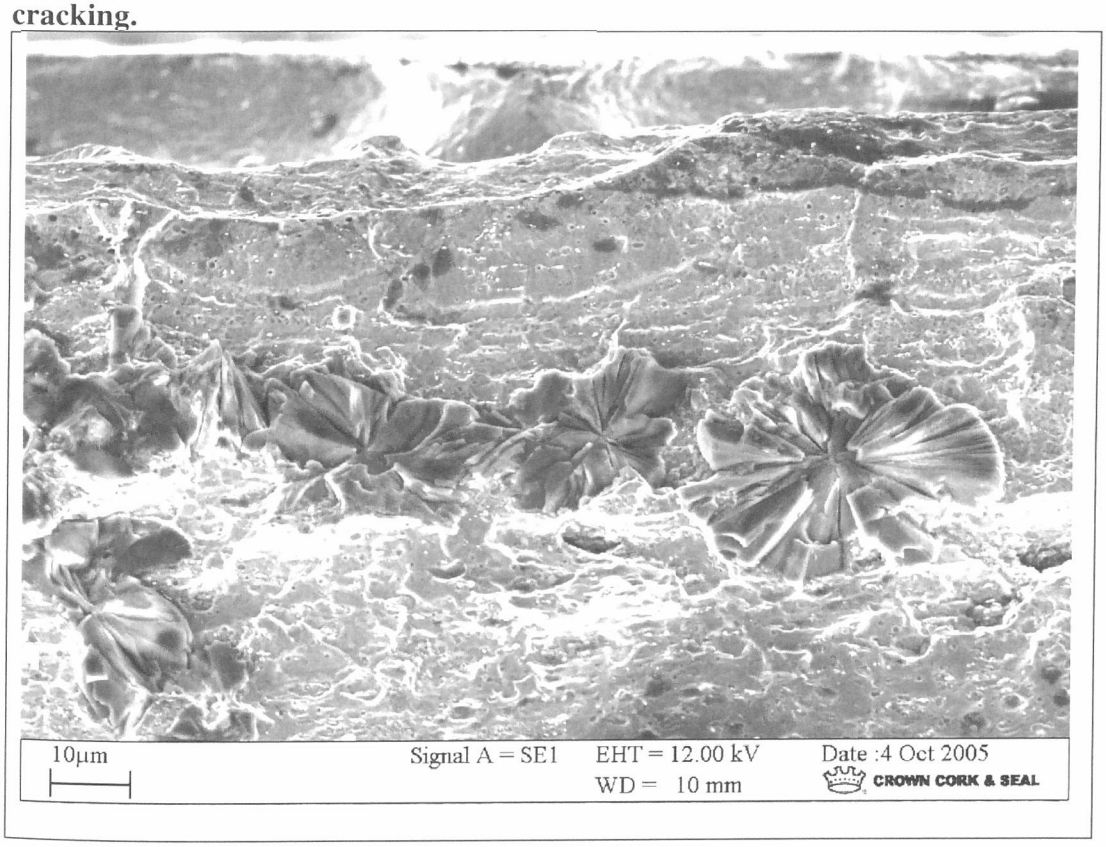
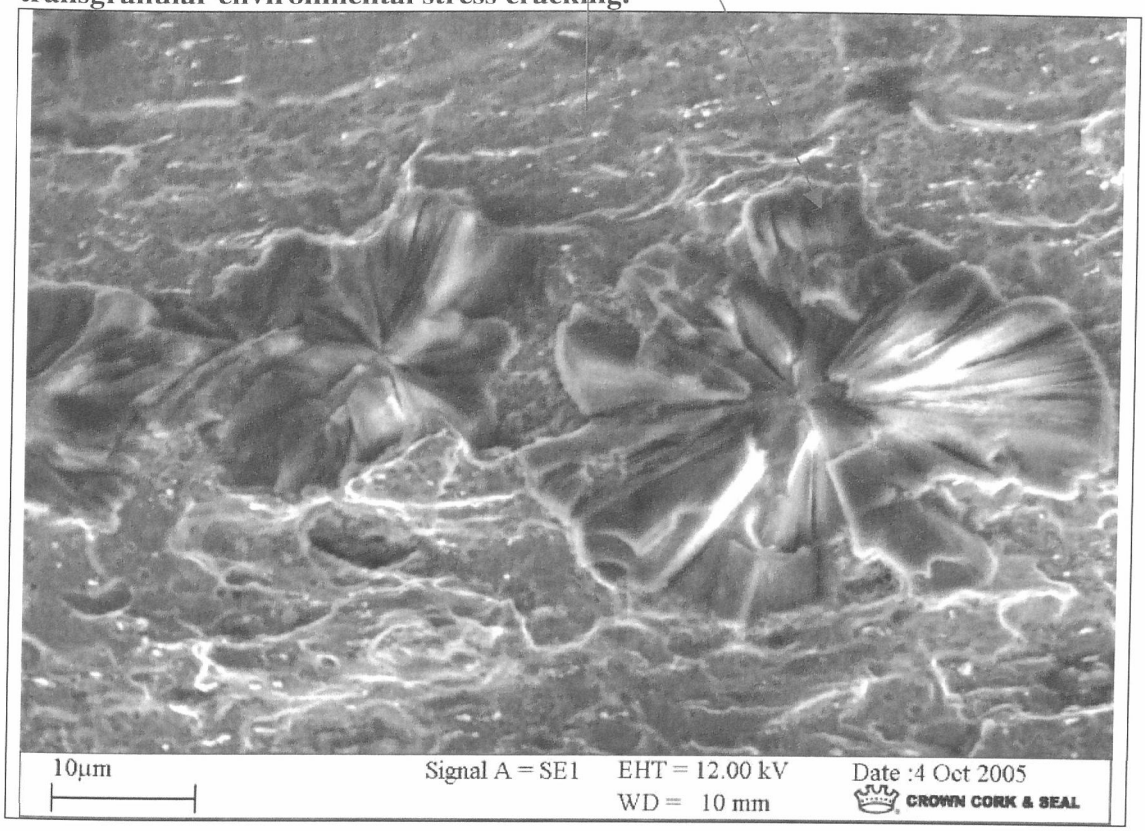


Figure 34: Sample ssrttu041. Slow Strain Rate Tested Sample: Tuna Brine, non acidified. Larger magnification view of ledges and fan shapes consistent with transgranular environmental stress cracking.



Continued on next page for acidified variables...

The acidified variables showed degrees of replication of what was shown for non scratched samples. One of these is shown for each acid, Figures 35 and 36 below.

Figure 35: Sample ssrttu043. Slow Strain Rate Tested Sample: Tuna Brine acidified with acetic acid to pH 4.67. View of fracture surface near notch area showing zone of low ductility, and some ledges consistent with transgranular environmental stress cracking.

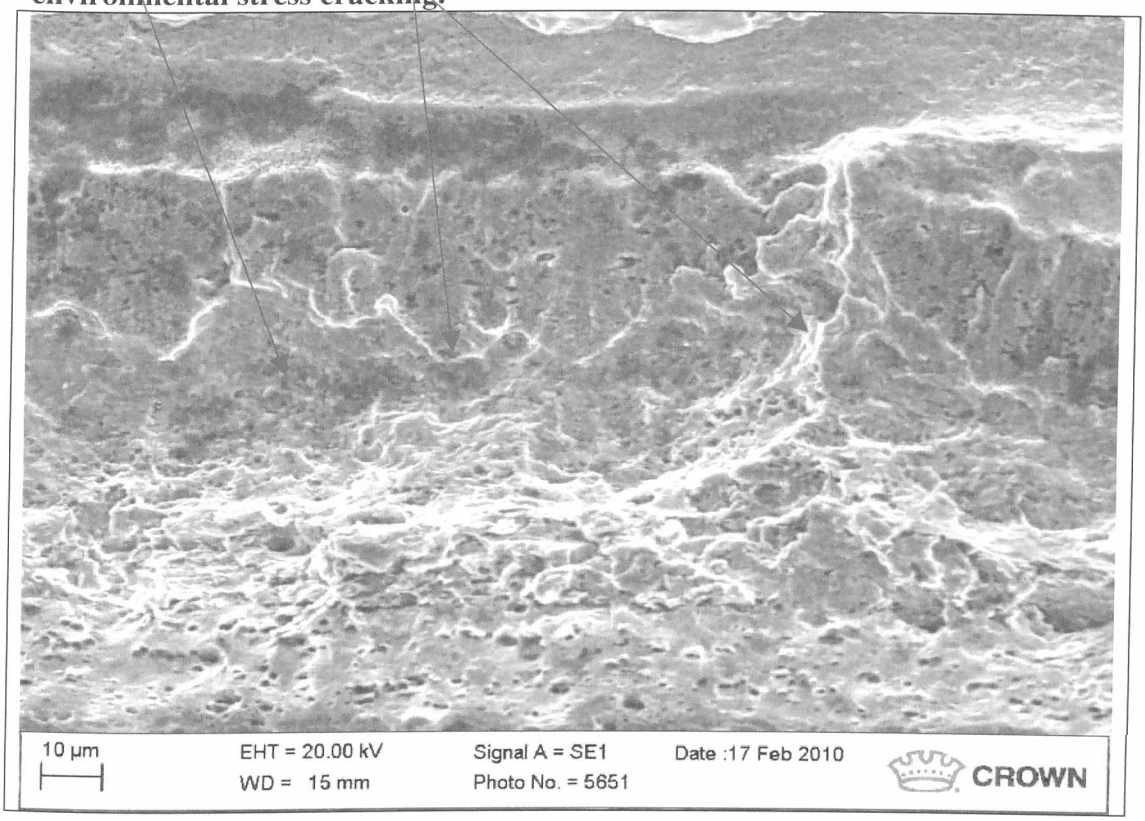
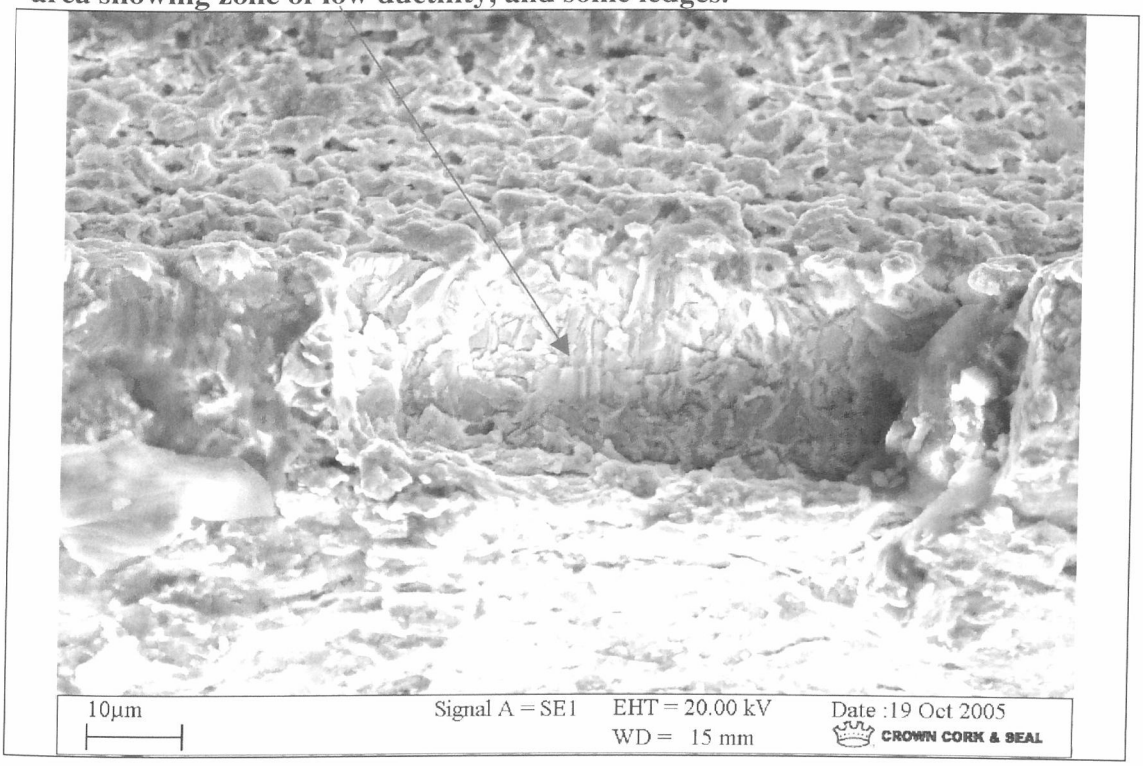


Figure 36 is shown on the next page.

Figure 36 Sample ssrttu040: Slow Strain Rate Tested Sample: Tuna Brine acidified with hydrochloric acid to pH 4.66. View of fracture surface near notch area showing zone of low ductility, and some ledges.



To summarise the scanning electron microscopy evidence, with respect to the non scratched acidified samples, these groups showed visible evidence of loss of ductility at the notch vicinity, and cases of fracture ledges or steps consistent with transgranular environmental stress cracking. On the limited non acidified samples tested the evidence of equivalent effects was inconclusive.

For samples to which a controlled scratch had been applied, at least one clear case of loss of ductility and appearance characteristic of trans-granular environmental stress cracking was demonstrated, no ssrttu041 for non acidified Tuna brine. For the acidified samples, the acetic acid case example, ssrttu043, Figure 35, showed loss of ductility and ledge conditions similar to non scratched samples. The hydrochloric acid acidified case, Figure 36, showed a local zone of ductility loss only.

2.4.6 Product Analysis: Tuna Brine: Anions and Cations.

Two of the pots of tuna brine form the bulk used for the tests were subject to analysis for anions and cations, as well as pH, this analysis being conducted by the Crown Analytical Laboratory. The anion analysis was by Ion Chromatography and the Cation alaysis was by an Inductively Coupled Plasma Method .The data obtained is tabulated below in Tables 22 and 23:

Table 22: Anion Analysis Data for Tuna Brine used in Slow Strain Rate Tests.Data in parts per million.

Anion	Pot 42	Pot 75	Values from comparison source For Tuna*
Chloride	8900	8900	4100
Nitrate	<10	<10	<10
Phosphate	3100	3000	4450
Sulphate	130	120	50
pH	6.05	5.85	5.8

* No data available for anions as opposed to elemental values in "The Composition of Foods", by McCance and Widdowson[32], so these values are from alternative shop purchased tuna cans used in other laboratory tests in 2003.

Table 23: Cation Analysis Data for Tuna Brine used in Slow Strain Rate Tests.Data in parts per million.

Cation	Pot 42	Pot 75	Values from reference[29] for DrainedTuna brine
Sodium	7111	6225	3200
Iron	24	23	10
Aluminium	0.5	0.5	No value
Calcium	84	63	80
Zinc	1.1	1.5	7
Manganese	<0.1	<0.1	Tr
Lead	<0.1	0.1	No value
Copper	<0.1	<0.1	0.5
Magnesium	325	255	270
Chromium	<0.1	<0.1	No value
Potassium	2156	1774	2300
Titanium	<0.1	<0.1	No value
Nickel	<0.1	<0.1	No value
Cobalt	<0.1	<0.1	No value
Tin	<0.1	<0.1	No value
Selenium	<0.1	<0.1	0.78

For the **anion** data the samples used in the present work showed a very high chloride level relative to the shop purchased comparison lot peviously measured. The sulphate content also showed an increase, but the phosphate level was lower in the present samples. pH was quite close to past samples. The main observation from this data was that the phosphate chloride balance was measurably different in the comparison cans from this used in the tests reported above. More pitting tendency in the samples presently tested can be a consequence of the higher chloride level.

Regarding the **cations**, where comparisons could be drawn with reference information on the composition of foods[32], sodium was notably high which accords with the rather high chloride content observed in these samples, while magnesium, calcium and potassium were not excessively far removed from the reference values. Copper which could plate out on steel and lead to galvanic action as a cathode was very low. Zinc and selenium which can assist hydrogen entry into steel were lower than reference values. Iron was notably high in the samples and a low level of aluminium was found. Other elements were present at a very low level or below the detection limit of the analysis. Later work in Section 3 covers a wider range of cation analysis than the above.

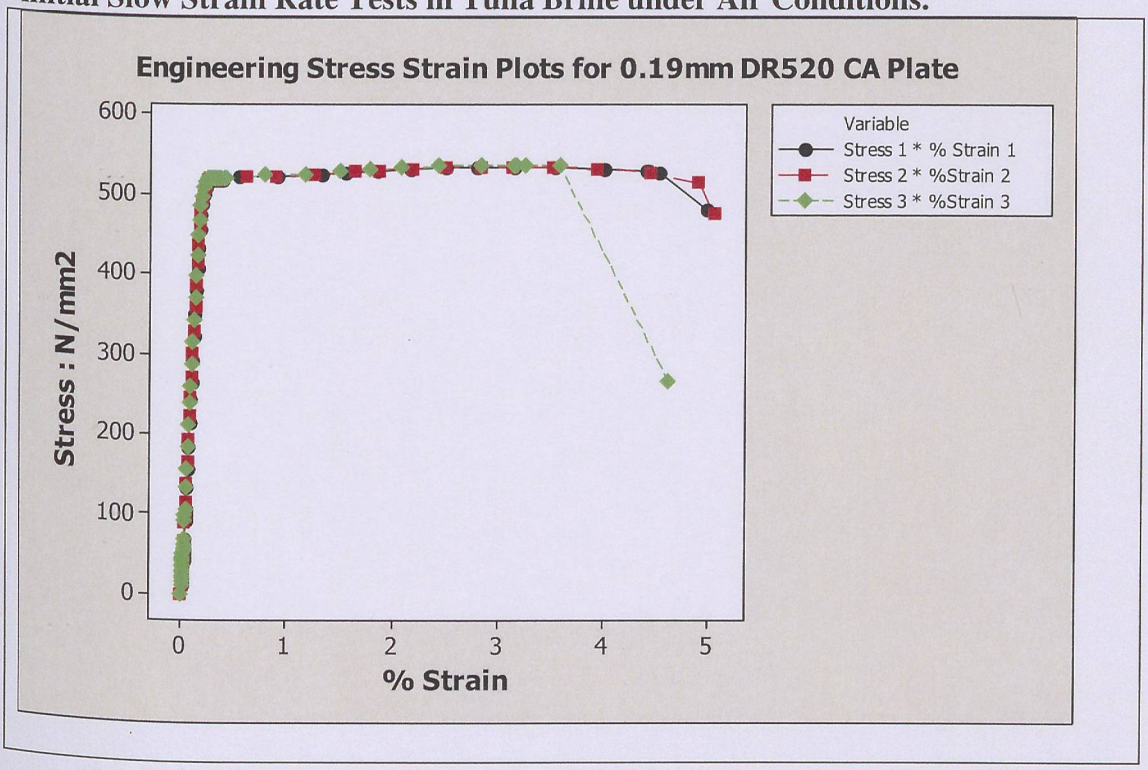
From this initial data the only rather high anion was chloride, which will aid pitting and two of the species analysed known to aid hydrogen entry into steel, zinc and selenium, were not present at exceptional levels. Phosphate anion which is an environmental stress cracking promoter was again not at an exceptional level by comparison with the control shop purchased sample. However, phosphorus was also identified by Evans[33], alongside antimony and bismuth, as favouring the passage of hydrogen through iron.

2.4.7 Tensile Properties of eccs Test Material.

Stress / strain curves were determined by way of Engineering Stress – Strain data obtained using the initial cross sectional area and an 80 mm gauge length. Samples of

the 0.19mm DR520CA material type were tensile tested as normal un-notched 'dog bones' on a Zwick Tensometer, under standard testing conditions according to DIN EN 1002-1 standard. The specimens were as shown in Section 3, Figure 38, except that no notches were present. The data are shown in plot 11 below.

Plot 11: Engineering Stress Strain Plots for 0.19mm DR 520 Material used in initial Slow Strain Rate Tests in Tuna Brine under Air Conditions.



From the above Engineering Stress-Strain plots, it was apparent that the DR520CA material showed a % elongation between around 4.7% and just over 5%, and that a plateau was observed after yielding i.e. a suggestion of conditions close to elastic-perfectly plastic up to the stage of final necking. At this stage of the work the true stress strain plots were not estimated but this has been done for the DR 620CA materials discussed in Section 3. However, it can be suggested that this form of plot having a behaviour close to plateau after yielding may give rise to an onset of necking after a very small extension beyond yielding.

2.4.8 Steel Composition Analysis

This analysis was carried out on a sample of the DR520CA material by Corus at Scunthorpe, and the data are tabulated below in Table 24 together with a target specification for this continuously cast type of material used as a stamping steel.

Table 24: Steel Composition Analysis by Wt% for 0.19mm DR520CA Plate Used for Tests on Tuna Brine in Section 2 Work.

Element	C	Si	Mn	P	S	Cr	Mo	Ni
% by weight	0.07	0.009	0.21	0.011	0.008	0.028	0.003	0.014
Target	0.12	0.03 max	0.30-0.50	0.020 max	0.020 max	0.08 max	0.02 max	0.08 max
Element	Al	As	Co	Cu	Nb	Sn	Ti	V
% by weight	0.028	0.002	0.001	0.014	0.003	0.006	0.002	<0.001
Target	0.02-0.08	0.01 max	0.02 max	0.08 max	0.02 max	0.02 max	0.02 max	0.08 max
Element	Nitrogen	B						
% by weight	0.005	0.0003						
Target	0.008 max							

The results have shown that the steel was essentially within the general purpose steel targets for a stamping quality material. The manganese content was below the target, but the limits here mainly concern behaviour of material for welding where the manganese content should not be too high such as over 0.35% as it can assist weld splitting risks during subsequent can flanging, but values as low as 0.18% are acceptable. The sulphur content of concast packaging steels is normally extremely low, so that a very high manganese content would not be required for reaction with the sulphur. A multiple for manganese of 10x sulphur content or more has been considered desirable, which was fulfilled by the above steel. These types of steels are generally very clean with extremely low levels of inclusions such as sulphides. The above steel was also very low in arsenic which is a catalytic recombination poison related to

hydrogen ingress, and also low in phosphorus. Low phosphorus has always been a requirement in packaging steels especially in the past where acid fruits were packed. This is logical given the link with hydrogen ingress[33] for this element. In relation to elements cited by Parkins et al[45] as capable of improving resistance to certain forms of environmental stress cracking, e.g. chromium, nickel and titanium, all of these were far below the 1% level recorded by Parkins[45] as necessary to promote a mitigating effect on environmental stress cracking.

2.5 Discussion of Initial Results.

At this stage, the investigation had shown that using Tuna Brine as the test medium, with some evidence of loss of ductility and environmental stress cracking could be shown sporadically using non acidified product and notched specimens, using the slow strain rate method at the Open Circuit Voltage as determined, and under air conditions. The best examples were observed for specimens to which a scratch across the width of the sample had been applied at the notch apex. Using the tuna media acidified to pH between 4.5 and 5.0 with acetic acid or hydrochloric acid, further evidence of ductility loss and some transgranular environmental stress cracking, apparent from step fractures or ledges,could be discerrned for both media and for scratched or non scratched specimens. The double reduced eccs steel used was of a high temper DR520 with relatively low ductility, elongation around 5% or below, and having with a chemical composition indicative of high purity. Elements such as chromium and titanium cited by Parkins et al [45], as consistently improving the cracking response of ferritic steels, were present at levels far below the order of 1% or even 0.75% quoted in certain instances as being necessary to improve cracking resistance in particular environments. Haggman[46] had identified some beneficial effects on copper present at 0.08-0.12% related to pitting studies, but this concerned steels which pre-dated the present

generation of continuosly cast materials having very low levels of sulphur as well as phosphorus. In earlier materials, the binding reaction of copper with these elements may have been the reason that a benefit was identified.

Pitting loop tests confirmed that tuna brine could be expected to display a pitting tendency and no distinctive passivation effects on the anodic polarisation curves during fast and slow sweep polarisation studies were observed. Hence, the slow strain rate tests at the Open Circuit Voltage showing some tendency to loss of ductility and probable envornmental stress cracking effects, are likely to be consistent with a hydrogen cracking mechanism. The analytical work has shown a high chloride level expected, to promote pitting and a significant phosphate content. Scott Smart and Proctor[16] had observed a loss of ducility at low anodic overpotentials in ferritic steels immersed and stressed in phosphate media. However, the food media such as fish are very complex and no individual constituent can be cited as having caused an environmental stress cracking effect without corroborative evidence to fit the circumstance. The cation analysis has not been exhaustive in respect of catalytic poisons and more detail on this is examined and discussed in Section 3.

Regarding the statistical analysis, the evidence from the correlation matrix showed that if test data for two acids was combined the Integrated current parameter, $I_{a2,}$ was significantly correlated with media difference for both scratched and non scratched samples. The final analysis was therefore confined to samples acidified with acetic acid, the data for hydrochloric acid and non acidified samples being too limited. From this subset statistical analysis, a number of strong correlations were observed for non scratched samples, namely the direct correlaton of time of test with specimen extension, and the inverse relationship of time of test with E_{rms2}. Time of test was the closest estimate of failure time, which could not be exactly pinpointed at this stage of the work, this being overcome for Section 3 tests. Integrated current was strongly inversely

correlated with maximum load, but not with time of test. For scratched samples, the significant correlations with time of test concerned the direct effect of extension and of OCV.

For non scractched samples, E_{rms2} proved to be a strong regression predictor having an inverse relationship with failure time and as an alternative, a combination of OCV, E_{rms2} and I_{a2} was suggested as a candidate supported by the partial least squares test for regression.

The mean failure time for scratched samples was observed to be greater than for non scractched for the acetic acid sub group, and this may have been because of more widespread corrosion taking place on the scratched samples, whereas the failure of a notched sample will be significantly determined by behaviour at the notch vicinity. Again, this may be why for scratched samples the relationship with time to failure was domnated by extension and no strong predictive relationship with electrochemical parameters was shown.

2.6 Conclusions from Initial Experimental Findings.

1. Some evidence of environmental stress cracking was produced sporadically using tuna brine by slow strain rate tests under air conditions, using notched specimens of DR520CA eccs packaging steel tested at the Open Circuit Voltage. Acidification of the product was also used and this reproduced the effect. Much test data were discarded during early work due to uncertainty about observations, inconsistency of results, or the absence of a meaningful outcome.

   The occurrence of product pitting action and corrosion after the test, and before dis-assembly and examination of samples, was probably contributory to

protracted uncertainties at this stage. The product had a rather high chloride content of over 0.8%.

2. Using tuna brine acidified with either acetic or hydrochloric acids to pH in the order of 4.5-5.0, loss of ductility and some evidence of transgranular environmetal stress cracking evident from fractographic steps or ledges, were effects produced using the same 0.19mm DR520 continuously annealed eccs plate. These effects were observed with non scratched samples or samples 'scratched' in a controlled way.Tests which produced the effects described using non acidified or acidified product were also conducted at the Open Circuit Voltage.
3. The plate used was commercial 0.19mm DR520CA eccs steel of a high purity chemical composition, typical of continuously cast non nitrogenised packaging steel.
4. Electrochemical tests on the product indicated a pitting tendency from pitting loop tests, and the absence of any clear suggestion of passive conditions arising on the anodic sweep, although some arrests in these curves were recorded.
5. The implication of the tests and observations points to a hydrogen ingress related loss of ductility and environmental stress cracking effect. Loss of ductility e.g. at low anodic overpotentials has been observed with phosphate media[16] , but the food media involved, while containing phosphate are rather complex in composition. At this stage of analysis, apart from phosphorus, present as phosphate, only a low level of zinc has been identified as an additional element having the potential to assist hydrogen entry into steel, Catalytic poisons such as arsenic antimony and bismuth[33] have been analysed in later stages of work. Low levels of hydrogen sulphide are likely to be generated by product sterilisation,

but may have been absent under the type of test practised using drained product brine.

6. Evidence of statistical correlations and predictive regressions for time of test, involving physical and/or electrochemical data was found for acidified media, analysed in detail for the tuna variable having added acetic acid. The parameters of extension, maximum load, E_{rms2} (potential noise), and Ia_2 (Integrated current-time) were among those which featured in inter parameter correlatons, and some candidate regressions for time of test were then identified.

For the acetic acid group tested as non scratched samples, E_{rms2} was a strong inverse regression predictor for time of test as a single parameter. An alternative candidate regression for further study involved potential noise, E_{rms2}, OCV, and integrated current, I_{a2}.

Regarding scratched samples, it was found that the overall statistical evidence linking electrochemical parameters to time of test was weak relative to specimen extension, this being the strongest predictor of time of test. This was suspected to be due to a probable reduction in local intensity of corrosion effects at the notch resulting from scratching across the specimen width at this location.

Slow Strain Rate Test Data for Initial Tuna Brine Samples Tested under Air Conditions. ('Non scratched' samples).

Sample ssrttu number	Specimen condition	Acidification used	Time of test : (hours)	pH start	pH end	OCV (millivolts) vs N/10 calomel electrode.	Maximum load: (KN)	Exten-sion (mm)	Delta BC* (cm)	E_{rms2} (Volts)	I_{rms2} (Amps/cm^2)	I_{a2} : Log_{10} current density (amps/cm^2) * time: s	Gauge (ins)
046	failed	acetic acid	38.80	4.63	4.63	-698	0.7401	0.883	0.0215	3.72e-5	4.3599e-5	-6.7089e5	0.0073
047	failed	acetic acid	37.82	4.68	5.05	-703	0.581	0.843	-0.0005	5.03e-5	2.1375e-4	-4.9014e5	0.007325
048	failed	acetic acid	26.43	4.65	4.93	-688	0.540	0.623	0.0015	8.318e-4	1.6767e-4	-5.4288e5	0.00735
049	failed	acetic acid	35.96	5.02	5.13	-698	0.923	0.806	0.006	2.324e-4	1.3333e-4	-7.2051e5	0.0073
050	failed	acetic acid	40.25	5.03	5.30	-686	0.870	0.820	0.003	4.52e-5	1.4949e-4	-6.8445e5	0.00735
051	non failed	acetic acid	38.61	5.05	5.11	-697	0.900	0.737	0.001	6.82e-5	1.0029e-5	-8.2018e5	0.0074
052	failed	hydrochloric acid	40.88	5.02	5.13	-681	0.891	0.957	0.010	1.028e-4	4.426e-5	-8.5241e5	0.0074
053	non failed	hydrochloric acid	46.61	4.63	4.62	-690	1.020	0.924	0.0025	4.34e-5**	8.2212e-6	-1.001e6	0.0074
054	failed	hydrochloric acid	52.34	5.01	4.93	-714	0.873	1.054	0.0005	5.8768e-4	1.4572e-4 **	-9.6146e5	0.00745
055	failed	hydrochloric acid	32.31	4.56	4.58	-702	0.752	0.503	0.0105	4.20e-5	2.9694e-5	-6.8126e5	0.0074
056	failed	none	35.75	5.83	5.81	-729	0.746	0.671	0.0175	3.2191e-4	unreliable	-7.0907e5	0.007475
057	non failed	none	71.78	5.94	5.67	-726	0.680	1.421	0.011	3.0587e-4	2.0806e-4	-9.7763e5	0.0074

* Small changes in specimen dimensions measured after fracture by re assembly of test pieces can result in small errors giving negative change data points.** values at 200,000 seconds only. The letter 'e' donotes a power of 10 multiple indicated.

Slow Strain Rate Test Data for Initial Tuna Brine Samples Tested under Air Conditions. (Samples 'scratched' across one face at the notch region).

Sample ssrttu number	Specimen condition	Acidification used	Time of test : (hours)	pH start	pH end	OCV (Millivolts) vs N/10 calomel electrode	Maximum load: (KN)	Extension (mm)	Delta BC (cm)	E_{rms2} (Volts)	I_{rms2} : ($Amps/cm^2$)	Ia_2 Log_{10} current density ($amps/cm^2$)* time :s	Gauge (ins)
034	failed	acetic acid	62.545	5.06	4.71	-680	0.981	1.400	0.0065	4.7414e-5	4.2447e-5	-1.8889e5	0.0072
035	failed	acetic acid	45.653	5.04	5.02	-696	1.014	1.014	0.013	3.9316e-5	1.9167e-5	-4.5453e5	0.00725
036	failed	acetic acid	35.785	5.09	4.97	-705	0.915	0.830	0.024	3.8937e-5	8.5724e-5	-4.7312e5	0.0074
037	failed	hydrochloric acid	43.481	5.10	5.10	-724	0.915	0.989	0.019	3.6049e-5	1.3712e-4	-7.0281e5	0.007325
038	failed	hydrochloric acid	41.736	5.06	5.12	-710	0.985	0.916	0.021	7.2865e-5	9.5054e-6	-8.8044e5	0.0073
039	failed	hydrochloric acid	39.243	4.66	4.66	-692	0.709	0.883	0.023	2.0128e-4	1.4344e-4	-7.6994e5	0.00735
040	failed	hydrochloric acid	43.279	4.66	4.66	-696	0.879	0.979	0.020	4.4809e-5	1.4812e-4	-6.9466e5	0.007375
041	failed	none	38.75	5.87	5.76	-758	0.895	0.920	0.012	4.1833e-5	1.0092e-4	-4.7169e5	0.00735
042	failed	none	35.246	5.80	5.75	-768	0.743	0.814	0.016	7.6581e-5	3.1436e-4	-5.2735e5	0.0074
043	failed	acetic acid	35.843	4.67	5.03	-697	0.503	0.806	0.015	9.7554e-5	2.0545e-4	-5.0373e5	0.00735
044	non failed*	acetic acid	22.047	4.68	6.01	-659	0.259	0.476	0.005	9.5821e-5	1.4895e-3	-2.7282e5	0.00735
045	failed	acetic acid	45.173	4.67	4.72	-707	0.956	1.006	0.0105	8.5493e-5	8.7174e-6	-9.5873e5	0.0073

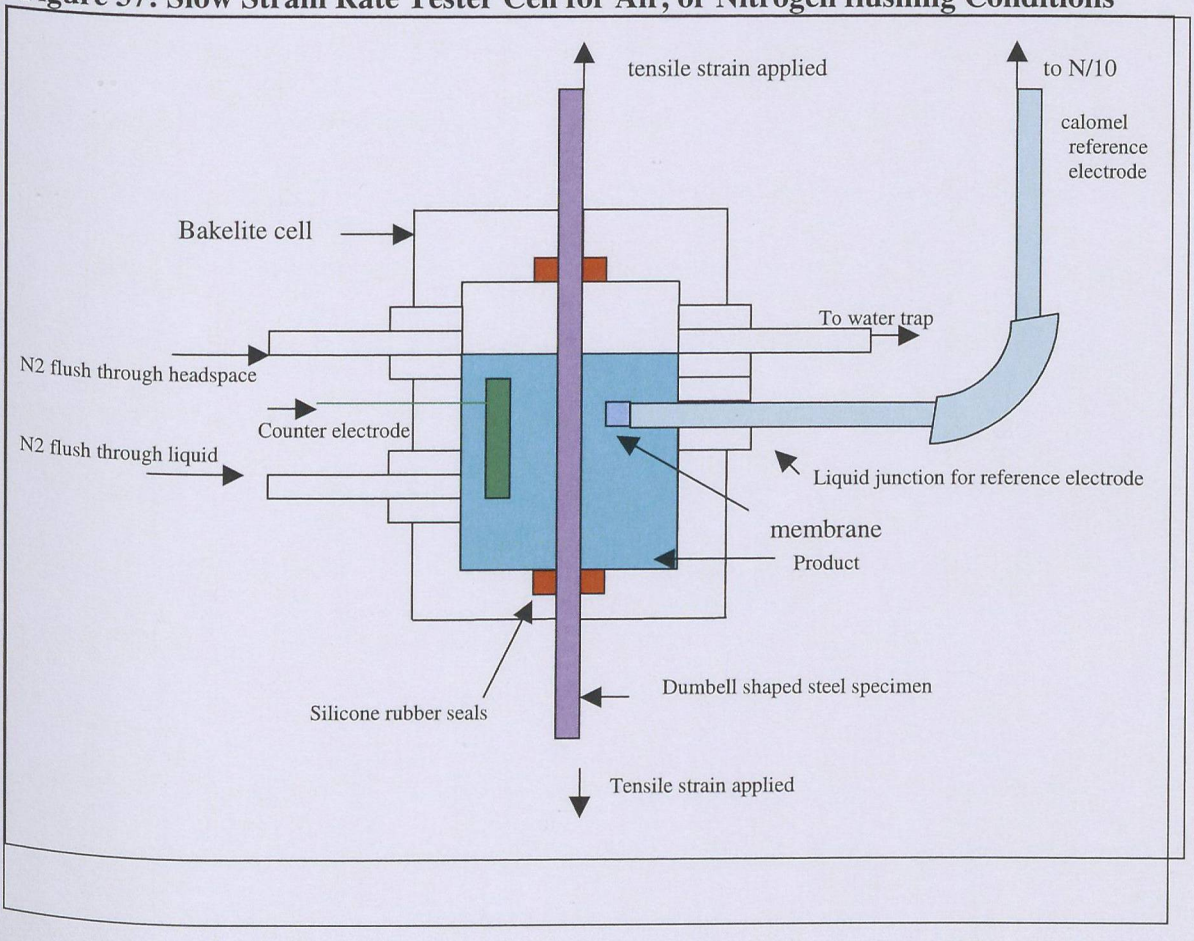
* badly pitted sample

3 Section 3: Experimental Work

3.1 Introduction: Slow Strain Rate Testing and Test Programme

An electrochemical cell was manufactured from bakelite, having internal dimensions of 59mm x 29mm x 30mm. This is illustrated in Figure 37. A liquid junction was provided linking the cell to an N/10 calomel reference electrode. A counter electrode manufactured from platinised titanium was positioned on the opposite side of the tensile test specimen, which was centrally positioned.

Figure 37: Slow Strain Rate Tester Cell for Air, or Nitrogen flushing Conditions



The cell was sealed by silicone rubber seals and in setting up the tests, the seals were lubricated with trace amounts of Mace Food Oil at the specimen ends, to prevent excess

friction which would interfere with the tests. The cell was provided with junctions to enable gas flushing with nitrogen through the liquid or through the headspace when required. It was encased in Aluminium foil for each test and this was earthed to reduce any extraneous induced currents. Before each test, the cell was washed thoroughly with hot water and scrubbed to remove any solid residues. The cell was assembled into a KH slow strain rate tensile testing machine. The tensile specimens were of standard 175x25mm dimensions, tapering smoothly to 12.5mm width, being formed by stamping in an automated press. The specimens were then notched at the mid point on either side using a hand press, the same notch tool being used to form both notches by reversing the sample. The notch positions were precisely controlled by a specimen holder having pegs, so that the notches were disposed in the corresponding positions on opposite sides of the specimen, and with any burrs on the same surface. The notches were of a 90 degree angle and having 0.15mm radius at the apex. The specimen surfaces were lightly wiped with cotton wool soaked in acetone to remove the surface lubricant, di octyl sebacate, which is applied in plate manufacture. The specimen edges including notch edges were then protected with an air drying lacquer, 'lacomite' (from the Canning Co, Birmingham) applied with a brush, followed by stoving at 60°C for 10 minutes. Using a travelling microscope, all specimens were measured before the test and again following the test for the parameters shown in Table 25 calculated from data points A-H in Figure 38. Figure 38 illustrates the specimen and notches.

The cell was bolted together with the face having any burrs pointing away from the counter electrode, for consistency in the experimental process. When the cell had been assembled, it was filled with the test liquid using a syringe via a top cell aperture, the filling being to level with the top aperture, which required approximately 47cm^3 of the solution which had been thawed from stock deep frozen at –20°C.

The test liquids had been extracted from tins and bulked for the tuna in brine and salmon in brine products purchased as commercial retail brands in shrink wraps, all being labelled cans, as follows:

a) Sainsbury's Tuna Chunks in Brine: 400gram 3 piece welded side-seam cans.
   BBE 2006. Produced in Spain for Sainsbury's. 99mm diameter cans

b) John West Wild Red Salmon (also declared as containing salt): 418 gram deep drawn 73mm dia cans.
   BBE2012. Salmon, Alaska, USA.

These cans were opened, the liquid drained and bulked into 5 litre quantities, which were stirred using a glass rod, and then poured into 125ml screw top plastic analytical pots in quantities of over 100mls, which were then closed and deep frozen at –20°C. The salmon product showed an oily layer on top of the aqueous phase, which was not observed for the Tuna product. All the slow strain rate tests were conducted in a temperature controlled room at 20+/- 2°C. The cross head speed tensile speed throughout the test was 5.7×10^{-6} mm/sec. This was fractionally below a strain rate of $5.78 \times 10^{-6}\ sec^{-1}$ for a material undergoing a 3% tensile strain over a 50mm gauge length in 72 hours. Each tensile specimen was measured for points A-H in **Figure 38** before and after the tests using a travelling microscope, allowing dimensional changes of the notch gaps, as well as the necked specimen length A-D, and width change E-F to be determined. The material thickness for each type of plate was also recorded; the local thickness changes at the notch regions being determined by microscopy after the tests. The slow strain tensile grips were of a design and construction so as to provide insulation between the specimen and the testing machine. The electrochemical cell was

connected to a Solartron 1286 electrochemical interface operated using DC Corrware Software (from Princeton Applied Research, Bracknell) via a Compaq Computer. Prior to each test , the Open Ciricuit Voltage (OCV) was determined over 30 Minutes, recording 5 points per second, and sufficient stability was considered to exist if the OCV did not vary by more than10 millivolts within a minute at the end of this period. For samples tested under low air conditions using nitrogen flushing, initial gas flushing was undertaken through the liquid for at least 12 hours prior to the test at a minimum flow rate of $3cm^3$ per minute measured by a flow meter. At the end of this time, and prior to OCV measurement, the nitrogen flushing was changed from through the liquid to via the headspace. Flushing via the headspace was then continued at a minimum rate of $3cm^3$ per minute throughout the test.

After the test was run, the electrochemical data was saved together with the load, time and extension data from the slow strain machine recorder. The specimen was removed as soon as was practicable after the test, washed in de-ionised water and air dried. The specimens were re-measured for points A-H , after placing them on the travelling microscope glass with the fracture edges in contact.

The following programme of testing was conducted:

i) 0.16mm DR620 CA Eccs drawing quality - 6 under high air and 6 under low air(N_2 flushing conditions) for each product.

ii) 0.18mm DR620 CA Eccs stamping quality - 6 under high air and 6 under low air(N_2 flushing conditions) for each product.

iii) 0.235mm DR620 CA Nitrogenised steel; Eccs stamping quality - 6 under high air and 6 under low air(N_2 flushing conditions) for each product.

Note: All of these tests were run but not all were run to failure. The analysis of results mainly concerns fully failed samples. For the tuna group tested under air conditions sufficient partially failed samples were achieved to enable estimation of crack growth rate.

Figure 38: Tensile Test Specimen for Stress Corrosion Cracking: Schematic.

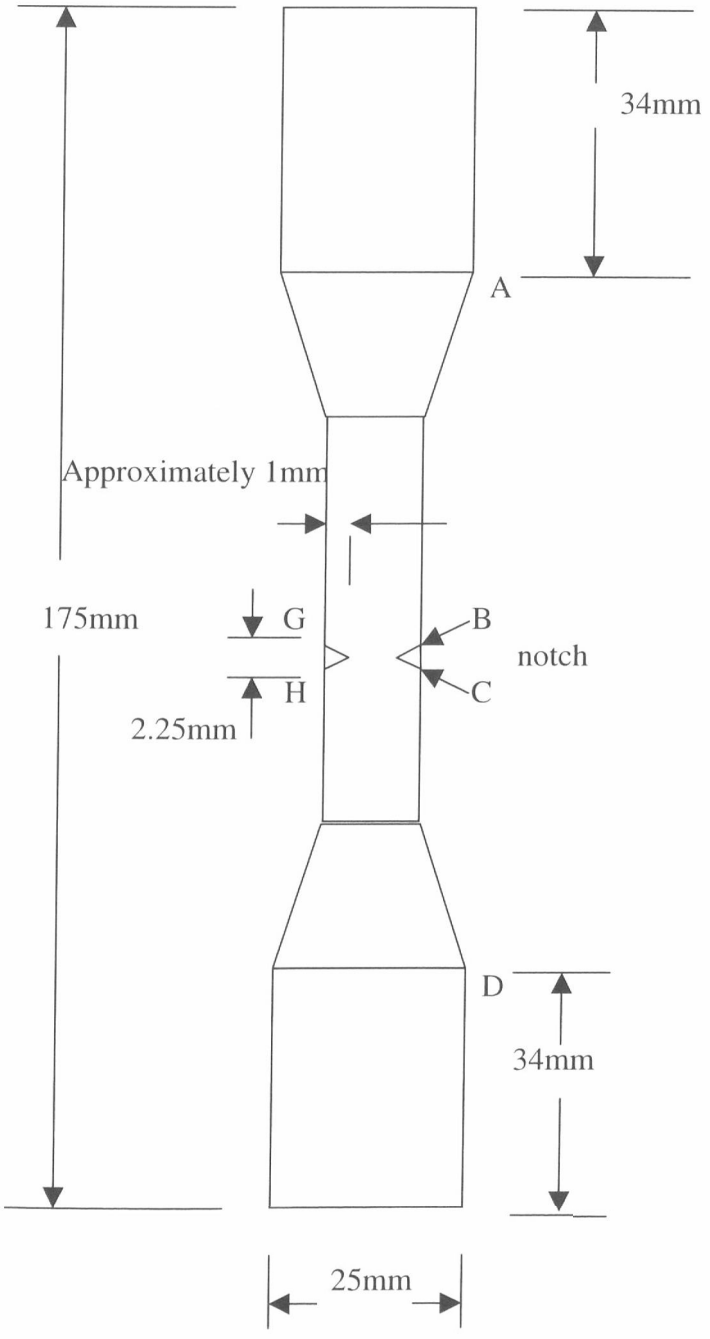


Table 25: Parameters Determined in the Course of Slow Strain Rate Testing.

Item	Symbol	Unit	Description
	Dimensional parameters		
1.	AD	cm	Reference length of test sample.
2.	Delta AD	cm	Change in AD distance resulting from test.
3.	BC	cm	Starting height of notch at 1st edge.
4.	Delta BC	cm	Change of notch height following test.
5.	Delta BC corr	cm	Change of notch height following test, corrected for gap.*
5.	HG	cm	Starting height of notch at 2nd edge.
6.	Delta HG	cm	Change of notch height following test.
7.	Delta HG corr	cm	Change of notch height following test, corrected for gap.*
8.	EF	cm	Distance between notch apexes acros specimen width
9.	Delta EF	cm	Change in distance EF following test.
10.	gauge	ins	Thickness of specimen.
	Other physical parameters		
11.	Initial load	Newtons (KN)	Initial reference value from tensometer, taken as zero.
12.	Maximum load	Newtons (KN)	Peak value in slow strain rate test.
13.	Change of load	Newtons (KN)	Nett load applied in course of test.
14.	M1//: Mechanical work.**	Newton.m	The area under the tensile load-extension plot up to the peak load.

*The notch height gap correction is the subtraction of the gap which exists after testing between the fractured components at the notch, due to the greater ductility of behaviour away from the notch region. This gives a revised notch extension value according to fracture behaviour at the notch region only.

**M1=M*C, where M is the area under the tensile load-extension plot up to maximum load, and C is a calibration factor for the KH Slow Strain Rate Tester Load Cell. For the KH tester, C had the value 0.95 for test loads from 0.0 to 1.0KN and 0.975 for test loads from 1.1 to 2.0KN. M values are shown on Appendices 7-10, paras 3.24 –3.27 of Section 3.

Table 26: Parameters Determined in the Course of Slow Strain Rate Testing.

Item	Symbol	Unit	Description
15.	d	mm	Starting cross-head displacement value before test.
16.	D	mm	Displacement at maximum load.
17.	D1	mm	Final displacement.
18.	Em	mm	Extension at maximum load.
19.	Ef	mm	Extension at failure.
	Chemical and		
	electrochemical		
	parameters		
20.	pH start	-	pH at start of test.
21.	pH end	-	pH at end of test.
22.	T1	deg C	Product temperature at time of initial pH.
23.	T2	deg C	Product temperature at time of final pH.
24.	T	deg C	Ambient room temperature during test.
25.	OCV	Millivolts	Open circuit voltage of specimen determined over 30 minutes before test, with reference to N/10 calomel reference electrode.
26.	E_{rms1}	Volts	Root mean square value determined for potential distribution during the test, up to the point of maximum load.
27.	I_{rms1} ***	$Amps/cm^2$	Root mean square value for current density determined during the test, up to the point of maximum load
28.	Ia_1***	Log_{10} current density ($amps/cm^2$) * time (seconds)	Integrated current-time value, up to time of maximum load.

*** Electrochemical parameters were normalised to a surface area of $1cm^2$.

3.2 Results

3.2.1 Notes on Statistical Methods used

i) Statistical correlation implies a linear relationship between two parameters, and the correlation may be direct (+ve coefficient) or inverse (-ve coefficient). The absence of correlation does not necessarily signify the absence of *any* statistical relationship between parameters.

ii) If two parameters have a correlation coefficient of 0.5 or above, it is thought unlikely that one could change independently of the other, and hence care must be exercised in this respect in the formulation of any multiple regression equations.

iii) For the purposes of initial consideration, correlations giving P values ≤ 0.100 have been considered as significant.

iv) Best Subsets regression and use of Mallows Cp statistic.

The consideration of choice of best subsets for regressions has been based upon a number of criteria defined in detail in the **Appendix 1.** Briefly these were:

- The use of R^2 and R^2 (adjusted) values as guidance to maximise % of variability explained by the 'independent' variables or candidate predictors.
- The statistical significance of the overall regression and candidate predictors fitted, indicated by the 'P' value.
- The use of Mallows 'Cp' statistic.

The regression fits were also examined in terms of the distribution of residuals and the existence of a central tendency or not, together with whether the residuals followed a normal distribution.

The statistical correlations obtained from tests involving **Tuna Brine** are shown on **Appendices 2 and 3.**

3.2.2 Statistical Correlations : Tuna Brine : Slow Strain Rate Tests: Air Conditions

See Appendix 2, Pages 1 and 2 for Data.

There were direct inter-correlations of the parameters 'gauge', 'change of load', 'extension', 'time to maximum load' and 'time to failure', all of which were significant

at the 5% level or higher. The parameter of 'Mechanical work' representing the area under the load extension plot up to the maximum load, showed direct inter-correlations with all of the above parameters. 'Mechanical work' could therefore be used in a regression model instead of combinations involving the first four of the above mentioned parameters, avoiding collinearity arising from, these variables.

The current – time integral, I_{a1}, showed inverse correlations with 'change of load', 'extension', 'time to load maximum' and 'time to failure', the latter three all highly significant.

The 'Mechanical work', M, has shown in addition a direct correlation with Open Circuit Voltage (OCV), and an inverse correlation with 'integrated current', I_{a1}.

Among other parameters, the notch height changes ('delta BC' and/or 'delta HG') or corrected, 'corr', versions, only showed sporadic correlations, 'delta HG' with 'OCV', 'delta HG corr' with 'pH start', and 'Delta BC' with gauge. The electrochemical potential root mean square parameter, 'E_{rms1}', showed one inverse correlation with 'pH start'. The specimen reference length, 'Delta AD', also appeared to be a weak predictor in terms of range of correlations, but one highly significant correlation with 'Delta BC' was recorded. 'pH end' did not show any significant correlations.

3.2.3 Statistical Correlations : Tuna Brine : Slow Strain Rate Tests: Nitrogen Flushing Conditions. See Appendix 3 Pages 1 and 2 for Data.

The direct inter-correlations of 'gauge', 'change of load', 'extension', 'time to load maximum' and 'time to failure' were repeated as for high air conditions. The correlation of 'Mechanical work' , M, with all of the above was repeated. 'Mechanical work' showed inverse correlations with 'OCV', 'I_{rms1}' and 'Ia_1'. For 'OCV' this was a reversal of the effect under air conditions.

pH has only shown one individual correlation, this being an inverse one between 'pH end' and 'extension'.

'Delta AD' showed more correlations with other parameters than under air conditions, these being direct ones with 'Delta BC', 'change of load', 'time to maximum load', and 'Mechanical work' and inverse with 'I_{rms1}'.

In contrast to tests under air conditions, the tests having nitrogen flushing have revealed a significant number of correlations involving the notch height change dimensions, 'Delta BC' and 'Delta HG', with other physical parameters of 'gauge', 'change of load' and 'extension', as well as 'time to maximum load' , 'time to failure' and 'mechanical work' all recording direct correlation effects. For 'I_{rms1}' and 'Ia_1', significant inverse correlations with notch dimensional change were found. For most correlations, the 'uncorrected' notch dimensional change parameters were involved, but for 'Delta Hgcorr' there were five significant correlations with other parameters, which included 'time to failure' (direct effect), and 'OCV' and 'Irms' as inverse effects.

The statistical correlations obtained from tests involving **Salmon Brine** are shown on **Appendices 4 and 5.**

3.2.4 Statistical Correlations : Salmon Brine : Slow Strain Rate Tests: Air Conditions. See Appendix 4, Pages 1 and 2.

As in the case of Tuna brine , direct inter-correlations were again observed between gauge, 'change of load', 'extension', 'time to load maximum' and 'time to failure', with 'Mechanical work' showing direct correlation with all of these as before. 'Mechanical work' also showed an inverse correlation with the notch height change, 'Delta HG corr', and with 'OCV' and 'Ia_1'.

For the change in specimen length 'Delta AD', correlations were limited to notch height change, 'Delta BC'. and 'Delta BC corr'. 'Delta HG corr' showed a significant number

of direct correlations with physical parameters including 'extension' and 'time to failure' , and inversely with integrated current, 'Ia_1' and 'Mechanical work'.

The change in correlation for 'Delta Hg corr' concerning on the one hand 'extension', 'time to failure' and 'time to maximum load' (direct), and on the other, Mechanical work, (inverse) may be a reflection of difficulty of attaining accurate re-measurement of dimensional change for fractured specimens. This difference in behaviour is considered further under the best subsets regressions section.

The most frequent correlation between physical and electrochemical parameters concerned the current- time integral value, 'Ia_1', which was found to correlate inversely with five of the above inter-correlated physical parameters as well as with 'Mechanical work' and notch height change invoving BC. 'pH start' showed one weak indirect correlation with E_{rms1}, an an odd inverse correlation for 'pH end' with gauge was recorded.

From these data , the correlations relevant to the key elements of the investigation were likely to be those involving 'Ia_1' and 'Mechanical Work'. The 'Ia_1' parameter does not define the direction of the current. A positive current signifies anodic dissolution with pitting possible, whereas a negative current implies decomposition of substances at a surface e.g. hydrogen gas or OH^- ions, or of alternative species from the complex media, and would require an electrochemically balancing deposition of other species such as metal ions. In practice, the log current- time plots tended to comprise behaviours alternating between positive and negative current observations in the course of the tests.

3.2.5 Statistical Correlations : Salmon Brine : Slow Strain Rate Tests: Nitrogen Flushing Conditions. See Appendix 5, Pages 1 and 2.

The low air, nitrogen flushing condition, would be expected to be much closer to the filled pack condition than the 'air conditions'.

For the nitrogen flushing condition, the inter correlations involving 'time to maximum load', 'time to failure', 'change of load', 'extension' and 'gauge' were replicated as for air conditions, all being direct relationships found to be significant at $P \leq 0.001$. Again, the inverse correlations with 'Ia_1' were observed with the above five parameters, all being statistically significant at $P < 0.001$ level.

The physical parameters of gauge and 'change of load' showed direct correlations with 'pH start' and 'pH end' at $P<0.100$.. 'E_{rms1}' and 'I_{rms1}' each showed correlation with 'pH end', and for 'Ia_1', there was an inverse correlation with 'pH start'.

3.2.6 Summary of Main Points of Correlation Evidence for Tuna and Salmon Brines

i) The larger the integrated current 'Ia_1', the shorter the test duration, and the lower the specimen 'extension', measured by cross-head movement in the tests. *This applied to both products under both environmental conditions.*

ii) The greater the 'Mechanical work', as determined up to maximum load, the longer the time to failure, again applicable to both products and environmental conditions.

The 'Mechanical work' term should allow those differences in failure times which may be linked to gauge differences between material lots to be taken into account in any regressions proposed. Gauge was directly correlated with time to failure in all 4 subsets.

iii) Notch dimensional change:

For **Tuna brine**, the notch height change showed only sporadic correlations for *air conditions*, but *for nitrogen flushing conditions*, the notch height changes 'Delta BC' and 'Delta HG' showed direct correlations with ' time to failure' and 'Mechanical work', and inverse correlations with integrated current 'Ia_1' and current noise, 'Irms'.

For **Salmon brine**, under *air conditions*, only the notch height change 'Delta HG corr' showed a significant number of correlations including a direct one with 'time to failure',

and an inverse one with integrated current, 'Ia_1', and similarly an inverse one with 'Mechanical work'. This will be considered in more detail later.

For salmon brine under *nitrogen flush* conditions, 'Delta BC' and 'Delta BC corr' showed inverse correlatons with integrated current , and direct relationships with 'time to failure' and 'Mechanical work'. 'Delta Hgcorr' was directly correlated with 'time to failure', but did not show any correlation with 'integrated current' or 'mechanical work'.

iv) pH in general did not show a great number of correlations, but for salmon brine under low air conditions, there were significant direct correlations for pH end with 'E_{rms1}' and 'I_{rms1}' $_{as}$ well as with pH start, and an inverse one between Integrated current, 'Ia_1' and pH start. Odd correlations involving pH, difficult to explain, were with 'gauge' and 'change of load' for the same subset.

3.2.7 Regression Predictions for Time to failure using 'Best Subsets' Method: Tuna Brine Product.

The parameters determined were examined for inclusion in best subsets regressions initially for time of failure with tuna brine product. The top ten subsets, including those having highest R^2 and R^2adj values for air and nitrogen flush conditions are recorded in Tables 27 and 28 below.

Table 27: Regression Matrix: Tuna Brine : Air conditions : Completely failed specimens.

Subsets	Rsq	Rsq adjusted	Mallows Cp	Standard deviation	pH start	OCV	dBC	dBC corr	dHGx	dHG corr	dAD	E rms_1	$Irms_1$	Ia_1	M1 Mech work
1	94.8	94.3	1.8	2.9041											x
2	72.2	69.7	48.8	6.7044										x	
3	96.4	95.6	0.6	2.5482									x		x
4	96.3	95.5	0.7	2.5739										x	x
5	97.4	96.5	0.4	2.2643						x				x	x
6	97.1	96.1	1.1	2.4011			x						x		x
7	99.0	98.6	-1.0	1.4581	x					x				x	x
8	98.2	97.3	0.7	1.9908	x	x				x					x
9	99.1	98.4	0.9	1.5314	x			x		x				x	x
10	99.1	98.4	0.9	1.5390	x					x			x	x	x

Table 28 Regression Matrix : Tuna Brine : Nitrogen flush conditions: Completely failed specimens.

Subsets	Rsq	Rsq adjusted	Mallows Cp	Standard deviation	pH start	ocv	dBC	dBC corr	dHGx	dHG corr	dAD	E rms_1	$Irms_1$	Ia_1	M1 Mech work
1	85.4	84.3	17.7	3.2592										x	
2	83.1	81.8	22.3	3.5084											x
3	91.7	90.3	7.4	2.5603							x			x	
4	90.9	89.4	8.8	2.6734										x	x
5	92.8	90.9	7.1	2.4831			x				x			x	
6	92.7	90.7	7.3	2.5032	x					x					x
7	94.8	92.7	5.2	2.2161	x					x				x	x
8	94.1	91.7	6.7	2.3677	x								x	x	x
9	96.2	94.1	4.5	2.0002	x				x	x		x			x
10	95.9	93.6	5.1	2.0814	x				x	x				x	x

Note : In the headings,the letter 'd' as a prefix to dBC, $dBC_{corr,}$ dHG, dHg_{corr} and dAD, refers the change in value delta of these parameters as defined in Table 25

3.2.7.1 Regression Predictions for Time to Failure: Tuna Brine : Air Conditions: see Table 27 for subsets considered in this paragraph

The best subsets table indicated that for sets 1 and 2, each of the variables explained a high level of variability, but for subset 2, the Mallows value was well above the guideline (number of predictors +1), indicating omission of important variables. While subset 1 would be a candidate regression as a single regression predictor, a key point of the study was to establish any candidate regression(s) involving a combination of physical and corrosion related parameters. For subset 3, the regression failed the data subsetting statistical fit test fit test and showed an irregular distribution of residuals. For subset 4 combining the parameters from subsets 1 and 2, the residual, showed a central tendency and passed the fit test, and this subset was chosen as a candidate. Subsets 5-10 all showed irregular distributions of residuals, although in each case the fit test was satisfactory. Among these, subset 7 was selected as a second candidate on account of the combination of highest R^2 adjusted value, low Mallows Cp, and lowest standard deviation of residuals.

Best Fit Regressions selected and shown below: Subsets 4 and 7 from Table 27:

Subset 4: (see Tables 29-31 for statistics).

The regression equation was:

Time to failure: Tuna :air (hours) = 21.2 + 40.6*M1(Mechanical work: N.m)

$-9.0e\text{-}6 * Ia_1$ ($\log_{10}$ current density: amps/cm^2 x time secs).

Table 29: Subset 4 : Regression Statistics/

Predictor	Coefficient	SE Coef	T	P
Constant	21.186	2.700	7.85	0.000
M1	40.628	5.054	8.04	0.000
Ia_1	$9.01e^{-6}$	$4.50e^{-6}$	-2.00	0.073

R^2= 96.3% R^2(sq adj) = 95.5% R^2 pred = 91.8%

Table 30: Subset 4: Analysis of Variance for regression

Source	Degrees of freedom	Sum of squares	Mean square	F ratio	P value
Regression	2	1714.31	857.15	129.38	0.000
Residual error	10	66.25	6.63		
Total	12	1780.56			

Table 31: Subset 4: Unusual Observations

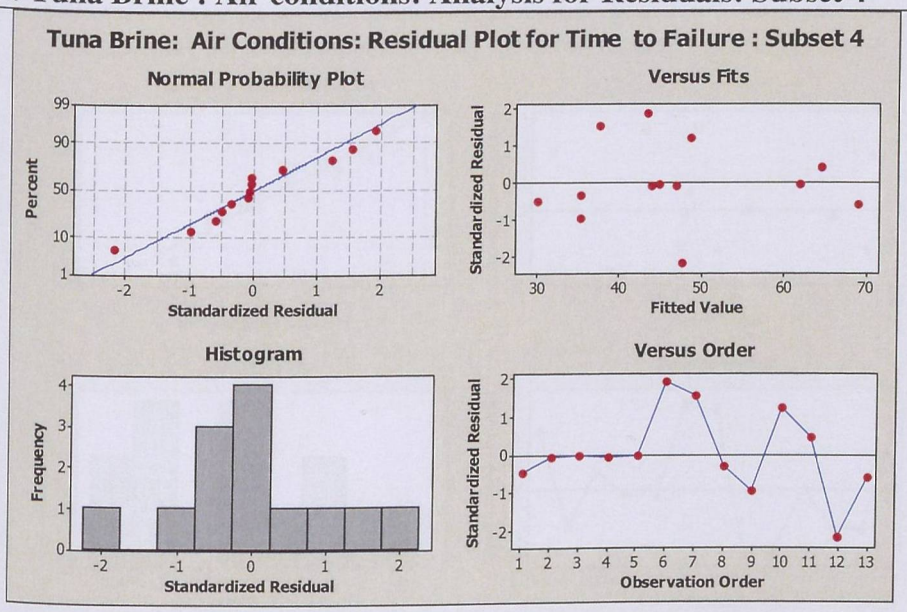
Observation	M1: Mechanical work	Time to failure: hrs	Fit	Standard error of fit	Residual	Standardised residual
12	0.491	46.695	47.628	1.231	-4.933	-2.18R

R denotes an observation with a large standardized residual.

No evidence of lack of fit (P >= 0.1).

For this regression, therefore, all parameters were significant at the 10% level or higher, with the overall regression significant at 0.1%. Over 90% of the variability in time to failure could be explained by the recorded data (R^2 adjusted), and for the predicted behaviour. The statistical fit test was satisfactory. The residuals followed a pattern having a substantially central tendency with some deviance from normal behaviour, and observation 12 has shown a high residual.

Plot 12: Tuna Brine : Air conditions: Analysis for Residuals: Subset 4



Plot 12 indicated that the initial observations gave the closest fit.

Subset 7: (see Tables 32-34 for statistics).

Time to failure: Tuna Brine : Air conditions (hours) = 488 + 35.7* M1

$- 1.2\ e^{-5}$* Ia_1 + 431* dHG_{corr} -79.9*pH start.

Table 32: Subset 7 : Regression Statistics

Predictor	Coeff	SE Coef	T	P
Constant	487.6	126.6	3.85	0.005
Mech work	35.730	3.092	11.56	0.000
Ia_1	$1.118\ e^{-5}$	$2.7e^{-6}$	-4.37	0.002
Delta HG corr	430.55	90.34	4.77	0.001
pH start	-79.93	21.59	-3.70	0.006

R^2= 99.0% R^2 (adj) = 98.6% R^2 pred = 96.38%

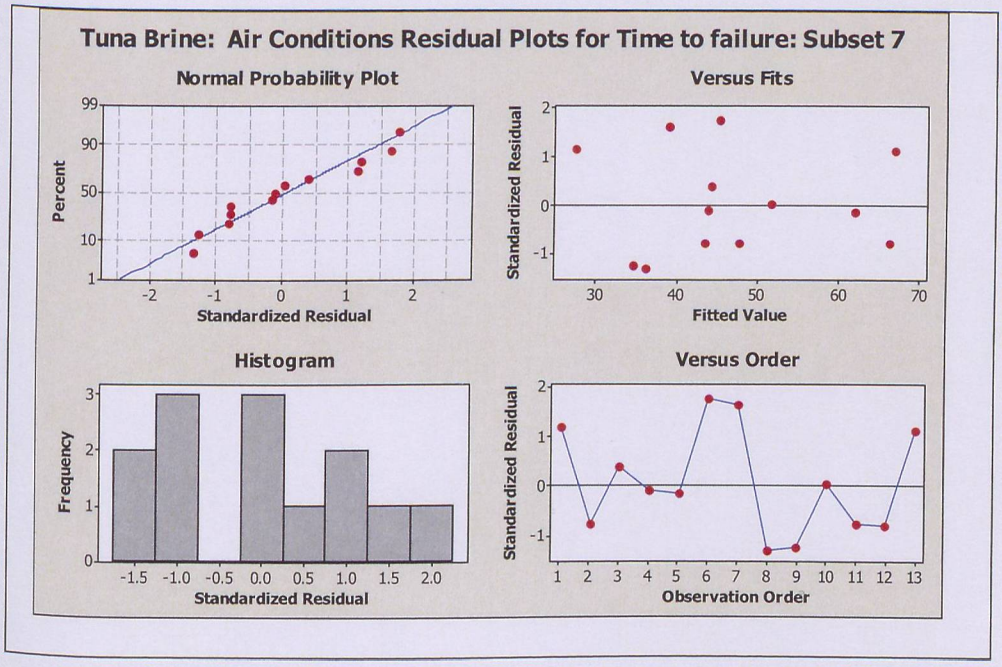
Table 33: Subset 7 : Analysis of Variance

Source	DF	Sum of squares	Mean square	F ratio	P value
Regression	4	1763.55	440.89	207.38	0.000
Residual error	8	17.01	2.13		
Total	12	1780.56			

There was no evidence of lack of fit. P > 0.100. The residual plots are shown as Plot 13.

Table 34: blank

Plot 13: Tuna Brine : Air Conditions: Analysis for Residuals: Subset 7



The residual plots show some skewness in the distribution on the histogram. While the general trend of the normal probability plot was close to linear, departures were evident with local changes of slope. The changes of slope would suggest an unidentified variable.

The group of subsets examined above for Tuna Brine under air conditions has shown a predominant influence on time to failure of Mechanical Work, and although the addition of other parameters raised R^2 by very small amounts, some candidate regressions which met the fit test were identified.

3.2.7.2 Regression Predictions for Tuna Brine : Nitrogen Flush Conditions. See Table 28 for subsets considered under this paragragh.

In this case the best subsets data showed that a greater proportion of variability in time to failure was explained by the integrated current time value, I_{a1}, and the mechanical work of deformation, than for air conditions. Refer to R^2 values in table 28. Again, the Mallows Cp values were too high for these parameters to be satisfactory as single regression predictors, indicating that in either case other predictors require to be added. Preferred subsets as candidate predictor combinations were numbers 7 and 9, combining high R^2 adjusted values with low standard deviation and Cp values at or below the number of parameters plus one.

Subset 7: (see Tables 35-37 for statistics).

Time of failure (hours) : Tuna :(N_2 flush)= - 216 + 26.5*Mechanical Work M1 (N.m) - $1.2*10^{-5}$*Ia_1 ($\log_{10}$ current (amps) * time (seconds)) + 158*Delta Hgcorr (mm) + 41.2*pH start.

Table 35: Subset 7 : Regression statistics

Predictor	Coeff	SE Coef	T	P
Constant	-216.43	96.52	-2.24	0.049
Mech work	26.516	7.013	3.78	0.004
Ia1	-0.00001175	0.00000585	-2.01	0.072
Delta Hgcorr	157.66	74.82	2.11	0.061
pH start	41.2	16.66	2.47	0.033

R^2= 94.8% R^2 (adj) = 92.7% R^2 pred = 83.97%

Table 36: Subset 7 : Analysis of Variance

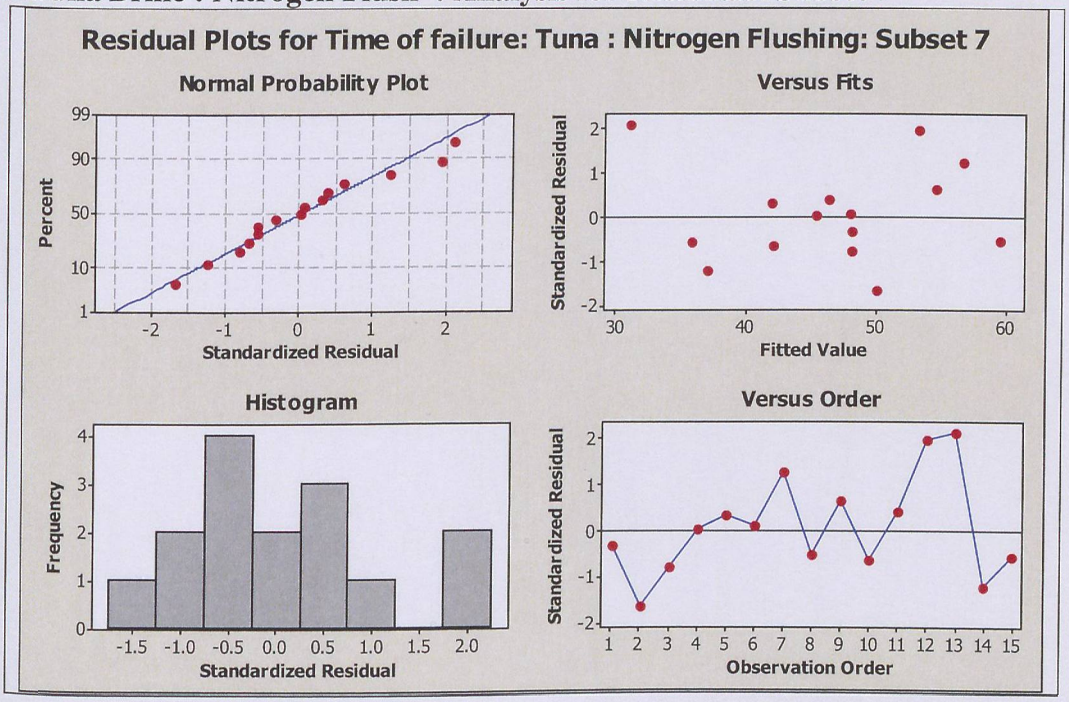
Source	DF	Sum of squares	Mean square	F ratio	P value
Regression	4	895.31	223.83	45.57	0.000
Residual error	10	49.11	4.91		
Total	14	944.43			

Table 37: Subset 7 : Unusual Observations

Observation	Mechanical work: Tuna N_2 flush	Time to failure: hrs	Fit	Standard error of fit	Residual	Standardised residual
13	0.101	34.680	30.920	1.322	3.760	2.11R

R denotes an observation with a large standardized residual.
No evidence of lack of fit (P >= 0.1).

Plot 14: Tuna Brine : Nitrogen Flush : Analysis for Residuals: Subset 7



Subset 9: (see Tables 38-40 for statistics).

The regression equation was:

Time of failure(hours) = - 375 + 40.0* Mechanical work M1 + 125207* erms(volts) – 423*DeltaHG (cms) + 467 * Delta HGcorr(cms) + 69.1* pH start.

Table 38: Subset 9 : Regression Statistics

Predictor	Coeff	SE Coef	T	P
Constant	-375.34	84.79	-4.43	0.002
Mech work	40.032	4.250	9.42	0.000
erms	125207	49795	2.51	0.033
Delta HG	-423.0	159.1	-2.66	0.026
Delta HG corr	466.6	109.8	4.25	0.002
pH start	69.08	14.42	4.79	0.001

R^2= 96.2% R^2 (adj) = 94.1% R^2 pred = 75.17%

Table 39: Subset 9 :Analysis of Variance

Source	DF	Sum of squares	Mean square	F ratio	P value
Regression	5	908.42	181.68	45.41	0.000
Residual error	9	36.01	4.0		
Total	14	944.43			

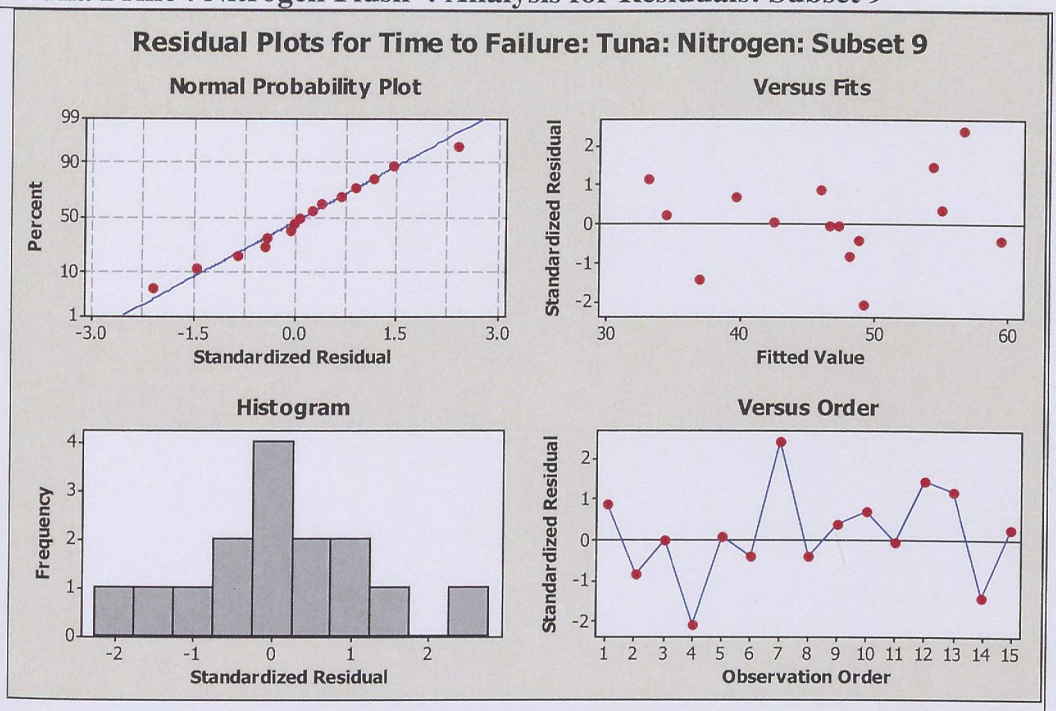
There were two unusual observations having large standardised residuals denoted by R in the table below, from which it is apparent that one was high and one low:

Table 40: Subset 9 : Unusual Observations

Observation	Mechanical work: Tuna N_2 flush	Time to failure: hrs	Fit	Standard error of fit	Residual	Standardised residual
4	0.398	45.380	49.235	0.791	-3.855	-2.10R
7	0.593	58.560	56.581	1.825	1.979	2.42R

There was no evidence of lack of fit in the lack of fit test : P >0.100.

Plot 15: Tuna Brine : Nitrogen Flush : Analysis for Residuals: Subset 9



3.2.8 Regression Predictions for Time to failure using 'Best Subsets Method:

Salmon Brine Product.

After having established numerous statistically significant correlations at $P \leq 0.100$ between some individual parameters and time to failure, the data sets for salmon brine obtained under air and nitrogen flushing conditions were examined for linear regression prediction for time to failure by the method of best subsets. The mini-tab statistical package was used. Starting from the least number of predictors, this analysis gave the following top ten subset predictions for high air and low air (N_2 flush)data sets respectively in tables 41-42 below.

Salmon Brine: Table of Best Subset Regression Combinations for Prediction of Time to Failure in Slow Strain Rate Tests.

Table 41: Regression Matrix: Salmon Brine : Air conditions : Completely failed specimens

Sub-set	Rsq Salmon: air	Rsq adj	Cp	s	pH start	pH end	OCV	dBC	dBC corr	dHG	dHG corr	dAD	E rms_1	I rms_1	Ia_1	M1 Mech work
1	89.7	88.8	-1.0	4.0779												x
2	79.0	77.2	8.4	5.8269											x	
3	94.1	93.0	-1.0	3.2223											x	x
4	92.0	90.5	-1.0	3.7544		x										x
5	96.0	94.8	-2.5	2.7939	x	x										x
6	95.4	94.0	-1.9	3.0005		x									x	x
7	97.0	95.6	-1.3	2.5546	x	x						x				x
8	96.8	95.4	-1.2	2.6306		x					x		x			x
9	97.9	96.6	-0.2	2.2563		x					x	x	x			x
10	97.7	96.2	0.0	2.3688	x	x				x		x				x

Note : In the headings,the letter 'd' as a prefix to dBC, dBC_{corr}, dHG, dHg_{corr} and dAD, refers the change in value delta of these parameters as defiined in Table 25.

Table 42: Regression Matrix: Salmon Brine : Nitrogen flush conditions : Completely failed specimens.

Sub-set	Rsq	Rsq adj	Cp	s	pH start	pH end	OCV	dBC	dBC corr	dHG	dHG corr	dAD	E rms_1	I rms_1	Ia_1	M1 Mech work
1	88.7	87.9	-2.2	3.8913											x	
2	86.9	86.0	-0.6	4.1873												x
3	91.6	90.3	-2.7	3.4814											x	x
4	90.3	88.8	-1.6	3.7361							x				x	
5	93.5	91.8	-2.3	3.1920	x						x				x	
6	92.5	90.7	-1.7	3.4155	x										x	x
7	94.7	92.8	-1.4	2.9909	x		x				x				x	
8	94.0	91.8	-0.8	3.1999	x						x				x	x
9	95.0	92.6	0.3	3.0488	x		x				x			x	x	
10	95.0	92.5	0.3	3.0574	x		x				x				x	x

Note : In the headings,the letter 'd' as a prefix to dBC, dBC_{corr}, dHG, dHg_{corr} and dAD, refers the change in value delta of these parameters as defiined in Table 25

3.2.8.1 General Observations.

Each analysis has shown that the great majority of variability observed in time to failure was attributable to the individual factors of 'mechanical work' and the '$\log_{10}$current-time' integral, I_{a1}, taken up to the point of maximum load. Examination of correlation has shown that the 'mechanical work' gave direct correlation and the '$\log_{10}$current-time' integral I_{a1} an inverse correlation, with time to failure, each being significant at the 0.1% level. Regarding the I_{a1} parameter, the relationship with time to failure is discussed in Section 3 paragraph 3.9.6 a)-e), regarding the combination of negative Ia_1 values (see Appendices 6-9) and the inverse effect.

Due to direct inter-correlations having been established between gauge, extension to failure, change of load and mechanical work, all significant at P= 0.1% or a higher level, the mechanical work term may be used as a single predictor combining the effect of these parameters. In analyses where the parameters of 'mechanical work' and Ia_1 were combined without other predictors added, a lack of fit test showed significance at the 5% level or higher.

3.2.8.2 Regression Predictions for Salmon Brine : Air conditions. See Table 41 for Subsets considered under this heading.

Lack of fit tests showed significance for regression subsets 1,3,4,5 and 6. For subset 2, a non normal distribution of residuals was clearly apparent, with an accompanying high Mallows Cp value, signifying important parameters missing. For regressions 7 and 8 the fit tests were acceptable. Regressions 9 and 10 may be considered over fitted. Subset 7 was the best in terms of fit and R^2 predicted values, Subsets 7 and 8 are detailed below.

Best Fit Regressions selected: Subsets 7 and 8 from Table 41:

Subset 7: (see Tables 43-45 for statistics).

The regression equation was:

Time to failure : Salmon: air : hours = 117 + 73.4 * M1(Mech work) +

4.45*Delta AD - 50.7* pHstart + 36.8 *pH end.

See tables below for regression statistics and analysis of variance:

Table 43: Subset 7 Regression Table

Predictor	Coeff	SE Coef	T	P
Constant	116.75	83.60	1.40	0.196
Mech work	73.434	4.373	16.79	0.000
Delta AD	4.45	2.587	1.72	0.119
pH start	-50.69	14.41	-3.52	0.007
pH end	36.751	9.602	3.83	0.004

S= 2.55464 R^2 = 97.0 % R^2(adj) = 95.6% R^2 predicted = 86.89%

Table 44: Subset 7 Analysis of Variance

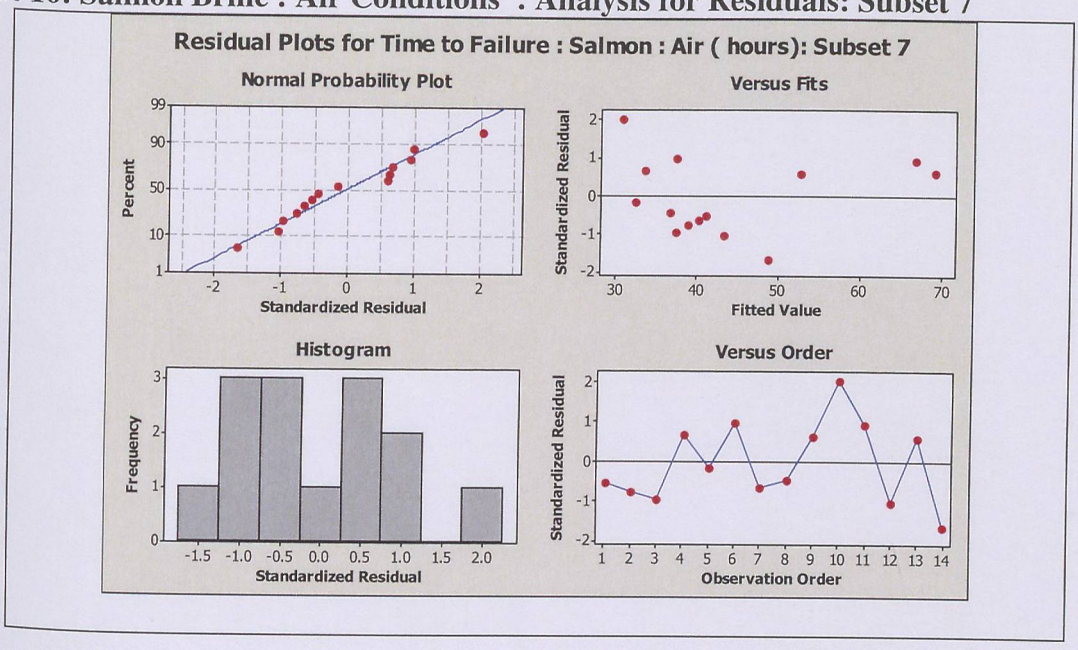
Source	DF	Sum of squares	Mean square	F ratio	P value
Regression	4	1879.22	469.80	71.99	0.000
Residual error	9	58.74	6.53		
Total	13	1937.95			

Table 45: Subset 7 Unusual observations: Mechanical Work: M1

Observation	Mechanical work M1	Time to failure: hrs	Fit	Standard error of fit	Residual	Standardized Residual
10	0.172	34.940	30.533	1.356	4.407	2.04R

R denotes a value with an unusually high standardized residual.
No evidence of lack of fit. (P>=0.1).
See Plot 16 below for residuals. These did not follow a normal pattern very closely, and there were indications of two distributions.

Plot 16: Salmon Brine : Air Conditions : Analysis for Residuals: Subset 7



Subset 8: (see Tables 46-47 for statistics).

The regression equation was:

Time to failure : Salmon : air (hours) = - 124 + 52.3* M1(Mech Work) +

6991* $E_{rms\,1}$+ 368*Delta HG_{corr} + 24.3 *pH end.

Table 46: Subset 8 Regression Table

Predictor	Coeff	SE Coef	T	P
Constant	-123.75	54.39	-2.28	0.049
M1 Mech work	52.303	6.974	7.50	0.000
E_{rms1}	6991	2424	2.88	0.018
Delta HG_{corr}	368.1	134.5	2.74	0.023
pH end	24.315	8.869	2.74	0.023

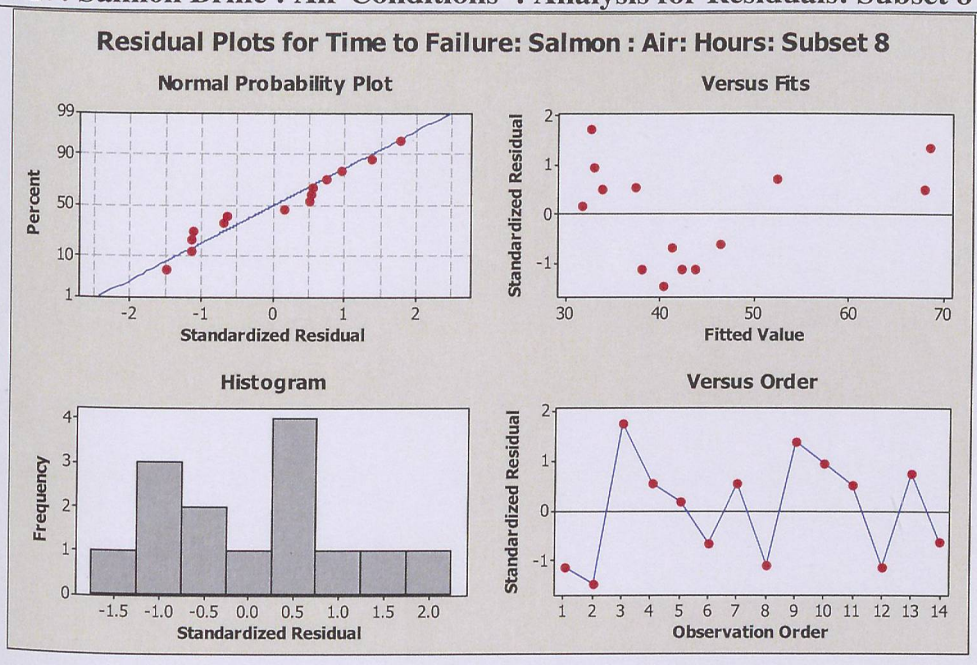
S= 2.63056 R^2 = 96.8 R^2 (adj) = 95.4 R^2 predicted = 89.68%

Table 47: Subset 8 Analysis of Variance

Source	DF	Sum of squares	Mean square	F ratio	P value
Regression	4	1875.68	468.92	67.76	0.000
Residual error	9	62.68	6.92		
Total	13	1937.95			

No evidence of lack of fit. (P>=0.1). Significance was shown for all individual parameters at 5% or a hogher levels, with R^2 for predicted data close to 90%. This regression again showed some bias in the distribution of residuals. See Plot 17 below.

Plot 17: Salmon Brine : Air Conditions : Analysis for Residuals: Subset 8



3.2.8.3 Regression Predictions for Salmon Brine : Nitrogen flush conditions.

See Table 42 for subsets considered under this heading.

For these conditions, the individual candidate predictors of integrated current , Ia_1, and Mechanical Work (M1) each gave statistically significant regressions, subset numbers 1 and 2. Once again when combining these two predictors in subset 3, significance was observed in a lack of fit test. For Subsets 4 and 5, combining Ia_1 with additional parameters each produced acceptable fits, with subset 5 producing a central tendency in residuals. Subset 6 again combining Ia_1 and Mechanical Work, M1, with an added parameter, produced a lack of fit with statistical significance at the 0.1% level. Subsets 7 and 8 produced acceptable fits with subset 8 combining Ia1 and Mechanical Work (M1) with notch dimensional change and pH. Subsets 9 and 10 would probably be over fitted.

Details are recorded below for three of the better fitting candidate predictor subsets, numbers 5, 7 and 8. Out of these, subsets 5 and 8 have show a central tendency in the

residual plots, but 'Delta GH corr' has shown up as an inverse predictor in these tests, whereas it was a direct predictor under air conditions. See later comments.

Subset 5: (see Tables 48-50 for statistics).

The regression equation was:

Time salmon failure: nitrogen flush: (hours) = 264 - 0.000046 * Ia_1 ($\log_{10}$ current density (amps/cm^2)x time (secs)) – 366* Delta HG corr(cm) - 40.2* pH start.

Table 48: Subset 5 Regression table

Predictor	Coeff	SE Coef	T	P
Constant	264.4	104.9	2.52	0.027
Ia_1	-4.591e-5	3.91e-6	-11.75	0.000
Delta HG corr	-367.8	148.0	-2.49	0.029
pH start	-40.15	16.64	-2.41	0.033

S = 3.19244 R^2 = 93.5% R^2 (adj) = 91.9% Predicted R^2 = 86.21%

Table 49: Subset 5 Analysis of Variance

Source	DF	Sum of squares	Mean square	F ratio	P value
Regression	3	1754.04	584.68	57.37	0.000
Residual error	12	122.30	10.19		
Total	15	1876.34			

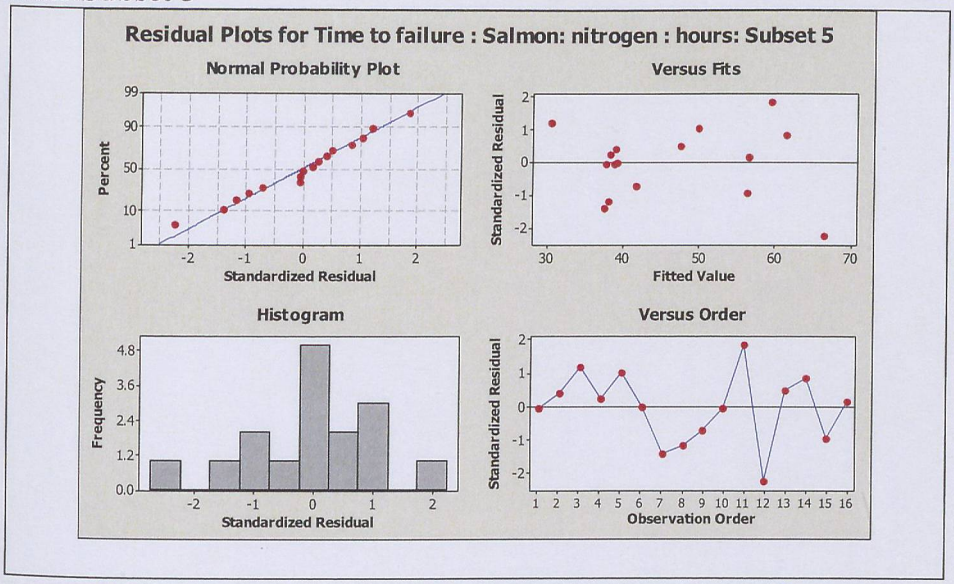
Table 50: Subset 5 Unusual Observations

Observation	Ia_1	Time to failure: hrs	Fit	Standard error of fit	Residual	Standardised residual
12	-1332700	61.290	66.542	2.192	-5.252	-2.26R

R denotes an observation with a large standardized residual.

No evidence of lack of fit (P >= 0.1).

Plot 18: Plot 6: Salmon Brine : Nitrogen Conditions : Analysis for Residuals:Subset 5



Subset 7: (see Tables 51-53 for statistics).

The regression equation was:

Time to failure (salmon): nitrogen (hours) = 160 - 0.000047*Ia_1 -

485*Delta HGcorr - 0.208*OCV - 49.4*pH start.

Table 51: Subset 7 Regression table

Predictor	Coeff	SE Coef	T	P
Constant	160.5	118.1	1.36	0.202
Ia_1	4.725e-5	3.77e-6	-12.54	0.000
Delta HG corr	-485.4	157.40	-3.08	0.010
OCV	-0.2083	0.1301	-1.60	0.138
pH start	-49.38	16.68	-2.96	0.013

S= 3.00302 R^2 = 94.7% R^2 (adj) = 92.8% Predicted R^2 = 87.76%

Table 52: Subset 7 Analysis of Variance

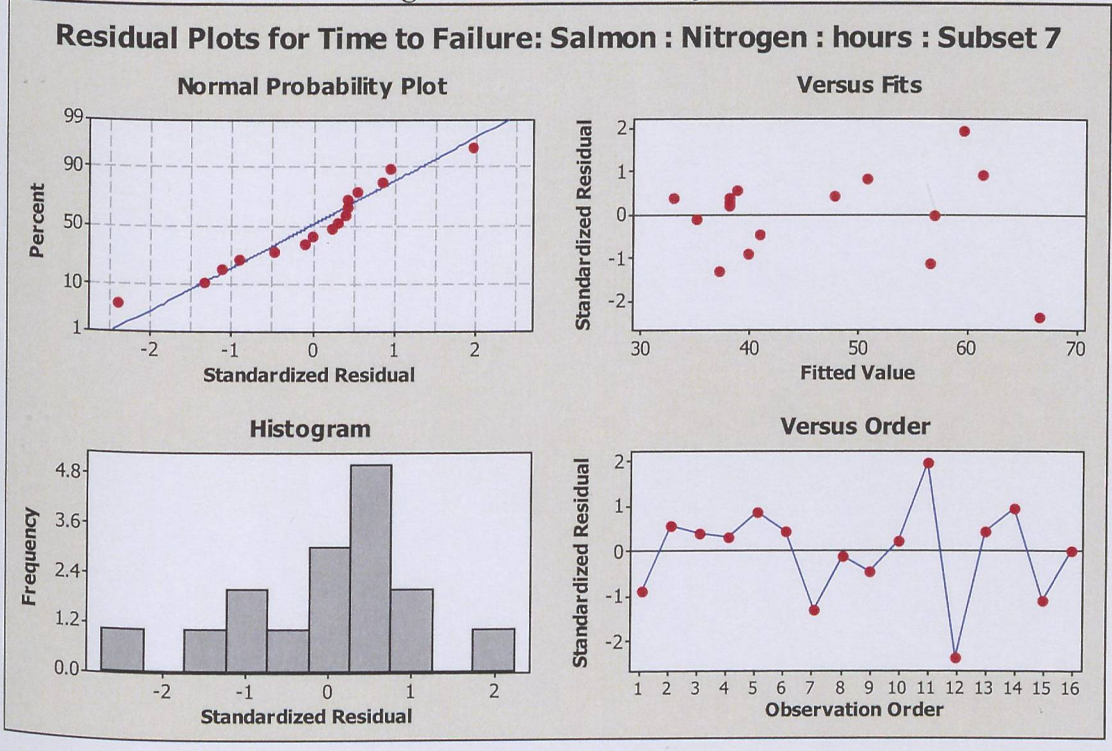
Source	DF	Sum of squares	Mean square	F ratio	P value
Regression	4	1777.14	444.29	49.27	0.000
Residual error	11	99.20	9.02		
Total	15	1876.34			

Table 53: Subset 7 Unusual Observations

Observation	Ia_1	Time to failure: Hrs	Fit	Standard error of fit	Residual	Standardized residual
12	-1332700	61.290	66.559	2.062	-5.269	-2.41R

R denotes an observation with a large standardized residual.
No evidence of lack of fit. (P> = 0.1).

Plot 19: Salmon Brine: Nitrogen Conditions: Analysis for Residuals: Subset 7



Subset 8: (see Tables 54-55 for statistics).

The regression equation was:

Time to failure = 229 + 10.0*M1 (Mechanical Work) - 0.000037*Ia_1

- 282*Delta HG corr - 34.2*pH start.

Table 54: Subset 8 Regression table

Predictor	Coeff	SE Coef	T	P
Constant	229.2	111.2	2.06	0.064
Mech work	10.0	10.25	0.98	0.350
Ia_1	-3.662e-5	1.030e-5	-3.56	0.005
Delta HG corr	-282.2	172.4	-1.64	0.130
pH start	-34.16	17.77	-1.92	0.081

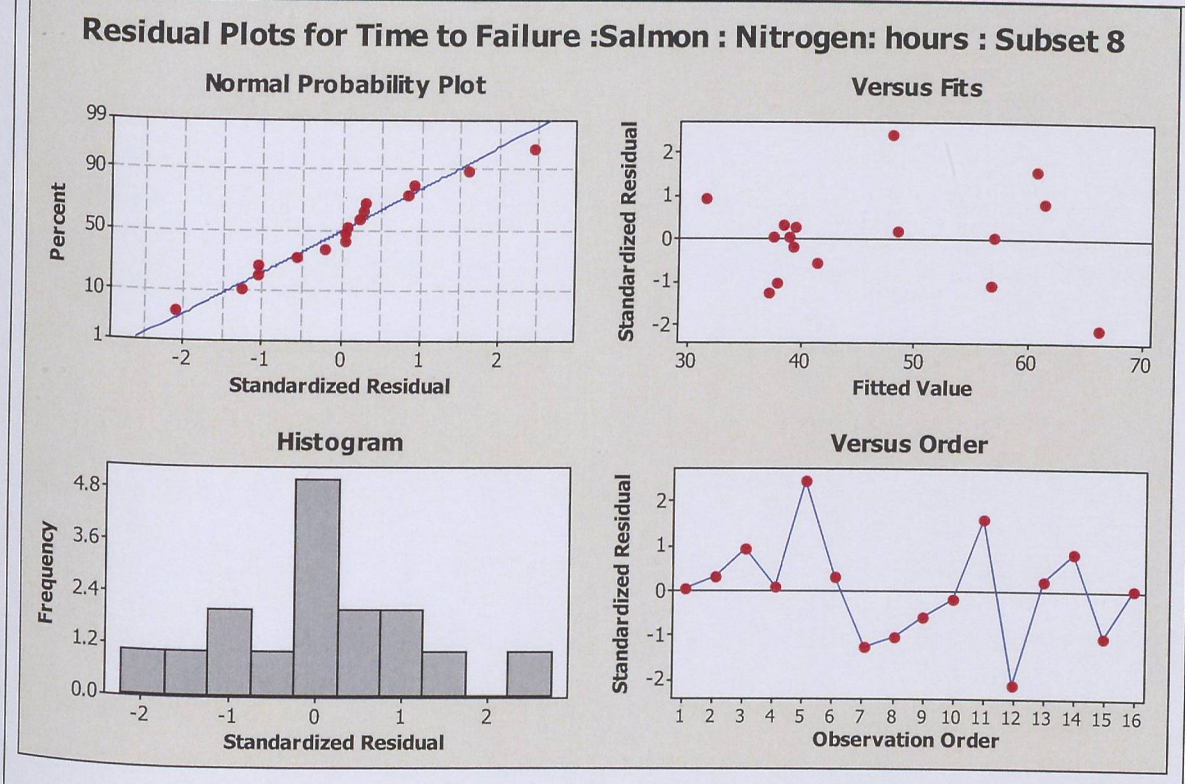
S= 3.19897 R^2 = 94.0% R^2 (adj) = 91.8% R^2 predicted = 81.16%

Table 55: Subset 8 Analysis of Variance

Source	DF	Sum of squares	Mean square	F ratio	P value
Regression	4	1763.77	440.94	43.09	0.000
Residual error	11	112.57	10.23		
Total	15	1876.34			

No evidence of lack of fit. (P>=0.1).

Plot 20: Salmon Brine: Nitrogen Conditions : Analysis for Residuals: Subset 8



3.2.9 Summary Comments on Regression Data: Tuna and Salmon Brines.

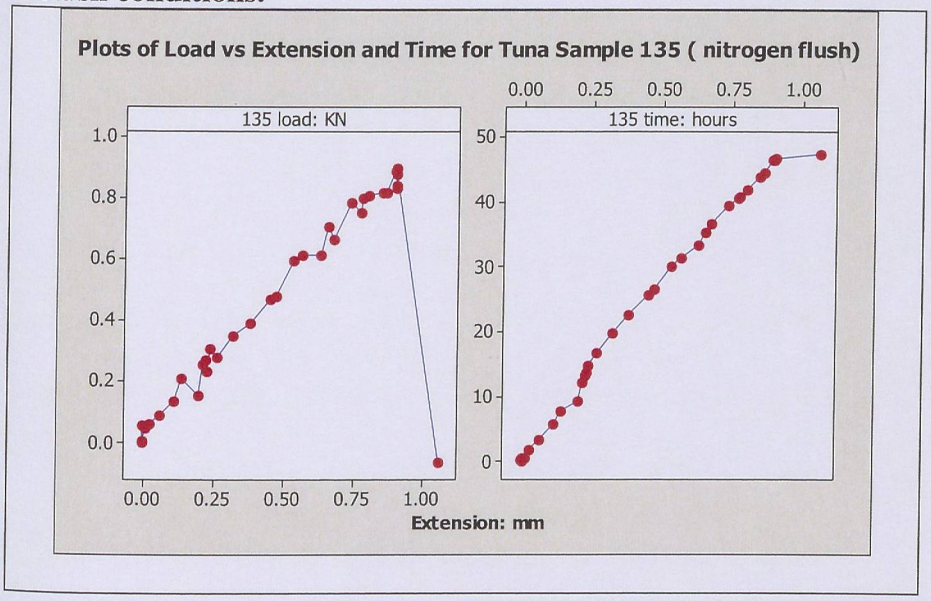
The failure process measured has included physical and electrochemical corrosion parameters, and the correlation matrix has shown that for both products and high air or low air (nitrogen flushing) conditions, direct correlation with time to failure of the Mechanical Work measurement, M1, existed, as did inverse correlation of the current – time integral Ia_1 (See paragraph 3.6.9 a)-e) for more detailed comment concerning the combination of negative values of this parameter and inverse behaviour with respect to time to failure). Although these individual parameters each explained around 70% or

more of variability in time to failure (and when combined in linear regression models, more than 80% of variability based on R^2 data all four main categories), there was generally a poor regression fit unless additional parameters were added. In the case of Tuna Brine under air conditions , however, the regression fit test was acceptable when the two above mentioned predictors were combined. In some of the candidate regressions an acceptable regression fit was obtained with just one of the parameters, M1 or Ia_1, combined with other parameters e.g. Tuna, nitrogen flush conditions, subset 9, or Salmon, nitrogen flush condition, subset 7. However, this introduced a new difficulty in the case of regressions with salmon where Delta HG_{corr} was included, the effect being shown as direct for air conditions and inverse for nitrogen flushing, relative to the correlation matrix which showed a direct effect in both cases. Examination of the regression behaviour of this parameter alone on time to failure for salmon brine revealed that the effect was direct for air conditions, but biased by a minority of data points, whereas the overall effect was neutral for low air conditions. This parameter would be rather operator sensitive in measurement, the test pieces being manually set under a microscope after failure. Delta HG_{corr} would be expected to be responsive to Mechanical Work, M1, on account of both elastic and plastic deformations which affect the result , but it could also be affected by corrosion in the vicinity of the notch, and again by the fact that the notch edge was lacquered and would have a small meniscus, and again by any environmental stress cracking which may have occurred in the notch vicinity. The correlations of Delta HG_{corr} with Mechanical Work and Ia_1 were inverse and statistically significant for salmon under air conditions only, so the investigation required to recognize this observation, while taking note of the potential limitations in measurement accuracy.

The evidence of some tests in which failure was incomplete suggested that crack initiations developed quite late in the failure process e.g. after around 90% of the failure

time. In conjunction with the trend in the tensile curve for rapid failure after reaching peak load, and close to linear tensile behaviour of most load extension plots up to maximum load, e.g. see plot 21 below, a likelihood existed that crack initiation took place at around the peak load level. A degree of noise in the plot was attributed to the load cell behaviour. This had a 50KN capacity and was run in these tests at under 2KN.

Plot 21: Load vs Extension and Time for Tuna sample ssrt 135 tested under nitrogen flush conditions.



From the candidate regression models detailed above, a limited number have shown a close to balanced central tendency of the residuals. These were Tuna (air conditions, subset 4), Tuna (nitrogen flush conditions, subset 9) and Salmon (nitrogen flush conditions, subset 8). There was not a very high degree of consistency of the subsets between these cases overall, but there was a strong tendency for the same individual prarameters to feature in at least two regressions. The parameters of Mechanical Work,M1, Integrated current, Ia_1, notch dimensional change, Delta Hg corr, and pH start, featured in a significant regressions for three of the four main conditions tested, combining product types and high or low air conditions. I_{a1} was not a chosen parameter for the salmon brine / air conditions subset.

Regarding pH, while the products differed by around 0.4 units the use of two single products with the chosen subsets treated separately would not be very likely to reveal effects very distinctively.

3.2.10 Estimation of Crack Growth Rate for Tuna Brine samples tested under Air Conditions using Slow Strain Rate Test Data

Using the regression method of 'best subsets' on the Minitab package for the same parameters as were used for time to failure, a better fitting relationship overall was obtained for crack growth rate than for time to failure for the Tuna product tested under air conditions. This regression included a number of additional partially failed samples from tests which were stopped prematurely to examine for crack length. This was the only subset having a sufficient number to complete this form of analysis. The regression equation selected as having the best fit on the same basis used as for previous cases is shown below, with statistical details in tables 56-58.

Log_{10} (crack growth rate: air conditions: Tuna) mm/second = -27.5 +1x10-6* Ia_1 – 5222*irms + 22.8*Delta HG –0.0313*OCV.

Table 56: Regression Table

Predictor	Coeff	SE Coef	T	P
Constant	-27.502	8.286	-3.32	0.006
Ia_1	$1.22e\text{-}^{6}$	$3.3e^{-7}$	3.70	0.003
I_{rms}	-5222	2444	-2.14	0.052
Delta HG	22.434	6.727	3.34	0.005
OCV	-0.03127	0.01082	-2.89	0.013

R^2= 84.7% R^2 (adj) = 80% R^2 predicted = 69.96%

Table 57: Analysis of Variance

Source	DF	Sum of squares	Mean square	F ratio	P value
Regression	4	5.3231	1.3308	17.95	0.000
Residual error	13	0.9638	0.0741		
Total	17	6.2869			

Table 58 Unusual observations.

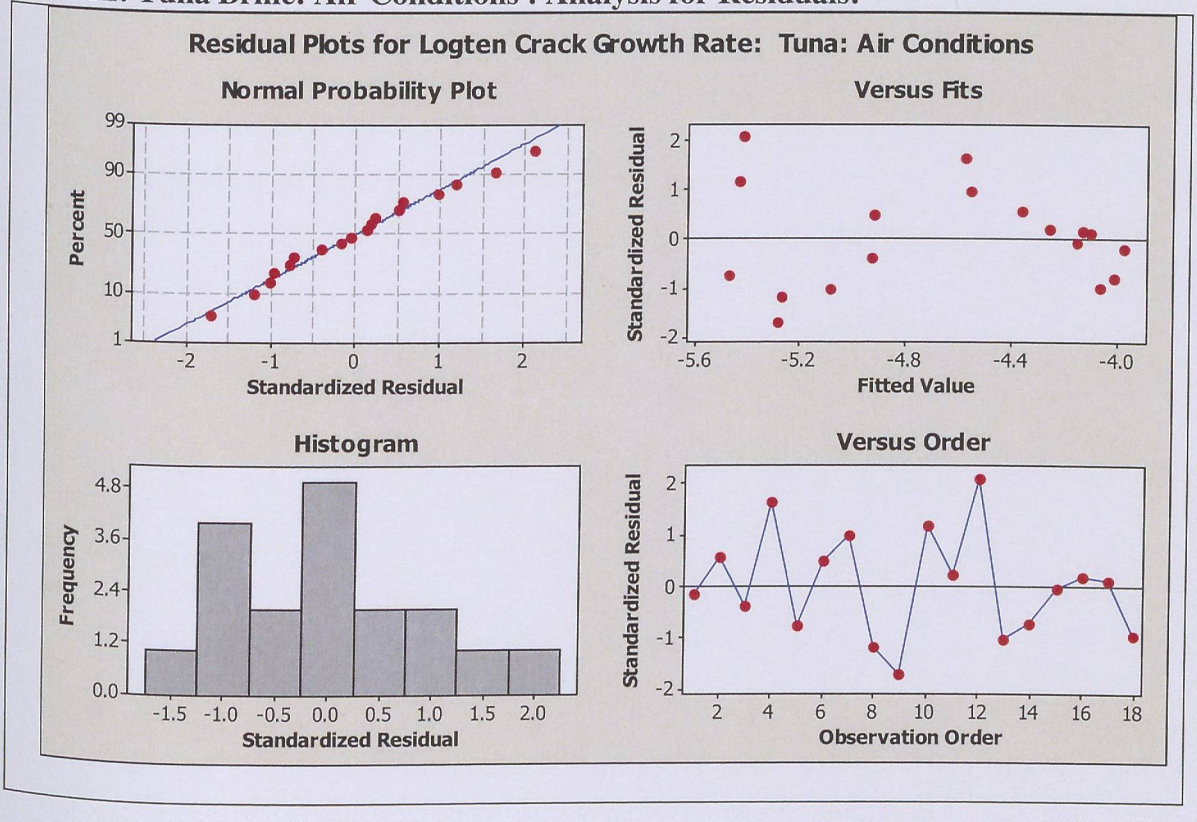
Observation	Ia_1	Log ten crack growth	Fit	Standard error of fit	Residual	Standard residual
12	-1343100	-4.9440	-5.4229	0.1509	0.4789	2.11R

R denotes an observation with a large standardised residual.

All parameters were therefore significant for this regression at at least 10% , with R^2 for predictions at almost 70%

The analysis of residuals is shown in Plot 22 below

Plot 22: Tuna Brine: Air Conditions : Analysis for Residuals:



From Plot 22, the residuals followed a close to normal pattern with a central tendency and fair balance. The residuals versus the order of observations indicated that observation 12 gave a large residual, but there was no evidence of lack of fit in the fit test, with $P > 0.1$.

It would be logical that more integrated current, if positive, would increase crack growth rate. In this case, notch change, deltaHG, has also shown up as a positive physical parameter which would be expected as a response to Mechanical Work, M1.

3.2.10.1 Stress Intensity factor for the Experimental Notch Case

It is established knowledge that crack growth rate shows a relationship with the stress intensity factor. The stress intensity factor has been determined by Herzberg[72] as a scale factor to describe the magnitude of the crack tip stress field. For an infinitely large cracked plate this author defines the parameter as:

$$K = \sigma \sqrt{\pi a}$$

where :

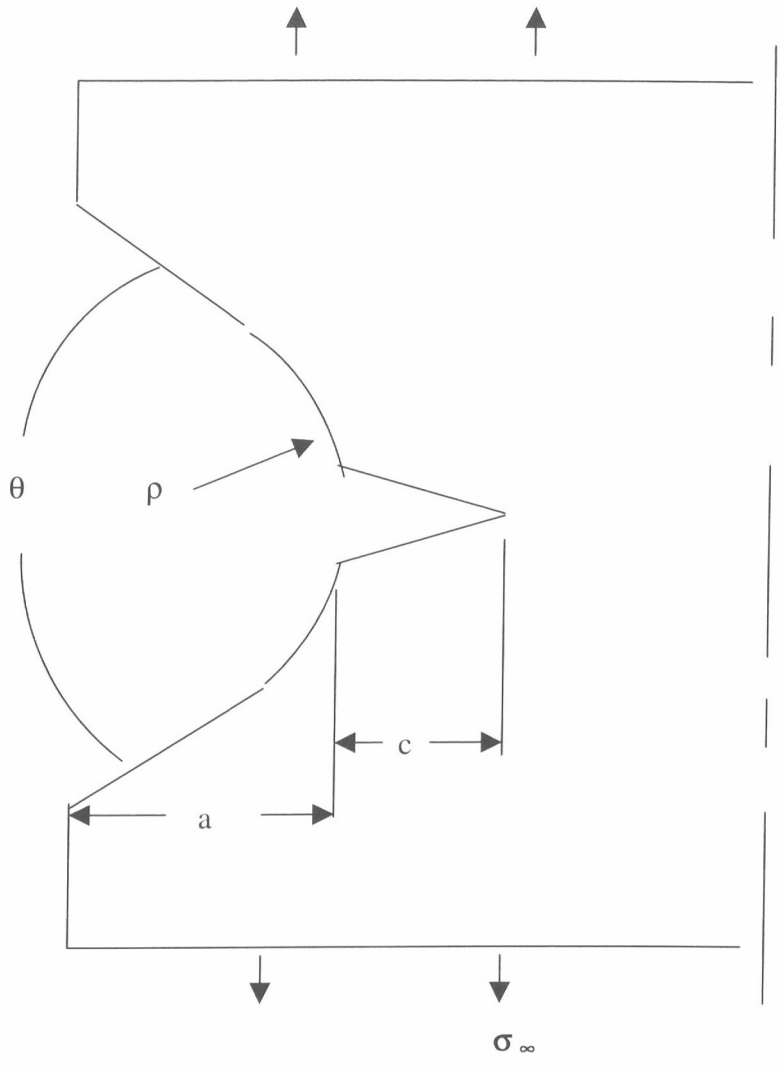
σ is the applied stress

and

a is the crack length.

For cases involving particular geometries in a construction, a geometric constant has to be included and researchers have defined K values for a wide variety of specimen geometries in terms of their dimensions and types of flaw, which are taken into account. H Nisitani and M Isida[80] have described a formula for the Stress Intensity Factor K_I for the case of an angled edge notch having a radius at the root from which a small crack has initiated. This is illustrated below in **Figure 39** , and the geometric constant which is modified by the notch angle, notch depth, notch root radius and crack length is shown on Appendix 11

Figure 39: Notch and Stress Intensity Factor Calculations



Stress Intensity Factor $\mathbf{K_I = F4 * \sigma_\infty * \sqrt{\pi}(a + c)}$

where:

K_I is the Stress intensity factor: Mpa$\sqrt{m}$.

F4 is a geometric constant determine from the notch angle, the c/a ratio and the ρ/a ratio.

σ_∞ is the applied stress : Mpa

a is the notch depth (mm x 10^{-3})

c is the crack depth beyond the notch (mm x10^{-3})

ρ is the notch radius (mm x10^{-3})

θ is the notch angle (deg).

Appendix 3 shows the detail for the geometric constant and the calculation of the values used in the case below for Tuna Brine.

The above formula was used to determine K_I , and tested for statistical regression with crack growth rate, alongside other predictors for eight data sets for Tuna product tested under air conditions. For these cases, the eight tests were terminated before final fracture and were found to have much less than 50% of the specimen width showing a crack. The following points were taken into account:

a) The tests conducted lead to a very slight bias in the equipment such that the cracks tended to emanate from one notch preferentially, mainly that defined by GH. On this basis a formula based on a single notch was considered a reasonable starting estimate in this circumstance, as only one crack initiated.

b) The relevant load is that applied to the whole specimen width used to estimate the stress at the section EF which defined the specimen width between notches.

c) The stress used was that based upon the maximum load and the initial width and thickness of the specimen across EF.

d) The geometric constant was moderated by the c/a ratio and the ρ /a ratio.

The estimated values of K_I made are shown on **Appendix 3.**

3.2.10.2 Statistical Analysis and Prediction for Log Crack Growth Rate Incorporating the Stress Intensity Factor Estimate and slow strain rate test data.

The data obtained was examined initially for correlation of $\log_{10}$ crack growth rate with the K_I estimate, the electrochemical parameters E_{rms1}, I_{rms1}, Ia_1 , and pH , notch height change. The correlation matrix is shown below.

Table 59: Statistical Correlation Matrix for Crack Growth rate including Estimated Stress Intensity Factor.

Parameters		*Log $_{10}$ crack growth rate. mm/sec*	*E rms: Volts*	*I rms$_1$: amps/cm^2*	*Ia$_1$: Log$_{10}$ current density (amps/cm^2) x time(secs)*	*K_I : Mpa√m.*	*Delta HG; cms*	*Delta HG corr: cms*	*pH start*	*pH end*
E_{rms}	coefficient	-0.159								
	P value	0.706								
I_{rms1}	coefficient	0.373	-0.340							
	P value	0.363	0.409							
Ia_1	coefficient	0.417	-0.039	**0.700**						
	P value	0.304	0.927	**0.053**						
K_I estimate	coefficient	**0.713**	-0.432	0.038	-0.036					
	P value	**0.047**	0.285	0.929	0.933					
Delta HG	coefficient	**0.742**	-0.218	0.087	-0.025	0.620				
	P value	**0.035**	0.604	0.837	0.953	0.101				
Delta HG	coefficient	**0.742**	-0.218	0.087	-0.025	0.620	1.0			
corr	P value	**0.035**	0.604	0.837	0.953	0.101	-			
pH start	coefficient	0.021	0.634	-0.277	-0.378	-0.209	-0.045	-0.045		
	P value	0.961	0.091	0.507	0.357	0.619	0.915	0.915		
pH end	coefficient	**0.695**	0.243	0.528	**0.626**	0.099	0.216	0.216	0.261	
	P value	**0.056**	0.563	0.178	**0.097**	0.816	0.607	0.607	0.532	
Mechanical	coefficient	-0.140	-0.141	**-0.680**	**-0.911**	403	0.242	0.242	0.156	-0.556
Work,M	P value	0.741	0.739	**0.064**	**0.002**	0.322	0.563	0.563	0.712	0.152

From this matrix the key observations were:

a) Log_{10} crack growth rate showed direct correlations significant at 10% or a higher level with K_I , Delta HG, Delta HG $_{corr}$ and pH end, but no significant correlations with mechanical work, M1, Ia_1, or electrochemical potential, current parameters.

b) Delta HG and delta HGcorr were inter-correlated. Mechanical work and showed inverse correlations with two electro-chemical parameters.

c) It should be feasible to obtain a regression model for log_{10} crack growth rate.

A best subsets regression for log_{10}crack growth rate with 6 parameters gave the matrix in Table 60 below:

Table 60: best subsets regression for log_{10}crack growth rate

Number	R-sq	R-sq(adj)	Mallows Cp	Standard deviation	K_I	Delta HG:	pH end	I_{rms1}	I_{a1}	M1: Mech work
1	55.0	47.5	70.6	0.24261		x				
2	50.9	42.7	77.4	0.25346	x					
3	90.3	86.4	14.2	0.12370	x		x			
4	84.9	78.9	23.0	0.15378		x	x			
5	97.1	94.9	4.8	0.075297	x	x	x			
6	90.8	83.9	15.2	0.13422	x		x			x
7	98.5	96.6	4.4	0.062127	x	x	x			x
8	98.2	95.8	5.0	0.068277	x	x	x		x	
9	99.0	96.5	5.7	0.062872	x	x	x	x		x
10	98.7	95.3	6.2	0.072353	x	x	x		x	x

From this data the evidence showed that while DeltaHG and K_I account for very significant proportions of variability in log_{10}crack growth rate, the Mallows Cp values for these parameters and their combinations including pH were much higher than the subset integer criteria. The regression giving marginally the highest R^2 adjusted value with the Mallows integer closest to the number of subsets plus one, or below, was **subset 7**. The data for this regression is shown below.

Subset 7 (see tables 60-61 for statistical details)

The regression equation was:

Log_{10}Crack growth rate = - 27.2 + 7.20*10^{-4}* K_I + 42.4*DeltaHG +

3.70*pH end – 0.481*M1 (mechanical work).

Table 61: Regression Table

Predictor	Coeff	SE Coef	T	P
Constant	-27.234	4.468	-6.09	0.009
K_I	$7.2e^{-4}$	$1.3474e^{-4}$	5.24	0.014
Delta HG	42.4	3.96	3.96	0.029
pH end	3.6983	0.7606	4.86	0.017
Mechanical work	-0.4815	0.2839	-1.70	0.188

S= 0.0621267 R^2 = 98.5 R^2 (adj) = 96.6

R^2 predicted = 70.76%.

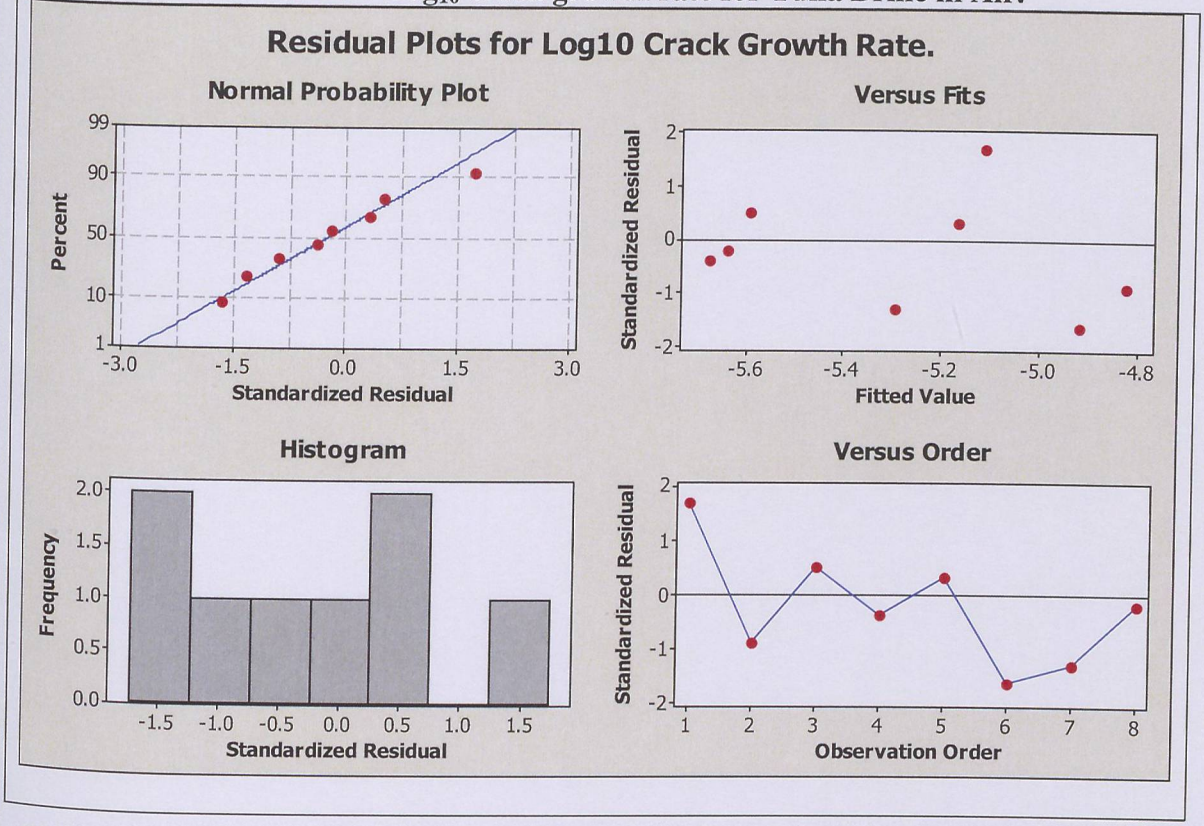
Table 62: Analysis of Variance.

Source	DF	Sum of squares	Mean square	F ratio	P value
Regression	4	0.77349	0.19337	50.1	0.004
Residual error	3	0.01158	0.00386		
Total	7	0.78507			

Thus, the variability of the crack growth rate observed is well accounted for by the regression parameters, but overall prediction was limited and more data and analysis would be need to improve prediction. The ANOVA table showed that the regression was significant at the 1% level. The mechanical work parameter was not significant as an individual parameter in the regression table.

There was not enough data for a lack of fit test. The residual plot is shown below as Plot 23. the residuals were mainly close to linear on the normal probability plot, but there was not a strong central tendency in the distribution.

Plot 23: Residual Plot for Log_{10} crack growth rate for Tuna Brine in Air.



3.2.10.3 Summary Comments on the Crack Growth Rate Estimates for the case of eccs Steels Tested in Tuna Brine Tested using the Slow Strain Rate Method under Air Conditions.

The evidence of the form of the tensile plots together with that of samples removed from the slow strain rate tests before complete failure, suggested that cracking initiated at quite a late stage in the test, and probably around the maximum load level, given that at or beyond the maximum load an abrupt change on the plot occurred followed by relative relatively rapid failure.

On the basis of the behaviour observed, while the time to complete failure of the specimens could be fitted to linear models with very substantial proportions of

variability explained, the crack growth rate would not be expected to be linear. For the tuna brine samples tested under air condition, sufficient data were obtained to formulate initial candidate relationships for crack growth rate. The R^2 values for predictions for the two selected cases were similar, but a better distribution of residuals was obtained using the larger amount of data available for the initial regression excluding K_I, and this regression had also included integrated current as a predictor. Further tests providing more substantive evidence would be required to establish a better prediction involving the K_I parameter.

3.3 Microscopy:

3.3.1 General Observations on Development of Fractures

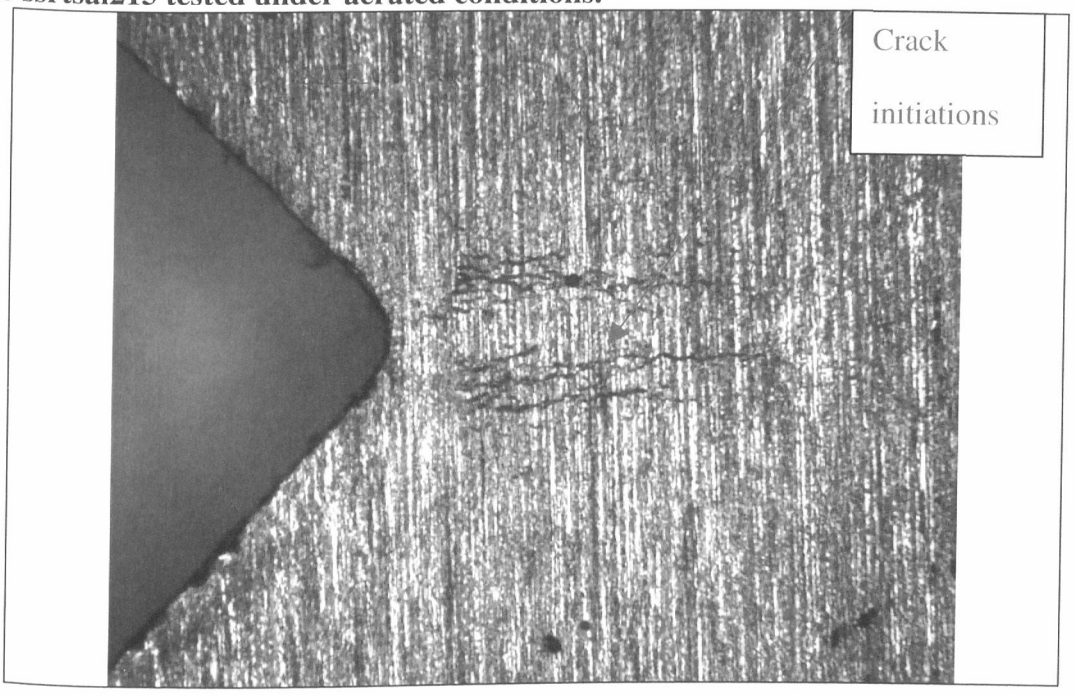
The failures have been examined using a combination of lower power microscopy and scanning electron microscopy.

The evidence of slow strain rate tests in the Tuna and Salmon Brine product media used has suggested that the development of the failure follows a sequence of steps listed below with effects illustrated in subsequent paragraphs:

a) Tensile loading leading to an essentially linear load extension plot, or a predominance of results displaying this, up to the point of maximum load.

b) Pitting took place in regions ahead of the notch apexes, at other points of relative weakness in the eccs protective system, and at scratches.

Figure 40: Example of cracks developing from elongated pits in salmon brine sample ssrtsal215 tested under aerated conditions.



c) Cracking was initiated at or slightly ahead of the notch apex region, e.g. **Figure 40.** As the notch edge had a coating of lacquer applied with slight meniscus formation, the favoured region for crack initiation tended to be just ahead of the notch apex coincident with one of the bands of pits. This was identified by observations on the minority of specimens from a number of tests which were terminated before complete failure took place.

d) The initial 1-3mm of cracking was characterised by evidence of reduced ductility to a variable extent affecting both product types and air/ low air test conditions. At the fracture boundaries close to the surface ahead of the notch, discrete regions showing fractographic 'steps' characteristic of environmental stress cracking were observed with salmon product under high air conditions, and to a lesser extent under low air conditions. For the Tuna product, while there was evidence of loss of ductility at the notch region where fracture initiated, the evidence of any environmental stress cracking was mainly far less certain than for salmon product. Some of the uncertainty arose due to additional corrosion after failure took place.

e) On control samples of each material which were tested in Mace Food Oil, thus excluding any effect due to moist air or corrosive liquid, there was evidence of much greater ductility at notch regions corresponding to those which had shown loss of ductility in the product brine test media.

f) For materials subject to tests in product brines, after the initial 1-3mm of fracture length running from one notch region, usually the notch designated 'HG', a more ductile condition was observed over the remainder of the failure, usually evident from necking behaviour.

g) The evidence from those specimens which were removed from the tests before complete failure suggested that cracking was likely to have been initiated late in

the test and quite probably around the peak load condition, this being consistent with predominantly linear behaviour in the load extension plot or behaviour very close to this up to the maximum load. Subsequent to the peak load condition being reached, the tensile load plot tended to drop very steeply with failure occurring quite rapidly. If a crack had initiated very early in the test, non linearity in the tensile plots, arrest behaviour, or interrupted peaks would have been be expected.

3.3.2 Observations on Control Samples Tested in Oil.

Slow Strain Rate Tests were performed on each test eccs plate material in Mace Food Oil as a control, the oil being used to eliminate any effect of moisture. The tests were performed at the same crosshead speed and following the same measurements and procedure as for the test samples.

These samples were then examined for fractography by SEM and examples of the images are shown below, Figures 41-52.

Samples were :

Item	Code	Description	Figures
1.	SSRT260	0.18mm DR 620CA plate	41-44
2.	SSRT261	0.235mm DR 620CA plate	45-48
3.	SSRT262	0.16mm DR 620CA plate	49-52

Figure 41: ssrt 260 control at notch end B

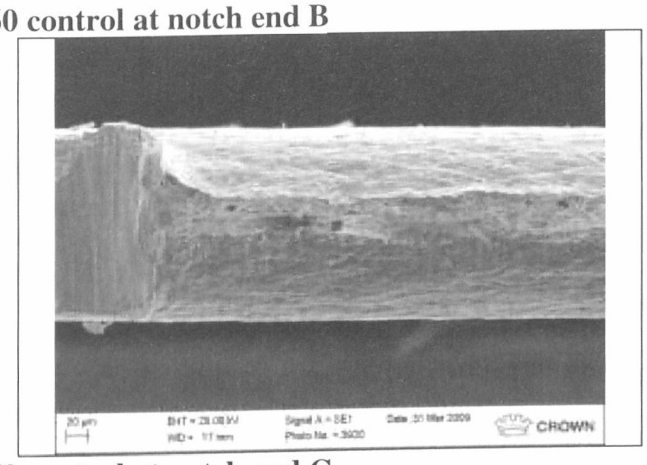


Figure 42: ssrt 260 control at notch end G

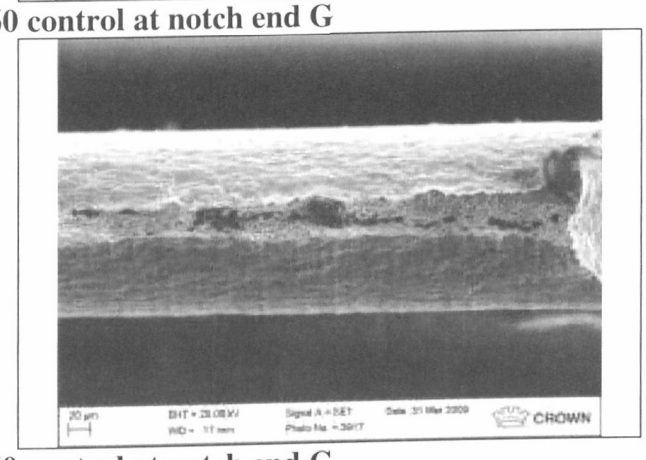


Figure 43: ssrt 260 control at notch end C

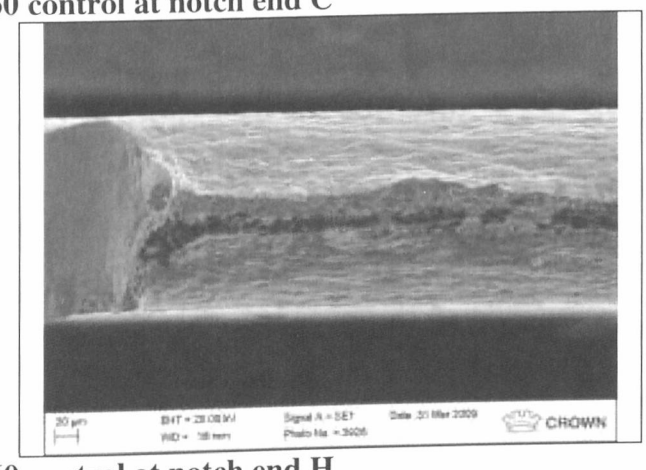


Figure 44: ssrt 260 control at notch end H

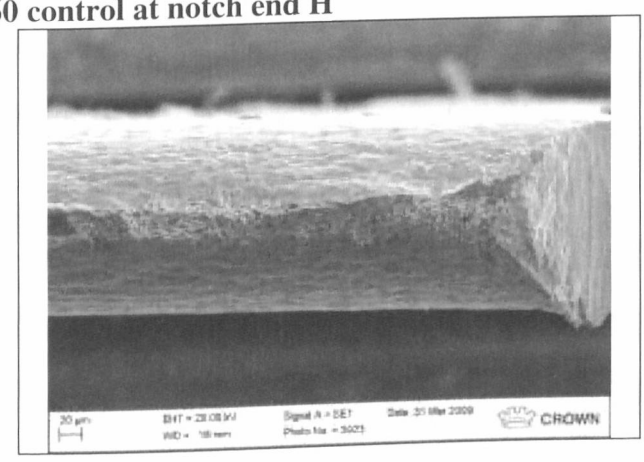


Figure 45: ssrt 261 control at notch end G

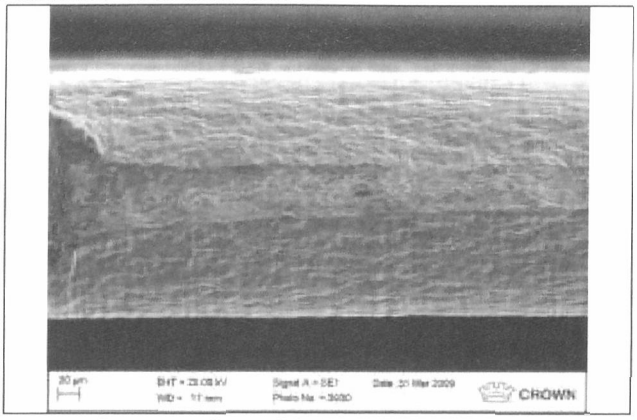


Figure 46: ssrt 261 control at notch end B.

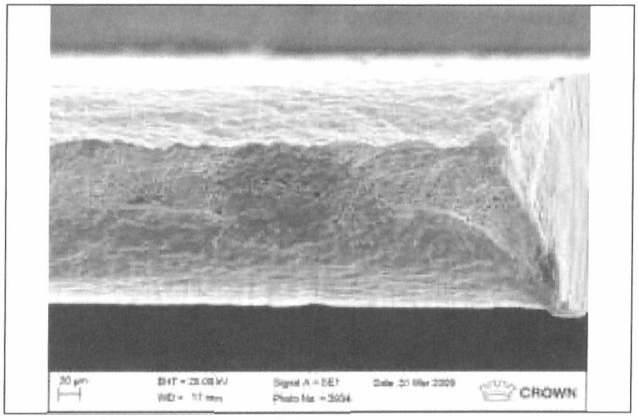


Figure 47: ssrt 261 control at notch end H

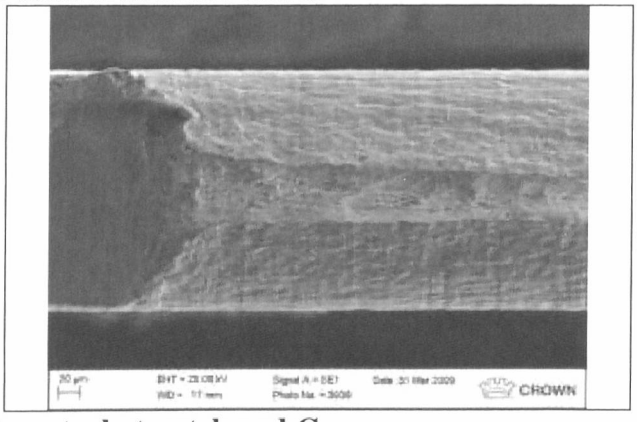
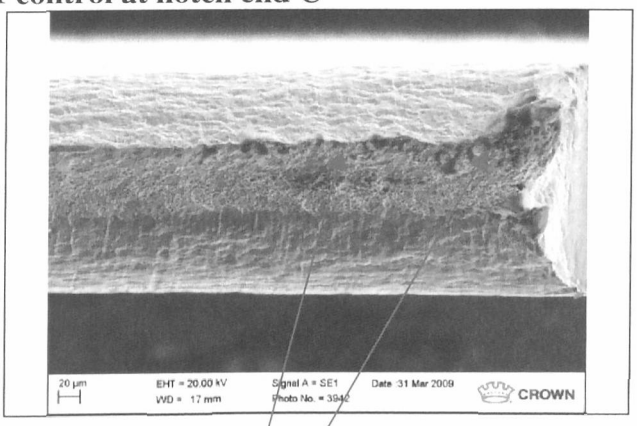


Figure 48: ssrt 261 control at notch end C



Regions of severe work hardening inferred

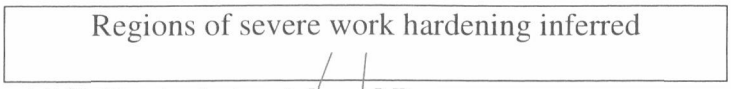


Figure 49: ssrt 262 Control at notch end B

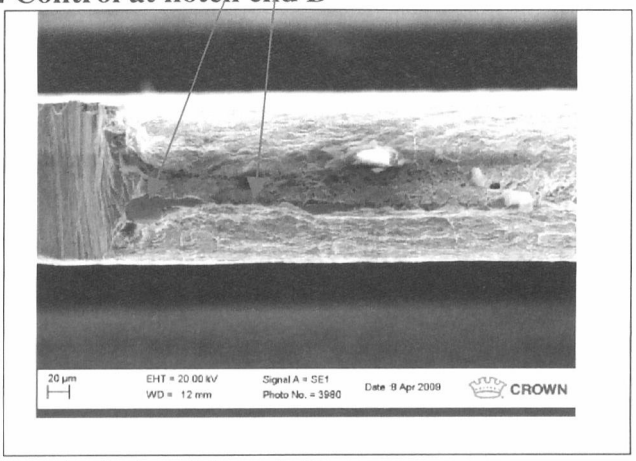


Figure 50: ssrt 262 control at notch end G

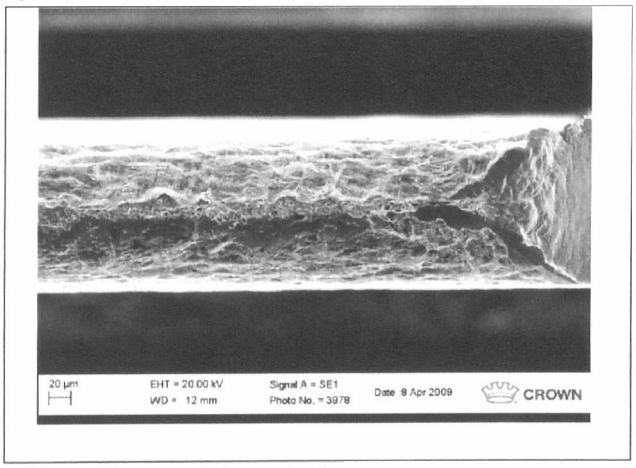


Figure 51: ssrt 262 Control at notch end C

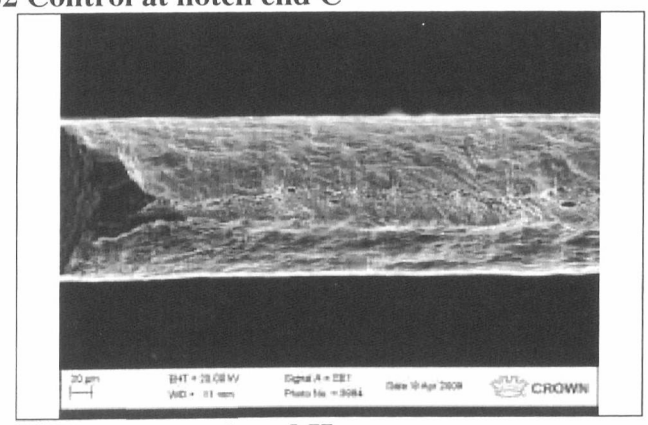
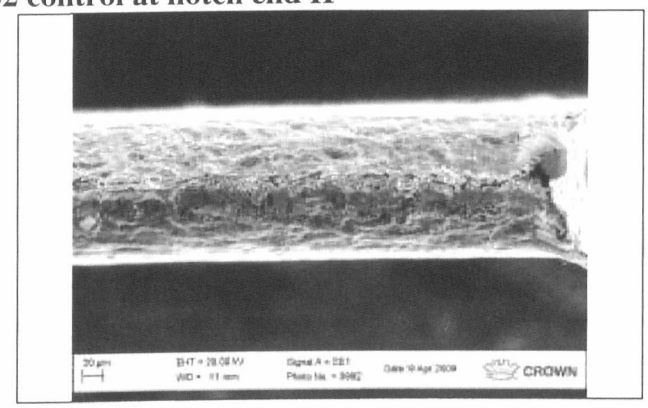


Figure 52: ssrt 262 control at notch end H



Each of these samples showed a very substantial measure of ductility and necking at either notch before fracture in the slow strain rate processs, so providing a reference base of comparison with later examples exposed to the two product media. The sections all showed regions of fracture near the notch apex which had a smooth appearance suggesting that work hardening of these regions has given rise to discrete areas of very low ductility at the point of fracture. The effect was found to be common to test specimens throughout the study whether or not tested in product brines, and again was later observed on parallel sided 'dog bone tensile test specimens. Also, some discrete regions away from notch area showed the effect e.g. **Figures 48 and 49.**

The metal thinning was measured at each notch extremity across the failure section to compare with the value at the mid region of the adjacent un-fractured sloping notch edge, and the % gauge reduction determined. The data has been used for comparisons with failures on samples subject to slow strain rate tests in the product media.

3.3.3 Observations on Slow Strain Rate Tested Samples in Tuna Brine: Air Conditions.

(In the photographs the ssrt code number was the sample, the upper case letter the notch field of the fractured sample, B,C,G, or H, and the lower case letter the photo suffix, plus the original magnification, where shown).

The initial observation was of a repeated difference in appearance between the two notched regions on individual specimens, one showing an apparent low ductility or loss of ductility over e.g. 1-3mm (mainly at the notch indentified as 'HG') . See example in **Figure 53.** The opposite notch typically showed a significant measure of ductlity (usually notch 'BC') e.g. **Figure 54.** This observation was substantially repeated for all three plate types used and for air conditions and nitrogen flush test conditions.

The fracture region commonly displayed a complex failure condition comprising to varying degrees the elements described and illustrated below:

a) A series of small crevices or elongated pits acoss the surface almost perpendicular to the direction of tensile load, **Figure 53**, in addition to more random pitting elsewhere, with one notch showng low ductility, and the second notch greater ductility, **Figure 54.**

Figure 53: Test sample srttuo116: Tuna sample at notch 'GH': air conditions. Low ductility at fracture. 0.18mm plate

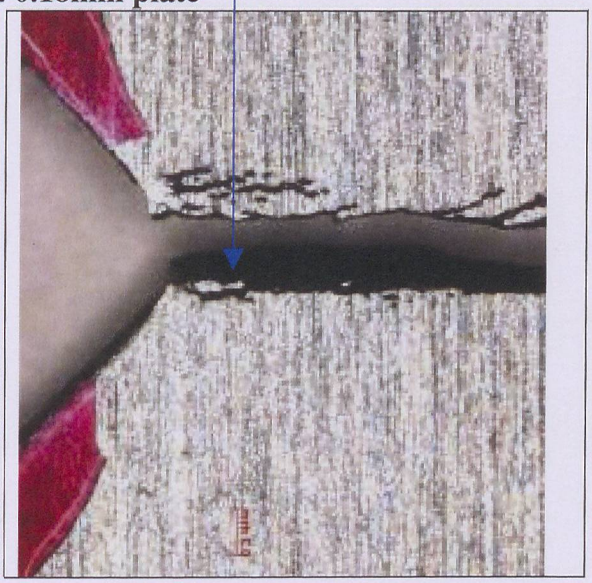
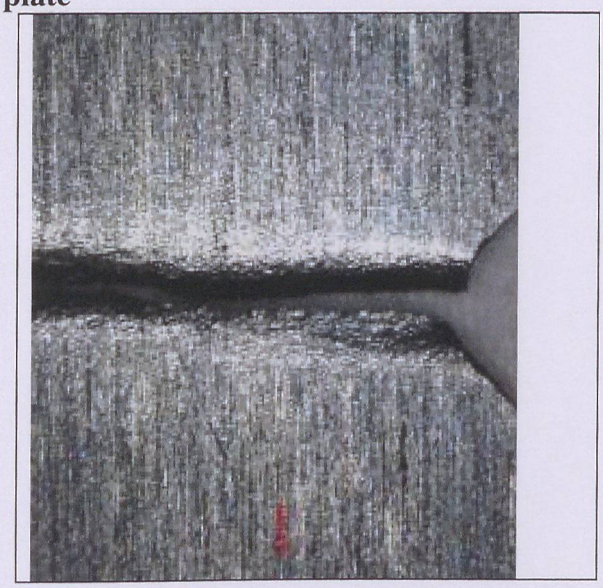
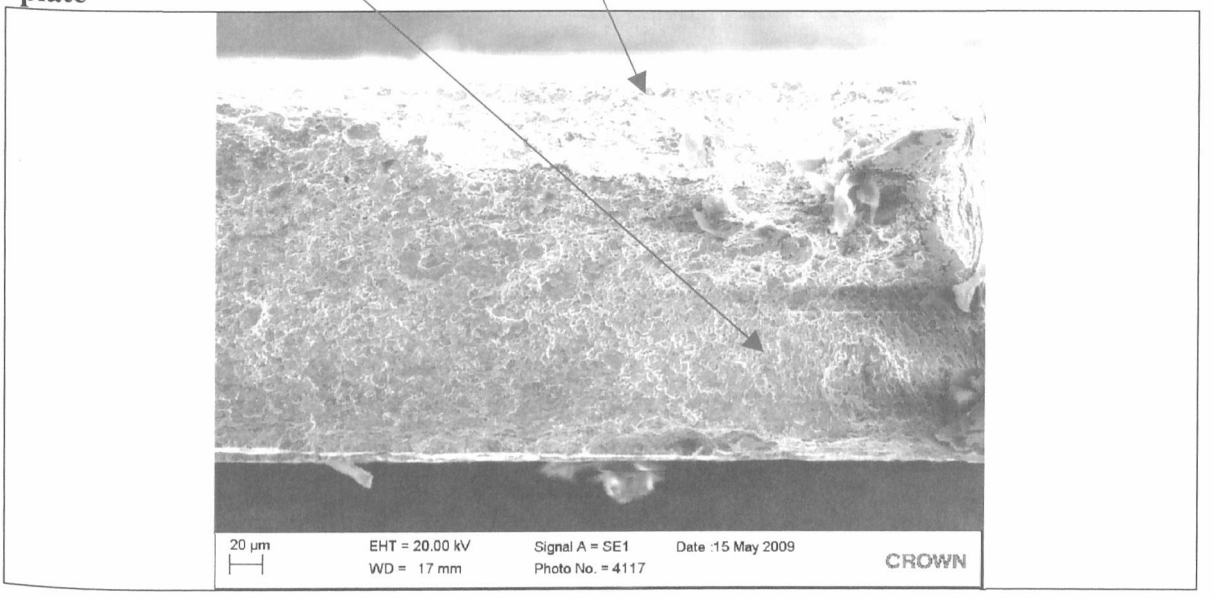


Figure 54: Test sample ssrtTu0116 : tuna sample at notch 'BC' showing a ductile condition. 0.18mm plate



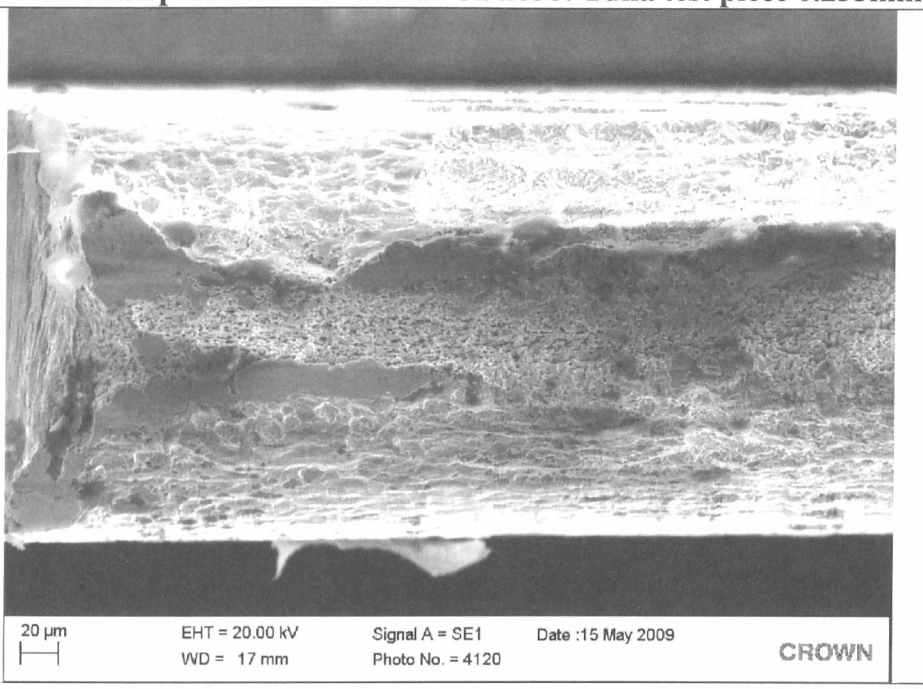
b) Close to the notch apex at the notch end indentified as 'HG', there were regions of low ductility, accompanying some pitting or corrosion at the surface region, .

Figure 55: Test sample ssrttuo163:Ha: test piece from tuna brine: x650. 0.235mm plate



At the opposite end notch 'BC', it was common for a much more ductile effect to be observed at the failure surface with visible necking, **Figure 56.** Note that there were discrete regions of the fracture edge showing a smooth surface which were similar to those identified in 'control' specimens such as e.g. **Figure 48 and 49,** and therefore probably indicated a mechanical work hardening effect of the cold reduced steel, rather than one which can be conclusively linked to an environmental stress cracking effect.

Figure 56: Test sample ssrttuo163:Notch Ca x650: Tuna test piece 0.235mm plate.



c) Ahead of the notch apex and below the surface, pits or crevices formed, some small discrete areas displaying low ductility or local zones of brittle appearance, characteristic of environmental stress cracking, were observed in individual cases. See **Figures 57 and 58.**

Figure 57: Tuna sample Ssrttuo163Bc ; air conditionsx4000: brittle zone near notch along specimen edge, appearance out of character with general evidence. 0.235mm plate.

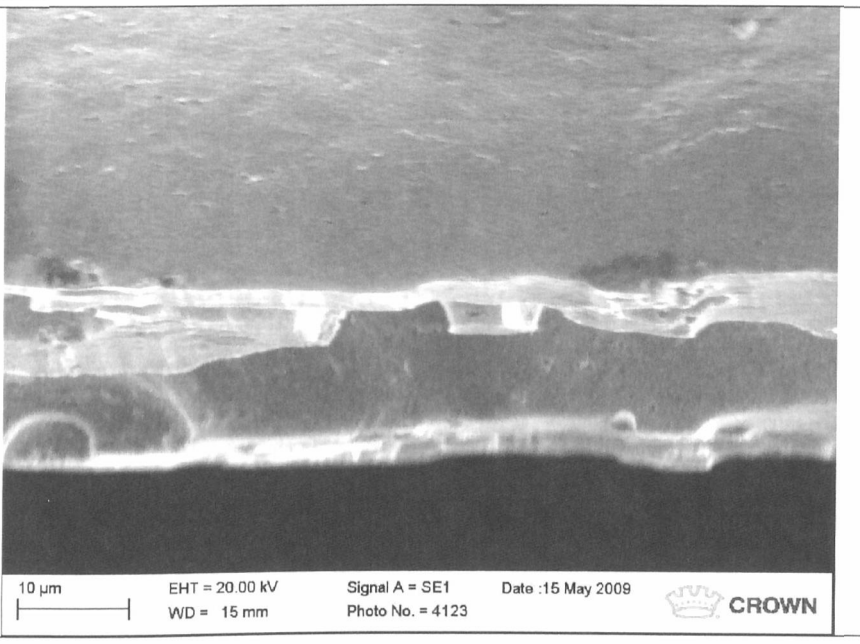
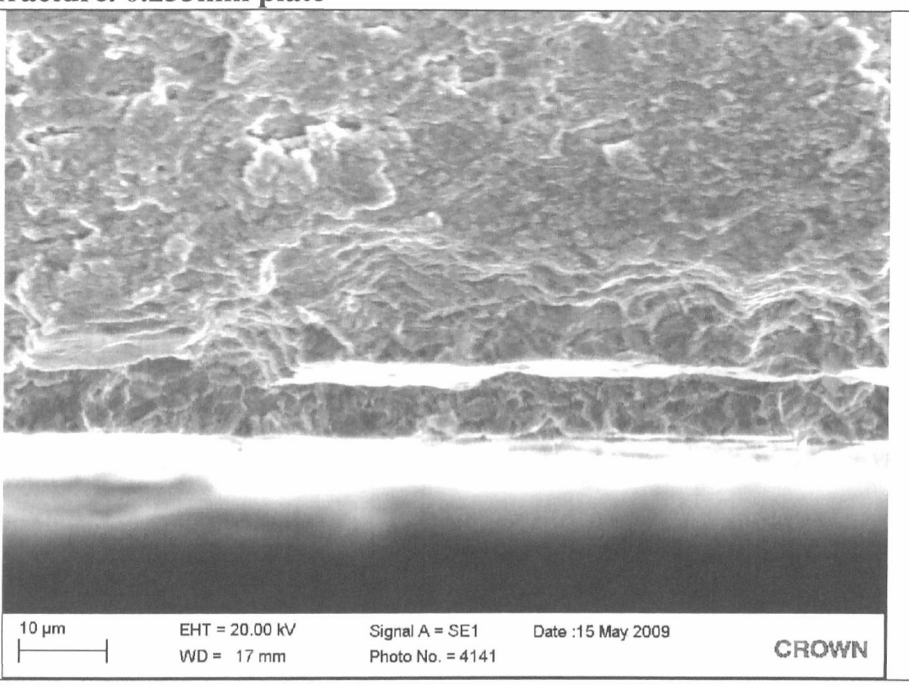


Figure 58: test sample ssrttuo163Ge x3000: Low ductility zone along fracture edge with step fracture. 0.235mm plate



These zones having steps, represented cracking associated with loss of ductility and probable environmental stress cracking in local regions. Further examples below showed very small discrete areas ahead of the notch on sample ssrttu116, **Figures 59 and 60,** showing probable environmental stress crack initiation, and very considerable loss of ductility at one notch 'BC', **Figure 61** , in comparison with high ductility at the opposite notch 'GH' , **Figure 62.**

Figure 59: Tuna sample 116Gb x2500: fracture zone showing discrete area of probable environmental stress cracking initiation. 0.18mm plate.

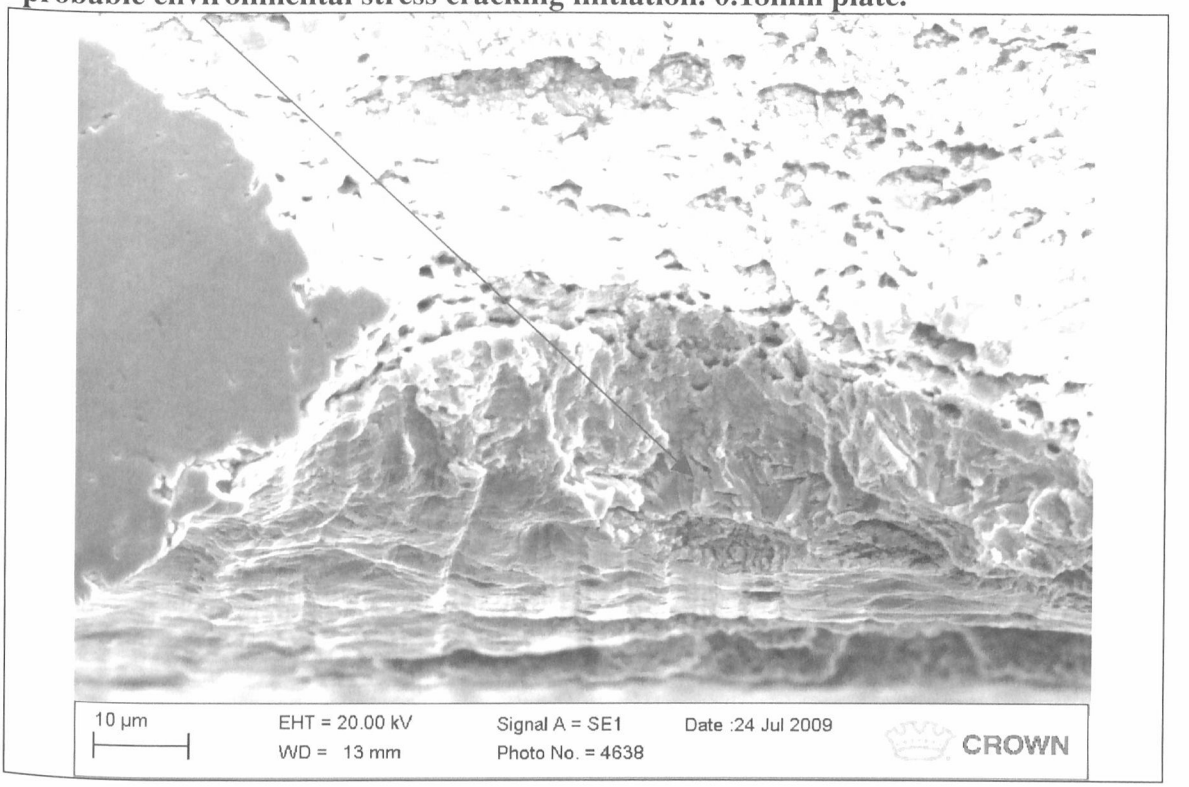
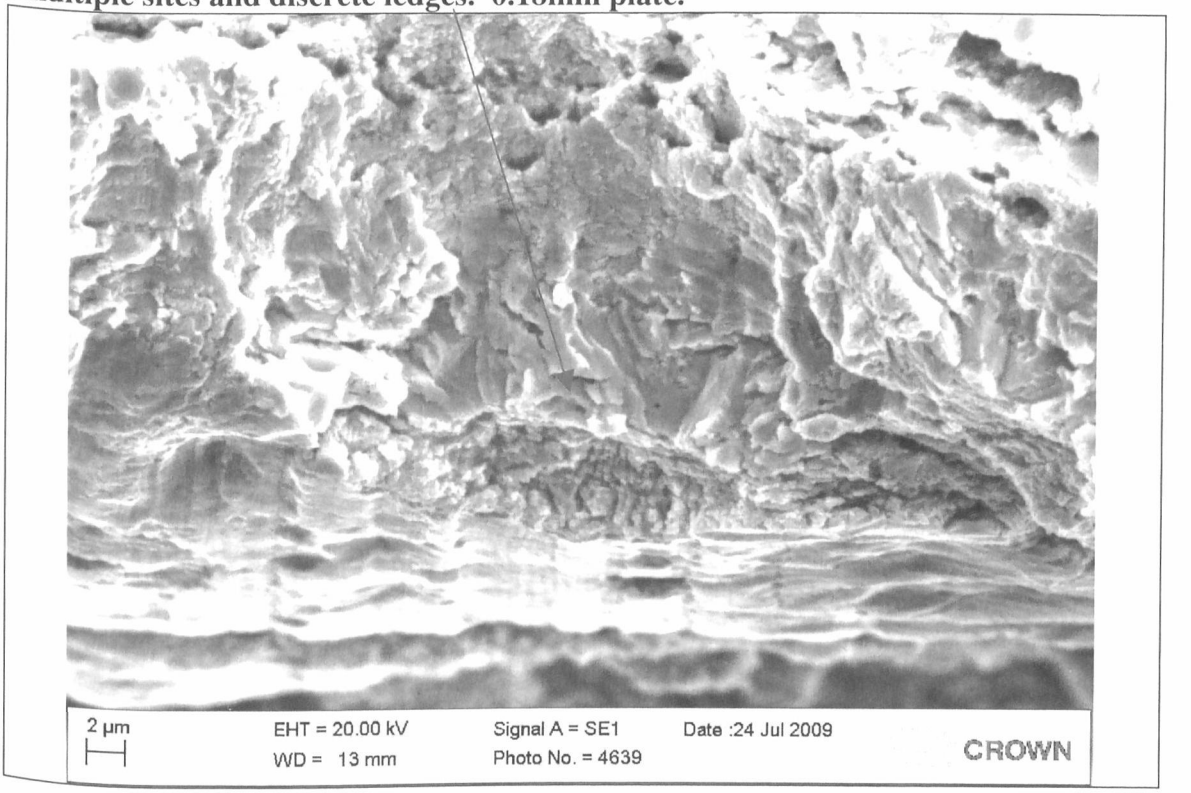


Figure 60: Tuna sample 116Gc x5000 Tuna : Higher magnification: Fracture zone showing discrete area of probable environmental stress cracking initiation- multiple sites and discrete ledges. 0.18mm plate.



Figures 61 and 62 show further examples of images of 0.235mm plate tested in Tuna Brine under air conditions, which illustrated the loss of ductility at one notch preferentially in comparison with the opposite notch.

Figure 61: Test sample ssrttu0164Ba x650: Tuna product : air test conditions, showing low ductility: 0.235mm plate

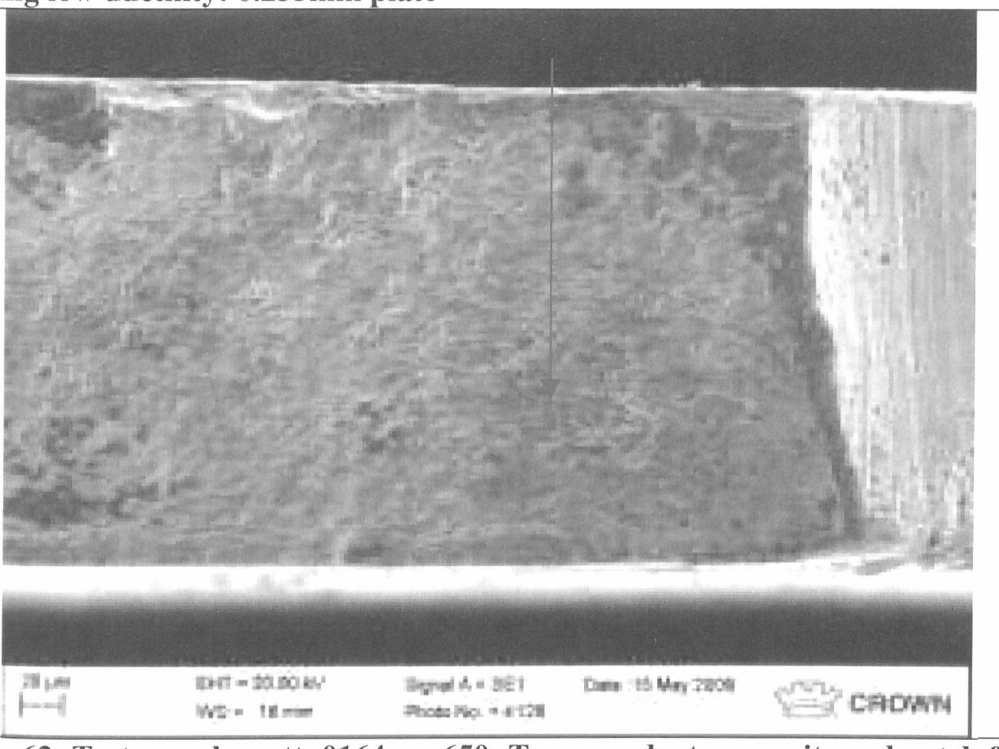
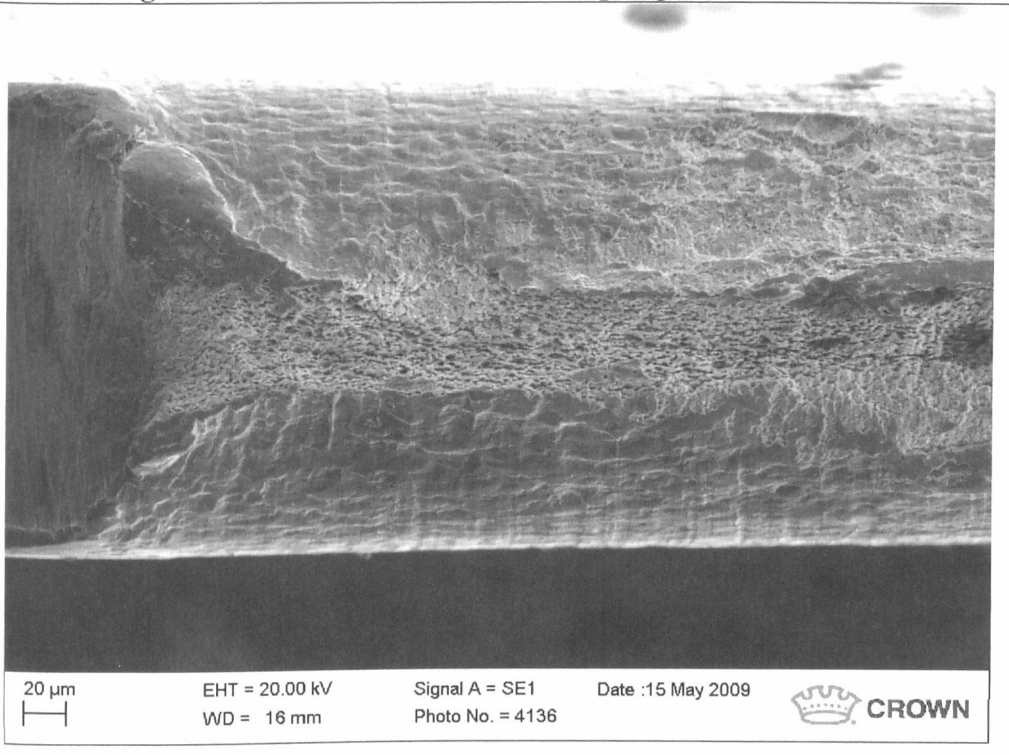


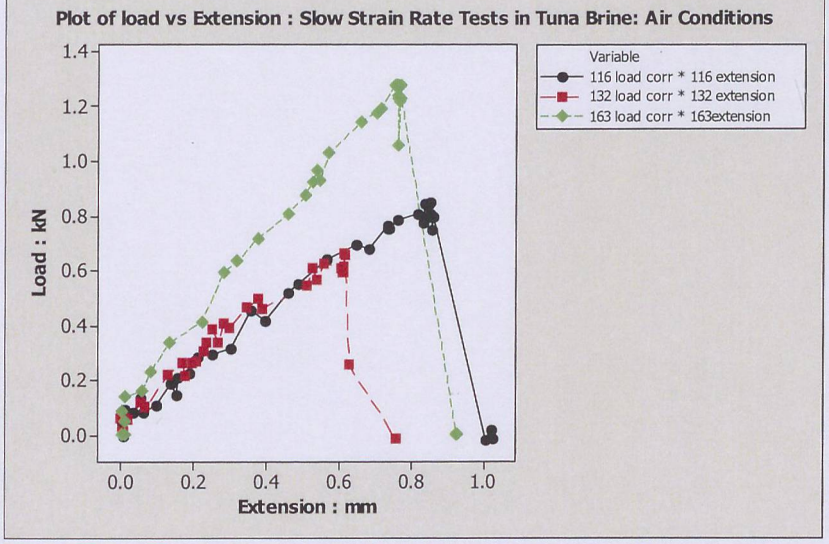
Figure 62: Test sample ssrttu0164ga x650: Tuna product , opposite end notch from figure 25 showing ductile behaviour with cone / cup regions in the central band.



3.3.4 Slow Strain Rate Tensile Load - Extension Plots for Tuna Brine Tests: Air and Nitrogen Flushing Conditions.

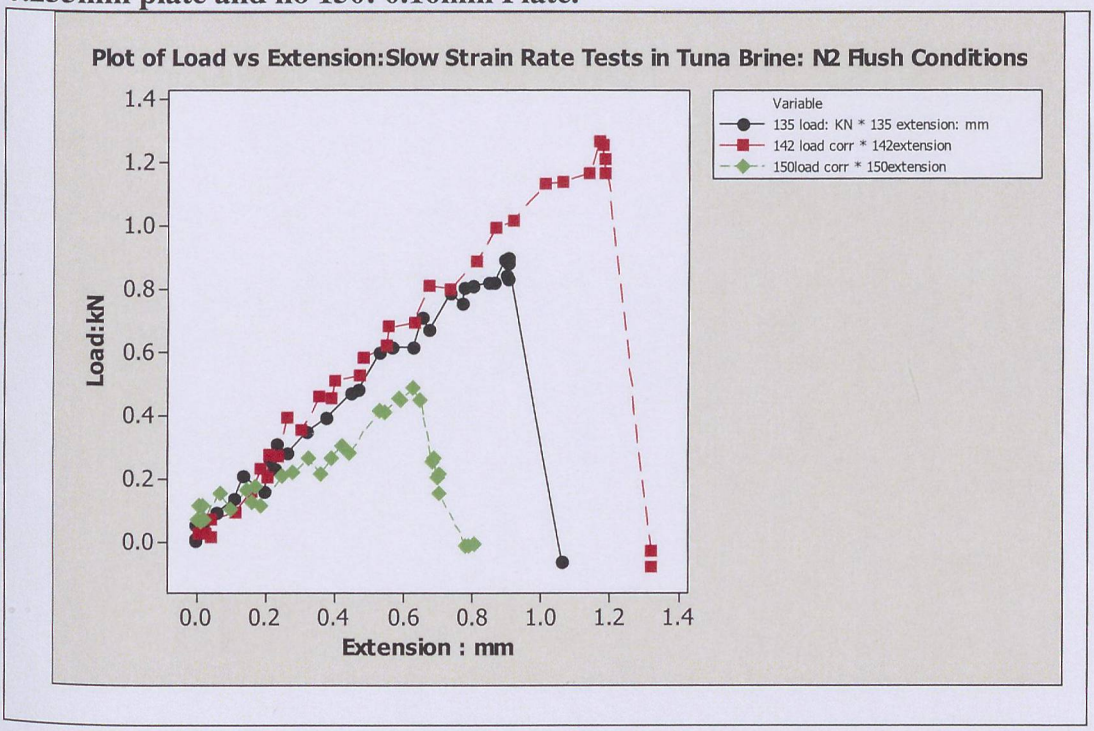
The tensile load – extension plots from the slow strain rate tests from one example of each plate gauge are recorded below, for tests on Tuna Brine in Air, **Plot 24** and low air, nitrogen flush conditions, **Plot 25.**

Plot 24: Load vs Extension Plots from tests for Tests in Tuna Brine; number 116: 0.18mm plate , no 132: 0.16mm plate and no 163: 0.235mm plate: Air Conditions.



Plot 24 showed similar trends for each material, with close to linear behaviour as the load increased, allowing for some noise in the equipment and any effects due to pitting which took place, followed by a sharp fall from peak load leading to failure.

Plot 25: Load vs Extension Plots from tests for slow Strain RateTests in Tuna Brine (nitrogen flushing conditions); ssrt no 135: 0.18mm plate , number 142: 0.235mm plate and no 150: 0.16mm Plate.

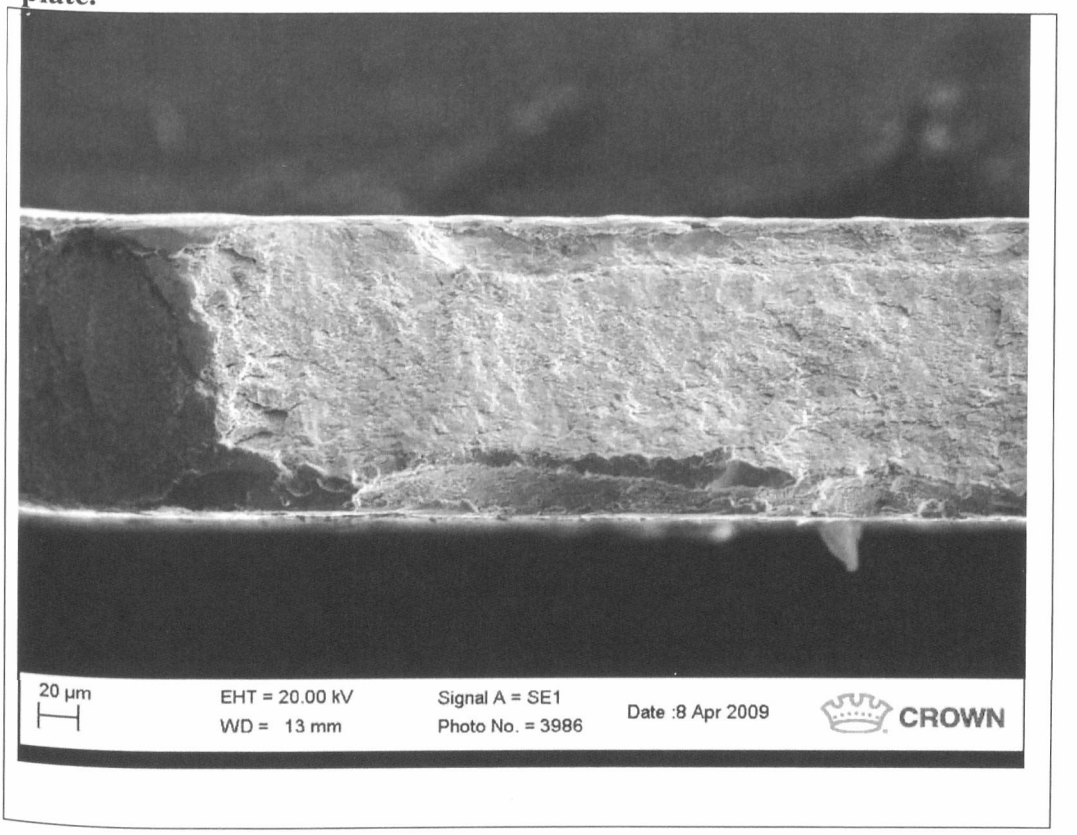


For Plot 25 under low air conditions, behaviour under nitrogen flush conditions was rather similar to that for air conditions for the corresponding materials, being close to linear up to the maximum load. The pattern of the plots under both high and low air conditions showing relatively linear behaviour supports the case that cracking is likely to have initiated in the region of peak loading, then leading to rapid failure.

3.3.5 Microscopy Observations on Slow Strain Rate Tested Samples in Tuna Brine: Nitrogen Flush Conditions

Under low air conditions, the loss of ductiliy was typically still evident at one notch region, such as the example in Figure 63 below. This includes a part fractured but retained segment at the lower edge.

Figure 63: Slow Strain rate Tested Tuna Sample ssrtt Tu150 Ha: x600. 0.16mm plate.



At the fractured region close to the top edge along from the notch a discrete area could be observed which displayed evidence of parallel plateau and ledge morphology, Figures 64, and 65 (higher magnification) . These conditions are similar to examples described in literature[79] as characteristic of cleavage fracture in low carbon steel. However, the width affected in Figure 63 can be seen to be quite small at around 20 microns. These were occasional observations among lots, apart from the loss of ductility highlighted above. In many cases too much pitting or general attack had taken place after the failure, to distinguish other effects.

Figure 64: Slow Strain ratetest sample: ssrttu150Ha x3500: top edge.

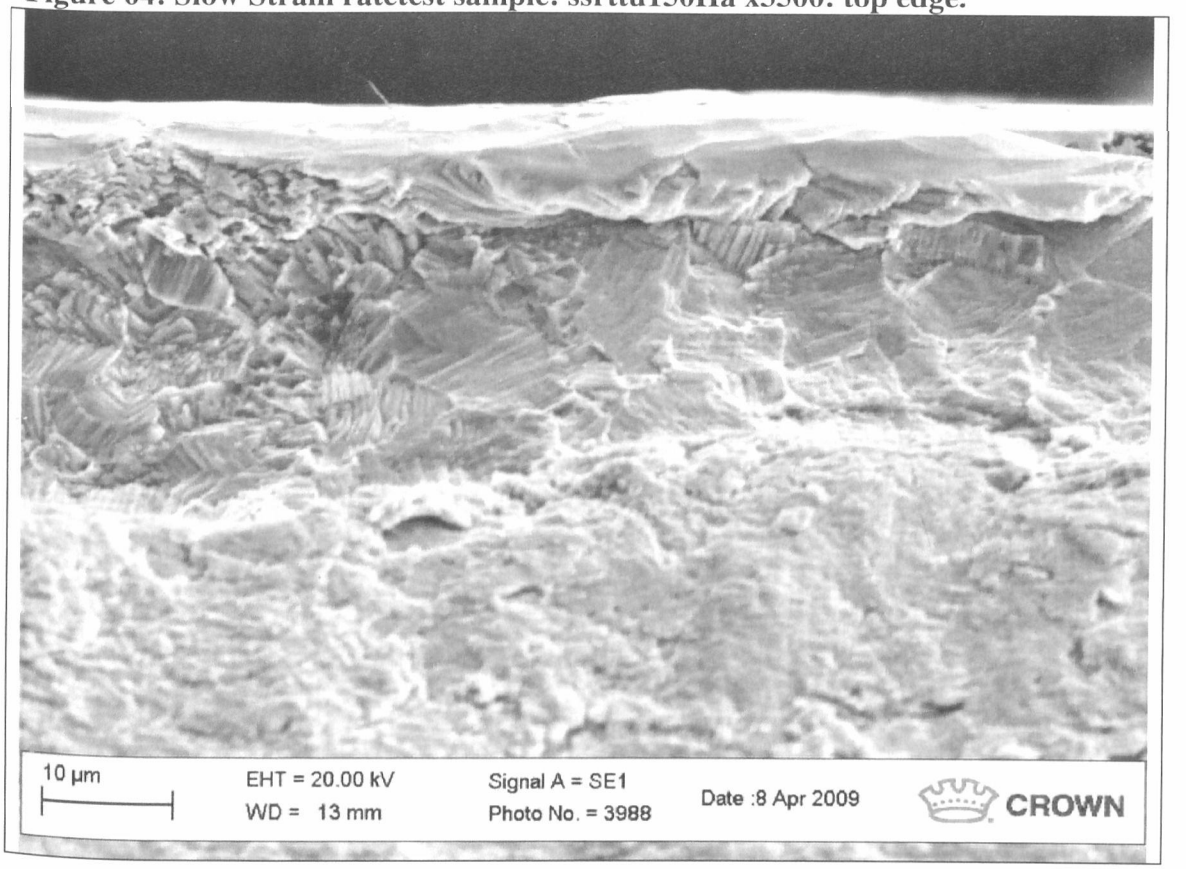
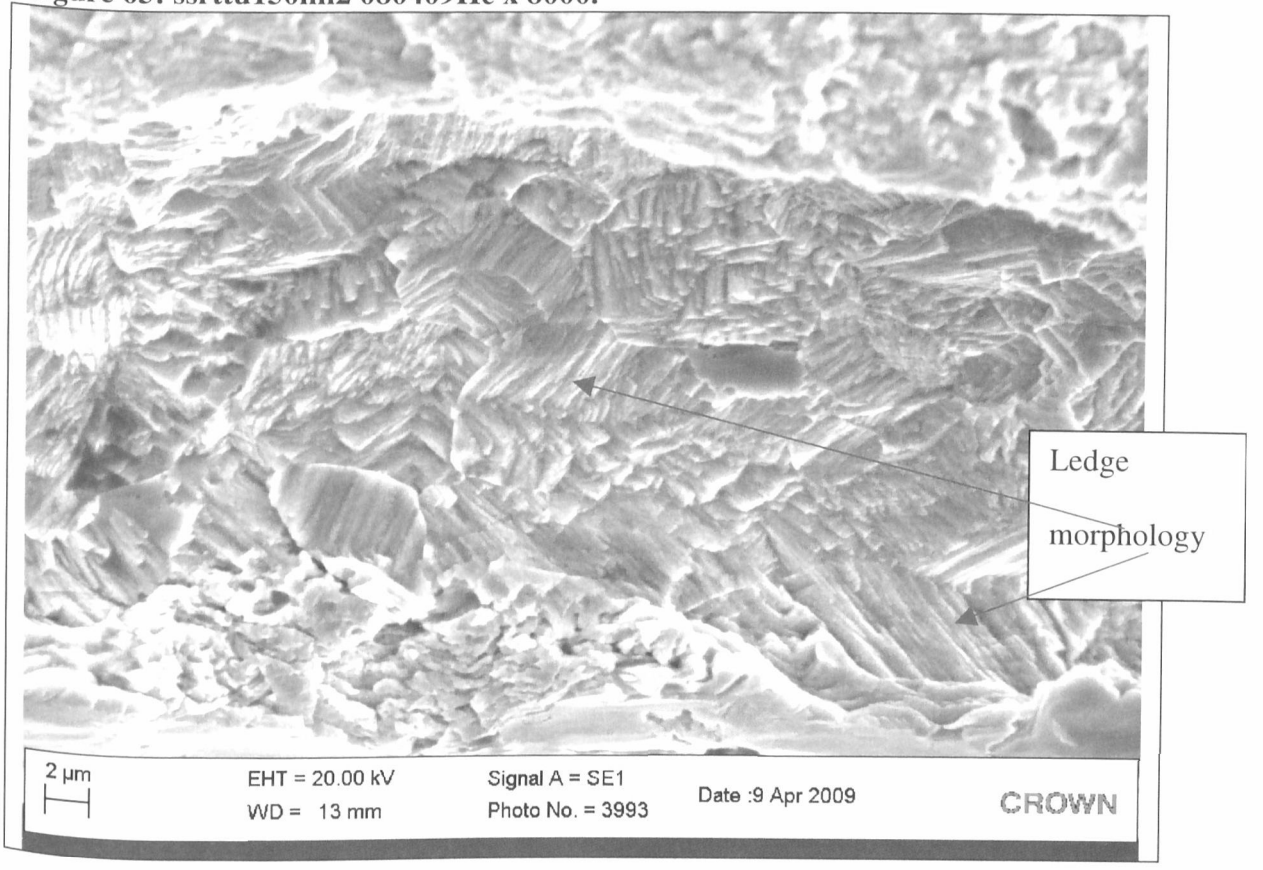


Figure 65: ssrttu150nn2 080409Hc x 8000.



3.3.6 Microscopy: Slow Strain Rate Tested Samples: Salmon Brine: Air Conditions.

The observations for salmon samples were quite similar to those for Tuna brine in respect of low ductility at one notch region.

Figure 66 below shows a predominantly ductile condition at the notch 'BC' but displayed a region of smooth fracture surface in the immediate vicinity of the notch Apex. This was similar to the work hardening effect reported for control samples.

Figure 67 shows a low ductility condition on the same sample at the notch 'GH'.

Figure 66: Salmon Brine slow strain rate test sample: ssrtsal211Ca:ductile condition.

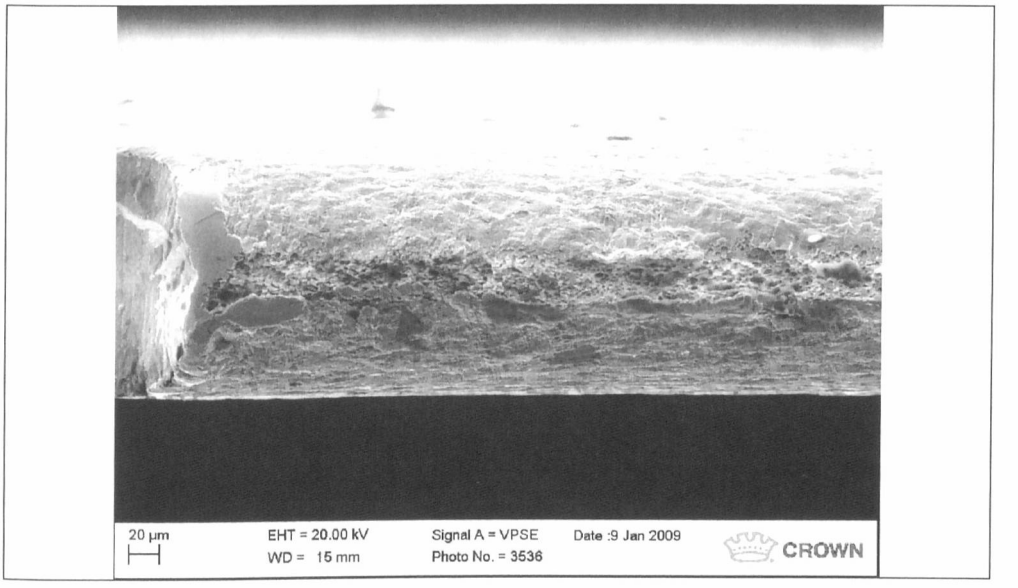
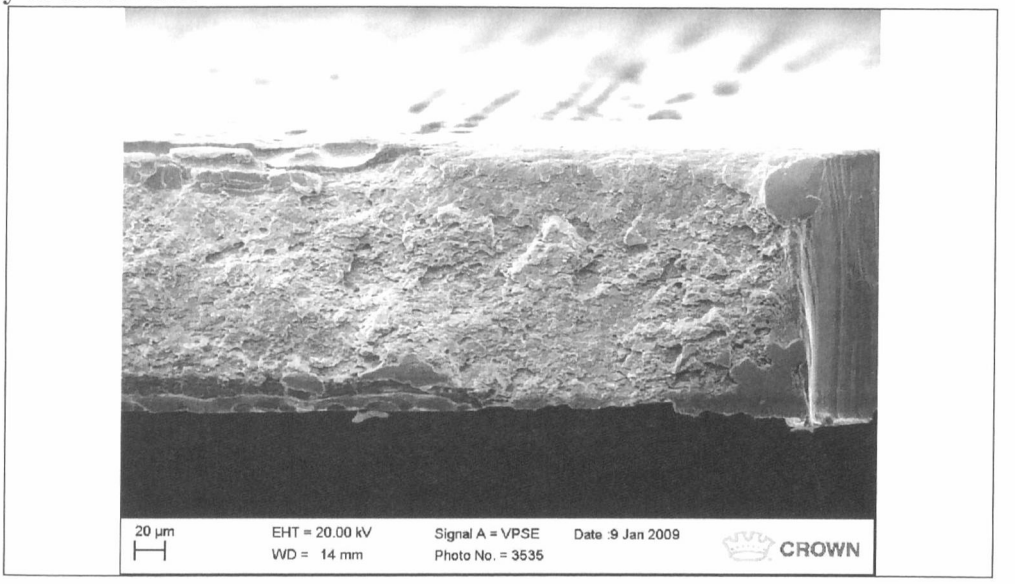


Figure 67: Salmon brine slow strain rate test sample: Ssrtsal211, Ha: loss of ductlity at notch GH



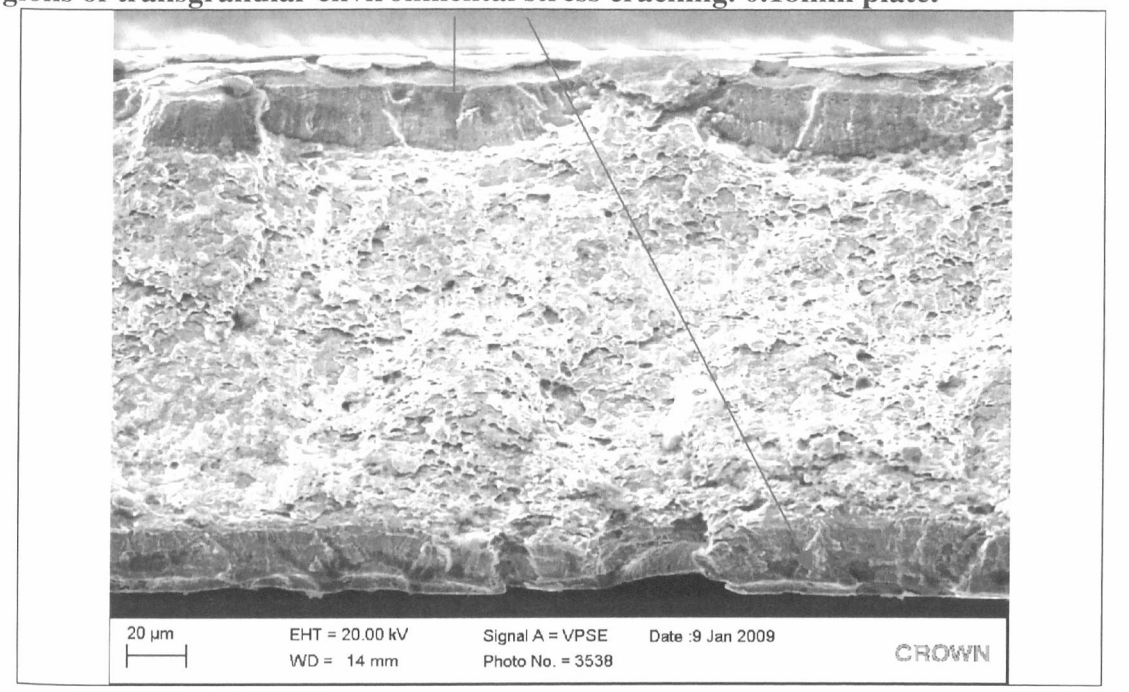
On the surface of this specimen ssrtsal211, towards the low ductility notch end, GH there were separate and distinctive effects comprising the following:

At the notch apex there was a region at one or in some cases both surfaces which indicated very low ductility corresponding to the effects discussed regarding Figure 64 and for control samples.

Ahead of the notch, there were small areas at one or both surfaces which showed conditions charactersistic of transgranular environmental stress cracking, penetrating over short distances from the surfaces such as around 20 microns. These are identified in **Figure 68.**

Similar examples were observed for each different plate and are recorded in the succeeding Figures 69 and 70, with the load-extension plots overlaid in one set of plots, in **Figure 69.**

Figure 68: Test specimen ssrt sal211, Gb0.18m DR 620CA plate image showing regions of transgranular environmental stress cracking. 0.18mm plate.



Larger magnification views of the sample ssrtsal211 are shown in **Figures 69 and 70** having regions showing appearance characteristic of transgranular environmental stress cracking involving ledges and river patterns which can arise from multiple crack initiations and crack coalescence.

Figure 69: ssrtsal211hb090109x2000 Top edge from Figure 68Transgranular environmental stress cracking. Ledges and river pattern effects

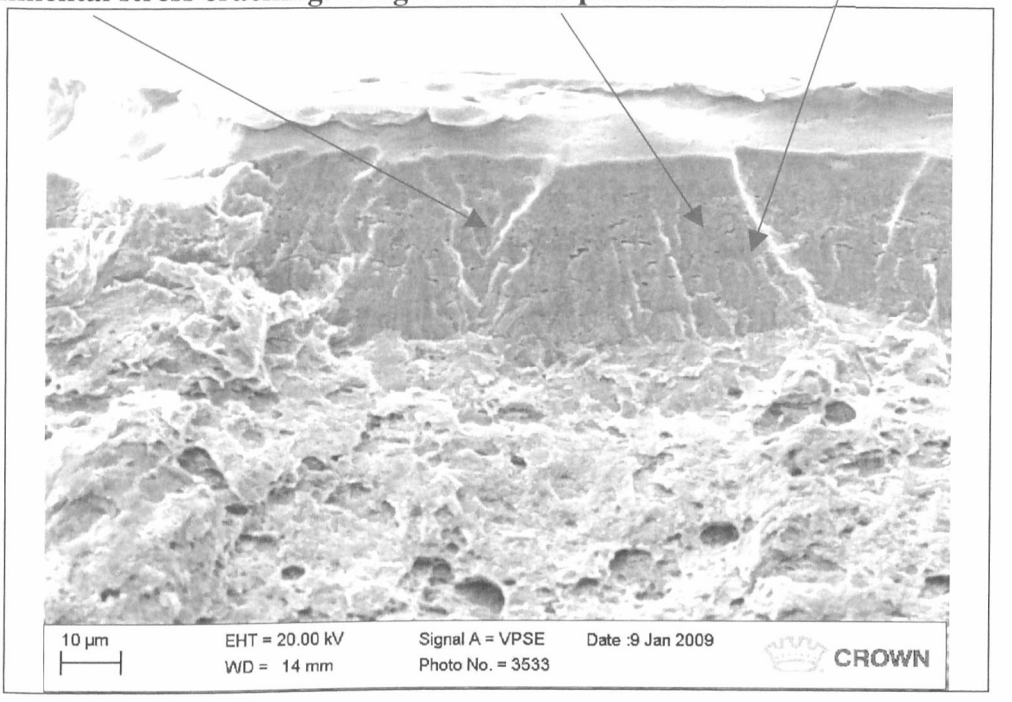
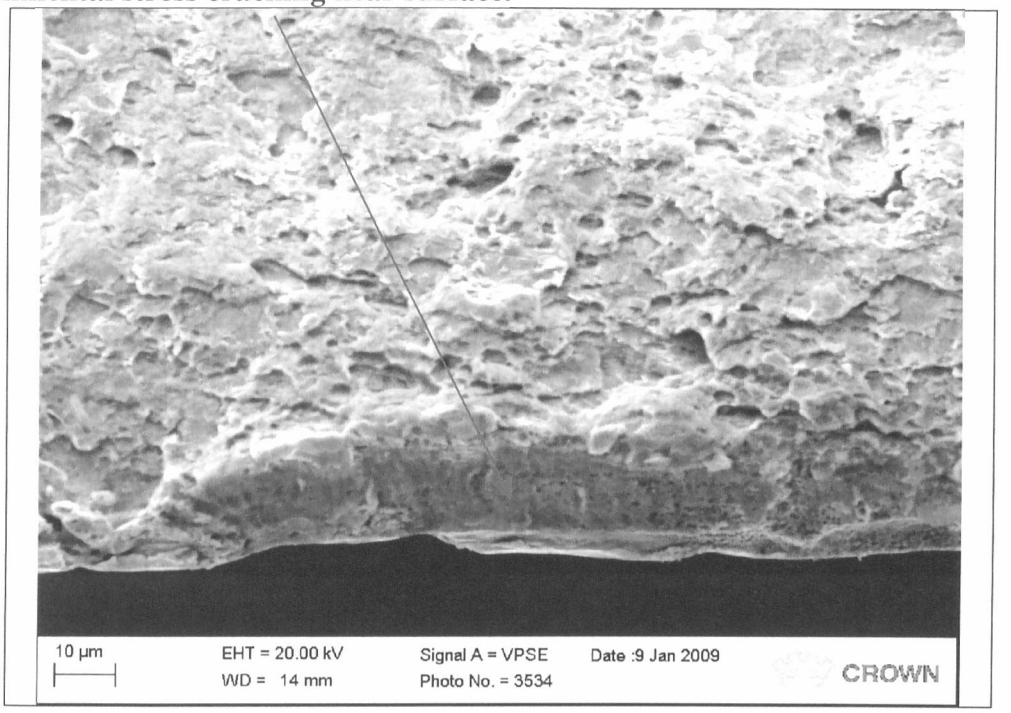


Figure 70: Sal211,Hc x200. Lower edge from Figure 68, showing small band of environmental stress cracking near surface.



The type of condition environmental stress cracking reported above for the salmon sample was replicated in other samples of different gauges, tested in salmon brine under air conditions. Examples of these are shown below in Figures 71-74 for 0.16mm DR620 drawing grade plate, number ssrtsal206 and 0.235mm DR620 end materials (number ssrtsal 208). The tensile load – extension plots for these cases are discussed in para 3.3.8.

Figure 71: Salmon sample ssrtsal 0206Ha: Tested in air: 0.16mm DR 620 CA plate, showing fractography near notch including fratography characteristic of transgranular environmental stress cracking.

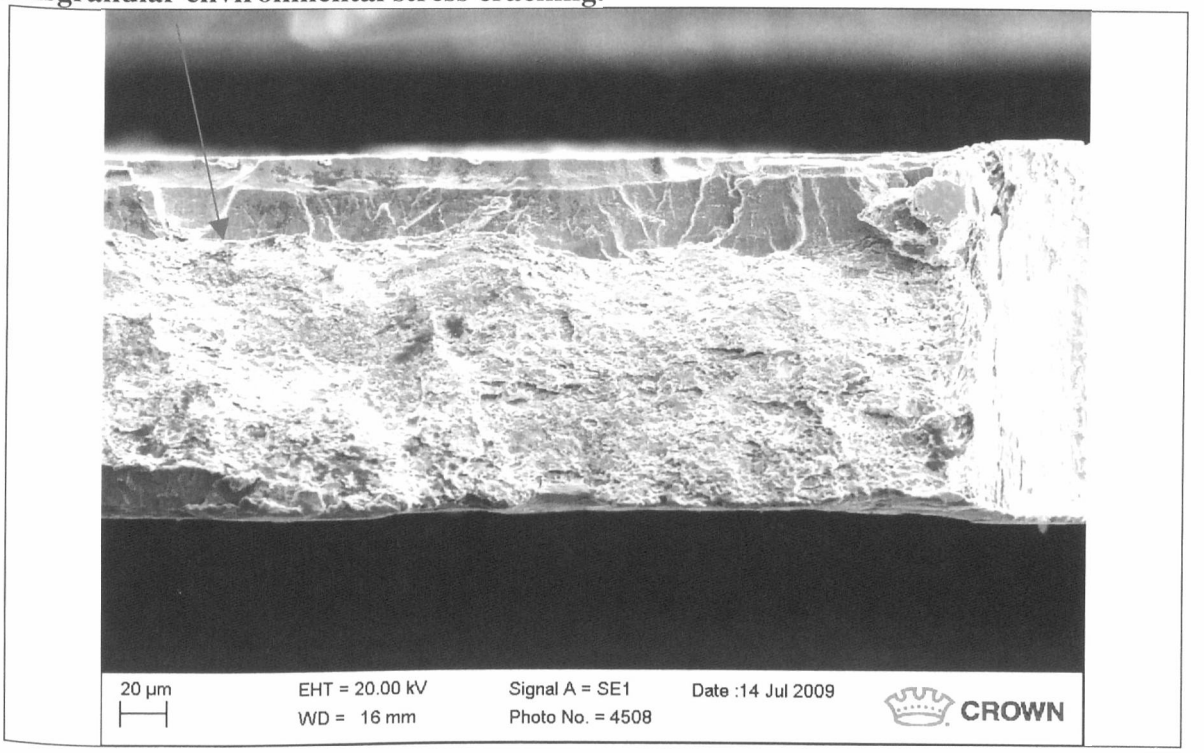


Figure 72:Salmon sample ssrt sal 0206H: Tested in air: 0.16mm DR 620 CA plate; larger magnification view of the fractographic characteristic of environmental stress cracking from Figure 35, with more ductile conditions beneath.

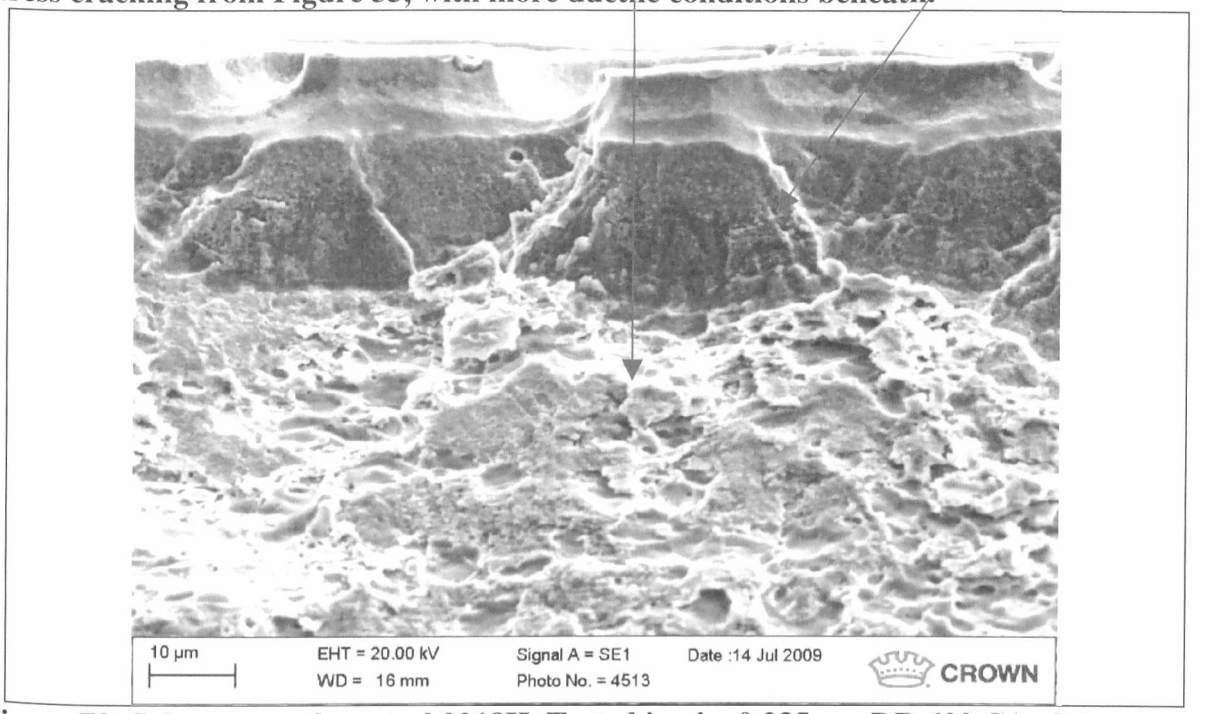


Figure 73: Salmon sample ssrtsal 0218H, Tested in air: 0.235mm DR 620 CA plate, showing fractography near notch characteristic of trans-granular environmental stress cracking.

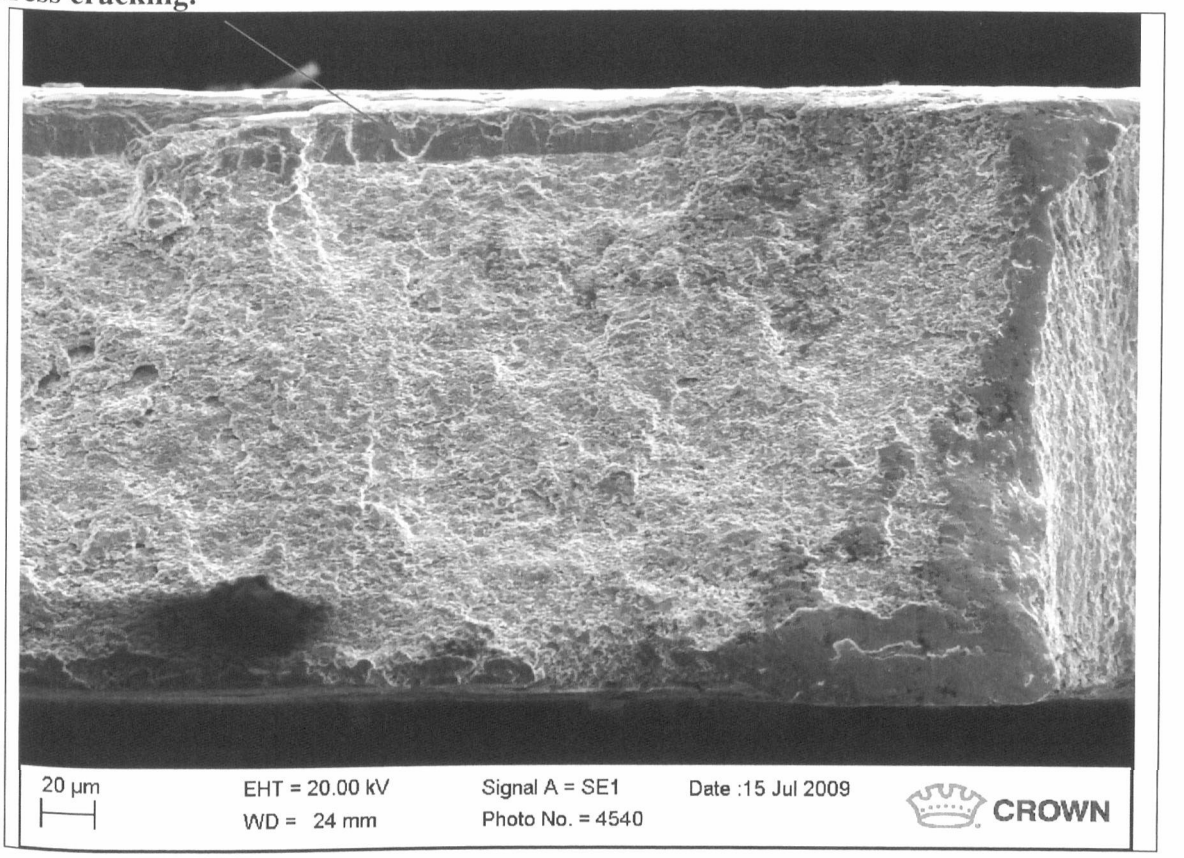
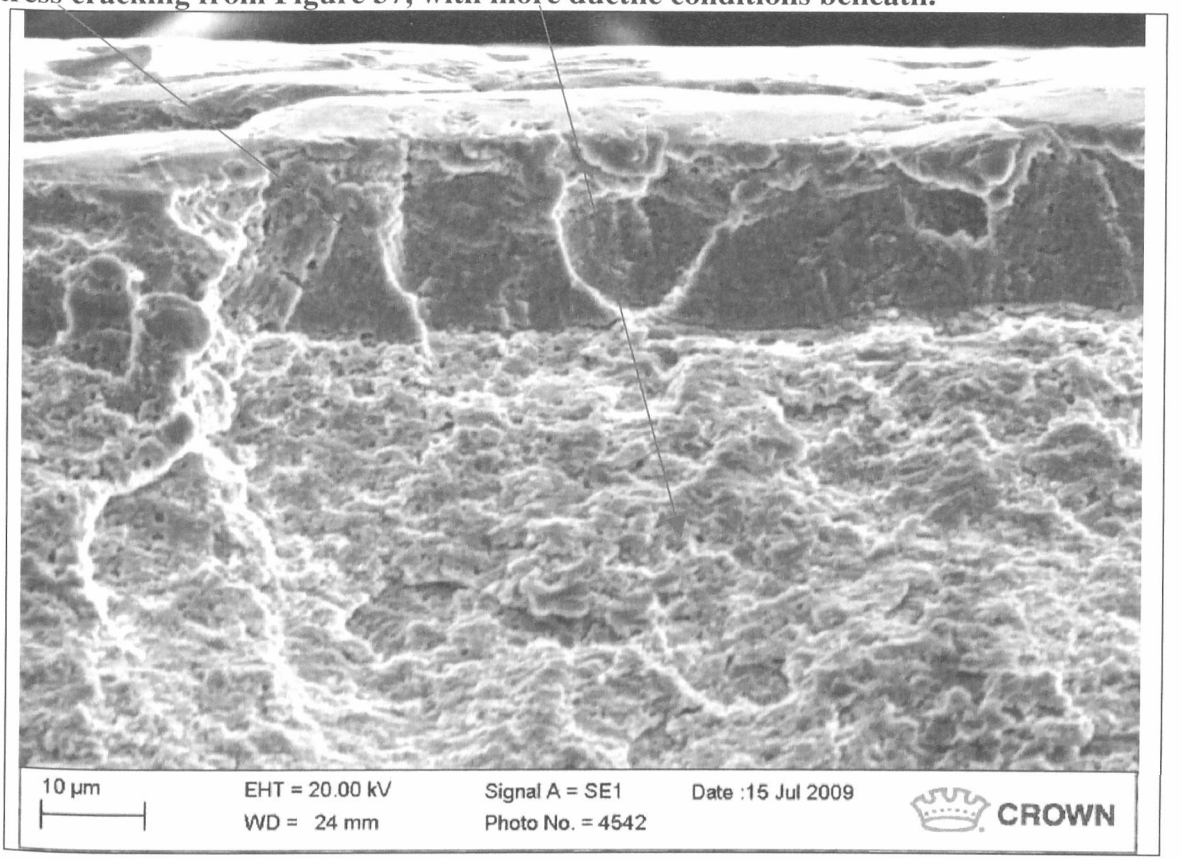


Figure 74: Salmon sample ssrt sal 0218H: Tested in air: 0.235mm DR 620 CA plate, larger magnification view of fractography characteristic of environmental stress cracking from Figure 37, with more ductile conditions beneath.



The Figures 67-70 and 71 –74 collectively provided strong evidence that for each material type subject to slow strain rate testing in Salmon Brine under air conditions, Environmental Stress Cracking took place over part of the fracture surface. The slow strain rate load-extension plots for specimens tested in brines showed behaviour close to linear, without clear evidence of plastic strain up to the point of maximum loading, but there did appear to be some plasticity in the two of the control tests.

3.3.7 Microscopy: Observations on Samples subject to Slow Strain Rate Tests in Salmon Brine: Nitrogen Flush Conditions.

In examination of salmon brine samples tested under nitrogen flushing conditions, the general observation was again of occasional evidence has been found showing discrete areas of environmental stress cracking. Examples are shown below for the three materials, 0.18mm, 0.16mm and 0.235mm steels tested.

Figure 75: Salmon sample ssrt sal 228He: x1000 : Test under nitrogen flushing conditions: 0.18mm DR 620 CA plate, showing trans-granular cracking regions characteristic of environmental stress cracking at either edge, with more ductile regions in between.

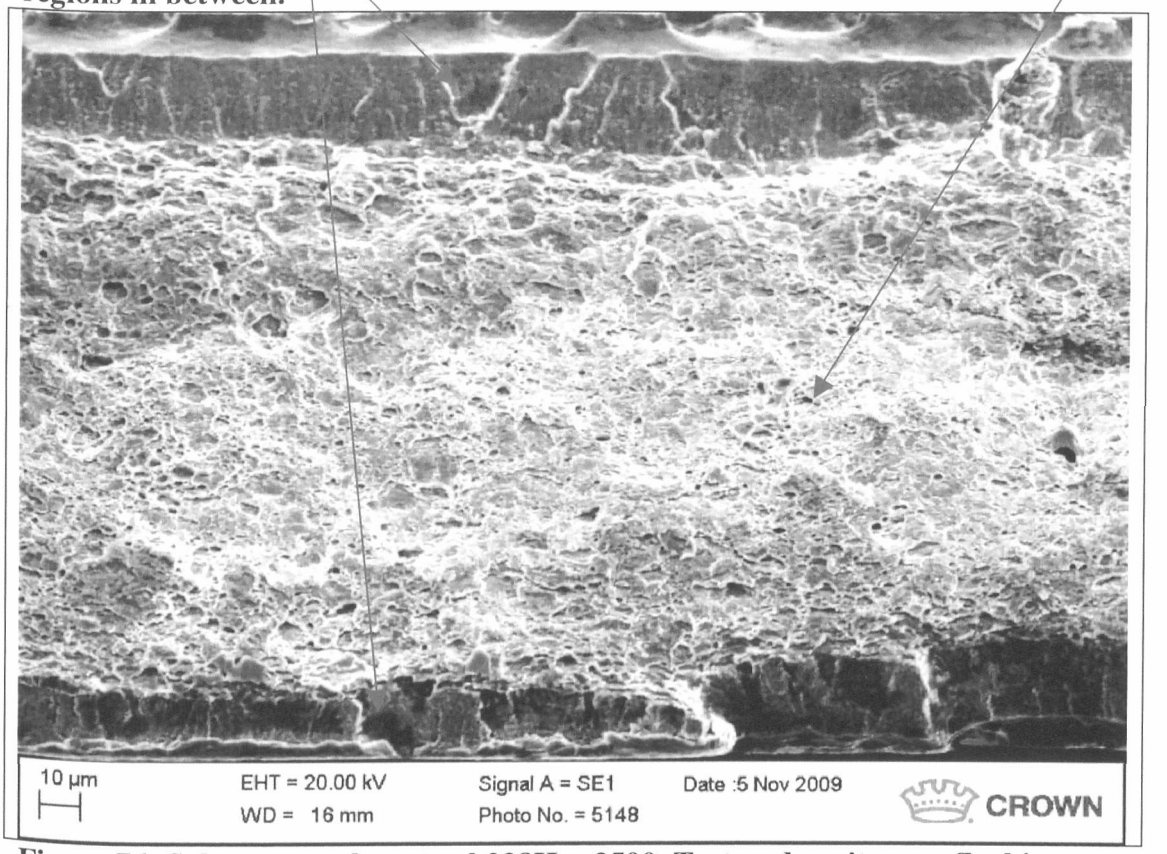


Figure 76: Salmon sample ssrt sal 228H: x2500. Test under nitrogen flushing conditions: 0.18mm DR 620 CA plate, larger magnification view of fractography at top edge from Figure 39, with evidence of trans-granular environmental stress cracking

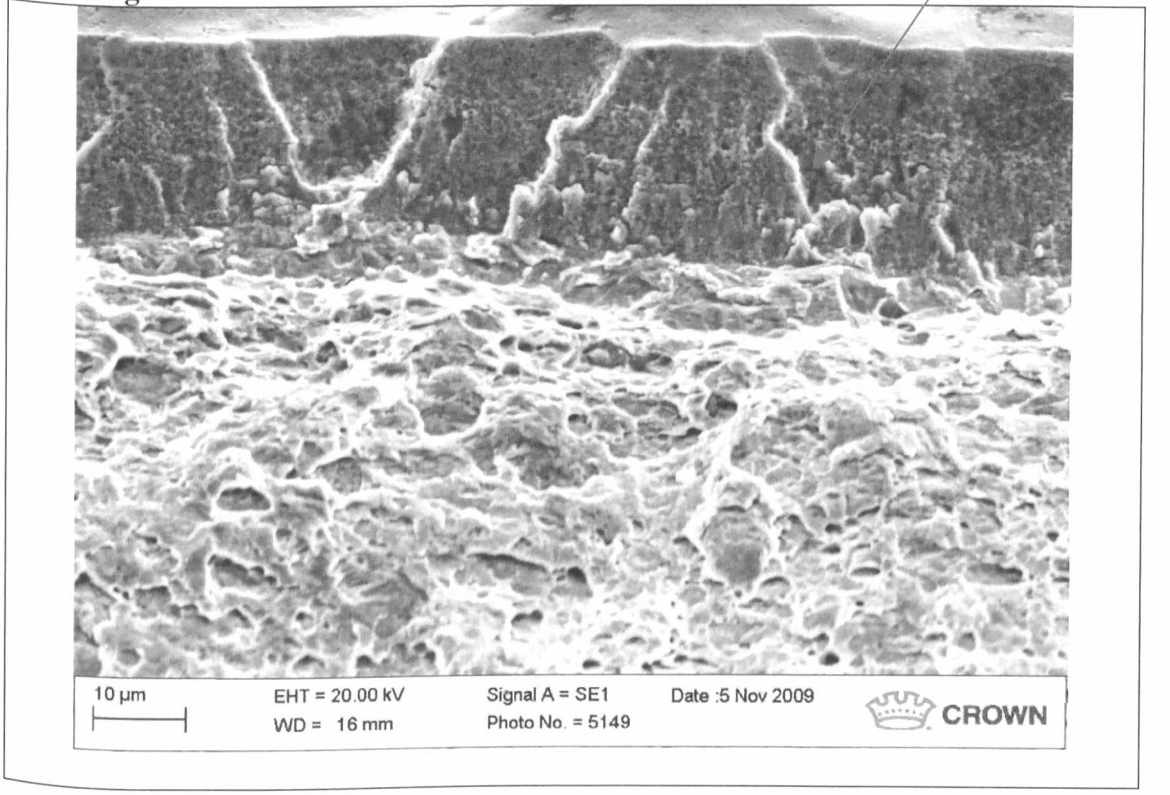


Figure 77: Salmon sample ssrt sal 232Bcx2500: nitrogen flushing conditions: 0.16mm DR 620 CA plate, large magnification view of fractography at edge , with indications of trans-granular environmental stress cracking near edge.

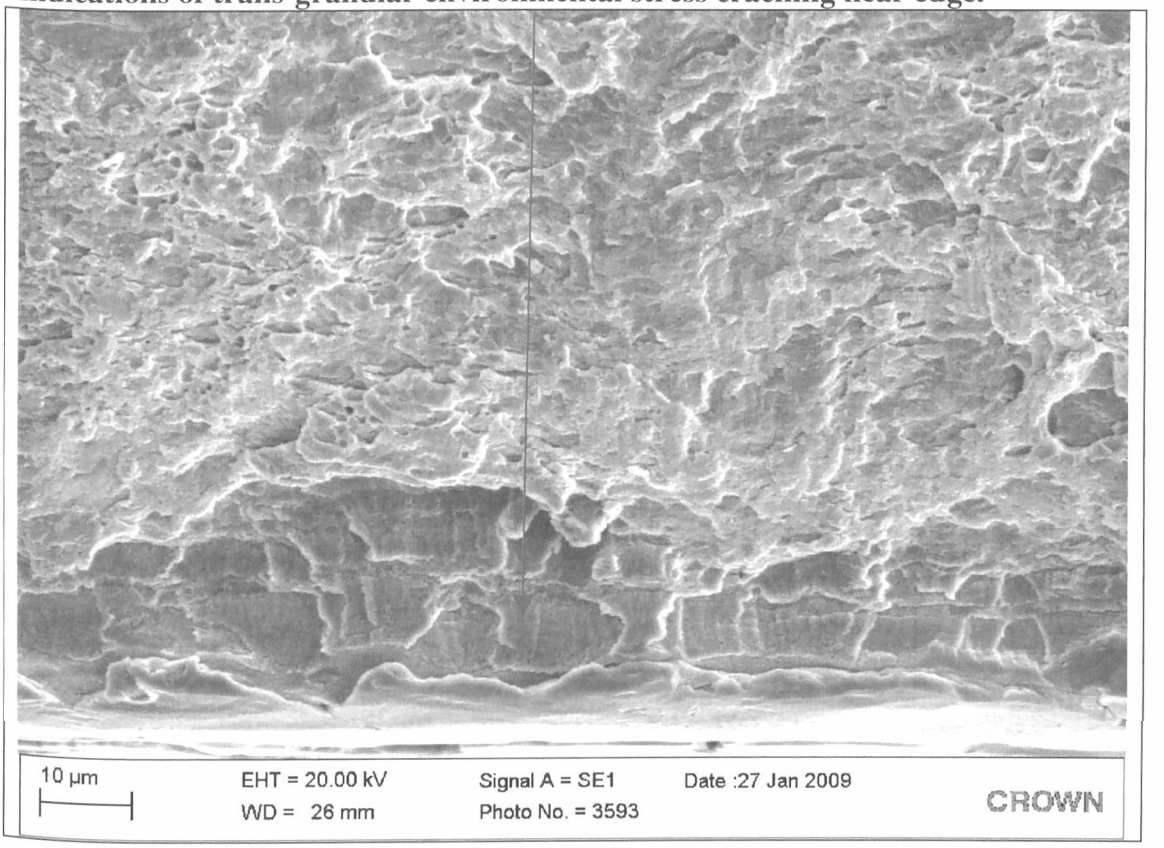
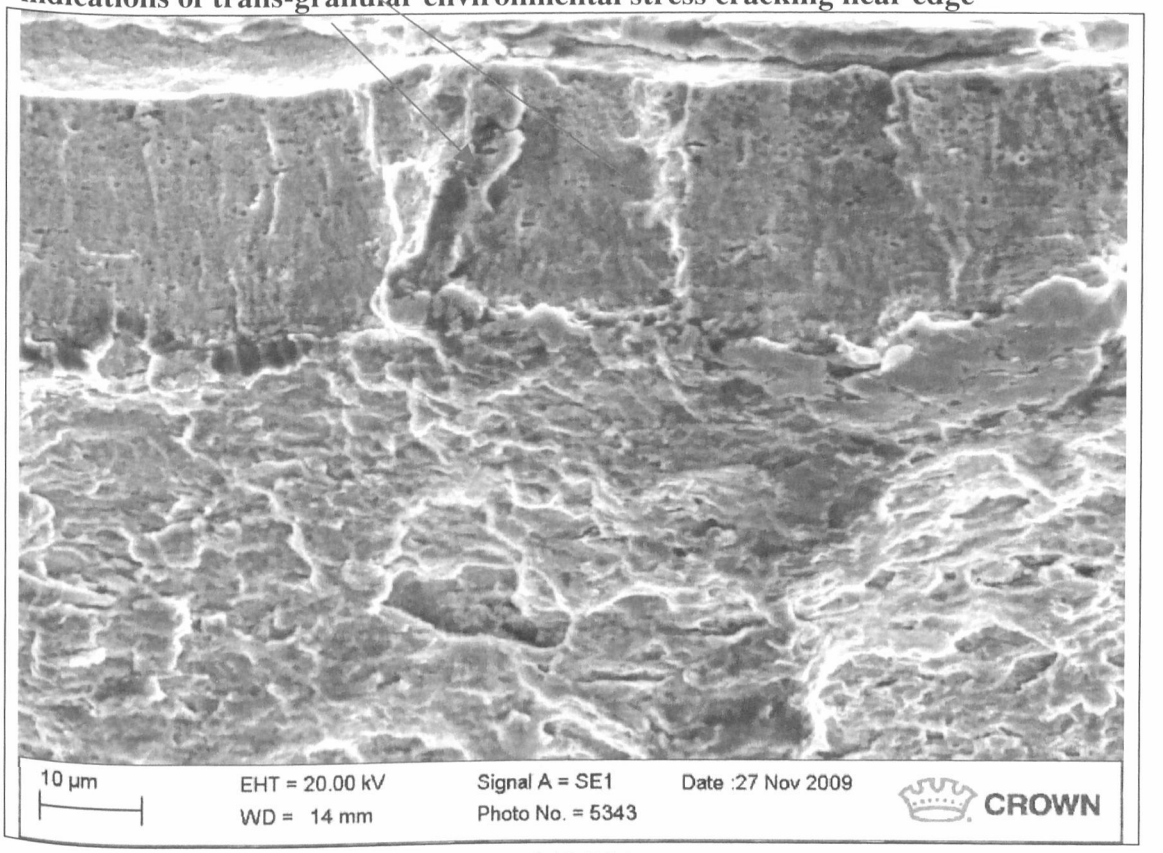


Figure 78: Salmon sample ssrt sal 238Bcx2000: Nitrogen flushing conditions: 0.235mm DR 620 CA plate, large magnification view of fractography at edge , with indications of trans-granular environmental stress cracking near edge

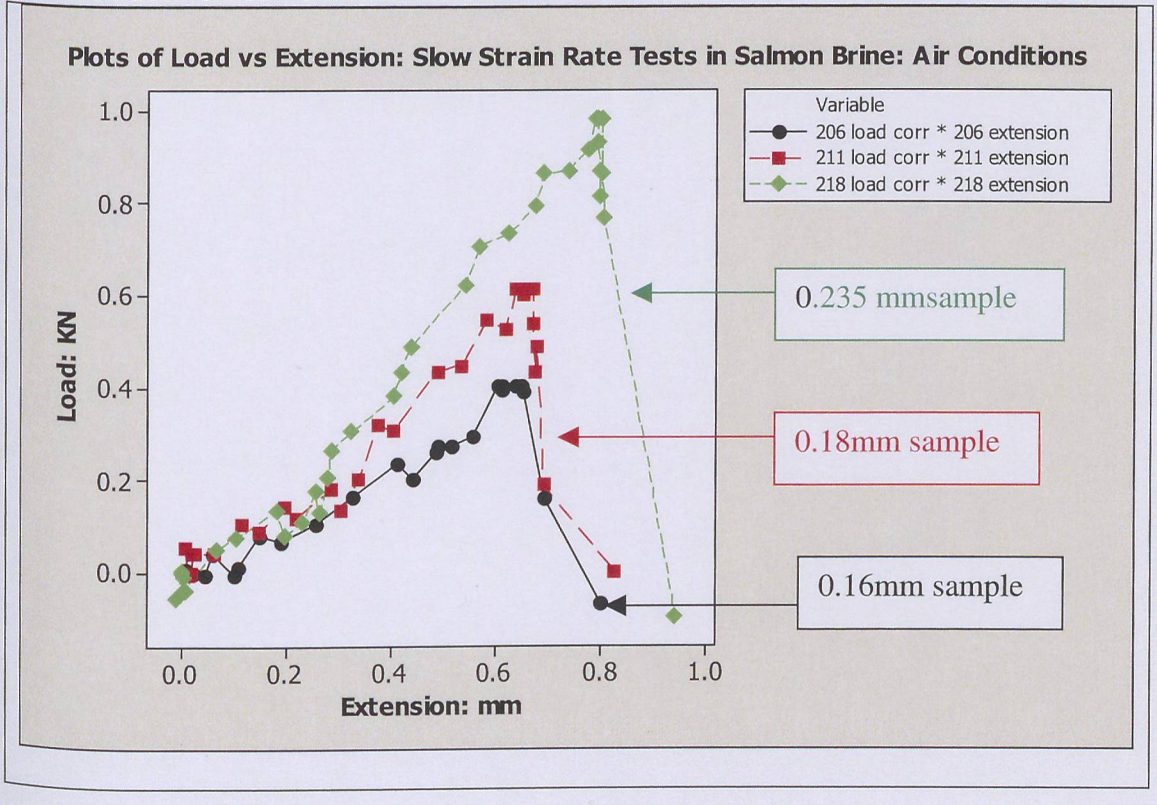


From these images, Figures 75-78, some evidence of trans-granular environmental stress cracking effects has been detected on individual samples from each plate type.

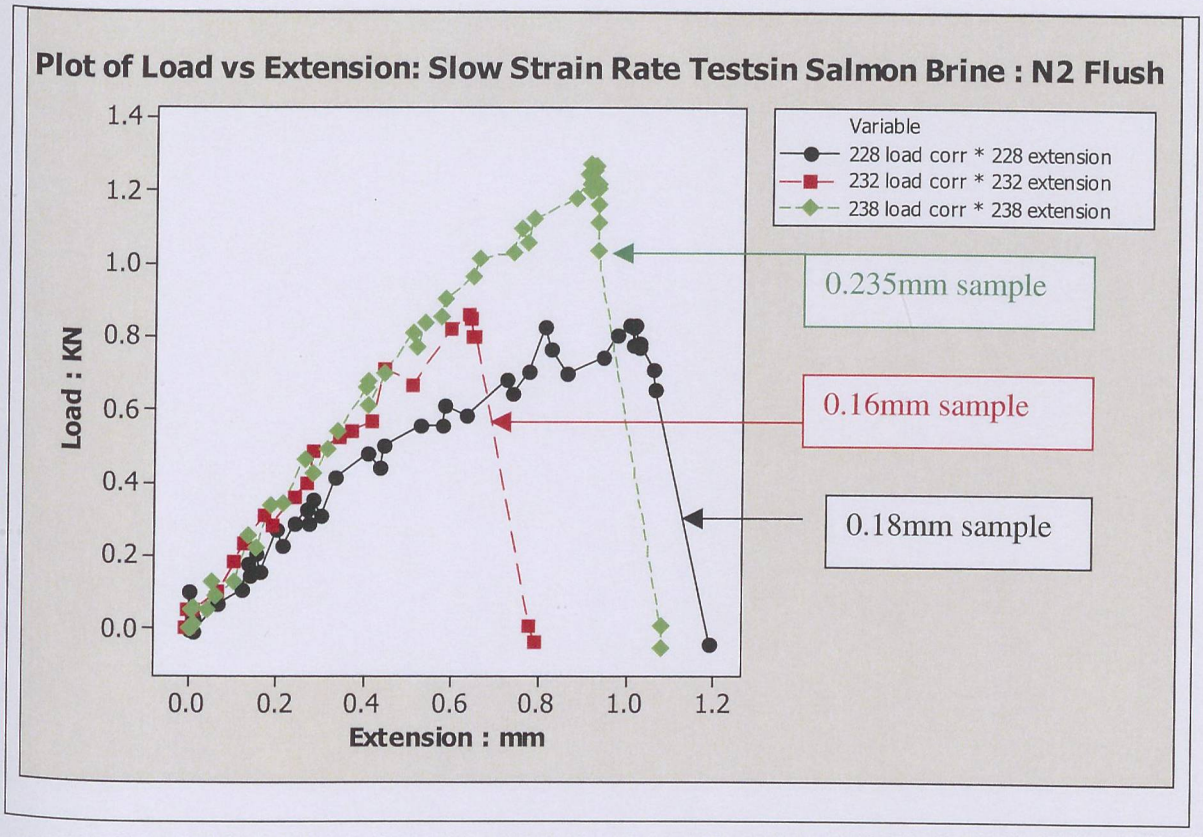
3.3.8 Tensile Load – Extension Plots for Salmon Samples Subject to Plots for Samples Subject to also Strain Rate Tests in salmon Brine and control Samples Tested in Oil

The tensile slow strain rate load-extension plots are shown below in Plot 26, for one sample of each eccs steel material type tested in Salmon Brine in air, and on Plot 27 for one sample of each gauge tested under nitrogen flushing conditions.

Plot 26: Tensile Slow Strain Plots for Sample ssrt sal 0206 (0.16mm DR 620CA plate; 0211 (0.18mm DR 620CA plate) and 0218 (0.235mm DR 620CA plate), tested in Salmon brine under air conditions.



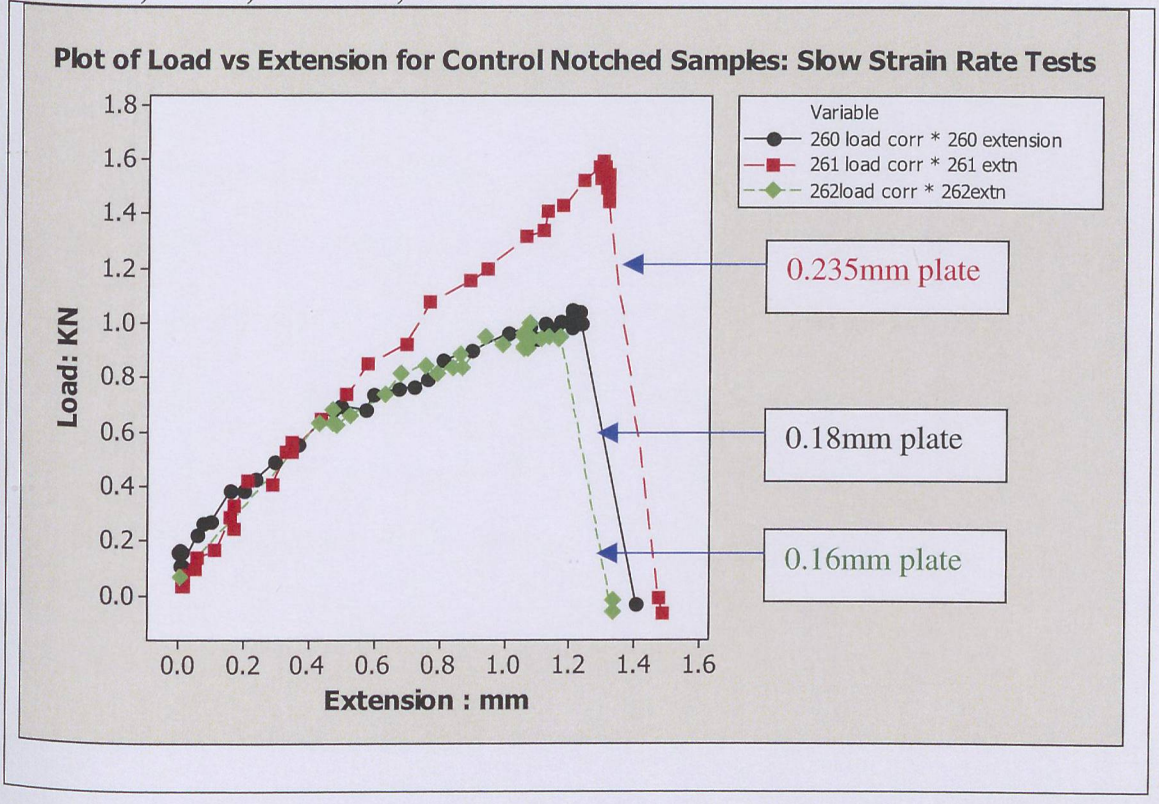
Plot 27: Tensile Slow Strain Plots for Sample ssrt sal 232 (0.16mm DR 620CA plate; 228 (0.18mm DR 620CA plate) and 238 (0.235mm DR 620CA plate), tested in Salmon brine under air conditions.



The individual plots for air conditions, Plot 26, each showed sharp falls in load after attainment of the maximum value. The load-extension data recorded up to maximum load in each of these cases fitted a linear regression model, significant at P= 0.000, with R^2 adjusted at $\geq$96.0%, indicating substantial conformance to a linear condition, although noise was visibly apparent, and sample ssrtsal 211 appeared to show increasing slope after the initial stage. Such effects might result from small slippage in the self tightening tensile grips at the initial stage. For the samples tested under nitrogen flush conditions, Plot 27, the 0.18mm and 0.16mm samples reached similar peak loads. Otherwise the general behaviour was quite similar to that for high air conditions in that after the peak load was reached a sharp fall in load took place for each gauge without much plastic strain.

The tensile tests for control samples tested in Mace Food Oil are shown in Plot 28 below for comparison, again one for each material type used.

Plot 28: Tensile Slow Strain Plots for Control Samples Tested in Oil: No 260: 0.18mm , no 261, 0.235mm , no 262 : 0.16mm.



The control plots showed a number of features to compare with those tested in product brines, as follows:

a) There was much less noise on the control plots than for samples tested in e.g. salmon brine under air conditions or nitrogen flush conditions, and this may be due to an influence of pitting in the former lots.

b) The 0.18mm and 0.16mm samples showed a measure of plasticity in the plots which was not clearly apparent in the 0.235mm material sample. For the samples tested in salmon brine shown in Plots 26 and 27 , there were no substantial plasticity effects, but observations are tempered by the noise and probable effects of pitting. The 0.235mm plate was of a nitrogenised steel

type showing a slighly different tensile plot to the other steels in control tensile tests. See later section.

c) A sharp 'angled' drop in the tensile plot has occurred for each of the controls, Plot 28, whereas for materials tested in salmon brine under air conditions, Plot 26, in two cases there were vertical arrests before final failure. Under nitrogen flush conditions, Plot 27, the vertical arrest was repeated for the 0.235mm sample. This is quite a marginal distinction. The differences in behaviours for samples tested in salmon brines were not of such obvious magnitude as to be an indicator of the involvement of environmental stress cracking, which was apparent from fractography in part of the cross sections on each of the 6 samples tested in salmon brine for which plots are shown above.

3.4 Metal Thickness Reduction Data at Notch Regions for Samples Subject to Slow Strain Rate Tests.

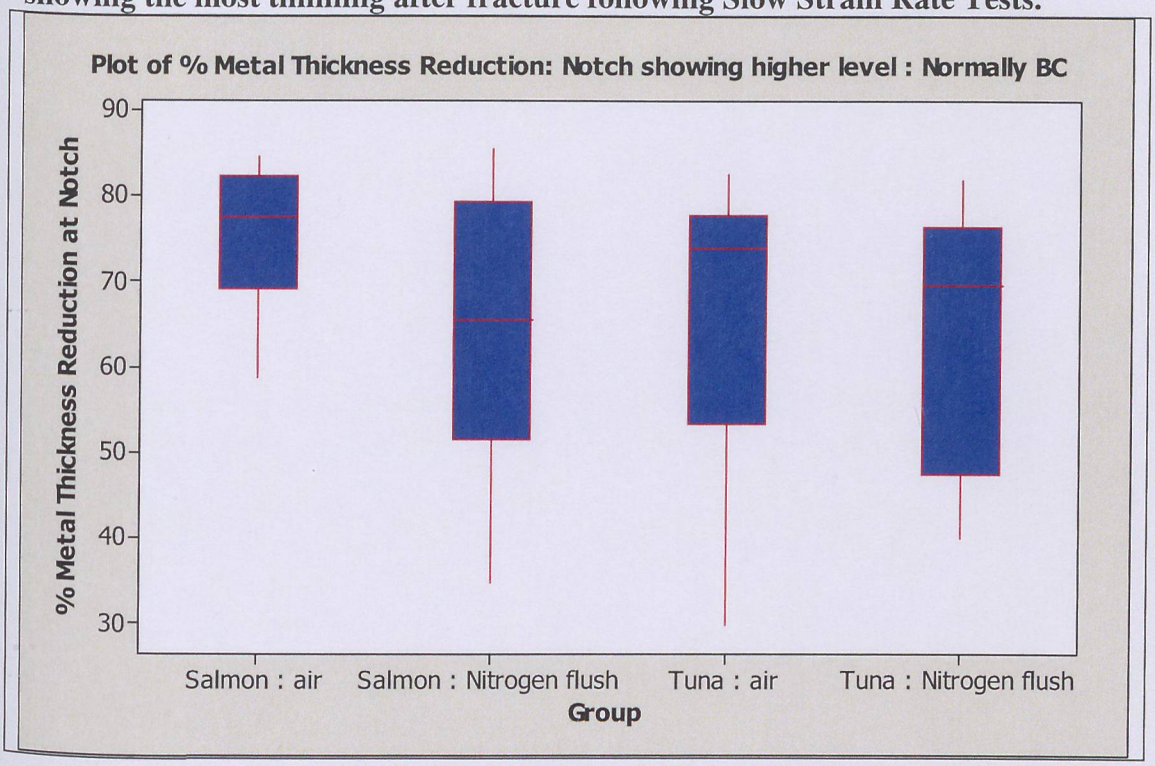
These data were important to corroborate observations of loss of ductility recorded as photomicrographs. Using SEM, thickness data were obtained at the fracture surfaces at either notch end at either face after the slow strain rate tests, in comparison with the mid region of adjacent notch edge, and a % gauge reduction value calculated. The average value of data for the two faces at each notch end compiled for at least 11 samples per product and air / low air condition, was used for comparisons. The samples measured spanned all gauges used in each subset. A previous observation was of a degree of bias in notch thinning behaviour on specimens tested in product brines, leading to one end showing a far smaller thickness reduction than the other. The data has therefore been treated as two separate lots, namely, that for the least ductile end, most commonly the 'GH' notch, and that for the more ductile end, most commonly the BC notch.

The data are summarised below for the product and air/ low air sub groups for the two notches.

a) **Mean % thickness reduction values at Notch showing the greater ductile behaviour, typically notch BC, on samples from slow strain rate tests in Product brines.**

The data are summarised in Plot 29 below for a minimum of 11 samples per product and air/ low air condition. Except in the case of salmon under air conditions the data sets either did not follow a normal distribution or were a poor fit.

Plot 29: Summary data boxplot for % Metal Thickness reduction at Notch showing the most thinning after fracture following Slow Strain Rate Tests.



From the plot it can be seen that in all groups at this notch the metal thickness reduction was substantial, over 50% on average in each case, and that the most consistent behaviour was observed for the Salmon group tested under air conditions. The basic statistics are summarised in the table 63 below:

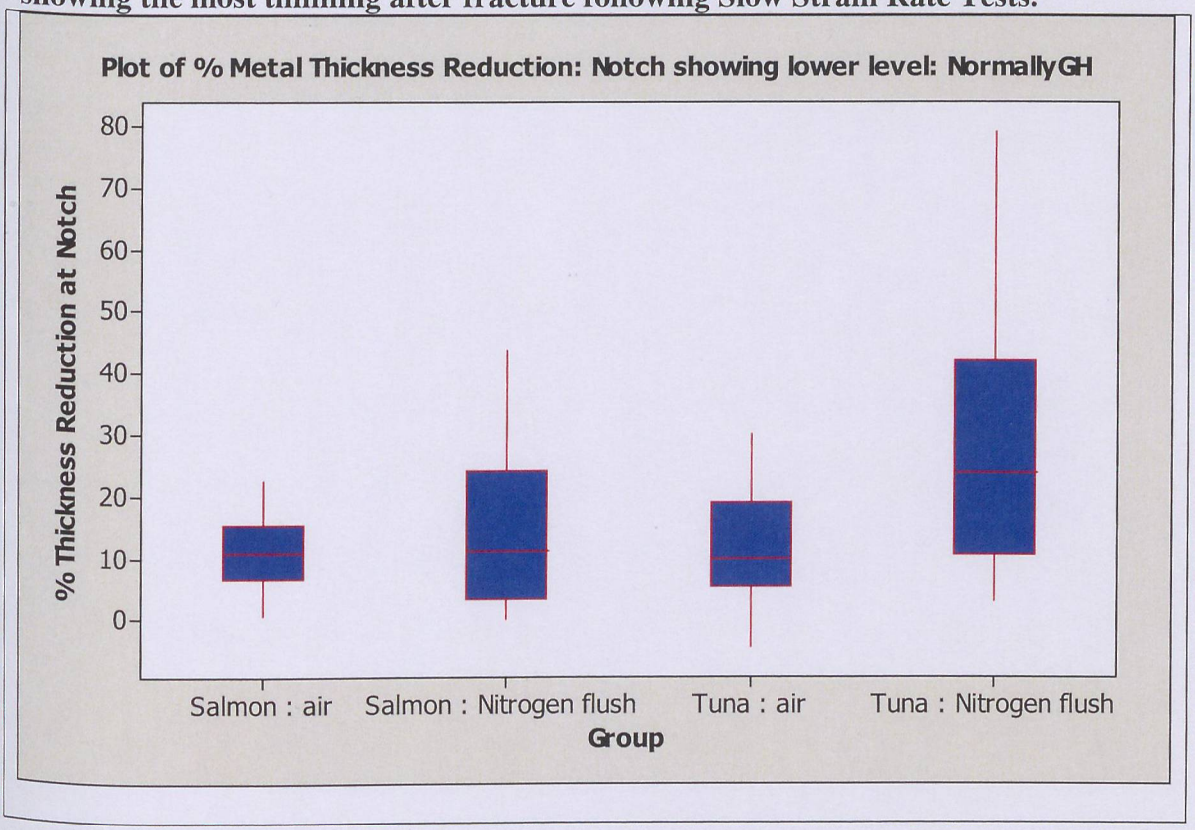
Table 63: Summary Statistics for Plot 29 lots: % Metal Thickness Reduction at Notch

Group	Number of samples measured	Mean % thickness reduction at notch	Sample standard deviation	Minimum	Maximum
Tuna : air conditions.	12	67.14	16.88	29.73	82.53
Tuna : nitrogen flush.	15	63.58	14.78	39.85	81.81
Salmon: air conditions.	11	75.24	8.23	58.68	84.45
Salmon: nitrogen flush.	13	65.19	17.17	34.70	85.53

b) Mean % thickness reduction values at Notch showing the Least ductile behaviour, typically notch GH, on samples from slow strain rate tests in Product Brines.

The corresponding metal thickness reduction data at the opposite notch showing least thickness reduction, commonly the notch designated GH.

Plot 30: Summary data boxplot for % Metal Thickness reduction at Notch showing the most thinning after fracture following Slow Strain Rate Tests.



It can be seen in Plot 30 that the metal thickness reductions were on average much lower than for the opposing notch data shown in Plot 29, with the Salmon group tested under air conditions showing the most consistent behaviour, and the variability increasing for either product type when nitrogen flush conditions were used. As the loss of ductility will be expected to relate to corrosion effects and any uptake of hydrogen

which occurred, the results are an indication that the degree of this effect took place in a less consistent way under nitrogen flushing conditions.

The basic statistics corresponding to Plot 30 are shown in the table 64 below:

Table 64: Summary Statistics for Plot 30 lots: % Metal Thickness Reduction at Notch

Group	Number of samples measured	Mean % thickness reduction at notch	Sample standard deviation	Minimum	Maximum
Tuna : air conditions.	13	11.62	9.68	0	30.02
Tuna : nitrogen flush.	15	27.66	22.87	2.79	78.91
Salmon: air conditions.	14	10.99	5.73	0.56	22.35
Salmon: nitrogen flush.	15	13.60	12.98	0	43.44

As the majority of data sets were either non normal or showed a poor fit to normality, the metal thickness reduction values were not compared using the ANOVA test.

c) **Metal thickness reduction data for Control Specimens of each material subject to Slow Strain Rate Tests in Mace Food Oil at the same rate as for Test Specimens**

Two samples of each material was tested in Mace Food oil using the same set up as for specimens tested in brines. The corresponding Microscopy data were determined as for the samples tested in brines, and in this case a comparison was made between values at the two notches. The data are summarised below in Plot 31, followed by the statistical analysis table. In this case the data for notches BC and HG were within normal limits based upon the Anderson Darling test and a one way analysis of variance test was made.

Photomicrographs showing the notch thinning for examples of each material, corresponding to three of the samples used in this test were shown as Figures 41-52.

Plot 31: Summary data boxplot for % Metal Thickness reduction at Notches for Control specimens after fracture following Slow Strain Rate Tests in Mace Food Oil.

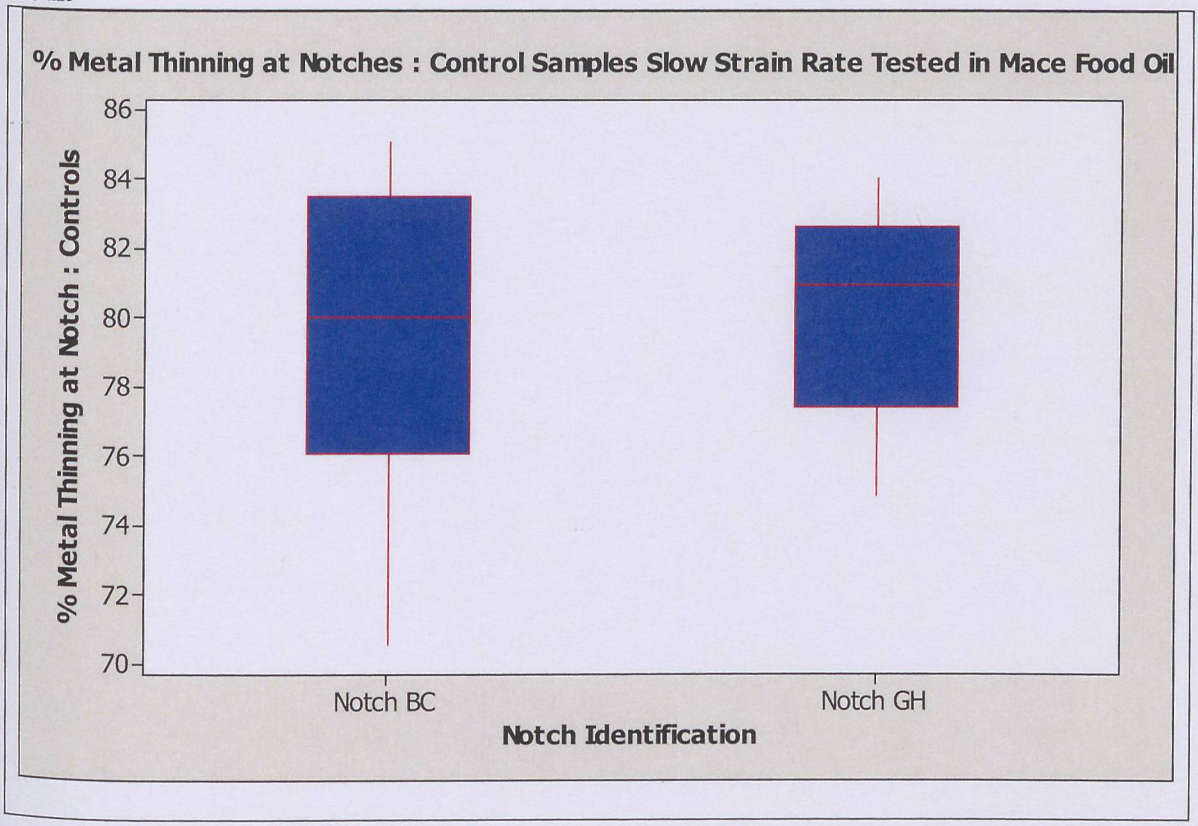


Table 65: Table of Analysis of Variance Data: Control Samples Totalling Six, two per Plate type.

				Individual 95% CIs For Mean Based on Pooled StDev
Level	N	Mean	StDev	--------+---------+---------+---------+-
Notch BC	6	79.418	5.029	(---------*---------)
Notch GH	6	80.200	3.317	(---------*---------)
				--------+---------+---------+---------+-
				77.5 80.0 82.5 85.0

Pooled Standard Deviation = 4.260

Table 66: Statistical detail

Source	Degrees of freedom	Sum of squares	Mean square	F ratio	P value
Notch	1	1.8	1.8	0.1	0.757
Error	10	181.5	18.1		
Total	11	183.3			

From the plot and statistical data, the following points were apparent:

i) The metal thickness reduction was very high at both notches, signifying pronounced necking with greater consistency recorded for the 'GH' notch.

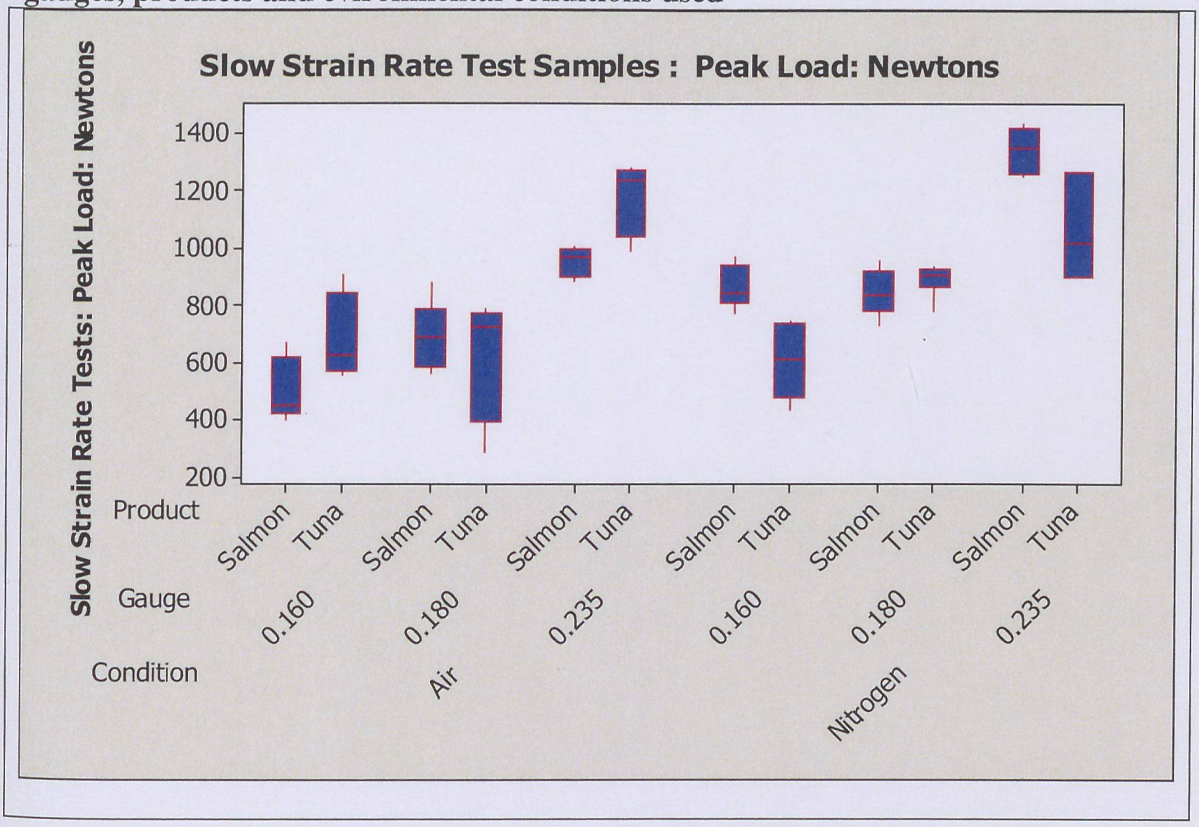
ii) There was no significant difference in the mean level of metal thinning between the two notches.

iii) The significant loss of ductility affecting at least one notch in the slow strain rate tests with product brines was not an artefact of the test, but a real effect due to the combination of corrosion and any interaction of stress.

3.5 Observations from Peak Load Values for Slow Strain Rate Test Groups Tested in Product Brines.

The peak loads for sub groups are summarised in the Plot 32 below with comments beneath:

Plot 32: Summary of Peak Loads recorded in Slow Strain Rate Tests for material gauges, products and evironmental conditions used



From this plot several important points could be deduced, as follows:

i) For air conditions the mean level of peak loads increased with increasing gauge, and higher mean peak loads were observed for tuna relative to salmon for respective gauges by varying margins.

ii) For low air (nitrogen flush conditions), it can be seen that there was some reversal of peak load behaviours between salmon and tuna products, for the lowest and highest gauge materials. This has not been accounted for, unless because of a change in surface film forming characteristics affecting corrosion

iii) There were inidications of interactive behaviour of environment and possibly plate in the data, noting that for the 0.18mm steel the mean peask loads showed the least differention between product groups under both nitrogen and aerated test conditions

3.6 Predictive Estimation of Strains and Stresses by Finite Element Analysis (FEA) Studies.

3.6.1 Explanatory Introduction

In order to conduct this type of analysis, the component under examination has to be broken down into discrete sub units called elements. These are joined at shared points called nodes. The combination of elements and nodes form a 'mesh'. The choice of element configuration to form the mesh depends on the geometry of the sample and the detail of the stress system e.g. 2 dimensional plane stress, axi symmetric, or 3 dimensional. In the work reported here, a 2 dimensional plane stress system and alternatively, axisymmetric conditions have been used for particular models chosen. The FEA method is one which predicts approximate solutions, and which should be cross verified by other methods. In this work, the elemental displacements have been based upon a material description of behaviour i.e. the element deforms with the material. This is termed 'Legrangian'.

The analysis of the physical process by FEA method predicts the displacement of nodes, and strains within the structure are then calculated in incremental stages. These strains are related to stresses via the stress strain curve for the material. There are two ways in which the analysis is commonly done, as follows:

a) The Implicit Method.

This method embodies the principle of an external load(s) applied to a structure, resulting in an internal load(s) and displacements, and is most suited to situations where linear elastic conditions predominate, and any non linear conditions are either limited, or local non linear behaviours are well controlled. Non linear conditions lead to a larger number of computations being required, as part of which changes to the 'stiffness' of the structure have to be calculated. The term 'elemental stiffness' applied to linear behaviour is a function of Young's modulus , modified, for example, for the unit length of a round bar by multiplication by the cross sectional area, and expressed per unit length of the element.

Force = stiffness x displacement.

The 'stiffness' of a element, for example, in a round bar is defined as :

$$\text{stiffness} = EA/L$$

where :

E = Young's modulus.

A = The cross sectional area.

L = The element length.

When non linear conditions become increasingly extreme, either a very large number of computational steps are required, or the model system fails because the matrix equations defining the model solution are not in equilibrium. This condition may be defined as 'non convergeance'. The term 'convergeance' means that the matrix equations describing of the stiffness properties of the elemental structure are satisfied. The properties of the structure include not just those of the material and any tool interaction behaviours, but also the choice of element. Certain types of element permit reduced integration which saves computational time. This is done by calculation involving a reduced number of integration points, but situations may occur where deformation modes take place that do not cause straining at the integration point(s). This leads to a

phenomenon called 'hourglassing' and mesh distortions, which may be overcome by the addition of an artificial degree of stiffness to the structure, termed 'hourglass control'.

The process of calculation is divided into solution increments, and equations relating strains to loads are solved at the end of each solution increment to define the strains produced. In turn, the strains are related to stresses by tensile property curves and Poisson strain effects for elastic behaviour. The tensile property plots should be true stress – strain plots.

From the above, the implicit method is suitable for modelling the application of e.g. a load applied to a tensile test piece. It may also be suitable for application to some more complex but well controlled forming operations involving sheet. In practice, it may be found that effects such as variable surface friction and deformation create non equilibrium conditions which lead to a malfunction of the model.

b) The Explicit Method

This method is based upon enumeration of the effects of a stress wave propagation through a component or structure. The force resulting from the stress wave leads to a finite acceleration of nodal movement(s) within the structure imparting a velocity to the nodal movement, leading to a strain rate. The integral of strain rate with respect to time determines the finite strain change $d_{E,}$ from which the total strain in an element can be enumerated. Under elastic conditions the stress is then calculated using theYoung's modulus relationship, but if plasticity also applies, the overall material property relationship must be used. Within the structure, the net force acting on a second

successive element can be used to calculate the new acceleration, the integration of which with respect to time leads to a new velocity and corresponding strain rate from which the strain in the second element is determined, the procedure continuing through successive elements.

The important distinction between the explicit and implicit solver relates to the stiffness calculation for the latter. In the implicit case a constant acceleration of nodal movement per time step is assumed. This means that the calculation of nodal deflection will be dependent on force and $(\text{stiffness})^{-1}$, and is determined at the end of each solution increment. In the case of the explicit solver the nodal displacement at the end of each time step is calculated by integration of acceleration with respect to the time increment (acceleration = force /mass), the resulting nodal velocity being used to determine the strain rate and hence the strain by integration with respect to time. This is then related to stress in the case of elastic conditions by the Young's modulus relationship, but in this case it can be independent of the stiffness matrix equations.

The method depends on a stable time increment being established related to the speed of a sound wave in the material. The wave speed 'c' is defined for a material as $c = \sqrt{E/\rho}$, where:

E= Young's modulus.

and ρ = density of the material.

When c has been determined , the stable time increment is defined by

$$t_{stable} = \text{element length}/ c$$

The shortest element dimension should be used.

The explicit method while calculating nodal movements, does not require the solution

of simultaneous equations for the complete property changes of the structure at the end of each increment, which enable the limitations of the implicit method for e.g friction conditions to be overcome.

The computational time step may be low for the explicit method and a large number of time steps and run time needed for models. If the analysis is then run faster than the stable time increment, this amounts to an increase of mass of the model components ('Mass Scaling') . The result may be that excess kinetic energy is generated, and a less accurate prediction of final behaviour is likely. The package enables the kinetic energy fraction to be enumerated as part of the total internal energy, and this should desirably be no greater than 10% of total energy for a reeasonable prediction. Simulia have advised a 5% limit for the Abaqus package.

Elements

Element types for can forming operations are normally solid elements e.g. brick structure with nodes at the corners, or shell elements having nodes at the mid points of the short axis dimension. A shell element can permit integration of thickness changes in some circumstances where a solid element does not e.g. in a plane stress case. Plane stress elements apply when the thickness of the body is small relative to its planar dimensions, the analysis being two dimensional. To a degree the Abaqus Simulia package helps by limiting the choice of elements or self selection, according to model type.

Where complex geometries occur it may be necessary to employ a free mesh rather than a structured one. An example is the notched tensile model, where on account of the geometry of the notch including a small radius at the Apex, the use of a structured mesh initially was found to give computational problems, with the model not being

completed. A 'free' mesh which better accommodates small geometric features over a wider spectrum of locations was found to function satisfactorily.

Anisotropy

The materials in this study were cold reduced steels, and would be highly anisotropic. In the case of the tensile notched specimen and other models run in this work, only the material tensile properties measured parallel to the grain have been used. The property measurement matched the tensile condition used for slow strain rate testing throughout the study. See later section. Work on other conditions was not completed, but some modifications to the final strain mesurement were explored.

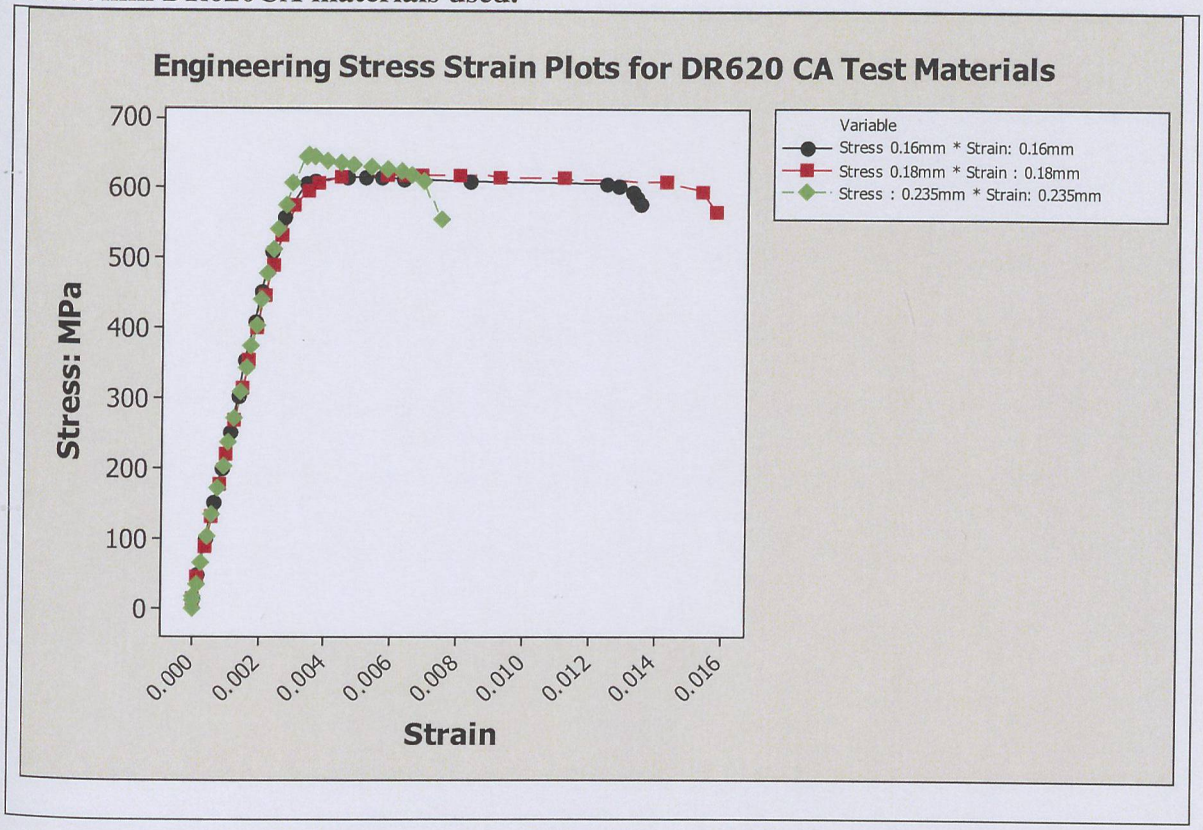
3.6.2 Plate Tensile Properties: Engineering-Stress Strain Plots and True Stress Strain Estimation Studies on DR620 CA Plates used in Product Brine Slow Strain Rate Tests.

The normal practice for determining data for stress / strain curves on tinplate and eccs materials is by way of Engineering Stress – Strain data obtained using the initial cross sectional area and an 80 mm gauge length. Samples of each material type were tensile tested as normal un-notched 'dog bones' on a Zwick Tensometer, under standard testing conditions according to DIN EN 1002-1 standard. The strain rate used was 0.0025 sec^{-1} (= 0.25% /sec).

The specimens corresponded to those shown in Figure 38, except for the absence of notches in the standard DIN test.

In the case of double cold reduced steels, the Engineering Stress Strain tensile plots below, Plot 33, showed that beyond the yield point, a negative slope existed on each curve, and such conditions have been found to be incompatible with the operation of the modelling package under tensile conditions such as pulling the notched test piece.

Plot 33: Engineering Tensile Stress Strain Plots for 0.16mm , 0.18mm and 0.235mm DR620CA materials used.



Three significant features of the plots were apparent:

a) The plots for the 0.16mm and 0.18mm materials showed indications of a very slight negative slope within a short margin of strain beyond yielding implying an onset of necking. For the 0.235mm material, there was a distinctly negative slope after a very small increment of strain beyond yielding.

b) The sudden drop in the curve very close to the failure point shows that severe necking occurred at a late stage, and not as a more gradual process such as in more ductile materials..

A negative slope implies that from slightly beyond the yield point strain, the material can be deformed without any increase in load. In practice, it is known that degrees of work hardening typically occur leading to some load increase with strain. A true stress-strain plot has to be used for Finite Element Modelling. Several exploratory stages have

been followed to try to determine true stress strain plots for the DR 620CA materials which are summarised below.

a) Practical Determinations.

These were conducted on three additional specimens per material , these being the peak load sample, a sample removed from the test at an intermediate point between the peak load and failure, and the failed sample. Measurement of the fracture surface for thinning was made using scanning electron microscope (SEM), and for other samples digital gauges were used to measure width and thickness. Because of too few increments and the need to amalgamate data from several tests, the method was thought to be inaccurate for intermediate points. However , the final fracture stress in each case was estimated from SEM measurement of sample thickness and caliper measurement of width. The following data in table 67 for examples of true fracture stress and applied loads were determined for each material.

Table 67: Final fracture Stress of Standard Tensile 'Dog Bone' Test Pieces: No notches.

	0.16mm DR620CA eccs Drawing Steel	0.18mm DR620CA eccs Stamping Steel	0.235mm DR620CA eccs Nitrogenised Stamping Steel
Fracture Stress: N/mm^2	2114.3	2433.6	2278.5
Tensometer Load applied to cause fracture of specimen: Newtons	1222.6	1382.9	1807.8

Similar 'dog bone' test pieces having two notches, as used for slow strain rate testing, were pulled under DIN EN 1002-1 conditions on a Zwick Tensometer for comparison. These gave the follwing loads to cause fracture, shown in table 68:

Table 68: Data: Final fracture Stress of Standard Tensile 'Dog Bone' Test Pieces, having two notches, each 1.06mm deep.

	0.16mm DR620CA eccs Drawing Steel	0.18mm DR620CA eccs Stamping Steel	0.235mm DR620CA eccs Nitrogenised Stamping Steel
Tensometer Load applied to cause fracture of notched specimens: Newtons	1086.9	1208.5	1611.87

The FEA models were used initially for notched sample simulation, to examine how closely the stresses predictions at the notch apex under tensile loading which caused specimen failures on the Zwick tensometer, would match the true fracture stress determinations for un-notched standard tensile samples.

Alternative Measurement of the Final Fracture Strain using the Erichsen Cupping Method.

Following consultation with experts within Crown CT, this was considered a better representation of fracture strain appropriate to drawing conditions to which the materials are subjected. Also, as metals work harden when strained, it was thought unlikely that the plateau region after yielding would still be realistic for a true stress/ strain plot, although further work might need to be done.

Six plate samples per material were tested by the Erichsen method, and the sample profiles traced at 10x mag. A plastic strained region 120mm wide was used to estimate the strain. The increases in plastic strains were compared with failed samples from original tensometer engineering stress strain measurements parallel to the grain. The data are shown in table 69 below.

Table 69: Data from Erichsen Cup Draw Test: 6 Samples perTest

	0.16mm DR620CA eccs Drawing Steel	0.18mm DR620CA eccs Stamping Steel	0.235mm DR620CA eccs Nitrogenised Stamping Steel
Depth of draw to failure: mm	2.82 (2.5-3.3)	3.6(3.1-4.2)	4.15(3.9-4.5)
Estimated plastic strain to failure from 10x trace.	0.0354(0.025-0.0417)	0.052(0.0319-0.0625)	0.0555(0.0458- 0.0667)
Total strain from engineering stress – strain plots	0.013450	0.0158075	0.0074350
Estimated plastic strain from Enginnering Stress-strain plots	0.011115	0.01316	0.0046925

From these data, the Erichsen cupping values and plastic strain estimates were in order of gauge, whereas the engineering tensile stress strain data gave a lowest strain value for the 0.235mm material. The plastic strain estimate using the Erichsen method showed a multipying factor for plastic strain of over 3x for 0.16mm plate, 3.95x for 0.18mm plate and over 10x for the 0.235mm material, relative to the standard tensile result.

b) Numerical Algorithm Estimates of True Stress-Strain Behaviour.

Reference to Dowling[71] described the following power relationship:

σ true $= H \varepsilon_P{}^n$

where:

σ true is the true stress

ε_P is the plastic strain.

n is the strain hardening exponent.

H is a number termed the strength coefficient.

The execution of the method requires a log stress – strain plot for plastic deformation which should be linear. However, plots based upon data obtained using equations **a1** and **b1** below were found to very wide departures from linearity for each material and did not appear obviously capable of immediate application.

Dowling[71] describes other relationships for true stress and strain estimates, based on an assumption of constant volume for plastic strain, as follows:

$\sigma_{true} = \sigma (1+ \varepsilon)$ **(equation a1)**

where

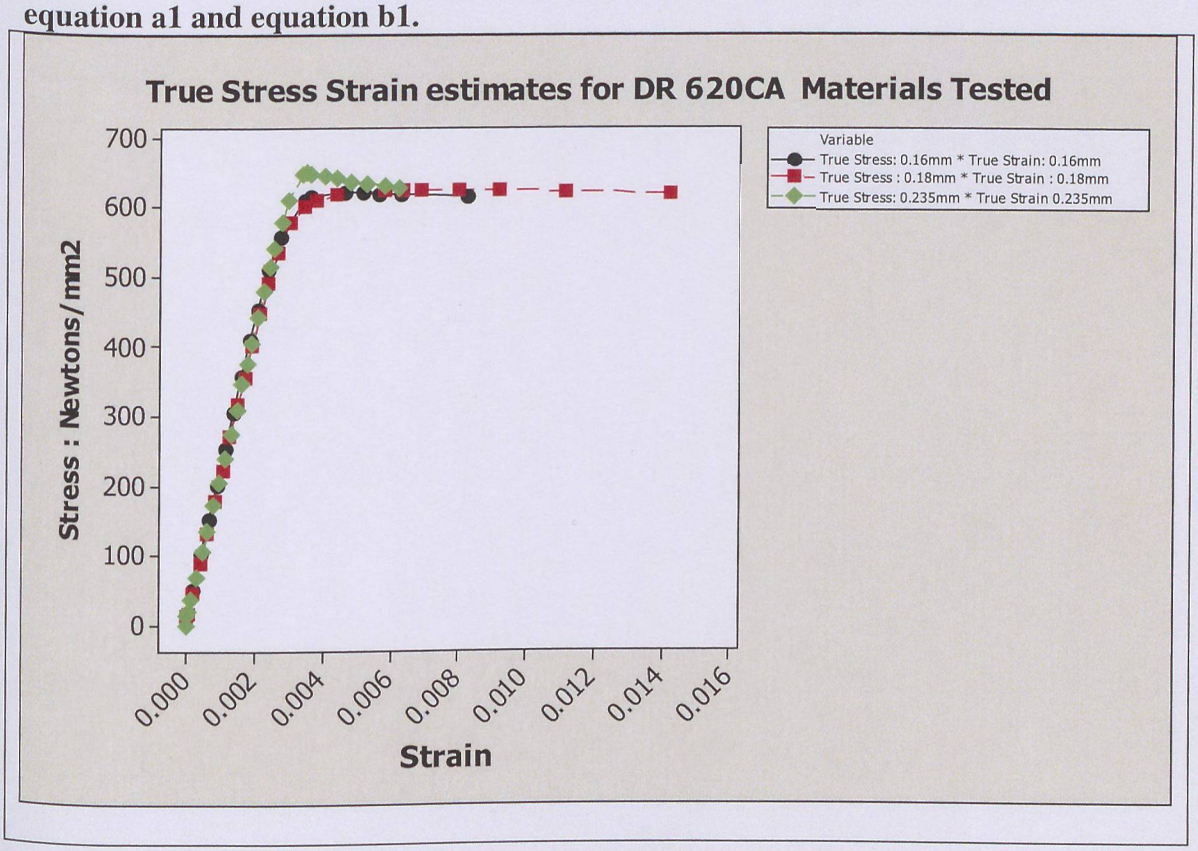
σ_{true} is the true stress.
σ is the engineering stress.
ε is the engineering strain.
and

$\varepsilon_{true} = \ln (1+ \varepsilon)$ **(equation b1)**

where ε is as described above.

The stress relationship (equation a1), was indicated as applicable for stresses above 2 x yield stress. The plots using these relationships were nevertheless examined as other options had proved unsatisfactory e.g. due to irregular strain markings beyond the yield point of these materials, it was difficult to determine a single representative thickness value. Using equations a1 and b1 above the curves shown in Plot 34 were derived.

Plot 34: True Stress Strain estimates up to the point of necking, based upon equation a1 and equation b1.



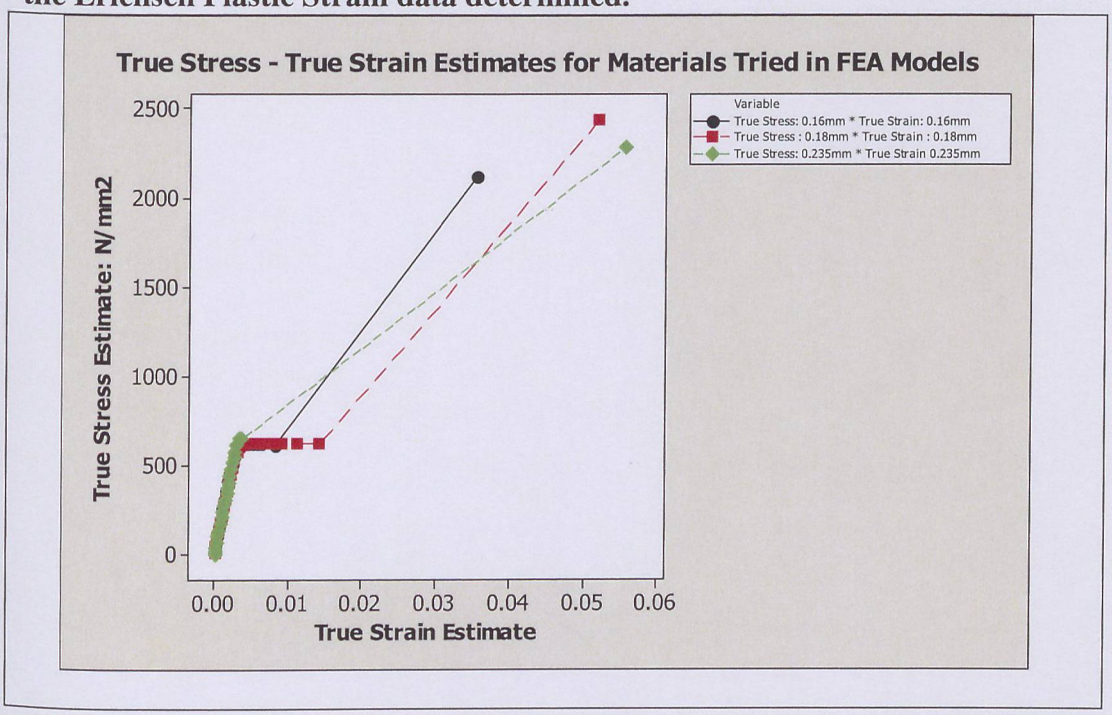
Identification : black : 0.16mm plate ; red 0.18mm plate; green 0.235mm plate.

In the case of the 0.16mm and 0.18mm plates, the form of plots suggested elastic perfectly plastic material behaviour up to the point of pronounced necking. In the case of the 0.235mm nitrogenised steel, the plot still showed a negative slope indicating the start of necking, and no satisfactory conclusion was reached enabling a soundly validated stress strain plot to be used in Finite Element Models. The fact that the plots show such a small change from the engineering stress strain plots reflected the low level of strains observed before necking. The plastic strain estimates tended to show a fractional reductions using equation b, and Dowling[71] comments that beyond the maximum stress, equations **a1** and **b1** are not applicable where necking is occurring. However , if the elastic-perfectly plastic indication prior to necking is approximately true, it may be a reasonable first estimate to include the plateau region prior to necking. In the absence of any better method having been established in this work to suit these materials, the data above for the plateau region based upon equations **a1** and **b1** was amalgamated with the final true fracture data and Erichsen strain values to failure, to examine stresses in the notch tensile model and the correlation between peak stress at the notch and tensile failure load of the notched specimens.

3.6.3 Final Estimate of True-Stress-Strain Plots achieved.

The True Stress Strain plot estimates obtained using the above are shown below in Plot 35.

Plot 35: True Stress- True Strain Estimates. Plots combining practical fracture stress determinations with engineering stress strain data modified using the constant volume assumption for plastic strain. Final strain values are means from the Erichsen Plastic Strain data determined.



While these plots were not smooth true stress – strain curves, to achieve much better plots is likely to require a longer exercise requiring a lot of sampling and practical measurement, or digital monitoring of thickness change in the tensile test. The latter would need to be done on a notched sample to ensure the site of necking to measure

c) Notch Height Strain from Tensile Tests.

As a further etimate of strain to fracture which could be applied to models for conditions parallel to the grain, the three notched tensile control samples tensile tested on the Zwick machne under standard conditions were measured for notch height strain

as an average of the two notches per material. notch strain = notch height extension/ original notch height. These values were as shown in table 70:

Table 70: Notch Height Strain from Tensile Tests

Sample	0.16mm DR620CA Plate	0.18mm DR620CA Plate	0.235mm DR620CA Plate
Notch strain from Zwick Tensometer Standard Test	0.08811	0.08155	0.0124

These results showed a degree of inconsistency with respect to gauge, but is can be seen that the strain values were higher than for the Erichsen samples which had fractured parallel to the grain.

These values were used as alternative final strain estimates in a model of the notched specimen tensile behaviour.

Models of the notch tensile sample were then run with each material and the two alternative fracture strain options, Erichsen values and notch strasin values.

The results were examined for agreement of the peak notch stress with the tensile final fracture true stress of a standard tensile sample, when the tensile load applied corresponded to that which failed the notched specimen on the Zwick tensometer.

3.7 Model Examples Selected for the Study :

1. Notch tensile specimens to match the slow strain test work.
2. An 83mm diameter drawn redrawn can such as would be used for Tuna product.
3. A 73mm dia easy open end shell formation.

3.7.1 Model 1: Notch Tensile Sample Used in Slow Strain Rate Testing Under Tension.

This was initially set up using the Abaqus system in the form of a ¼ geometry model of the test piece but having a reduced overall height of 3mm, as shown in Figure 79 below.

Figure 79: Diagram of Model Set Up

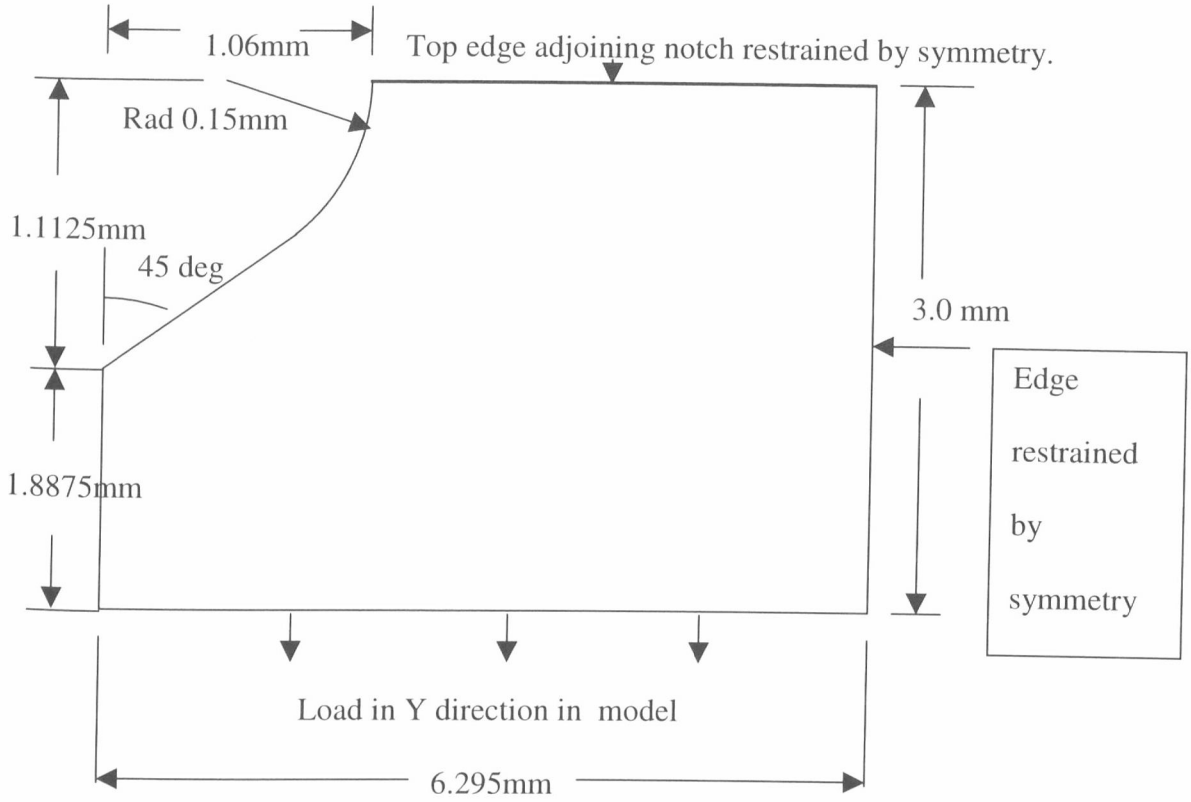


Table 71: Details of the model are shown in the table below

Item	Parameter	Description
1.	Model method	Abaqus standard: Static
2.	Set up	2D Plane stress
3.	Load applied	Uniaxial displacement
4.	Mesh	Quadratic solid element dominated: Abaqus version 6.8-1: CPS8R; free mesh.
5.	Step time	0.5 seconds.
6.	Loading	Successive models run at loads of 150- 600 Newtons applied at the bottom edge
8.	Validation of set up	No errors reported by package.
9.	Number of incrementations.	Automatic : maximum 500.
10.	Material properties	Young's modulus from tests conducted.
	0.16mm plate: E	207490 N/mm^2
	0.18mm plate: E	201642 N/mm^2
	0.235mm plate: E	210359 N/mm^2
11	Poisson's ratio	0.3

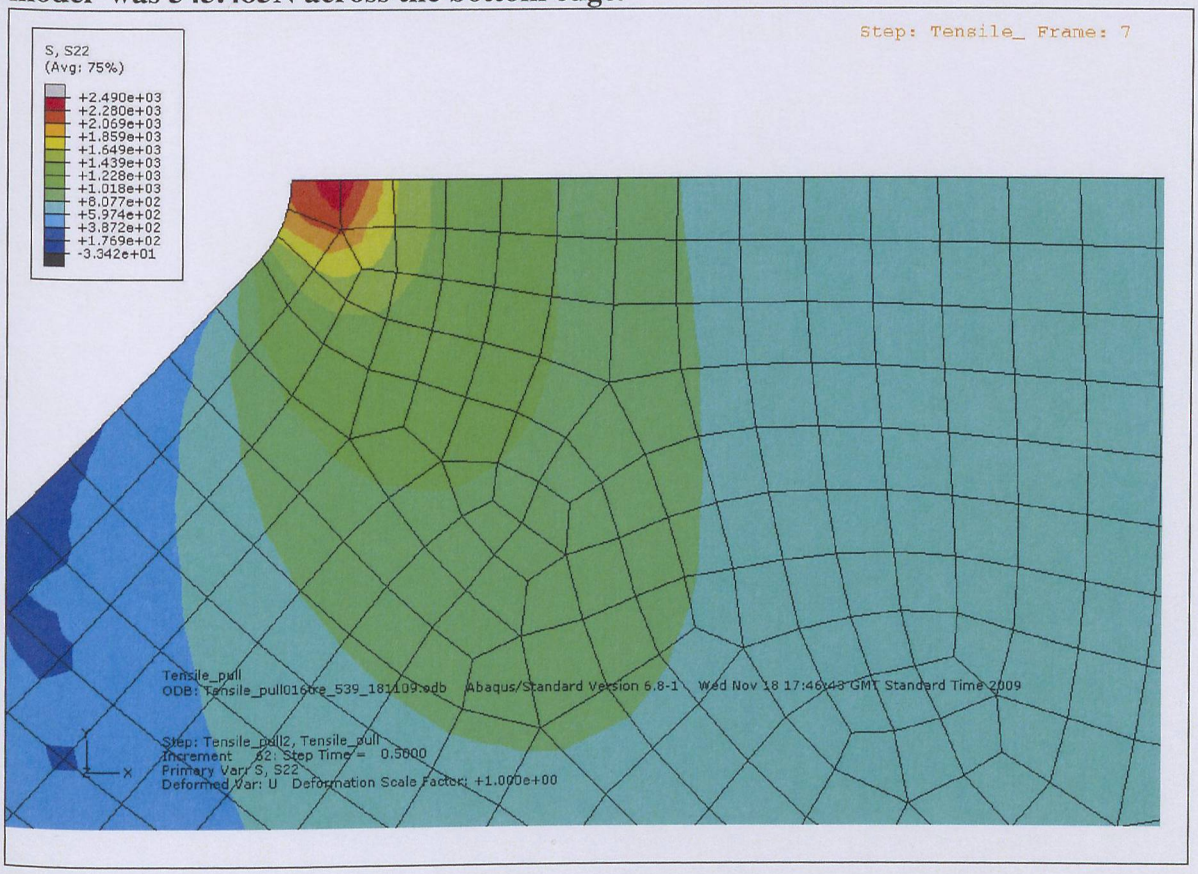
The sample is pulled in uniaxial tension, but by virtue of the notch a two dimensional state of stress, plane stress, is expected. Under the conditions described the model ran satisfactorily.

3.7.1.1 Notch Tensile Model Results.

The results are presented in the plots below as the stress distribution in the 'y' direction (S22) for the maximum load applied, for each of the three materials examined. There are two images for each gauge, one modelled with the Erichsen peak strain and one with the notch strain as peak strain. The results are reviewed at the end of the section.

0.16mm DR620CA Plate Model Utilising Erichsen Cupping Value for Final Strain in True Stress-Strain Plot.

Model 1, Image 1: 0.16mm DR 620 CA Material : Material data using Erichsen cupping value as final strain. The measured True fracture stress was 2114N/mm^2 using a standard tensile sample. The Y direction load applied to the half width model was 543.485N across the bottom edge.



The above image of the 0.16mm model shows that for the completed model having a tensile load of 539.6N/mm2 (543.485N) applied to the bottom edge over half the width (1086.9N across full width) the peak stress in the 'y' direction , S22 , had reached between 2280 and 2490 Mpa (N/mm^2) at the notch apex region. The principal stresses at

the notch apex are shown below in Table 72. S33 is zero as there is no stress normal to a free surface for a plane stress condition. A two dimensional state of stress was shown to exist.

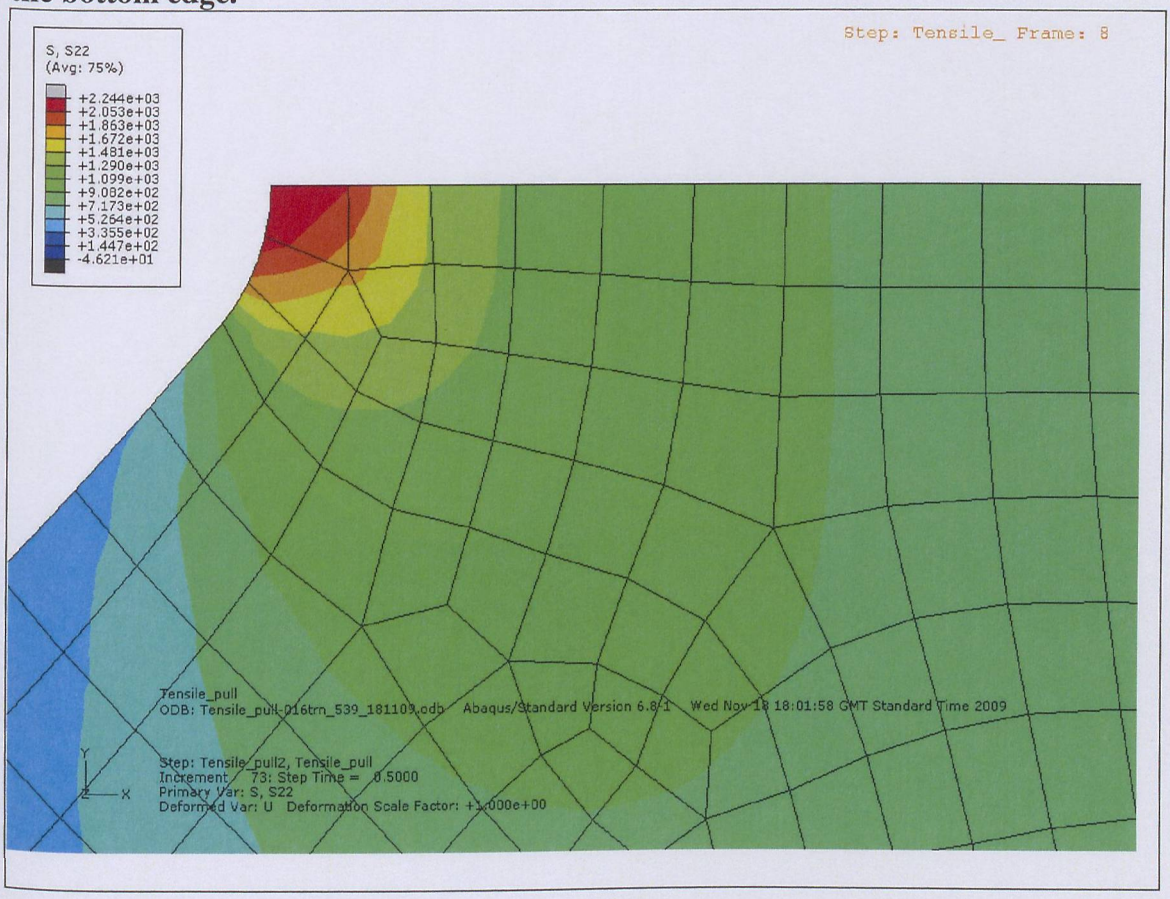
Table 72: 0.16mm DR 620 CA Sample. Data are : Stresses in MPa

	S11	S22	S33
Notch apex peak stress:	834-932	2280-2490	0.0

The mean stress at the notch in the y direction was thus 2385Mpa. The model was re-run using the 'notch strain' value for the material entry corresponding to the failure stress, to examine whether the prediction was improved. The plot and table 73 of predicted peak stress values at the notch apex are shown below.

0.16mm DR620CA Plate Model Utilising Notch Height Strain from Slow Strain Rate Test as Estimate for final Strain in True Stress-Strain Plot.

Model 1, Image 2: 0.16mm DR 620 CA Material: Modifed failure strain criteria utilising failure strain of a notched tensile sample measured from notch height strain. The y direction load applied to the half width model was 543.485N across the bottom edge.



The principal stresses at the notch apex are shown below in Table 73:

Table 73: 0.16mm DR 620 CA Sample. Data are : Stresses in MPa

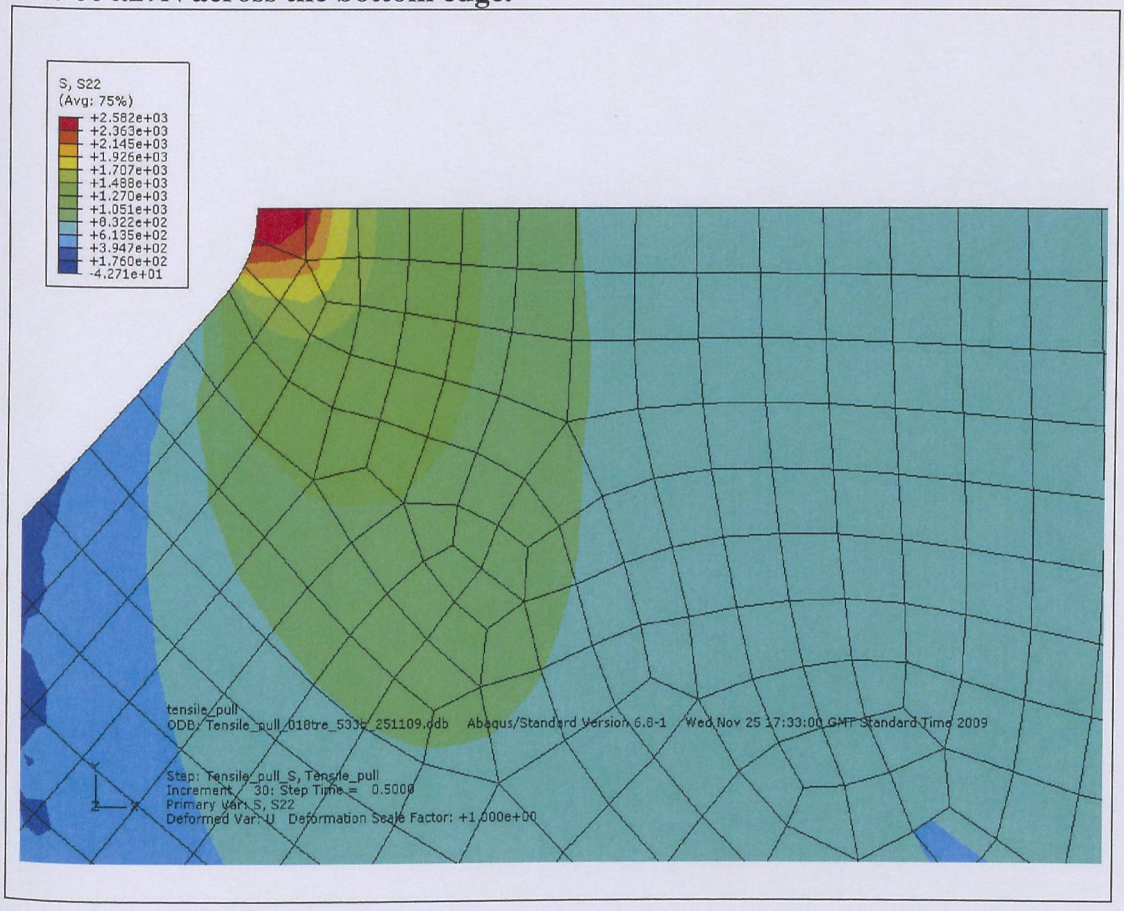
	S11	S22	S33
Notch apex peak stress	633-714	2053-2244	0.0

This model gave an average value for S22 of 2148.5MPa and relative to the estimated true fracture stress of 2114Mpa .

3.7.1.2 Notch Tensile Model Results: 0.18mm DR620CA Plate.

0.18mm DR620CA Plate Model Utilising Erichsen Cupping Value for Final Strain in True Stress-Strain Plot.

Model 1, Image 3: 0.18mm DR 620 CA Material: Stress prediction using final strain value from Erichsen test. The measured failure true stress was 2433.6Mpa for standard tensile sample. The y direction load applied to the half width model was 604.27N across the bottom edge.



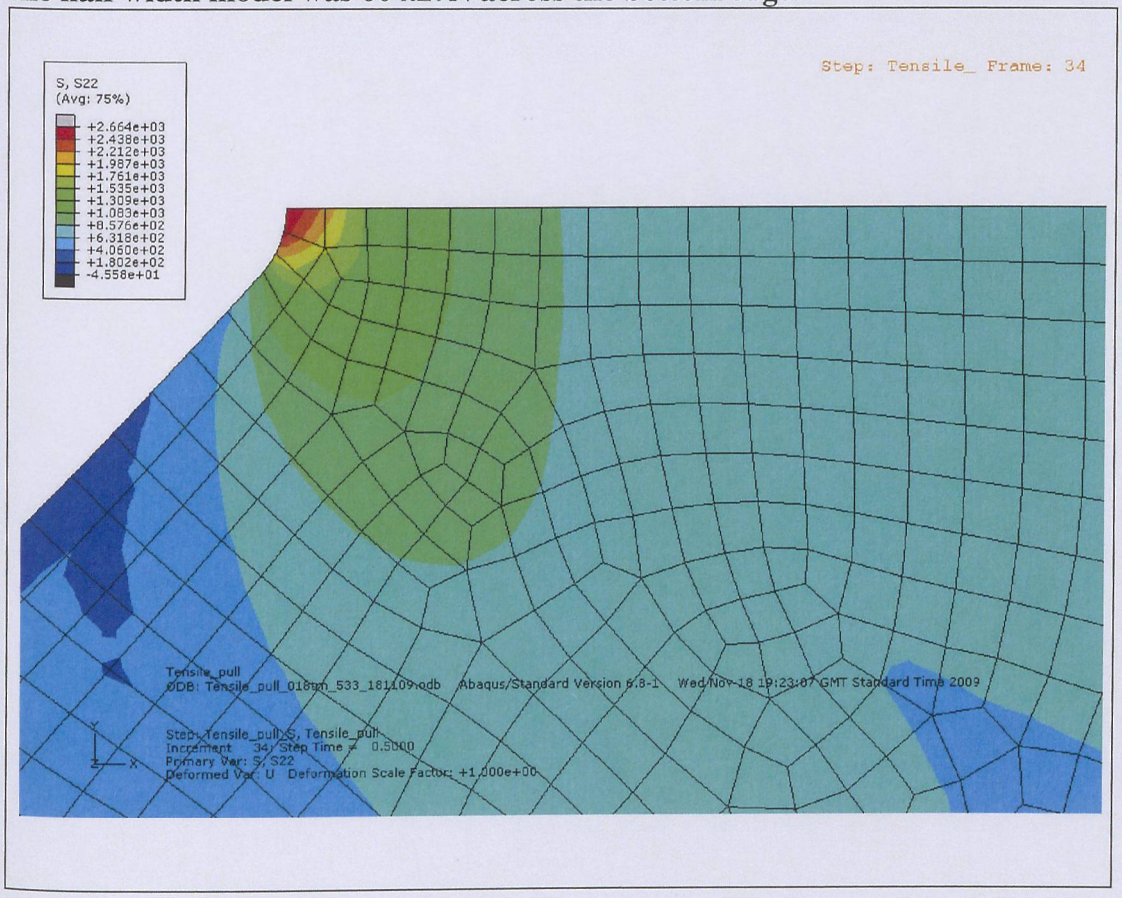
The above image of the 0.18mm model shows that on the completed model having a tensile load of 533.3N/mm2 applied to the bottom edge over half the width (equivalent to

1208N load across full width). The peak stress in the y direction, S22, had reached between 2453 and 2681MPa at the notch apex region. The principal stresses are shown in Table 74 below.

Table 74: 0.18mm DR 620 CA Sample. Data are : Stresses in MPa

	S11	S22	S33
Notch apex peak stress	839-938	2453-2681	0.0

Model 1, Image 4: 0.18mm DR 620 CA Material: Stress prediction using final strain value from notched tensile slow strain tests. The y direction load applied to the half width model was 604.27N across the bottom edge.



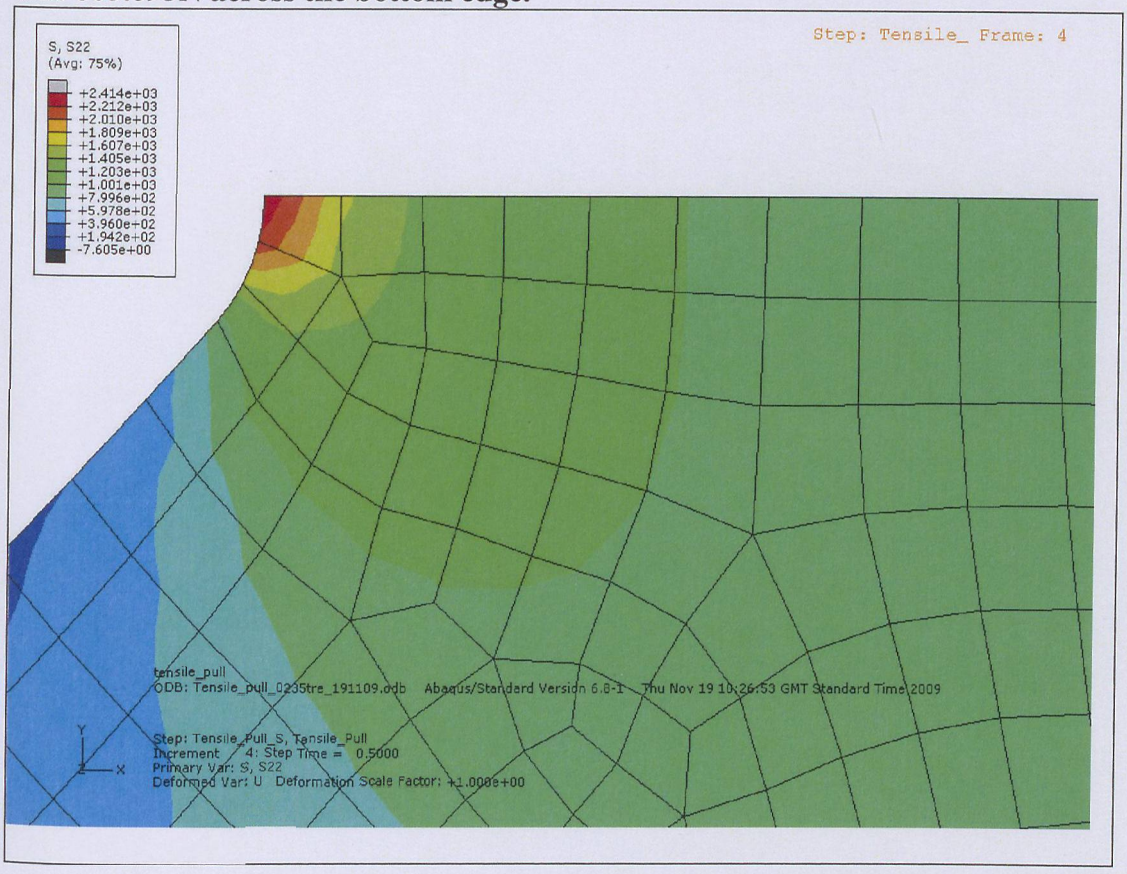
The principal stresses at the notch apex are shown below in Table 725

Table 75: 0.18mm DR 620 CA Sample. Data are : Stresses in MPa

	S11	S22	S33
Notch apex peak stress	675-759	2438-2664	0

3.7.1.3 Notch Tensile Model Results: 0.235mm DR620CA Plate.

Model 1, Image 5: 0.235mm DR 620 CA Material. Stress prediction using final strain value from Erichsen test. The measured failure true stress was 2278.5Mpa for a standard tensile sample. The y direction load applied to the half width model was 805.895N across the bottom edge.

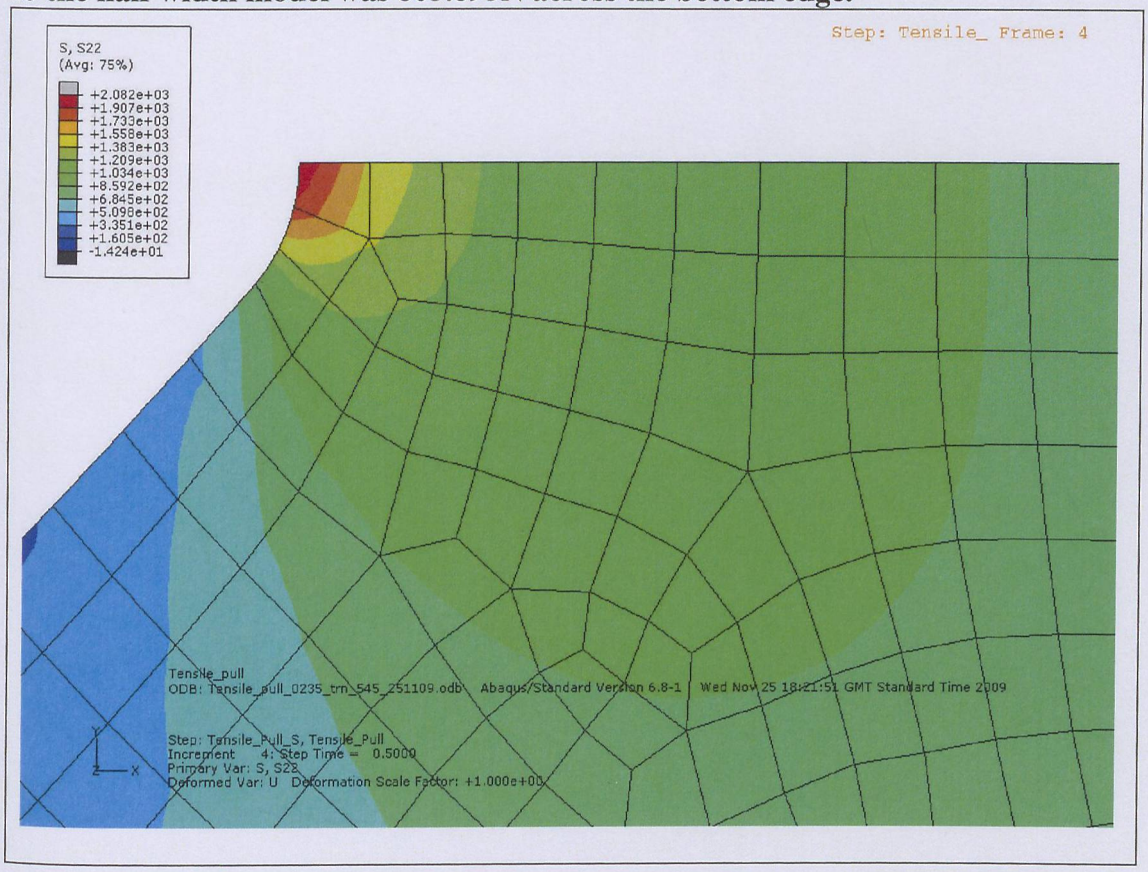


The above image of the 0.235mm model shows that on the completed model having a tensile load of 805.895N applied to the bottom edge over half the width (1611.79N across full width) the peak stress in the 'y direction ,'S22', had reached between 2212 and 2414 Mpa(N/mm^2) at the notch apex region. The principal stresses at the notch apex are shown below in Table 76.

Table 76: 0.235mm DR 620 CA Sample. Data are : Stresses in MPa

	S11	S22	S33
Notch apex Stress	550-642	2212-2414	0

Model 1, Image 6 0.235mm DR 620 CA Material. Stress prediction using final strain value from notched specimen slow strain test. The y direction load applied to the half width model was 805.895N across the bottom edge.



The principal stresses at the notch apex are shown below in Table 77.

Table 77: 0.235mm DR 620 CA Sample. Data are : Stresses in MPa

	S11	S22	S33
Notch Apex Stress	504-575	1907-2082	0

3.7.1.4 Summary of Stress Predictions for Notched Specimens compared with True Fracture Stresses measured on Standard un –notched Tensile Specimens.

The comparisons are shown in Table 78.

Table 78: Stress Predictions for Notched Specimens Compared with True Fracture Stresses measured on Standard un -notchedTensile Specimens.

Sample	**0.16mm DR 620CA Plate**	**0.18mm DR 620 CAPlate**	**0.235mm DR 620 CA Plate**
True Fracture Stress from standard tensile sample: N/mm^2.	2114.3	2433.7	2278.5
Peak notch stress mean predictions, S22, for tensile loads causing failure of notched specimens			
Peak Stress prediction (N/mm^2)using Erichsen test strain data.	2385	2473	2313
Peak stress prediction (N/mm^2) using notch strain data.	2149	2551	1994
Prediction errors, %, using Erichsen test strain to failure.	+12.8%	+1.59%	+1.54%
Prediction errors, %, using notch height strain to failure.	+1.62%	+4.82%	-12.6%

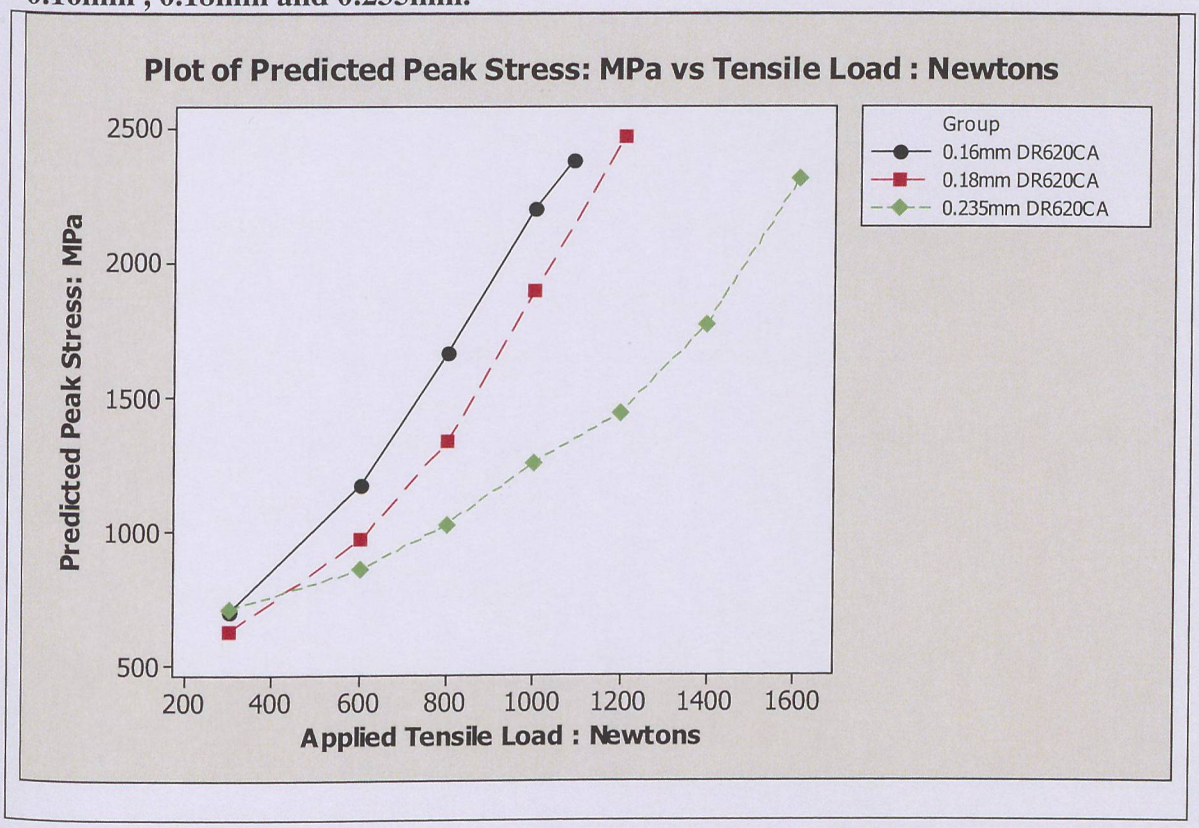
The results showed that using either the Erichsen data or the notch strain data to support the generation of true stress strain plots, relatively good or poor predictions maybe achieved in individual cases indicating that more work needs to be done. To achieve much more genuine data would require real time monitoring of the thickness change as the tensile test reaches necking using micrometers or optical devices.

As the Erichsen strain measurements were thought likely to be more consistent than those for notch strain, the material behaviours including the Erichsen strain values were used with the 0.16mm plate for the Drawn Redrawn Can Model and with the 0.18mm data for the Eo shell model.

The above results represent an initial mechanism by which a cross check between modelling predictions for stress and tensile information from two parallel tests can be achieved.

Plot 36 below summarises the predicted Y direction peak stress at the notch as a function of the tensile load applied to the full width of a test piece i.e. 2x that for the half width in the model.

Plot 36: Notch Tensile Specimen Model: Predicted Peak Streses for loads applied to a full width Tensile Specimen, for each of the DR620CA materials modelled , 0.16mm , 0.18mm and 0.235mm.



The loads shown do not exceed those which approximate to that which gave predictecd stress levels close to the true failure stresses established from tensile tests on standard tensile dogbones. In order to demonstrate metal thinning and true simulated fracture the models require to be re run using a shell element in place of the solid element used.

3.7.2 Model 2: 83mm Dia Drawn Redrawn Can with Redraw Height of 50mm.

3.7.2.1 Introduction

This type of can is produced for food products such as tuna in brine. A typical size is 83mm dia x 45mm high. The first stage is a cup draw from the blank to an overall diameter of 103.4mm x height of 48mm. This is followed by a redraw using a punch of 83.65mm diameter and a second draw ring, in a redraw tool having a height of 50mm, but a range of redraw heights to provide different finished can heights is possible. The third stage is base profiling achieved by two concentric plugs. The can would then be trimmed and flanged before double seaming. The plate used is 0.16mm DR620 CA material of drawing quality, and the process is carried out on lacquered plate. The explicit dynamic method of modelling was used this being best able to handle complex drawing operations.

3.7.2.2 Stages of Formation and Times

The stages of formation are summarised below in Table 79, after the blank disc has been cut.

Table 79: Stages of Formation and Times

Stage	Description	Times in model. (seconds)
1.	Draw ring holds down blank against draw sleeve.	0.2
2.	Punch P1 forms cup to 103.4mm diameter.	0.214
3.	Redraw tools engage cup and 2nd draw ring holds cup base against redraw sleeve.	0.3
4.	Plug P2 redraws container to 83mm dia.	0.30
5.	Base profiling tools engage.	0.3
6.	Base profiling tools form base shape.	0.3
7.	Base profile tools withdraw	0.1

In order to perform the model the redraw tools for stages 3 and 4 were actioned from inside the blank draw punch, the punch P1 being inactivated after stage 2. Again the base profiling tools were actioned for stages 5and 6 from within the redraw tools the redraw punch, P2, being inactivated after stage 4.

3.7.2.3 Model Details.

The model details are shown in Table 80:

Table 80: Model Details

Item	Parameter	Description for Model
1.	Model method	Explicit dynamic
2.	Set up	Axisymmetric
4.	Mesh : Element type	Abaqus CAX4R
5.	Number of elements through thickness	6
5.	Incrementation time	$5x10^{-7}$ s.
6.	Loading	By tool displacements only
8.	Validation of model set up	Automatic
9.	Friction coefficients	0.06: tangential contacts
10.	Material Properties	
	Plate type	0.16mm DR620CA material
	Young's modulus result	207490N/mm2
	Poisson's ratio	0.3

Note that the tensile stress strain plot used, as tested on the notch tensile case, Model l, gave a prediction of peak tensile stress just under 13% below the estimate true fracture stress from practical determinations.

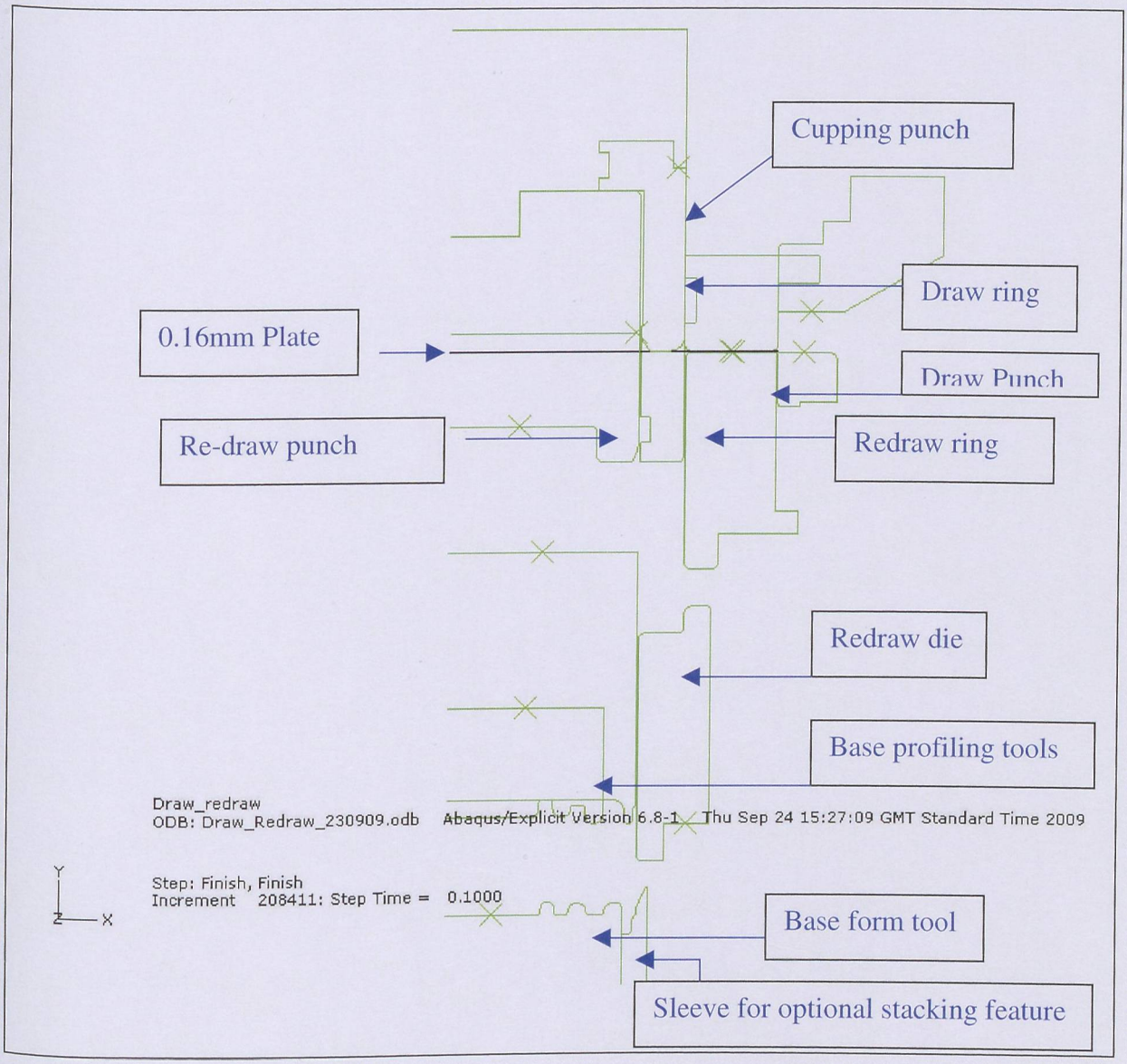
The material properties were as used for the 0.16mm plate in the notch tensile model. The model ran to completion with no errors reported. Mass scaling was used due to very long computation time with automatic time incrementation e.g. over 1 day. For this model, the mass scaling would not function when it was attempted to apply it to a plate set defining the body material, and it was run by application on a whole model basis. The run might need to be repeated when the reason for the difficulty is found. The

friction level of 0.06 is a common level used in Crown CT for simulation of metal fabrication processes.

3.7.2.4 Overview of Tooling Set up

The tooling set up is shown below. All drawings were fully re constructed from hard copy originals.

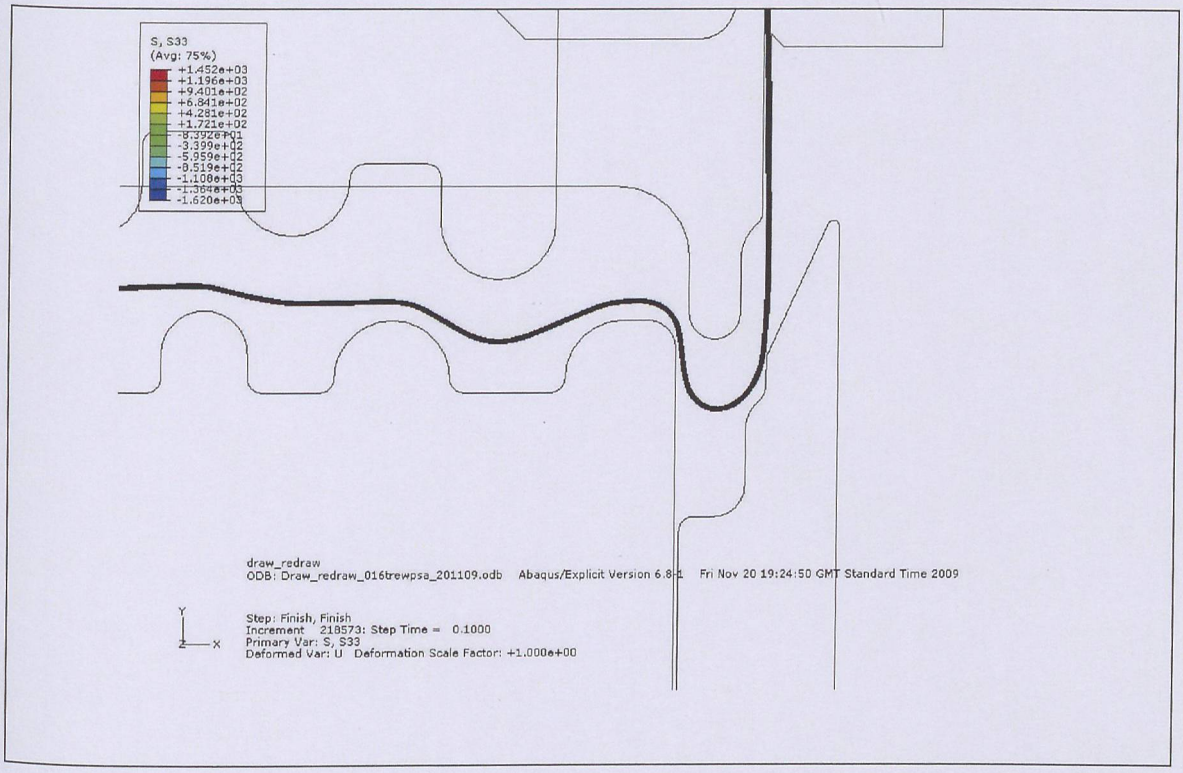
Model 2, Image 1: DRD Model : Overview of Tooling Set-up



3.7.2.5 Images of Stress Contours from Model with Stress Tabulations for S33, S22 and S11 Directions.

In the succeeding figures, images are presented and stress estimates defined.

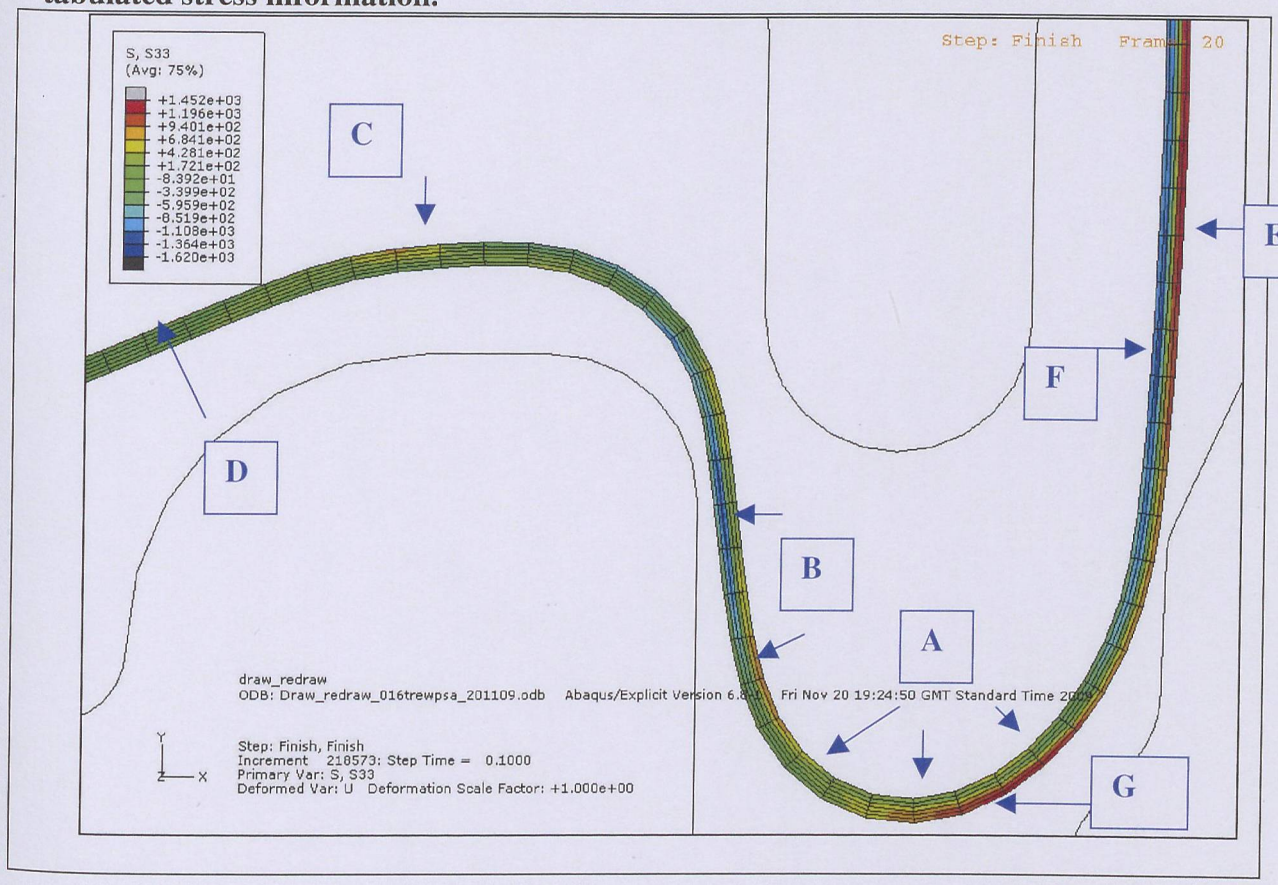
Model 2, Image 2. Bottom rim region and countersink with adjacent beading: general appreciation.



In image 2 at low maginification the normal bottom end beading is shown. After the tool disengagement some springback occurred and this lead to some increase in the hoop stress S33 at the outer base rim region identified as G in Image 3.

Model 2, Images 3-6. Bottom rim radius region and reverse wall with principal stresses S33 for the Z direction (hoop stresses), S22 for the y direction, and S11 for the X direction. A summary of stresses is given beneath each plot in Tables 81-83, and Table 84 summarises the stresses. The energy plots are shown as Model 2 Image 7 . Note that all stress predictions applied the model after tools were released from contact at the bottom rim region.

Model 2, Image 3: DRD Can : Base Rim Region: General Appreciation of Form at Base Rim: 'z' Direction Stresses : S33. Regions idetified by letter relate to tabulated stress information.



Model 2, Image 4: DRD Can : Base Rim Region: Base Rim enlarged, showing high predicted tensile hoop stress, S33, at reverse wall: 684-940MPa

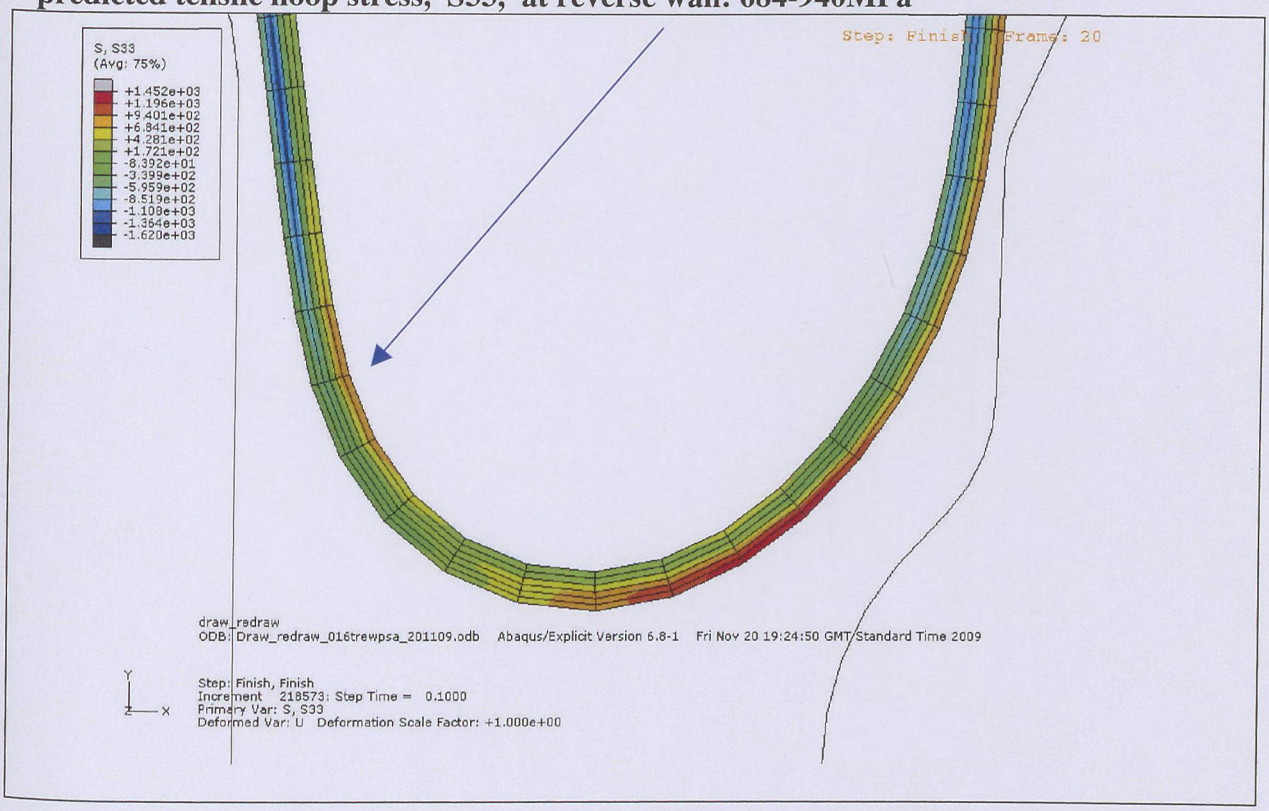


Table 81: Table of S33 (Hoop Stresses) on Drawn Redrawn Can Stress Predictions : Mpa: +ve = tension / -ve = compression

Location	S33 Stresses
A. Inner bottom rim radius	- 8.392 to + 172.1
B. Inner reverse wall	- 8.392 to + 940.1
C. Inner countersink region	+ 172.1 to + 940.1
D. Inner bead region	- 595.9 to + 172.1
E. Outer wall lower	+1196 to +1452
F. Inner wall lower	- 851.9 to - 1108
G. Outer bottom radius	1196 to +1452

From these data, there were regions in tension towards the extremeties of the bottom inner rim radius, A, and the inner reverse wall, B. At the inner wall this would be likely as some expansion is required to form the wall. Major tensile effects were at the outer

wall and radius which would not affect internally initiated environmental stress cracking. The inner countersink and bead regons showed some local tensile sites.

S22 Stresses are shown and tabulated on the next page:

Model 2, Image 5: DRD Can : Base Rim Region: Base Rim enlarged, showing 'y' direction, S22, stresses, which were mainly compressive, but showed high tensile stresses at the outer wall of 1085-1371MPa.

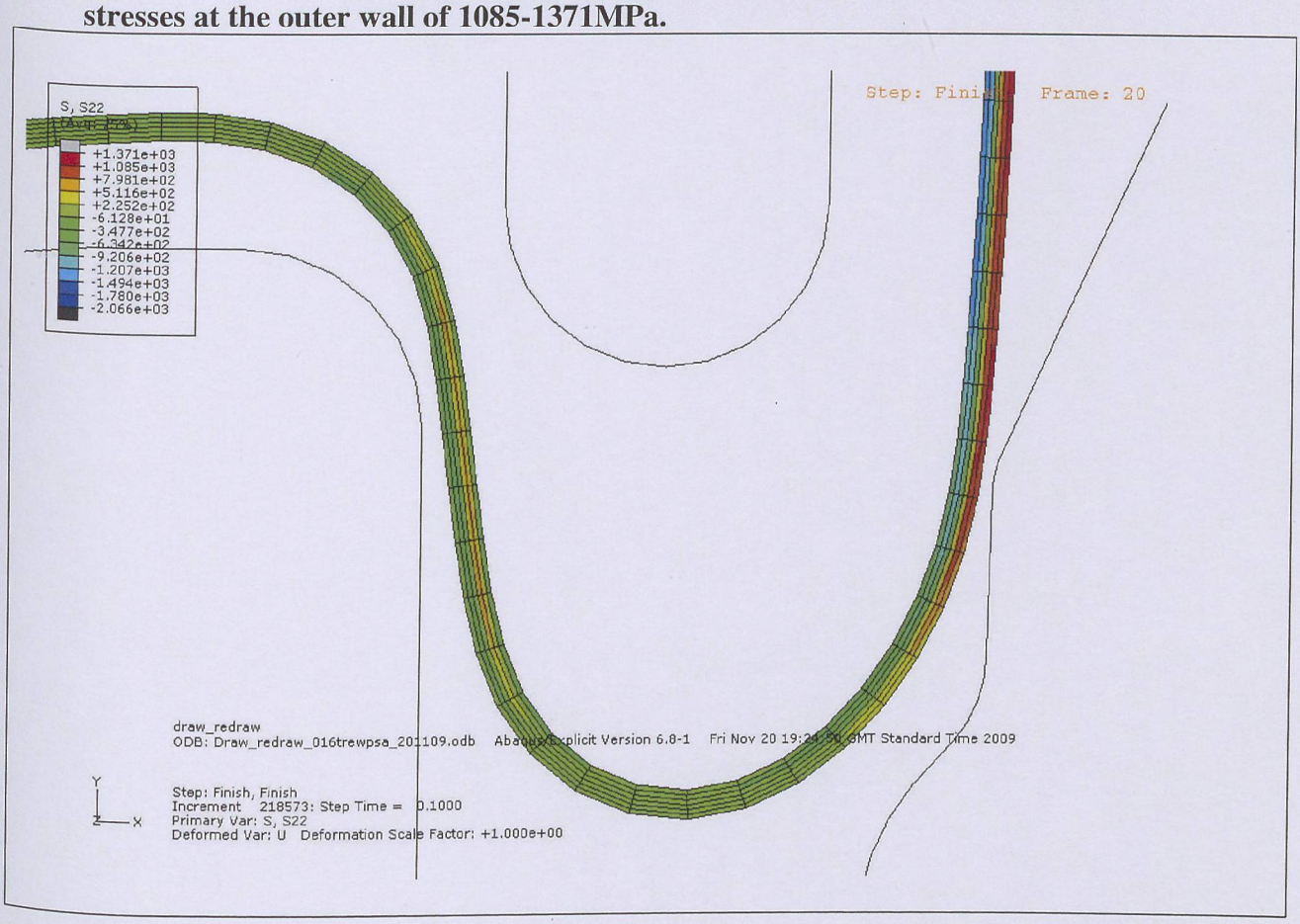


Table 82: Stress Predictions : MPa: +ve = tension , -ve = compression

Location	S22 Stresses
A. Inner bottom rim radius	- 347.7 to -61.28
B. Inner reverse wall	- 347.7 to -61.28
C. Inner countersink region	- 347.7 to -61.28
D. Inner bead region	-347.7 to -61.28
E. Outer wall lower	+1085 to +1371
F. Inner wall lower	- 1297 to - 1494
G. Outer bottom rim radius	-347.7 to +798.1

S22 stresses were tensile at the outer wall and outer bottom rim radius only

S11 stress predictions are shown on the next page

Model 2 Image 6: DRD Can : Base Rim Region: Base Rim enlarged, showing 'x' direction, S11, stresses, which were mainly compressive, but showed some tensile behaviour at the the outer rim bottom radius.

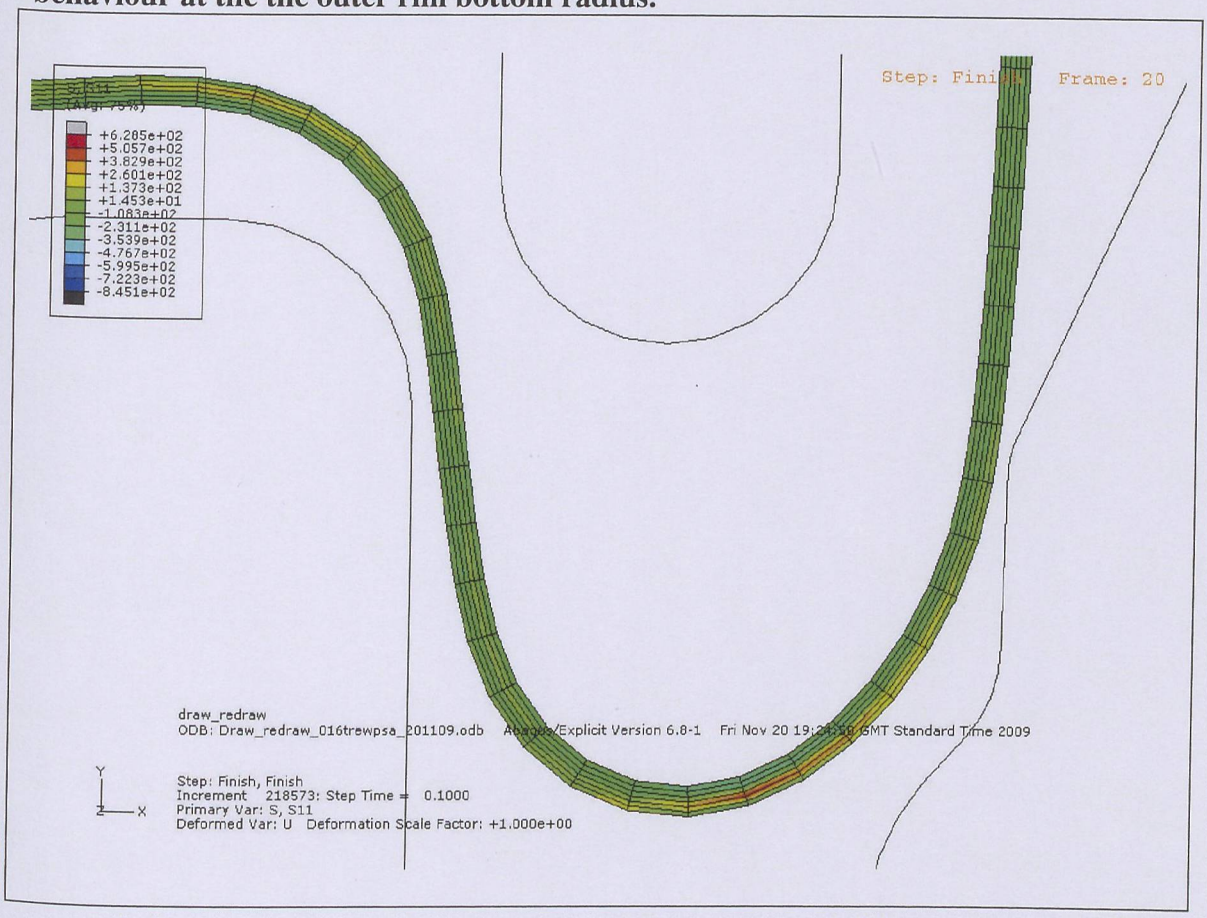


Table 83: Stress Predictions : MPa : +ve = tension , -ve = compression

Location	S11 Stresses
A. Inner bottom rim radius.	- 476.7 to +14.53
B. Inner reverse wall.	- 108.3 to +14.53
C. Inner countersink region.	- 108.3 to +14.53
D. Inner bead region.	-108.3 to +14.53
E. Outer wall lower.	-108.3 to +14.53
F. Inner wall lower.	- 108.3 to +14.53
G. Outer bottom rim radius.	+137.3 to +260.1

The 'x 'direction tensile stresses were of a very low order whre these have been predicted for inner surfaces.

3.7.2.6 Drawn Redrawn Can Model: Summary Table for Predicted Stresses.

The results are shown in table 84.

Table 84: Stress Predictions :MPa : +ve = tension , -ve = compression

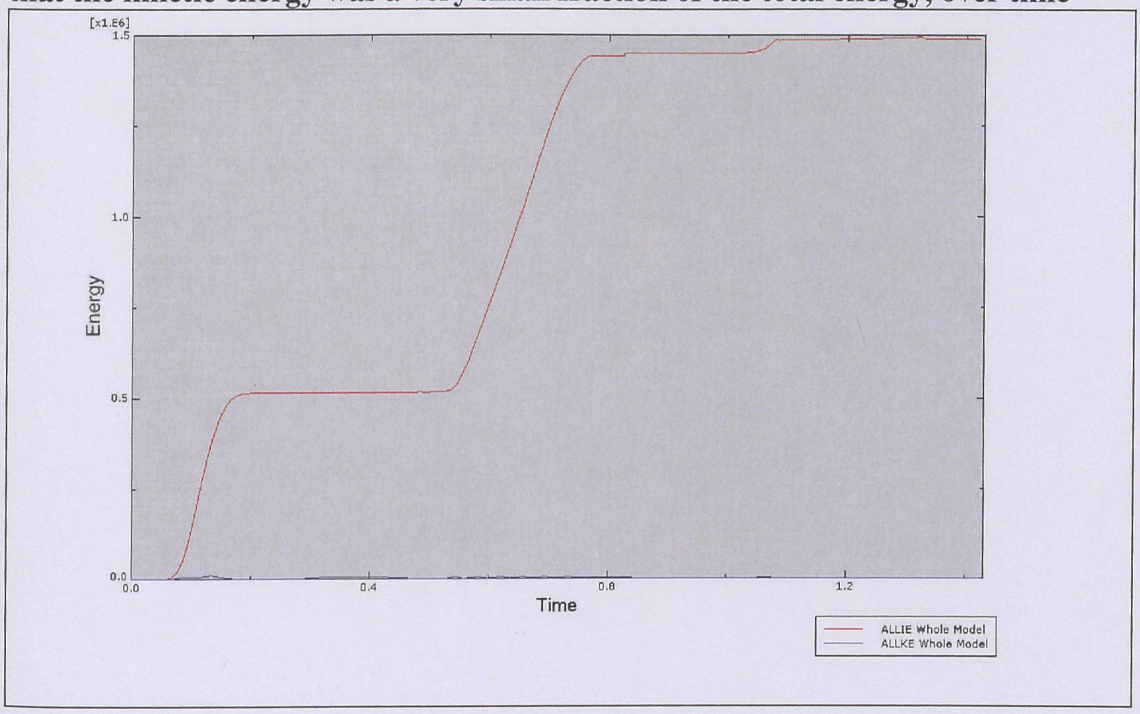
Location	S11 Stresses	S22 Stress	S33 Stresses
A. Inner bottom rim radius.	- 476.7 to +14.53	- 347.7 to -61.28	- 8.392 to + 172.1
B. Inner reverse wall.	- 108.3 to +14.53	- 347.7 to -61.28	- 8.392 to + 940.1
C. Inner countersink region.	- 108.3 to +14.53	- 347.7 to -61.28	+172.1 to + 940.1
D. Inner bead region.	- 108.3 to +14.53	- 347.7 to -61.28	- 595.9 to + 172.1
E. Outer wall lower.	-108.3 to + 1.453	+1085 to +1371	+1196 to +1452
F. Inner wall lower.	- 108.3 to +1.453	- 1297 to - 1494	- 851.9 to - 1108
G. Outer bottom rim radius.	+137.3 to +260.1	-347.7 to +798.1	1196 to +1452

The results have shown that the major tensile stresses affecting internal regions were in the hoop direction, S33 at the inner reverse wall and countersink region. A complication is that the predictions indicated stresses above the yield point of the plate, which was around 558MPa, whereas literature on the subject of residual stresses[37] has stated that any stresses above yielding are relieved, since residual streses are considered as elastic stresses. More study of this aspect is thus required to reconcile this key aspect. Where the values above the yield point were recorded, they tended to occur through part of the plate thickness only.

Kinetic Energy as a Fraction of Total Internal Energy for theWhole Model.

The plot for these parameters is shown as Model 2, Image 7 below.

Model 2 Image 7 :Kinetic Energy vs Internal energy for the whole model showing that the kinetic energy was a very small fraction of the total energy, over time



The unit of energy for the model will be millijoules as the mass density is in tonnes per mm^3. The result shows that the kinetic energy fraction, ALLKE, grey- blue line, appeared to be empirically below 10% of ALLIE, the total internal energy, red line, for the whole model. The model requires to be re-run when it functions with mass scaling applied to the plate set.

3.7.3 Model 3: 73mm Dia Easy Open End Shell for Processed Foods

3.7.3.1 Technical Explanation

The explicit solver is more practical than implicit because of problems of convergeance when the implicit solver is used under mechanical contact conditions.

The choice of element within the package has an association with the point of integration. The element chosen for the easy open end model was CAX4R which is integrated for displacements at the centre of the element. The term 'hourglassing' is used to describe the effect by which an element shape can change e.g. from a rectangle

to a trapezium without a change in the dimension along the central axis. The CAX4R element is used with hourglass control, adding stiffness to reduce the effect. An axisymmetric model form was used which applies loadings around a 360 degree circumference.

The basic stages and times in the model are are shown in Table 85.

3.7.3.2 Easy Open Shell Formation Sequence and Timing

Table 85: Easy Open Shell Formation Sequence and Timing

Stage	Operation	Time (seconds)
1.	Punch action	0.06
2.	Tools withdrawn	0.02

The model was run for the 0.18mm DR620 CA plate only.

The model detail is shown below. Frictional contact between tools and plate was treasted as tangential, with the interaction property coefficient of friction set at 0.06.

The draw ring spring load acting against the punch and plate was set at 450 Newtons.

3.7.3.3 Easy Open End Shell Model Model Details.

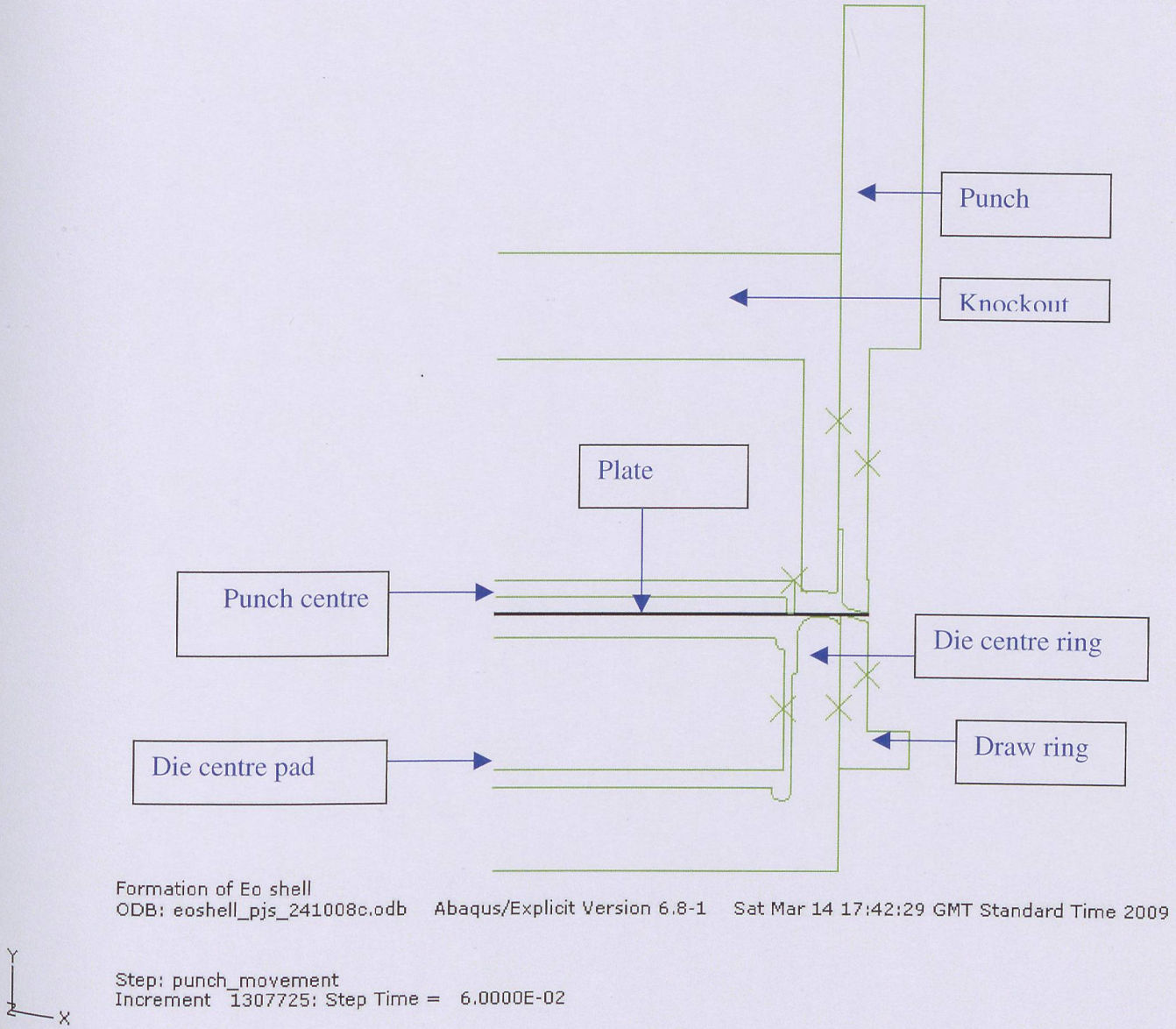
The model details are shown in Table 86:

Table 86: Easy Open End Shell Model Model Details

Item	Parameter	Description: Optimised Time Model
1.	Model method	Explicit dynamic
2.	Set up	Axisymmetric
4.	Mesh : Element type	Abaqus CAX4R
5.	Number of elements through thickness	4
5.	Incrementation time	$5x10^{-7}$s.
6.	Loading	By tool displacements only: smooth step conditions.
8.	Validation of model set up	Automatic
9.	Friction coefficients; tools/ plate	0.06 : Tangential contact
10.	Plate properties	
	Material	0.18mm DR620CA eccs
	Young's modulus result	201642 N/mm^2
	Poisson's ratio	0.3

The tool plan is shown in the model tooling image below, Model 3, Image 1, followed by an explanation of the end formation.

Model 3, Image 1: Overview of Tooling for East Open End Shell Model.



In the formation of the EO shell, the model starts after the blank has been cut. The press operation takes in around 0.060 seconds , during which time the punch and the punch centre move simultatneously, the punch compressing the blank against the draw ring, with material being drawn into the shell as the punch penetrates towards the die centre

pad. At the instant when the punch reaches bottom dead centre the knockout touches the plate at the draw ring. This point has been checked out a number of times, and it is a feature of the technology that the material is drawn between the punch and draw ring over the die centre ring and not involving another ironing force impinging at the die centre ring region. In this case the punch centre shown was a special one used with a reduced bottom outer radius to produce test samples for stress corrosion susceptibility tests by packing. This should represent a condition worse than normal manufacture.

3.7.3.4 Model Images and Stress Predictions.

The regions at which stresses have been recorded are identified by letter code in Model 3, Image 2, applicable to all results sets.

The images of the EO shell model for principal stress predictions in 'x', 'y' and 'z' directions are stated below:

Model 3, Image 2 : S11 stresses: X direction stress.

Model 3, Image 3 : S22 stresses: Y direction stress.

Model 3, Image 4: S33 stresses: Z direction or hoop stresses.

Model 3, Image 2 indicates the sites at which stresses were recorded.

Summaries of the predicted stress data are shown in Tables 87-90.

Energy plots are shown as Model 3, Image 5.

Model 3, Image 2 : EO Shell :0.18mm DR 620 CA Plate. Principal Stress S11, 'x' direction. Model after tool disengagement. Enlarged view of countersink region.

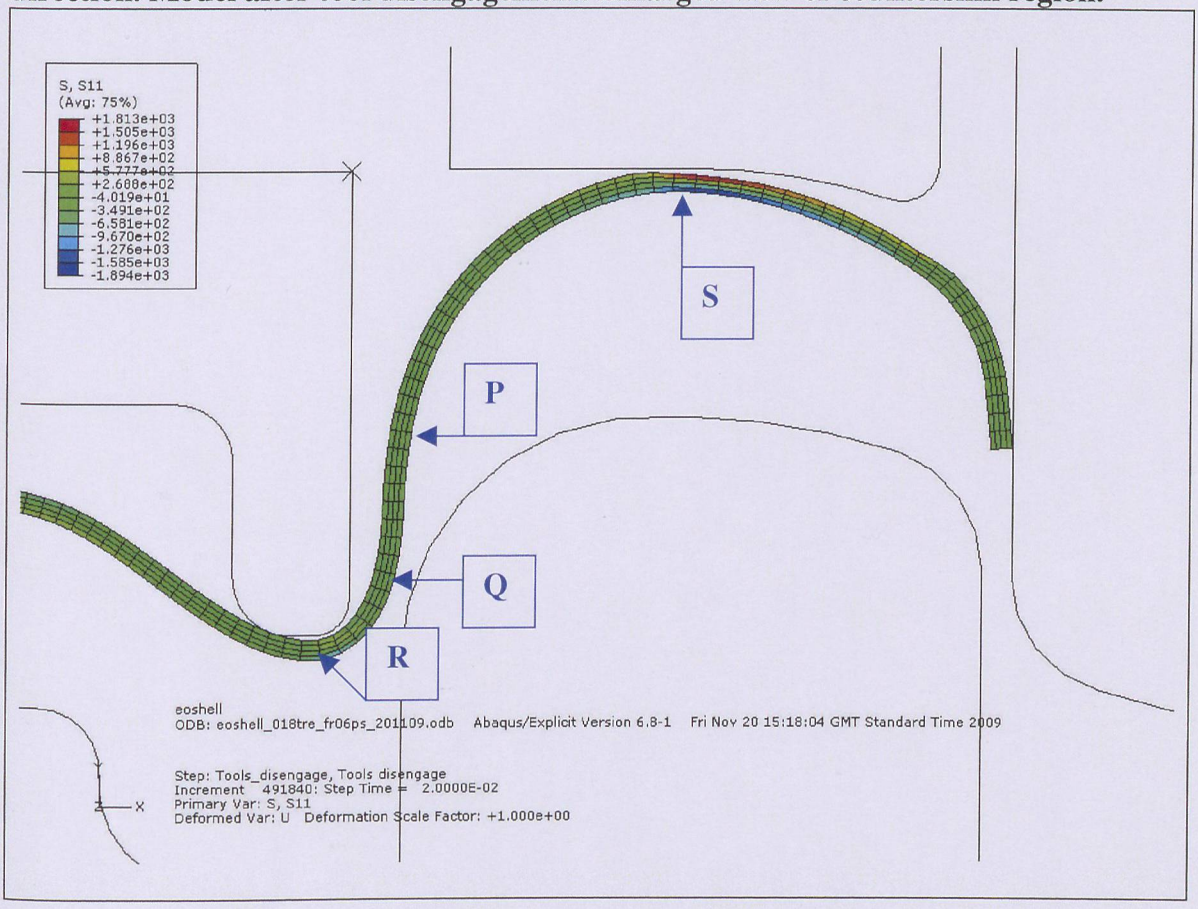


Table 87: Model 3, Image 2: Summary of S11 ('x' Direction) Stress Predictions:

Location	S11 Stresses: MPa
P. Countersink wall	-4.019 to + 268.8
Q. Countersink wall / radius	-4.019 to + 268.8
R. Countersink radius bottom	-967 to + 268.8
S. Top of countersink interior	-1894 to - 1585

+ve = tension , -ve = compression.

The table above indicates that some tensile stresses in the 'x' direction can occur at the countersink wall.

Model 3, Image 3: EO Shell : Principal Stress S22, ' y' direction : Model after tool disengagement. Enlarged view of countersink region.



Table 88: Model 3, Image 3: Summary of S22 ('y' direction) Stress Predictions:

Location	S22 Stresses: MPa
P. Countersink wall	+ 513.2 to + 732.6
Q. Countersink wall / radius	+ 583.6 to + 293.9
R. Countersink radius bottom	- 144.9 to - 293.9
S. Top of countersink interior	+ 952 to +1171

+ve = tension , -ve = compression.

'y' direction tensile stresses were predicted at the countersink wall region and the top of countersink interior.

Model 3, Image 4: EO Shell :Principal Stress S33: hoop direction, 'z'. Model after tool disengagement: Enlarged view of countersink region.



Table 89: Model 3, Image 4: Summary of S33 ('z' Direction) Stress Predictions:

Location	S33 Stresses: MPa
P. Countersink wall	+ 183.7 to + 556.3
Q. Countersink wall / radius	+ 556.3 to + 928.8
R. Countersink radius bottom	- 188.8 to - 183.7
S. Top of countersink interior	+ 556.3 to +928.1

+ve = tension , -ve = compression.

For the internal end surface, tensile hoop stresses were predicted at the countersink wall and countersink wall – bottom radius junction.

3.7.3.5 Summary Table Combining all Stress Predictions: Comments on Model 3.

The summary is shown in table 90.

Data are : Stress Predictions in Mpa: +ve = tension/ -ve = compression

Table 90: Summary Table Combining all Stress Predictions and Comments on Model 3.

Location	S11	S22	S33
P. Countersink wall	-4.019 to + 268.8	+ 513.2 to + 732.6	+ 183.7 to + 556.3
Q. Countersink wall /bottom radius region	-4.019 to + 268.8	+ 583.6 to + 293.9	+ 556.3 to + 928.8
R. Countersink radius bottom	-967 to + 268.8	- 144.9 to - 293.9	- 188.8 to -183.7
S. Top of seaming panel radius interior	-1894 to -1585	+ 952 to +1171	+ 556.3 to +928.1

From the model study the main observations have been as follows:

i) For the 'x' directon, S11, the stresses were either compressive, or where the range encompassed tension, the levels were well below the yield stress values for the plate.

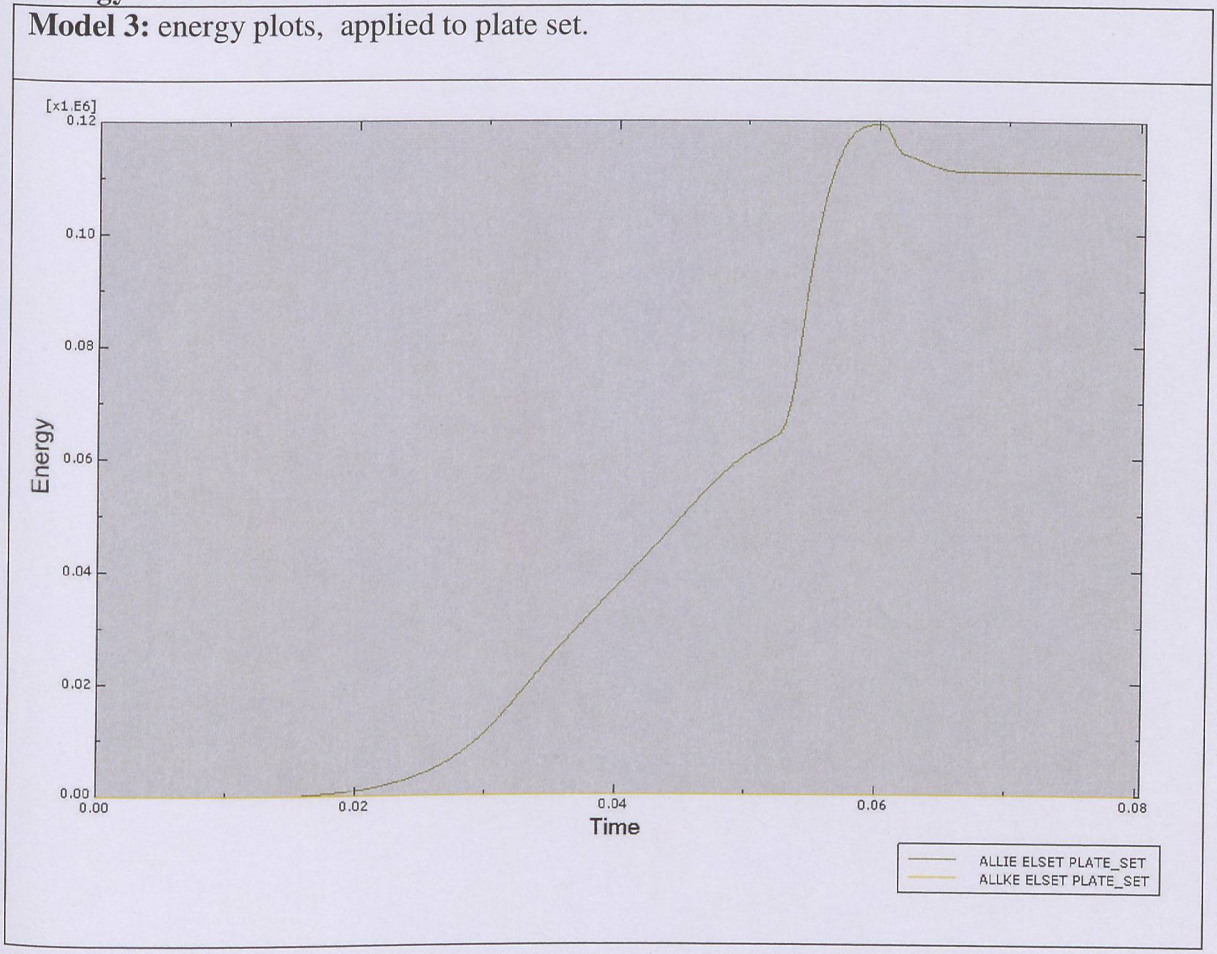
ii) For the 'y' direction , S22, the countersink wall showed tensile stress values ranging from below to above the yield stress, but at the countersink wall radius region, the effect became compressive at the bottom of the countersink radius.

iii) For the 'z' direction (hoop stress), S33, a predominance of tensile stresses was predicted including the countersink wall and the wall/ radius region.

iv) The upper region of the countersink corresponding to the point of impact of the knockout at the end of the press cycle, point S, has shown evidence of high tensile stresses at the interior for the S22 and S33 directions. For this region, there was particular sensitivity to the tool setting and timing and if as in this case, the knockout impacts too much and the top of the countersink, the stresses at this point and probably at the countersink wall would be increased

3.7.3.6 Total Internal Energy and Kinetic Energy Fraction Plots vs Time for Easy Open Shell Model, and Comments

Model 3 Image 2: Eo shell model: Plot of Total Internal Energy and Kinetic Energy vs Time for
Model 3: energy plots, applied to plate set.



The energy unit will be millijoules. The plot shows that the kinetic energy, yellow line ALLKE PLATE_SET was a very small fraction of the total internal energy, ALLIE, green line, empirically below 10%, so that the model should be acceptable from this standpoint.

3.8 Product Tests and Analyses.

3.8.1 Electrochemical Tests on Tuna and Salmon Brine Products.

The objectives of these tests were to characterise tuna and salmon brine behaviours, under the following conditions:

a) DC 'fast' and 'slow' sweep polarisation.

b) Pitting loops.

The dc fast and slow sweep tests constitute a method which has been used to determine susceptibility to environmental stress cracking under anodic conditions. During early work concerning Tuna Brine, Section 2, tests under both high air and low air (nitrogen flushing) conditions, had established that the Tuna Brine tested did not show any clear evidence of paassive conditions on the anodic sweep under slow sweep conditions. The pitting loops were a method of characterisation to compare pitting tendency, pitting being a precursor to many circumstances of environmental stress cracking failure. Tuna brine had shown a pitting tendency.

3.8.2 Experimental Details

a) 'Fast' and 'Slow' Sweep Polarisation

These tests were carried out on 1cm^2 samples of 0.18mm DR620CA electro chrome coated steel (eccs) material, using material as supplied, and also abraded using1200 grit, being placed in cells holding two electrodes of each type, one of each being subject to polarisation sweeps at 1000mV/min and the second at 10mV/min, the tests being repeated for high air conditions and

for low air by means of nitrogen flushing. The test material was from the same sample lot as was used for the slow strain rate tests on 0.18mm gauge DR620CA eccs steel material. The products used were thawed from the same deep frozen stock of pots as were used for the slow strain rate tests except that for this work the products were vacuum filtered before the tests to remove solid residues. The test cells were each held for 12 hours overnight before the tests commenced. All tests were preceded by checking the Open Circuit Voltage (OCV) for stability, which was typically within 5mv or less. An N/10 calomel reference electrode was used.

In the case of reduced air conditions, nitrogen flushing was performed through the liquid over at least 12 hours prior to the test at a minimum flow rate of $3cms^3$ / minute via a flow meter. The N/10 calomel reference electrode was then inserted into the cell and gas flushing continued for 2 hours at $15cm^3$ per minute through the liquid. During the test the flushing was changed to through the headspace and maintained at a minimum of $3cm^3$ per minute. To perform the polarisation sweeps the OCV was monitored for 1 minute followed by 600 seconds hold at –500mV vs N/10 calomel reference electrode, based upon refrence information consulted[16], the sweep then being started from this point through to 500mV noble of OCV. SEM and XRA examination was performed on the electrodes after testing. The results are summarised below.

b) Pitting Loops

Pitting loops were performed using further samples of the same product variables, with cell preparations and electrodes as used for the fast and slow sweep polarisation tests. A 4 x $1cm^2$ electrode cell was again used into which two 1200 grit abraded eccs electrodes we inserted together with two eccs electrodes. The material used was the 0.18mm DR620CA variable only. The sequence involving gas flushing with nitrogen for 12 hours, insertion of the reference electrode and

further gas flushing for 2 hours was repeated. The products were thawed from the same frozen bulk stock and vacuum filtered through Whatman type 54 filter paper prior to the tests. The tests were performed in steps as shown in the table 91 below:

Table 91: Pitting Loop Tests.

Step	Description
1.	Open Circuit Voltage (OCV) monitoring 1000 seconds vs N/10 calomel reference electrode
2.	Potentio-dynamic sweep from –250mv wrt OCV to + 1000mv at 0.4mv /sec(24mv/minute)
3.	Reverse potentio-dynamic sweep from +1000mv vs OCV to –500mv wrt OCV at 0.4mv / sec

Duplicate runs were made for each electrode type. Because of the very significant and more irregular noise behaviour on the abraded eccs electrodes, results are presented for the un-abraded eccs electrodes alone.

3.8.3 Discussion of Results

3.8.3.1 DC Fast and Slow Sweep Polarisation Curves General Observations.

Some rather noisy current behaviours have occurred, especially in the slow sweep polarisation tests with both products, this being more prevalent on the abraded eccs material than for eccs material tested as received. Complex food media containing amino acids would be expected to show adsorption behaviours on account of either a the residual positive charge on the nitrogen atom, or due to the COO^- group bearing a residual negative charge on the oxygen atom. Most current noise in the tests was observed on the cathodic side of the open circuit potential, but some extended to the anodic side. A further phenomenon of the results was the negative potential shift related

to OCV in several instances for the fast sweeps, relative to the observation that initial OCV values for fast and slow sweep samples showed predominantly good agreement. The main observations which were made are summarised below for eccs samples. The levels of noise on the abraded steel samples were generally far to high to permit detailed consideration and these plots have not been included.

3.8.3.2 DC polarisation Plots for Salmon Brine Tested under Air Conditions and Nitrogen Flushing Conditions : See Figures 80 and 81.

The results in Figure 80 showed that under slow sweep conditions a degree of arrest occurred in the anodic curve at intermediate over-potentials, but the comparison of currents between the two curves at this region was just within one order of magnitude.

Figure 80: Salmon Brine : Air Conditions: Fast and Slow Sweep DC polarisation curves for 0.18mm DR620CA eccs material.

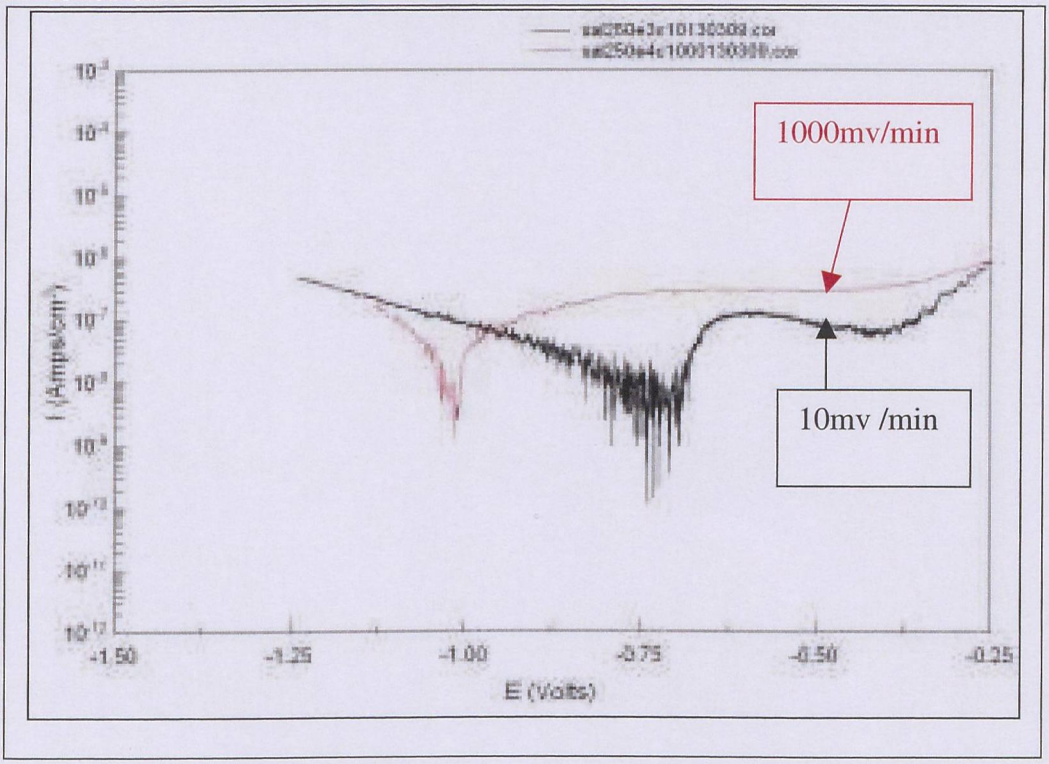
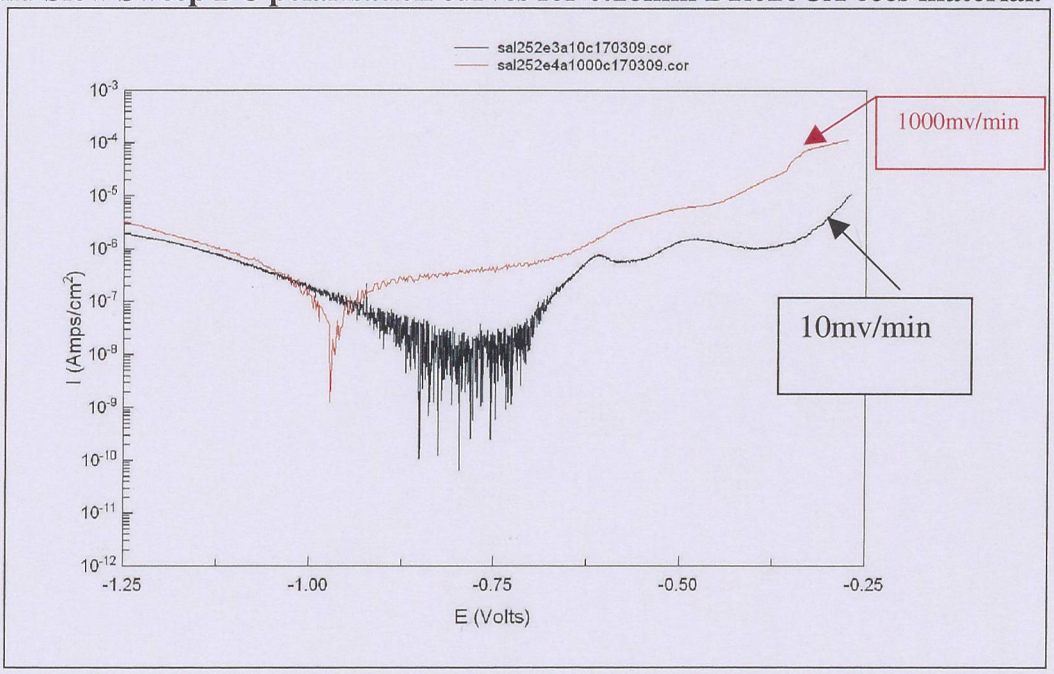


Figure 81: Salmon Brine: Reduced Air Conditions: (nitrogen flushed cell). Fast and Slow Sweep DC polarisation curves for 0.18mm DR620CA eccs material.



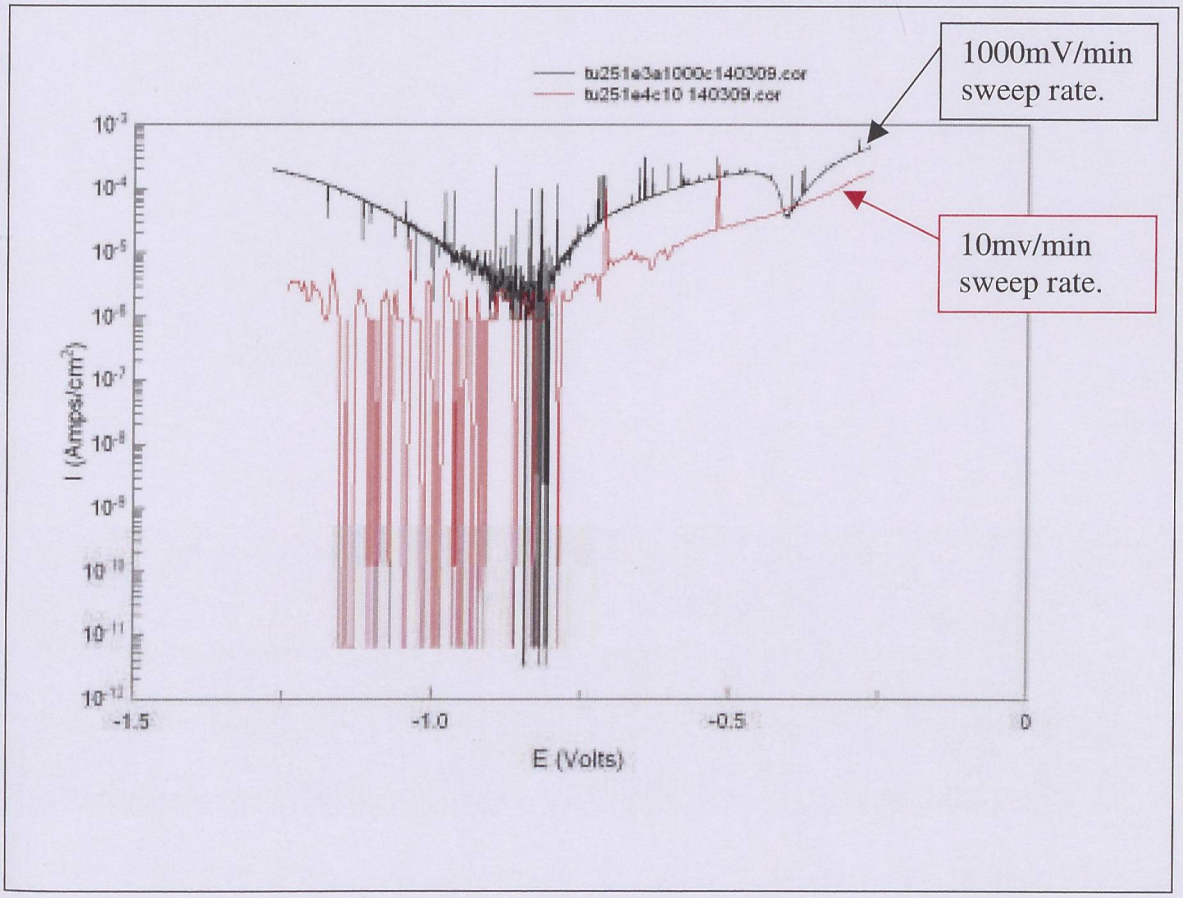
The reduced air condition plots, Figure 81, again showed degrees of arrest behaviour on the anodic slow sweep curves. The anodic current difference between the two plots at the arrest regions was again within one order of magnitude for the arrest at intermediate over-potential, and was slightly more that one order at higher over-potential. The increased anodic currents relative to high air conditions may indicate less film formation under anodic conditions allowing faster attack in salt media.

3.8.3.3 DC polarisation Plots for Tuna Brine Tested under Air Conditions and Nitrogen Flushing Condition: See Figures 82 and 83.

Under air conditions, Figure 82, the tuna brine has given higher anodic currents than salmon, (Tuna had a greater chloride level), with a high degree of current noise in the cathodic region on the slow sweep curve. There was a current 'arrest' behaviour on the

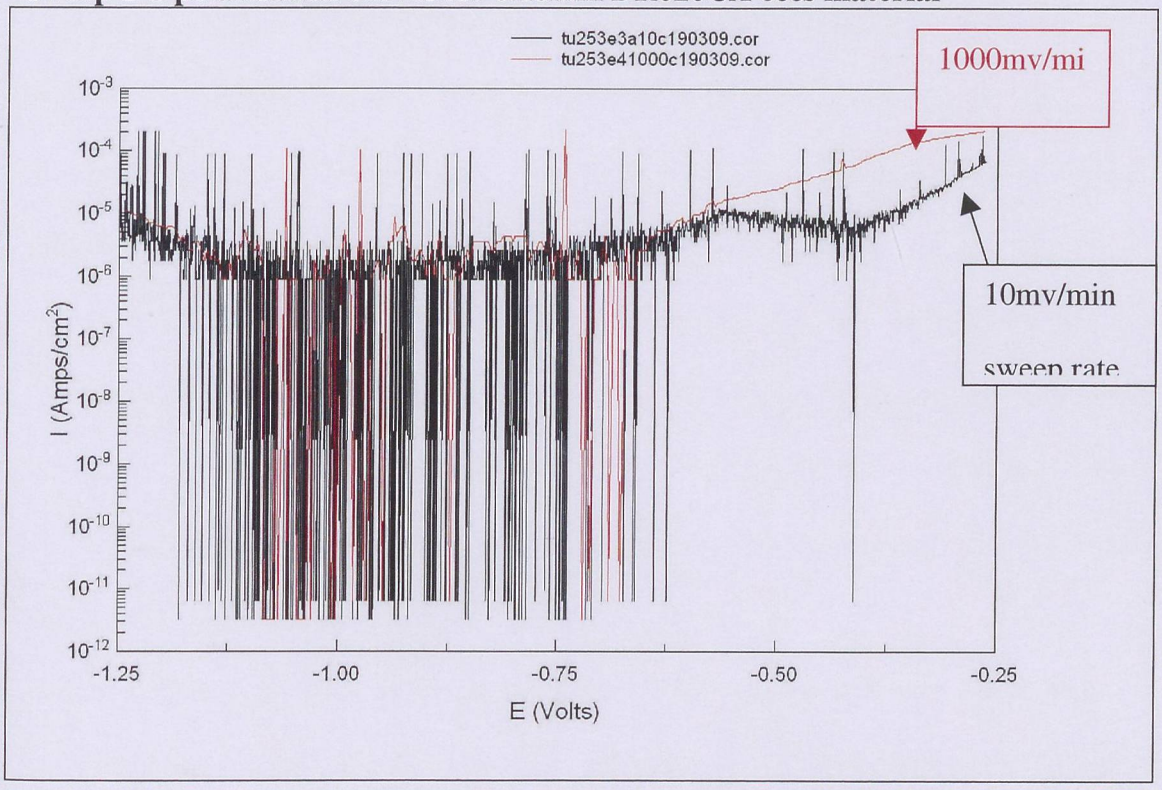
fast sweep plot at high anodic over-potential. The anodic current difference between the two plots was within one order of magnitude.

Figure 82: Tuna Brine : Air Conditions: Fast and Slow Sweep DC polarisation curves for 0.18mm DR620CA eccs material.



Under low air conditions, Figure 83, the Tuna Brine samples have produced very noisy polarisation plots and interpretation is not very practicable beyond noting that the difference in current between fast and slow sweeps reached about one order of magnitude, and at high over-potential (> - 600mV) with a degree of arrest behaviour present on the slow sweep plot.

Figure 83: Tuna Brine Tested Under Nitrogen flushing conditions. Fast and Slow Sweep DC polarisation curves for 0.18mm DR620CA eccs material



The above plots for Salmon and Tuna have not shown any pronounced arrest behaviour of the anodic slow sweep curves and while further work may be worthwhile to examine risk behaviour under anodic conditions, the evidence above was not thought to not provide strong or conclusive indications of active /passive conditions on the anodic curves.

3.8.3.4 Pitting Loops for Salmon and Tuna Brines Tested under Air Conditions and Nitrogen Flushing Condition:

Figures 84-85 show the plots for salmon brine tested on eccs for high air and reduced air conditions. These pitting loops showed active corrosion behaviour of the anodic curve with positive hysteresis which was an indicator of pitting behaviour, there being

no evidence of passivity or re-passivation on the return loop segment before the current noise region close to the rest potential. The outward anodic sweep displayed some arrest behaviour on both low and high air samples, but little difference was apparent in currents between the respective plots. Given the presence of an eccs coating with limited exposure of steel, the difference between high and low air behaviour in a short term test may not be unexpected.

The pattern of behaviour for the Tuna product, Figures 86-87, was quite similar to that for salmon in terms of the general form of the plots, again showing positive hysteresis in the anodic curves and noise bands similar to those for salmon product. However, there was some inconsistency between the two plots for tuna brine under low air conditions, and there was less arrest behaviour on the anodic curves.

In conjunction with behaviour observed in the fast and slow sweep tests, sufficient evidence has emerged to suggest that the current noise behaviour was not an artefact of the manner of execution of the test, but a real effect likely to be attributable to adsorption behaviours within the products. While the greater effect was on the cathodic side of the Open Circuit Voltage, there were degrees of effect on the anodic side.

Figure 84: Salmon Brine : Air Conditions: DC Polarisation Pitting Loop Curves for 0.18mm DR620CA eccs material. Duplicate runs.

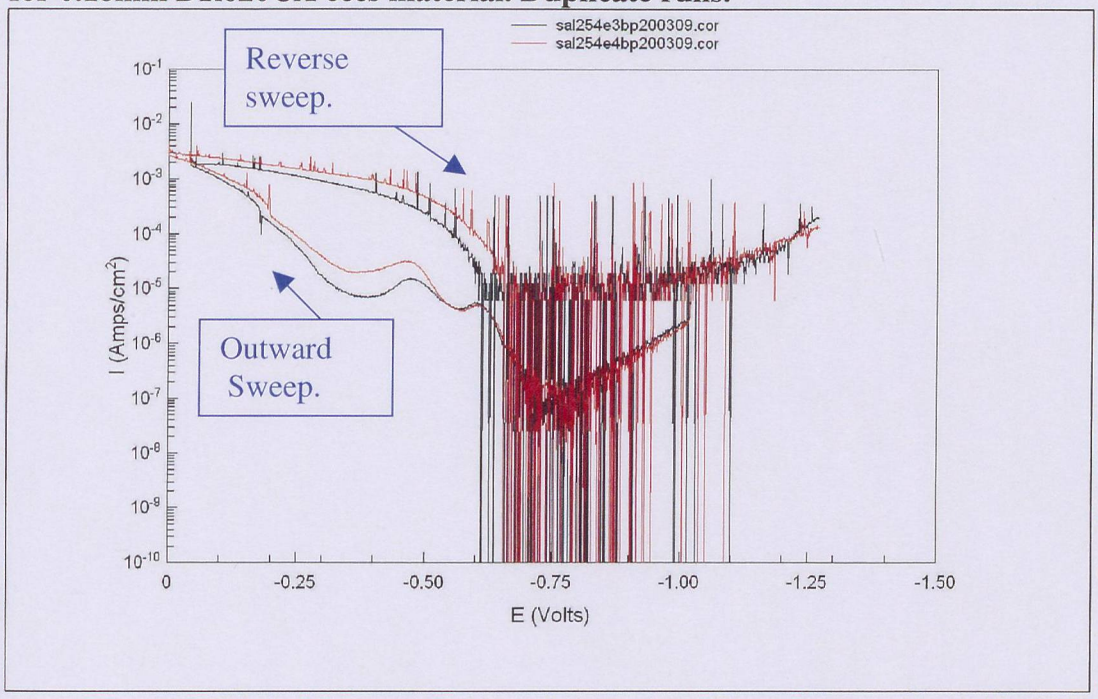


Figure 85: Salmon Brine : Nitrogen flush Conditions: DC Polarisation Pitting Loop Curves for 0.18mm DR620CA eccs material. Duplicate runs.

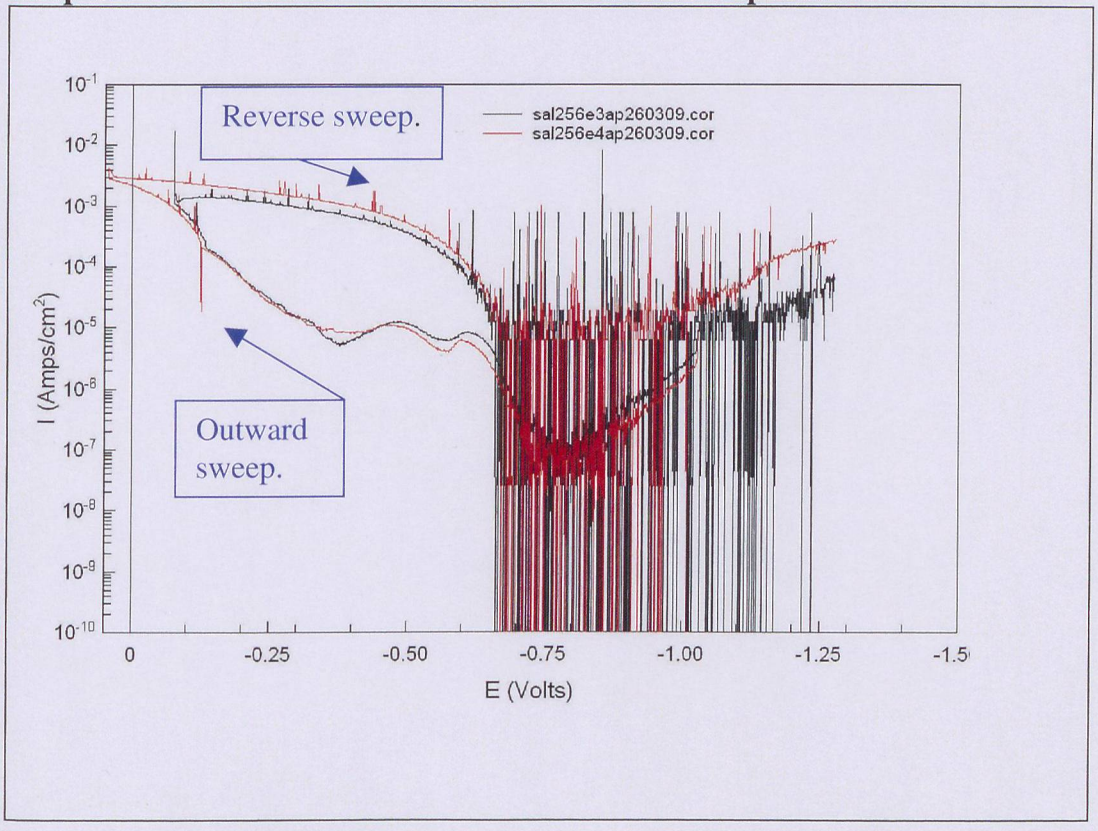


Figure 86: Tuna Brine : Air Conditions: DC Polarisation Pitting Loop Curves for 0.18mm DR620CA eccs material. Duplicate runs.

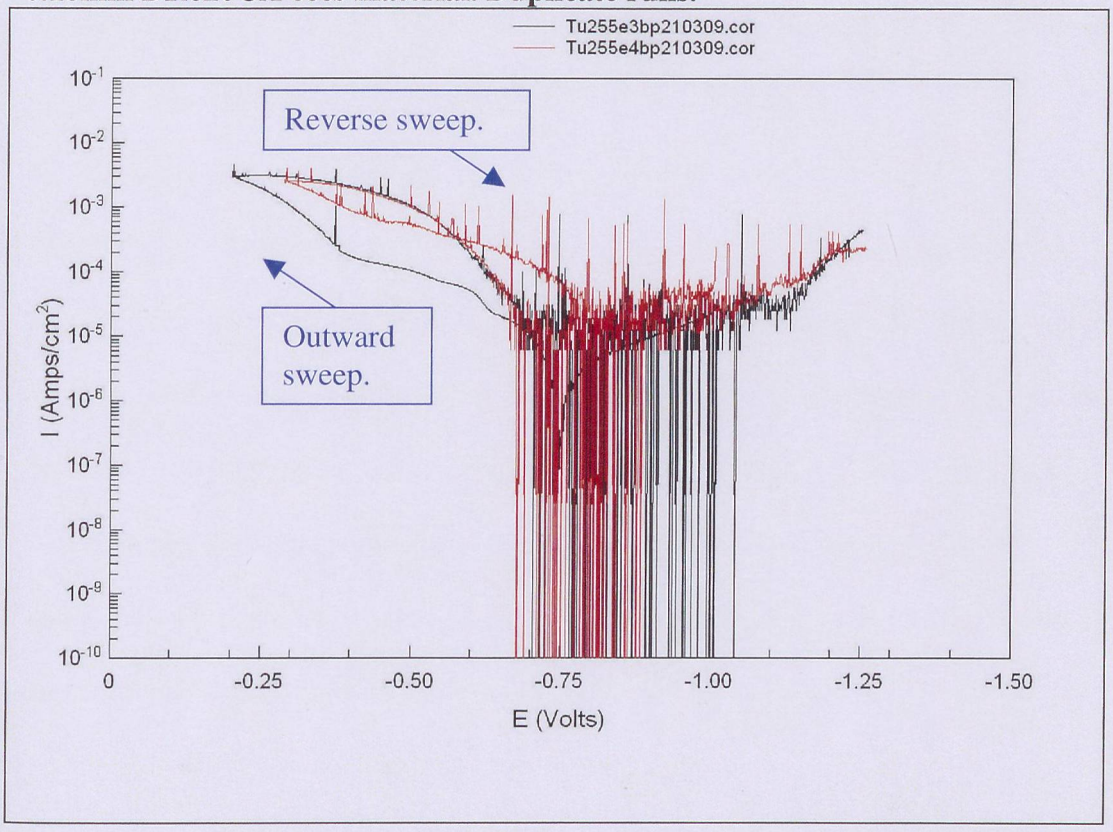
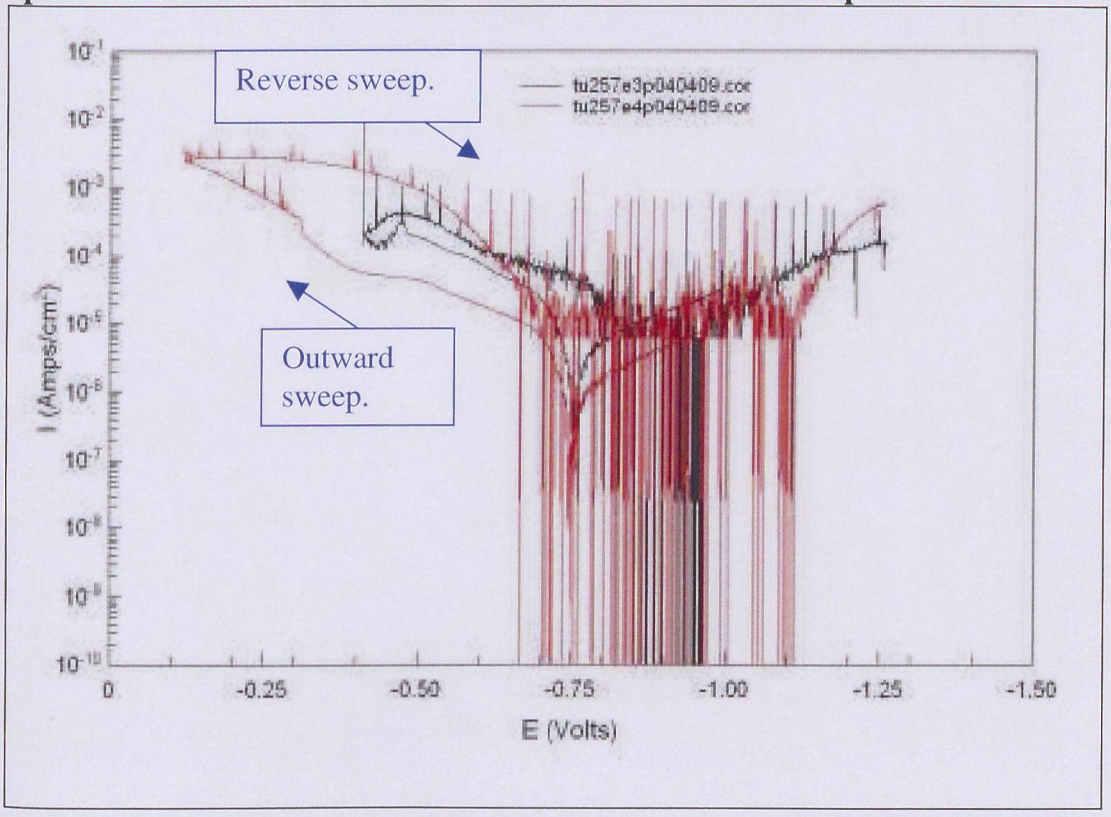


Figure 87: Tuna Brine : Nitrogen Flush Conditions: Fast and Slow Sweep DC polarisation curves for 0.18mm DR620CA eccs material. Duplicate runs.



3.8.4 Observations from XRA Studies using SEM equipment on Electrodes from Electrochemical tests in Salmon and Tuna Brines :

3.8.4.1 Electrodes from Slow Sweep Polarisation Tests.

The initial XRA examinations were made on one sample each of abraded eccs and non abraded eccs electrodes which had been subject to the slow sweep dc polarisation tests at 10mv/ minute in salmon and tuna brines respectively under low air conditions, as described above, finishing on the anodic side of open circuit voltage. These variables would be closer to that involving can conditions than samples tested under air conditions. The samples had been rinsed with distilled water after the tests. A list of observations of elements identified in Table 92 below:

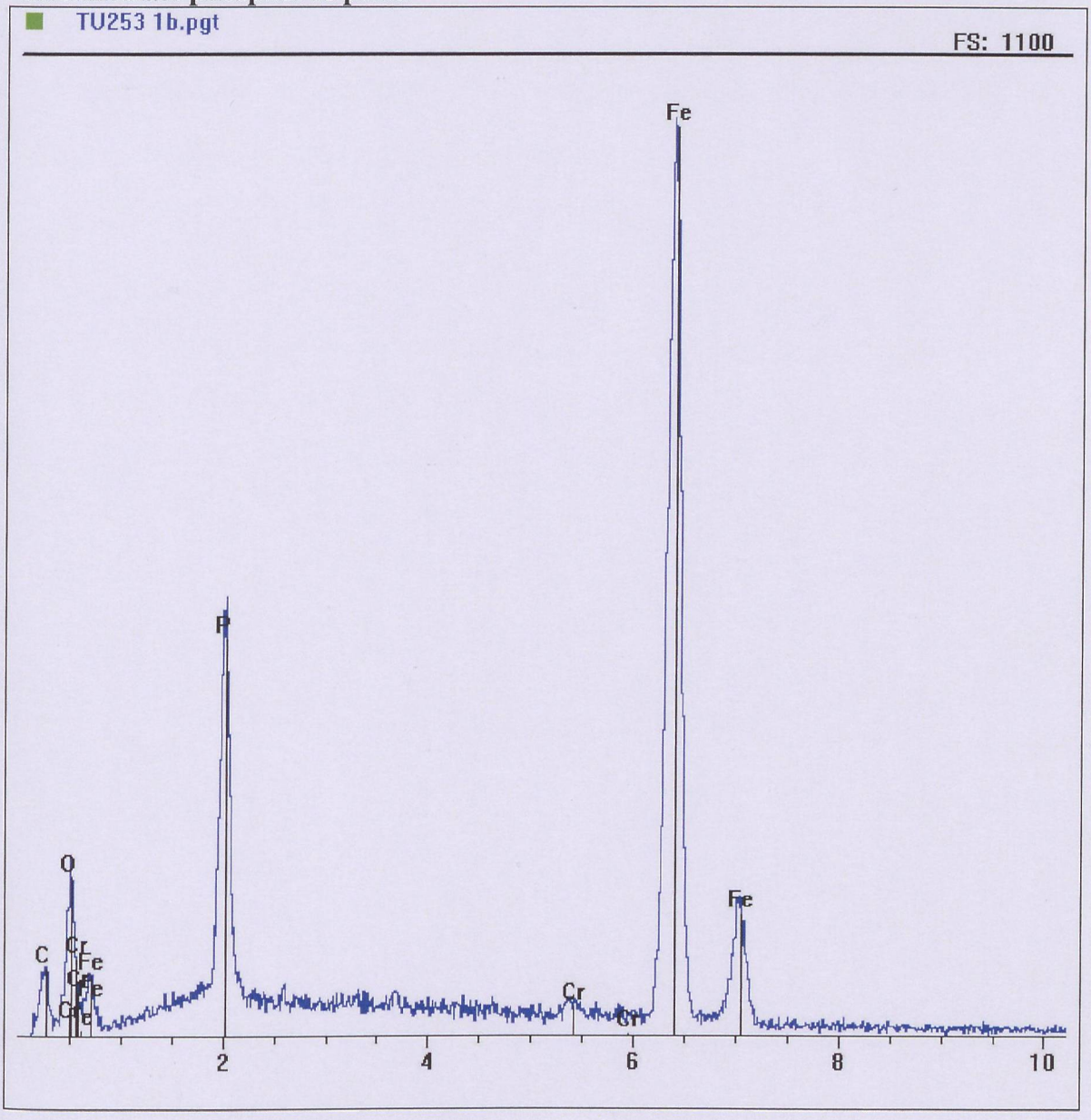
Table 92: List of observations of elements identified

Item	Sample	Scan	Major peak	Minor Peak	Trace
1.	Salmon 252. N_2 flush	Electrode1 abraded eccs/ scan 1r	Fe.	Cr, P, O, C.	
2.	Salmon 252, N_2 flush	Electrode 3, eccs/ scan 3r	Fe.	Cr, C	-
3.	Salmon 252, N_2 flush	Electrode 3, eccs/ scan 3r2	Fe.	Cr,	-
4.	Tuna 253, N_2 flush	Electrode 1, abraded eccs scan 1b	Fe, Intermediate peak: P	Cr, O, C	-
5.	Tuna 253, N_2 flush	Electrode 1, abraded eccs scan 1b2	Fe.	Cr, P, O	C
6.	Tuna 253, N_2 flush	Electrode 3, eccs/ scan 3b.	Fe	Cr	-
7.	Tuna 253, N_2 flush	Electrode 3, eccs/ scan 3b2.	Fe	Cr	-

A major peak was taken as one showing over 50% of the full scale deflection for counts. An intermediate peak would be one exceeding one third of full scale deflection. Iron was a consistent observation in this respect, which would be expected. It was apparent that the observation of phosphorus for either product was only made on the abraded samples. In addition to iron, identification of Chromium would be likely from the surface coating or from the steel. Carbon and Oxygen have been observed in some

cases; carbon could be associated with steel or product, but was more likely to be associated with product where the observation was more than a trace. Oxygen would arise from corrosion of the steel surface, or possibly product residues e.g. phosphate or amino acid residues. Sulphur detection might be a less likely observation after anodic polarisation. Some residues may have been removed by rinsing with distilled water. Scan 1b from item 4 showing the high phosphorus peak is reproduced in Figure 88 below.

Figure 88: Tuna Brine: Cell 253: Electrode 1: abraded eccs , Scan 1b, showing intermediate phosphorus peak.



3.8.4.2 XRA Observations on Electrodes from Pitting Loop Tests.

XRA observations were made on samples subject to pitting loop tests in a similar manner to those for fast and slow sweep polarisation tests. The pitting loop tests concluded on the cathodic side of the Open Circuit Voltage, and again had all been carried out on the 0.18mm DR 620 CA steel. These samples were examined to include both high and low air conditions. Again a major peak was taken as at least 50% of full scale defection, and an intermediate peak as over one third of full scale deflection. The observations are summarised in the table 93 below:

Table 93: XRA Observations on Electrodes from Pitting Loop Tests.

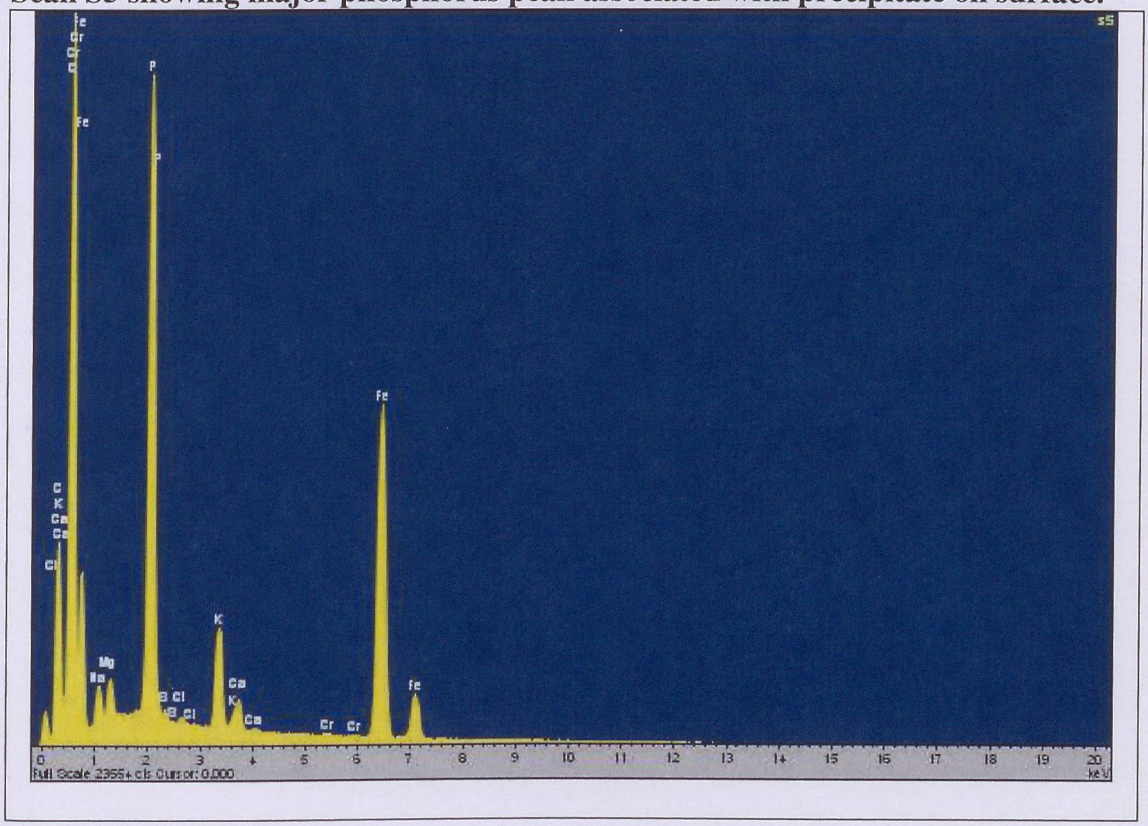
Item	Sample/ cell number.	Sample:	Scan number	Major peak	Intermediate peak	Minor Peak	Trace
1.	Salmon 254. air conditions	abraded eccs surface precipitate	s1 s2 s2b	Fe Fe Fe, P	Fe, O, Cr, F Fe, P Fe	- K, Cl, Na, F K, Cl, Na	Cr, K, Cl, P, Na,S. S, Ca
2.	Salmon 254, air conditions	Eccs precipitate/ surf precipitate	s3 s4 s5	Fe Fe. P, Fe, Cr, O	Fe Fe, Cr Fe, Ca, Cl, K, C.	Fe, Cr, C. Fe, Cr, P,O,K,C Fe ,K, Cl, Na, Mg, Ca	Cr ,P K, Na Cr, Cl,S
3.	Salmon 256, N_2 flush	abraded eccs precipitate	s11 s12	Fe Fe,Cr, O	- -	Fe, Cr, P,O,C Fe, P, Mg ,C	Cr Cr
4.	Salmon 256, N_2 flush	Eccs white deposit	s13 s14	Fe Fe	Fe, Fe, Cr, O	Fe, Cr, C. Fe, Cr, K, P,C	Cr K,Na
5.	Tuna 255 air conditions	abraded eccs deposit white deposit	s6 s7 s8	Fe Fe Fe	Fe, Cr,O Fe,Cr,O Fe,Cr, O	Cr , C Fe, Cr, C , Fe, Cr, C,	Cr,S Cr Cr
6.	Tuna 255, air conditions	Eccs surface pit	s9 s10	Fe Fe	Fe -	Fe, Cr ,P,O,C Fe, Cr, P,O,C	- Al
7.	Tuna 257, N_2 flush	Abraded eccs precipitate. small deposit	s15 s16 s17	Fe Fe,O Fe	Fe Fe,P, -	Fe, S, O,C. Fe, Ca, Mg, C. Fe, Ca, P,C	- - -
8.	Tuna 257, N_2 flush	Eccs pit	s18 s19	Fe Fe	Fe. -	Fe, Cr. Fe, Cr, P, Al, O,C.	C -

The results of these XRA analyses showed the following main points:

1. Apart from iron, the observation of chromium is expected for eccs and may also be observed for abraded eccs given that some chromium is present in the steels. Chromium was observed in most scans for both products.

2. Phosphorus has been a frequent observation common to both products, present in one or more scans for all salmon electrodes and for three out of four tuna electrodes, thus including high and low air conditions, and with some major peaks on salmon samples accompanying high air conditions and surface deposits or precipitates. The scan S5 (sample 254) associated with a surface precipitate is shown in Figure 89 below.

Figure 89: Cell 254: Salmon brine: Air condition pitting test sample eccs electrode. Scan S5 showing major phosphorus peak associated with precipitate on surface.



Examples of surface pitting and deposits are recorded below for one sample each tested in Salmon and Tuna brines, Figure 90-91 which had been subject to pitting

loop tests under air conditions. The much greater level of deposits on the salmon sample was apparent.

Figure 90: Salmon sample 254 , air conditions test , showing precipitations found to be phosphorus rich.

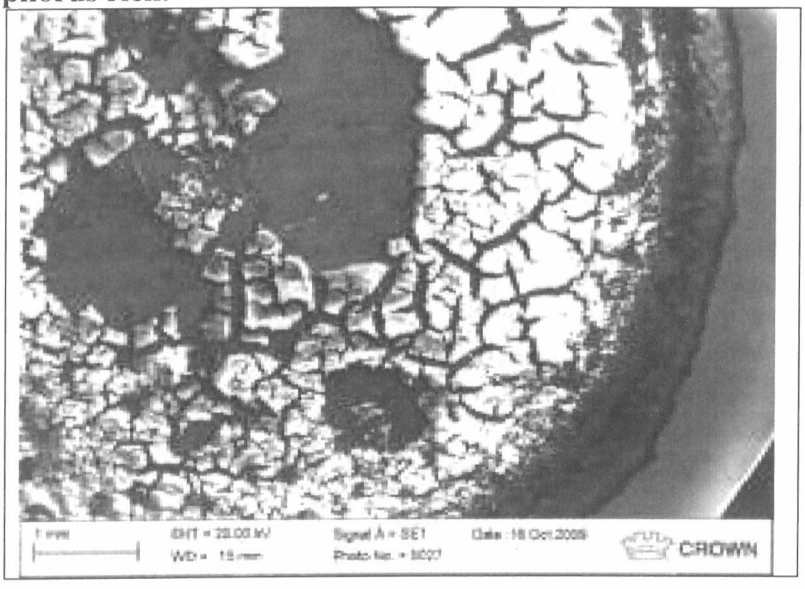
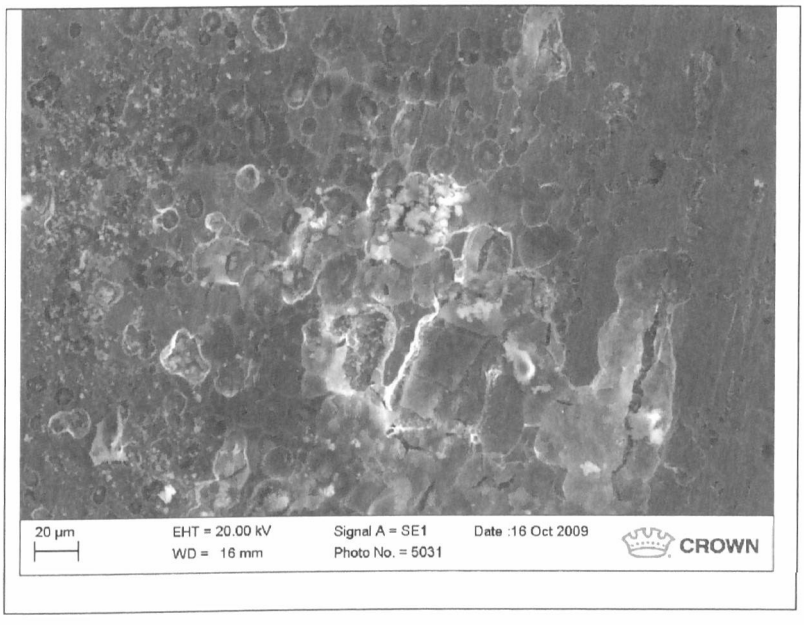


Figure 91: Tuna sample 255, air conditions test, showing corroded and pitted surface.



3. In the case of salmon product, sodium potassium and magnesium were observed for high and low air conditions, these being constituents of product or water forming the brine content. Calcium was observed for air conditions, again likely from product residue, being a constituent of bone and of some soluble salts in

aqueous media. For tuna, calcium and magnesium were detected for low air conditions only with likely sources as for salmon product.

4. Sulphur was an occasional observation for both products, for high air conditions with salmon and both aeration conditions with tuna. Sulphur derives from product proteins such as cystine or methionine and when present as HS- ions is considered for act as a catalytic re-combination poison for hydrogen. No identification of arsenic, antimony, bismuth or selenium was made in these tests, these also being catalytic recombination poisons for hydrogen.
5. Fluorine has been an occasional observation requiring follow up in the context of the product. Carbon and Oxygen may be from product, or in the case of carbon, low levels in steel. Oxygen can be part of corrosion products e.g. rust or an iron phosphate formed at a surface or pit.
6. Aluminium has been an occasional observation for Tuna brine product.

In the context of environmental stress cracking behaviour, phosphorus as phosphate has been linked to observations of loss of ductility of steels[15] at low anodic over potentials, and Evans identified phosphorus as a hydrogen ingress promoter for steel. Sulphur may be critical, depending on the constituent compound or ion regarding hydrogen ingress for steel.

3.8.5 Chemical Analyses of Product Brines for Anions and Cations.

The analysis of salmon and tuna products for anions and cations as drained brines was subcontracted to Chipping Campden Food Research Association. Two pots each from the frozen bulk were analysed. The laboratories are UKAS accredited. The data is recorded in Table 94 below.

Data in mg per litre

Table 94: Chemical Analyses of Product Brines for Anions and Cations

Element or Anion	Tuna Pot 130	Tuna Pot 144	Reference Values*	Salmon Pot 208	Salmon Pot 243	Reference Values*
Anions						
Chloride	11900	12100	5500	7300	7400	7300
Nitrate	<10	<10	-	<10	<10	-
Phosphate	4300	4400	-	5800	5900	-
Sulphate	145	150	-	80	80	-
Cations						
Arsenic	0.78	0.78	-	0.23	0.19	-
Antimony	<0.01	<0.01	-	<0.01	<0.01	-
Bismuth	<0.01	<0.01	-	<0.01	<0.01	-
Calcium	119	114	80	44	41	910
Copper	0.15	0.12	0.5	0.05	0.05	0.5
Iron	91	92	10	0.60	0.51	6
Magnesium	355	360	270	210	225	250
Manganese	0.26	0.26	Tr	0.01	0.01	
Potassium	2310	2330	2300	4020	4050	2600
Selenium	0.13	0.14	0.78	0.04	0.04	
Sodium	9460	9540	3200	4350	4460	4300
Zinc	0.98	0.89	7	0.31	0.29	8
Phosphorus	1580	1600	1700	2030	2050	1700
pH	5.97	5.98		6.30	6.37	

* Reference values were taken from 'The Composition of Foods', by McCance and Widdowson [32]. The values are guidelines from commercial product analyses.

The analyses showed that for each product a substantial measure of consistency was observed between data for two different pots chosen at random from the original bulk make up lots. This would indicate that the test work is likely to have been valid for comparisons across the range of the three eccs plate materials tested with each product involving many sample pots. The tuna product was much older than salmon regarding best before dates of the products in the original tins. Hence it may not be surprising that the iron content was high for tuna.

In terms of aspects of the data which may be relevant to an occurrence of environmental stress cracking or a form of hydrogen cracking, the following observations were made:

i) There was no significant level of nitrate present in either product.

ii) Phosphate anion level was higher for salmon product than tuna by an average of 1500mg/litre or around 34.5%. Phosphate has been a associated with loss of ductility of stressed steel at low anodic overpotentials[15],[16].

iii) Greater amounts of chloride and also sulphate were present in tuna product, and these species promote pitting which is a common precursor to cases of environmental stress cracking. The elements which have been cited as catalytic poisons in the context of the hydrogen recombination reaction are arsenic, antimony, bismuth and selenium[33]. Zinc[33] was also reported to assist hydrogen entry into steel. Of the catalytic poisons, there were no significant levels detected for antimony and bismuth. Small amounts of arsenic and selenium were found in both products, but were higher in the tuna product. Zinc was present in both products as a minor constituent.

iv) Copper was higher in tuna than salmon, and it is known to chemically bind sulphur and phosphorus when used in steels. In the context of product behaviour in steel cans, it can aid pitting by galvanic action if it plates out on steel.

v) Manganese was higher for tuna, but no significance has been attributed, unless by binding of sulphur in which case the influence is likely to be negative.

vi) pH was confirmed as higher on salmon by between 0.3 and 0.4 units, so that in the context of hydrogen generation, the salmon product requires increased electrochemical action to attain a local pH below around 5.7, cited in literature as an important threshold.

vii) Phosphorus was determined as around 28% higher for salmon . Further study is necessary to understand the precise significance of this data in comparison with the anion value.

Calcium magnesium and sodium were all higher for tuna, but potassium was higher for salmon with no significance known at this stage, related to the type of failure in question.

3.8.6 Headspace Gas Analysis Data from Tuna and Salmon Can Stock used to Provide Product Brine Bulks.

Three cans of each product were examined by the Crown Technology Analytical Laboratory and the results obtained are shown in Table 95 below.

Table 95: Headspace Gas Analysis Data

Sample	Volume of gas collected (mls).	% of each gas collected				Sum of %
		O2	N2	CO2	H2	
Tuna 1	43	0.35	65.1	2.4	32.2	100
Tuna 2	47	0.81	59.9	2.3	37.0	100
Tuna 3	50	0.24	64.6	2.4	32.8	100
Salmon 1	22	0.26	89.6	8.8	1.4	100
Salmon 2	22	0.18	90.1	8.5	1.2	100
Salmon 3	22	0.23	85.3	12.7	1.8	100

From this data it was apparent that for both products, a significant level of hydrogen was generated in the packs of each type during storage. In the case of the tuna packs, by the time of the measurement these were well past the 'best before date' and the proportion of hydrogen was high, and much larger than for salmon in brine. The salmon product has recorded a higher CO_2 level. Earlier comment on this subject[19] indicated that for CO_2 to be contributory, high pressures e.g. 2.5Kg/cm^2 as well as synergistic behaviour with water and CO were necessary, as opposed to typical vacuum conditions in cans.

3.8.7 Steel Analyses for 0.16mm , 0.18mm and 0.235mm Gauge DR620CA eccs Plates used in Slow Strain Rate Test Programme.

This was subcontracted to Minton, Treharn and Davies, Cardiff, who are a UKAS accredited laboratory.

The analysis was performed on each of the steel types used in Slow Strain Rate Testing and the results are shown on Appendix 6. All steels were found to conform to compositional requirements for respective eccs steel types which were;

0.16mm DR 620 CA: drawing quality steel.

0.18mm DR 620 CA: stamping quality steel.

0.235mm Dr 620CA: stamping quality nitrogenised steel.

Packaging steels have very low levels of residual elements to help ensure optimum corrosion resistance to a wide range of environments, and are commonly of an Al killed continuously cast type.

3.8.8 Microstructural Characterisation of Steels Used in Slow Strain Rate Test Programme, and Comments.

Several Strips of each material were cut parallel to the grain direction, mounted in bakelite, diamond polished and etched in 2% nitric acid in methanol. The micro-structure was examined with observations recorded below, followed by typical fields for each material.

a) The low carbon 0.16mm steel, Figure 92, had a comparatively larger grain size and lower level of precipitated carbides than the other two materials. A proportion of grains tended to be less angular to a degree, relative to the other materials, which is expected to aid ductility. However the material as a whole showed a high degree of variability in grain size.

b) The 0.18mm DR620CA stamping quality steel, Figure 93, showed a significant level of precipitates which would be mainly carbides in addition to a finer grain size than the 0.16mm drawing steel. Again there was high local variability in grain size and the larger grains were less angular.

c) The 0.235mm nitrogenised steel, Figure 94, showed the highest level of density of precipitates parallel to the grain, and predominantly the most angular grain shape among the three types examined, and again finer grain size than the 0.16mm drawing quality steel.

   Nitrogen is an interstitial element in steel, but can also give rise to precipitation of nitrides.

Figure 92: 0.16mm DR 620Continuously annealed eccs steel. This material was a low carbon material suitable for fabricating into Drawn Redrawn Cans.

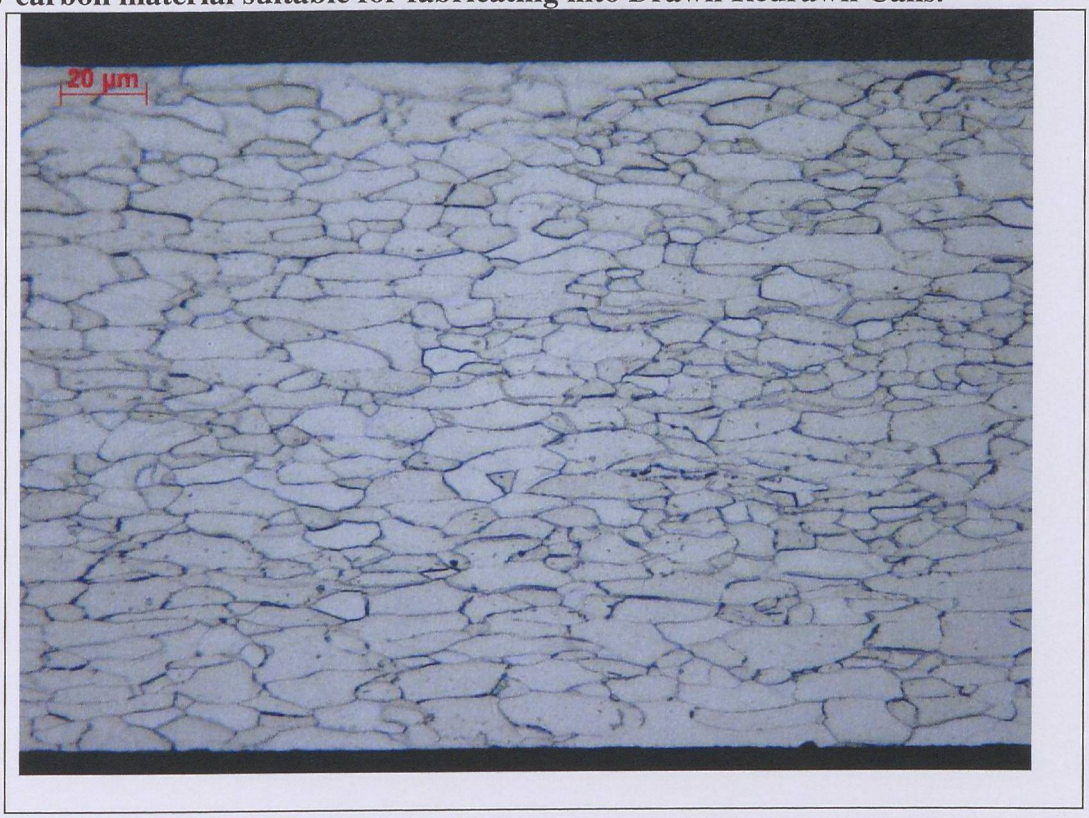
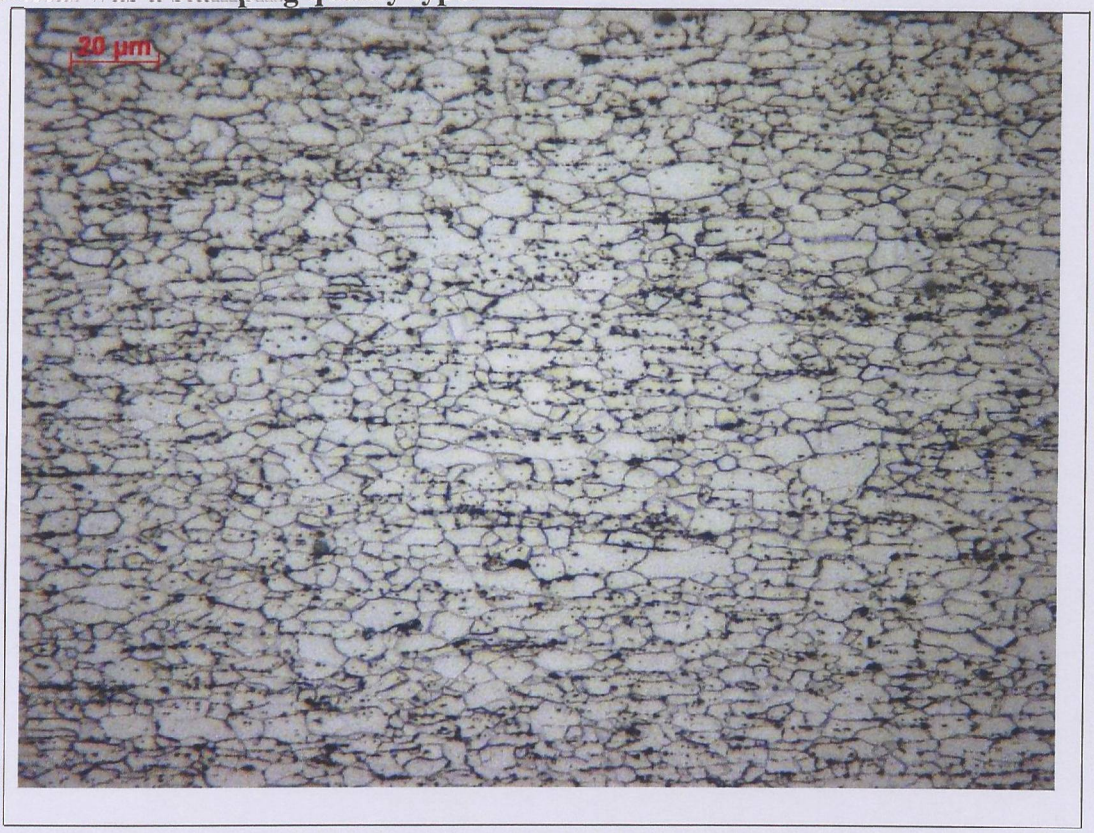


Figure 93: 0.18mm DR 620Continuously annealed eccs steel. This material was a stamping quality type.



Figure 94: 0.235mm DR 620 Continuously Annealed Nitrogenised eccs steel. This material was a stamping quality type.



From the microstructure a major distinction existed between the larger grain drawing 0.16mm steel with low precipitation of carbides, and the other two steels. The 0.235mm nitrogenised steel has shown similar or slightly finer grain size than the 0.18mm steel nitrogenised, with more precipitation than for the latter.

The Erichsen cupping data indicated that while the differences in compositions and structures between the 0.16mm drawing steel and the other two materials are designed to confer drawing ability at the very low gauge of the former, the higher gauge 0.18mm and 0.235mm steels still showed a higher a measure of overall ductility using this drawing test, although the tensile elongation properties measured parallel to the grain were lowest for the 0.235mm sample, based on individual results on Plot 33.

3.9 Discussion of Investigations

3.9.1 The Development of Cracking and Failure: Initial Observations on Corrosion Behaviour.

During early work it was observed that some propensity for loss of ductility and small degrees of suspected environmental stress cracking could be detected following slow strain rate testing at the Open Circuit Voltage, using either tuna brine product or tuna brine acidified by addition of either hydrochloric or acetic acid. It is not thought that the distinction in behaviours between acids based upon limited observations was sufficient to say that one was clearly more effective than the other in producing low ductility or environmental stress cracking effects.

In this work, Section 2, DC polarisation tests showed that both tuna brine product would be expected to give rise to pitting, but there was no very distinctive behaviour during anodic polarisation to show that a pre-disposition to active- passive conditions (unstable passivity) would be highly likely. However, there were some arrests in the slow sweep curves at intermediate and high overpotentials, and more investigation would be needed to indicate the true behaviour of these regions under tensile stress conditions. Later electrochemical testing in Section 3 on both Tuna and Salmon brines using the same methods as before, confirmed similar trends in both product brines showing pitting tendencies. Again, some 'arrest' behaviour was observed on anodic sweeps for high or low air conditions with each product, but without clear evidence of active / passive conditions being likely.

Based upon the observations from initial work, giving indications of a likelihood of a hydrogen related mechanism leading to loss of ductility, the main experimental study has concerned characterisation of behaviour of tuna and salmon products under slow

strain rate test conditions. The tests were conducted at a fixed potential, corresponding to the Open Circuit Voltage, as determined at the start of the test.

It was shown by analysis of filled cans from the same lot used in this study, that hydrogen gas was generated by both tuna and salmon brine products in steel cans over time.

The test potential having been fixed, when the slow strain rate test commences, according to local conditions existing at points on the surface of the metal due to e.g. local surface heterogeneities, local film differences, or concentration gradients of species such as dissolved oxygen, the resulting effect can be the generation of electrochemical cells and the onset of corrosive action. If the entire specimen was at the true open circuit voltage, and no local potential variations could occur, then no attack would be expected, as no net current flows to or from the electrode at the open circuit voltage. The potentiostat showed a finite potential distribution around the set potential indicated by an E_{rms} value over the slow strain rate test time. The open circuit voltage (OCV) as initially determined, had also showed a finite distribution over the time of measurement, so that the setting of a fixed potential at the end of the stabilisation time, meant that the set potential could show a difference from the true OCV at an instant in time, leading to a finite current.

Corrosive action could therefore be expected to develop at scratches or points of relative weakness in the passivation film or in the edge protection, such as may have been caused in handling samples, or prior to receipt of the plate, or at weakly protected edge points. Potentio-dynamic dc polarisation tests indicated that for tuna brine media, the steel having an eccs surface film was typically found to be slightly cathodic to abraded eccs steel (e.g. by around 10mV), so that any surface damage leading to steel exposure would be expected to lead to some acceleration of local attack under aqueous conditions in the presence of aggressive anions.

As the tensile slow strain extension and loading slowly increased, the chromium/chromium oxide passivation film on the surface would be weakened or locally fractured under strain, and to a greater extent ahead of the notch regions where local strains would be increased. Pits were observed to develop on specimens of Tuna or Salmon product under high or low air conditions. The pits were observed to become elongated ahead of the notch apex regions, but were not exclusive to these regions with either product.

Over time, the combination of tensile strain applied and pitting gave rise to eventual initiation of fracture at least one notch. A complicating influence would be the meniscus arising from the edge protection lacquer, so that the region of initial attack in the notch vicinity tended to be ahead of the notch and the meniscus, e.g. Figure 40.

3.9.2 Behaviour at Notches

Observation of the fractures under a low power microscope (10x-20x mag) indicated that the metal associated with the crack regions at one notch displayed a much lower level of ductility than at the second notch (e.g. Figures 84-87), or than elsewhere along the failure distance. This was later confirmed by fractographic evidence for both products under high and low air conditions.

The microscopic evidence further indicated that away from the failure initiation region at a notch showing ductility loss, typically of around 1mm running from the notch, relatively more ductile conditions were observed along the sample fractures.

The specimens were set up in a consistent way relative to the initial dimensional characterisation, and it was suspected that the notch behaviour difference was linked to the specimen hanging at a very slight angle to the vertical in the test machine when set up with both grips fixed. These were of a very heavy construction and were attached to flat faced junction pieces fitted to the slow strain rate tensometer.

Specimens subject to the tests with either product under high or low air (nitrogen flushing) conditions were characterised for estimated % thickness reduction at both notch regions. Variable loss of ductility was a feature for both products and test conditions, primarily at one notch region on each sample relative to control specimens tested in oil. The control specimens of each material showed relatively similar physical effects for both notches, without evidence of the same low ductility effect for specimens tested in product brines.

3.9.3 Evidence from Fractography.

Distinctive evidence of environmental stress cracking was observed for salmon brine product in all 3 plate materials under aerated test conditions, and under low air conditions. The environmental stress cracking observations comprised a combination of 'ledges' and brittle appearance just below one or both surfaces ahead of the notch apex, but the central region of the fracture then showed greater ductility. These effects provided evidence characteristic of a hydrogen cracking mode which has been proposed as requiring an incubation time[50] for atomic hydrogen in the metal to concentrate and reach a critical level at a stressed region such as a notch, providing an initiation point for cracking. For tuna product, while all material groups showed degrees of loss of ductility for high air or low air test conditions, the evidence of environmental stress cracking was mainly too uncertain to draw a conclusion . Probable degrees of environmental stress cracking identified by ledge effects were observed on one sample each under high and low air conditions for the 0.235mm plate. Part of the uncertainty could have been due to corrosion after the failure event. Some marginal levels were suspected from photo-micrographic observations e.g. Figures 60 and 65, but these represented very small areas close to the plate surface.

3.9.4 Evidence from Product Chemistry and X Ray Analysis(XRA).

In the literature review, compositional aspects of fish were reviewed, with a number of aspects highlighted, including the following:

i) The breakdown of sulphur bearing amino acids during heat processing which can liberate hydrogen sulphide and in addition other organic sulphides such as di methyl sulphide and methyl mercaptan[7]. Hydrogen sulphide is recognised as a catalytic hydrogen recombination poison[33], with an explanation given that adsorption of the catalyst prevents the species adsorbing at the surface to recombine. As a result of this, a

concentration gradient of hydrogen atoms is built up, leading to diffusion of atomic hydrogen into the metal.

In the course of X Ray Analysis work in this study, using the Scanning Electron Microscope, no large sulphur peaks were identified, but samples subject to pitting loop tests did reveal low level sulphur identification by XRA. No corresponding detection was made on samples subject to dc anodic slow sweep polarisation curves. Any volatile sulphides would escape detection by this method, and after the pitting loop tests, when cells were dismantled, there was some empirical indication of sulphurous odours involving salmon and tuna products.

ii) Apart from any hydrogen sulphide generated by amino acid breakdown, [7,25] catalytic hydrogen re-combination poisons have been cited as arsenic, antimony bismuth and selenium, with zinc also identified as an element which promotes hydrogen entry into steel. This study has shown that small amounts of arsenic and selenium as well as zinc were present in both products. These elements would be candidates for inclusion in tests to try to mimic the product effect.

iii) It is established knowledge that the phosphate anion has been associated with environmental stress cracking of steels under anodic conditions[15]. Smart Scott and Proctor[16] had also observed that at potentials more negative than –550mv (vs saturated calomel electrode), a considerable loss of ductility was observed.

In this work, loss of ductility has been a consistent observation in slow strain rate tests with both products and each material type. Phosphate anion has been a common constituent in both products and at an increased level in salmon product. Chloride has also been at a significant level in both products, but higher in tuna. However, the peak corrosion currents on the anodic curves of the pitting loops have not shown much difference between products, Figures 84-87. The balance between these two anion levels was of higher phosphate and lower chloride in salmon product.

iv) The electrochemical pitting loops as well as the slow sweep polarisation curves have demonstrated that a pronounced noise behaviour was repeatable in the cathodic region and to a lesser extent in the anodic region of the polarisation sweeps, suggesting a strong intervention of adsorption behaviours. Apart from inorganic species of cations or anions which may adsorb at the metal surface, the amino acids have the potential to adsorb by virtue of residual charges on nitrogen atoms (positive charge) and oxygen atoms(negative charge). As amino acids form large chain molecules, it would be thought more likely that inorganic cations would be the most active in this respect. However, in view of the pronounced noise behaviour of products in polarisation studies the inclusion of selected cases in a further experiment would be worthwhile. Histidine has been described as present at a relatively high level in tuna product which has been found prone to some practical cases of environmental stress cracking.

v) The test work concerned two products with pH values differing by around 0.4 units. In the course of slow strain rate tests and other electrochemical tests a pH drop typically took place. Measurement at the start and end of tests showed that the mean drop for slow strain rate tests was under 0.1 units for tuna brine, and was under 0.3 units for salmon brine considering both air and nitrogen flush conditions , with no individuals recording a drop of 0.5 units. The opinion of a Micobiologist was sought, and it was considered unlikely that bacteriological growth would have been very significant. Generation of any sulphide ions by this mechanism may assist the action of catalytic poisons.

3.9.5 Evidence from Correlation and Regression Information from Slow Strain Rate Tests.

The two parameters providing the most consistent correlations with time to failure in slow strain rate tests were the current-time integral, Ia_1, up to the point of maximum load (inverse correlation) and the area under the load-extension plot up to maximum load (Mechanical Work, M1), which showed direct correlation.

This observation leads to a summary of three fundamental findings of the study, as follows:

1. The correlation and regression relationships of integrated current, Ia_1 and Mechanical Work, M1, (both defined up to the point of maximum load), with time to failure of the slow strain rate specimens, for the 4 main sub groups of salmon and tuna brines tested under high air and nitrogen flush conditions.
2. The fractographic observations using SEM showed significant loss of ductility at one specimen notch per sample preferentially, typically over around 1mm, again for all 4 main sub groups identified, and involving all plate lots.
3. The SEM studies revealed evidence of a trans-granular environmental stress cracking mode of failure just ahead of the notch region on salmon samples tested under air conditions and nitrogen flushing conditions. The evidence mainly took the form of ledges and areas of brittle surface appearance.

In the tuna product sub-groups for air or nitrogen flushing conditions, the evidence of environmental stress cracking was either limited e.g, by very small areas affected, or inconclusive, sometimes because of additional corrosion, or possible product residues. However, one sample of the 0.235mm plate for each of high air and nitrogen flush conditions (numbers ssrttuo163, Figures 57-58, high air, and ssrttu150, Ha/Hc, N_2 flush Figures 64-65), showed some evidence indicative of

trans-granular environmental stress cracking, or probably so, Figure 57 indicating an apparent local brittle condition. These samples featured the 0.235mm nitrogenised plate. Tuna sample ssrttu116 tested under air conditions, featuring 0.18mm plate, showed what was interpreted as a possible environmental stress cracking effect in a small region, Figures 59-60, but this was rather uncertain due to additional corrosion.

3.9.6 Regression Predictions for Time to Failure in slow Strain rate tests, Based upon Integrated Current-Time Data and Mechanical Work.

Considering the 4 main sub groups referred to for prediction of time to failure on the basis of regression equations involving the parameters of Integrated Current –Time data, Ia_1, and Mechanical Work (M1), the following comparative results were obtained:

Table 96: Regression Equations for Time to Failure in Slow Strain Rate Tests.

Item	Description	Mean failure time: hours	Predictive Regression Equation
Group 1.	Salmon brine: high air	43.43	$Tf = 12.8 + 46.9x\ M1 - 2.1x10^{-5} \times Ia_1$
Group 2.	Salmon brine : low air.	46.11	$Tf = 16.2 + 20.1x\ M1 - 2.3x10^{-5} \times Ia_1$
Group 3.	Tuna brine: high air.	46.75	$Tf = 21.2 + 40.6x\ M1 - 9.0x10^{-6} \times Ia_1$
Group 4.	Tuna brine: low air.	46.52	$Tf = 21.4 + 22.2x\ M1 - 2.0x10^{-5} \times Ia_1$

Where:

Tf is time to failure in hours.

Mechanical work 'M1' is in Newton.m (the area under the load-extension plot up to maximum load).

Ia_1 is the $\log_{10}$ current - time integral in units of $\log_{10}$ current (amps) x time (seconds), normalised for a specimen surface area of $1cm^2$, again up to the time corresponding to the maximum load point.

The $\log_{10}$ values for the Ia_1 parameter multiplied by the time have given consistently negative results, (see Section 3 , Appendices 7-10, as well as as Section 2, Appendices 1 and 2), so taking this into account, the inverse relationship of Ia_1 with time to failure became direct. The interpretation made here is as follows:

a) The integrated value parameter for Ia_1 was determined as $\int y\,dx$, where 'y' represented the current axis and 'x' the time axis. This integral would not define the direction of the current.

b) A log integer for current values below 1.0 amp yields negative values. Most current values during tests involved multiples of values ranging between 10^{-6} and 10^{-2} amps. Instantaneous currents in the 10^{-5} amp range were very common.

c) The visual evidence displayed by tuna and salmon brine test plate samples after slow strain rate tests indicated that pitting had occurred, and the electrochemical pitting loop tests predicted a pitting tendency. From this evidence a substantial measure of positive current must have existed.

d) The failure effects shown from fractography have revealed a combination of mechanical elements , pitting and in at least the cases displayed in this report, some partial environmental stress cracking effects or low ductility.

e) From the above it follows that the Integrated Current Parameter, Ia_1, has represented an effect operating in parallel with mechanical work in the regression predictions for overall failure time. If the current

were relatively high and pitting or a combination of pitting and environmental stress cracking were substantial, the time element would be reduced. On the other hand, if the corrosion currents were very low and pitting and any environmental stress cracking effects were minimal, then the time dimension within Ia_I would be expected to be much larger, and a different balance in the parameter would exist.

On the basis of the above, it is possible to explain the net direct effect of the integrated current parameter in a regression relationship for time to failure. Supposing again that corrosion currents were very large such that the $\log_{10}$ value for Ia_I became positive, then provided that an inverse correlation with time to failure had still been shown involving such data, a true inverse effect could exist.

Regarding the above candidate regressions, three have shown close similarity in the values of the current –time integral, Ia_I, (excepting Group 3), and the coefficients for 'Mechanical Work' followed a pattern related to high or low air test conditions.

The indications from practical observations and the form of load extension plots were that crack initiation probably took place at a late stage in the tests, likely to be around the peak load stage. Given this indication, and the fact of the most important evidence of low ductility was associated with the start of fracture, data for mechanical work and integrated current after the maximum load point was thought likely to be of less critical significance than that up to the maximum load, although the values over the total failure time could still be examined at a later stage.

A high degree of similarity in mean failure times has been observed for all but the salmon group tested in air, Group1, in the above table. A normality test (the Anderson Darling Statistic) showed that failure times were highly unlikely to be normally

distributed for the two salmon variables (P=0.019 for nitrogen conditions and P<0.005 for air conditions.)

No similar statistical significance at 5% or a higher significance level was shown for the tuna groups, providing more evidence of degrees of difference between product behaviours.

Table 97 below shows the summary of regression parameters for the above 4 data sets, identified as Groups 1-4.

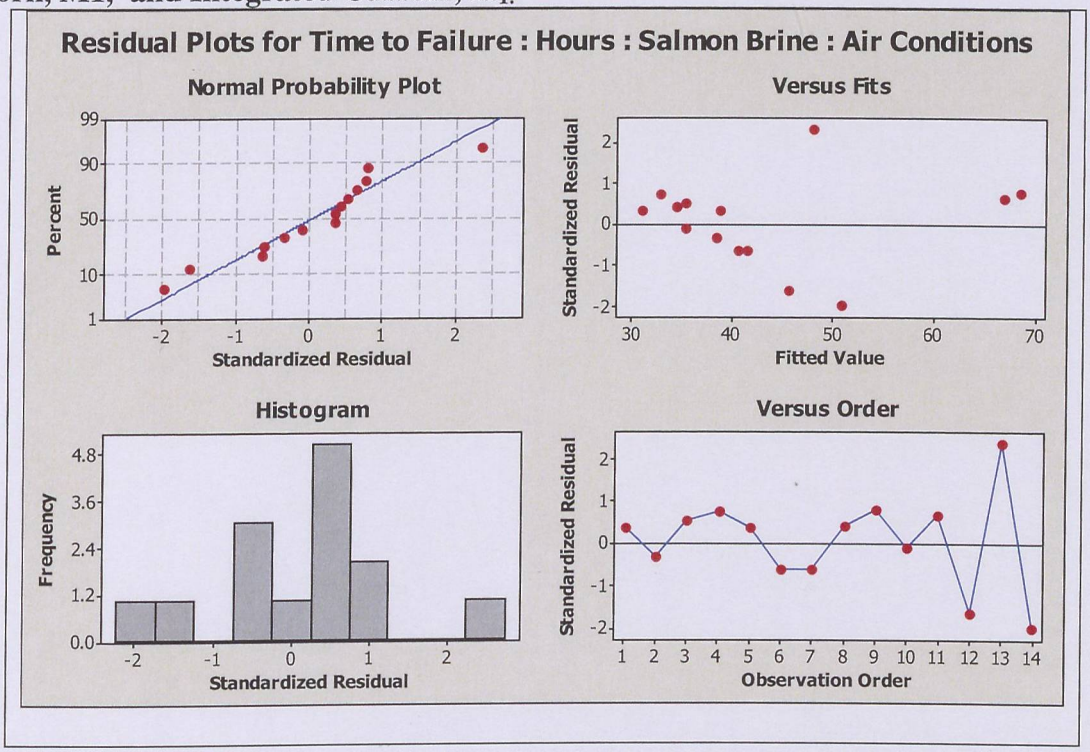
Table 97: Statistical Parameters for Respective Data Sets in Groups 1 to 4.

Item	Regression Data set	R^2	R^2 adjusted	R^2 for predicted values	S: Standard deviation of residuals	P value for regression
1.	Salmon brine: high air	94.1	93.0	87.21	3.22	0.000
2.	Salmon brine: low air.	91.6	90.3	83.07	3.48	0.000
3.	Tuna brine: high air.	96.3	95.5	91.8	2.57	0.000
4.	Tuna brine: low air.	90.9	89.4	85.57	2.67	0.000

All regressions were highly significant (P=<0.001) and with R^2 and R^2adjusted values indicating high proportions of variability in time to failure accounted for. Three data sets showed R^2 for predicted times to failure were above 80%. However, in all cases the residuals were not found to be closely approximated to a normal distribution. Given the objective of the study to better understand environmental stress cracking in food cans, the prominent cases for further consideration were salmon under air conditions, and again under nitrogen flushing conditions, these being the cases where more distinctive evidence of environmental stress cracking was observed. The residual plots for the regressions using the predictors of

mechanical work, M1 and Ia_1 are shown below for these two conditions, Plots 37-38.

Plot 37: Regression Residuals for Time to failure in hours of Salmon Brine, subject to Slow Strain rate Testing under Air Conditions as a function of Mechanical Work, M1, and Integrated Current, Ia_1.



The analysis recorded one unusual observation, number 13, having a large standardised residual, as follows in Table 98:

Table 98: Unusual observations

Observation	Mechanical work: M1	Time to fail: hours	Fitted value: hours	Standard error of fit	Residual	Standardised residual
13	0.455	53.9	48. 16	2.184	5.74	2.42

The lack of fit test was significant at P=0.000.

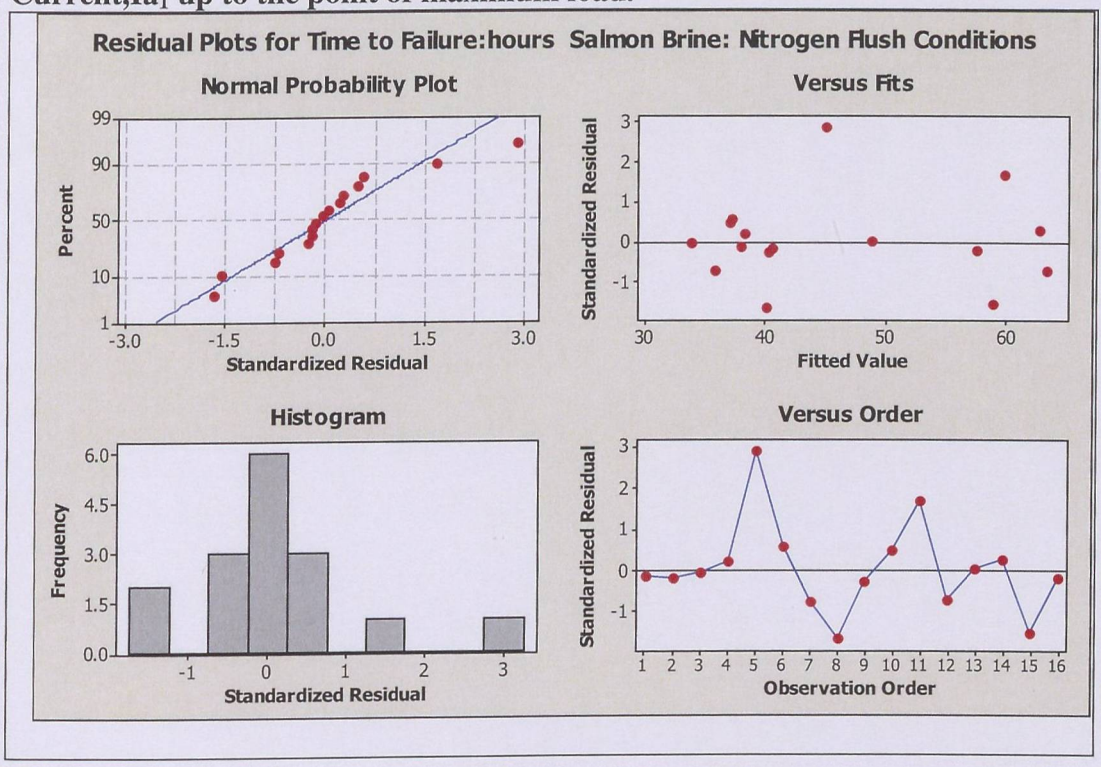
A significant proportion of the residual data were quite close to a normal pattern. A central tendency of residuals was shown, but there was a degree of positive bias. The values giving high positive or negative residuals corresponded to intermediate failure times. The higher residuals in the last three tests were associated with the

0.235mm material, but one of the samples tested with this material did not give a high residual. Thus the conclusion of this analysis is that the two chosen parameters asccount for the majority of variability in time to failure, but the overall fit was not satisfactory on account of a small minority of data points suggested by the residuals plot.

From earlier consideration of data, correlations of notch height change, Delta HG $_{corr}$, with Time to failure (direct), Mechanical Work,M1 (inverse), and integrated current, Ia_I (inverse) were noted (Appendix 4, page2). These correlations were not repeated for the other sub groups, except for a weak correlation of Delta HG corr with time to failure for Tuna brine under nitrogen flush conditions. The strength of the correlations of this parameter for salmon under air conditions may be an additional indicator of the contribution of environmental stress cracking to determining the failure time, which is not easily reconcilable from fractography work alone, as some specimens suffer additional post failure corrosion. Future work should include attention to the notch height change parameter. It has been noted that notch height change is a particularly difficult parameter to measure accurately after failure, as was evident from some negative values recorded

The corresponding residual plots for the regression for salmon under low air conditions, table 96 item 2, are shown below in Plot 38.

Plot 38: Regression Residuals for time to failure of Salmon Brine under Nitrogen Flushing Conditions as a function of Mechanical Work,M1, and Integrated Current,Ia_1 up to the point of maximum load.



This regression recorded one unusual observation, having a large standardised residual, as shown in Table 99 below.

Table 99: Unusual Observations

Observation	Mechanical work: M1	Time to fail: hours	Fitted value: hours	Standard error of fit	Residual	Standardised residual
5	0.334	53.04	45.031	2.122	8.009	2.9

In this case again an imtermediate failure time was involved. The overall lack of fit test was significant at P= 0.026.

The residual plots for the time to failure prediction for salmon brine under low air conditions again showed that a significant proportion of data displayed only a limited departure from a normal distribution. The residuals also showed a central tendency, this time at zero, but there was a single very high positive residual, and this sample was of a different material to the high residual cases for air conditions. In this case an 0.18mm sample showed a longer failure time than other samples of the corresponding gauge. A

conceivable reason was some sample slippage in the tensile grips, which was a difficulty in a minority of cases.

The pattern of the majority of residual observations would suggest that the chosen model is probably the best available based upon the results achieved, but it has some limitations.

A suggested combinastion of reasons why a minority of results within a number of regression models have tended to undermine the predictions are:

i) A minority of samples may have suffered finite slippage in the mechanical tensile grips leading to longer failure time than might otherwise have been the case.

ii) In using lacquer at the edges of the eccs specimens and especially at the notch edge, it is not possible to avoid small anmounts giving rise to meniscuss effects at the adjacent faces, and with the peak stress developing at the notch edge, this may have influenced the location and rate of corrosive attack.

iii) The specimens had a variable amount of metal exposure on their faces due to damage, and the rate of attack will also have been affected by permeation of salt containing species through points of relative weakness in the eccs protective film. For these reasons the true area exposed to corrosive attack will have varied and the local intensity of attack e.g. at the notch region might also have been affected to a degree.

Given the above observations, the data for the tuna in brine, air conditions tests, Table 27, subset 4, did meet the data subsetting statistical fit test using the parameters of Integrated current and Mechanical Work together.

This study has included some work involving estimation of the stress intensity factor, K_I, and its application to crack growth rate estimations applied to the case of Tuna brine

under air conditions. While time to failure data has been fitted to linear models with statistical significance, the observations inferring crack initiation at late stage of the tests were clearly not consistent with a linear process, and a regression fit for $\log_{10}$ crack growth rate was achieved using the K_I estimate with limited data points. However, an alternative and better model was fitted for $\log_{10}$ crack growth rate for the full 18 point dataset of the corresponding test condition using I_{a1}, I_{rms1}, Delta HG and OCV. This gave an R^2 value for predicted data of 69.9%.

Related to observations made in initial studies, section 2, a full re appraisal has still to be carried out , but apart from some test condition differences from the present work, the Integrated Current and noise, I_{rms2} values were derived from the entire test time and not up to peak load. At that stage of work , the precise failure point was not known, as it had not been identified from the sudden load drop at the failure point. It is not, therefore, surprising that some differences in results have occurred.

3.9.7 Stress Prediction Studies by Finite Element Modelling

A major difficulty was encountered in attempting to establish true stress strain plots for the double reduced eccs steel plates used. This has not been fully resolved and requires much more work to achieve good plots.

Approximations have been attempted by a combination of the following:

a) Practical determination of the true failure stress involving SEM measurement of fracture dimensions.

b) Approximations to true stress and strain values in the region beyond the yield point, based upon information according to Dowling[71]. Attempts to determine the strain hardening exponent were not successful, as non linearity of the log stress strain plots for plastic conditions was encountered for each material.

c) Final fracture strains were measured using two methods ,namely, Erichsen cupping tests, and strain measurements on notched tensile plates as used in slow strain rate testing , but instead pulled parallel to the grain direction on a Zwick tensometer.

The fracture stresses and alternative fracture strain estimates were combined with True stress - True strain plots obtained using equations based on the constant volume assumption for plastic strain and stress, but these equations would not be truly valid for the circumstances encountered where an extensive region of the plot may lie beyond the point of maximum stress. Slight necking after a small strain increment beyond yielding had occurred, associated with an elastic - perfectly plastic approximation of properties for at least two materials, up to the stage of sudden and severe necking. The nitrogenised steel showed a slightly greater negative after the maximum load point than the other materials.

Each of the approximations was tested to predict the stress at the notch tensile sample apex, after loading to match the practical failure load. The predicted stress was compared with the true failure stress measured for standard 'dog bone' test specimens The stress predictions agreed with the practical determinations variously between 13% and under 2%. Finite Element Analysis Models of Draw Redrawn Can forming , and Easy Open shell forming were then carried out using the Erichsen approximation for failure strain. These models were run on the basis of 'boundary condition' movement and 'smooth step' progressions within true fabrication stage times for all key forming movements. They should be re-run to verify whether the same answers are obtained using applied velocity movement instead.

3.9.8 83mm Diameter Draw-Redrawn Can Model: Base Rim and Wall Stresses and Comparison with Notch Tensile Test Piece Results.

The vulnerable area of the can from past experience is the bottom rim, should it become dented and then be subject to fluctuating stacking loads in transport. In the Finite Element Model, the plate material tested (0.16mm DR620CA), showed significant tensile forces at the bottom rim radius in the S33(hoop) direction.

Other inner surface regions in tension were the bottom countersink wall and the adjacent countersink bottom and beading, also in tension in the hoop direction. The wall stress can be reconciled with the final forming at the can base requiring some radial expansion. The highest stresses within these areas tended to occur at the countersink base region and the countersink wall.

The outer can wall showed very high tensile stresses in the S22 and S33 directions. These stresses were predicted to be well above the yield point, as were the highest values at points such as the countersink reverse wall. Such a finding is in conflict with literature referred to earlier in this study[43], indicating the stresses termed 'residual

stresses' are relieved if they exceed the yield point. Further consideration of this aspect is required beyond this study.

The stresses predicted at internal regions of the drawn-redrawn cans were all well below those predicted in tensile notched regions for specimens having the same properties, and subject to tensile loads approximating to the fracture strength.

3.9.9 73mm Diameter Model for Easy Open end Shell: Comments.

For this model the stress predictions were of significant tensile stresses in the countersink area with high values in the S22 and S33 directions, and some peak value predictions exceeding the yield stress. The bottom of the countersink radius showed predictions of either lower tensile values or compressive stresses.

The peak stress point at the top of the seaming panel would be indicative of what could happen, if the 'knockout' strikes this point before the press operation is at bottom dead centre.

3.9.10 Stress Predictions from Notched Tensile Models.

The modelling of the notched tensile samples did not include corrosion, so that the predictive stress data obtained does not necessarily relate to that which would exist in samples subject to slow strain rate testing under corresponding loads. Some attributes related to failures and corrosion behaviour identified in this work have corresponded to those associated with hydrogen cracking. For this type of failure sometimes termed 'delayed failure embrittlement', a minimum stress can be expected, below which failure should not occur. To define such a level would require further work necessitating e.g. the testing of specimens with larger notch angles than in the present specimens, say 120 degrees and 150 degrees, to help identify the boundary where absence of ductility loss or embrittlement ceases to occur. Parallel stress modelling of the notch modifications would

provide further predictions based on uncorroded samples, which can then be compared with the forming stress predictions. The stress concentration factor for the 90 degree v notch used was estimated to be in the order of 3.5 which was considered very high, and the use of the larger notch angles suggested is a potentially very important to assist predictions of reduced risk conditions.

3.10 Section 3, Appendix 1.

Use of Statistical Terms and Consideration of Candidate Predictors for Linear Regression Models.

A source of reference used for statistical guidance was :

Ref 81: John O. Rawlings; Sastry G. Pantula and David A, Dickey; Applied Regression Analysis, 2nd edition, Springer , 2001. ISBN 0-387-98454-2.

In this work a number of statistical terms have been condsidered in the context of predictions for time to failure and crack growth rate. These are defined below.

Correlation: The Pearson correlation value, together with the P value indicating significance level in the Minitab package.

The P value is also used in the Minitab package for other significance tests including regression table and Analysis of Variance tables for the regression functions.

$P = \leq 0.100$ signifies significance at 10% i.e. less than 10% probability that the observation concerned arose by chance based upon the statistical method used, and involving any assumptions and/or limitations of the method in its application.

$P = \leq 0.050$ signifies significance at 5%.

$P = \leq 0.010$ signifies significance at 1%.

$P = \leq 0.001$ signifies significance at 0.1%.

In relation to correlation coefficients and the subsequent selection of predictors, if a correlation coefficient between two predictors is 0.5 or higher it is improbable that one paramater can change independently of the other. This is information understood by the author based upon previous discussions with a statistical consultant. Refer to TR11405[72] reference 5.

Linear Regression Predictions: The method of 'best subsets' has been used from the Minitab package, with the following indicators of suitability of subsets.

R^2 : The coefficient of determination. This is represented by

$$R^2 = \frac{\text{Sum of squares (for regression)}}{\text{Sum of Squares (Total).}}$$

This is the proportion of the variability of the dependent variable explained by the independent variables in the model. R^2 will increase as additional parameters are added to the model. A judgement is required regarding the benefit of adding variables where the relative increaee in R^2 becomes small.

R^2 adj: The adjusted coefficient of determination.

$$R^2 \text{ adj} = 1 - \frac{\text{Mean square (Residuals)}}{\text{Mean square (Total)}}$$

This has the effect of removing the impact of degrees of freedom and the resulting values can be better compared for models having different numbers of parameters. As variables are added the value reaches an upper limit. The simplest model with R^2 adjusted around the upper limt should be used.

S = The standard deviation of the residuals. Smaller 'S' values will be associated with better fitting models

Mallows Cp Statistic[81].

This is an estimate of the standardised total mean squared error of estimation for the data set being considered.

$$Cp = \frac{\text{Sum of squares (residual)}_p}{S^2} + 2p' - n$$

where:

Sum of squares $(\text{residual})_p$ is the residual sum of squares for the p variable subset being considered.

S^2 is an estimate of σ^2

When the model is correct Cp is approximately equal to p'

When important variables have been omitted Cp is larger than p'.

As variables are added Cp decreases towards p' and then falls below or fluctuates around p'.

p' = p+1 , where p was the number of independent variables used in the regression.

P' denotes the total number of parameters in the model.

n is the sample size, being the number of tests or observations made.

It is quite possible for Cp to be negative. If a model has a very high R^2 value,, then Cp will be negative if the number of data points is greater than 2x the number of parameters fitted.

'Lack of Fit Test': This was taken from the option in the minitab package, and 'data subsetting' was the normal choice. Significance in the data subsetting test normally indicates curvature in the predictive model. i.e. if P is significant at <0.1 for the model, it is suggesting that there is curvature in the data.

Other Statistical Methods used.

In certain cases where the number of test replicates was very limited, an alternative to the best subsets method required to be used. This was for initial studies reported in Section 2. In these cases a combination of the stepwise regression from the Minitab package and the partial least squares method was used.

Standardised Residuals[81] : These were used in the residuals plots. Dividing each residual by its standard deviation gives the standardised residual.

Stepwise Regression Procedure[81]

"The subset models are identified sequentially by by adding or deleting the variable that has the greatest impact on the residual sum of squares. The stepwise methods are not guaranteed to find the best subset for each subset size, and the results produced by different mehods may not agree with each other."

Least Squares Criterion used for Regression[81]**.**

The principle involved here is that the computation takes place such that the resulting coefficients for the constant term and parameter multiple are such that the sum of squares of the residuals for the predicted dependent variable is minimised.

3.11 Section 3, Appendix 2, Page 1

Tuna in Brine: Correlations from SCC Tests: Air Conditions

.Factors Correlation values P values	Delta AD (cms)	Delta BC (cms)	Delta BC corr (cms)	Delta HG (cms)	Delta Hg corr. (cms)	Gauge (ins)	Change of load. (KN)	Extension to failure. (mm)	Time to load max: (hrs)	Time to failure (hrs)	OCV: (Milli-volts)	E rms_1: (Volts)	I rms_1* (Amps)	Ia_{1*} log_{10}I amps x time: secs	pH start	pH end
Delta AD																
P																
Delta BC	**0.789**															
P	**0.001**															
Delta BC corr	0.399	**0.776**														
P	0.177	**0.002**														
Delta HG	-0.185	0.018	-0.064													
P	0.546	0.954	0.835													
Delta HG corr	-0.164	-0.084	0.007	0.459												
P	0.591	0.784	0.981	0.115												
Gauge	0.202	**0.557**	0.421	0.324	0.132											
P	0.507	**0.048**	0.152	0.279	0.667											
Change of load: KN	-0.011	0.366	0.201	0.405	0.191	**0.789**										
P	0.971	0.218	0.511	0.170	0.531	**0.001**										
Extension	-0.175	0.046	-0.112	0.272	0.204	**0.622**	**0.735**									
P	0.568	0.880	0.717	0.368	0.505	**0.023**	**0.004**									
Time to load maximum.	-0.164	0.092	-0.057	0.257	0.238	**0.619**	**0.811**	**0.979**								
P	0.591	0.766	0.854	0.396	0.434	**0.024**	**0.001**	**0.000**								
Time to failure.	-0.158	0.097	-0.062	0.274	0.215	**0.635**	**0.809**	**0.987**	**0.998**							
P	0.605	0.752	0.841	0.364	0.480	**0.020**	**0.001**	**0.000**	**0.001**							

* Electrochemical parameters were normalised to $1cm^2$ for all test groups for the slow strain rate tests.

3.12 Section 3, Appendix 2, Page 2

Tuna in Brine: Correlations from SCC Tests: Air Conditions

Factors Correlation values P values	Delta AD (cms)	Delta BC (cms	Delta BC corr (cms)	Delta HG (cms)	Delta Hg corr (cms)	Gauge (ins)	Change of load. (kN)	Extension (mm)	Time to load max: (hrs)	Time to failure (hrs)	OCV: (volts)	E_{rms1}: amps	I_{rms1}: (amps /cm^2)	Ia_1: $\log_{10}$I amps/ cm^2 x time: secs)	pH start	pH end
OCV	0.013	0.324	0.208	**0.603**	-0.070	**0.573**	**0.569**	0.403	0.371	0.401						
P	0.966	0.280	0.495	**0.029**	0.821	**0.041**	**0.042**	0.172	0.213	0.174						
E_{rms1}	-0.142	-0.106	0.010	-0.061	-0.157	-0.379	-0.138	0.035	0.046	0.042	-0.165					
P	0.644	0.731	0.975	0.842	0.608	0.179	0.653	0.910	0.881	0.892	0.591					
I_{rms1}	-0.087	0.229	0.214	0.448	0.160	**0.498**	**0.539**	-0.022	0.063	0.061	0.383	-0.264				
P	0.777	0.452	0.484	0.125	0.602	**0.083**	**0.058**	0.944	0.838	0.844	0.196	0.384				
I_{a1}	0.072	0.035	0.288	0.099	0.069	-0.332	**-0.549**	**-0.851**	**-0.849**	**-0.850**	-0.073	-0.077	0.288			
P	0.814	0.909	0.340	0.748	0.824	0.268	**0.052**	**0.000**	**0.000**	**0.000**	0.812	0.802	0.340			
pH start	0.285	0.154	-0.013	0.167	**0.674**	0.196	0.065	-0.106	-0.095	-0.104	-0.208	**-0.532**	0.254	0.179		
P	0.345	0.616	0.966	0.5869	**0.012**	0.521	0.833	0.730	0.758	0.736	0.495	**0.061**	0.402	0.558		
pH end	-0.076	0.148	0.442	0.383	0.360	0.239	0.002	0.077	0.041	0.045	0.464	-0.203	-0.029	0.309	-0.067	
P	0.806	0.630	0.130	0.196	0.227	0.431	0.996	0.803	0.895	0.884	0.110	0.505	0.925	0.305	0.828	
Mech work, M	-0.086	0.209	0.035	0.297	0.160	**0.747**	**0.898**	**0.952**	**0.968**	**0.974**	**0.512**	-0.063	0.189	**-0.797**	-0.055	0.043
P	0.781	0.493	0.909	0.324	0.602	**0.003**	**0.000**	**0.000**	**0.000**	**0.000**	**0.074**	0.837	0.537	**0.001**	0.858	0.889

3.13 Section 3, Appendix 3, Page 1

Tuna in Brine: Correlations from SCC Tests: Nitrogen Flushing Conditions .

Factors Correlation values P values	Delta AD (cms)	Delta BC (cms)	Delta BC corr (cms)	Delta HG (cms)	Delta Hg corr. (cms)	Gauge (ins)	Change of load. (kN)	Extension (mm)	Time to load max: (hrs)	Time to failure (hrs)	OCV: (Milli-volts)	E rms_1 (Volts)	I rms_1 (amps /cm^2)	Ia_1: log_{10}I amps/ cm^2 * time: secs	pH start	pH end
Delta AD																
P																
Delta BC	**0.796**															
P	**0.000**															
Delta BC corr	-0.289	-0.264														
P	0.296	0.342														
Delta HG	0.141	0.394	-0.222													
P	0.615	0.146	0.427													
Delta HG corr	0.052	0.041	-0.033	**0.755**												
P	0.855	0.885	0.906	**0.001**												
Gauge	0.366	**0.476**	-0.123	**0.727**	**0.471**											
P	0.180	**0.073**	0.662	**0.002**	**0.076**											
Change of load: KN	**0.673**	**0.570**	0.132	**0.491**	0.328	**0.580**										
P	**0.006**	**0.027**	0.640	**0.063**	0.232	**0.023**										
Extension displ	0.382	**0.528**	0.414	**0.441**	0.424	**0.543**	**0.540**									
P	0.160	**0.043**	0.125	**0.100**	0.115	**0.036**	**0.038**									
Time to load max	**0.449**	**0.564**	0.118	**0.608**	**0.467**	**0.776**	**0.707**	**0.838**								
P	**0.093**	**0.029**	0.675	**0.016**	**0.079**	**0.001**	**0.003**	**0.000**								
Time to fail	0.427	**0.544**	0.137	**0.588**	**0.454**	**0.745**	**0.644**	**0.885**	**0.983**							
P	0.112	**0.036**	0.626	**0.021**	**0.089**	**0.001**	**0.010**	**0.000**	**0.000**							

3.14 Section 3, Appendix 3, Page 2

Tuna in Brine: Correlations from SCC Tests: Nitrogen Flushing Conditions

Factors Correlation values P values	Delta AD (cms)	Delta BC (cms)	Delta BC corr (cms)	Delta HG (cms)	Delta Hg corr (cms)	Gauge (ins)	Change of load. (kN)	Extension (mm)	Time to load max: (hrs)	Time to failure (hrs)	OCV: (Milli-volts)	E_{rms1} (Volts)	$I\ rms_1$ (amps /cm^2)	Ia_1 $\log_{10}$I amps/cm^2 x time: secs	pH start	PH end
OCV	-0.160	-0.094	0.023	**-0.704**	**-0.833**	**-0.705**	**-0.462**	**-0.461**	**-0.636**	**-0.616**						
P	0.569	0.739	0.934	**0.003**	**0.000**	**0.003**	**0.083**	**0.084**	**0.011**	**0.014**						
E_{rms1}	0.128	0.339	-0.082	**0.508**	0.080	0.551	0.386	0.225	0.365	0.351	-0.161					
P	0.649	0.216	0.771	**0.053**	0.776	0.033	0.155	0.420	0.181	0.199	0.567					
I_{rms1}	**-0.564**	**-0.457**	0.099	**-0.486**	**-0.528**	**-0.644**	**-0.624**	**-0.517**	**-0.722**	**-0.663**	**0.567**	-0.168				
P	**0.029**	**0.087**	0.724	**0.066**	**0.043**	**0.010**	**0.013**	**0.049**	**0.002**	**0.007**	**0.027**	0.550				
I_{a1}	-0.196	**-0.454**	-0.158	**-0.612**	-0.414	**-0.671**	**-0.510**	**-0.786**	**-0.926**	**-0.924**	**0.573**	-0.391	**0.569**			
P	0.483	**0.089**	0.574	**0.015**	0.125	**0.006**	**0.052**	**0.001**	**0.000**	**0.000**	**0.026**	0.150	**0.027**			
pH start	0.090	0.221	0.022	-0.078	0.227	-0.092	0.001	0.289	0.272	0.361	0.081	-0.158	0.155	-0.314		
P	0.751	0.428	0.939	0.783	0.415	0.743	0.998	0.297	0.326	0.186	0.773	0.573	0.582	0.254		
pH end	-0.103	-0.176	-0.364	0.103	0.023	0.093	0.104	**-0.574**	-0.141	-0.283	-0.078	-0.040	-0.056	0.166	-0.382	
P	0.715	0.529	0.182	0.715	0.936	0.742	0.712	**0.025**	0.615	0.307	0.783	0.889	0.842	0.555	0.160	
Mech work M	**0.527**	**0.638**	0.123	**0.602**	0.342	**0.818**	**0.808**	**0.775**	**0.942**	**0.911**	**-0.576**	0.407	**-0.678**	**-0.854**	0.167	-0.051
P	**0.044**	**0.011**	0.663	**0.018**	0.212	**0.000**	**0.000**	**0.001**	**0.000**	**0.000**	**0.025**	0.132	**0.005**	**0.000**	0.552	0.855

3.15 Section 3, Appendix 4, Page 1

Salmon in Brine: Correlations from SCC Tests: Air Conditions

Factors Correlation values P values	Delta AD. (cms)	Delta BC. (cms)	Delta BC corr. (cms)	Delta HG. (cms)	Delta Hg corr. (cms)	Gauge: (ins)	Change of load: KN	Extension to failure: mm	Time to load max. (hours)	Time to failure; (hours)	OCV: Milli-volts	$E_{rms1.}$ (Volts)	$I_{rms1:}$ amps /cm2	$I_{a1;}$ $\log_{10}$I amps/ cm^2 * time: secs	pH start.	pH end.
Delta AD																
P																
Delta BC	**0.962**															
P	**0.000**															
Delta BC corr	**0.963**	**0.926**														
P	**0.000**	**0.000**														
Delta HG	-0.049	-0.019	0.069													
P	0.868	0.948	0.814													
Delta HG corr	-0.025	0.452	**0.460**	0.421												
P	0.934	0.105	**0.098**	0.134												
Gauge	-0.142	0.189	0.374	0.346	0.437											
P	0.629	0.518	0.188	0.226	0.118											
Change of load: KN	-0.241	0.380	**0.511**	0.354	**0.474**	**0.844**										
P	0.407	0.180	**0.062**	0.215	**0.087**	**0.000**										
Extension to failure.	0.024	**0.514**	**0.538**	0.333	**0.708**	**0.758**	**0.872**									
P	0.935	**0.060**	**0.047**	0.245	**0.005**	**0.002**	**0.000**									

3.16 Section 3, Appendix 4, Page 2

Salmon in Brine: Correlations from SCC Tests: Air Conditions

Factors Correlation values P values	Delta AD: (cms)	Delta BC; (cms)	Delta BC corr (cms)	DeltaHG (cms)	DeltaHG corr; (cms)	Gauge: (ins)	Change of load; KN	Extension (mm)	Time to load max: (hrs)	Time to failure. (hours)	OCV: Milli-volts	E_{rms1} (Volts)	I_{rms1}: amps/ cm2	I_{a1}; $\log_{10}$I amps/ cm^2 * time: secs	pH start	pHend
Time to load max	0.033	**0.677**	**0.638**	0.369	**0.784**	**0.521**	**0.681**	**0.875**								
P	0.910	**0.008**	**0.014**	0.194	**0.001**	**0.056**	**0.007**	**0.000**								
Time to fail	0.041	**0.674**	**0.644**	0.383	**0.788**	**0.540**	**0.685**	**0.879**	**0.999**							
P	0.889	**0.008**	**0.013**	0.176	**0.001**	**0.046**	**0.007**	**0.000**	**0.000**							
OCV	-0.009	-0.338	-0.389	-0.108	-0.162	-0.166	-0.141	-0.089	-0.054	-0.063						
P	0.977	0.237	0.170	0.713	0.581	0.570	0.632	0.789	0.854	0.830						
E_{rms1}	-0.132	0.346	0.214	0.040	0.187	-0.089	0.207	0.237	**0.536**	**0.509**	0.282					
P	0.653	0.225	0.462	0.892	0.522	0.761	0.477	0.416	**0.048**	**0.063**	0.328					
I_{rms1}	0.138	-0.153	-0.128	-0.271	0.439	**0.146**	0.107	0.325	0.206	0.200	0.148	0.004				
P	0.638	0.601	0.663	0.348	0.116	**0.619**	0.716	0.256	0.479	0.492	0.613	0.990				
I_{a1}	-0.085	**-0.667**	**-0.588**	-0.266	**-0.646**	**-0.280**	**-0.542**	**-0.733**	**-0.897**	**-0.889**	-0.149	**-0.632**	-0.119			
P	0.772	**0.009**	**0.027**	0.357	**0.013**	**0.332**	**0.045**	**0.003**	**0.000**	**0.000**	0.611	**0.015**	0.684			
pH start	0.068	-0.090	-0.079	0.245	-0.213	0.288	0.200	0.204	-0.099	-0.090	-0.009	**-0.485**	-0.187	0.235		
P	0.818	0.760	0.789	0.398	0.464	0.319	0.493	0.485	0.735	0.760	0.976	**0.078**	0.522	0.419		
pH end	0.066	0.270	0.054	-0.128	-0.249	**-0.508**	-0.404	-0.188	-0.121	-0.126	-0.118	-0.131	-0.296	0.118	0.420	
P	0.824	0.351	0.854	0.664	0.391	**0.064**	0.152	0.520	0.679	0.667	0.689	0.656	0.305	0.688	0.135	
Mechanical work, M.	-0.059	**0.582**	**0.623**	0.390	**-0.743**	**0.749**	**0.876**	**0.960**	**0.944**	**0.947**	**-0.095**	0.399	0.238	**-0.808**	0.022	-0.287
P	0.841	**0.029**	**0.017**	0.167	**0.002**	**0.002**	**0.000**	**0.000**	**0.000**	**0.000**	**0.747**	0.157	0.413	**0.000**	0.940	0.321

3.17 Section 3, Appendix 5, Page 1

Salmon in Brine: Correlations from SCC Tests: Nitrogen Flushing Conditions

Factors Correlation values P values	Delta AD (cms)	Delta BC (cms)	Delta BC corr. (cms)	Delta HG. (cms)	Delta Hg corr. (cms)	Gauge. (ins)	Change of load: KN	Extension at failure: mm	Time to load max. hours.	Time to failure. hours.	OCV: Milli-volts	$E_{rms1;}$ (Volts)	$I_{rms1;}$ Amps / cm^2.	I_{a1}: $\log_{10}$I amps/ cm^2 * time: secs	pH start	pHend
Delta AD																
P																
Delta BC	-0.196															
P	0.466															
Delta BC corr	-0.138	**0.928**														
P	0.611	**0.000**														
Delta HG	0.283	-0.218	-0.008													
P	0.288	0.417	0.976													
Delta HG corr	0.042	0.223	**0.437**	**0.565**												
P	0.877	0.407	**0.090**	**0.023**												
Gauge	-0.157	**0.591**	**0.632**	0.104	0.130											
P	0.562	**0.016**	**0.009**	0.700	0.631											
Change of load: KN	-0.239	**0.660**	**0.632**	-0.246	-0.063	**0.914**										
P	0.373	**0.005**	**0.009**	0.359	0.818	**0.000**										

3.18 Section 3, Appendix 5, Page 2

Salmon in Brine: Correlations from SCC Tests: Nitrogen Flushing Conditions

Factors Correlation values P values	Delta AD (cms)	Delta BC (cms)	Delta BC corr. (cms)	Delta HG (cms)	Delta Hg corr. (cms)	Gauge. (ins)	Change of load. KN	Extension at failure: mm.	Time to load max. (hours)	Time to failure. (hours)	OCV: Milli-volts	$E_{rms1.}$ Volts	$I_{rms1.}$ amps /cm^2	Ia_1: log_{10}I amps/ cm^2 * time: secs	pH start	pH end
Extension failure	-0.135	**0.581**	**0.621**	-0.046	0.221	**0.817**	**0.759**									
P	0.619	**0.018**	**0.010**	0.865	0.411	**0.000**	**0.001**									
Time to load max	-0.232	**0.558**	**0.548**	-0.126	0.052	**0.869**	**0.822**	**0.887**								
P	0.387	**0.025**	**0.028**	0.641	0.849	**0.000**	**0.000**	**0.000**								
Time to fail	-0.251	**0.546**	**0.541**	-0.138	0.040	**0.872**	**0.829**	**0.889**	**0.999**							
P	0.348	**0.029**	**0.030**	0.609	0.883	**0.000**	**0.000**	**0.000**	**0.000**							
OCV	-0.107	-0.020	-0.235	**-0.724**	-0.374	-0.298	0.021	-0.248	-0.045	-0.049						
P	0.694	0.943	0.380	**0.002**	0.153	0.263	0.938	0.354	0.869	0.857						
E_{rms1}	-0.160	-0.013	0.073	-0.351	-0.265	0.311	0.393	0.272	0.215	0.252	-0.064					
P	0.553	0.961	0.789	0.183	0.321	0.241	0.133	0.309	0.424	0.346	0.815					
I_{rms1}	-0.158	-0.185	-0.282	**-0.656**	**-0.459**	-0.330	-0.134	-0.168	-0.170	-0.155	**0.447**	**0.550**				
P	0.558	0.493	0.290	**0.006**	**0.073**	0.211	0.621	0.534	0.529	0.567	**0.082**	**0.027**				
I_{a1}	0.306	**-0.532**	**-0.576**	0.044	-0.176	**-0.867**	**-0.844**	**-0.870**	**-0.935**	**-0.942**	0.059	-0.257	0.237			
P	0.249	**0.034**	**0.020**	0.873	0.515	**0.000**	**0.000**	**0.000**	**0.000**	**0.000**	0.830	0.336	0.377			
pH start	-0.353	-0.022	0.059	0.086	-0.196	**0.479**	**0.454**	0.242	0.389	0.412	-0.174	0.412	-0.025	**-0.545**		
P	0.180	0.936	0.828	0.751	0.467	**0.061**	**0.077**	0.367	0.137	0.113	0.520	0.113	0.926	**0.029**		
pH end	-0.236	0.200	0.193	-0.336	-0.240	**0.495**	**0.591**	0.279	0.353	0.373	0.122	**0.757**	**0.471**	-0.370	**0.475**	
P	0.379	0.458	0.473	0.204	0.371	**0.051**	**0.016**	0.295	0.180	0.155	0.653	**0.001**	**0.065**	0.158	**0.063**	
Mech work, M.	-0.224	**0.631**	**0.610**	-0.175	-0.003	**0.929**	**0.957**	**0.843**	**0.931**	**0.932**	-0.008	0.295	-0.198	**-0.918**	**0.452**	**0.485**
P	0.404	**0.009**	**0.012**	0.518	0.993	**0.000**	**0.000**	**0.000**	**0.000**	**0.000**	0.977	0.267	0.462	**0.000**	**0.079**	**0.057**

3.19 Section 3, Appendix 6

Chemical Analysis of Three Steels used in Slow Strain Rate Tests:

Material	C%	Si%	Mn%	P%	S%	Cr%	Mo%	Ni%	Al%	Cu%	As%	Co%	Nb%	Sn%	Ti%	V%	N%
Steel Type 1.	0.006	<0.01	0.21	0.013	0.018	0.07	<0.01	0.02	0.03	0.03	0.004	0.005	0.005	0.006	0.002	0.003	0.004
Steel Type 2.	0.05	,0.01	0.26	0.014	0.007	0.06	<0.01	0.01	0.04	0.01	0.003	0.03	<0.001	0.005	0.001	0.002	0.001
Steel Type 3.	0.063	0.01	0.24	0.016	0.012	0.07	<0.01	0.01	0.04	0.02	0.003	0.003	<0.001	0.003	<0.001	0.002	0.011
Target: Steels 1,2	0.12 max	0.03 max	0.30-0.50	0.02 max	0.02 max	0.08 max	0.02 max	0.08 max	0.02-0.08	0.08 max	0.01 max	0.02 max	0.02 max	0.02 max	0.02 max	0.02 max	0.008 max
Target: Steel 3	0.02-0.09	0.03 max	0.55 max	0.02 max	0.02 max	0.08 max	0.02 max	0.08 max	0.01-0.05	0.08 max	0.01 max	0.02 max	0.02 max	0.02 max	0.02 max	0.02 max	0.010-0.015

Steel Type 1 was an 0.16mm DR620 continuously annealed drawing quality steel having very low carbon, eccs coated, and would be used in lacquered form for drawn- redrawn cans such as fish cans, manufactured e.g. in France or Thailand

Steel Type 2 was an 0.18mm DR620 continuously annealed material, eccs coated, suitable for end stamping such for food non easy open ends e.g. for animal foods, meat , fish , or vegetables in lacquered containers.

Steel Type 3 was an 0.235mm DR620 continuously annealed steel suitable for end stamping such as for larger food ends of 99mm diameter containing the same products as steel type 2.
All three steels were within their respective specifications for steel chemistry.
DR means double cold reduced steel.
ECCS means electro chrome coated steel, the chromium level applied to each surface typically being between 50 and 130mg/m^2.

3.20 Section 3, Appendix 7

Slow Strain Test Data for Tuna Brine samples Tested under Air Conditions.

Sample ssrtTu0 number	Time to failure: (hours)	pH start	pH end	OCV (Millivolts) vs N/10 calomel electrode	Delta BC (cm)	Delta BC_{corr}* (cm)	Delta HG* (cm)	Delta HG_{corr}* (cm)	Delta AD* (cm)	E_{rms1} (Volts)	I_{rms1} (Amps/cm^2)	Ia_1 (Log_{10} current density (amps/cm^2)* time (secs)	Mechanical work. M (N.m)	Gauge (ins)
113	28.73	5.87	5.80	-761.00	0.0230	0.0090	0.0230	-0.002	0.035	5.9731e-5	1.7389e-5	-5.6417e5	0.087268	0.0073
114	46.55	5.87	5.83	-768.00	0.0070	0.0010	0.0170	0.007	0.0085	4.0862e-5	1.8978e-5	-9.4615e5	0.419958	0.0072
116	44.63	5.83	5.73	-775.00	0.0345	0.0195	-0.0015	-0.0045	0.0415	9.9356e-5	1.4227e-5	-9.7750e5	0.361675	0.0070
117	43.61	5.92	5.77	-773.00	0.0385	0.0115	0.0245	0.0135	0.069	4.9695e-5	1.7366e-5	-9.2550e5	0.350702	0.00725
119	61.77	5.87	5.78	-776.40	0.0260	0.0175	0.0180	0.0065	0.010	5.4048e-5	3.0169e-5	-1.2853e6	0.715124	0.0094
124	46.42	5.91	5.91	-757.00	0.0305	0.0225	0.0320	0.020	0.017	5.2850e-5	1.0533e-4	-4.8089e5	0.436976	0.0094
130	40.99	5.84	5.80	-769.27	0.0110	0.0020	0.0230	0.0020	0.002	5.9812e-5	4.7881e-5	-7.9123e5	0.222243	0.00626
131	34.39	5.88	5.78	-768.86	0.0130	0.0090	0.0170	0.0080	-0.011	5.2929e-5	3.6770e-5	-7.0160e5	0.189145	0.00603
132	32.95	5.87	5.77	-770.10	0.0180	0.0140	0.0155	0.0030	0.020	6.6698e-5	4.3931e-5	-6.5002e5	0.201935	0.00624
133	51.64	5.86	5.71	-769.40	0.0080	0.0000	0.0370	0.0105	-0.008	1.0847e-4	5.2580e-5	-9.5917e5	0.462172	0.00631
161	65.47	5.83	5.94	-722.20	0.0320	0.0180	0.0380	0.0050	0.0165	7.0120e-5	3.1490e-5	-1.1062e6	0.821583	0.0091
163	42.69	5.87	5.73	-744.39	0.0385	0.0170	0.0295	-0.0025	0.0365	4.1558e-5	1.2957e-4	-7.1919e5	0.491391	0.00945
164	67.93	5.89	5.68	-753.29	0.0180	-0.002	0.0205	0.0055	0.015	4.8548e-5	6.1909e-5	-1.4117e6	0.866880	0.00923

Notes: * Small changes in specimen dimensions measured after fracture by re-assembly of test pieces can result in small errors, giving negative data points for notch height change values or change in AD values.
The letter 'e' donotes a power of 10 multiple indicated.

3.21 Section 3, Appendix 8
Slow Strain Rate Test Data for Tuna Brine Samples Tested under Nitrogen Flushing Conditions.

Sample ssrtTu number	Time to failure: (hours)	pH start	pH end	OCV (Millivolts) vs N/10 calomel electrode	Delta BC* (cm)	Delta BC_{corr}* (cm)	Delta HG (cm)	Delta HG_{corr}* (cm)	Delta AD (cm)	E_{rms1} (Volts)	I_{rms1} (Amps/cm^2)	Ia_1 (Log_{10} current density (amps/cm^2)* time (secs)	Mechanical Work. M. (N.m)	Gauge (ins)
134	47.47	5.87	5.81	-774	0.0195	0.0080	0.0270	0.0145	0.0145	4.5221e-5	1.6123e-5	-9.0768e5	0.368467	0.0072
135	46.64	5.87	5.84	-778	0.0240	0.0140	0.0255	0.0155	0.0325	4.3177e-5	1.8590e-5	-9.7417e5	0.403648	0.0071
136	46.54	5.87	5.84	-774	0.0290	0.0115	0.0150	0.000	0.045	4.0809e-5	3.0397e-5	-9.3792e5	0.441600	0.00715
137	45.38	5.87	5.84	-774	0.0285	0.0165	0.0220	0.010	0.063	6.2274e-5	2.1104e-5	-6.6434e5	0.398025	0.0071
138	42.54	5.80	5.87	-772	0.0220	-0.0090	0.0180	0.006	0.043	5.4635e-5	6.2511e-5	-7.2123e5	0.377454	0.0072
139	48.15	5.86	5.86	-775	-0.0020	0.000	0.0120	0.004	0.002	4.3739e-5	4.6897e-5	-9.3866e5	0.427728	0.0072
140	58.56	5.86	5.76	-775	0.0330	0.0210	0.0305	0.0075	0.033	1.0203e-4	8.8664e-6	-1.2552e6	0.593408	0.0094
142	59.06	5.93	5.80	-774	0.0435	0.0170	0.0230	-0.003	0.0645	5.3746e-5	1.2091e-5	-1.0707e6	0.739487	0.00943
145	55.51	5.86	5.84	-785	0.0220	0.0060	0.0330	0.030	0.032	4.7327e-5	8.9726e-6	-1.0127e6	0.489314	0.0095
146	40.81	5.88	5.90	-764	0.0270	0.0125	0.0165	-0.0025	0.025	4.3788e-5	6.5789e-5	-7.8110e5	0.285318	0.00625
147	47.24	5.88	5.66	-770	0.0270	0.0985	0.0155	0.006	0.0285	4.4616e-5	9.5550e-5	-8.4195e5	0.366741	0.0062
148	55.86	5.99	5.71	-772	0.0225	0.0100	0.0135	0.0035	0.0390	3.8201e-5	6.0277e-5	-1.0452e6	0.380439	0.0062
149	34.68	5.84	5.77	-767	0.0160	0.0095	0.0025	-0.0055	0.0380	3.6047e-5	4.1586e-5	-4.2060e5	0.100959	0.00625
150	34.70	5.91	5.86	-769	0.0140	0.0090	0.0125	-0.008	0.005	5.5685e-5	1.6729e-4	-6.0878e5	0.151734	0.00623
151	34.67	5.87	5.79	-770	0.0070	0.0070	0.0195	0.0015	0.006	4.8310e-5	1.2531e-4	-5.4296e5	0.141015	0.0063

* Small changes in specimen dimensions measured after fracture by re-assembly of test pieces can result in small errors, giving negative data points for notch height change values or change in AD values.

The letter 'e' donotes a power of 10 multiple indicated.

3.22 Section 3, Appendix 9
Slow Strain Rate Test Data for Salmon Brine Samples Tested under Air Conditions.

Sample ssrtsal number	Time to failure: (hours)	pH start	pH end	OCV (Millivolts) vs N/10 calomel electrode	Delta BC* (cm)	Delta BC_{corr}* (cm)	Delta HG (cm)	Delta HG_{corr}* (cm)	Delta AD (cm)	E_{rms1} (Volts)	I_{rms1} ($Amps/cm^2$) .	Ia_1 (Log_{10} current density (amps)* time (secs)	Mechanical Work. M (N.m)	Gauge (ins)
0203	39.77	6.29	6.15	-791	0.0255	0.0140	0.0195	0.0105	0.0220	6.6878e-5	1.4713e-4	-7.1023e5	0.231924	0.0060
0204	37.34	6.40	6.27	-769	0.0135	0.0040	0.0265	-0.0005	0.0145	6.2140e-5	1.0942e-4	-7.2316e5	0.217848	0.00595
0205	36.74	6.33	6.13	-774.04	0.0085	0.0040	0.0150	-0.004	0.0235	5.5990e-5	1.3556e-4	-7.0696e5	0.157620	0.0060
0206	34.87	6.33	6.22	-765.75	0.0255	0.0120	0.0015	-0.0015	0.0290	5.8758e-5	1.0357e-4	-6.6971e5	0.121102	0.00595
0207	31.87	6.28	6.10	-769.40	0.0025	-0.0035	0.0085	-0.001	0.0005	5.6244e-5	2.3400e-4	-5.6285e5	0.131532	0.0060
0209	39.50	6.36	6.08	-765.50	0.0145	0.0085	0.0310	-0.0025	0.0100	5.8458e-5	1.1182e-4	-7.6455e5	0.264152	0.0068
0210	38.66	6.25	6.04	-776.65	0.0260	0.0260	0.0140	0.001	0.0290	1.2986e-4	9.5608e-5	-7.6450e5	0.247097	0.0069
0211	35.57	6.23	6.00	-771.23	0.0065	0.0005	0.0168	0.0043	0.0130	4.9444e-4	1.6913e-4	-5.6784e5	0.204990	0.0069
0212	70.16	6.23	6.10	-768.60	0.0345	0.0200	0.0185	0.0115	0.0510	1.2177e-3	1.3677e-4	-1.3088e6	0.597918	0.00695
0213	34.94	6.30	6.00	-766.44	0.0005	-0.0060	0.0360	0.0035	-0.0005	5.5011e-5	8.0984e-5	-6.7660e5	0.172347	0.00693
0216	68.57	6.32	6.02	-769.24	0.0255	0.0205	0.0350	0.0280	0.3145	1.3520e-4	2.4069e-4	-1.1198e6	0.651063	0.0092
0218	41.14	6.37	6.00	-770.27	0.0125	0.0070	0.0040	0.001	0.0240	7.5107e-5	2.0171e-4	-6.8871e5	0.392890	0.00913
0221	53.90	6.39	6.16	-785.75	0.0240	0.0185	0.0340	0.006	0.0120	4.4951e-5	8.6049e-5	-6.6231e5	0.454518	0.0092
0222	44.97	6.33	6.02	-776.62	0.0185	0.0130	0.0260	0.0015	-0.0005	7.2768e-5	1.0127e-4	-8.4310e5	0.432077	0.00919

* Small changes in specimen dimensions measured after fracture by re-assembly of test pieces can result in small errors, giving negative data points for notch height change values or change in AD values.

The letter 'e' donotes a power of 10 multiple indicated.

3.23 Section 3, Appendix 10

Slow Strain Rate Test Data for Salmon Brine Samples Tested under Nitrogen Flushing Conditions.

Sample ssrtsal number	Time to failure: (hours)	pH start	pH end	OCV (millivolts) vs N/10 calomel electrode	Delta BC* (cm)	Delta BC_{corr}* (cm)	Delta HG* (cm)	Delta HG_{corr}* (cm)	Delta AD (cm)	E_{rms1} (Volts)	I_{rms1} (Amps/cm^2)	Ia_1 (Log_{10} current density (amps/cm^2)* time (secs)	Mechanical Work. M. (N.m)	Gauge (ins)
223	37.48	6.38	6.01	-793.29	0.005	0.003	0.0475	0.0105	0.1705	4.2128e-5	6.3080e-5	-7.2392e5	0.262763	0.0069
224	39.91	6.33	6.08	-784.54	0.0225	0.0155	0.026	0.0195	0.0365	9.4497e-5	1.2452e-4	-7.8159e5	0.326707	0.0069
225	33.68	6.42	6.10	-794.90	0.0145	0.0075	0.0285	0.0045	0.010	7.6757e-5	5.2766e-5	-5.5223e5	0.252958	0.00681
226	38.88	6.35	6.13	-778.00	0.0160	0.0065	0.0195	0.0035	0.3020	7.6287e-5	9.7497e-5	-6.5282e5	0.358125	0.00685
228	53.04	6.40	6.02	-783.60	0.0180	0.010	0.0205	0.0060	0.0095	5.8988e-5	1.2223e-4	-9.7212e5	0.334125	0.00693
230	39.07	6.43	6.16	-773.16	-0.0135	-0.028	0.0190	-0.0025	0.0290	3.9246e-5	1.5776e-4	-6.9556e5	0.258965	0.00591
231	33.35	6.38	6.10	-776.00	0.022	0.0045	0.0160	0.0005	0.0260	5.9111e-5	1.2225e-4	-6.4055e5	0.250245	0.00595
232	34.81	6.45	6.15	-772.50	0.0115	0.0065	0.022	0.0120	0.0055	3.8412e-5	9.3925e-5	-8.0437e5	0.276642	0.00599
233	39.41	6.37	6.14	-776.00	0.0205	0.0155	0.0130	0.0060	0.0315	1.2832e-4	1.5781e-4	-7.6542e5	0.333060	0.00598
235	38.57	6.35	6.16	-770.90	0.025	0.007	-0.0005	-0.0045	0.032	6.0424e-5	2.2319e-4	-6.0157e5	0.360355	0.0060
236	64.66	6.40	6.14	-777.54	0.0285	0.017	0.0155	0.0035	0.0235	4.0343e-5	6.9077e-5	-1.1603e6	0.858050	0.00905
237	61.29	6.37	6.10	-778.15	0.032	0.0220	0.0135	0.0090	0.0260	6.9006e-5	3.3095e-5	-1.3327e6	0.838823	0.00906
238	48.98	6.38	6.33	-782.32	0.030	0.0200	0.0300	0.0090	0.0290	4.6993e-5	8.1786e-5	-9.2209e5	0.580106	0.00908
239	63.61	6.50	6.28	-783.845	0.031	0.0215	0.026	0.0100	0.0350	4.1830e-5	1.1017e-4	-1.3416e6	0.796875	0.00915
240	53.94	6.55	6.14	-784.780	0.0255	0.0175	0.029	0.0030	0.0180	3.9851e-5	4.1604e-5	-1.2196e6	0.740745	0.00929
241	56.90	6.51	6.51	-782.38	0.0185	0.0130	0.0065	-0.0005	0.0020	5.3498e-3	2.3152e-4	-1.1597e6	0.742224	0.00910

* Small changes in specimen dimensions measured after fracture by re-assembly of test pieces can result in small errors, giving negative data points for notch height change values or change in AD values.

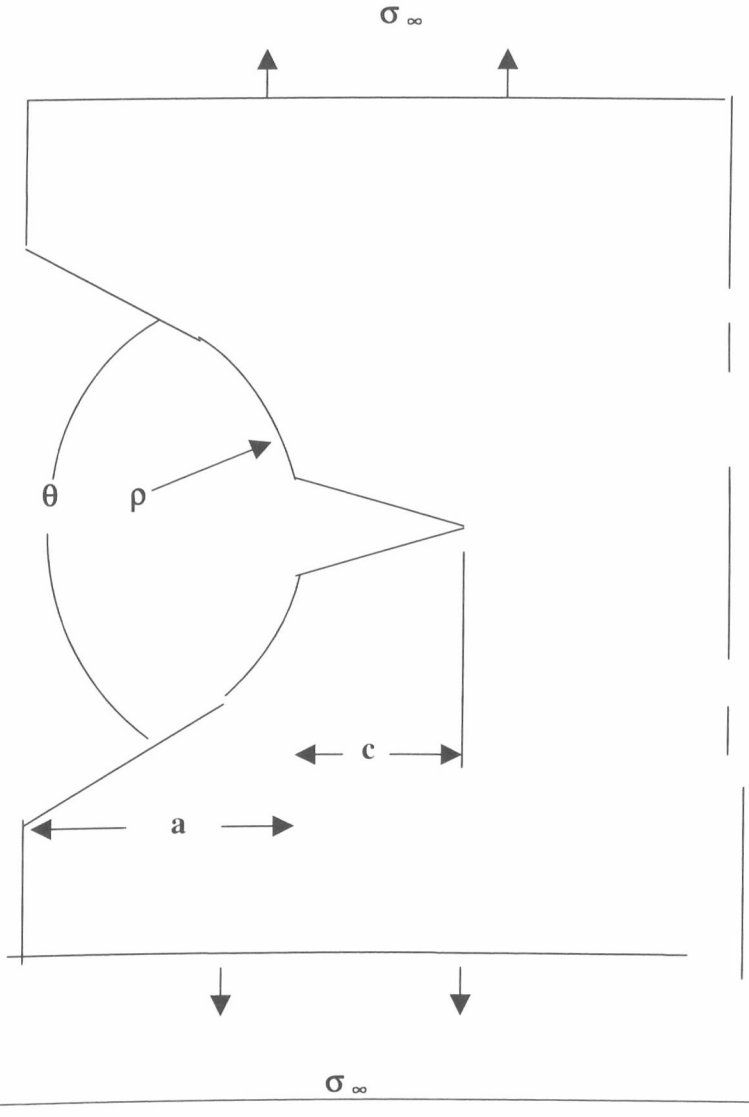
The letter 'e' donotes a power of 10 multiple indicated.

3.24 Section 3, Appendix 11, Page 1 of 3

Environmental Stress Cracking Studies .

Notch detail and Stress Intensity Factor estimations for Partially Cracked Specimens on Steels Tested in Tuna Brine under Air Conditions.

Notch detail related to calculations on Page 2 of 3



Calculation of Stress Intensity Factor Estimates - K_I

Tuna in Brine : Air Samples : Partially Cracked.

Sample number	a: mm	c: mm	(a+c): mm	c/a	Plate thickness: mm	F4	Area of cross section mm^2	Maximum tensile load, P : KN.
115	1.06	2.376	3.436	1.316	0.1854	1	1.88181	0.755
118	1.06	2.048	3.108	1.932	0.1842	1	1.86973	0.650
120	1.06	0.552	1.612	0.521	0.23876	1	2.423414	0.940
121	1.06	0.2855	1.3455	0.269	0.2431	1	2.449195	0.879
123	1.06	1.392	2.452	1.313	0.24003	1	2.43915	0.991
125	1.06	2.850	3.91	2.689	0.2388	1	2.4239	0.992
128	1.06	0.80	1.86	0.755	0.15951	1	1.61903	0.896
129	1.06	0.3235	1.3835	0.305	0.1590	1	1.61395	0.770

Sample number	Stress:σ N/mm2	π(a+c): mm	$\sqrt{\pi(a+c)}$	$K_I = F4 * \sigma_\infty * \sqrt{\pi(a+c)}$ $N.mm^{-3/2}$	Mechanical Work Estimate to maximum load: ½ * P* extension: N.m
115	401.21	10.7989	3.28616	1318.440	0.558400
118	347.64	9.768	3.12538	1086.510	0.401760
120	387.88	5.06628	2.25084	873.060	0.343602
121	358.89	4.2287	2.0564	738.021	0.436424
123	406.29	7.70628	2.7760	1127.860	0.472280
125	409.26	12.28857	3.5505	1434.661	0.688448
128	553.42	5.84571	2.4178	1338.060	0.597710
129	477.09	4.34814	2.08522	994.838	0.554785

Geometric Correction Factor F4 : Details for use in the calculation of Stress Intensity Factor.

For the 90 degree notch, used F4 approximated to 1.

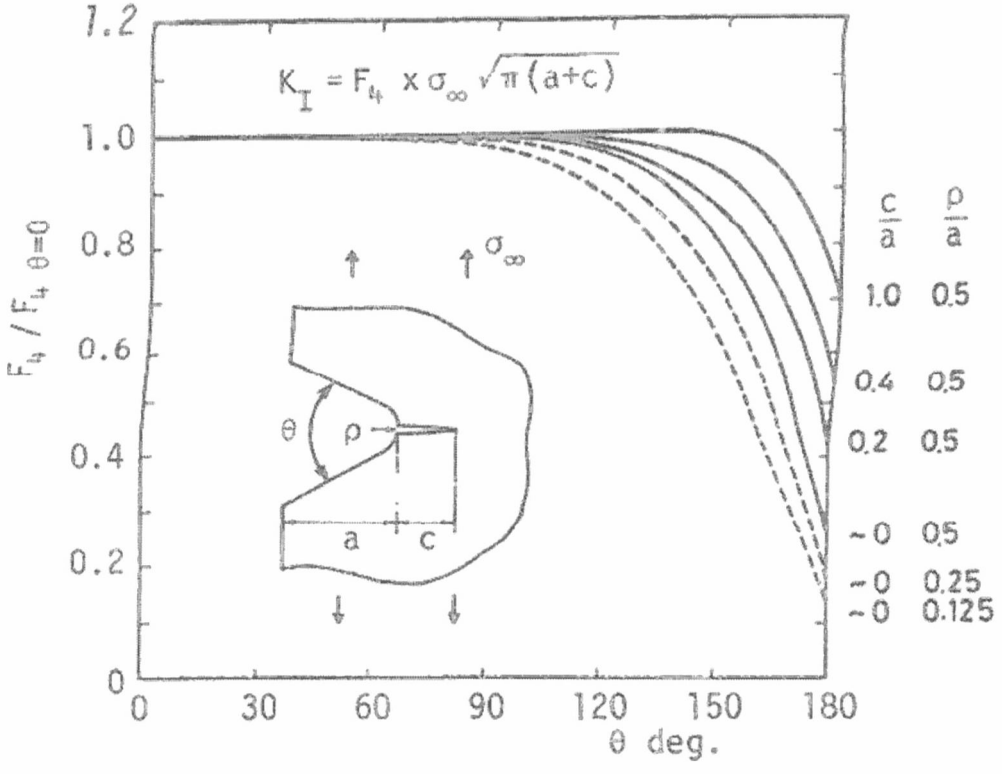


Fig. $F_4/F_{4\,\theta=0}$ as a function of θ

4 Section 4: Conclusions and Recommendations

4.1 Conclusions.

4.1.1. The theoretical mechanism of failure involving cans of fish or meat products involves the initiation of localised corrosion at stressed regions in lacquered cans, which are likely to have either some sites of metal exposure, or points of relative weakness in the protective system. The localised corrosion leads to occluded cells which give rise to acidification. Subsequently hydrogen entry into the steel would be promoted by catalytic hydrogen recombination poisons. Prior work[1-3] had considered mechanisms and included discussion of hydrogen sulphide with some data, but did not explicitly state 'hydrogen embrittlement' as the cause of failures. Other limited lab test work on meat products[9] had reported indications of hydrogen embrittlement.

4.1.2. The present study has generated the following evidence from lab test work to support the theoretical mechanism.

a) Loss of ductility accompanied by regions of transgranular brittle cracking was observed in eccs DR 620CA plates subjected to slow strain rate tests in drained tuna or salmon brines, but with more substantial evidence for salmon brine. The tests were performed at the open circuit voltage, using sub groups including air and nitrogen flushing conditions for respective products.

b) Localised corrosion observed ahead of the notch apex preceded the cracking. Pitting loops showed positive hysteresis of the anodic sweeps for both tuna and salmon brines, consistent with a pitting tendency.

c) In the case of salmon brine, all three types of eccs DR620CA steels were found to show regions of brittle cracking under both aerated and nitrogen flushed test conditions, while the evidence for the tuna product was more limited.

d) Loss of ductility measured using notch thickness data, indicated mean thickness reductions of 11-28 % at the crack initiation notch after tests in product brines. The variability of this data was higher for tests under nitrogen flushed conditions than for air conditions. These values compared with approximately 80% mean thickness reduction for similar tests in pure food oil as controls.

e) The failures were of a partially brittle nature over approximately 1mm running from the notch fracture initiation, and typically displayed increasingly ductile conditions away from this region, both along the specimen width and through the thickness. Such effects are characteristic of a hydrogen embrittlement or a 'delayed failure' embrittlement mode.

f) The load-extension plots from slow strain rate tests were essentially linear up to the point of maxumum load, after which a sharp fall in load was observed preceding the failure, the indication being that crack initiation took place at a late stage of the test, probably under the maximum load condition.

g) Potetio-dynamic polarisation curves at fast and slow sweep rates did not provide any clear evidence of active-passive behaviour on the anodic sweep, normally associated with stress corrosion cracking, although some 'arrests' in the plots were noted.

h) Analytical work showed that in addition to phosphate anion which has been associated with loss of ductility in carbon steel, [15,16] low levels of the catalytic hydrogen recombination poisons[33] arsenic and selenium were present, as well as zinc which promotes hydrogen entry into steel. Elemental phosphorus is also mentioned [33] in the same context. The literature search also indicated that the breakdown products of cystine[25] can lead to generation of hydrogen sulphide which acts as a catalytic hydrogen recombination poison. Hydrogen gas was also measured in cans of both product types used to prepare the product brines.

This study has therefore provided strong evidence to support the occcurrence of a hydrogen embrittlement mechanism leading to failures in eccs steel or tinplate fish cans.

4.1.3 Regarding the generation of component strains and stresses in manufacture, lab test work[76-78] preceding this study showed that material strains leading to necking e.g. at end countersink regions, causing around 8% plate thickness reduction, enhanced the risk of failure in DR520CA eccs plates. Laboratory work[78] involving DR620CA plates indicated that around 10% 'necking' at the countersink region showed measurably increased failure risk, relative to around 4% gauge reduction. Apart from any effects on the organic coating and metal exposure level, high 'necking' strains would be consistent with a tendency to the generation of voids around 2nd phase particles, which could then provide sites for nucleation of hydrogen gas and cracking failure. This may be a factor contributory to the uncertain predictibility of this failure type, and is suggested as a subject area for further study to reduce material related risks. Also, it may help to explain some earlier observations to the effect

that increasing 'plasticity reserve[2]' improved resistance to cracking. No obvious hydrogen blisters were seen during slow strain rate tests in this study. While these might not be observed with very high temper materials, the influence of other decohesion mechanisms[50] involving hydrogen is not ruled out.

4.1.4 Correlation and Regression studies involving the physical and electrochemical parameters of the slow strain rate tests for salmon and tuna brines from the main experimental programme, Section 3, showed that two parameters figured very prominently and consistently, namely.

a)Mechanical Work : M1(The estimated area under the load extension plot up to the maximum load).

b)The Integrated Current Density – Time parameter, Ia_1, comprising the area under the Log_{10} Current – time plot, up to the point of maximum load.

Significant regression relationships for these parameters with time to failure could be derived for all four main test groups of salmon and tuna brines under air and nitrogen flushing conditions. All of these cases achieved statistical R^2 adjusted values for respective regressions of over 80%.

The integrated current parameter, Ia_1, showed and inverse 'negative' relationship with failure time. The influence of this parameter was interpreted on the basis that increasing current densities will be expected to be associated with relatively lower test failure times and vice versa, with this parameter acting as a parallel influence to Mechanical Work. It should be emphasised that the failures displayed only a partially brittle condition. If very large currents were observed, these would lead to positive values of the Ia_1 parameter, with an anticipated true inverse effect on test time, but this would be subject to the same correlation being maintained with failure time as has been observed in this work.

The overall statistical fit test for regression with time to failure for these two parameters combined was not satisfactory, except for one sub group (Tuna brine, air conditions) the test indicating evidence of curvature where lack of fit was identified. For the individual candidate regressions selected from the best subsets test in Section 3, satisfactory fits were obtained for the 4 sub groups comprising product type and air or nitrogen flushing conditions, when either one or both of the above key parameters were selected in conjunction with other predictors, but with some inconsistencies noted in the signs of the coefficients of the additional parameters between regression candidates.

4.1.5. Regarding the initial experimental slow strain rate test work involving Tuna Brine, Section 2, the main data on which regressions for time of test could be examined concerned Tuna Brine acidified with acetic acid. The principle finding was that $Erms_2$ (potential noise distribution) was a candidate predictor for time of test for 'non scratched' specimens. For the category of tests where specimens were purposely 'scratched' across one specimen face at the notch region, specimen extension was dominant as a regression predictor for time of test, and electrochemical factors became weak predictors. This was thought to be because of the wider distribution of corrosion effects across the specimen width at the scratch, and there was some increase in mean failure time. However, degrees of loss of ductility and environmental stress cracking effects were detected among both 'non scratched' and 'scratched' samples. At an early stage in pilot studies it had been observed that the introduction of a sharp scratch across one face of the eccs plate sample running from the notch using a scribe did appear to contribute to the occurrence of SCC with tuna brine, but the later systematic tests in Section 2 were carried out with a purpose made scratching tool giving a wider scratch with perhaps less locally intense effects. The use of acidified test media was limited to Section 2 studies, and to achieve a reconciliation of predictive effects between acidified and non acidified media would require further work.

4.1.6. Three types of commercial double reduced (DR 620) continuously annealed electro chrome coated steel plates were used in the main experimental programme, Section 3, namely, a drawing quality 0.16mm material, a stamping quality 0.18mm plate, and a nitrogenised stamping quality 0.235mm plate. Each showed evidence of environmental stress cracking when subject to slow strain rate tests with salmon brine under air or nitrogen flushing conditions. If the generation of voids around second phase particles was an effect critical to this form of failure, it would help to explain why continuous straining can be a very severe test in practice. Constant load testing over long time periods as an alternative was not thought practical with perishable foods, but may be viable with synthetic media.

4.1.7.From the tensile test behaviour of the three plate types used, the indications were that two materials, the 0.16mm DR620CA drawing steel and the 0.18mm DR620CA stamping grade material, approximated to elastic- perfectly plastic conditions up to the stage of severe necking immediately prior to fracture. For the 0.235mm DR620CA nitrogenised material, a negative slope observed on the tensile plot within a small strain increment after yielding was not overcome by attempts made to estimate the true stress- strain plot. Elongation values for each material were all relatively low e.g. at around 1.6% or less , based upon an 80mm gauge length, so that risks of necking behaviour in fabrication are likely to exist, and especially if any manufacturing aspects were out of control. Evidence accumulated prior to and during deductions from this study, has emphasised the importance of minimising 'necking' effects to reduce potential failure risks.

4.1.8. Finite element stress predictions were made for notch tensile specimens for each plate used, and repeated for selected plates in a drawn redrawn can model and for the forming of an easy open end shell.

Because the Finite Element Modelling process is likely to be highly sensitive to the fine detail of conditions defined by individuals, and the accuracy of the material properties, it is safer to use the information generated on a comparative basis with one or other form of 'control' system or test. On this basis, the present work gave the following indications:

a) The tensile models for notched specimens could predict peak stresses at the notch associated with failure for standard dog-bone tensile samples, variously to between 13% and under 2% of true stress values estimated for the materials used. This depended on estimation of plastic fracture strain values using either the Erichsen method, or a strain determination from a notched tensile sample.

b) For the drawn re-drawn can formation, significant tensile stresses were predicted at the bottom inner reverse wall and at the inner countersink region of the base in the hoop direction, S33.

c) For the easy open end shell formation, the peak predicted tensile stresses were primarily at the countersink wall and radius region, either in the hoop direction, S33, or the 'y' direction, S22.

Some of the finished component stress predictions showed values above the yield stress of the materials, which were in conflict with literature[43] stating that residual stresses are relieved if they exceed the yield stress. Further work concerning this aspect will be needed.

4.2 Recommendations

Steps towards more effective prevention of this form of can failure are the investigation of:

1. Optimisation of the material and tool aspects to minimise 'necking' at key strain points in cans or ends.

2. Measures to avoid abnormal sources of stress in handling and shipping, such as bottom rim denting of 2 piece cans, excess stacking loads and /or cyclic loads during shipment, overhangs on pallets, and avoidance of residual in can pressures involving e.g. animal foods (carbon dioxide pressures). Prepare a Best Practice Document.

3. Can protection aspects. Prevent under-cured coatings, and local score marks at regions of significant forming stress.

4. Examination of the relationship between the second phase particle distribution, density and grain structure in steel, with strain and susceptibility to cracking in adverse environments. Identify the most advantageous structure to use from available options.

5. Use the notched tensile slow strain method to attempt to identify lower risk conditions through material or notch angle changes which reduce stress concentration, with parallel finite element prediction of stresses. Plate thickness reduction at the notch after failure is one indicator of locally brittle or ductile behaviour.

P.J.Smith

28th July 2010

5 Acknowledgements.

The support and help from the following people is acknowledged and appreciated.

1. To my supervisor, Professor Hocking, for training and guidance and very helpful discussions.
2. To Toby Ashton, Rachel Hayes and Gwen Wixey, Crown CT, for training and guidance on SEM.
3. To Rachel Hayes of Crown CT for XRA scan support.
4. To Martin Watson of Crown CT and Stephen King of Simulia for Training and guidance on FEA Modelling.
5. To Dr Paul Butler, Crown CT, for his support in enabling me to undertake this work, and helpful discussions.
6. To Dr Mike Cochran, Crown CT for many helpful discussions on Biochemistry and Corrosion over many years.
7. To my Manager, Alex Dachs, Crown CT, for his ongoing support, interest and reviews of the documentation.

This work took place over ten years mostly during evenings and weekends.

6 Reference List

Number	Detail
1	M. Tsurumaru, K Masuda and Y Yamamoto; Proceedings of 5th International Tinplate Conference, London, 1992, Paper 19, P222.
2	J Nekvasil and J Pitter: proceedings of 5th International Conference, London, 1992, Paper 17, Page 190.
3.	C D Kim and E J Helwig; Stress Corrosion Cracking of Tinplate and other Tin MillProducts; evaluation of Tinplate Performance in Petfood ; Proceedings of 5th International Tinplate Conference, London, 1992, Paper 20, P236.
4.	C J Cron ,JH Payer and RW Staehle; Dissolution Behaviour of Fe/Fe_3C structures as a function of pH, Potential and Anions; An electron Microscopy Study. Corrosion, vol 27, 1971.
5.	R N Parkins in : Corrosion 3rd Edition, Edited by Shreir, Jarman and Burstein, P 8.34- 8.35. (1994)
6.	C. Exartier; Arcelor Internal Report on Stress Corrosion Cracking in Food Cans: May 2002.
7.	L. Schutte; Precursors of Sulphur Containing Flavour Compounds; Critical review; Food Technology, vol 14, P457-505, 1974.
8.	Alan H Varnam and Jane P Sutherland; in Meat and Meat Products, Technology Chemistry and Micobiology , 5th edition (1995), P169-170 Cured meats; Chapman and Hall.
9	R Newman; Stress Corrosion of Welds in Cans: Laboratory Report dated March 1993, concerning tests on Chicken in Brown Sauce and Steak and Onion Casserole; UMIST Corrosion and Protection Centre.
10.	Fox and Cameron; Food Science , Nutrition and Health, 6th Edition, P184, 1995. (Edward Arnold)
11.	C E Bodwell and PE McClain in: The Science of Meat and Meat Products , 2nd edition, PP93-99, edited by JF Price and B Schweigert, WH Freeman and Company San Francisco ISBN0 7167-0820-5, 1970.
12.	R.N Parkins in Corrosion, 3rd Edition, edited by Shreir , Jarman and Burstein;Vol 1, P 8.20 (1994) (Butterworth Heineman.)
13.	Metals Handbook, 9th edition , Vol 13; Corrosion, P152, ASM International.
14.	M Henthorne and R.N. Parkins;. Some aspects of the Influence of Structure Upon Stress Corrosion Cracking and Grain Boundary Corrosion in Mild Steel; Br Corrosion Journal, Vol 2, P186, September 1967.
15.	R. N. Parkins, N. J.H. Holroyd and R. R. Fessler, Stress Corrosion Crackin of Carbon steels in Phosphate Solutions; NACE,Vol 34, No 8, Aug 1978.
16.	N.R.Smart, P.M. Scott, and R.P.M. Proctor. Re-passivation Kinetics and Stress Corrosion of Mild Steel in Phosphate Solutions : Corrosion Science , Vol 30, No 8/9, P877-901,1990.
17.	J.M. Sutcliffe , RR Fessler, W.K. Boyd, and R.N. Parkins. Stress Corrosion Cracking of Carbon Steel in Carbonate Solutions : Corrosion: NACE, Vol 28, P312-320 (1972).
18.	R.N. Parkins and R Usher. Journal of Applied Chemistry, 9, P445 (1959).

Number	Detail
19.	M Kohawa and S. Negata, Trans-granular Stress Corrosion Cracking of Mild Steels and Low alloy Steels in the H_20-CO-CO_2 system. Corrosion, NACE, No 12 , P427-428.
20.	R. Levermore e mail report on Gas Chromatography Sulphur Analyses in Canned Foods, dated 18.06.03.
21.	Kane , Wilhelm and Oldfield ; Review of Hydrogen Induced Cracking of Steels in Wet H_2S Refinery Service. Proceedings of the International Conference on Interactions of Steels with Hydrogen in Petroleum Industry Pressure Vessel Service, Paris , 1989,P7-15(Published in 1993).
22.	Germit N. Buchheim; Exon Research and Engineering Company; Florham Park New Jersey, Article in Oil and Gas Journal July 9, 1990, based upon Paper presented at the National Petroleum refiners association refinery and Petrochemical plant Maintenance Conference, May 23-25, 1990.
23.	M Elboujdaini in Uhlig's Corrosion Handbook 2nd Edition, Chapter 12, P 205-214, (2000).
24.	Jeorg Gutzeit(Amoco Research Centre): Cracking of Carbon Steel Components in Amine Service; Article based upon Paper presented at the NACE Western Canada Regional Meeting, Calgary, Alberta, Feb 20-23,1990; published in Materials Performance, vol 29, 9, p154-157, 1990.
25.	J. Bjarnasson and K. J. Carpenter: Mechanisms of Heat Damage in Proteins, 2, Chemical Changes in Pure Proteins; British Journal of Nutrition; vol 24, 1970 P313-329.
26.	Scholberl, A (1941) Chem. Ber.74B,1225.
27.	Scholberl, A and Eck, H (1936). Justus Liebigs Annln Chem.522, 97.
28.	John M. Deman: Principles of Food Chemistry: 3rd edition, 1999 (Aspen), pages 120-128
29.	Alan H. Varnam and Jane P Sutherland; Cooked Meat and Cooked Meat Products; Chemistry, Chapter 6 Pages 259-260 in Meat and Meat Products, Technology Chemistry and Micobiology, 5th Edition (1995),(Chapman and Hall).
30.	Price J.F. and Schweigert, BS (eds)(1987) The Science of Meat and Meat Products, food ansd Nutrition Press, Wesport,CT.
31.	Maurice E Stansby: Proximate Composition of fish, in : Fish in Nutrition; International Congress , Washington DC , 1961, Edited by E Heen and R Kreuzer, published by fishing News(Books)Ltd, 1962.
32.	The Composition of Foods; McCance and Widdowson, Sixth Summary Edition; The Royal Society of Chemistry, Cambridge, 2002, ISBN 0-85404-428-0.
33.	U.R.Evans: the Corrosion and Oxidation of Metals, Edward Arnold , 1960, pages 394-404.
34.	H.O.Hultin; Chapter 5, Oxidation of Lipids in Sea-foods, P49 in: Seafoods ; Chemistry , Processing , Technology and Quality, Edited by F Shahidi and J.R Botta; First edition ,1994.
35.	C.D.Kim and E.J.Helwig: Stress Corrosion Cracking of Black Plate Contaminated in Ethyl Alcohol, The Chemical Packaging Review, 1991, **2,** No 2 PP30-33.

Number	Detail
36.	Richard W Hertzberg: Deformation and Fracture Mechanics of Engineering Materials:, 4th edition; Wiley, (1996) PP315-321.
37.	G.N. King and RA Jarman: Outline of Fracture Mechanics in: Corrosion , 3rd Edition, Edited by Shreir, Jarman and Burstein, Vol 1 P8: 218-8: 214. (1994).
38.	R.N.Parkins : Mechanisms of Stress Corrosion Cracking; in Corrosion , 3rd Edition, Edited by Shreir, Jarman and Burstein, Vol 1 P8.1-8.29. (1994).
39.	Rice JR : A Path Independent Integral and Approximate Analysis of Strain Concentration by Notches and Cracks. Journal of applied Mechanics: June 1968 p379-386 (Trans ASME).
40.	N J Petch : The Cleavage Strength of Poly-crystals: Journal of the Iron and Steel Institute, vol174, P25-28 (1953).
41.	Petch NJ and Stables P: Delayed Fracture of Metals under Static Load; Nature , vol 169, pp842-843, 1952.
42.	Jian Lu et Al : Handbook of Measurement of Residual Stresses, Society for Experimental Mechanics, Fairmount Press, (1996) Chapter 5: X ray Diffraction Method, PP71-133.
43.	George E Dieter ; Mechanical Metallurgy, Mcgraw Hill, 1961, P393-418.
44.	A Review of The Finite Element Method: Abaqus Manual, 6-5 Getting Started; P 1-13 to1-18.abaqus , Inc 2004.
45.	R.N. Parkins, PW Slattery and B.S. Poulson; The effects of alloying additions to Ferritic Steels on Stress Corrosion Cracking resistance; NACE; Corrosion Vol 37, P650-664, 1981.
46.	J. Haggman : The Role of hydrogen in The Corrosion of Tinplate Cans : The Proceedings of The 2nd International Tinplate Conference, London , (1980) paper 36: PP400-405. International Tin Research Institute.
47.	W. Hume Rothery: The Structure of Alloys of Iron: An Elementary Introduction; 1st Edition , (1996), Pergammon Press Ltd, P49 : Grain Boundary Structure and Segregation.
48.	S Harada, Kochizuki, and Ban , Kawasi Steel Corporation, Japan; the effect of surface enriched elements in killed steel on Tinplate Corrosion Resistance; Proceeding of the 2nd International Tinplate Conference 1980paper No 29 pages 316-
49.	PR Swann: dislocation substructure vs Trans-granular Stress Corrosion Susceptibility of Single Phase Alloys; Corrosion; Houston Texas vol 19, PP102-112 (1963).
50.	A R Troiano: The role of Hydrogen and other Interstitials in The Behaviour of Metals: Trans ASM , vol 52, PP54-80 (1960).
51.	E.G. Coleman, D Weinstein and W Rostoker: On a Surface Energy Mechanism for Stress Corrosion Cracking; Acta Metall, vol 9 , PP491-496 (1961).
52.	A.N. Stroh : The Formation of Cracks in Plastic Flow; Proceedings of the Royal Society ;Vol 232, PP548-560, 1955.
53.	E.H.Dix, Acceleration of the Rate of Corrosion by High Constant Stresses. Trans American Institute of Min and Met Engineers, vol 137, PP11-40 (1940).

Number	Detail
54.	M Pourbaix: Localised corrosion behaviour and Protection Mechanisms; Corrosion Chemistry within Pits Crevices and Cracks, edited by A Turnbull. NPL Conference Proceedings Oct 1984.
55.	J.C. Scully: The Electro Chemical Parameters of Stress Corrosion Cracking; Corrosion Science , vol 8, Pp513-523 (1968).
56.	R.N Parkins: Factors Influencing Stress Corrosion Crack Growth Kinetics: Corrosion ; NACE; vol 43,no3, March 1987
57.	Y.-Z Wang Corrosion Fatigue in : Chapter 13 PP 221-232: Uhlig's Corrosion Handbook, 2nd Edition, edited by R Winston Revie, John Wiley, (2000).
58.	P.M.Scott; Corrosion Fatigue, Chapter 8.6, Pages 8.143-8.180 in Vol 1, Corrosion, 3rd Edition, Edited by Shreir, Jarman and Burstein;// Butterworth Heinemann, 1994. ISBN 0-7506-1077-8
59.	R.N. Parkins; Stress Corrosion Spectrum: British Corrosion Journal,Vol7, PP15-28, 1972.
60.	R.B.Hughes; Journal of Science of Food Agriculture, vol 15, May 1964, PP290-292.
61.	V.S.Sastri; An Overview of Corrosion Inhibition, Chapter 3, PP 39-40. In :Corrosion Inhibitors, Principles and Applications, John Wiley, 1998, 54.
62.	IL Finar , Organic Chemistry 5th edition, 1967, Thioephene, PP 790-792.
63.	G Marc Loudon , Organic Chemistry, 3rd Edition, 1995,Organic Sulphides PP343-345, ISBN0-8053-6650-4.
64.	JGN Thomas, The Mechanism of Corrosion Prevention by Inhibitors, P17.41 in Corrosion 3rd Edition , edited by Shreir, Jarman and Burstein, 1994.
65.	Weast, Handbook of Chemistry and Physics, 61st Edition , 1980-1981. Physical Constants of Organic Compounds., Section C.
66.	B. Sun Pan and J. –M. Kuo section 7.3.3 ; Sulphur Containing Compounds PP103-104 in : Seafoods : Chemistry , Processing , Technology and Quality, 1st Edition, Edited by F Shahidi and J.R.Botta, Blackie Academic and Professional, Chapman and Hall, 1994.
67.	J. M.West; A general Model for Stress Corrosion Crack Propagation; Metal Science Journal, 1973, Vol 7, PP169-172.
68.	Richard W. Hertzberg ; Fracture Toughness Determination and Elastic-Plastic Analysis with The J Integral; section 8.11, PP359-369 in : Deformation and Fracture Mechanics of Engineering Materials, 4th Edition, John Wiley 1996. also : Hydrogen Embrittlement Models: Section 11.1.1 PP 488-492.
69.	George E Dieter, Jnr, Section 19-10. Residual Stresses in Rolled Products, Chapter 19 in : Mechanical Metallurgy, McGraw-Hill Book Company , 1961, P503-504.
70.	D.K.Felbeck and A G Atkins, Fracture of Very Thin Sheets, Ch 14, P341-342, in Strength and Fracture of Engineering Solids,2nd Edition, 1996, Prentice Hall, ISBN 0-13-856113-3
71.	N.E. Dowling; True Stress Strain Interpretation of the Tension Test, pp126-134, section 4.5; Mechanical Behaviour of Materials, 3rd Edition , 2007, Prentice Hall, ISBN 0-13-186312-6.

Number	Detail
72.	R.W. Hertzberg; Deformation and Fracture Mechanics of Engineering Materials; 4th edition, Chapter 7, Page 273-274, and 321-333;J Wiley, 1996, ISBN 0-471-01214-9.
73.	R.E.Peterson, Stress Concentration Factors, John Wiley & Sons , NewYork, 1974, P 27-39 . ISBN 0-471-68329-9
74.	WE Hoare, E S Hedges and T K Barry; The Technology of Tinplate, Edward Arnold(London) 1961, Pages 311-312.
75.	J.H.Westerbrook: Segregation at Grain Boundaries, Table 1 , Some Effects of 3rd Element Modifiers on Segregation; Met Reviews, 1964, Vol 9, PP415-471.
76.	P.J.Smith; Environmental Stress Cracking in Processed Food Cans: Summary State of Knowledge on Prediction of Failure: Crown Technology Technical Record no TR11405.
77.	P.J.Smith; 96mm Dia Neo ends: Stress Corrosion tests and Examination of Factors affecting SCC End Performance with four 0.235mm DR620 ECCS Plate Variables. Crown Technology Technical Record no TR11710.
78.	P.J.Smith; Environmental Stress Cracking: Food Cans: Summary Report on Test Data. TR12077 Draft. Crown CT Project File z809.
79.	R.W. Hertzberg; Deformation and Fracture Mechanics of Engineering Materials; 4th edition, Chapter 8.2, Pages 321-333, J Wiley, 1996, ISBN 0-471-01214-9.
80.	H.Nisitani and M Isida; Simple Procedure for calculating K_I of Notch with crack of arbitary size and its application to Non Propagating Fatigue Crack, Proc. Joint JSME-SESA Conference on Experimental Mechanics (1982) Part 1, pp150-155.
81.	John O. Rawlings; Sastry G.Pantula and David A, Dickey; Applied Regression Analysis, 2nd edition, Springer , 2001. ISBN 0-387-98454-2.